AN INVESTIGATION OF COAL GASIFICATION BY RAPID HEATING TECHNIQUES

BY

M. AZHAKESAN B.Sc. M.Sc.

under the supervision of
Professor A. Williams, B.Sc., Ph.D.,
C.Chem., F.R.S.C., C.Eng., F.Inst.E.,
F.Inst.Pet., F.I.Gas E.

A thesis submitted in accordance with the requirements
for the degree of Doctor of Philosophy
in the University of Leeds.

Department of Fuel and Energy,
The University,
Leeds, LS2 9JT

March, 1988

ACKNOWLEDGEMENTS

A professor once said in his inaugural lecture, "Research is an intensely social affair". The author acknowledges if not wholly, but substantially the force of the above statement and expresses gratitude to all those who have contributed to the work reported herein. The author thanks all the technical staff of the Fuel and Energy department including R. Holt of the Electronics workshop. The author acknowledges many helpful suggestions and discussions with colleagues and with Mrs. Patricia Murdoch who has long been involved with coal pyrolysis modelling.

The author thanks Professor Alan Williams for his patient guidance.

Thanks are due to British Gas PLC for a grant which allowed the work reported to be carried out.

Finally, the author thanks with gratitude Mrs. Joan Cope for the typing of this thesis and to my brothers Sajeev and Sunil for their assistance, financial and otherwise towards the preparation of this thesis.

ABSTRACT

The phenomena of rapid pyrolysis has been investigated using the techniques of high speed electrical heating, fluidised bed heating, and high speed photomicrography. Secondary probes such as scanning electron micrography (SEM), gas chromatography, elemental and proximate analysis and FTIR spectroscopy have provided useful information for the subsequent analysis of the phenomena of rapid pyrolysis.

Total yields, time resolved gas yields and time resolved physical changes under dynamic conditions of particle heating have been collated by the use of gravimetric, gas chromatography and cine photography techniques.

Representative gas yields and total mass yields from the coals tested have been analysed by the use of an overall independant single reaction model and a multiple parallel reaction model. The results indicate that the evolution characteristics of classes of gas products show similiarity between the high volatile, low rank bituminous coals tested. The character of the product distribution and yield suggest that a series of complex, sequential and parallel reactions

are occuring with competitive reactions exerting an influence on product distribution.

Heating rate exerted an influence on product distribution even for the case of minimal mass transfer limitation conditions (simulation of single particle packing condition under vaccum conditions, using fine particles, 75/90um). There is thus a suggestion of diffusional limitations operating at high heating rate conditions. Total or ultimate yields show insensitivity to imposed heating rate over the range 10 - 5,000 °c/s.

Overall yields and photomicrography results suggest that the initial depolymerization reaction is a rapid low activation energy reaction. Product distributions reported suggest a large range of product types originating from substituted functional groups on the coal macro-molecule including long chain unsaturated groups. Secondary cracking reactions at high energy flux conditions contribute to severe cracking of the monomer units released from the liquified coal/char resulting in soot yields of differing types in the hot zones of the fluidised reactor.

CONTENTS

Chapter 1

THE CENTRALITY OF ENERGY TO THE ECONOMY

1.1 INTRODUCTION

With the beginning of the era of rapid industrialisation spearheaded by the Northern nations at the turn of the century, the problems of energy supply and demand has increasingly taxed the Governments of rich and poor nations alike.

The 50's and the 60's bought in their wake[1], rising levels of consumption and expectations fuelled by rapid technological advances concurrent with rapid economic growth. The consequent increase in energy demand and the demonstrably strong coorelation between rate of energy usage and various indicators of economic health has made energy a central issue in economic planning[3] and even in the political affairs of nations.

From an economic viewpoint, the fuel consumer is influenced by availability and security of supply, unit price, fuel cleanliness and ease of handling, disposable costs of waste products, energy density per quantity of fuel and legislation associated with each fuel[3].

The Arab/Israeli war of 1973 and to a lesser extent the Iranian revolution of 1979 put in jeopordy both security of supply and price stability of the most widely used fuel, oil, resulting in unpredictable movements of both price and availability. The resulting instability has had deliterious effects on the economies of various groups of nations, namely the major industralised Western nations, newly industrialising nations and ironically the economies of nations whose major currency earner happens

to be oil.

Despite rapid advances in alternative energy sources such as nuclear power, solar photovoltaic cells, wind turbines, fuel cells and hydroelectric power generation among a host of other energy sources, studies[1,3] have indicated that hydrocarbon fossil fuels will continue to play a major role concomittant with increasing energy demand.

Against a background of rising energy demand worldwide and an expectation of the inevitable decline of intensively exploited oil and gas resources, various multi-national energy companies [7,8] and governments[5,6] are turning towards the abundantly available reserves of coal.

1.2 Coal as Source of Bulk Chemicals and Energy

The use of coal worldwide as both a source of heat, light and as a source of gas and liquids is anything but new.[4,9] Indeed, the history of the gas industry in the U.K., owes its origins to gas produced by the thermal pyrolysis of coal. The consequent founding of a gas industry at the turn of the 19th century saw an uninterrupted growth of the gas industry to the present day, a process culminating in the creation of a vigorous British Gas Plc in 1987.

Besides its historic and current role as an energy source, coal was, up to the 1960's, the most important raw material for the manufacture of organic chemicals[11]. Coke oven gas, benzole and coal tar (from both gasworks and coke ovens)[9,11] provided the raw material for a whole host of products ranging from

pharmaceuticals, dyestuffs, pesticides, binders and electrode carbon. Coke production for metallurgical purposes in conjunction with tar and benzole for the production of aromatic chemicals remains an important route to date in many countries.

Coal is a complex, heterogeneous, sedementary rock with varying compositions of an admixture of organic and inorganic matter (Southern Hemisphere coals, the so called "Gondwana" coals may have up to 30% mineral matter associated with the organic part). Thus, the chemistry of all coal conversion processes must encompass an initial degradation step, or breakdown into smaller molecules. Degradation inevitably leads to a division of products into hydrogen rich and hydrogen poor (relative to say CH_4; see fig.1) vis-a-vis the organic carbon framework. Reference to fig.1[6] clearly illustrates the central problem associated with coal conversion to liquids/gases, i.e., the low H/C atomic ratios. Even in combustion processes, the H/C atomic ratio will determine coal combustion reactivity and ignition mechanism, among other factors.

The central problem of efficient utilization of available 'H' or the necessary addition of excess and relatively costly 'H' is then the focus of most research effort in coal conversion processes. There are three principal routes to coal degradation; carbonization/pyrolysis, synthesis and hydrogenation.

The first route has a long history (vide infra) and involves thermal treatment in the absence of air to produce volatizable products richer in 'H'. The second route based mainly on early German work involves degrading the solid to gaseous $CO + H_2$ and

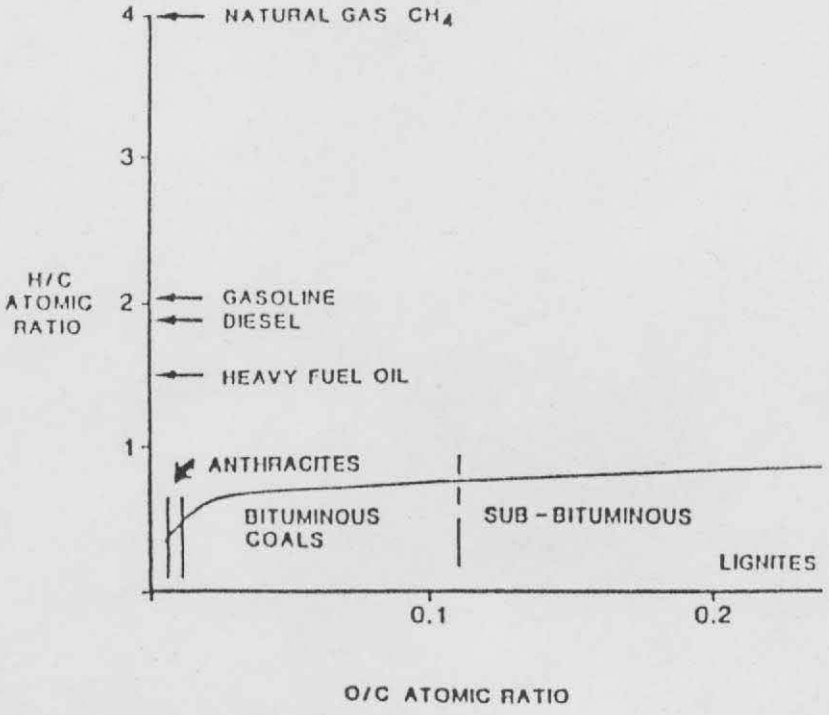

FIG. 1 Hydrogen to carbon ratios

consequently synthesising the required products catalytically via appropriate processes. The third route can be effected in two ways, either by the liquefection route via the addition of 'H' rich liquid (often delivered from coal liquids themselves) or the direct gasification of the coal by molecular 'H' gas under conditions of high temperature and pressure with/without the presence of solvents.

A variety of subprocesses are being tested[4,12] all of which are essentially derivants of the above three generic processes.

The workable reserves of coal at existing mines alone in the U.K., are estimated[(84)] to be in the region of 4.5×10^9 tonnes, are of good quality (i.e., relatively low ash), well distributed throughout the U.K., and as such can support a large part of the energy demand for the U.K., well into the 21st century.[(1)(3)]

Introduction of new mining techniques using machinery, began in the 1950's and even newer more efficient machinery (telechiric coalface cutting and handling) has seen the proportions of fine coal produced in mining rise from 20% - 30% in the 1970's to probably double this figure in the years ahead.[(10)]

This has important consequences for the type of coal conversion processes envisaged.[(10)] In the 1950's Russian work[(13)] on coal recognised this aspect of coal mining and set in train studies to utilize the coal fires so produced. Pulverized coal combustion is a process based solely on very finely crushed coal and early work, such as the Russian, including early B.C.U.R.A. work along

with U.S. research had given rise to high expectations of enhanced yields arising from processing of fine coal material in low density, disperse phase systems.

1.3 Philosophy and Purpose of Current Work

The impetus for the work undertaken and reported in this thesis stems from a continuation of coal research undertaken in the Fuel and Energy Department on the fundamental aspect of coal thermal decomposition over a number of years.

The emphasis of this work has been on British coals,[14,15] which in very broad terms are of a similiar nature to coals of similiar age in the Northern Hemisphere. Further, British Gas (Sponsor) which operates the slagging gasifier at Westfield, Scotland requires compilation of data on treatment of coal fines which have been injected separately into the vessel, being essentially a fixed bed system, treating lump coal. It is also assessing other, potentially thermally efficient[10] reactor systems such as fluidised bed and entrained flow systems which may prove to be the likely candidates for future coal gasification systems.

Finally, it is to be noted[16] that any basic or applied research on coal would be potentially beneficial as a source of data for any coal conversion processes, processes which in the view of the author seem to possess similiarities of a fundamental nature.

Many authors[16,18,19,20] have emphasised the importance of careful coal characterization in terms of origin and preparation of samples for study. Where possible this warning has been heeded.

Chapter 2

COAL PROCESSING SYSTEMS

An overview of the nature of the processes encountered in dealing with a heterogeneous solid reacting in a multiphase system, subjected to the effects of temperature, pressure and time history in that enviroment is presented in this chapter. A brief description of relevant reactor systems appropriate to the thrust of work undertaken in the present study is also presented.

2.1 System Parameters

A number of factors dictate the choice of a particular reactor system. In the introduction to this work some of the larger issues that might lead to the choice of coal as a starting point for conversion to more convenient fuels such as oil and gas had been touched on (vide infra). These issues are what one might call macro-system parameters encompassing economic, political and resource considerations. A further macro feature which has a more dircect bearing on the choice of a particular and/or multiplicity of processing systems and thus a particular reactor system is that of environmental considerations. All energy processing and production systems lead to unavoidable pollution of the environment in varying degrees, either thermal or material in kind. Such consideration have led to an asessment of more efficient reactor systems such as fluidised beds,[34][3][37] entrained flow systems[36,3,41,43] and the more

thermally efficient fixed bed systems such as the British Gas Lurgi gasifier.[42,40] These systems, under development by various companies, utilities and often supported by Government grants operate in many countries. The major operational goals defined for these systems are as follows:

- near complete gasification/conversion of a wide variety of coals;
- high reactor throughout;
- high thermal efficiency and efficient heat recovery;
- production of required product with minimum effect on environment;
- net production of energy (taking into consideration energy requirements for system operations) should be positive and comparable to liquid and gas production systems[44]

2.1.1. Features of Solid/Environment interactions

The prime consideration with regard to the technical utilization of coal, is that it is a highly concentrated form of solid matter. As the desired objective is to degrade the solid to more manageable forms (i.e., smaller molecules) such as liquids or gases, it therefore follows that some form of energy "hammer" must be applied to effect decomposition. Normally mined coal in lump form is subjected to mechanical treatment (i.e., a mechanical "hammer") to reduce its size before utilization in

say a pulverized combustion plant. A parallel analogy[45] can be made with regard to the application of a "thermal hammer" to the macromolecular solid structure of coal. All conversion processes involving coal, be it pyrolysis, gasification, liquefaction or combustion is therefore initiated by the application of heat to the solid coal in some form of chemical reactor (vide infra). As temperature is a intensive property derived from the application of a heat source, we may say that the coal is being subjected to a temperature "hammer". The heat source may be applied in situ in gasification processes by partial combustion of the organic part of coal and is known generically as an autothermal process. Indirect application of heat,[43] for example by nuclear heat to the coal/reactor system is known as a allothermal process.

The nature of the solid/environment interactions are dictated by the type of processing entailed and the reactor system chosen to attain desired products.

Thus, production of small molecules, say gases would require application of an intensive thermal hammer or high temperature, rapid heating, or putting it another way, a high thermal flux in a relatively short time interval.

Alternatively, if we desire a less extensive fragmentation of the molecular solid structure, we would subject the coal material to a light thermal hammer, such a process would entail moderate temperatures applied over a longer period of time resulting in a mainly carbonaceous residue with some production of gas and liquid, as in slow pyrolysis/carbonization processes.

If the production of liquids was the goal, then a moderate "thermal hammer" may be applied, perhaps in the presence of solvating agents as in the "H" donor process[45] and other liquefactic processes.[3]

Thus far we have identified six technological parameters in coal processing systems, namely reactor type, residence time, diluent fluid material (liquid or gas), nature of reactant material, temperature and heating rate ("thermal hammer").

The quantity and type of product distribution resulting from coal treatment is a function of the operating system parameters. Before attempting to examine these operational aspect in more detail, the relevent parameters are listed as follows:

- Pretreatment of the coal such as comminution and exposure to air/moisture[21,22,23] or other chemicals
- particle diameter
- particulate density/fuel bed thickness
- rate of heating of solids
- exposure time at the processing temperature
- effect of sweep gas
- rate of cooling of products
- effect of external pressure
- structure and morphology of sample investigated

2.2 Physical Transfer processes

The physical transfer processes involved in coal processing systems are heat and mass transfer including fluid mechanical aspects associated with pneumatic feed lines and flow patterns in individual reactor systems. All the parameters noted above and to be elaborated henceforth apply equally to laboratory scale studies and in particular to pyrolysis or thermal decompostion studies which is the particular process under study with respect to the work reported herein.

a) Heat Transfer Processes

As noted, the transfer of heat to the particulate coal material is the starting point for all conversion processes and as such deserves particular attention. Much of the confusion in the literature concerning the difficulty of decoupling the effects of heating rate from the final equilibrium temperature attained by the coal particle(s) may be traced to a lack of insight in this area.

In particular, there is a difference between heat source temperature and the rate of heat transfer,[46] belatedly recognised by the later studies of Solomon[35] and increasingly so by others[47,48,49,50,30] including the author of this current work.

In the reactor systems of interest, the mode of heat transfer depends very much on the reactor configuration and the fluid mechanical flow regimes encountered.

Conventionally, heat transfer is effected by conduction,

convection and radiation. Conductive heating throughout the target volume of the material may be particularly effective by unconventional heating techniques such as Ion and electron heating, R.F. and microwave heating, compressive heating (gases), mechanical heating by friction (liquids and solids)[46] and electrical heating (solids).

Tne problem of defining particulate temperature stems from a number of reasons. Most systems depend on measuring the temperature of the environment around the particulate matter, particularly so in dispersed phase flow systems. However the temperature so measured may well be a function of solids loading[48] or frictional heating of the thermocouple used to detect the temperature. The use of two colour pyrometry techniques[35] has improved the position somewhat, but problems of interpretation arise owing to the screening effect of sooty volatile clouds of decomposition products around the particle(s). Further complications are caused by the fact that CO_2 and H_2O products are also significant radiators at high temperatures.

The basic problem of heating a particulate, reacting solid in a defined time period is to be able to substain a sufficient heat flux that will cross the particle/environment boundary, to sustain that heating rate history. In order to do so, there must be very good contact between particle and heat source or the heat flux must be highly directed and concentrated as in laser heated systems. An excellent

review of the conceptual pitfalls encountered in various heat-transfer situation may be found in reference 46.

Owing to the complex hydrodynamic flow patterns in flow reactors, particles may be subjected to a range of temperature regimes and residence times dependant on whether the reactor flow field patterns are plug flow, turbulent or intermediate.[34,49,50] Further, rates of heat transfer may be enhanced by the use of solid material such as sand in fluidised beds,[67] by which means several hundred times more heat may be transfered than by hot gas at the same source temperature. The hydrodynamics of the reactor system affecting heat transfer are particle and carrier gas nature, extent of particle dispersion, extent of mixing of feed carrier gas streams[64,65,70] and primary, reactor gas streams, including the nature of feed injector geometry (in terms of location and number.)

Both convective heat transfer to a solid by hot fluid and radiation heat transfer from hot radiating walls can be reduced if particles are introduced into the reactor in a concentrated stream due to mutual particle/particle interaction. Secondary effects such as particle sintering in such dense steams at the high reaction temperatures encountered can lead to catastrophic changes in both hydrodynamic and reaction mechanism characteristics. Thus, defluidization can occur in fluidized beds caused by large sintered lumps, changes in char residence times in entrained reactors and secondary cracking and volatile matter capture by char can occur in all reactor systems.

Thermal properties in disperse, multiphase systems refer to effective values dependant on both nature of fluid and solid.

"Effective" physical properties such as thermal conductivity, difussivity (α_s) and specific heat (Cp), depend on porosity of particle, or for particle bed/streams on the porosity of the gas/particle composite. Thus, physical properties of the gas blanket, surrounding pressure, environment temperature and changing porosity of the reacting solid (or solid/gas composite where separation between particles determine porosity) determine it's temperature response.

At sufficiently low pressures, high temperatures and small particle size (e.g., fragments of devolatalised coal/ and soot/tar fragments), the particle is no longer surrounded by fluid continium. The resulting estimates of convective and diffusive rates, based on emperically derived relations such as Nusselt's number no longer hold.[52,66] Two effects arise from the atomistic nature of the fluid, namely velocity slip and temperature jump,[66] both of which lead to a reduction in convective heat transfer coefficient to the particle. When the relative velocity between particle and fluid is near zero, the effect of velocity slip disappears, whilst the temperature discontinuity at the fluid/particle interphase persists. For larger particle sizes, relative motion between particles and fluid is increased and enhances Nusselt's number.[50,66]

In certain reactor systems such as cyclone[27] reactors,

fluidised beds and even entrained flow systems,[35] particle convective motion brings particles into intermittent contact with the hot solid reactor surfaces. Such short contact times can lead to much enhanced heat transfer rates from the high thermal fluxes encountered.

b) Mass Transfer Effects

The physico-chemical, heterogeneity of coal with it probable 3-D polymeric nature, degrades under the action of heat into an increasingly porous matrix with consequent flow of gases/vapour through the developing pore structure. A reactive organic solid subjected to sufficiently high heat flux can pass into an "ablative" mode of reaction where decomposition occurs in depth of a certain thickness located at the particle surface and a thermal wave tied to the surface propagates into the material at it's intial temperature.[24,54]

Internal pressures may rise with evolution of gases and this so called 'blowing'/'pyrolysis wind' will place a limit on absorbed heat/flux[54,55] depending on the driving hydrodynamic pressure[32] developed from 'bottled' gas formation. Further reduction in heat transfer may result from liqui and gaseous product thickening of the boundary layer. Alternatively , the surface may reach sufficiently high temperatures to reradiate heat to its surroundings, depending on other things, its surface to volume ratio, shape and temperature with respect to its environment.

Evaporative cooling via a form of distillation boiling or subsaturation boiling as in a drying process could occur.

Owing to the highly structure dependant properties of coal in that it is porous, composing of distinct physico-chemical components (macerals) of differing thermal responsiveness and also layered in some respects (the more mature coals are highly oriented fused ring platelets) results in a profoundly complex pattern of mass transfer modes.

Gases produced may be expelled by jet like efflux[69,70,72,32] or pressure driven flow; soluble or permeable molecules can be released by bulk diffusion, driven by concentration gradients. With the onset of chemical decomposition reactions, gradients of concentrations may arise from different species superimposing diffusion velocities on mass mean flow velocities.

Coupled to natural defects in structure, gas formation may occur by phase change or chemical degradation in depth and may create cracks through which fluid may seep if other channels (e.g., pores) are not readily available. Coal particles that swell, melt and flow under the influence of heat, release gases through bubble formation followed by eruption at the particle surface.[54,73] Large mass losses in the form of volatiles can give rise to significant changes in the hydrodynamic character of the reactor/reactant system.

Phase changes caused by endothermic reaction and processes such as melting, solidification, sublimation and vaporisation may cause a qualitative and quantitative shift in heat and mass flux flow across the particle/environment interphase.

c) Chemical Process

Chemistry is the study of transformation of matter. The study of chemical transformations are based on the the application of thermodynamics and chemical kinetics to the system under study. Information as to the extent of reaction completion may be obtained with respect to the degree of thermodynamic equilibrium attained under reaction conditions of space, temperature and pressure.

Most gasification reactions considered require the imposition of high temperatures and pressures owing to the low reactivity of the highly carbonaceous coal solid and/or thermodynamic considerations.[74] The reaction conditions considered depend on the product mix desired. Direct production of methane requires the gasifier to be operated at high pressure, at high steam or (H_2)/coal ratio and the lowest acceptable temperature.

If CO and H_2 are the desired products, then low steam or (H_2)/coal ratio is fed in at low pressures at the highest attainable temperature, for complete gasification.

The physical transformation of coal under heat to a porous semisolid-liquid state with production of gaseous

volatiles due to pyrolysis reactions must result in a continuously shifting chemical environment. Under conditions of rapid heating, suspended particles and even captive ones, (see subsequent photographs) can fragment catastrophically following swelling and generation of extreme porosity due to rapid devolatalization at rising temperature levels.

A number of studies have also indicated that rapidly devolatalising coal releases highly reactive volatile 'C', leaving in it's turn, (under rapid heating conditions) a highly porous reactive char. (Reference may be made to the early work of Dent[75] at Leeds University, that of Johnson[76] and Howard, J.B.) In effect the subsequent hydrocracking reactions of volatiles and char gasification may be considered independently of each other. Catalytic reactions could occur on the surface of ash enriched char such as the water gas shift reaction.

Thermodynamic considerations, however, provide no information on the rate of chemical changes. To consider the effect of time on the rate of equilibration of chemical reaction we have to apply chemical kinetic techniques.

The kinetic study of dynamic solid state decompostion, however, in contrast to reactions in gases or solutions has to be elucidated with respect to the structure and morphology of the sample being investigated. Decomposition of solids represents a complex sum of simultaneously interdependant processes (vide infra).

Whereas the evaluation of over-all measurements of theoretical models leads to mostly artificial, theory dependant (i.e., not to reaction specific kinetic data) and to rather ambiguous mechanistic models, the careful elucidation of the microscopic processes by independant quantitative as well as qualitative techniques yield a framework for understanding of the kinetics.

It has been accepted practice to assume that organic solid decompostions proceed by an irreversable, first order decompostion process.[77] In a solid material, rate of decompostion is probably fixed by the rate of energy transfer. Energy of activation for internal rearrangements or bond breaking will depend on the accumulation of sufficient vibrational energy in the solid structure. Thermal energy is thus transferred into atomic oscillations increasing in magnitude as the temperature rises, resulting in localised centres of reaction[53] within the solid. This process will in turn depend on the vibrational coupling between different parts of the solid, i.e., the rate of reaction and it's temperature dependance will be a function of the structure of the solid (hence the necessity of the following morphology of the reacting solid). Large structures present in coal molecules with large numbers of vibrational modes can probably spread energy very rapidly through the coal structure.

Widespread variation in rate can be traced to either structural differences among coal samples or to the kinetic factors of energy of activation or entropy of activation.

In Eyring's activated complex theory of reaction rates, the pre-exponential factor for a unimolecular reaction has been estimated to be $10^{13}/s$ from the following relationship:[78]

$$A = \frac{RT}{hAv} \times e^{\Delta S''/R} \approx 10^{13}/S$$

$\Delta S''$ is the entropy of activation; Av = Avogadro's No.; h = Planck's constant. The pre-exponential factor, A had been computed for simple molecules. However a large reduction in entropy can result from the formation of an activated complex for complicated multistructured molecules, in which case the pre-exponential factor can be considerably below the assumed value (i.e., $<<10^{13}/S$.)

Further, the energy of activation will depend on the strength of the bond that is being broken and formed in the transistion state, and can be strongly influenced by factors such as solvation. Thus activation energies may vary by amounts ranging from 40 - 320kJ/mole. At room temperature, this variation in activation energy could give rate constants which differ by a factor of 10^{50}.

But, as noted earlier, solid state reactions, particularly for highly structured entity such as coal, the interpretation of rate data is an ambig ous affair. P.C. Yellow[77], in an excellent review of this area in 1965 brought attention to this long standing problem of assigning a meaningful 'Activation Energy' to rate processes encountered in solid state reactions. Indeed, many physically controlled processes such as the variation of viscosity with temperature, product layer formation,[17,79] rates of drying and cooling among

others may be approximated by the Arhenius-like equation

$k \equiv A \exp(-E/RT)$.

Most of these physical processes are of an activated diffusion type where the diffusion coefficient will change with temperature in a way similiar to the reaction rate constant (i.e. $k \equiv D$, the diffusion coefficient). For a more complete description of the problems encountered, references 79 and 80 should be consulted.

Further problems arise, in that in a decomposing solid, product fragments and vapours will have to find suitable paths for escape, i.e., to devolatalise. In the initial stages of pre-softening, heavy material released may be trapped within the solid structure unless cracks or natural fissures/pores exist to help its removal.

In the later stages, large fragments may have difficulty diffusing through thickening product layer. The question then arises as to whether the rate process observed is that of the 'intrinsic' pyrolysis rate or that of the 'devolatalization' rate which will be affected by the fluid-mechanical nature of the decomposition products. Are the two processes equivalent? There is a distinction then between rate of production of volatiles and the rate of their removal from the reaction zone.

The major factor of reaction variable is that of temperature which can cause a shift in reactions from simple disproportionation to more vigorous cracking & condensation polymerization at higher temperatures. Cracking reactions

may be sensitive to the presence of catalytic surfaces, which may include reactor surfaces.

Reactions can proceed simultaneous to temperature rise of the solid and this will lead to nonisothermal mass loss, where heating history may have a profound influence on the course and extent of reaction. Indeed, if heating rate has been found to be a variable of importance in coal processing systems, then clearly we are dealing with a nonisothermal process with its attendant difficulties with regard to elucidation of rate parameters.

2.3 Information Required For Reactor Design

Design of reactor systems depend on a stepwise procedure[29] whereby data on product distribution and yield based on feedstock character (chemical nature) coupled to thermodynamic information on reaction probabilities are tied to rate studies of the reaction process.

Interpretation of the rate studies and product distribution variation with temperature, time and imposed conditions of pressure, heat flux and diluent gas/liquid on the coal processing method chosen depends on a clear understanding of coal structure as a physical and chemical entity.

It is also necessary to try to separate and decouple the effects of 'primary' and 'secondary' reactions which may be a complicated function of equilibrium temperature of solid, residence time of products in hot zones and the temperature time history to which the coal had been subjected. Yield, product

distribution and mechanism of the reaction may be controlled and understood if such a separation is possible.

The question also arises as to whether the reaction is chemically controlled or physically controlled and the conditions that could arise where oscillations between such states are possible[33] as a function of changing conditions in a processing system. Such unstable multiple states may also be characteristic of the elementary chemical steps of the conversion system studied.

It is clear from the preceding discussions that the study of a general coal conversion process is a complex undertaking. However, the process under study in this work, rapid pyrolysis being of such fundamental and decisive influence in all coal conversion processes, needs to be probed from a number of vantage points and a data base built for it's eventual elucidation.

The discussion touched on physical transformations of the particulate and it is thus useful to follow by a battery of optical methods (e.g. S.E.M., photography etc.,) the dynamic kinetic transformations encountered.

Kinetic studies should be interpreted to provide information on reactor sizing in terms of lengths of heating and reaction zones.

Owing to the hetrogeneity of the coal and the complexity of the physical transfer phenomenae affecting the coal pyrolysis process many workers have suggested[52,53,54] a parallel study using qualitative and quantitative methods to help pinpoint the relevant characteristics of the process.

Care has to be exercised in the gathering,[20] preparation, storing[21][23] and use of the coal sample in any study concerning coal. This is a direct consequence of its physical heterogenity and evidence of 'structure' (porosity, defects and nonisotropic nature). Thus preparative procedures such as comminution and sizing have to be carefully assessed in[55,56,57] in the provision of a representative sample.

2.4 Extant Coal Processing Systems

Historically, including research on newer processes in the last 15/20 years, the number of coal conversion processes are enormous in variety and number. Generically they are of three types (vide infra) namely direct pyrolysis, synthesis and degradation of coal structure via direct or indirect hydrogenation. The routes chosen depend very much on resource/ political considerations (e.g. South Africa), market considerations and economics of processes vis a vis primary fossil fuel prices.

Present markets include domestic and industrial heating, power generation and coking for steel production.

Medium term future markets would include SNG for pipeline gas distribution, combined cycle power generation using low to medium C.V. gas, manufacture of chemicals in the petrochemical industry and liquid fuels for transport (petrol, diesel oil and jet fuel). The major markets by the year 2000 expected in the areas of petrochemical feedstocks, transport and industrial process heat have been estimated by British Coal, reproduced here in table 1.[81]

Table 1. Major Future Uses of Liquid Fuel by Year 2000

	Oil Demand ($x10^6$ tonnes)	
Industrial process heat	7	
Petrochemical and other non energy users	31	
Light road vehicles	31	
Other: Transport	18	Total: 77

However, in the long term future, integrated coal conversion/energy production complexes are likely candidates. The reasons stem from a) the nature of coal whose degradation/reaction results in production of char, tar liquids, gases and 'waste products' such as recoverable sulpher, ash (dry or slag form) and ammonia. All these can be utilized in one way or other as either fuel or process chemicals. b) thermodynamic limitation in plant operations can result in waste heat from the various process which can be recovered in part by using the concept of combined cycle power generation.

In this manner, reactive char from say flash pyrolysis processes[37] (an example is the OCCIDENTAL process) can be burned in pulverized coal boilers without derating with respect to normal coal feed. Hot gases from the gasification chamber can be burnt in a gas turbine to generate electricity. The hot gas exiting from the gas turbine, coupled to excess heat from the gasifier can be used to raise steam to power a steam turbine to produce more electricity.[38] Alternatively hydrogen may be manufactured by gasification of the char, for use in upgrading liquid fuels (hydrotreating), thus conserving expensive hydrogen.

Such processes have been studied, for example the COGAS process, a successor to the COED pyrolysis process,[37,81] the COG (coal/oil/gas) solvent extraction/hydrogenetion process, synthesis processes as in SASOL[82] (SASOL 1,2&3 produce a large range of transport fuels and chemical feedstocks) and most recently the Cool Water, IGCC (integrated gasification combined cycle) plant operated by the Electric Power Utility of Southern California.[38] The IGCC plant has received glowing reports in the press and has been hailed as a pointer to the future in terms of environmental performance, thermal efficiency and flexibility of operation, all expected features of integrated coal conversion plants. The British Gas slagging gasifier has been mooted as a potential candidate for integrated combined cycle power production.

The huge number of coal conversion processes is such that it is impossible to do justice in assessing their potential here. The following references provide ample source for perusal, namely, refs: 4,5,7,8,10,11,36,37,38,40,42,43,44,81 and 82.

Some of the reactor types and process parameters are summarised below.

2.4.1 Coal Conversion Parameters

In terms of thermal efficiency, pyrolysis provides the most efficient route to liquids production from coal, with efficiencies up to 80-90% compared to 50-70% for direct and indirect liquefaction processes.(37) Reactor systems used in the newer processes are mainly fluidized bed reactors or as in the Occidental process,

entrained flow reactors. A variant is the Rockwell International process which uses rocket motor technology. Residence times vary from tens of milliseconds to tens of seconds for fluidised beds. Temperatures vary from 316°C (1st stage of multistage COGAS process) to 1000°C. Pressures vary from about 1 bar to 145 bar for the various processes.[81]

In fluidised bed processes the coal feed may be contacted by non-reactive/reactive hot gases, or by recirculated hot char (German Lurghi-Rhurgas process) or inert, solid heat carrier as in the Toscoal[38] process. Most of the above processes use crushed, small particle sized feed.

A number of solvent extraction/hydrogenation processes are under study. These processes aim at a high conversion to liquid fuels by providing hydrogen in both molecular and solvent form. High conversion is effected non selectively, by breakages of the linking structures between coal macromolecules and eventual opening of ring structures. The extent of reaction is governed by temperature, hydrogen pressure and contact time, and the particular product distribution is governed by use of suitable catalysts.

Solvents are generally used to extract trapped material in the coal and are of three types, nonspecific solvents, specific solvents and degrading solvents. Specific solvents can extract up to 40% of the coal at temperatures as low as 200°C and is believed to be the main component of volatile matter evolved in heating coal. (Note: this is a contentious issue and is the subject of much debate with a direct bearing on coal constitution). Degrading

solvents are capable of extracting up to 90% of coal at temperatures around 400 °C. Thus pyrolysis contributes to the degradation of the coal structure whilst the solvent disperses and hence, retards polymorization reactions. Both inter and intra molecular reactions can occur in the presence of these solvents which are often themselves fractions of coal tar such as anthracene oil. Most of these processes are conducted under high pressure and use crushed coal[81] feed.

Coal gasification technologies and processes have been developed and commercialised for a long time. Generically, the different type of gasifiers can be classified as follows:

- Fixed bed gasifiers producting dry ash or slag (British slagging gasifier)
- Fluidized bed gasifiers producing dry or agglomerating ash (Note: high rates of heat transfer in fluidized beds can result in depressed fusion points for the ash).
- Entrained flow gasifiers yielding dry ash or slag during primary gasification (Shell-Koppers gasifier,[36] Texaco coal gasifier).
- Molten bath gasifiers (CO_2 Acceptor process using calcined limestone or dolomite as heat for gasification and selectively removes CO_2 and H_2S from the synthesis gases).

Other possible reactor systems are cyclone[27] reactors and ultra rapid fluidised reactor[28]. Normally, coal gasification

systems aim to manufacture high calorific value SNG to produce pipeline quality gas, particularly for gas utility operators. However, low C.V., gas may be used for electric power production in either combined cycle turbogenerators or direct firing in gas boilers. Production of CO and H_2 in gasification systems can be upgraded to a range of petrochemical products via the well understood Fischer-Tropsch reactions. Other upgrading processes include ethylene/propylene conversion using zeolite catalysts (Mobil/BASF process).[36]

Fixed beds generally accept lump coal with an admixture of up to 30% fines in the British slagging gasifier. Most of the other processes use coal feed in pulverized coal fines form (entrained beds; fluidised bed feed tend to be larger), fed in dry form or as coal/H_2O, coal/oil slurries. Operation is normally at high temperatures and relatively high pressures. Residence times in flow reactors are short, of the order of tens of milliseconds. (Entrained flow beds)

An important feature of some of these processes is the application of dispersed flow solids handling using gas as transport medium. Reference to figure 2 shows two forms of this solids handling aspect, namely particulate dense phase fluidization and entrained flow.

Fig 2: Flow Reactor Systems

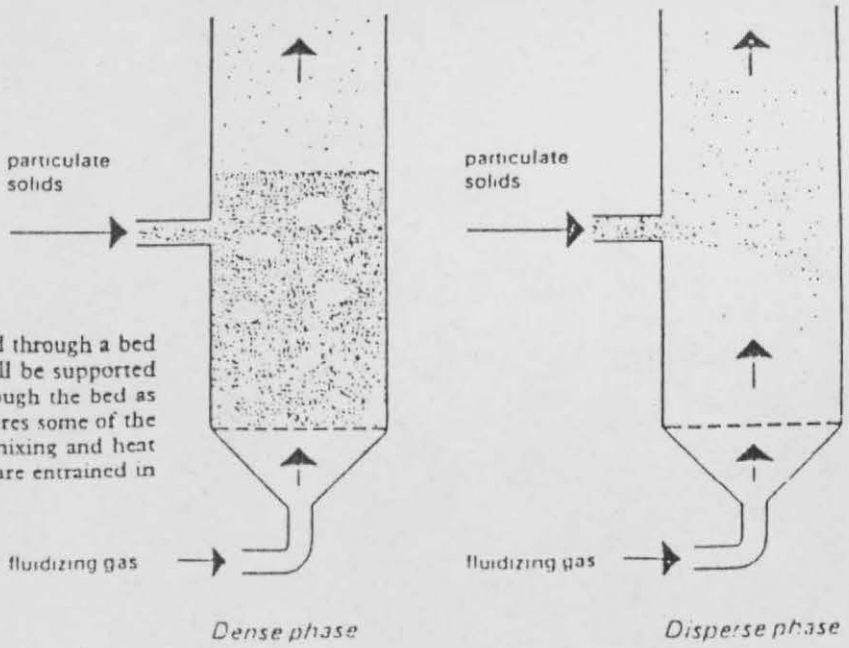

Forms of fluidization If gas is passed upward through a bed of particles with sufficient velocity, the bed will be supported by the gas stream and excess gas will pass through the bed as bubbles. This is termed a fluidized bed and shares some of the properties of a boiling liquid, including good mixing and heat transfer. At higher gas flow rates, the particles are entrained in the gas stream and removed from the vessel.

Solids handling in this manner allows for convenience in pneumatic tranport lines, efficient gas/solids mixing, high rates of heat transfer and uniformity of temperature distribution in the reaction zone. However there are problems of solids residence time control in fluidised beds and problems over agglomeration during pyrolysis (vide infra)

Chapter 3

PHYSICO-CHEMICAL ASPECTS OF COAL CONSTITUTION

Coal can be considered as an 'organic rock' if one is referring to Northern Hemisphere hard coals ('soft' coals possess significant associated moisture), and exclude Southern Hemisphere 'Gondwana' coals which are of a different age, associated with higher inorganic mineral matter and tend to be associated with a considerably higher inertinite content. Distribution and type of flora, geological history, diagentic and metamorphic processes including localised geological events produce that entity generically defined as coal. It is thus no surprise to learn that there is still fierce controversy in reconciling conflicting interpretations concerning studies of coal constitution and origin.

3.1 Origin, Diagenesis and Metamorphosis of Coal

An explosive evolution of land plant at the beginning of the carboriferous period followed by accumulation of plant debris provided the setting for the evolution of coal deposits. The major periods of coal formation are documented in figure 3. (ref. 85). There are two broad belts of coalfields from the older Carboniferous-Triassic Periods: a broad chain of large coalfields of carboniferous age extends from the U.S.A., through Western and Eastern Europe, the U.S.S.R., and into China; A second chain of Permo-Triassic coalfields is found in the Southern Continents, South America, Southern Africa, India,

FIG.3 AGE OF COAL MEASURES

GEOLOGICAL ERA	SYSTEM PERIOD	APROXIMATE MEAN AGE (YEARS)	RANK OF COALS FORMED
UPPER PALEOZOIC	CARBONIFEROUS	250×10^6	BITUMINOUS
	PERMIAN	210×10^6	CARBONACEOUS ANTHRACITES
MESOZIC	TRIASSIC	180×10^6	BITUMINOUS
	JURASSIC	150×10^6	BITUMINOUS
	CRETACEOUS	100×10^6	SUB-BITUMINOUS + BITUMINOUS
TERTIARY	EOCENE	60×10^6	LIGNITES + SUB-BITUMINOUS
	OLIGOCENE	40×10^6	LIGNITES
	MIOCENE	20×10^6	LIGNITES
QUATERNARY	PLEISTOCENE	1×10^6	PEAT ONLY

Australia and Antartica. Fully two thirds of the world's total reserves, all highly coalified (high rank) bituminous coals are of the carboniferous variety.[84] Reconstruction of continental configuaration at the end of the Permain period (225 x 10^6 years ago) showed that Northern Hemisphere coals were in fact formed in tropical swamps whereas Southern Hemisphere coals were formed from different flora consitent with formation in temperate southern latitudes. (see fig. 4 below)

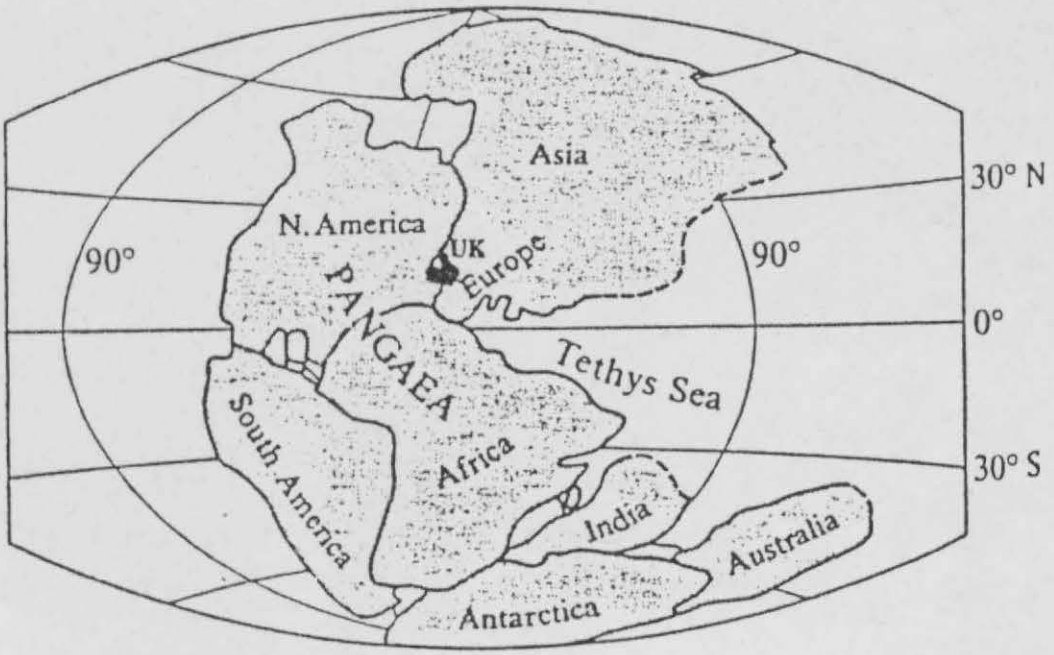

Fig. 4 Reconstruction of the continental configuration at the end of the Permian period 225 ma.

The coalfields are formed by sequences of sedementary rocks, with small coal layers (1-10%) sandwiched between variable alternations of shales, siltstones, sandstones and fossil soils

such as seat-earths.[84,85] Various terrestial fauna and flora such as root stock, plant stem, foliage, fish, bivalves/mussels (freshwater fauna), spores, pollen, fruit algal remains, including some marine fauna in low lying areas (most of the U.K., was covered by shallow seas during the latter carboniferous period) may be associated with the sedimentary layers. This rythmic pattern of sedementary deposition is referred to as cyclothems. Hence, different areas of coal measures are associated with varying environments of flora and fauna.

The changes that transform, mainly plant tissues to coal are effected through the sequential events of diagenesis (bacterial/ biochemical degradation process) through to formation of peat followed by metamorphosis over millions of years by the agencies of temperature and pressure (resulting from the accumulating overburden). The main constituents of coal forming plant structures, are tabulated below (Table 2) and some of the chemical structures of these coal precursors are shown (fig. 5).

Table 2. Plant Composition Precursors to Peat Formation

Plant Tissue	Compounds Present	% of Tissue	Avge. Ult. Analysis					Typical Empirical Formula
			C	H_2	O_2	N_2	S	
	1. Cellulose	45 - 65	44.4	6.2	49.4	-	-	$(C_6H_{10}O_5)n$
Wood	2. Lignin	20 - 40	63.2	6.1	30.7	-	-	$C_{10}H_{33}O_{11}$
(Xylen, Cortex)	3. Water + proteins in soln.	12 - 16	53.5	7.0	22.0	15.5	2.0	$C_{72}H_{112}N_{18}O_{22}S$
	4. Resins	0.5 - 15.0	80.0	10.0	10.0	-	-	$C_{20}H_{30}O_2$
	5. Waxes	0.2 - 4.0	82.0	14.2	3.8	-	-	$C_{29}H_{60}O$

The polymeric constituents of cellulose and lignin,

Cellulose

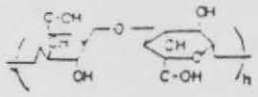

Protein

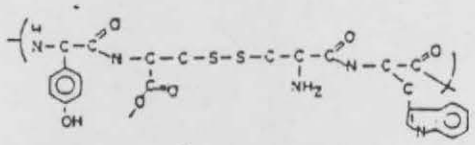

Waxes

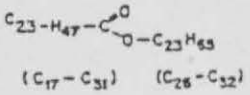

Resins

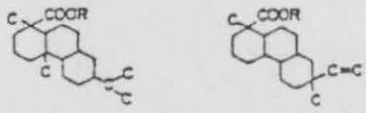

Terpenes

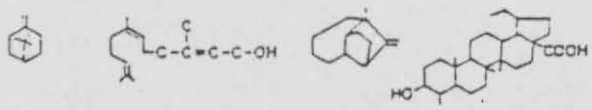

Sterols

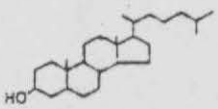

Flavonoids

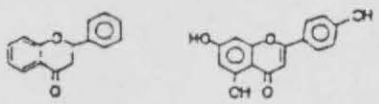

Tannins

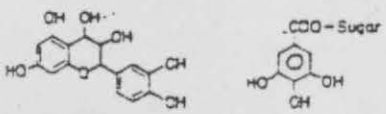

Lignins

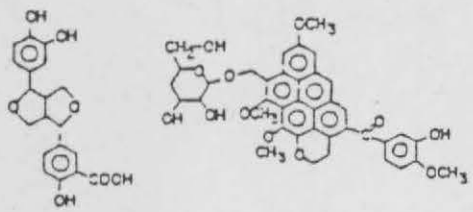

Alkaloids

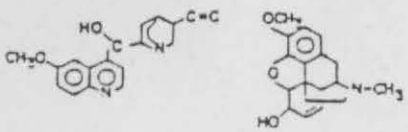

Structures of coal precursors

Fig. 5

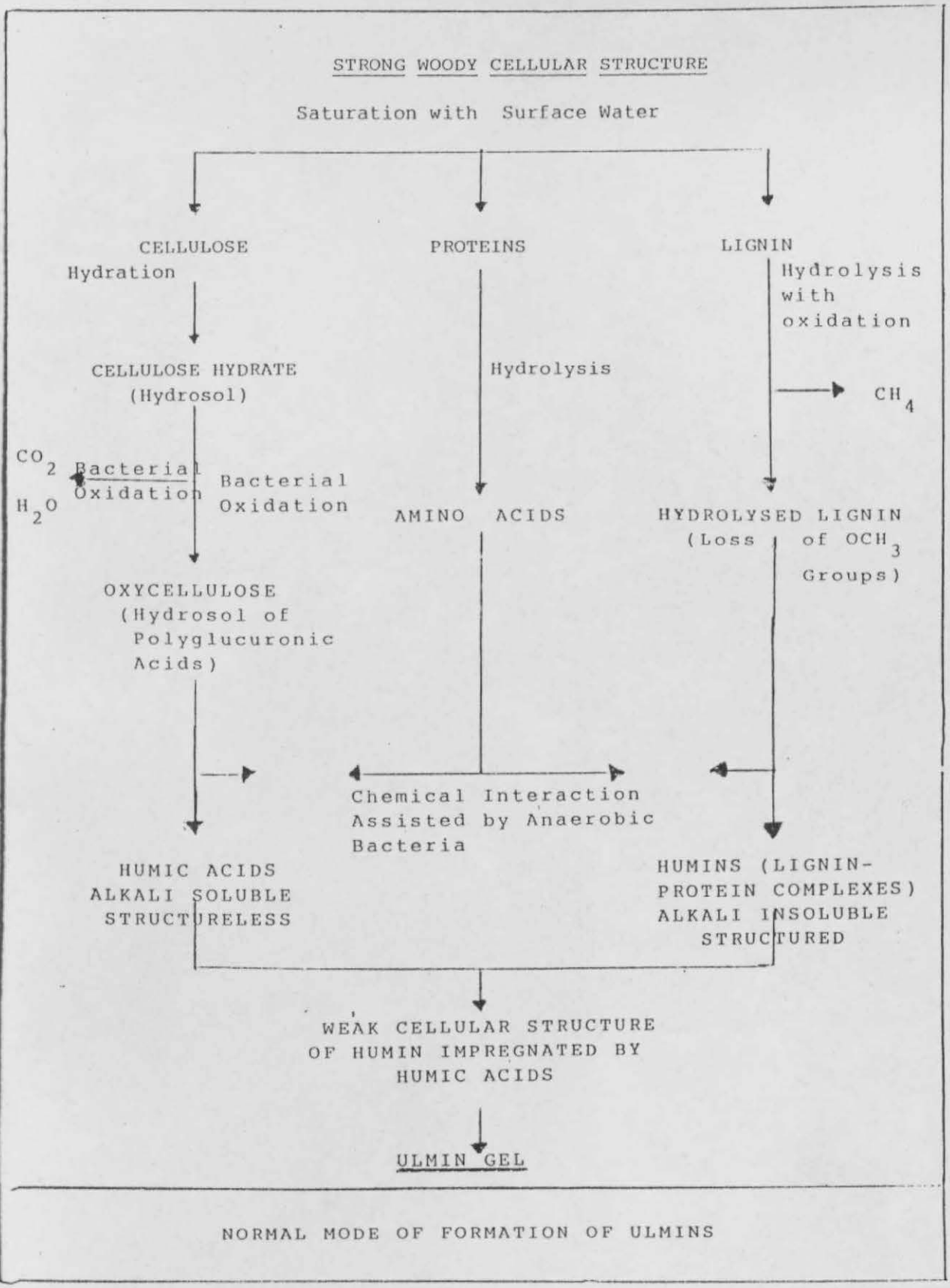

Fig. 6: Diagenetic processes leading to gelification.

the former alicyclic in nature (saturated rings), the latter, aromatic, with various 'O' functional groups attached to the respective ring structures make up the major precursors to coal formation. Proteins are complex molecules containing 'N' and 'S' and reaction of these with the degradation products of cell walls give humic acids which precedes the formation of ulmic gels in the peatification stage. 'Biochemical gelification' occurs during the peat/soft brown coal stages under varying conditions of alkalinity, oxidation, water supply etc. (refer fig. 6) give way to 'Geochemical gelification' in the metamorphic stage to eventual formation of the black lustrous Vitrinite component of bituminous coals, which is the major component of Northern Carboniferous coals.

Plant constituents which are most resistant to diagenesis up to the sub-bituminous coal stage (75-80%C) are those of waxes, resins, tannins, flavanoids, alkaloids and those cellulosic/ lignitic cell walls impregnated with these substances. Some of these materials contribute towards the aliphatic components of coal precursors. (Tannins, however are a mixture of high M.W. compounds possessing phenolic character and are also part of Vitrinite formation).

Other pathways to coalification, resulting in the 'sapropelic' coals (boghead and cannel which do occur in the U.K.) have somewhat different properties such as higher volatility, evidenced by higher 'H' content, are not covered in this review.

Following diagentic processes through to 'peatification', metamorphic processes acting over time transform the peat through successive stages to ultimatately graphite given sufficient time, temperature and pressure. These transformation processes result in progressive chemical and physical changes reflected by

elemental composition changes (fig. 1), volatile matter content changes, reactivity towards oxidising, hydrogenating and alkaline reagents, density and pore structure variations and changes in plastic properties (in the gelification stage preceding Bituminization).

The rate of chemical change is determined by time, temperature and pressure, the latter having the effect of bringing reacting insoluble groups into sufficient proximity to react and to retard rate of reactions resulting in volatile product evolution.

Thermodynamic considerations concerning compositional changes with reference to free energy of formation of H/C will indicate that formation of simple molecules are favoured with concurrent carboneaceous residue formation,[91] (fig. 7)

Thus, dehydrogenation and deoxygenation proceeds with CH_4, H_2O and CO_2 generation. This maturation process leads to a classification parameter of coal known as coal rank reflecting it's degree of metamorphosism from the original plant material. Ultimately, metamorphosis leads to a homogenisation of the coal substance by the anthracitic stage where fossilized remnants of plant material known as Macerals lose their separate identity.

Abnormal metamorphic processes such as contact with igneous rock intrusions, regional metamorphic events (folding, faulting, mountain formation) can give rise to either abnormally accelerated metamorphosis or regional variations in coal seam ranking. The prime effect on rank is temperature and in accordance with Hilt's Law, rank increases with depth as temperatures increase with depth. Temperatures of 150°C-350°C are associated

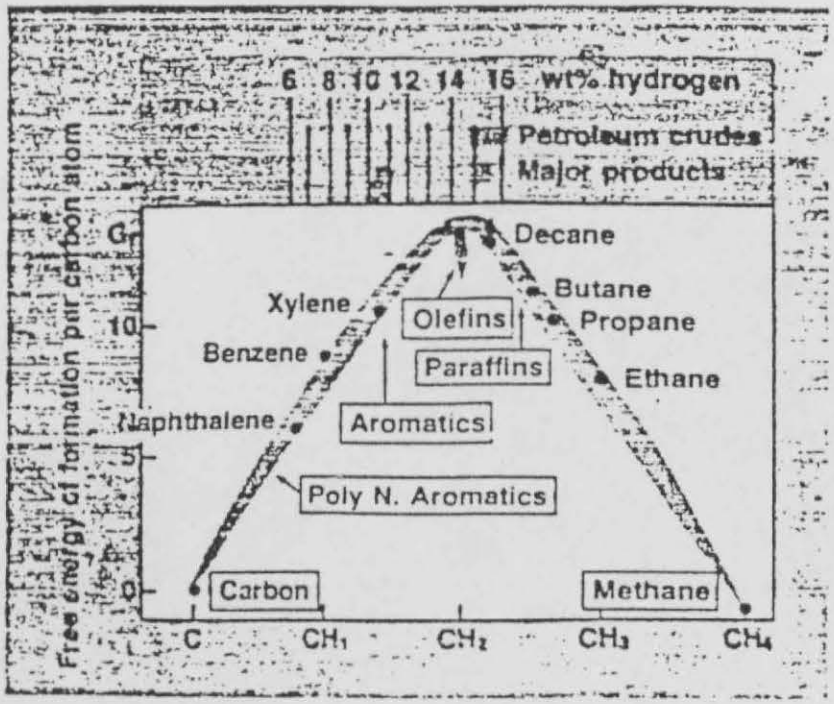

Fig. 7 How composition determines the free energy of formation of hydrocarbons

with this stage of coal formation. Chemical reactions proceed via simple dehydration, decarboxylation, dehydroxylation leading to condensation reactions[83] to subsequent, slow aromatization through cyclization and dehydrogenation of non aromatic structures at the high temperatures experienced by the high rank coals. These chemical and physical events have a profound parellel with the pyrolysis process to be discussed later.

3.2 Coal Viewed as a Mineral Rock

The variations in flora and fauna, diagenetic and metamorphic processes result in the formation of coals with different macro-features in the form of visible banded/layered structures classifiable as lithotypes. Unbanded coal is generally of post-cretaceous age,[83] but not necessarily so.[87] In the science of coal petrography, under the Stopes-Heerlen system of maceral (counterpart of inorganic rock minerals) classification the following petrographic organization of coal 'type' is encountered.

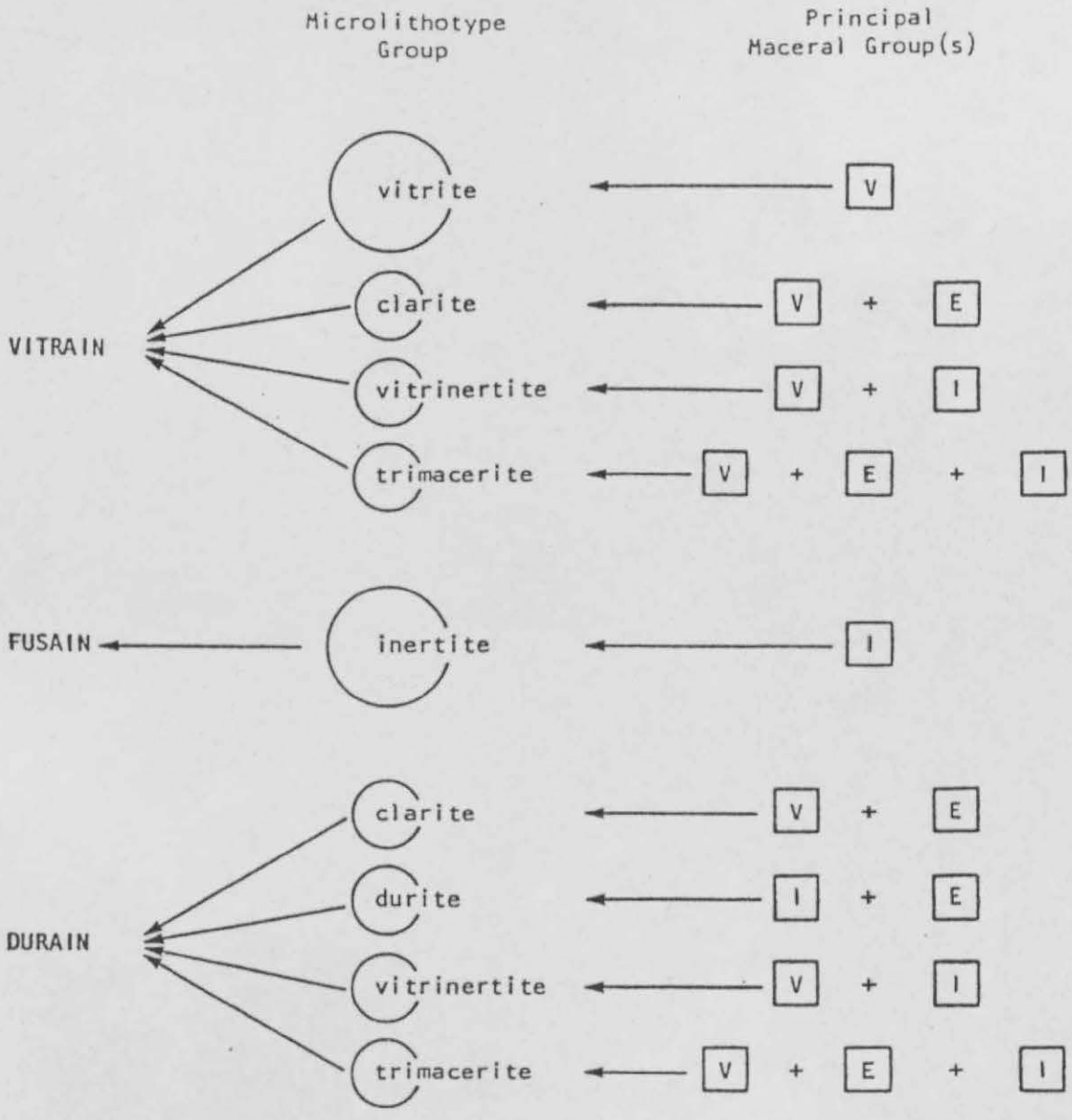

Fig.8 The petrographic 'organization' of coal.

Fig. 9 The macerals and maceral groups of coal (after Mackowsky, 1975)

Maceral group	Symbol	Maceral	Composed of or derived from
Vitrinite	V	Collinite	humic gels
		Telinite	wood, bark and cortical tissues
Exinite	E	Alginite	algal remains
		Cutinite	leaf cuticles
		Resinite	resin bodies and waxes
		Sporinite	fungal and other spores
Inertinite	I	Fusinite, Semifusinite	'carbonized' woody tissues
		Macrinite[b]	unspecified detrital matter, >10 µm
		Micrinite	unspecified detrital matter, <10 µm
		Sclerotinite	fungal spores and mycelia

Fig. 10

Macerals suggest new coal classification method

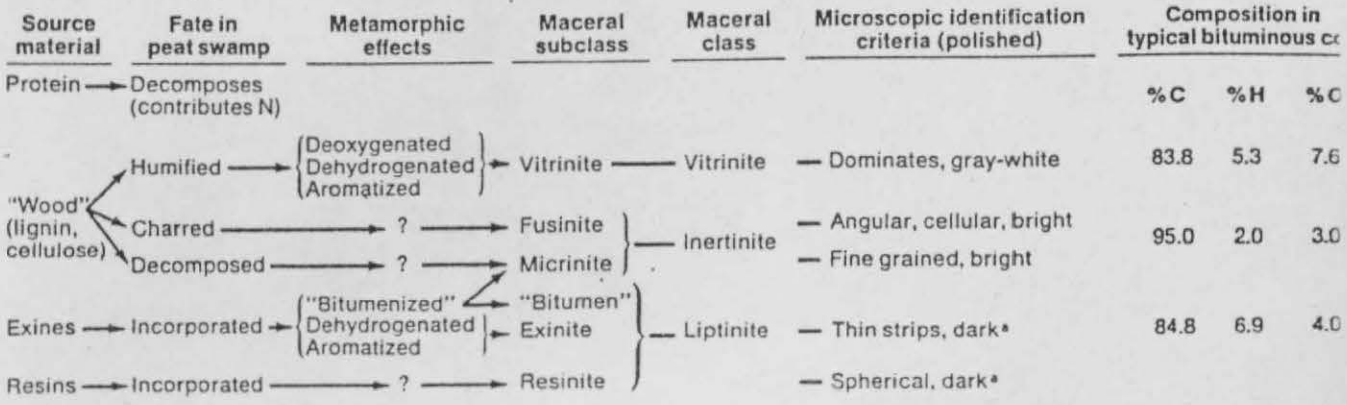

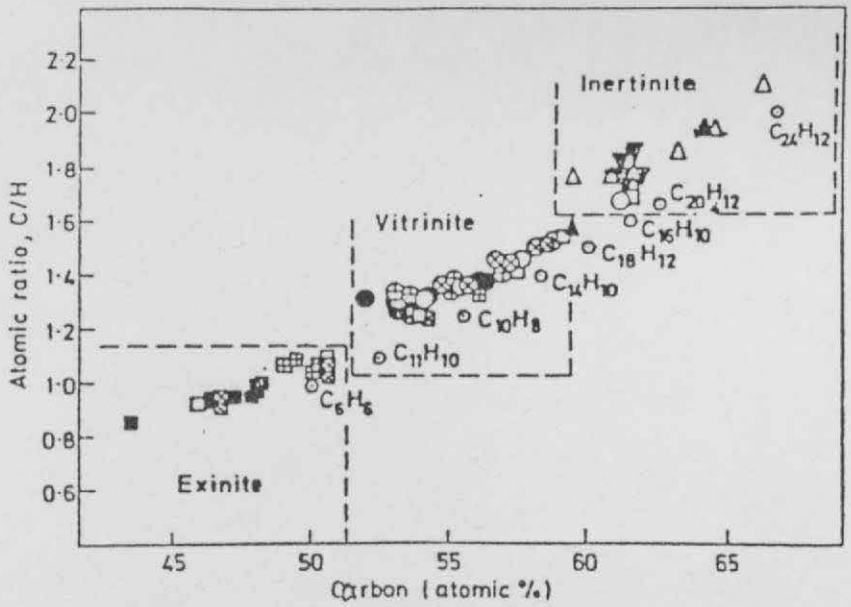

Fig. 11 Diagram of atomic C/H ratio vs atomic percentage of carbon (C_{at})

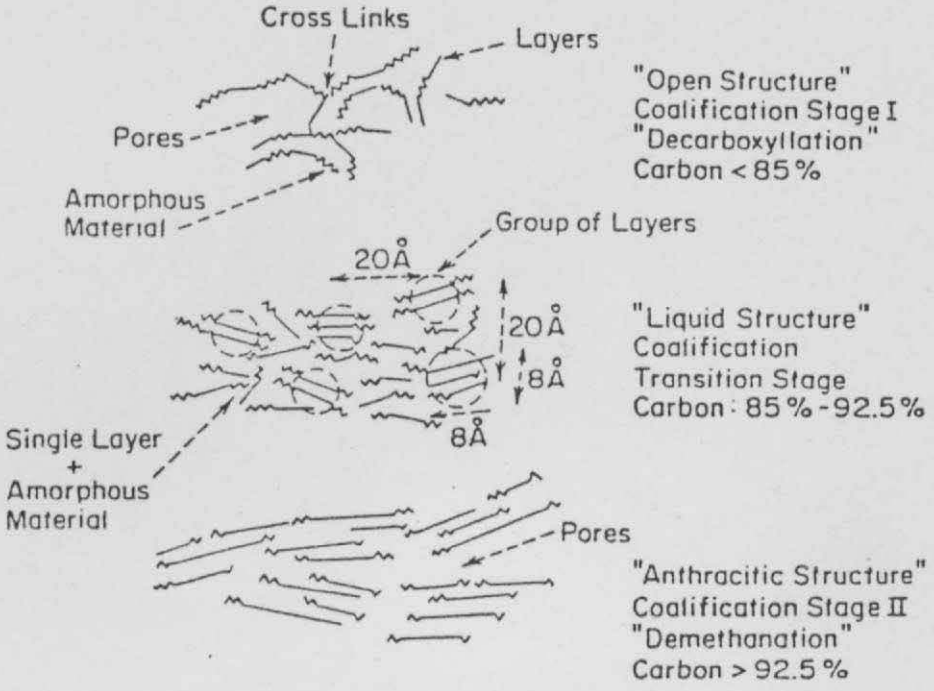

Fig. 12 Schematic illustrating coal structure during coalification Stage I or decarboxylation *(top)* – "open structure"; transition stage *(center)* – "liquid structure"; and coalification Stage II or demethanation *(bottom)* – "anthracitic structure."

Lithotypes and microlithotypes which are association of microscopic maceral groups represent the gross physico-chemical heterogeneity of banded coal.

The macerals are the microscopically distinct phases recognizable under reflected light microscopy and are organically and physically distinct (1-100μm size). They are in part visible, coalified plant remains with form and/or structure still preserved at the bituminous coal stage. They are also in part, degradation products where plant origins cannot be recognized anymore. Figures 9 [83] and 10 [88] summarises the origins, components and processes connected with the maceral groups. These macerals differ in volatile content, density, resistance to abrasion, and reflectivity. When classified by elemental compositional features of C/H ratio against atomic C% Kessler [89] was able to characterize the differing chemical compositions of the macerals into indentifiably distinct groups reflecting their individually different coalification paths. (see fig. 11) In banded coals, vitrinite is the main constituent, usually larger than 70% and whose relectivity variations with coalification is sufficiently regular to be a good indicator of rank.

Vitrinite originated from humic acid fractions of humic substances, which are dark coloured compounds of complex character of varying molecular weights and solubilities containing O, H, N and C atoms embedded in aromatic ring structures. Major 'O' functionalities are present as OH and COOH functional groups.

The inertinite Maceral group is relatively rich in 'C', of low 'H' content and highly aromatic compared to Exinite or Vitrinite even though it has evolved from the same original plant material as Vitrinite.[86] This can be traced to a more severe diagenetic or metamorphic processes encountered by the inertinite group. However, some of the inertinite Macerals are more reactive than previously thought, particularly micrinite and some Southern hemisphere inertinites.

Exinites originate from relatively 'H' rich plant material and therefore possess higher aliphatic content and 'H' content and significantly enhanced plastic deformation when subjected to heat. Although Extinites only account for between 5-15% of bituminous coals against 60-80% for Vitrinites, they can have a significant effect on coal morphology and reactivity in thermal processes, particularly as they are usually well distributed randomly thoughout the coal structure in small (micron size) to medium to large accretions.

The organic matrix of Macerals are punctuated with various pores of differing size and shape (10^{-5} - 10^{-9}nm) and the matrix is often fractured into crevices and cleats. (ref. 90, fig. 2). These cleats and crevices are defects which may play a role in voltatile mass transport and perhaps the 'peeling', exavaporative transport

behaviour observed and speculated on by the current author and others.[53]

The cleats, crevices and pores may often be filled with accretions of inorganic mineral matter. Mineral lenses and nodules also occur at the boundaries of the lithotypes. Mineral matter may originate from either inorganic constituents of the coal forming plants or adventitious inorganic matter introduced into coals by natural transport processes of wind and water during the diagenesis state or during the metamorphic stage where mineral matter is incorporated into the coal by an epigenetic process (deposits occur in defect cavities).

British coals are associated with mainly clay minerals, accounting for 60-80% of mineral matter associated with coal, particularly Kaolinite, transformed by epigenetic changes to Illite. Next to clays, the most important group of impurities are carbonates such as siderite ($Fe\ CO_3$) and ankerite ($Ca(Mg,Fe)(CO_3)_2$). Sulphur is present mainly in the form of pyrite and marcasite ($Fe\ S_2$). Other elements associated with coal impurities occur in traces including germanium, arsenic and uranium. Some of the metals such as Boron Ca,Na form organometal complexes, particularly in younger coals with 'O' functional groups.

Chlorides, sulphates, and nitrates are also incorporated by epigenetic process into the coal material.

3.3 Physical Aspects of Coal Structure

For a complex porous material such as coal, physical properties may exert a direct effect on measurements such as porosities (void volume of solid), density and stress/strain

relationships which themselves are a function of the chemical molecular structure of coal.

However, a distinction may be made between chemical and physico-structural changes effected during coalification (diagenetic and metamorphic processes). Porosity falls rapidly in the early stages of coalification due to loss of moisture by compressive overburden accumulation and drying. Post Brown coal stage coalification is reflected predominantly by elemental atomic changes and volatile matter content changes.

Because of the variation in coalification behaviour of the microscopic components of coal, i.e., Macerals (vide infra), differences occur in physico/chem., properties within and between particulate coal components.

3.3.1 Gross Overview of Physical Features

The vitrification of plant material results in Maceral types such as collinite (collinite and telinite are the major constituents of the Vitrinite Maceral group and which make up 60-80% of carboniferous coals) with a gel like structure with the cell lumens filled with colloidel humic gel precipitated from the humic solution This gel like structure has implications for the chemical constitution of coal (particularly in relation to the 2 component model) and its behaviour in thermal liquefaction and pyrolysis processes where dissolution by heat can transform the gel into sol (dispersion of solid in a liquid), paralleling the gelification stage of coal formation.

The Macerals differ in hardness, ash content, volatile content, density, porosity and very likely electrical, heat transfer properties (Cp, k) and physical deformation to applied stress.

In terms of density, micrinite (inertinite group, 1.41-1.46g/cm^3)> Vitrinite (1.32-1.37g/cm^3)> Exinite (1.2-1.35g/cm^3). Fractures and fissures occur in Vitrinite and is highly brittle in comparison to Exinite which is tough and resistant to fracture. Some components of Inertinite are charcoal-like and friable and some are extremely hard and highly reflective optically. Thus, components of Inertinite and mainly Vitrinite fracture easily to accumulate in the finer fractions when subjected to grinding. Grinding in air (in the presence of 'O' produces fines prone to agglomercation which can be avoided by grinding under cooled N_2 (see Chapter 5, experimental section). Fractures occur due to shrinkages generated by moisture and V.M., loss in the coalification process and directed by tectonic stress, including overburden pressure. Apart from grindability, the permeability of coal is highly related to the cleats and fractures which along with the pore size distribution will dictate mass transfer into and out of the particle. Like most of the properties of coal there is variation of these and other properties with coal rank (or coalification degree). Variation of porosity and density with rank (or %C d.a.f.) show a minimum of about 87-88%C which may represent a degree of pore closure brought about by coalification changes.[83,107]

The elucidation of pore structure and surface areas of coals present partially unresolved ontroversies due to the effects of activated diffusion and inbibation/coal-sorbent interactions encountered in the methods of measurement. The problem is that coal posesses a complex molecular sieve-like pore structure with large pores (macropores of several 100Å) to transitional pores

of $\sim 40\text{Å}$ which are linked by 5-8Å pores (micropores). Micropores predominate for medium to high rank coals (50-80% of total void volume)[83] whereas 75% of void space of low rank coal (<75%C) is associated with macro-pores. The second problem is that 'O' functional groups of particularly low rank coals interact strongly with polar sorbents. It is also not clear to the author how meaningful porosity and surface area measurements can be in a gel-like solid with substantial amounts, type and variations of trapped material in the pores/fractures including accretions of mineral matter in the same area. Nevertheless, the magnitude of the pore dimension represent useful information insofar as inbibation/exudation through solid material may be discounted in mass transport. The mean free path of gas/vapours which is related to its molecular weight will encounter changes in continiuum to Knudsen diffusion in the pore structure.

Surface area which are related to porosity range from tens of M^2/g to < 300 M^2/g.

Oxidative weathering can result in blocking of pores by 'O' absorption, pronounced in low rank coals and subsequent reduction in coal reactivity. Water association with the coal will depend on coal porosity, 'O' functionalities and type of inorganic matter present. Degassing of coal can result in partial collapse of the gel-like pore sturcture (or possibly blockage at narrow pore mouths by released trapped material in larger pores).

Of the Macerals Fusinite is probably the most porous with a broad range of pores (5-50nm), with Vitrinite possessing the finest porosity and Exinite being the least porous.

Certain physical properties show variation with bedding plane orientation. For example, electrical conductivity and thermal expansion coefficients[83] are higher pependicular to the bedding plane, the latter about twice as high compared to the parellel bedding plane . Thermal conductivities are higher parallel to the bedding plane and are also dependent on V.M., moisture content and properties of gases entrapped in the pore structure.

The study of coal by X-ray techniques began in the 1930's and after much reinterpretation[83,80] has provided 'ball park' figures for aromatic ring sizes, stack heights of ring layers and inter layer spacing. The interpretation of the diffraction spectra resulted in the structures represented in figure 12,[93] which is a reflection of the coalification stages of the metamorphosising coal material. The ordered layers represent aromatic crystallites and the amorphous 'C' may be associated with alkyl groups, -COOH,-OCH. and other non aromatic entities. Several points of interest may be noted:

1) Increasing orientation of the rings parallel to the bedding plane due to overburden pressure and the gradual coalesing of the aromatic clusters through loss of aliphatic side chains with coalification.

2) Groups of layers about 7-8 Å across and 20Å apart (for 85-92.5%C) for high rank Bit. coals reminescent of the pore sizes encountered here, including the reflection of large scale porosity associated with the 'open structure' X-ray picture of lower rank coals.

3) There may be a range of weaker bond interactions between the individual layers, ranging from 'H' bonds to weak Van der Waals interactions to dipole/dipole interactions which keep the solid phase together.

5) Other, stronger crosslinks via covalent bonding may arise as coalification proceeds provided by etheric, methylene and S bridges wrought by condensation reactions. [an area of controversy]

6) The stack heights range from 1 ("open structure") to > 2 for "liquid structure" to a sudden jump to much higher values at high C% (>93%C). These values indicate Polynuclear aromatic ring size of 2-4 pericondensed rings in coals of C content 80-92%.

Overall, the similiarity of C-C spacing and inter layer spacing to graphite suggest that lamellae structures similiar to graphite exist in coals and that these layers increase with 'C' content.

There is some indication that [83] the X-ray interpretation overestimates the actual aromatic layer sizes or that it may equally be reconciled with Alicyclic ring systems. Confirmation of the above picture is dependant on complementary information gained from NMR, FTIR, ESR and wet chemical studies.

3.4 Chemical Aspects of Coal Structure.

The chemical structure of coal, it has to be said, remains an area of darkness, with profound disagreements as to its primary organic structure. Thus, between 1972-1976 Chakrabarty and co-workers (including N. Berkowitz) engaged in fierce debate

with dissenters in the pages of 'Fuel' on the basis that coal was primarily a diamond-like polyamantine, alicyclic ring system. They based their conclusions on oxidation studies of coal using a relatively mild and highly specific oxidant Sodium Hypolchlorite. NaOcl does not cleave aromatic rings and can distinguish between sp^2 and sp^3C hybridisation. The crux of their argument was that, evidence of sp^3C suggested polyamantine as a likely structure amongst a host of possible forms. Further it has already been pointed out that X-ray studies of coal could equally be assigned to alicyclic ring systems as aromatic ones (vide infra). There is also indications from the work of Whitehurst[94] that high aromaticity in coal products (often taken as proof of coal aromaticity, in processes such as short-contact time liquefaction and vacuum or fast pyrolysis) is the result of the processing itself and not an intrinsic property of starting coal material. Also, heats of combustion of large polyamantine structure or partial isomerization of the same to Benzenic rings would be equivalent to coal heat of combustion. Further study[94] indicates that coal is highly reactive to 'H' doner (which could even be the Vitrinite material itself[95]) solvents such as Tetralin, which 'liquifies' the coal easily with little Hydrogen consumption (0.3-0.5%H). Chakrabarty further pointed out that coals easily oxidise and that solubility increased with bascity of solvent which is atypical of aromatic ring systems.

Nevertheless, the X-ray interpretations of C-C spacings including interlamellar spacing could equally sit well with a 2-D graphitic fused ring structure with layers held to each other by weak forces. [Note: The bigger the ring sizes, the stronger the Van der Waals forces].

Elemental coal composition suggests that several statistically preferred skeletal features such as, 2-4 ring structures, [83] condensed or otherwise with short/long sidechains can equally exist as much as polyamantane structures [94].

Chemical degradation methods such as oxidation, hydrogenation etc. seek to break the coal down into recognisable fragments and then reassemble the now more tractable fragments to arrive at the original structure. There is however, some evidence that certain oxidative studies, for example $Na_2 Cr_2 O_7$ oxidation studies by Hayatsu et al at temperatures near 250°C can give rise to aromatization of the coal structure by 'H' rearrangements or condensation reactions.

Direct characterization techniques have been applied to study coal by non-intrusive methods such as solid state NMR and FTIR spectroscopy, including ESR and as mentioned earlier, X-ray spectra.

The nature of solid, amorphous, black coal results in spectra which is complicated by broadening and overlapping. In theory, NMR should provide information on fractions of aromatic ^{13}C and ^{1}H in solid coals and thus allow estimates of coal aromaticity fraction.

Enhanced high resolution spectra from NMR employing dipolar decoupling, crosspolarization, magic angle spinning to enhance sensitivity and remove hetronuclear dipolar broadening and chemical shift anisotropy are used [98]. However, it is not clear if all the C is being polarized (i.e. being 'seen') owing to proximity to stable free radicls centered on relatively large polyaromatic H/C rings. This would increase the aromaticity values. However, nonpolarized 'C' could also be in polyamantine

structures and the resulting error would decrease aromaticity values. ESR studies on coal materials [96] indicates that the concentration of free radicals decreases in the order, Fusinite (Inertinite Group) >Vitrinite >Resinite (Exinitic Group) It was noted earlier that Inertite components may have been subjected to charring processes during coal metamorphosis. Hence it could easily have been highly aromatised, resulting in greater stabilization of free radical structures over large ring structures. Thus, interpretation of aromaticity is not necessarily an easy task by 'whole coal' analysis using spectral methods.

The ESR data is also debatable. Heteroatoms such as 'O' and 'N' in the coal framework posessing unpaired electrons would also contribute to the coal free-radical spectra (including any residual air in the sample) which would make resolution of the composite spectra difficult.

Despite the reservations expressed above, certain trends can be established which suggest that data from various sources such as FTIR, NMR,[98,83] chemical degradation studies,[97,90,99] including ESR provide sufficient similiarity to infer the presence of aromatic structures in coal. The important trends to note are 1) increasing aromaticity with rank (or %C) 2) increasing aromaticity with respect to Macerals where Intertinite>Vitrinite >Exinite which are both consistent with increasing coalification and coal genesis patterns. Overall, one can say that extremes of coal rank reflect extremes of aromatic/aliphatic carbon skeletal structure and the possibility of quite significant polycondensed saturated rings for low rank coal to highly aromatic structures for Anthracitic

coals. Significant variations in localised aromaticity and aliphaticity may occur for structures present in the medium to high volatile ranks coals. The number of aromatic rings per cluster size may be no more than 1-3 for coals 75-86%C, increasing rapidly to 5-6 rings for coals with %C>90%.[98] (refer Table 3).

3.4.1 Two-Component Model of Coal

The title describes a concept of coal structure that has persisted from the early days[60] stemming from Wheeler's work (using rapid and vacuum pyrolysis of coals) to that of Holden and Robb's mass spectrometry[60] study of coal carbonization (1958), through to Vahrman's solvent extraction studies (1969/1970) and Hayatsu et al's study of trapped molecules in coal,[101] to a series of papers in the 80's by Given,[102,103] Larsen[98] et al and others.[105,106] In more prosaic times gone by, Wheeler comments ".... coal contains 2 types of compounds, of degrees of ease of decomposition, the one yielding paraffinic H/C and the other yielding H2 with greater difficulty". This was dubbed the 2 component theory of coal constitution favoured by many, including Essenhigh to explain ignition phenomena, pyrolysis products noted at low temperatures (150-250°C) and solvent extraction from mild to more severe extractions. Latterly, this has been elevated to the status of the "moleculer sieve" structure with a "mobile" phase trapped inside a relatively rigid 3-D macromolecular structure. Mobility has been deduced from ^{1}H NMR studies of molecular motions of 'H' in the coal structure. Reference 102 provides a complete, by no means resolved debate by participants from 3 continents (U.S.A., Australia and Europe) on whether

Table 3

Structural Parameters of Coals

Coal	C (%)	H_{ar}/C_{ar}	H_{al}/C_{al}	Minimum average aromatic cluster size
Anthracite	93.0	0.23	2.06	30
Pocahontas #4	90.3	0.35	1.91	6
PSOC 268	86.5	0.36	1.75	3
Powellton	85.1	0.36	1.38	3
PSOC 124	83.8	0.31	1.69	1
PSOC 351	83.5	0.36	2.42	3
PSOC 501	83.4	0.32	2.31	3
PSOC 103	82.9	0.38	1.59	3
PSOC 640	82.7	0.31	2.34	3
PSOC 330	82.0	0.33	1.74	3
PSOC 170	82.0	0.34	2.14	3
Bumik 40660	81.3	0.35	2.11	3
Upper Mich	81.0	0.34	1.45	2
PSOC 212	79.4	0.31	1.91	3
PSOC 155	77.9	0.42	1.32	1
Star	77.0	0.34	1.89	2
PSOC 308	76.6	0.36	1.78	2
Lovilia	75.0	0.33	1.48	2

TABLE 4 COMPOSITIONAL VARIATIONS WITH RANK.

	% C
Peat	
Brown Coal	
Lignites	60-75
Subbituminous	75-80
Bituminous	80-91
Carbonaceous	91-93
Anthracites	93-95

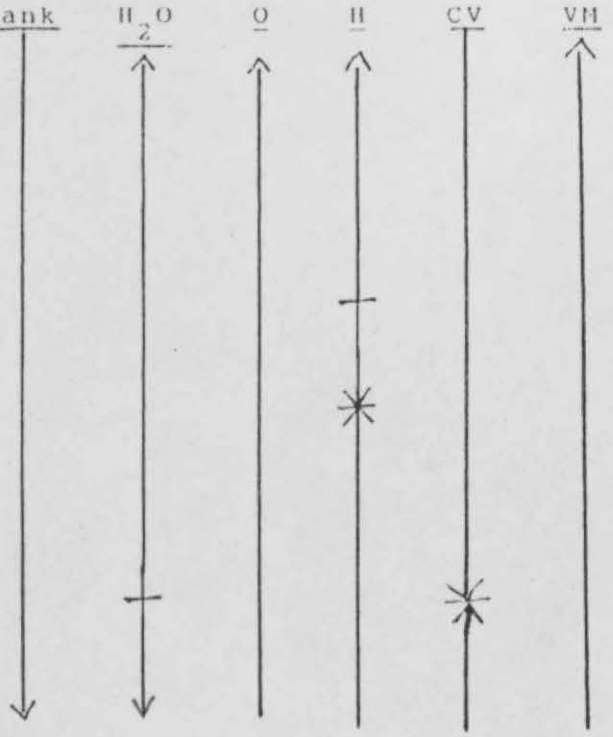

Note: 1) All components on d a.f. basis

2) Arrows indicate direction of increase

3) Adapted from ref. 85

4) The above classification is intended to show trends due to coalification and other classifications may be found in the literature.

coals contain a 'substantial fraction' (<50%) of relatively small molecules clatharated within the debatably 3-D, semi-rigid macromolecular network. Further, the question was raised by Given of the enhanced extractability of coals when shock heated, resulting in enhanced yield and speed of extraction. (This is a most interesting point and some studies of space-filling models of coal structures by Spiro, [107] observations of crumpled Lamallae sheets of carbonized coal [108] and some SEM studies by the author, all point toward this aspect of coal constitution).

With reference to the 'trapped' material, this has been deduced to be a complex series of compounds of a homologous series of n-alkyna pthalenes, furan and phenols, containing side chains of C_1-C_{22} and higher[102] alphatics including alicyclic and hydroaromatics and 2-3 ring fused aromatics, Heteroatomic thiopnenes and derivatives [101] (141 compounds isolated by Hayatsu etal). Anna Marzec et al, in their extraction study isolated over 300 compounds [110] with a wide range of molecular weights (700-800 amu, with 200-600 amu molecules predominating). A paper on CS_2 extraction of a suite of U.K., coals including M.Main (ref. 109) indicated the presence of n-alkane up to C_{50} chain lengths with other material of a wide range of molecular weights extending up to 1200 amu. 1-3 ring alkylated aromatics and polycyclic rings up to 10 rings such as ovalene and coronene, albiet in low concentrations were found.

A recent paper (ref. 106) finds some support for the latter study in finding stable, polycondensed species in the 'mobile'

phase in a suit of American coals.

3.4.2 Nature of Interaction between "Trapped" and "Rigid" Structure

Non valence bonds, chiefly electron donor interactions, 'H' bonds and Van der Waals interactions between aromatic planes (V. short range force) are assumed to hold the trapped molecules in the gel/isogel macromolecular structure. EDA interactions arise due to irregular electron density in the macromolecules and is determined by the presence of various functional groups with heteroatoms, O,N,S and C atoms with different hybridization of valence electrons. Separate structural blocks can posess various sets of sites which show electron donor properties (acid groups) and electron acceptor properties (basic groups). The acid/base nature of these structural sites depend on the chemical composition of the functional groups, their surroundings and aromaticity of the macromolecules. Larsen estimated that 'H' bonds between the 2 phases exceeds the number of macromolecular covalent crosslinks by a factor of four. P.C. Painter et al, applying FTIR techniques, indicate that the principal 'H' bonded groups in low and medium rank coals involve 'H' bonded chains or cyclic complexes of OH groups, some OH---ether bonds and a few OH---- basic N bonds.

Weak 'H' bonds and EDA bonds require quite low values for bond breaking of the order of 20-30 KJ/mole which explains high disintegration rates in solvents of bituminous coals at modest temperatures <100-350°C.

The crosslinking units in the macro-molecular structure are however likely to be covalent etheric, methylene, alicyclic

and hydroaromatic bridges (which have buckled structures) or more labile S-S bridges. The effect of 'S' in bridge stuctures can result in unusually thermally reactive response indicted by enhanced plastic flow including dissolution in appropriate solvents.

Before leaving this area of coal structure it must be said that the high quantity of trapped molecules assumed by Marzec and others could arise from part of the macromolecular structure becoming sufficiently flexible in the presence of solvents, thus contributing to the 'mobile H' content of coal detected by ^{1}H NMR. Therefore, disruption of secondary interactions between trapped material and 3-D macromolecular structure by solvents may be interpreted in two or more different ways. Further, certain coal/extract solvent interactions cause partial disintegration of the macromolecular structure. This contributes to the smaller molecular component parts of the trapped molecules and resultant overestimation of the trapped component. Moreover, the aspect of 3-D linkage is controversial because of uncertainty in applying solubility parameters or Flory-Huggins parameters to swelling experiments in support of cross linked macromolecular structures in coal.

3.5 Coal as a Physically Entangled Network

Interpretations of coal plasticity including swelling in solvolysis can be interpreted as an unravelling of an aggregation of molecules of large molecular weight distribution. Thus, larger molecules in strerically hindred or inaccessible parts could be prevented from swelling in powerful solvents whereas other parts of the structure imbibes and swells. Certain polymers melts and plasticise by an unravelling of intertwined chains.

Evidence for physical entanglements comes from a number of sources. In Sternberg's coal alkylation studies,[83] where aspects of this process were noted and thought to arise from steric hinderance phenomana is interpreted by Berkowitz to arise from highly assymetric physical entanglements. In this context it is noted that application of Sternberg reductive alkylation by Ignasiak [83] et al to coal was accompanied by release of atomic 'H' (about 20% from coal and the rest from solvent). Molecular weight distribution analysis of the products of coal by Sternberg reductive alkylation and the very different Friedel-Crafts acylation of coal by Hombach et al resulted in a very similiar high MW product distribution for both reactions. This was interpreted as a simple solvolysis of the coal resulting in a molecular weight distribution of coal plus added groups. From this Hombach concluded that coal was a mixture of large linear macromolecules. However, Larsen[(90)] has criticised this on two counts. Firstly, he concludes that the MW distribution results from reductive alkylation of depolymerized coal fragments and not the parent coal i.e., bonds have been cleaved in the parent coal (at possibly C-C and ether linkages). There are no clear reasons given for Friedel-Craft acylation results and any possibility here for coal bond breaking and further to the similiarity of MW distributions for the 2 reaction products.

Secondly, he cannot see how linear macromolecules can be held together without large intermolecular interactions as provided, for example by entanglements. Hence, by implication an alternative interpretation incorporating physical entanglements would be acceptable.

In this context one can envisage long chains being folded on to themselves in compact/roughly globular loops held by various kinds of bonds between different parts of the chain. (The stability of the structure could be preserved by those interactions discussed in section 3.4.2 and possibly stronger ionic and weakly covalent interactions between the 'trapped' material in coal and sourrounding macromolecules). This gel structure picture can be easily distrurbed by acidity, metallic salts, temperature changes and gas intercalation. This could explain the high solubilities of coal in some solvents, other reactions involving Lewis acids and also the release of trapped material concomittant with 'coagulation'/polymerization of the macromolecular part by thermolysis. Here, heat will favour macromolecule/macromolecule, interactions over weak 'macromolecule/smaller trapped molecule' bonds. Once the macromolecule is joined at one point their proximity will lead to more bonds once intercalated material is lost. Such interactions and structure occur in large, natural protein molecules. These features coupled to their similiar response to heat has caused the author to speculate thus in the preceding paragraph. However, as noted by Barton and Lynch, [102] a high degree of entanglement rather than covalent cross-links would prevent larger molecular sections of coal from dissolving in some powerful swelling solvents.

Further evidence of physical entanglements come from solvolytic extraction studies of coal at low temperatures.[83] Such features as swelling of coals and mutual alignment of coal lamellae by later metamorphic processes (compressive overburden accumulation with time) can be explained by physical entanglement without invoking 3-D cross linking. The alignment process could occur by

a progressive disentanglement by increased compression (helped by partial brakage of weak structures in coal skeletal structure? Demethylation, decarboxylation and cyclodehydrogenation at hydroaromatic parts of coal could be invoked as in Mazumdar et al).

3.6 An Alternative View of Coal Structure

An alternative viewpoint of coal structural parameters which reconciles rank changes with extant structural data is that of Mazumdar et al whose views are significantly different in certain key aspects. Whilst retaining generally accepted views on aromaticity indexes, elemental distribution and presence of hydroaromatic groups, they maintain the following, based on collated structural papameters of coal and their own studies:

1) Based on a differing view of dehydroxylation via atomic 'H', the authors maintain that coal structure up to anthracite cannot be 3-D/cross -linked 'polymer' as generally postulated as a possibility (Re: Van Krevelen Larsen et al). The authors quote the responsiveness to softening of high rank coals and organic substitution reactions such as nitration as reasons against extensive condensation by this rank. Further, onset of dehydre-genation of hydroaromatic part of coal at about 83%'C' with concommitant liberation of atomic 'H' could eliminate hydroxyl groups by the same mechanism and so avoiding cross linking.

2) The linkages between structural 'units' is envisaged to be γ-pyrone in the lignitic stage to δ-pyran during coalification. Etheric linkages do

not occur until the 85%C stage via hydro-splitting of γ-pyran. Other linkages occur via single methylene bridges or C-C bridges. (Note: Refer to Tsai, ref. 111, page 95 which shows an anamolous increase of etheric 'O' from subit. coal to Bit. coal and also refer to fig. 18).

3) The disposition of the hydroaromatic moity is viewed as a side chain to the aromatic coal nucleus which allows cyclo-dehydrogenation/cyclisation reactions during coalification which would facilitate the features mentioned above including increased aromatization with rank. It is to be noted that other 'models' of coal have been envisaged with tetralin, decalin and/or dihydro-anthracene as the basic structural unit and are universally based on coals of 'C' of 80-83%.

Overall, it must be said that Mazumder et al's representations in particular hydroaromatic placing, which facilitates production of nascant 'H' can explain mechanism of 'capping' of radicalised coal fragments split off in thermal processes. Moreover it sits well with x-ray diffraction features of coal rank changes (e.g., orientation of parallel packing of lamallae, etc.) and also finds some support in Spiro's space filling models.[107] Spiro, however invoked 3-D cross linking via extra methylene bridges and aliphatic hydroaromatic including alicyclic protrusions from extended planar aromatic regions covalently bonding the layers together. Consequently thermolysis is envisaged as freeing the locked lamallea by the breaking of 'weak' covalent bonds attaching the protrusions to

the lamallae. Thus the lamallae is able to 'slide' over the intercalated fragments which act as 'mobile' spacers (see fig. 20)

It should be noted that Spiro and Mazamder et al, have underplayed the effect of physically 'trapped' material known to be present in coal (the debate centres only on the magnitude of the amount so intercalted; vide infra). Therefore it is possible to explain, substantially, coal thermolysis and extractability, including coal structural features and changes by retaining the main ingrediants of lamaller planarity, hydroaromatic features and including 'trapped' material (small MW aromatics, long chain aliphatics, etc) whilst discounting 3-D cross linking. Essentially we hark back to that old concept of the 2 component theory of coal constitution minus 3-D cross linking. The forces holding such a structure would be those discussed in section 3.4.2 (vide infra).

One further criticism of Mazumdar's models is the lack of consideration of 'S' heteroatom which can have profound effects on reactivity, particularly the highly siscile S-S bridge, if present. Both Berkowitz and Attar have stressed the importance of 'S' as a heteroatom. However it is noted that 'S' is readily interchangeable [111] with 'O' in some of the bridge groups and ring structures including their substituents.

3.7 Heteroatom Functionalities

The heteroatom functionalities range from 'O' in ketonic/carboxylic, etheric, quinonic and phenolic groups to 'S' in thiophenic and such like heterocyclic rings and possibly present as bridges. 'N' heteroatoms probably occur in pyrrolic and pyridine structures. Organomentallic bonds may exist giving

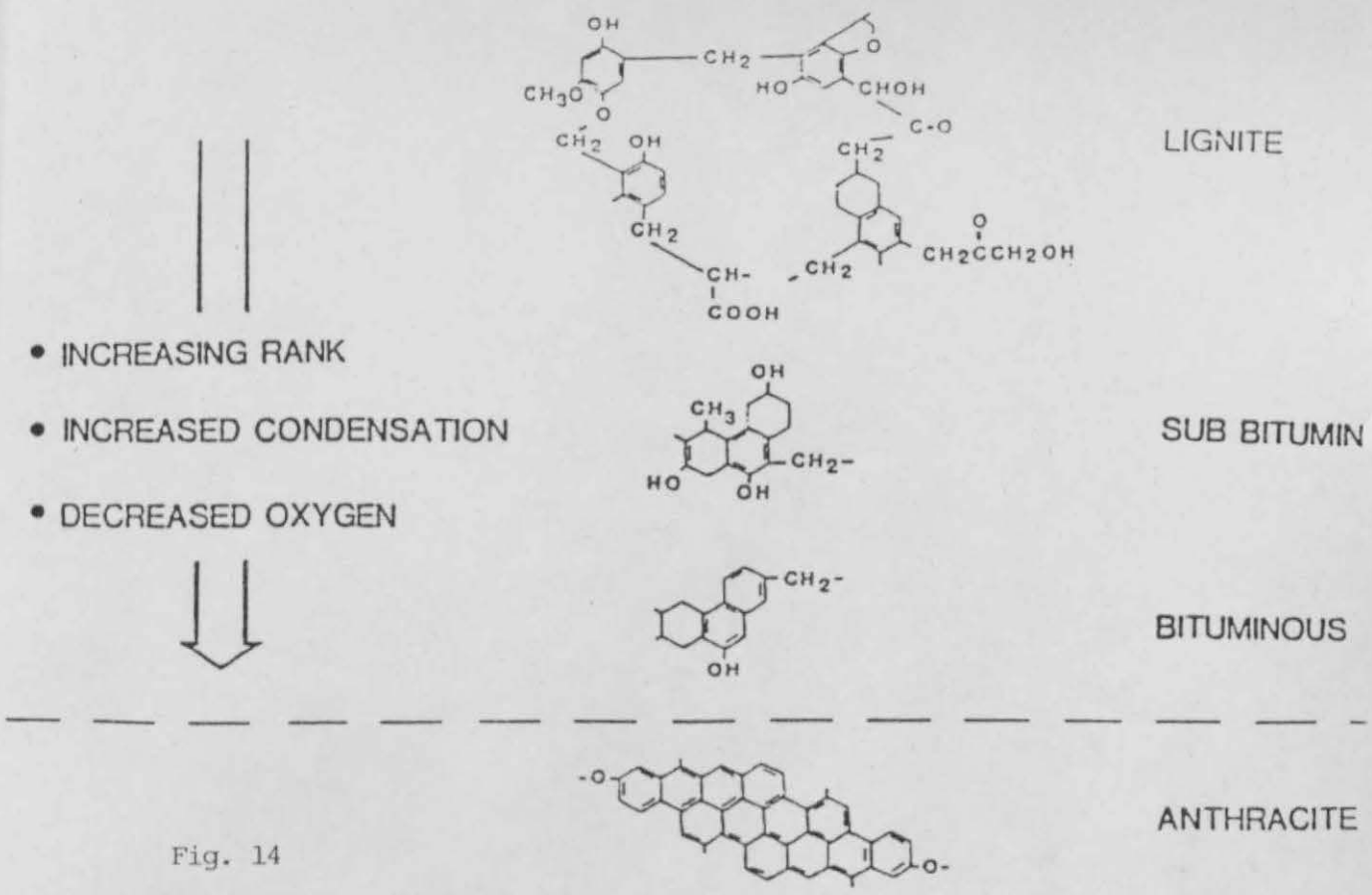

Fig. 14

Relationship between rank and aromaticity

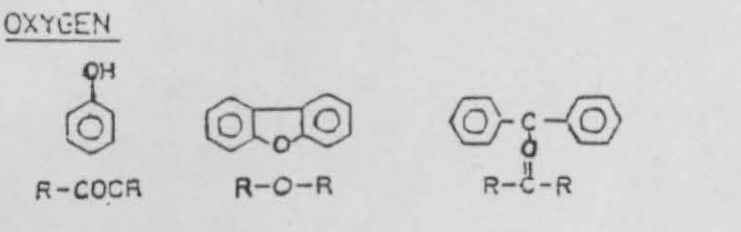

Fig. 15 *Functional groups found in coal*

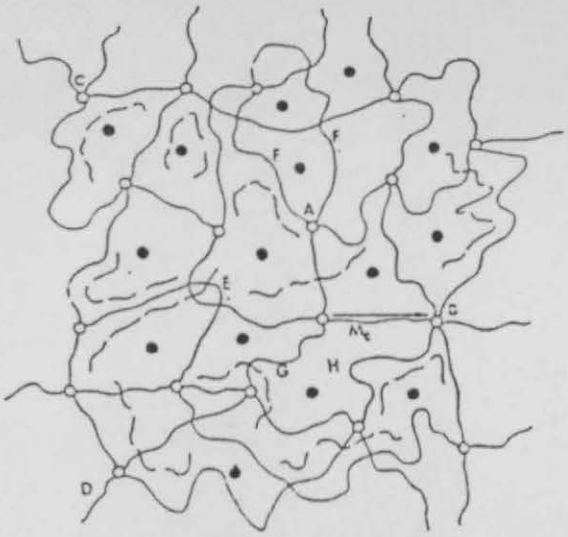

Fig. 16 Simplified representation of the crosslinked structure of coal including possible defects. ——: Chains participating in network structure; — — — —: extractable (unreacted or degraded) chains; O : crosslinks (junctions); ● molecules of swelling agent; $\bar{M}_c$: molecular weight between crosslinks; A: tetrafunctional crosslink; B: multifunctional crosslink; C: unreacted functionalities; D: chain end; E: entanglement; F: chain loop; G: effective network chain; H: mesh size.

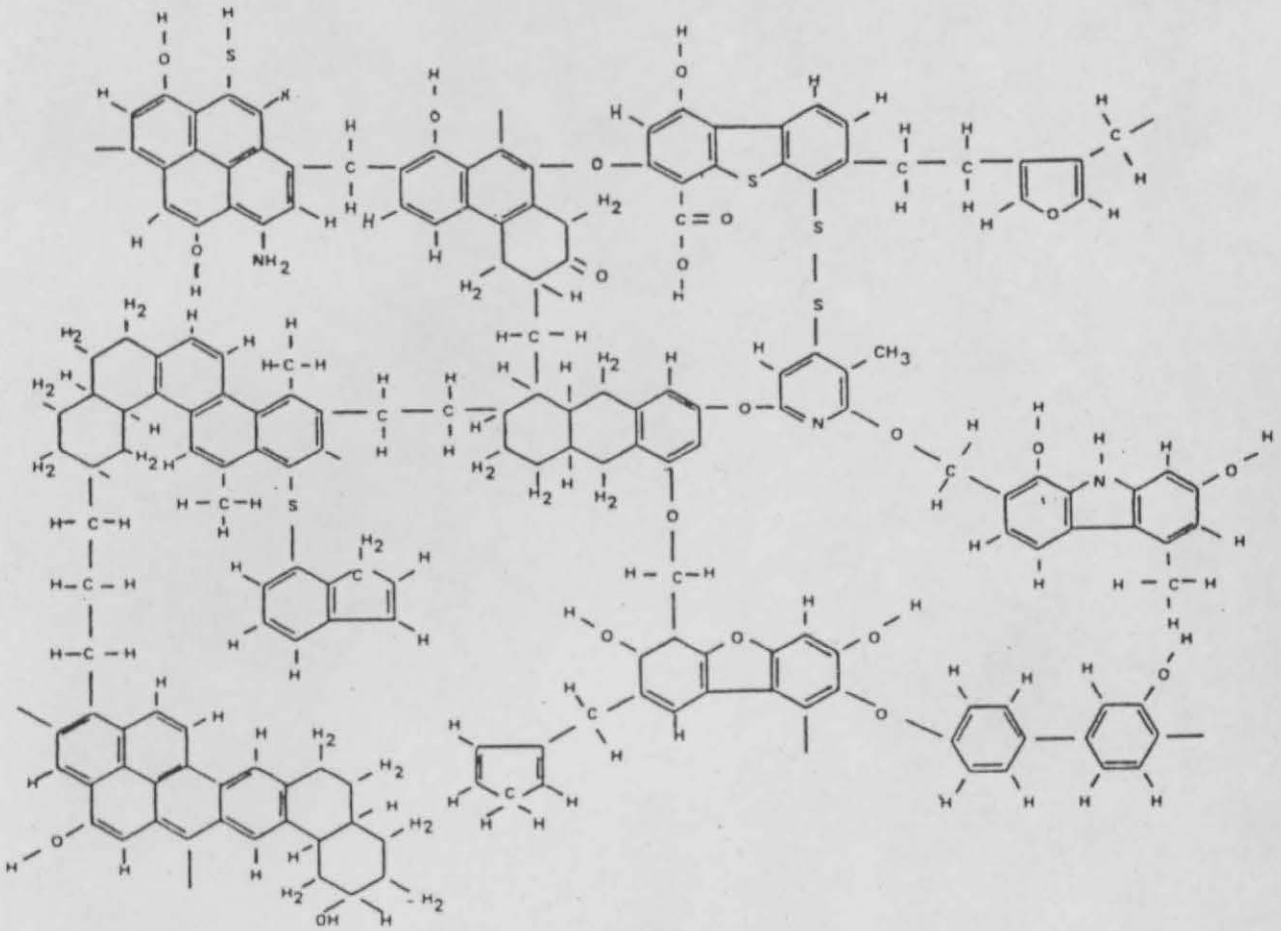

Fig. 17 Schematic representation of structural groups and connecting bridges in bituminous coal (by W. H. Wiser, *in* Sternberg, 1975)

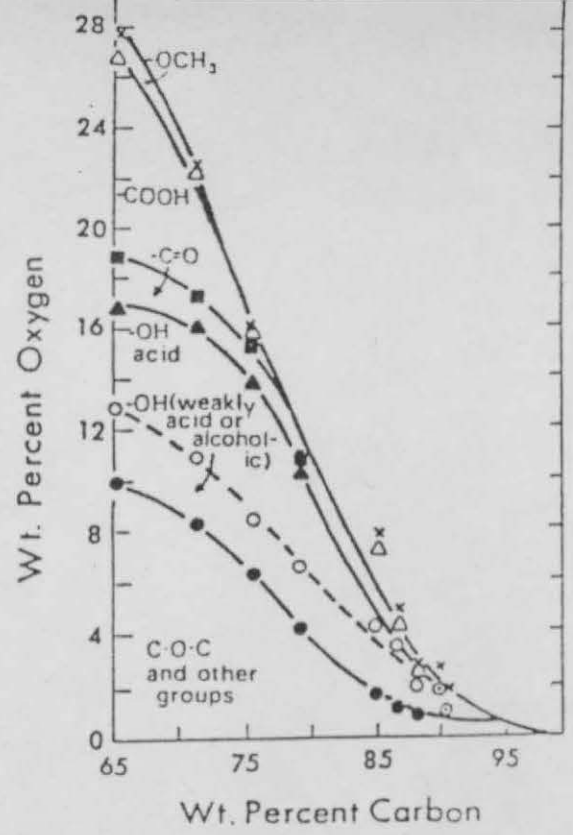

Fig. 18 Oxygen functional groups in coal

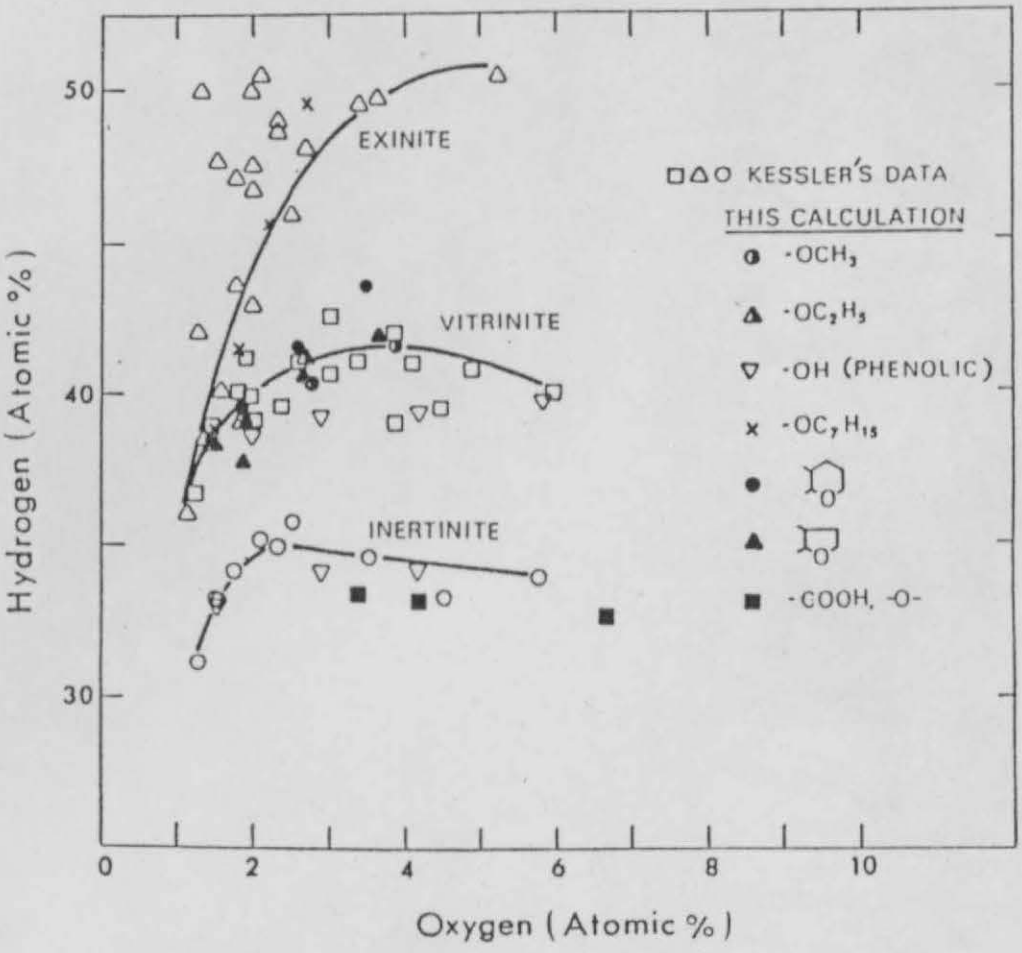

Fig. 19 Hydrogen to oxygen contents of coal maceral groups and oxygen functional groups in coal

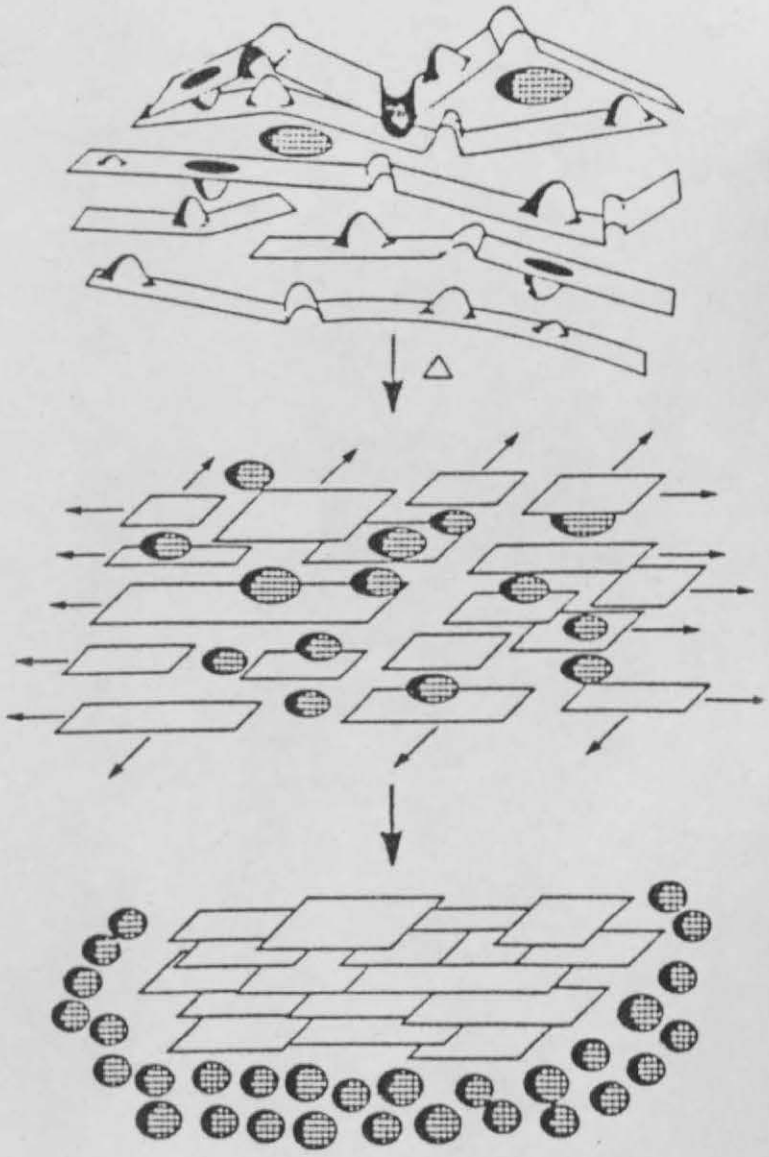

Fig. 20 Schematic illustration of coal pyrolysis. Initially the molecules exist in lamellae with flat aromatic planes interrupted by aliphatic protrusions. Next, thermolysis results in enhanced parallelism of aryl planes accompanied by two-dimensional mobil Finally, when lubricating fragments and gases diffuse from the planes, the char and pore system of the semicoke develops

Re: Spiro et al

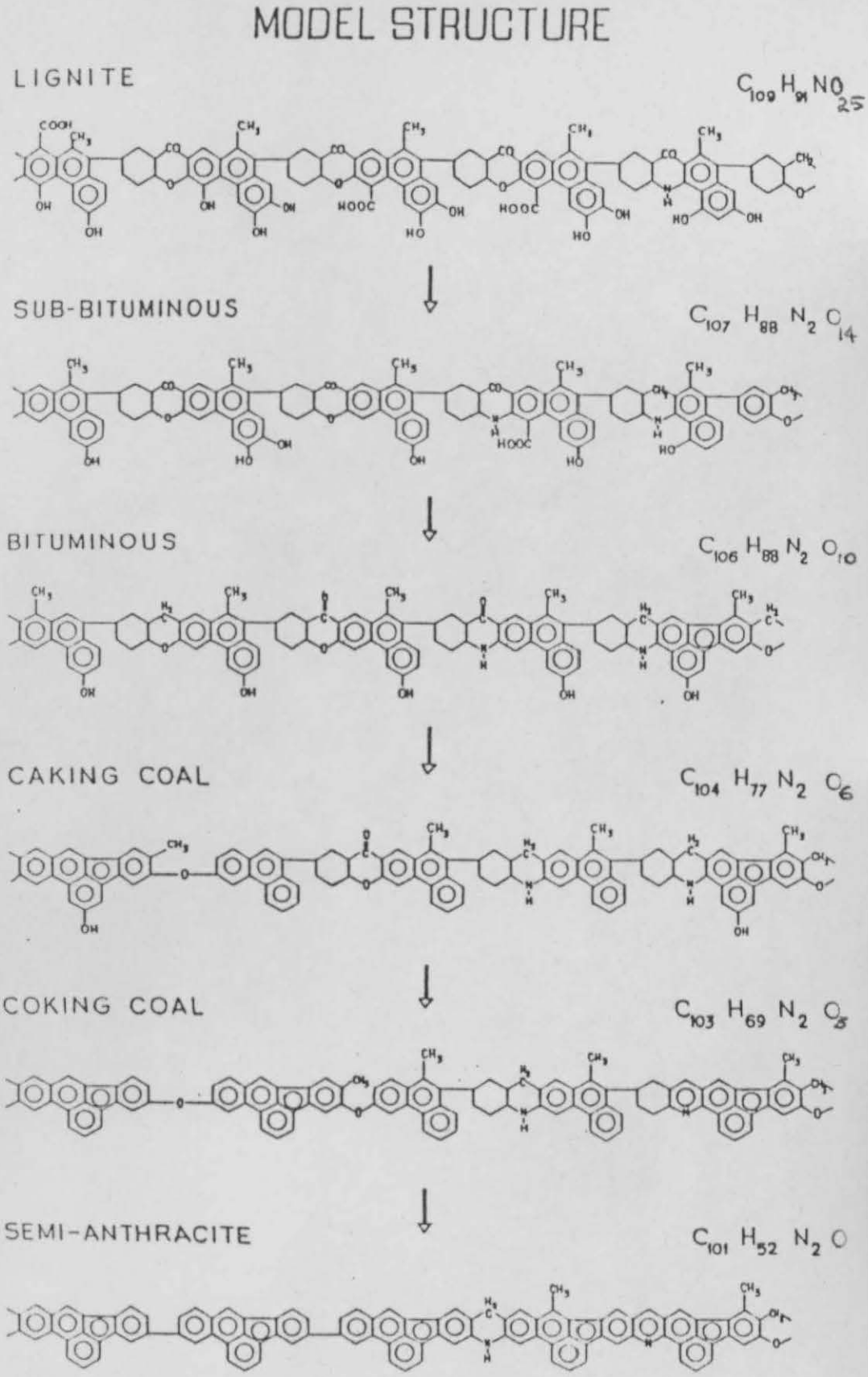

Fig. 21. Model Coal Structures (Mazumdar et al)

Table 5. (Mazumdar et al)

– Structural properties of the proposed models at different rank levels.

	Model I	Model II	Model III	Model IV	Model V	Model VI
Molecular formula	$C_{109}H_{91}NO_{25}$	$C_{107}H_{88}N_2O_{14}$	$C_{106}H_{88}N_2O_{10}$	$C_{104}H_{77}N_2O_6$	$C_{103}H_{69}N_2O_3$	$C_{101}H_{52}N_2O$
%C	72.1	79.1	82.2	86.1	89.5	92.6
H/C	0.835	0.82	0.83	0.74	0.67	0.515
$\%O_{OH}$	9.7	5.9	5.2	2.2	Nil	Nil
$\%O_{COOH}$	5.3	1.97	Nil	Nil	Nil	Nil
$\%O_{CO}$	3.5	2.95	2.1	1.1	Nil	Nil
$\%O_{C-O-C}$	3.6	2.95	3.1	3.3	3.5	1.2
f_a	0.605	0.673	0.68	0.75	0.845	0.95
f_{bar}	0.275	0.224	0.226	0.17	0.107	Nil
$f_a + f_{bar}$	0.88	0.897	0.906	0.92	0.952	0.96
f_{CH_3}	0.046	0.047	0.047	0.039	0.029	0.02
H_{ar} /C	0.13	0.22	0.24	0.27	0.35	0.41
(H/C)(non-aromatic)	1.53	1.66	1.74	1.80	2.06	2.75
(H/C) aromatic	0.21	0.33	0.35	0.36	0.41	0.42
$\frac{H_{CH} + H_{CH_3}}{H_{CH_2}}$	1.04	0.96	0.90	0.88	1.0	1.5
Average No. of Carbon per aromatic cluster	13.2	14.4	14.4	15.6	17.4	24.1

rise to ionic type bonds which can result in formation of oxidation activity centres and reactive/catalytic centres, particularly for brown coals/low rank coals.[112] Some of the possibly representative features present in coal are represented in figs.[13,19] 14, [6] 15 [94] 16 [97] and the Wiser model of Bituminous coal (fig.17).

The presence of heteroatom functionalities has implications for reactivity and pollutant formation during coal processing. In particular, 'O' being the major heteroatom has a key role in structural distribution and reactivity. 'N' is evenly distributed and appears to be partitioned in a regular manner in the products of char tar or gas. It's effect on reactivity is not clearly known.

The major functional groups are methoxyl ($O-CH_3$) carboxyl (-COOH), carbonyl (-C=O), hydroxyl (-OH), etheric (C-O-C) and heterocyclic 'O' (part of 5 & 6 C membered rings). The distribution and amount of 'O' show rank variations in accordance with coalification changes resulting in H_2O and CO_2 losses (in the low rank Bituminous to semi-Anthracite stage, evolution of CH_4 results in increasing aromatization of the coal).

Methoxyl [111] groups disappear early in the coalification process followed in order by carboxyl, carbonyl, acid hydroxyl, weakly acid/neutral hydroxyl groups and the remaing groups. (See fig.18, from ref.111). Thus, carboxyl, carbonyl and phenolic hydroxyl groups are present in low rank coals and absent in high rank coals.

Certain 'O' functionalities show anamolous trends and thus etheric 'O' are present in both low and high rank coals.

In higher rank coals the major part of 'O' is incorporated as linkages between aromatic groups (in so called 'caking' coals) and in heterocyclic structures. Alcoholic hydroxyl groups (weakly acidic) are present in both low rank and higher rank coals. (refer Table 4 for an overview of rank indicators).

Using Kessler's replotted diagram of Van Krevelen's coalification diagram (H/C Vs O/C). Tsai et al have calculated the dependence of %atomic 'H' on % atomic 'O' resulting from addition to coal of each of the above-mentioned 'O' functional groups for Macerals of a high rank Bituminous coal (see fig.19). Their conclusions are as follows:

1) Exinitic 'O' content increases primarily due to increase in higher molecular weight aliphatics (see ref.95 for indications of aliphatics up to C50)

2) Increase of 'O' in Vitrinite was attributed to methoxyl and ethoxyl/alcoholic 'O' and heterocyclic (5/6 'C' rings) and possibly phenolic 'O'.

3) Increase of 'O' in Inertinite is attributed to carboxylic, phenolic 'O' and etheric 'O' cross-links of the aromatic lamallae.

The 'S' heteroatom is divided between the inorganic (mainly pyrites and marcasite) and the organic phase and its distribution in the organic phase may be a function of rank and thus geology. Most of [90] the 'S' is incorporated in aromatic ring structures (aryl, thiophenic and condensed thiophenics) 'S' is present in organic structures as Thiol (-SH) disulphide (S-S), aliphatic sulphide (R-S-R), thiophenic and aryl sulphide.

The distribution of 'N' functionalities in coal is not well known as much as its distribution in the products of coal processing. 50-75% of 'N' is present in pyridine and quinoline derivatives according to A. Attar (ref.90, page 165).

The distribution of heteroatoms, in particular 'O' and 'S' exerts a profound influence on the extent and reactivity of most coal processing. Coal softening/caking and volatility in purely thermal processes as well as extractability in solvents can be dictated by the polarity of the 'O' and 'S' groups including their aromatic or aliphatic incorporation in the coal structure. These aspects will be touched on in subsequent sections.

3.8 Conclusion and Comments

It is clear from the preceding review that a mountainous task awaits the coal research community attempting to clarify and cohere structural aspects of coal which could help to interprete key aspects of coal responsiveness to processing conditions.

Studies indicate that coal is a complex mixture of diverse molecular entities i.e., the molecular species removed progressively from them differ in kind as well as size (re: Maceral differences arise from origin, metamorphosis within a particular rank and between ranks). This, in the words of Berkowitz, defines the utility of 'statistically average structures'. One should not therefore put too much weight on structural models other than as a visual aid to deliniate the kinds of structural features that could be encountered. (see figs. 21 and Table 5 for Mazumdar et al's model parameters)

It is only possible to surmise that a certain range of features occur in coal such that geological origin, physical structure (turbostratic lamallaes) and certain probable chemical structural features operate interatively to define the particular coal one is dealing with. Faced with a complex, possibly 'polymeric' possibly aggregative mixture of large molecular types, one may take refuge in the classical concepts of organic chemistry. Here we mentally analyse the molecule as consisting of a reaction centre/ centres to which are attached various substituents. Thus, nature of the reaction centre determines what reactions occur and nature of the substituents determine reactivity. Hence, we may look on coal as consisting of partially aromatised ring structures containing regions of alicyclics, hydroaromatic structures, short chain and long chain aliphatics, regions of unpaired electrons stabilized over ring structures, held together by a range of bond interactions. The bond interactions range from relatively weak 'H' bonds, electron donor/acceptor interaction, V n Waals forces and stronger covalent bridge structures of varying liability. The physical structure will then consist of oriented/buckled areas encompassing regions of varying porosity in partial entanglements and possibly 3-D cross linked gel structures. Long chain fatty molecules within entanglements or 3-D gel are probably folded on to themselves in compact/roughly globular shape. The shape will depend on various kinds of bonds between different parts of the chain and sourrounding environment in the shape of polar heteroatoms, other native chemical environment features (e.g., mutual replusion between structurally similiar molecules), shape and size of encompassing pores/fractures etc.

CHAPTER 4

REVIEW OF THE PYROLYSIS PROCESS APPLIED TO COAL

4.1 Overview of Pyrolysis

The literature highlights a trend away from low heating rate, high mass load studies of mainly coking coals to the study of a wider range of coal types, subject to higher heating rates in loadings approximating to dispersed, particulate densities.

Earlier studies were concerned mainly with the production of metallurgical coke and emphasis was placed on the coal-coke transition occurring during pyrolysis. Hence, 'carbonization' is a term normally applied to a process where interest centres on the production of solid coke. Concurrently, the production of gas for heating, lighting and the associated liquids for chemicals manufacture, utilised in major part, packed beds. These beds entailed higher residence time of vapour products in hot zones than the newer, higher heating rate, dispersed phase systems. A direct consequence of the differing conditions of processing is reflected in the distribution of products at the end of the processing steps.

The relative proportions of gas, tar, liquor and char for a given processing temperature differ, including the magnitudes of the respective yields. Further, the relative importance and extent of 'secondary' reactions vary to the extent that such reactions are enhanced in so called 'low heating rate' processes and supressed in higher heating rate processes.

Secondary reactions such as vapour cracking on reactant surfaces (coal-coke surfaces) or repolymerization reactions, lead to higher gas yields, enriched in unsaturates and to higher solid products enriched in carbon, either as soot or polycondensed aromatics. A similar effect will occur at high vapour residence times around heated areas removed from the reactant-bed zone.

Secondary effects which affect product distribution and type are particle size, coal type, temperature and nature of hot zones. Particle size, in parallel with bed depth, may affect the dynamics of heat and mass transfer mechanisms (which, if acquires sufficient resistance may control the rate of product formation and its distribution as opposed to chemical kinetic control.) The consequences are not only limited to product evolution history, but to interpretation of rate studies of the process.

Temperature is of fundamental importance in dictating the extent and rate of equilibration of the reaction process in the reactant-bed zone. However, at high temperatures, reaction rates are so fast that secondary cracking and/or repolymorization reactions are accelerated and desorption of products may become rate limiting. Secondly, even in dispersed systems, hot carrier gas streams effectively extend the reaction zone in space and thus in time, resulting in enhancement of secondary reactions. Thus, in some processes such as the CFP process[113] developed by Occidental Research Corporation for the production of coal liquids by flash Pyrolysis, hydrogenated recycle solvent is used to quench the highly reactive pyrolysis vapours. Such treatment supresses polymerization reactions by acting as a diluent and also as a vehicle for 'H' shuttling to prevent further reactions.

The nature of the hot zones can exercise a catalytic effect on the reaction products. Coked surfaces will enhance cracking of hydrocarbons (aliphatic) to olefins[116]. Metal surfaces with transition state metal components (Fe, Co, Mo, etc) may catalyse cracking reactions including CO hydrogenation[116]. Depending on temperature and vapour residence time in hot zones, cracking reactions can lead to varied forms and distribution of soot formation, dependant on reactor type[114, 116].

The preceding chapter on coal constitution will have given some indication of the complexity and structural variations inherent in variations of coal rank, type and geological origin. One would therefore expect, a priori, some distinctive influence of coal origin on the Pyrolysis process. Indeed, perusal of the literature from the early studies of Wheeler in [117-121, 19, 32, 33, 53, 60, 90, 99, 102] the 1920's through to the present day highlights sustained efforts to match coal conversion parameters to coal constitution. The importance of coal constitution can be gauged by the profound parallel between pyrolytic transformations of coal to a highly carbanceous char and the corresponding changes accompanying coal metamorphism from Peat to the Anthracitic stage.

The primary reaction conditions of time, temperature, and pressure differ in magnitude, resulting in differences that are dictated primarily by kinetic constraints. Thus changes that occur over extended periods of geological age, are accelerated in laboratory time scales.

With increasing temperature and time, melting, depolymerization, plasticisation (paralleling the gel-sol transition in early coalification) reactions concomitant with disproportionation

reactions leading to release of a range of gaseous and aromatic solid/liquid products are prevalent. The chemical changes accompanying these transformations are reflected by decreases in H/C and O/C atomic ratios including some rearrangements and partitioning of the 'S' and 'N' heteroatoms amongst the products. Increasing aromatisation of the carbon skeleton is reflected by increased carbon and, hydrogen aromaticities reflecting earlier loss of aliphatic 'H' and finally increased loss of aromatic 'H' at higher temperatures[122]. Internal rearrangements of 'H' within the hydroaromatic bridge structures, along with possible homolytic scission of these and other bridge structures such as polymethylene, etheric and sulphidic bridges aid in the evolution of heavier, large molecular mass species such as tar, and light H/C gas in competion with a propensity towards repolymerization. The latter process results in an increse in the size of the aromatic clusters which increasingly align themselves in parallel stacks of increasing depth with time and temperature. Such a process will be aided by increased external pressure.

A recent study of coals ranging from Peat to high rank bituminous coals from different geographical locations and thus of differing geological age subjected to Pyrolysis (maximum temperature, 550^{o}C) and optical classification reinforces the parallels between coalification and Pyrolysis. Comparison with the results of elemental analysis and Pyrolysis revealed the following trends. Early coalification led to loss of CO_2 and H_2O with O/C decreasing faster than H/C up to a rank bordering low rank and medium rank high volatile bituminous coals. Thereafter H/C decreases more than O/C, corresponding to a major loss of hydrocarbons. There is some indication that whilst the quantities

of H/C volatiles released may vary between coals of a particular rank, there is less variation in their distribution.

The major cause of such differences stem from variations of maceral distributions in the coals.

4.2 Effect of macerals on Pyrolysis behaviour

As a gross first approximation, one may consider coal to be a mixture of inert material (inorganics and Inertinite macerals) and the 'reactive' macerals, Vitrinite and Exinite. Indeed, liquifaction yields have long been correlated with total reactive maceral content, normally associated with Vitrinite and Exinite[124]. Latterly, such correlations have been sought for rapidly pyrolysed coal in a fluidized bed[(125)].

Important differences in plastic behaviour, fluid product yield (tars), coking capacity and rate of devolatization are reflected by the type of macerals referred to[86, 20, 60, 83]. Differences in coal reactivity show variations with rank which are also reflected by petrography rank variations. As noted earlier (vide infra) differences between macerals gradually disappear with increased coalification, reflecting a homogenization of the maceral composite making up the coal. Marked decrease in O/C and H/C atomic ratios with rank parallels a shift towards increasing aromatization of both the component maceral and of the heavier product fragments derived from pyrolysis of the particular maceral[(126)]. As reference 126 bears out, there are striking similarities between product fragments of Inertinite and Vitrinite macerals of similar 'C' content.

Perusal of the literature clearly shows that for coals of a particular rank, (below 90% 'C') there are marked differences in H/C atomic ratio, volatile matter content, plastic behaviour, specific gravity and other associated parameters[123-127, 86, 60, 34] It is therefore not surprising that coals of similar elemental composition result in differing extraction yields in liquifaction[124] or show differrences in plasticity[34] or yield in pyrolysis[60].

There is less variation in Exinite behaviour with coal rank, as their higher paraffinic content in the form of biomarker compounds such as alicyclic polyenic isoprenoids appear to render Exinites more resistant to coalification changes[126]. A study of the reactivity of British Coals in solvent extraction (ref 124) indicated that lower rank coals (NCB 802 & 902) were less sensitive to petrographic variation than to pre-oxidation. The latter process is likely to be an effect of ready 'O' reaction with the relatively larger proportions of 'O' functionalities present in such coals, leading to further cross-linking between units of the coal macromolecule and possibly the extractable material trapped therein. Pre-oxidation is an important consideration during sample preparations (grinding, storage) preceding and during Pyrolysis/liquifaction. Oxidation would then decrease yields, change the course and rate of decomposition (depending on rank) and decrease the extent and duration of plasticity (dependant on rank).

In general, the following trends are observed when the different macerals are subjected to heat in a variety of apparatus such as dilatometers, plastometers, thermogravimetric apparatus, static beds and flow reactors. Exinite is the most reactive,

showing considerably enhanced fluidity,[186, 60] a greatly increased[83] rate of mass loss and finally a much enhanced ultimate mass loss. It is also known that a large part of the Exinite evolves as tar, containing a certain amount of paraffinic[34] material (C_{20} and higher). The Vitrinite component show 'characteristics' intermediate between that of some of the more reactive Inertinites (Micrinite and Semifusinite) and Exinite. For a given rank of coal, the temperature interval of rapid mass loss and that of maximum rate of mass loss is situated in a relatively narrow range for all the macerals[93, 86]. However, the 'secondary' degasification period appears to be broadened over a larger temperature range in going from Exinite to Micrinite. Increases in rank of the parent coal cause a shift in the maximum rate of devolatization to higher temperatures for all the macerals, with the differences in thermal response homogenizing at high 'C' content (>90%'C')[60]. Plasticity, coking characteristics (softening, swelling, pore formation), tar yields, all follow the aforeseen trends with the Inertinite group of macerals showing the least reactivity. However, Micrinite and Semifusinite, particularly of southern 'Gondwana' coals occupy an intermediate position between Fusinite and Vitrinite in its coking behaviour[128]. A study of British and U.S. coals[126] indicated a Pyrolysis fragmentation pattern of products intermediate in character between Vitrinite and Fusinite, which suggests that some of macerals in the Inertinite suite such as Micrinite and semifusinite are more reactive than hitherto assumed. The presence of Exinite cannot be disregarded unless in very small quantities, owing to the profound effects it can impart to the general mobility, lubrication and swelling of the whole coal.

Whilst Vitrinite has been generally assumed to be chemically and physically homogeneous, this is not necessarily true. As pointed out in reference 77 it is possible that so called 'oily bitumens' soluble in chloroform and/or benzene and shown to be partially effective in plasticizing and liquefying the rest of the coal may have impregnated the Vitrinite, probably during the gelification stage of coal metamorphism. Further, Vitrinites often contain Exinitic inclusions[77, 86]. Kroger found by solvent etching of otherwise structurless Vitrinite, material embedded inside the cell walls consisting of waxes, resins and oxyhumins[68] (so called 'bitumens', see ref 77).

'Lacy' cenospheres obtained from Vitrinites in high heating rate studies[129-132] are reminiscent of this cellular structure described by Kroger. Such structure, showing interconnected thin walls inside an otherwise contiguous outer shell is more prevalent in lower rank coals [131, 132, 162] where one would expect the original plant cellular structures to be better preserved. However, fully 'excavated', hollow spheres are also obtained from such Vitrinites more prevalent with higher rank Vitrinites and Exinites [86, 129-132, 162] of all ranks (<90% 'C') termed 'Cenospheres' by Sinnat[132] and others.

It has been pointed out previously that owing to variable brittleness of the macerals, grinding to finer sizes will cause an aggregation of brittle Vitrinite and some of the more friable fusain components in the fines. Thus, rapid Pyrolysis in an entrained flow reactor[129] of varied particle sizes showed up enhanced mass losses in the larger particle size range resulting from a small increase in Exinite content. The implication is

that devolatization is strongly influenced by the development of plasticity which is much enhanced by Exinitic content.

A similar effect was noted in the dilalometric results of Kroger and Van Krevelen. Here, increased dilation was found for Vitrinite particles of diameter <200μm used by Van Krevelen as opposed to the finer particles used by Kroger (<40μm). The effect may be due to diminished mass transfer resistance for the finer particles (larger surface area is smaller diffusion path), the effect of complex packing patterns in the dilatometer (tighter packing and consequent resistance to mass transfer is known to enhance plasticity[130] analogous to a pressure effect[134]) or the presence of Exinite inclusions in the Vitrinite (it is extremely hard to effect complete separation of the macerals unless ground to very fine sizes).

Studies of gas evolution from macerals[93, 136] at low heating rates suggested some interesting trends. In Fitzgerald's paper, rates of flow of gases were measured with rising temperature. Total gas evolution showed an earlier and enhanced evolution at the lower temperatures for the Exinite with less 'CO' gas flows compared to both Vitrinite and Micrinite.

J. C. Macrae[136] heated Exinite and Vitrinite macerals of 'C' content (83% 'C') at temperatures below 350°C over a period of 118-180 days, that is, at very slow heating rates. Such slow heating at low temperatures simulates the low temperature coalification reactions better than most other studies. Thus, trends separating the various stages of volatile evolution was discernable. Pyrolysis of the Exinites proceeded in four well defined stages (1) H_2S evolution (2) CO_x evolution (3) saturated

and unsaturated evolution and[4] Hydrogen evolution. At higher temperatures, the evolution of H/C gases dominate to the extent of 91% of the gases at 330°C.

The Vitrinite showed a sharp acceleration in rate of gas evolution at about 308°C compared to a more gradual evolution at lower temperatures (unlike the Exinite which had much enhanced gas evolution rates at the lower temperatures). Unsaturated gases began to be evolved at 275°C for the Vitrinites as opposed to 215°C for the Exinites and in lower quantities and rates than from the Exinites (similar to Fitzgerald trends at higher temperature at higher heating rate, 1.8°C/min). However, the formation of unsaturated gases (presumably C_3's and C_4's) were similar for both Exinites and the Vitrinite in that these were released more rapidly than C_2 H_4. Noticeably production of H_2 from the Vitrinite began at such low temperatures as 250-270°C and an increase in rate was marked above 308°C.

H_2S evolution seemed to parallel other gaseous evolution in the Vitrinite with only 11% of the organic 'S' evolved up to 308°C, whereas 40.5% of 'S' had been lost at 332°C for the Exinites. From the products and nature of the curves, it appears that the gas producing functional groupings are similar in both Exinites and Vitrinites of similar rank, which is in agreement with Fitzgerald's work.

Liquid products were obtained from both Exinites and Vitrinites with light oils appearing at temperatures 110-250°C and heavy 'oils' starting at 203°C for the Exinite. Maximum rate of heavy liquid production occurred at about 313°C and yielded 3.6% H_2O, 2.3% light oils and 29.7% by weight of heavy oils.

The heavy oils were 90% neutral with the remaining fraction dominated by phenols.

Paraffins, naphthenes, aromatics, acids, phenols and bases were detected. Liquid production from the Vitrinite was interestingly at these low temperatures quite low with a maximum yield of 5.3% at 326°C. The heavy oil fraction was markedly phenolic in nature whilst the neutral oil fraction were similar in composition to that of the Exinites with, in fact 51% more unsaturated and aromatic H/C's than the Exinitic neutral oil.

Another interesting feature of this study is the indication of obvious plasticity of the exines even at these low temperatures and heating rates. The Vitrinite showed no sign of fluidity, although all residues retained the ability to form fixed cokes in a standard crucible test, but with indications of reduced coking ability.

There are a number of papers on low temperatures Pyrolysis, mostly at low heating rates, apart from that of MaCrae's[136] from the U.S.A.,[101, 59] U.K.[60, 137] and the Soviet Union[138] that provide important insights into the structure of coal in relation to coal pyrolysis reactions.

Certain trends emerge from a number of studies such as these which along with others[126,160,154,153,151,150,152,157,125] involving both slow and rapid heating, point to possibilities which may help resolve some of the current controversies surrounding coal Pyrolysis. Controversy abounds as to Pyrolysis mechanism as well as reasons for the huge disparities encountered in rate parameters[(161)]. Such disparities arise partially from the

disparate experimental techniques employed and partially from the heterogeneity of coal itself. Attempts to deconvolute one aspect from the other appears to be either selective in its approach (re: ref 161), dogged by controversy surrounding coal structure or even, cursory in the examination of the wealth of work stretching back over 60 years which may provide appropriate clues.

4.3 The relationship of coal extracts to general aspects of Pyrolysis

Earlier studies by MaCrae, Wheeler,[100] Girling,[137] Holden and Raff[60] has shown the existence of product evolution at low temperatures (150°C-320°C), ostensibly from Pyrolytic decompositions. However, the term Pyrolysis implies an extensive decomposition of the coal structure which leads to the evolution of a range of products in at least three differing phases (solid, liquid and gaseous) and gives rise to the phenomena of fusion, plasticity and resolidification observed in a number of coal types. Normally, plasticity is limited to coals of the 'liquid' structure denoted by Hirsch's X-Ray diffraction studies. However, there is no valid reason for the lack of fluidity in either the low rank, high volatile coals or some of the higher rank coals. Indeed under suitable conditions, e.g. rapid heating,[130, 162] such plasticity is observed for some of the lower rank coals, and further enhanced to the point of 'foamyness' for the medium ranked 'plastic' coals[86].

The observation of enhanced plasticity, and thus swelling in high heating rate studies is significant, in that this physical

effect may reflect more fundamental physico-chemical events which underlie the combined effects of plasticity and decomposition. Worthy of note also is the state of dispersion (particulate density) of the coal particles which lead to surprising effects. In general dispersed particulate systems are synonymous with high heating rate in reactors such as fluidized beds and entrained beds in which enhanced plasticity is encountered. However, it was noted that particles which normally plasticize in packed beds (e.g. coke ovens, giesler platometer and dilatometers) at low heating rates, ($<10^{-1}$ $^{o}C/S$) did not do so when heated at a similar rate in a mesh reactor[130] with the particles well dispersed. This anamoly highlights the probability that plastic measurements in such instruments as the giesler plastometer and experiments involving packed beds is partially due to sliding between the particles caused by exuded coal liquids coating the surfaces.

MaCraes paper provides trends in gas and liquid production that have been largely reflected in many subsequent studies of coal pyrolysis of widely varying heating rates.

It has been noted earlier (ch 3) that 'H' bonding plays an important part in keeping the coal structure together (about 4:1 ratio with respect to covalent bonding). Recent work by Solomon et al[164] using an entrained flow reactor (heating rates $\sim 10^{5}$ °C/S claimed) including work reported therein hints strongly at the importance of 'H' bonding disruptions as an initiator of tar/liquid evolution. [Reference to MaCraes work will show a markedly increased Pyrolytic H_2O, CO_2 and light oil production preceding H|C gas formation]. The results, for a Pittsburgh Seam Coal (83.5% C (daf), H/C=0.79) show Pyrolytic H_2O and CO_2 evolution

(from dehydration and decarboxylation) preceding the onset of fluidity. It was reported that significant tar evolution had occurred by this time.

Rapid swelling to cenosphere formation proceeds concomitant withrising rates of CH_4, CO and Pyrolytic H_2O which had reduced to a minimum at the onset of fluidity. Hydrocarbon gas and CO continues to increase past resolidification period (maximum swelling) whilst Pyrolytic H_2O decreases and CO_2 starts rising towards a second peak.

The reported features of multiple Pyrolytic H_2O, CO_2 and CO peaks have been noted in other studies of coal Pyrolysis at low heating rates where these features are better resolved. In fact, multiple sources of certain H/C gases[121] single ring compounds[137] and coal extracts[119] have been reported.

Reference to Girling[137], Meuzelaar et al[126], Romovacek et al[160], Studier et al[59], Vastola et at[167], Karn et al[168], Brown & Waters[165], Holden and Raff[60] along with MaCrae (vide infra), highlight recurrent aspects of coal decomposition worthy of note. The work referred to above, encompass Pyrolysis in regimes ranging from 1-3^{o}C/min (Ref 137 & 165) to laser flash heating of coal surfaces (estimated surface temperatures, about 1000-1200^{o}C at very high heating rates).

Brown & Waters, working with a suite of Australian (67.8% 'C', 83.0% 'C', 83.8% 'C' & 87.4% 'C') coals, conducted a comprehensive study, relating chloroform extracts to fluidity and rate of weight loss. The key points to note are as follows:

1) Apart from Brown coal (67.4% 'C'), the extract yield displayed 2 peaks. The initial yield of chloroform soluble extract amounting to more than half the total was released before and up to the temperature of softening (<300-350^{o}C). The remainder of the extract was released during the phase of rapidly increasing fluidity and rate of weight loss.

2) The temperatures of maximum rates of release of phase I and phase II extract increase with 'C' content of the parent coal.

3) Temperatures of final loss of extract coincide with the Giesler solidification temperature and generally precedes and almost coincides with the maximum rate of weight loss.

4) The H/C atomic ratio of the extracts were significantly higher than the parent coal and apart from Brown coal extract the atomic O/C ratio was somewhat higher than parent coal too.

5) The molecular masses of the extracts ranged from 440-570 and decreased with increased coal rank and the melting points of the extracts range from (90-175^{o}C).

Also noted were differences in extract yield with rank with a peak at about 88% 'C' and differences in yield with respect to geological origin. Many properties of coal form a variety of geological formations (e.g. Carboniferous, Cretaceous, etc) show a peak at about 85-88% 'C' which appears to support a particular view of coal structure, namely that the chemical effect of coal-ification is the result of a 3-D multifunctional polymerization process (Refer to fig (22) for an illustration of the variation of properties referred to above).

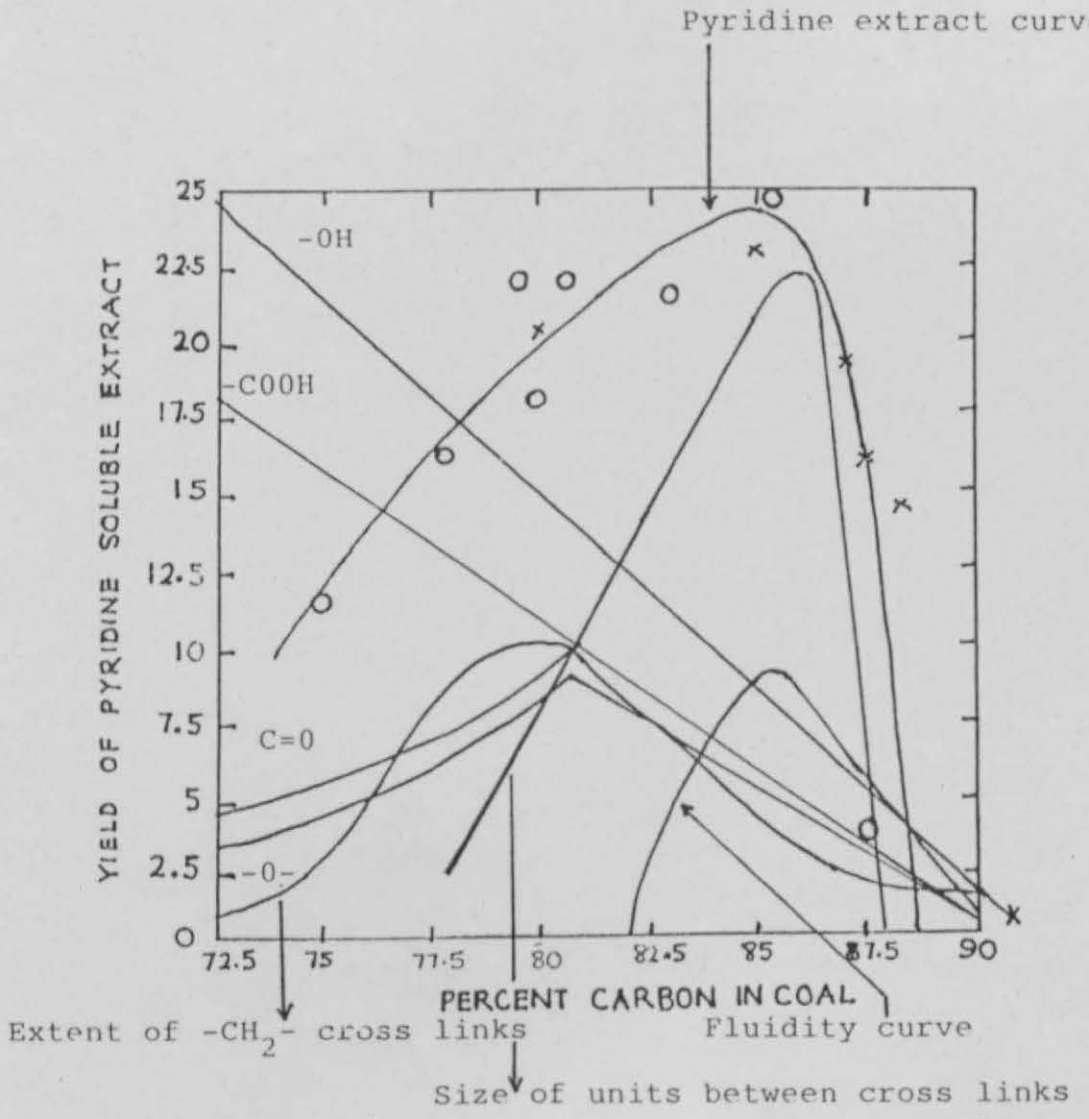

Fig. 22 Compilation of coal structural parameters as a function of coal rank. (Compiled by author from several sources; qualitative trends shown except for pyridine extract).

Also noted in the work was the observation of activated diffusion of extract material, dependant on coal pore size distribution of parent coal. As the apparent porosity shows a minimum at about 88% 'C', 'shock' heating to temperatures of softening (300-400^{o}C, in dense packings) was required to release the major part of the coal extract from coals of higher rank (80-90% 'C').

Apart from MaCrae, Holden and Robb including Girling also reported release of material at low temperatures. One of the important facets of these studies (refs, 137, 126, 160, 59, 167, 168, 60) is the prompt removal of products from the reaction zone which allows focus on 'primary' products. 'Primary' products are defined in the sense of minimising of 'secondary' reactions which can occur in hot zones, either in hot gas surroundings or on hot surfaces. However, 'secondary' reactions such as repolymerization and cracking on the hot coal surface or in depth may still be occurring, dependant on the rate of cooling of the solid body.

Holden and Robb report evolution of mainly aliphatic material, containing many cyclic structures in the temperature range 90-150^{o}C and alkyl aromatics between 150^{o}C-300^{o}C. Evolution of the aromatics reach a maximum at 84-87% 'C' corresponding to the region of minimum 'He' densities. (This feature indicates incidentally, the minimum in densities, porosities noted in this region may be a result of trapped material[2]).

At about 320^{o}C CH_4 was detected, along with a large release of alkyl phenols. The amount of phenols decrease with rank increase. (Refer to 'O' functional group distributions, Ch 3 and fig [22]). The release of alkyl phenols was assumed to be due to breakage of 'O' bridges. [Refer to MaCraes work, where

phenolic compounds were detected in the 'heavy' oil fraction along with $C_n H_{2n+2}$ H/C release at T > 275 ^{o}C].

Reference to Meuzalaar et al (British and U.S. coal macerals), also a mass spectroscopic study (In conjunction with curie point Pyrolysis at 610^{o}C and 122^{o}C/S heating rate), highlights the presence of alkyl phenols. Here, phenols and dihydroxybenzenes show a preponderance in Vitrinites with the amounts falling with increases in % 'C'. Further, the Fusinites were dominated by aromatic rings such as benzenes, alkyl benzenes, napthalenes, acenapthenes/biphenyls, phenanthrenes and anthracenes. Interestingly, an increase of parent rank of the macerals (Vitrinite, Semifusinite, Sporinite), reproduced substantially the changes in fragment pattern seen in going from Exinite to Fusinite. Exinite macerals were in the main dominated by alkenes and dienes which may explain the early release of alkenes noted in Pyrolysis studies over large ranges of heating rates.

The trends worthy of particular note are:

1) Preponderance of single and 2 ring products (C_6H_6 and Nepthalene) over 3 ring structures such as phenanthrenes/anthracenes with increases in coalification. The same features were reproduced in passing from Vitrinite to Fusinites. There was an increase in alkyl fragments (C_3-C_5 alkyls) with coalification as well.

2) The relative increase in 3 ring structures at high parent 'C' content (>91% 'C').

Work reported by Studier[59] et al on a Lignite (67.3% 'C'), Bituminous coal (77.8% 'C') and Anthracite (91.3% 'C') also gave rise to similar trends. Pyrolysis in vacuum at 150°C of the Bituminous coal produced volatiles where 90% consisted of $<C_6$ volatiles. The remaining 10% containing more than 200 compounds consisted of a mixture of aliphatics (alkanes/alkenes/alkynes/alkadienes), alicyclics (cyclohexane, cyclohexene, etc), hydroaromatics (Tetralin, Indan, etc) and aromatics (C_6H_6, neapthalene, etc) including 5% thiophenes. No 'O' or 'N' compounds were found.

Pyrolysis at 350°C indicated the following fragmentation patterns detected by a mass spectrameter. Benzene dominated in Lignite, followed by napthalene and a range of ring structures containing 'O' such as xanthone, dibenzofuran, anthroquinone, etc (2 ring and 3 ring structures). Bituminous coals were dominated by benzene followed by napthalene and phenanthrene and a range of 'O' containing structures as well as 'S' and 'N' containing ring structures. Anthracite consisted mainly of phenanthrene and an increase of 'N' and 'S' in fused rings were observed. The fragment pattern became simpler (i.e. consists of far less products) in passing from Lignite to Anthracite. A range of phenols (phenol, methyl and dimethyl phenol) were observed in the Lignites and Bituminous coal. It was noted that in the presence of clay minerals these phenols were converted to Benzene, Toluene and Xylene (BTX), thus pointing towards possible catalytic reactions that may occur during Pyrolysis.

Rapid Pyrolysis, using a molten tin both in a Czechoslovakian[160] study (gas chromatography used for detection of products) also gave rise to a similar pattern of product distribution.

Coals and macerals thereof were Pyrolysed at temperatures ranging from 500-925^{o}C. The coals ranged from Lignite to Bituminous to Anthracite (64.4% 'C' - 90.6% 'C'). Again, as in Studier et al, a simpler pattern of product distribution was noted with increase in rank. Further, the same pattern was reproduced for rising temperatures of Pyrolysis. Of particular interest were the increases of benzene and its derivatives such as toluene and m, p-xylene with increases in Pyrolysis temperature as well as rank. The latter trend runs through much of the previous work discussed and also apparent in the flash Pyrolysis tars derived from a spouted bed (Canadian Coals[149]). The Czech work resulted in the detection of a range of vapour phase products namely pentane and isopentane, various branched butenes, alicylics such as hexane, cyclopentane, cyclopentadiene, methyl substituted alicyclics and BTX. The most significant products were pentane and BTX followed by methylcyclopentane. In general, the ratio of nonaromatics to aromatics increases with decrease in rank and in similar fashion for the macerals where nonaromatics of a complex pattern dominated for the Exinites.

Girling, working with a suite of British coals, including Markham Main, and using a G.C. technique like the Czechs detected a host of aliphatic and aromatic compounds at temperatures lower than 100^{o}C. The coals he studied ranged from 78.5% 'C' to 91.6% 'C' covering NCB code ranks 101, 301, 401, 602, 501/502 and 902 (29-30mg samples of coal were heated to about 700^{o}C at a rate of 1^{o}C/min).

The care that Girling took in avoiding secondary reactions (small mass loads; sweeping of products with diluent gas, use of

cold traps) as well as sufficiently slow heating allowed the detection of features not reported previously. He grouped the compounds detected in 3 groups, (1) 'paraffins' ranging from C_3-C_{10} consisting of alkanes, (2) 'Olefins', C_4, C_5 & C_6 isomers up to Octene-1 and Nonene-1, (3) 'Napthenes', consisting of plain and alkyl substituted C_5 and C_6 alycyclir ring and (4) single ring aromatics and their derivatives (BTX, Ethylbenzene, trimethylbenenes, etc).

Although paraffins, napthenes and aromatics were seen to evolve at temperatures as low as 50^{o}C, there were 2 phases of release noted (Note the parallel with the chloroform extract yield of Australian Permian coals; Girling was working with carboniferous coals). The first phase yielding 1/2-1/3 of the total yield had a maxima in the region 150-300^{o}C and the second at 370-450^{o}C (corresponding, by comparison, with other work such as Giesler fluidity measurements and TGA mass loss studies to the region of increased fluidity and rate of mass loss).

Again the trends were consistent with the previous studies mentioned. The yields of liquid products appear to peak at 87.5% 'C' in accordance with fig 22 in terms of profile. (The magnitude of the yields were small ranging from 0.05%-3.1%). The points of interest to note are as follows:

1) Amount of aromatics emitted below 300^{o}C has a peak at 87.5% 'C' and falls away steeply thereafter.

2) Amount of aromatics emitted above 300^{o}C increased with rank up to 89%.

3) The higher olefins showed a single maxima at 370-450^{o}C (except for the low rank coal, 902) corresponding to a much increased rate of gas evolution.

4) Benzene and Toluene continued to evolve at higher temperatures following the cessation of most other volatiles (450->460^{o}C, dependant on rank).

5) Consideration of thermodynamic equilibrium calculations at 450^{o}C for the alkylated Benzene isomers indicated that such material was not released by a fragmentation (i.e. decomposition process) process but by physical desorption similar to the compounds released below 300^{o}C.

Solvent and steam assisted extraction studies by Vahrman on British coals in the early 70's confirms much of the speculations concerning the 2 component hypothesis of coal. In short, the view is that a considerably larger proportion of the coal substance than previously thought is loosely attacked/adsorbed in the surfaces of the coal in various pores. These relatively low molecular weight material (<600) can be detected in coal extracts (vide infra) and are also released easily on heating, to appear in the so called 'primary' tars (<600^{o}C tars). It is suggested that a substantial part of the primary tars is present 'as such' in the coal. Vahrman suggested that up to 23% may be present in the coal, dependant on rank. Later and current work in this area, by Polish, U.S.A. and Australian workers suggest higher figures up to 40-50%, dependant on the solvent used. Van Krevelen and co-workers including Dryden stated 30 years ago that different solvents possess varying effectiveness in extracting the coals, closely related to the rank of the coal. Further, preheating of

the coal prior to extraction resulted in a much enhanced yield[165,170] (An explanation is that heating 'loosens' up the coal structure by both thermal expansion and thermal agitation, bringing more of the material to the coal surface?). The effectiveness of different solvents may be gauged from fig 23.

It is well to reconsider at this stage the arguments put forward concerning extractable yield discussed earlier (Ch 3, ref 102). Whilst there is some debate concerning the high yields obtained by polar solvents such as Ethylene diamine, particularly for low rank coals containing large concentrations of oxygenated polar groups, there is insufficient evidence to invoke chemical rupture of the macromolecular structure to account for the high yields. Rather, there is evidence that the enhanced extractability in polar solvents is facilitated by disruptions of secondary bond interactions such as donor-acceptor (and other 'H' bonding) bonding of the small molecules to the 'rigid' macromolecular 3-D or entangled network. Further, as Given points out, vapours such as toluene among other solvents can diffuse or imbibe into the solid matrix accompanied by swelling. In this context, the behaviour of chloroform extract commonly equated with plasticity and coking of the coal[165,102,170] has been considered in detail by Brown and Waters[77]. They consider then, that fusible 'bitumins' ('oily' and 'solid' bitumens of MW<600, with melting points <200^{o}C) soluble in chloroform or benzene help to solvate and disperse part of the humins into a colloidal state. The humins are deemed to consist of two components, one, of colloidal dimensions (MW<600), soluble in polar solvents such as pyridene and the second of macromolecular dimensions not normally dispersible except by solvolysis (i.e. attack by reactive solvents e.g. by e^{-} donors

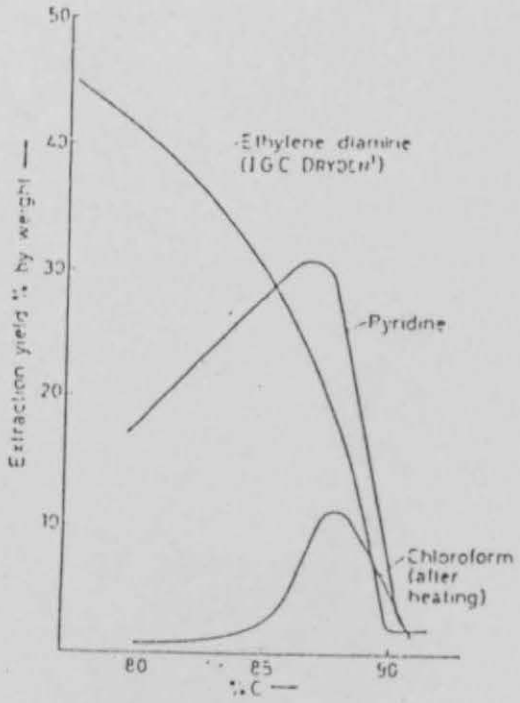

Fig. 23 effect on type of solvent on extraction yield
Re: Dormans et al

or 'H' donors causing partial breakdown of the 'rigid' structures).

It was noted that component one of the humins in conjunction with the bitumens makeup <40% of the pyridene extract of the whole coal. Thus fusion and liquefaction of the whole coal grain is achieved below the decomposition temperature (this depends on rank and 'O' content, and with coals of high 'O' content decomposition proceeds simultaneously to fusion, thus diminishing the range and duration of plasticity) to disperse colloidally or in suspension the 'insoluble' humins and other particles.

4.3.1 Initial hypothesis on possible mechanisms of Pyrolysis

Considered in conjunction with the vast range of products released at lowish pyrolysis temperatures (<350^{o}C), the yields and facility of solvent entraction yields, especially of 'shock' preheated coals and the large yields obtained from 'H' donor and even non 'H' donor solvents such as Anthracene/Phenanthrene, it appears that a larger part of the parent coal than previously thought may be detached with minimal chemical disruptions.

That is to say, relatively weak secondary bond disruptions such as electron-donor bonding, 'H' bonding and van der Waal interactions are affected. In that case the major gaseous products preceding fusion and solvation of the coal grain are likely to be H_2O and CO_2 from labile hydroxyl and carboxyl functional groups. The release of a range of low melting point aliphatic, alicycic, hydrocromatic and aromatic structures at low temperatures (<250-300^{o}C), probably coinciding with the first phase of chloroform entractable material (refer Brown and Waters

and Girling) acts to solvate and lubricate the more 'rigid' parts of the coal structure to the point of fusion. At this stage, owing to the coupled effects of thermal expansion and solvation leading to a more 'opened' up coal structure, and rising temperature level leads to an acceleration of secondary bond disruptions. The latter process probably has the twin effect of accelerating the disruption of the 'cage' structures trapping the low molecular weight material and increased solvation of the coal structure. Material is then evaporated continuously and/or desorbed by some mass transfer phenomena such as hydrodynamic flow or film diffusion the whole process being continuously fed by increased temperature rise and increased fusion of the coal grain. Some material is probably added to the pool of evaporating liquid mass by weaker Aryl-ether bond disruptions at higher temperatures, which probably give rise to the quantities of alkyl phenols noted at this stage (equally 'H' bonded phenolic groups could disrupt giving rise to more Pyrolytic H_2O as seen in Solomons flash heating study, vide infra).

Because of increased mobility of the lamallae in the coal grain, access to 'H' donating[106] groups and 'H' shuttling may be facilitated to stabilise any free radicals generated by more powerful chemical disruptions at the higher temperatures.

Overall, however, the hypothesis put forward based on the preceding discussion is that quite a large part of the coal in the form of tar may be released/absorbed by a combination of a physically activated process and low activation energy reactions involving weaker secondary bonds. It is likely that covalent bond breakage occurs to a significant extent only at the higher

temperatures corresponding to past-resolidification reactions (>450-500^{o}C), which probably gives rise to light H/C, CO and H_2 gas evolution.

The unlikelihood of the release of large fragments from the macromolecular part of the coal may be gauged by the following considerations. Firstly, owing to their size and multifunctionality larger fragments are likely to be attached to other parts of the coal skeleton by several bonds. Thus the release of large fragments involving fission of many bonds is less probable than the release of smaller fragments clatharated as such within the coal structure.

Such a fragmentation however may be envisaged at higher temperatures. Thus, a series of parallel and competing reactions involving fragment formation stabilization, evaporation and repolymerization may oscillate in dynamic competition at rising temperature levels.

Some material in Exinites and low boiling material such as napthalene may evaporate by sublimation and thus with minimal decomposition at the lower temperatures.

A Russian paper[138] describing coal Pyrolysis in a high vacuum provides considerable support for the hypothesis put forward. Here, coals heated at 10^{o}C/min to peak temperatures (400-600^{o}C), released desorbed CH_4 along with other condensible products (tar liquids) to a significant extent. The activation energies calculated ranged from 5-20 KJ/mole for condensible and non-condensible products (presumably CH_4). Support is drawn from previous Russian work which views coal as held together, not by covalent bonds but by a network of 'H' bonds and other weak intermolecular forces.

4.3.2 Structural aspects of coal relevant to coal Pyrolysis

Consideration of the Hirsch X-ray structures of coal provide some insights into possible decomposition routes. The X-ray studies along with chemical studies inform us that low rank coals (roughly up to 85% 'C', although a more representative classification would be based on H/C and O/C atomic ratios) of the Hirschian 'open structure' are dominated by single rings. For example, a vitrain of 85% 'C', has 60% of the lamallae layers as single rings, 28% of double rings and 12% of larger ring size. (Very recent work[109] of CS_2 extracts of British coals have indicated a small concentration of fused rings up to ten rings including ovalene and coconene. It is therefore likely that small concentrations of such large rings may exist, particularly in the Inertinite maceral groups, characterised by high aromaticities. There is evidence also (re: Chapter 3) that even high resolution NMR is not 'seeing' all the ring structures in coal).

In the low rank coals, the smaller lamallae are probably connected by more chemically crosslinked bridges ($-CH_2-$, $-CH=$) than higher rank coals, resulting in a higher degree of polymerization. Further, the large concentrations of 'O' functional groups (-OH, COOH, etc) will also result in much enhanced 'H' bonding.

In short, for the lower rank coals, any homolytic fission of weak bonds will release radicals of limited stability owing to limited reasonance stabilities. Thus, repolymerization is more likely before removal by vaporization. (A likely effect of high heating rate here would ensure enhanced vaporization over repolymerization reactions which would have insufficient time to render

completion as opposed to lower heating rates. This is probably one reason for plasticity observed in these normally non plasticising coals). A further reason for lack of plasticity and low tar yields probably stems from the large number of 'H' bonds which help to lock the coal structure together.

The mobility of the 'liquid' Hirschian structures (85-91% 'C') coincides with a much reduced crosslinked density. Here, the better oriented lamallae (parallel to bedding plane) are held together by increased van der Waal interactions, some 'H' bonding (from phenolic groups and CO groups present) and other interactions such as election donor interactions. As noted before, larger ring sizes enhance van der Waals interactions, helped by increased stacking of the lamallae with increase in coal rank. (At 89% 'c' up to 45% of rings are still on form of single rings and the rest largely paired layers with larger concentrations of 2-4 rings). Parallel with increased orientation of the lamallae is an increased amount of clatharated material evidenced by increases in extractable material and tar yields reaching a maximum at about 86-88% 'C' for carboniferous coals). It is interesting to note that both low angle X-ray scattering and Helium densities including porosities indicate a minimum in porosities at this region.

It is clear therefore, stable fluidity/mobility exhibited by these coals do not require the breakage of cross-link covalent bonds as envisaged by van Krevelen and which led to a sequential scheme of coal Pyrolysis, dependant on an initial, slow primary decomposition to produce thermally 'stable' but mobile units exhibiting plasticity. Rather, reduced crosslinks and reduced 'H'

bonding, leaving relatively weak van der Waal interactions will allow lamallae mobility and fluidity.

For coals of >91% 'C', ring sizes increase rapidly as well as lamallae orientation, which has two consequences. One is that increasingly oriented and enhanced porosities allow loss of fragments clatharated within the mesh structure of coal originating from coalification reactions. Hence, the steep fall off in extractable material and correspondingly low tar yields noted. The second consequence is the much increased van der Waals forces stemming from large oriented ring structures which lock and inhibit mobility and thus plasticity.

Whilst it may well be that a large part of the mass loss observed in Pyrolysis in the form of tars of a wide molecular weight range originates from loosely bound clatharated material and partial breakdown of the gel-like Vitrinite structure, is it likely that at temperatures >500^{o}C covalent bonds of varying labilities are being disrupted? The consistent appearance of particularly benzene and to a lesser extent derivatives of benzene in Pyrolysis products (BTX and isomers of xylene) at higher temperatures and increasing coalification in a number of studies (vide infra) suggest this possibilty. (However, Girlings contention that the alkyl benzenes were not products of fragmentation based on thermodynamic considerations must be borne in mind). Also the presence of large yields of non-condensible gases in the products (at temperatures >450^{o}C) especially alkanes, alkenes/alkynes, H_2 and CO are not reconsilable with simple desorption (but, as the Russian work and others[136,137,180] demonstrate, gases such as CH_4, C_2H_6 and C_3H_8 exist in the pore structure of coal, probably from previous coalification reactions).

A recent laser Pyrolysis study of a range of U.S.A. coals (78.8-90.4% 'C') may throw some light on the above speculations. There was uncertainty concerning the temperatures reached and the suggestion of significant ring fragmentation implies rather high temperatures in the heating period. Nevertheless there are some interesting results worthy of note. Among these are:

1) The presence of considerable amounts of 2 ring structures such as napthalene and its radical. The fragmentation pattern suggest the present of CH_2 linkages with up to 5 CH_2 groups for the low rank coals. (Methylene linkage apparently decrease with increased rank, see fig 22).

2) Significant amounts of C_6H_6 and the benzyl radical including the presence of CH_2 substituted linkages.

3) C_3-C_7 fragments were detected which were traceable to alkenes such as C_3H_6, C_4H_8 and C_5H_{10} and more interestingly to dienyls such as pentadienyl, hexadiene and cyclohexene. The characteristics of the dienyls point to fragmentation of the hydroaromatic portions of the 2 to 3 ring fused hydroaromatic structures. (Examples of such structures known to exist in coal are tetralin, 1, 2 or 1, 4 -dihydro-napthalene, 9, 10 -dihydrophenanthrene etc; olefins such as Butene-1, isomers of Butene-2, Pentene, hexene, Heptene-1, isomers of Heptene-2 and Octene and Nonene-1 were detected by Girling (vide infra). Apart from a low rank coal (NCB902), in most of the coals studied by Girling, significant olefin evolution were noted at temperature >300^{o}C, corresponding to temperatures close to suspected 'active' decomposition).

4) Significantly, little CH_4 was detected, although H_2O, CO /or C_2H_4 were detected. This was interpreted as the likelihood of CH_4 being a secondary product of decomposition.

The above study is interesting from the viewpoint of possible thermal decomposition patterns occurring during Pyrolysis. However, the relative absence of saturated alkanes, the presence of CO and the preponderance of alkenes suggest that quite high temperatures have been reached and the products are not necessarily as 'primary' as has been assumed. Many of the previous studies have pointed to significant aliphatics production at lower temperatures of Pyrolysis (<600^{o}C). In particular, Girlings work (including Holden & Robb among others) points to significant alkane evolution in the first phase (80-250^{o}C, corresponding to the initially easily desorbed products trapped near the coal surface. Alkanes were evolved at higher temperatures as well, along with napthenes and aromatics including fragments of alkanes substituted on aromatic rings (see ref: 126).

Therefore the significance of Vastola et als work lies in the possibilities that may arise from fragmentation of the 'rigid' part of the macromolecular structure of coal at high enough temperatures. Here, significant decomposition of hydroaromatic structures can result in higher alkenes (C_4 and higher) along with single and two ring compounds such as C_6H_6 and napthalene. Further, as much of the heteroatoms such as 'O', 'N' and 'S' are present in the saturated part of the fused rings (e.g. Dibenzofuran, fluorenone, benzoquizoline, etc), decomposition of the hydro-aromatics would release CO and N_2 which were detected by the mass spectrometer.

Before leaving this section, note is made of another flash heating study (Ref: Fuel, Vol 55, Jan 1976 pp 59 with supporting work by Ladner et al, Ref: BCURA Annual Report, 1966 pp 66). Bituminous coals (VM=45.9% and 17.6-29.4%) were subjected to light flash from a capacitor discharge lamp. The coal particles reached temperatures up to 1000^{o}C, dependant on flash energy received. Overall, it was suggested that Bituminous coals were composed of 2 different molecular types, a H/C rich ('H' type) and a dark ('O' type) compound. The latter was deemed to be a partially hydrogenated aromatic skeletal structure with high 'O' content mostly in the form of phenolic 'OH'. Supporting evidence was recalled from previous work (Holden & Robb, Brown and Waters, Vahrman, etc). From the preceding discussions it would appear that this is a simplified assumption. In fact as the Brown and Waters extraction work indicate, there is a fair amount of oxygenated species in the extracts. Further, previous British coal work show substantive proportions of heteroatoms in coal extracts which differ from the parent coals only in that the extracts exhibit a narrower range and less variability in amounts of heteroatom distribution with respect to rank origin (and a higher H/C ratio). As subsequent flash experiments have indicated it is not easy to distinguish between fragments of coal material originating between the two parts[146] (the 'mobile' and 'immobile' parts).

The following points are worthy of note:

1) As flash energy encountered by coal particles increased, the colour of the discharged material grew progressively darker.

2) At very high energies, coal particles 'exploded' into a gossamer like film, of colloidal dimensions (35nm diameter; however, as Ladner et al notes this gossamer material originated from vapour phase cracking reactions initiated by UV part of the flash spectrum).

It was concluded that low energy flash heating released loosely held, low MW (<500) compounds containing a disproprotionate amount of 'H' compounds (presumably long chain alkanes, hydro-aromatics, etc). High energy flash heating (implying higher surface temperature) caused an extensive 'detachment' of the smaller molecules from the macromolecular structure with minimal thermal decompostion. (Various SEM studies also suggest that substantial detachment can occur between macerals[129,132,162]. In particular, the Inertinite macerals are prone to such detachment and fragmentation[132]. Cracks[174] can appear in the Vitrinite at temperatures as low as 150-175^{o}C. Overall there is room for slippage/mobility between the macerals owing to differing thermal responses. The Exinitic material, with its high thermal lability and fluidity would also contribute greatly to the initial plasticisation and tar yield at low temperatures). Lastly, it was suggested that flash heating does not gasify much of the coal and the coal does not reach very high temperatures. The main response appears to have been evaporation/evolution of loosely held molecules by desorption/molecular diffusion in analogy with extraction studies. (There appears to have been an intermediate level of flash energy reuired to maximise liquids yield).

The latter observations concerning yield and yield character with regard to energy supplied are important factors, tied to

rate of energy supply in the form of heating rate. Thus, the effects of heating rate separated from problems associated with heat and mass transfer lead to subtle effects on the nature and yield of products.

4.4 Coal plasticity with regard to Pyrolytic reactions

In a seminal paper[175] Fitzgerald (1955), a one time co-worker of van Krevelen formulated a kinetic scheme of coal Pyrolysis consisting of 2 sequential first order reactions describing carbonization in the plastic state. Earlier, van Krevelen and co-workers had formulated a sequential scheme consisting of the following essential 'elementary' steps:

1) Coal complex $\xrightarrow[\text{decomposition}]{\text{slow}}$ Primary products + Residue

2) Primary products $\xrightarrow{\text{rapid}}$ Final products
   Residue $\dashrightarrow$ semi-coke

3) Semi-coke $\dashrightarrow$ coke

(2) and (3): secondary decomposition

Fitzgerald's work concentrated essentially on the second part of the reaction scheme coinciding with loss of fluidity and formation of semicoke.

Working with a range of British coals of widely varying caking properties (NCB301-702, temperature up to 470°C), including coals of quite indifferent caking properties, he concluded:

1) In the region of fluidity, (under isothermal conditions), fluidity changes may be described by 2 consecutive chemical reactions of first order.
   Coal $\xrightarrow[K_1]{V\ \text{Rapid}}$ fluid coal $\xrightarrow[K_2]{\text{rapid}}$ semicoke where $K_1/K_2 \simeq$ 3-4 for a highly caking coal.

2) The activation energy of the slower, second reaction was found to be ~ 209 ± 17 KJ/mole with a pre-exponential factor of 10^{15}-$10^{18}{}_5{}^{-1}$, for the 10 coals tested. The relative constancy of the rate parameters was implied to suggest that the nature of the carbonization process (reaction mechanism) was essentially the same for all coals. (Under the conditions of the test of dense packing; 5g samples of size <600 μm, contained in a Giesler plastometer).

The above quoted work sets in perspective the central importance of the coal-coke transition phenomena which is strongly influenced by Pyrolytic processes and which in turn influences the course and nature of Pyrolysis, at least in the case of Bituminous coals. (In the case of low rank coals such as Brown and Sub-bituminous coals, the situation is complicated by extensive cross links generated by 'H' and etheric links including organically linked mineral matter inclusions).

The range of phenomena touched upon in the preceding pages including coal extract yield phenomena, its relation to coal solvation, fluidity, pyrolytic mass loss rate, cenosphere formation/swelling and lamallae orientation are all closely inter-related and influenced by the development and decay of plasticity.

Fitzgeralds work can be criticized on a number of counts not least for the assumptions of minimal volatile matter evolution during measurements using the Giesler plastometer. Criticism concerning artificially generated, excess plasticity caused by the paddles of the Giesler plastometer beating the fluid coal into a foam has been voiced by Kirov[60]. Work by J C MaCrae with a different plastometer indicated that the rising period of rapid

fluidity (at 381^{o}C) was associated with evaporation of accumulated liquid film coating the coal particle surfaces (dp=75μm, packed into an annular space of 3mm width with a packing voidage of 40.5%). The film originated from the loosely bound extractable material and developed into a foamy bubble structure by evaporation of the lower M.W. material (The melting range extended from 160^{o}C to 22% >325^{o}C and the boiling range from room temperature to a high proportion (78%) boiling over 450^{o}C). Whilst the above criticisms are noted, they do not wholly invalidate Fitzgeralds study, which focusses attention on the period of fluid decay.

The latter process is thought to be associated with bond breaking and repolymerization reactions leading to increasing graphitization and the formation of a rigid coke. A similar study by Kirov et al[60] in concert with thermogravimetric studies (at low heating rates 1.5-6^{o}C/min) on Australian coals produced a remarkably similar result to Fitzgerald ($E_A \approx$ 228KJ/mole and $k_o \approx 10^{14} s^{-1}$). However, Kirov makes a number of points worthy of note:

1) The complexity of coal decomposition reactions renders the concept of reaction 'order' untenable. But, if so inclined, then 'order' rises with temperature (and thus with extent of reaction) and decreases with time (at a particular temperature). The latter decrease may be associated with physical processes associated with degassing.

2) Even if the overall process was not even approximately 1st order as commonly assumed, it was possible to regard one special part of the reaction, that of the liquid component becoming solid as 1st order. Thus, a distinction was made between observed volatile mass loss originating from disparate

processes (e.g. simple disproportionation,condensation physical ejection etc?) and the specific solidification reaction associated with the liuid-solid transition.

3) Granular softening was shown to be a physically reversible process[60,178] and appears to reach a similar level of fluidity (below 400^{o}C) irrespective of rank <88.5% 'C'. The viscosity measured suggested a polymer-like material in which molecules were highly associated in long chains. (Does this support entanglement model of coal structures?). The rapidity, reversibility and insensitivity to heating rate of the initial fluidity implies that the so called 'metaplast' release is not associated with a high activation energy chemical reaction process as assumed by both van Krevelen and Fitzgerald. (Previous discussions, (vide infra) and a number of studies in rapid heat transfer[179,60] reactors lend support to this along with interpretation of analysis offered by Brown & Waters[77] in regard to reconciliation of extraction yields to coal structure and plasticity).

4) Petrographic variations had little effect on the characteristic temperatures (maximum fludity, mass loss and solidification), but affects amount and rate of mass loss.

5) As the solidification reaction rate constant was relatively high, both time and temperature were deemed to be of importance and thus resolidification was expected to depend on heating rate (so deduced from a theoretical nonisothermal rate analysis and confirmed by low heating rate fluidity curves, which it must be noted could have given rise to heat and mass transfer resistances).

6) The solidification reaction was associated with the scission of side chains (aliphatic bridges between rings, alkyl substituents, etc) followed rapidly by a relinking process with mobility aiding development of 2-D graphitic sheets and eventually, formation of cross links to form an immobile 3-D structure.

Reference to Kirov's results indicate (re: Brown & Waters) that the temperature of maximum fluidity generally precedes and in some cases almost coincides with the maximum rate of mass loss (rank dependant). The resolidification temperature generally follows the former, the lag being dependant on rank (% 'C'). Some recent work in so called 'rapid, dilute' phase Pyrolysis studies [179,154,158] employing a novel, fast response plastometer and a strip mesh furnace [154] provides some support for this sequential scheme of Pyrolysis.

The rapid response plastometer study [179] (dT/dt=480K/S; MIT, J. B. Howard & Peter W. A.) represents an ingenious and laud ble attempt to combine and replicate past efforts at reconciling extraction yields (pyridine extractables) and volatile yields to Fitzgeralds consecutive scheme from the viewpoint of rapid Pyrolysis. The pyrolytic yields were obtained in a mesh strip furnace (enlarged version, 14 x 7 cm). The study appeared to substantiate past low heating rate studies employing usually, denser mass loadings. Extract yield curve follows substantially the mass loss curve with the former identified with the so called 'metaplast'. Initial softening was found to be independant of heating rate (range 50-700 K/S) as noted by Kirov et al. Molecular weight analysis suggested either repolymerization reactions

and/or selective evaporation of the lighter components of the 'metaplast' with duration of heating.

An analysis of the fluidity rise and decay curves at 450 K/S (T=> 500-800^{o}C) resulted in the following values:

Coal $\xrightarrow{k}$ metaplast; k_o=245/S, E_A=40.7 KJ/mole

Metaplast $\xrightarrow{k2}$ coke; k_o=2x10^{8}/S, E_A=133 KJ/mole

In analysing the results it is interesting that the activation energies obtained from the above study were quite low despite the assumptions of chemical generation and destruction of 'metaplast'. Either these values represent a truer picture of the Pyrolysis process where heat transfer limitations were minimised or transport processes have been rate controlling. At any rate, taking previous discussions into consideration one would be inclined to agree with the rate parameters generating 'metaplast', but may perhaps quarrel with the solidification parameters as being too low. Nonetheless, as a number of thermo-kinetic studies of organic compounds indicate, the dissociation energy of a Bond depends not only on the atoms forming the bond but also on the groups attached to these atoms. Thus, ring size, geometry of fused ring (linear/branched), degree of activition/deactivation imp rted to the bond by substituent nature (CH_3, CH_2-CH_2, OH, COOH, etc) and/or heteroatoms could result in substantially lowered bond dissociation energies.

A subsequent paper, reanalysing the MIT work in terms of more adjustable parameters such as a Gaussion distribution of melting points of extractable material, among other things resulted in revised activation energies (120 & 176 KJ/mole for the generation and decay of 'metaplast'). Reference to the fit of the model to

the experimental mass yield curves indicate that the experimental rate of mass loss is greater than the fit over a substantial part of the initial period. It appears, uncertainly that at least some part of the fluid 'metaplast' owes its yield to partial chemical decompostion of the macromolecular part of the coal inhibits acceptance of a high rate constant for the so called 'depolymerization' step by some authors.

But as studies by Oxley and Pitt[60,33] in apparatus where heat transfer rates are high (e.g. fluidized beds, entrained flow) and mass transfer limitations were minimized, the rate of release of extractable material was very rapid. Thus, perusal of the work of Pitt[(185)], Stone and Batchelor[(58)] and recourse to a range of disperse phase, high heating rate studies (so long as high heating rate is equated to adequate heat transfer to the particle sustained by particle size reduction, dispersion and energy transfer mechanism) will indicate a rapid initial loss of volatile matter. Indeed, analysis of the MIT results shows up substantial mass loss and fluidity rise during the heating period particularly at the higher temperatures (>500^{o}C), which is in accord with more recent work associated with the mesh[154-158] and entrained flow reactors.

Overall, a persistent neglect in considerations of heat and mass transfer phenomena associated with studies of rapid Pyrolysis and misinterpretation of previous work associated with relatively high mass loads and low heating rates simulating such conditions in coking ovens[175] has made it difficult to explain the observed effects of heating rate.

As an example, various kinds of dilatometers[33] used to provide information on aspects of fluidity (such as softening temperature, percent dilation, resolidification temperature, etc) indicate that all characteristic temperatures including extent of dilation are pushed to higher levels at increased heating rates. In fact the reasons can be traced to heat transfer limitations, resulting in the apparent shifts noted. (Ref: 33, pp 326-328).

4.4.1 Interactions of heating rate and mass transfer resistances

It is germane at this point to consider some aspects of the effect of heating rate before proceeding to look in more detail at possible pyrolytic reactions relevant to plasticity. Whilst it was known that rapid heating resulted in enhanced total volatile yields it was not known whether this was due to fundamental kinetic influences or due to transport effects. Very few studies have set out to test the questions begging on a comparative basis in the same study. However, an analysis by David Gray et al[183] of volatile yields in dense and dilute phases came to the conclusion that yield was strongly correlated inversely to particulate packing density. Recent work by Tyler et al[125] on tar yields suggest a similar conclusion. Increased particle densities provided room for repolymerization and/or cracking reactions which previous discussions (vide infra) concerning the efficacy of coke surfaces towards cracking will bear out. Further, the effects of coal swelling and exudations of material of a wide range of boiling points over the particle surfaces observed by MaCrae will result[177] in a congealed mass of reduced bed porosity. The combined effect would be to inhibit mass transfer of the heavier exudates likely

to contain heteroatoms such as 'O', 'N' and'S' in thermally resistant ring systems which are however, reactive to repolymerization.

Such a picture can be reproduced in so called dilute phase 'rapid' heating studies. Pitt's study of rapid Pyrolysis and some of the mesh studies provide grounds for such possibilities. Pitt[188] utilised a sand fluidised bed to which was fed 25g of particle size 250-500 μm. As subsequent work by Tyler and others working with entrained beds (e.g. Jenkins[47], Scaroni[50], etc) realised, including the author, feed rates had to be very dilute to avoid heat and mass transfer effects. Further, as Pitt's system only allowed collection of data 10 seconds after coal was fed to the reactor, his analysis was restricted to the latter part of the Pyrolysis process reflecting chemical cracking reactions as opposed to the larger, initial rapid mass loss.

Pitt's reported activation energies showed a peak at 209-230 KJ/mole (k_o=1.7 x 10^{12} - 5 x 10^{13} S^{-1}) for a bell shaped distribution of activation energies (giving rise to the picture of coal decomposition as a set of independant parallel reactions). This peak value is in accord with both Kirov's[60] and Fitzgerald's[93] rate parameters. This value corresponds closely with the average value of C-C bonds in mineral oils[60] and as Kirov has pointed out this suggests the specific reaction involving resolidification. A cogent review of coal Pyrolysis by Yellow[58] also pointed to the fact that tar cracking (which is probably released very rapidly and remains longer within the reaction zone in denser packings) reactions also indicated activation energies in the range noted for the above studies (188-230 KJ/mole). Recent studies of tar cracking also suggest similar values.

Effects noted by Freihaut[158,154] in a mesh furnace (heating rates <1000°C/S) such as temperature deviations associated with very rapid tar release during the earlier heating period can be partly explained by the dense loading adopted. Hence, even in reactor systems where conditions assist in suppressing secondary reactions, the rapidity and nature of the heavy products of devolatalisation can result in erroneous assumptions concerning the 'primariness' of the products if extra care is not taken to avoid secondary reactions. Reference to a study of agglomeration of coal particles of single layers by Klose and Lent[183] will provide support for the points of view set forth thus far. One other study which in the view of the author is the only one (other than David Gray et al's) which more by accident than intent clearly highlights the effect of mass transfer on devolatization partially uncoupled from heating rate changes is that by Geoffrey Fynes et al[166]. Here, comparison of relatively rapidly heated coal of thick bed dimensions (10g, dp=250-500 μm, dT/dt=5°C/S; tube dimension=8mm i.d.) compared to dense phase, slow heating rate Gray King assay indicated the following trends:

Coal	% C	Tar/gas (GK)	Tar/Liquor (GK)	Tar/gas (Tube)	Tar/Liquor (Tube)
Anthracite	93.6	0.087	0.67	2.0	10.0
Bituminous	81.8	1.23	1.80	6.33	9.5
Brown	70.7	0.49	1.28	4.60	2.3

The results show (reconstructed by author) that whilst the overall char yield (and thus volatile yield) is similar for both Gray King and tube reactor (because of the dense packing in both cases), the tar to gas and tar to liquor yields show considerable increases for the latter.

The enhanced yield of heavier liquids stem from quicker removal of products from the reaction zone in the 'rapid' heating reactor. As the temperatures reached were $<600^{o}C$ cracking to coke or 'C' is less important relative to removal of higher boiling components by selective evaporation of the lighter components and mild cracking to gas and liquor.

The above discussion highlights the observed effects of high liquids to gas yield noted in so called high heating rate studies. (Recourse to the flash heating studies suggest that high flash energies will result in a diminished liquids/gas ratio for reasons noted).

Clearly, in the last study, if bed thickness had been sufficiently thin thus improving both heat and mass transfer, then not only would we observe enhanced heavy/light products ratios, but also enhanced total yields.

4.4.2 Possible Pyrolytic decompositions associated with the liquid - coke transition

Plasticity is a property of coal much studied in the past giving rise to the consecutive reaction model based on very comprehensive studies of a range of Bituminous coals and model polymer compounds. Much of the work, led by the Dutch school of van Krevelen[170-173] and co-workers including Fitzgerald led to reassessment of extraction studies and the idea of coal structure as a 3-D polymerization process. The latter idea has been taken up by USA workers led by Larsen et al.

At room temperature, Vitrinite exhibits optical anisotropy (i.e. optical properties differ with light direction). On heating to the point just preceding softening, it's optical properties become uniform in all directions described as 'isotropic'. Throughout the plastic range (encompassing temperatures of softening to resolidification, the range being a function of pressure and possibly heating rate), reflectance increases. At the temperature of solidification the coal undergoes a transition to a state similar to a nematic liquid crystal or 'mesophase'. At this stage, optical anisotropy is regained and continues to increase with heating. The mesophase developes from a number of centres and spreads at the expense of the isotropic phase until coalescence occurs throughout the mass on resolidification. This is a state almost akin to a poly-crystalline substance. The mosaic texture represents a measure of local orientation and stacking of the aromatic layers. The dimensions of the stack depends on the size of the fused rings or lamallae. It is thus that low rank coals generally exhibit fine mosaic size whereas higher rank coals exhibit larger mosaic size reflecting the precursor ring sizes.

The presence of large concentrations of 'O' functionalities in low rank coals also give rise to smaller molecular orientation size.[186,188,189,108] Berkowitz's review[83] highlights a number of low temperature reaction possibilities involving the highly reactive groups present. Some of these are depicted below. (Berkowitz also suggest, low temperature reactions such as izomerization and cydization occur).

Fig 24 Low Temperature Reactions (<300°C)

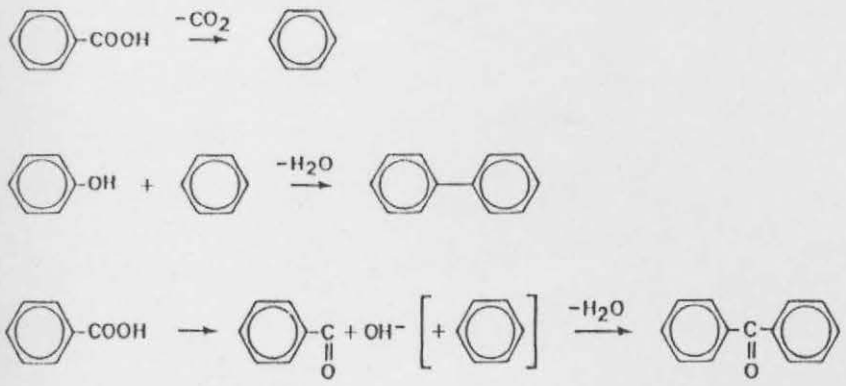

These simple group stripping and/or condensation reactions release H_2O, CO and CO_2, and for highly oxygenated coals can lead to significant crosslinking which may prevent coal softening and thus development of plasticity. The size and orientation capacity of lamallae during plasticity is a strong function of temperature 'O' and 'H' atoms, coal macromolecular structure (presence of hydroaromatic and fused ring distribution, nature and extent of cross-links) including nature and extent of extractable[106] material. Thus, a combination of 'H' donation/shuttling and/or free radical stabilization capacity of fused ring structures (e.g. pyrene, phenenthrene, Anthracene, coronene, etc present in both mobile and 'immobile' phases of the coal) will aid in solvation and mobility of the whole coal grain, the latter being a pre-requisite for effective molecular orientation.

4.4.2.1 Effects of heating rate on plasticity

The processes underlying increased plasticity at high heating rates may be viewed as follows:

If higher heating rate may be identified with a higher rate of thermal energy input, then the increased energy input will enhance molecular reorganization and ordering. This is so because the process of mesophase formation and growth by coalescence involves considerable relative movement of lamallae molecules.[186,187] It is possible that enhanced fragmentation of the molecular structure at high heating rates can lead to lower viscosities and thus mobility of the liquified material. A further consequence of high heating rate is that larger quantities of vapour/gas is released more violently in a narrower temperature/time interval leading to large 'vacuole' formation which results in the range of thin walled 'cenosphere' structures prevalent under these conditions.

Another effect of heating rate is the influence it exerts on the temporal elemental composition of the pyrolysing coal and thus on both its softening characteristic and extension of molecular orientation. Breaking down the heating/Pyrolysis stage into stages, stage one can be identified with granular softening and release of mainly 'O' groups which at high heating rates may be accomplished sufficiently promptly with the increased thermal energy, providing sufficient disturbance to the system to diminish and/or disrupt crosslinking reactions. Further, at fast heating rates overlap of the former phase may occur with rapidly increasing softening/fluidity concomitant with heavy H/C evolution and an acceleration of molecular orientation. Towards the end of this stage, with temperatures rising, increasing loss of side chains/ substituent groups will allow increased orientation of the lamallae and thus growth of fused ring dimensions by repolymerization culminating in decay of fluidity. The last stage of the process, following the major molecular reorientation and graphitization

noted will be a slow annealing and crosslinking of the lamellar stacks aided by 'H' and various heteroatom release in the form of gases such as HCN, COS, H_2S, mercaptans, etc.

4.4.2.2 Skeletal elemental changes in relation to Pyrolysis

Reference to a number of studies at high heating rates[190-196, 33,154,142,143,125,169] of elemental changes with Pyrolysis temperature will confirm the above picture. Thus reference to Freihaut et al highlights the fact that elemental 'N' loss in the char closely reflects volatization of 'N' in tar and gas. The acceleration of 'N' release as HCN gas was interpreted as tar cracking at the higher temperatures where a fall off in tar was noticed (peak tar yields in the mesh reactor under vacuum conditions occurs at about 600-750^{o}C, dependant on coal origin). Closer examination shows that the fall of 'N' in the char at higher temperatures suggest the possibility that both ring fragmentation in the coal/coke structure as well as tar cracking contributes to gas increase.

Freihaut further claimed that there was a close correlation between volatile yield and 'N' removed in the form of tar, gas and char. Work by Blair et al[(142)] also hint at significant 'N' evolution at high temperatures (800-1400^{o}C). Reference to his results clearly show however, that the slope of the 'N' loss is different from that of mass loss with respect to temperature, which fact does not tally with Freihaut's results. Blair et al noted that whilst yield varied substantially with temperature between different coals (73.8, 75.1 and 85.7% 'C'), the rate of the loss of 'N' with temperature was similar for all the coals.

The latter result does not find agreement with Freihaut who found the reverse.

Disagreement probably results in part from mass transfer differences stemming from differences of particle packing, particle size and method of heating. (Blair et al used single particles and multiple particles of dp=500-617 μm which could suffer temperature gradients at the high heating rates used ($20^{o}C/msec$). Further, the Blair studies utilised electrically heated graphite whereas Freihaut employed stainless steel and tungsten meshes. Moreover, the former used a diluent gas, argon and the latter's study was conducted at vacuum conditions at $1^{o}C/msec$. Particle sizes were 45-140 μm and loads of 10/25mg of coal).

Work reported by Peet et al utilising a dense phase fluidised bed and dilute phase drop tube resulted in the observation that volatile yield was linearly related to total 'S' release of the form: $S = \alpha \Delta W + C$. The constant α, was greater than unity suggesting that the organic 'S' was part of more labile structures than the rest of the organic material. (Organic 'S' constituted 88-93% of total 'S', the rest essentially in pyritic form). The study was conducted on New Zealand coals of particle size 106-250 μm at isothermal temperatures of 300-900^{o}C and residence times of 1½-30 seconds.

A point worth noting with coals of high 'S' content from a variety of geological formations[83,192,154,124] and rank is the enhanced plasticity including high mass and tar yields. Rapid heating of Canadian coals[149,198] (spouted bed reactor) and USA[154,158] coals (an Appalachian and Pittsburgh coal, in a mesh reactor)

of high 'S' content yielded tars of high aromaticity. As there is little data available on the nature of the high tar yields inherent in the volatile yields noted for the New Zealand coals it is not possible to ascertain the synonimity of high tar yield to high aromaticity as hinted by Freihaut et al. An important source of uncertainty arises here. Hence, some authors argue that yield is correlated to aliphatic 'H' content reflecting availability of 'H' (made available by cracking of labile aliphatic bridges, alkyl ring substituents and dehydrogenation of hydro-aromatic structures for radical stabilization). Support for this idea stems partly from early work of Solomon et al[143),(146)] working with USA coals in the mesh reactor, from Tyler[(124)(125)] and Calkins[199-202] et al (Australian and USA coals) working with fluidized bed tars and correlations obtained by Canadian workers[(153)] working from low heating rate, dense particulate Fischer assay conditions. Tyler and Furimsky[153] showed that a linear correlation existed between yield of tar and H/C atomic ratio for a wide range of coals which implies the aforementioned correlation. However, the Canadian work in particular found that yields from low rank coals (high 'O' and ash content) were severely overpredicted by the correlation. Interestingly, like Freihaut, Furimsky found a close relationship between parent coal and tar aromaticity, except that the yield/aromaticity relationship was diametrically opposed. The latter disagreement stems probably from two sources. One would be diminished mass transfer likely to occur in the packing conditions of the Fischer assay which would favour lighter products. The second reason may stem from differences of coal structure and geology as well as the distribution of 'S' in the various structures of the coal 'polymer'.

Freihaut found enhanced tar yields from Appalachian and Interior USA coals. The latter originate from the carboniferous period with the Appalachian coals having been buried to a higher depth and having generally medium to high 'S' levels. FTIR results indicate high aromaticity as well as higher tar yields for these coals compared to the Cretaceous period which show stronger aliphatic bands. (The Cretaceous coals are about 200×10^6 years younger than the Carboniferous coals).

If one considers the fact that the Canadian coals Furimsky worked with were also largely of the Cretaceous period, including the Australian coals (which also includes Permian coals of younger origin than Carboniferous coals), then the agreement between yield and H/C ratio noted for these coals is not surprising. Further, the incorporation of 'S' into more thermally resistant thiophenic structures may require increased coalification age which may explain high aromaticities in the liquids noted by Freihaut for his high 'S' Carboniferous coals. It is worth noting that the tar obtained from one of the high 'S' Carboniferous Canadian coals obtained by rapid heating in a spouted bed[149,198] was highly aromatic.

As noted above, Freihaut's work coupled with a number of related studies[198] of plasticity[187-189] and extractivity[106,77,124] suggest that yield may be equally facilitated by plasticisability, 'H' shuttling capacity and/or radical stabilization propensity of thermally stable fused ring structures. Further, if mass transfer resistances are supressed by use of flowing diluent gas or low pressures, than it is likely that an increased yield will also reflect higher aromatic liquid material as is noted in so

called 'rapid' heating rate studies (vide infra). The latter discussion, in conclusion suggests that higher tar yields were conducive with higher parent coal aromaticity in 'C' range 76-88%.

One further consideration concerning the 'S' heteroatom is the multitudinous manner in which 'S' structures can react within the condensed phase as well as the fact that gas phase products such as H_2S can react with both gaseous H/C as well as mineral matter (e.g. Carbonates and oxides of Ca, Mg and Fe) in the coal.[90,196] Shock tube studies of coal Pyrolysis indicated that at temperatures >727^{o}C, the reaction of H_2S with mineral matter was so fast that nearly all the H_2S was incorporated in the char even for times <2ms. The work of A Attar[90] in particular has indicated that there are several reactions that can tie volatile 'S' into the Organic matrix.

Attar has also highlighted the distinction between ease of gas phase mass transfer as opposed to the probability that many 'S' (and by analogy ther species) products are diffusion limited in the condensed phase. Studies by Doolan et al[197] of shock tube Pyrolysis of very fine coal particulates (dp<10 μm) produced lowish activation energies for a range of product gases, which they concluded stemmed from diffusional limitations. (Bearing in mind they were working at high temperatures 827^{o}C-1927^{o}C and high energy transfer rates it is quite likely that diffusion limitations may so arise).

Owing to the many forms that 'S' occurs in coal, as sulphates, pyrites and a variety of organic forms, the effect of 'S' on reactivity is particularly important. (Refer to refs: 196, 90, 190, 195, 194, 193).

The preceding discussion suggest that heteroatoms such as 'S', 'N' and 'O' may be distributed uniformly throughout the organic coal structure in a manner related to geological history. As the discussion had strayed to high temperatures (>700-800^{o}C) where significant evolution of heteroatoms (especially 'N' & 'S' and 'O' in form of CO) occur at the post resolidification stage of Pyrolysis, it is clear that decaying primary decomposition reactions are overlapping with secondary reactions including increased vaporization rates. At high heating rates it would therefore be difficult to distinguish between the three processes at even the intermediate temperature stage (500-600^{o}C) and thus to judge which of the three processes control the rate of devolatization.

A number of studies attempting to do so[209,210,211,212,213] by consideration of various mass transfer processes (evaporation/ subsaturation boiling, film diffusion/bulk diffusion, hydro-dynamic flow[32] etc) have produced ambiguous results. Vastola and co-workers[225] conducted a theoretical study of possible heat transfer situations by retaining a basic single overall reaction model (adjusting only the values of rate parameters E_A and k_o and ultimate yield) without attempting to propose a detailed scheme of Pyrolysis mechanism.

Rather, the latter group have concentrated on gathering data of yield and yield nature, utilising a range of analytical chemical techniques and reactor types simulating rapid heating yields.

4.4.2.3 Reactivities of various structural groups associated with coal decomposition

The key structural features of coal determining its reactivity may be related to the following basic features based on the preceding commentary, that is:

a) The major building block of coal are predominantly aromatic and hydroaromatic units with the relative proportions varying with coal rank.

b) There are heteroatoms situated at the edges of the blocks in the form of 'O', 'S', 'N' and 'H', which are released at higher temperatures (not counting the material loosely clatharated within pores/defects).

c) Extent and nature of cross links between the lamallae units which is a function of rank and whose extent determines the degree of 'polymerization' of the parent coal. It has been speculated that the degree of cross linking can increase with temperature of heat treatment arising from condensations of 'O' functional groups and 'S' group interactions.

d) Extent and nature of secondary interactions such as 'H' bonding, donor/acceptor bonds (acid/base), van der Waal bonding which varies with rank and heat treatment temperature.

The latter two features have been discussed at length and it remains to assess the nature and interactions of (a) and (b) on reactivity during Pyrolysis. Considerable study of fused ring systems from the viewpoint of thermochemistry[169] liquefaction and carbonization[188,99,189,108,116] have highlighted the following

facts. Consider the following simplified reaction scheme:

1) Coal-Coal⟶2 Coal• (weak linkage breakage)

2) Coal•⟶'H' capping and evaporation

⟶Collisional deactivation with 3rd body (e.g. diluent gas, reactor walls, etc) and evaporation

⟶Recombination in gas phase and condensed phase

Reaction pathways noted in (2) arise from probabilities for free radical stabilisation which may be influenced by (a) concentration of reactive edge atoms at building block edges, (b) mineral matter inclusions at edges and defects, (c) external pressure and particle bed depth, (d) vapour pressure (enhanced in vacuum and for curved surfaces) of stabilised lower M.W. fragments, (e) entrainment of V.M. by shear induced volatile flux combined with transient pressure assisted ejection (both probably assisted by high heating rates and plasticity).

Based on arguments presented in the preceding pages the author posits reaction (1) to occur to a significant extent and rate at higher temperatures (>450-500^{o}C) following low temperature dehydroxylation, decarboxylation, softening followed by rapid fluidity rise concomitent with heavy liquid evolution (vide infra). Alpha radicals produced via reaction (1) from various ring structures indicate that extension of the attached aromatic system increases the ease of bond breakage. This arises from the increased possibilities for resonance stabilisation of the radicals so formed and consquently leads to low values of several bond dissociation energies noted in coal decomposition (Refer to Gavalas, Ch 3 for a good discussion and reference [124] pp 302-303 for numerical illustrations of rates).

However, reactivity towards free radical formation, elimination of heteroatoms (including aromatic 'H') and resolidification/ repolymerization was noted to depend on:

a) geometry of ring system (linear, branched) and size

b) position on fused ring (edge positions)

c) nature of heteroatom substituent at edges

d) steric configuration of ring systems which may override reactivity parameters indictating ring growth. A review by Lewis[188] and studies by Walker[116,189] and others have shown that linear fused rings are more reactive than branched rings. For example anthracene is more reactive than it's branched isomer phenanthrene in terms of lower temperature of reaction and carbonization (i.e. increased aromatic 'H' loss and char formation by repolymerization).

Further, it is known that reactivity at the 'C', 9 & 10 positions of Anthracene is higher than any position in phenanthrene or biphenyl. Heating Anthracene in an autoclave to supress vaporization, it was observed that it melted at 128^{o}C forming an isotropic fluid whose viscosity fell sharply with temperature. At about 450^{o}C 'H' was released at the 9, 10 positions forming free radicals and thus leading to condensation reactions. With continuing 'H' elimination and increased condensation the fused ring structures reach sufficient size to realize van der Waal attractions to promote lamallae alignment. At this point anisotropic spheres (mesophase) appeared in the dispersed isotropic fluid, the former increasing in number and size until coalescence occurred to form bulk mesophase which quickly led to resolidification

to a brittle solid (semi-coke). In various graphitizing materials, large porosities are developed just before the semi-coke stage which aids orientation of lamallae (Refer to rapid heating rate chars produced by Hamilton et al [130] and Solomon et al [163] from coals which showed anisotropic mosaic features).

Polymerization reactions leading to increased ring sizes can occur in successive stages by elimination of H_2 as described for anthracene leading to either noncondensed polymers (units linked by single c-c bonds) or fully condensed polymers (planar fused rings). The polymerization path was found to depend on steric factors. In this context, Berkowitz's [58] work on 'H' release at temperatures above 500-600^{o}C has been interpreted as a reaction controlled by lamellar mobility (a physical process) reflected by an 'activation' energy of 33.5 KJ/mole. (This result is in variance with assumed mechanisms of aromatic 'H', release reflecting high activation energies calculated by Solomon et al and others.[58] However, as Yellow notes in his review, Berkowitz postulated his mechanism from subsidiary experiments whereas others either assumed a mechanism based on theoretical considerations and/or based on limited data).

Substituents on the aromatic rings can alter the course of polymerization leading to graphitization at higher temperatures. Substitution of 'N' at the 9, 10 positions in anthracene (phenazine structure) accelerates loss of 'H' and thus free radical production and thereby enhances carbonization rate relative to anthracene. Substitution by 'S' can result in generation of cross links in a similar manner to 'O' (vide infra). Alternatively 'S' can be incorporated into ring structures which remain stable until

high temperatures are reached when they can undergo polymerization reactions. 'S' heteroatoms incorporated into strained ring systems can be readily eliminated in the early stages of carbonization. (Refer previous section for 'S' reactions).

Substitution by 'O' functional groups such as 'OH' can increase the reactivity of the ring structure in a manner dependant on position of substitution. Thus, dissociation rates of 'OH' substituted cresol decreases in the order o-cresol>m-cresol> p-cresol. A combination of inductive effect (e^- withdrawing effect) and mesomeric effect (here, the e^- of the substituents are involved in e^- delocalisation), dependant on substituent nature is responsible for the changes in reactivity of substituted ring systems noted. Work reported by Gavalas from the viewpoint of thermal liuefaction and thermal decomposition of representative coal model structures such as cis - 9, 10 dihydronapthalene suggests that the latter and high temperature reactions involving phenolic radicals occur by concerted reaction pathways as opposed to the free radical mechanisms noted above.

In the above reactions, 'H capping', essential for stabilisation and thus evaporation of resulting low M.W. fragments from large parent macromolecule polymer is facilitated by internal 'H' rearrangements. Available 'H' is then added at the most reactive positions of the molecule. However, reference to the curie point Pyrolysis studies of Meuzelar[126] et al indicates increasing products of anthracene, phenanthrene, acenapthene and napthalene at increasing coalification (analagous to increased Pyrolysis temperatures). It is possible that these structures originate from low M.W. clatharated material which exerts a sufficient vapour pressure at T>400^{o}C to simply desorb/evaporate.

Further reactions can occur such as thermal rearrangements which can result in formation of more aromatic fused ring structures without loss of 'C' atoms ('H' eliminated)[188]. An example quoted by Lewis which involves loss of 'C' in the rearrangement reaction is that of methylene phenanthrene which results in the elimination of C_2H_2. The former rearrangement involves cydization of relatively unstable 5 membered rings such as acenapthylene and bifluorene to stable 6 membered rings.

In recounting the above processes, including the 'S' atom reactions noted in section 4.4.2.2, it is noted that several processes such as bond cleavage, molecular rearrangements, polymerization/ring condensation, substituent and heteroatom elimination, including gas phase/condensed phase interactions can all occur in parallel, either independantly or competitively. Lewis notes that the multiplicity of polymerization sites in aromatic molecules can lead to multiplicity of products. For example he suggests that 11 reaction products have been noted from simple dimerization of anthracene. With progress in reaction, the number of possible isomeric structures and thus, reaction possibilities increase rapidly.

Indeed, subsequent studies by Fitzgerald[93] emphasises the simultaneousness of the Pyrolysis process with the product of one reaction being the reactant of the next. Thus, his revised scheme is as follows:

$$\text{Coal} \xrightarrow[\text{V fast}]{k1} \text{metaplast} \xrightarrow[\text{rapid}]{k2} \left[\begin{array}{ll} \text{Primary tar} & \xrightarrow[\text{slow}]{kc} \text{Pitch} + \\ + & \\ \text{Semi coke} & \xrightarrow[\text{slow}]{k3} \end{array}\right] \begin{array}{l} C+O \rightarrow CO \\ \text{coke} + \text{gas} \\ C+2H_2 \rightarrow CH_4 \end{array}$$

Several points are worth noting which supports preceding hypothesis of tar release and subsequent development of the parallel, independant reaction models developed by Pitt, Anthony and Howard , and incorporated in some form by many authors in their reaction schemes for coal decomposition at high heating rates. He notes that:

1) Tars arise by distillation with little decomposition involved under vacuum conditions (fairly dispersed state and low pressures.

2) Self hydrogenation of semi coke observed by excess CH_4 production at temperatures >500^{o}C (This was observed by Berkowitz as well and whilst this is thermodynamically favoured at high pressures, the presence of 'freshly' generated reactive edge 'C' atoms along with possibly sufficient concentration of nascent 'H' generated by dehydrogenation of hydroaromatic structures could support this at low external pressures).

3) CO generated by high temperature reactions probably stem from thermally stable 'O' structures incorporated into fused rings of the semi-coke/coke structures by earlier condensation reactions.

4.5 General comments

Taken in total the previous discussions suggest a huge variety of reactions at a large range of temperatures ranging from 80^{o}C to above 800^{o}C. Whilst certain classes of reactions and products may be assigned to particular temperature intervals,

particularly H_2O/CO_2 release, heavy H/C release paralleling fluidity increases and subsequent resolidification reactions, it appears likely that at high heating rates, kinetic constraints would lead to an observation of overlapping multiple processes.

Reference to a number of high heat flux studies ranging from flame systems, laser heating, shock tube studies and entrained flow reactors indicate that the activation energies noted for both gas yields and particularly total yields are generally low. There is then a suggestion that at high heating rates where heat and mass transfer resistances are minimised, devolatalization rates are indeed very rapid, occurring during the period of heating up of particle to its peak temperature. Both fixed bed studies in mesh reactors (refer Freihaut, MIT work and entrained flow work of Sandoram et al and Maloney et al), entrained flow reactors fluidised beds and flame systems imply such a possibility.

However, the observations of Freihaut et al, among others of significant light gas yield (H/C gases and gases such as CO, HCN, etc) at the post rapid tar evolution stage indicte a sequential scheme of chemical decompositions for their release. The preceding discussions of resolidification reactions also suggest this possibility. But reference to gas yields as a function of time by Russian workers and by Johnson (Leeds University) including Chuckanov et al among others do not suggest an exponential relationship suggested by a first order decomposition process. The Russian work suggests either a $t^{\frac{1}{2}}$ or linear relationship as does Johnson's results. Clearly, the situation is quite complicated by such interfering factors as secondary cracking reactions (probably accelerated at the enhanced residence times

of particles at peak temperature for high heating rates). Further, as Doolen et al suggest, rapid devolatalization at high heating rates for even small particles (<10 μm) may be limited by diffusion of products, including light gases. Further, as the results of Berkowitz and discussion of the importance of steric factors for the condensation of ring structures resulting in 'H' gas release (Lewis[188]) show, physical factors play a part even at high temperatures.

Consideration of the large scale porosity evidenced by lacy and other cenospheres suggest that rate of devolatalization is limited by diffusion processes arising from a rapid generation of decomposition products. Despite high velocities of volatile evolution calculated by Blair et al[142] (based on pressure driven flow described by a form of Darcy's Law relating permeability to porosity), Atitmay et al[69] and Azhakesan[71] (volumetric jet efflux model with no holdup of volatiles generated) and recorded observations by Sharkey et al during laser flash heating, diffusion resistances may be yet operative in the condensed phase.

Observations by Attar on the importance of diffusivity in the condensed phase dependant on particle size, external pressure, vapour pressure and viscosity of the multiphase coal. /liquid/coke/ gas system suggest that the importance of diffusivity limitations cannot be overestimated. Observations of high activation energies have been traced to high mass load systems where the value of 50-55 K cal/mole may be identified with tar and or model polymer cracking activation energies. Such an observation can therefore arise in reactor systems where heat transfer lags and/or mass transfer resistances operate which can be a complex function of reactor geometry, feed density or particle packing.

Thus, Antal et al[31] discovered that decoupling of measured particle temperature from the actual temperature of biomass samples resulted in increased E_A values. Accounting for heat transfer effects by closer matching of mesured temperature to 'true' particle temperature resulted in lowered E_A values. Consideration of the rate equation for particular values of rate parameters will clearly highlight this effect as a lowered reaction rate when matching yield data to a measured temperature which actually overestimates the true particle temperature. Such artefacts can lead to choice of dubious models such as the varieties of two reaction model (Kobayashi et al, Nsakala et al) whose division of time and/or temperature dependant reaction parameters probably reflect heat transfer limitations.

It is however difficult to estimate particulate temperatures in a variety of rapid heating situations involving fine particulates. Observations at high heat flux conditions have suggested indications of temperature arrest of the particles during the devolatalization process. Thus a number of studies of Pyrolysis in fluidised beds (Atitmay et al[69] Azhakesan[71] dp>1000 μm) have indicated both large velocities of gas/vapour release and observations of low particle temperature (black against red heat bed) during the rapid devolatalization process. Measurements of particle temperature during relatively rapid heating by convection and radiation heating of single particles by Davies et al[204] (dp = 6.35 - 25.4 mm and T = 380 - 550^{o}C) indicated a temperature plateau of about 400-420^{o}C during a period of 'constant' weight loss. The latter period corresponded to heavy liquid evolution, after which (as in the fluidized bed cases) particle temperature rose to that of the surroundings.

The latter study is particularly interesting in that it was found that mass loss in the aforesaid period was found to be proportional to heat flux. Estimates of latent heat of tar and reaction heat suggested fairly large values of endothermic heat requirement. A study by Verfus et al[205] of rapid heating reaction heats of high volatile Bit. Coals suggest that reactions were endothermic over the range of temperature measurements with endothermicity rising at increased temperatures and rising extent of carbonization. (T = 600-800^{o}C; dp = 63-1000 μm range). The values quoted were higher than those generally assumed from extent information on such reactions gleaned from low heating rate, high mass load studies where, incidentally, the trend was one of decreasing endothermicity with decreasing extent of carbonization/ temperature.

Freihaut et al (including the author) has noted signs of temperature arrest for rapid rate heating of fine particles at 1000^{o}C/S. The temperature deviations coincided with period of rapid tar release and was accentuated by high coal volatile content. However, the results indicate that these deviations were dependant on imposed final temperatures. Simulations by Niksa et al and by the author of loading conditions in the mesh reactor suggest that such deviations can occur as a result of excessive local mass loadings. (Refer to Ch 6). Nevertheless, the nature of the deviations, dependant on coal volatility, coupled with numerous other experimental observations mentioned, admittedly, of larger particles suggest that significant cooling of the particle may be occurring due to heat carried away by vapour efflux.

Indeed, rapid, high heat transfer study of injected coal

particles into a stirred, preheated bed of ceramic balls by Peters[219] was interpreted in terms of constant rate of weight loss of zero order occurring during the period of temperature arrest. (dp = 0.2-2mm, T = 700-1100°C). The temperature arrest was estimated to be 330°C following which slow secondary degasification occurred. A reinterpretation by Mills et al[56] suggests a more reasonable figure of 497°C for the endothermic period. The relationship of yield to temperature was deduced as follows:

$$W\%(\text{mass } \%/s) = 5 \times 10^{-3}(T_B - 603)Do^{-0.26}$$

Where T_B = Bed 'driving' temperature

Do = particle diameter

The above relationship indicates a very weak particle diameter dependance and particle temperatures were theoretically estimated using rather large values of heat transfer coefficient, corresponding to Nu = 14. The Nusselt correlation implies an inverse heat transfer coeff (heat flux parameter) to particle diameter ($h \propto 1/D$) which is not reflected in the yield/diameter relationship. This probably reflects a different heat transfer mechanism (complex p-p contact ?) rather than the assumption of kinetic control assumed by Mills' interpretation.

A number of studies in flow reactors (all at temperatures >550°C) have indicated suggestions of devolatalization induced temperature arrest during heavy liquid efflux (Maloney et al Vastola et al[225]). The problems of interpreting such studies are numerous. Most of the studies had to resort to numerical simulations to assess particle temperatures during heat up, based on a dearth of suitable coal thermal properties appropriate to fine particulates. Further, problems arise (refer Ch 3) owing to

the complex heat transfer mechanisms operating in the various reactors. Heat transfer may be a complex of convective, conductive (wall-p, p-p, gas-p) and radiative mechanisms and generally increases with temperature. Finally, high reactor temperatures have been used, making it difficult to assess whether at the higher temperatures a different mechanism such as rate of volatile diffusion/evaporation becomes rate controlling and/or whether secondary reactions had interfered. Lastly, heating rate is a function of reactor temperature and mixing time of feed coal stream with reactor gas stream.

Quite drastic assumptions had been made concerning isothermality and heating rates of the single particle based on feed streams of variable density and gas/particle properties (interparticle and intraparticle porosities; gas and particle properties; particle loading). Clearly, for many of the studies, assumptions of very fast heating rates are incompatible with negligible weight loss during the heat up period for the particle sizes studied nor isothermality of particle. There is further, considerable difficulty in choice of heat-transfer mechanism assumptions which show differing particle size dependancy and it is doubtful whether single particle heat transfer models may be foisted on to multi particle streams.

Analysis of the mesh reactor systems loads to similar problems of interpretation and experimentation. Comparison of the work of a number of workers show significant variations in loading (in terms of mass per unit area of mesh loaded, particle size range, localisation of load mass). Early work by Solomon et al and Gavalas et al [19] which involved packing 50-200mg of coal

into a similar mesh area as used by others (e.g. Anthony & Howard and Suuberg used 5-10mg; Menster et al used microgram quantities; Freihaut packed 15-20mg into a small area, $\sim$ 2 cm^2) was claimed to represent a more accurate representation of 'isothermal' Pyrolysis at the high heating rates studied (650-1000^{o}C/S). Clearly the latter claim makes a nonsense of the meaning of applied heating rate to individual particles and was criticized by MIT workers.

Niksa also pointed out the difficulty of sustaining high heating rates to particles under low pressure conditions where the deficiency of interphase heat carrier such as diluent gas can lead to large temperature lags. However, Niksa's experimental procedures, whilst thorough presents particular difficulties in interpretation. His yield curves, including appearance of liquid yield at substantially higher temperatures than noted in a variety of studies (except Kobayashi et al) suggest heat transfer lags. These probably arise from the method of particle loading adopted (as mesh expands with heating, the particles will heap together) and thermocouple attachment procedure adopted (Refer Niksa thesis for interpretation). The suggestion of heat transfer lags, particularly at high heating rates and vacuum conditions probably result in his conclusions that (alone among other mesh studies) under these conditions total yield increases with heating rate (long residence time at peak temperatures) at higher temperatures. He was able to fit his data by a model accounting for heating rates which, significantly, utilised Kobayashi's data as support for his interpretation of yields during heatup, total yields at high heating rate and assumption of competitive reaction mechanism.

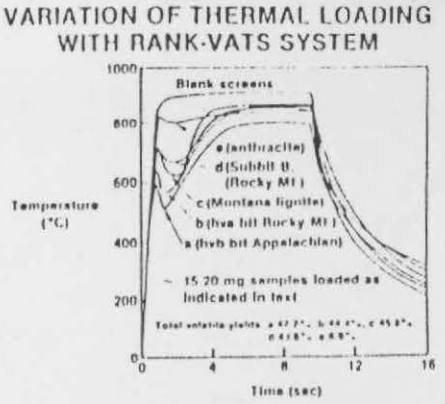

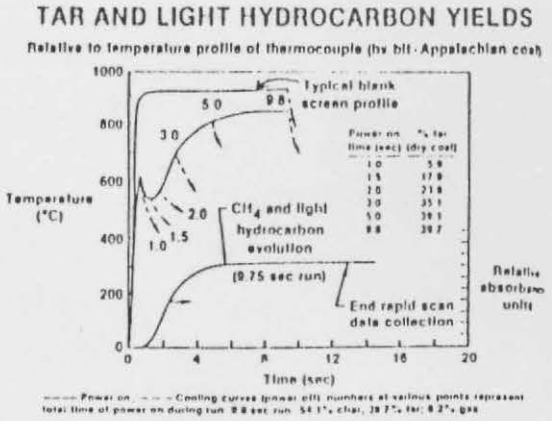

Fig. 27 Temperature deviations during coal pyrolysis in a heated mesh screen.
Re: Freihaut et al (Ref. 158).

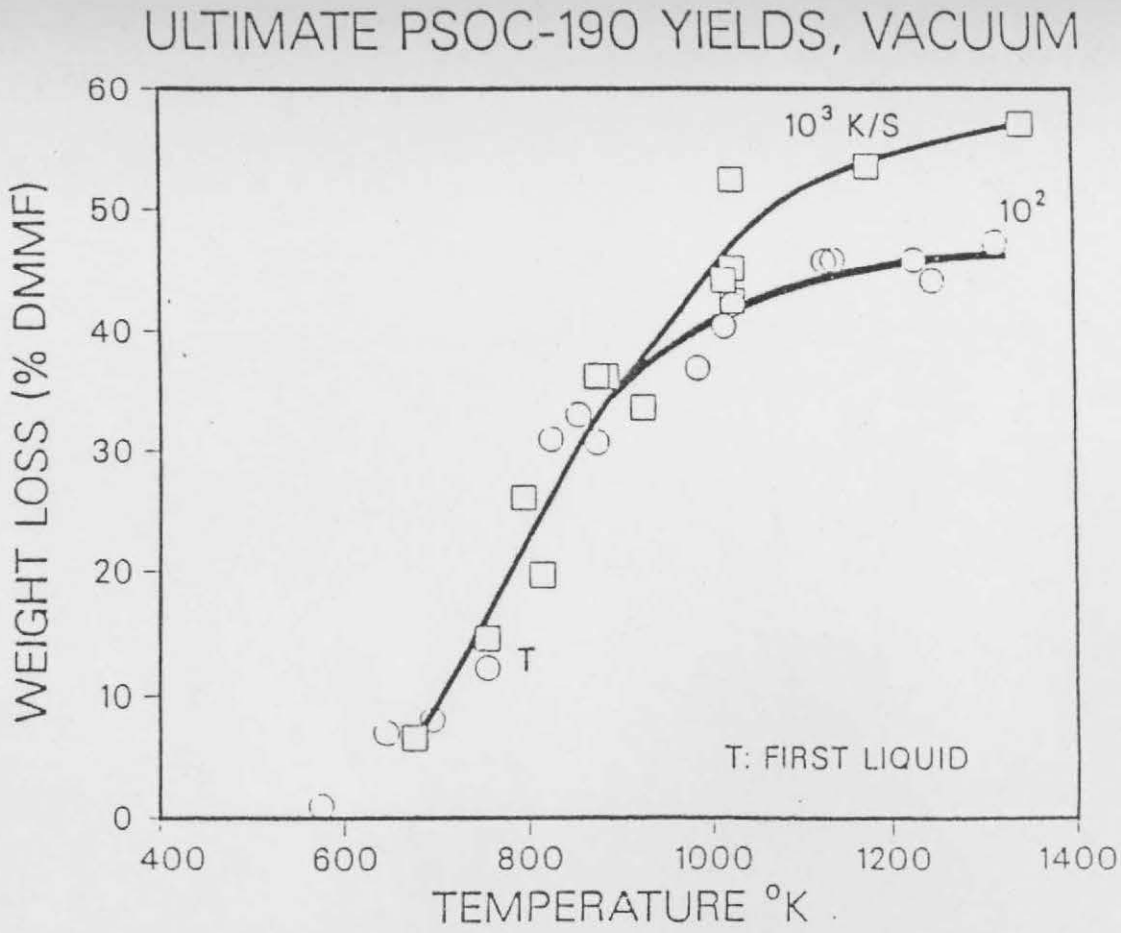

Fig. 25

Re: Niksa et al; yield at 30 seconds

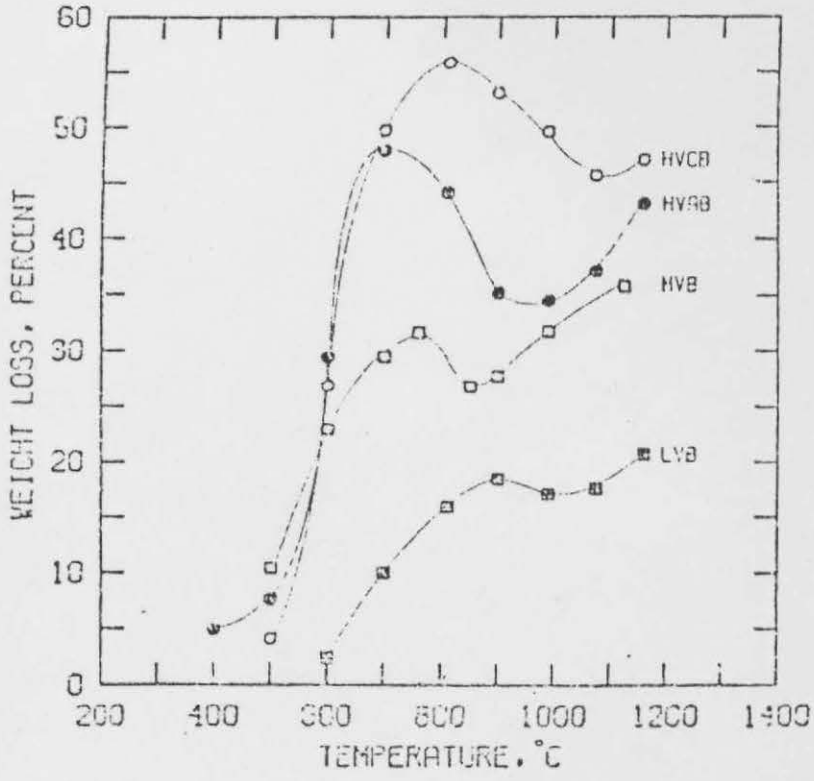

Re: 26 Menster et al

Vacuum pressure transient yields

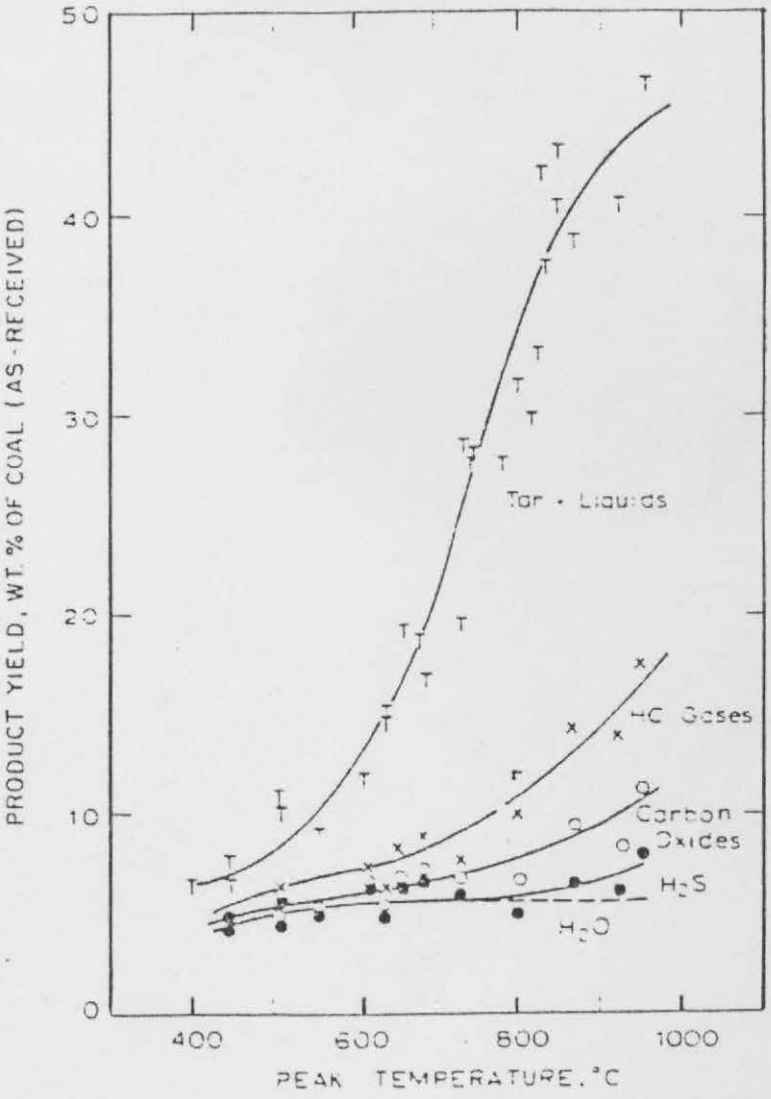

FIG. 28 Pyrolysis product distributions from bituminous coal heated to different peak temperatures [(●) H_2O and H_2S; (○) H_2O, H_2S, CO, and CO_2; (×) H_2O, H_2S, CO, CO_2 and all hydrocarbon gases; (T) total weight loss, i.e., H_2O, H_2S, CO, CO_2, all HC gases, tar and liquids. Pressure = 1 atm (helium). Heating rate = 1000°C/s].

Re: Suuberg et. al.

Kobayashi's system has been interpreted to suffer substantial heat transfer problems by subsequent studies of Solomon et al and others utilising entrained flow reactors.

Nevertheless, Niksa's experimental work and ideas on modelling[216] represent illuminating insights on both aspects of Pyrolysis work. Refernece to Menster et al[155] indicate yield curves, consistently reproducible for a variety of coal ranks which show features completely different from others. (A comparison of Niksa, Menster et al[155] Freihaut and Antnony et al is made in figs[25-28]). It is worth noting that Menster's experimental technique differs substantially from others in terms of particulate loading density and particle size range utilised. (Coal load = 100-370 µg; Vitrinite maceral used, of dp = 44-53 µm loaded onto a 304 stainless steel mesh, fashioned into a cylinder, 6 cm long and 0.12 cm diameter.)

As in all the mesh heating studies, Menster et al noted enhanced volatile yields at rapid heating rates in the temperature range 400-1160^{o}C. However, his total yields show maxima or plateaus (for Brown coal and low volatile Bituminous coal) at temperatures dependant on coal rank at a constant heating rate of 8250^{o}C/sec. At higher temperatures (>900-1000^{o}C), yields begin to increase again at a rate dependant on coal type (sharpest for high volatile and brown coal). Further, the rapid mass loss occurs over a narrower interval of temperatures for comparable coals (see Sauberg et al and Anthony and Howard) heated in mesh reactors. The latter may be a result of the vacuum conditions of Pyrolysis and significant mass transfer supressions entailed by Menster et all's closely sized, low loading densities.

Menster also attempted a more direct measure of particle temperature lags by recourse to heating of metals of known melting points.

Overall, the difficulties presented by the worryingly different features noted in the mesh studies to date are considerable in terms of interpretation. However, a closer examination of the work compared in terms of different procedures for particle loading will uncover a trend which suggests the importance of heat and mass transfer variations hinted at by the nature of the yield curves. Reference to the German mesh furnace studies (which include both single particle and packed load studies) as well as that of Hamilton et al (plasticity effects were studied as a function of heating rates to 1000^{o}C for a variety of Australian coals) yield such clues. These features will be analysed more closely in the subsequent chapters.

4.6 Conclusions

Comparison of rate parameters for coal Pyrolysis and other related biomass materials show a remarkable feature that activation energies increase with increases of preexponential factor. Noting this feature, in his book on nonisothermal Pyrolysis, Kock, and others who have noted this feature offer no good reason for this kinetic 'compensation effect'.

Interpretations of reaction rates based on the empirical Arrhenius relationship has its basis in homogeneous reaction kinetics. Here, the concept of reactant concentration, order of reaction (w.r.t. reactant concentration), temperature coefficient of reaction rate (E_A) and pre-exponential factor

have specific meaning when applied to simple molecules and aided by appropriate theories of reaction rates (vide infra).

However, the mechanism for acquisition of activation energy for decomposition reactions in a condensed phase system of high molecular mass, in near impossible steric configurations and physico-chemical environments, appears to be singularly puzzling. In the initial stages of heating, even if sufficient energies may be acquired via vibrational and rotational modes for activation, it is likely that the high viscosity of the system will result in severe diffusional limitations. It is likely then that any transient weakening of chemical bonds will reassert itself in recombination reactions.

Perhaps it is thus that true chemical reactions resulting in molecular weight reductions by bond dissociations could not commence until solvation and fluidization of the larger macro-molecular fragments of the coal occurs to effect sufficiently low viscosity levels.

Nonetheless, the evolution of the larger part of the coal in the form of 'primary' tars in this initial stage cannot be attributed to covalent bond disruptions. By virtue of its rapidity and minimal disturbance by chemical decompositions other than weak non covalent secondary bond disruptions it is likely that this is a desorption/vaporisation process. The overlapping of low temperature, highly reactive chemical reactions involving 'O' functional groups and H_2S release from Pyritic decompositions further complicate matters.

Reactions at rising temperature levels and loss of fluidity is probably affected by physical effects stemming from high rates

of heating, creating a more 'excited' and disturbed system. Suspected temperature arrest at temperatures below 500^{o}C (<625^{o}C at higher heating rates; re: Freihaut et al) probably arises from heat effects engendered by phase transitions, coupled with enthalpy of vaporization, melting, sublimation and solution.

At higher temperatures corresponding to resolidification and bulk mesophase formation, very complex series of competing and parallel reactions occur as evidenced by the preceding discussions. An assessment of experimental values of rate parameters interpreted by normal isothermal methods of kinetic analysis or by nonisothermal analysis produces a variety of rate parameters whether applied to total yield or individual volatile yield.

Application of a simplified overall single reaction model to a process that reflects such a diversity of molecular weight products cannot but bias rate parameters towards the heavier products. The complexity of the reactions and changing nature of reactions with temperature and time impedes decomposition of the elementary processes to a dynamic rate mechanism. Therefore, whilst there is an implicit sequentiality in the various processes leading from coal softening to resolidification and ultimately graphitization, it appears that it is unlikely that specific rate parameters can be assigned to specific reactions, particularly at high heating rates.

One way out of the dilemma has been to take refuge in parametric model fits of yield data to such models as the parallel reaction model among others. Here, it is postulated that a series of independant parallal reactions of a wide distribution

of activation energies occur each, commonly assumed to follow first order decomposition. (The latter assumption does not seem to have any particular justification other than possible mathematical tractability and historic custom).

The above picture holds that reactions with sufficiently low E_A values reflect rapid reactions/yield at low temperatures. Those with higher E_A values have minimal rates at these temperatures but increase at higher temperatures to contribute to the volatile yield. The analysis may be cast in a form which account for temperature/time variations and may be recast in a nonisothermal form where heating rate is incorporated as an extra parameter as in the analogous single reaction model. The model may be applied to individual gas yields by again assuming a broad distribution of sources (e.g. functional group and other structural sources) of differing E_A values.

The latter model has four adjustable parameters, namely, an assumed pre-exponential factor, mean activation energy (Eo), the range of an assumed distribution, normally assumed gaussian (usual to assume ±2 standard deviations width on either side of the mean) and an ultimate yield (Vo), dependant on assumptions of maximum possible source material giving rise to the material in question. Parametric least square fit by iteractive methods fit the experimental yield|time, temperature data to initially guessed values of ko, σ, Eo and Vo.

The latter model neatly sidesteps the dilemna of identifying specific elementary reaction steps linked together by a detailed dynamic model identified with a reaction mechanism. However, it's widespread use and popularity reflect it's utility as an engineering

model fit of data from a variety of sources for comparative purposes.

The utility of detailed multiple reaction models are, however, restricted in that sufficient data does not exist which can identify various key steps of the Pyrolysis process which can be unambiguously separated from effects of experimental technique, transport limitations and uncertainty regarding coal structure.

CHAPTER 5

5. Experimental Techniques, coal preparation and implementation of work undertaken

5.1 Overview

Uncertainties concerning aspects of coal Pyrolysis have been hinted at in the preceding review of the literature. Careful study of the literature points to deficiencies in experimental technique as the main source of error as Solomon's latest review appears to conclude.[161] The literature also reveals a somewhat piecemeal approach, in that few studies have attempted to piece together different aspects of the Pyrolysis process.

It has been pointed out by several authors in the field of solid state decomposition (vide infra), that a reaction mechanism can only be postulated by the integration of information obtained by subsidiary experiments. Thus the Berbau Forschung group[29,207] has undertaken over the years visual examination of dynamic coal structural changes under rapid heating in the same apparatus (mesh furnace) as used for product yield determination along with coal structural studies. Entrained flow reactors were also employed as an adjunct to the rapid heating studies.

It is difficult to even assess the validity of extant models without data that can be deconvoluted from the effects of transport processes or secondary reactions. Thus mechanisms postulated are endless with limited applicability to both experimental data let alone industrial demonstration plants. Solomon and Gavalas have postulated mechanisms based purely on

known homogeneous gas phase decomposition reactions relevant to organic compounds. The former has however considered aspects of mass transfer processes based on evaporation limitations.

Recourse to data from fluidized beds, shock tube studies and work by Menster and Freihaut in the mesh reactor clearly indicate the occurrence of secondary reactions at high temperatures. Freihaut's[154] results, conducted in vacuum for fine particles (40-140μm) suggest that tar yields suffer reduction at temperatures greater than 600-700^{o}C in a manner that depends on thermal stability of the tar formed, which is itself reflects parent coal aromaticity. Reference to the data of Tyler et al for fluidized beds suggest a similar dependance.

Uncertainty exists as to the nature of the secondary reactions observed. Other work reviewed by the author along with Tyler's study suggests a mechanism of tar cracking to gas and coke, including soot formation in fluidized beds. In the case of the static bed study, it is likely that polymerization of tars to form coke probably competes with cracking reactions. Studies by Suuberg et al[206] including model simulations by Attar [209] and Lewellyn suggest bubble nucleation, growth and escape along with evaporation supression could aid in both repolymerization and cracking in competition with decomposition reactions.

Attempts to incorporate features of activated decomposition repolymerization and other reactions occurring in sequence, simultaneously and competitively have been attempted by Reidelback and Summerfield and by Antal et al.[14] These models probably represent the key initial steps of coal Pyrolysis modelling before

attempts can be made to include more fundamental reactions pathways suggested by Gavalas and Solomon based on organic decomposition of various functional groups present in coal. Different models require diverse types of data. However, for the purposes of industrial research, definitions of the limits of variables such as particle diameter, transport limits, effects of temperature, and heating rate are adequate as a first step towards design purposes. Such information along with delineation of the Pyrolysis stages such as primary and secondary Pyrolysis ultimate and individual product yield, should help to clarify reaction mechanism options.

In order to measure the progress of a chemical reaction these are two essentially complimentary processes involved. In the first case we may measure some change in the property of the reactant. The methods utilized may be gravimetric, visual for example by some optical technique (light microscopy or SEM) and/or chemical examination of the partially reacted solid (e.g. I.R., N.M.R., etc).

To help identify the progress of individual steps of the reaction we may measure the change in the gases produced in the reaction as a function of reaction variables. The techniques of gas chromatography, infra red spectroscopy or size exclusion chromatography may be utilized among others. As we are interested in delineating as far as possible chemical reactions separate from transport processes, we have to choose conditions that assist elucidation of kinetic parameters based on measurements where the overall rate is controlled by chemical kinetics.

A sufficient temperature range needs to be studied and both external and internal mass transfer effects should be supressed. If one notes that in general, film diffusion coefficients vary as follows:

$D_i \propto$ (diluent gas velocity)$^{\frac{1}{2}}$ and $D_i \propto 1/p^n$, then operation at sufficient diluent gas flows and lower pressures should supress external mass transfer. Supression of internal mass transfer resistance may be effected by providing a short diffusion path for escape of generated products. This may be ensured by choosing a large volume to surface area ratio or small particulate size. The latter process, and to a lesser extent the former process depends on dynamic structural variations, product molecular weight range, heating rate sustained by the particle volume, particulate geometry including packing arrangements of particulate assembly. It is thus that visual, non intrusive techniques such as dynamic high speed photography (for fast reactions) and static scanning electron microscopy or light microscopy come into their own as useful adjuncts to the study of solid state reaction mechanisms.

The fundamental parameters controlling the reaction environment are temperature, pressure and time. Thus, for studies in the fast Pyrolysis regime, reproductibility entails careful control of these parameters by suitable instrumentation and experimental technique. In rapid Pyrolysis studies the effects of heating rate decoupled from peak temperature needs to be assessed to elucidate its effects on the reaction parameters. The following criteria therefore must be met, namely,

1) Small sample and particle size

2) Rapid temperature rise to peak value without overshoots of temperature

3) Accurate control over Pyrolysis period.

4) Sufficient heat flux to sustain desired heating rate.

Based on the above criteria, few experimental techniques can satisfy this as well as the electronically heated mesh technique originally developed by Loison et al.[157] Thus this versatile technique was employed, being refined from previous work conducted in the department[14-15] using a similar technique. Single particle studies were conducted by G R Johnson on a tungsten wire loop which provided much useful information (ref: 14). However, the heat transfer and geometry situation were different from the associated mesh studies.

In an industrial process, particles are subject to heat fluxes dependant on reactor gas stream and/or wall temperatures at invariably high temperatures (>600^{o}C). Uncontrolled heating rates, exponential temperature variations and residence time variations of both Pyrolysing solid phase and vapour phase may occur. Further, the transport processes are more complex and scope for secondary reactions are enhanced.

In terms of design, simplicity of operation and versatility the fluidised bed is a convenient reactor for Pyrolysis studies and has been mooted as a likely candidate for rapid Pyrolysis and gasification processes. Studies by Tyler et al in Australia and spouted bed studies in Canada suggest that scale up from

laboratory scale reactors to at least pilot plant sizes are reproducible in terms of yield and product distribution noted. Reference to the studies mentioned highlight some anamolies in elemental compositional changes between spouted bed and the fluidized bed work. Also, comparison of yields from a Pittsburgh coal, heated in a mesh at long residence times showed significant differences to that obtained in the fluidized bed work of Tyler[125] et al. The fluidized bed work reported by both Tyler and Essenhigh[72] show very high yields at low Pyrolysis temperatures compared to mesh reactors. (Comparison to entrained flow reactors is not possible owing to the dearth of data at temperatures below 600^{o}C. However, the improved entrained flow studies, taking into account heat transfer considerations indicate Pyrolysis times of tens of milliseconds at these temperatures).

Further, Tyler's work highlights very high yields of CH_4, linearly increasing with temperature up to 900^{o}C, the ultimate temperature of operation. This is in contradiction to most other studies. Clearly, these are intriguing features which need to be explored. Moreover, the fluidized bed study offered scope for larger yield of products which can give a better idea of yield variations with temperature. Yield size also enables subsidiary studies of tar (by elemental analysis/I.R. spectroscopy etc) and it's secondary reactions. Thus the fluidized bed was also utilised in the present study as a complement to the mesh study.

5.2 Selection of parameters of study

Consideration of the literature of experimental work and theoretical simulations of transport processes[206-213] suggested that, for single particles, coal type, heating rate, particle diameter, external pressure and peak temperature of particle interact in a complex way. The manner of the interactions may be such that transitions may occur between transport control and chemical control dependant on the relative magnitudes of the quoted parameters. Reference to Simons[32] highlights differences between softening coal and non softening coal noted by others which lead to differing mechanisms of transport processes that reflect on the relative magnitudes of the devolatalization rates compared to the 'intrinsic' Pyrolysis rate. He concludes, in essence that the maximum pressure generated within the particle as a consequence of volatile generation suggested the following relationship:

$$P_{max} \propto \frac{1}{k} \text{ and } \frac{1}{T} \text{ as } k \propto T$$

$$P_{max} \propto dp \; ; \quad k = \text{rate constant } (S^{-1})$$

For non softening coals, able to sustain high internal pressures, the fluid transport increases and transition to intrinsic Pyrolysis rate control may be attained. As softening coals cannot sustain high internal pressures, the reverse is likely to be true requiring very small particle size and also low pressures to avoid secondary reactions arising from supression of volatile evolution. Therefore, to observe Pyrolysis chemistry it appears advisable to choose weakly caking coals.

But other studies suggest that the limiting parameters are dictated equally by the transport mechanism assumed. Further, the diffusion coefficients of multicomponent products existing in a multiphase system depend on the molecular structure and phase of the species.

Consideration of the relevant time scales provide 'ball Park' figures for the heating rates sustainable by a particular size of particle. Comparison of the following time scales provide some indication:

1) External heating time scale dependant on heating mechanism and temperature of heat source.

$\frac{dp \times (spCp)}{hc \text{ (or } hr)}$ spCp = Volumetric heat capacity

hc/hr= Convective or radiative heat transfer coefficient

2) Internal heating time scale = $\frac{dp^2}{\alpha p}$; αp = Thermal diffusivity

3) Volatile Diffusion time scale = $\frac{dp^2}{D_i}$

D_i = effective diffusion coefficient of component i

D_i = f (molecular size, pore structure, coal viscosity and pressure).

4) Heating rate time scale:

i.e. t = Peak Temperature/dT/dt

5) Intrinsic Pyrolysis rate time scale = $^1/_k$

k = rate constant (S^{-1})

$k = ko\ A \exp(-E/RT)$

For observation of intrinsic Pyrolysis rate, equilibration of process (1) - (4) must be faster than (5).

As the physical parameters required vary by many magnitudes in the literature it is difficult to assess the above. But reference to experimental studies and transport model calculations combined with the above considerations allow some measure of choice. Reference to German work[207,218] indicates that for heating rates of 8-9000K/S, 75-150 μm represents the range of critical particle diameter. Gavalas suggests a critical particle diameter dependant on final temperature attained (80 μm for 827°C, dependant on assumed heat transfer coefficient and rate constant value). Anthony and Howard suggest larger values than the above for higher heating rates.

Overall, the choice of heating rate, particle diameters, coal type and pressure of operation was arrived at by a combination of the above considerations, availability of relevant apparatus (mesh sizes) and acquisition of well characterised coal from known sources.

Thus most of the work was carried out on low swelling, weakly caking coals of particle size 75-90 μm, namely Markham Main and Goldthorpe. The maximum sustainable heating rate was estimated to be <6000°C/S. Studies were conducted mainly at 1000°C/S. and 5000°C/S with some at 10°C/S and 200°C/S at both atmospheric and low vacuum conditions (0.5-5 torr) in the mesh reactor. Studies were conducted by measurement of ultimate yields and some tar yields under flowing gas conditions for atmospheric pressure tests.

Gas yields and ultimate yields were obtained under vacuum conditions and static diluent gas conditions in the mesh reactor. The diluent gas utilised were Argon and Helium. The effect of ultimate yield for variations of packing density, packing geometry

and particle size were also conducted initially to study side-effects such as transport limitations and secondary reaction processes.

Subsidiary experiments were performed such as dynamic high speed photography, static photography, SEM studies of chars and calibrations of temperature of mesh by melting point standard metals.

Elemental changes of tar and in some cases char, molecular weight distributions of tar and Fourier transform infrared spectra from both fluidised bed and mesh furnace were collated.

5.3 Coal selection, preparation and storage

Coal samples were obtained from two sources. The Midland Research station of British Gas PLC provided well characterized Markham Main coal samples of particle size 150-250 microns. Variations of particle size experiments were conducted on this coal originating from the Barnsley Seam. A range of other coals of varying coal ranks were obtained by the author from British Coal, courtesy of Dr A. H. V. Smith. These coals were obtained by coal geologists from freshly cut and lumps representative of the dull and bright componentns of the coal face. The samples were placed in N_2 filled plastic bags which were then sealed in tin buckets by means of soldering of the lid tops. Goldthorpe coal of rank 800 from the Shafton colliery was used along with Markham Main for the study. Both coals were low rank, high volatile Bituminous coals of low caking propensity (B.S. swelling number, 1-1½ for both coals).

Study of the literature (refs 55, 56, 219 and others) and advice from British Coal Scientists at Wath upon Dearne provided information on a final choice of grinding procedure including petrography techniques. Initial tests on a vibrating ball mill produced excessive fines production and lengthy grinding times for size reduction.

To reduce maceral differentiation between particle sizes and enrichment of finer particles by mineral matter accumulation, including the softer fusain components, careful procedures were adopted for particle characterization. To avoid 'O' pickup during coal particle reduction, crushing and grinding were conducted in a large sealed plastic bag in an atmosphere of flowing 'O' free N_2. The procedure adopted after extensive trials were as follows.

Initial size reduction to <2 cm sizes were conducted in an adapted screw feed meat grinder. Final size reduction was conducted in an electric moulinex coffee grinder. Tests on grinding times indicated that grinding for periods greater than 80 seconds produced excessive fines and agglomeration. Starting from a crushed top size of 1.8-2.1 cm, grinding for short bursts of 5-7 seconds produced a large fraction accumulating in the 150-212 μm sizes corresponding to the top size of the Markham Main sample obtained from British Gas. The total sample was then riffled using a riffler (sampling and preparation procedure followed recommended practice in B.S.1017 part 1 and other literature advice).

The procedure adopted for size reduction of the top size fractions 150-212 μm was the same for both Markham Main and

Goldthorpe coals thereafter. An optimum period of 20-30's was found for accumulation of desired particle size range 75-90 μm without excessive fines production. To avoid particle blockage of the test sieves, an optimum time of seven minutes sieving coupled to frequent gentle brushing of sieve/particle surfaces was found to be suitable.

Required sieve fractions were obtained for 90-125 and 150-212 μm fractions of the Markham Main coal along with the 75-90 μm fraction. The latter narrow size range of fine size was utilized for the majority of the study reported. It was found necessary to elutriate the coal particles in a small N_2 fluidized bed to remove fines adhering to the particle surfaces. Optimum times for this was found by bubbling the fines through H_2O and filter holders in sequence. The particles examined under light microscopy indicated clean, well separated particles with almost no adhering fines. Most of the particles were blocky cuboids with rounded surfaces in the main.

Coal particles were stored under N_2 gas in plastic containers and placed in a cool place. Some samples were stored under distilled H_2O. These latter samples were, in initial tests loaded as a wet slurry on to the mesh surfaces which were then dried under vacuum at $105^{o}C$ overnight in a vacuum oven. This was done as part of a progressive series of tests to determine the optimum packing configuration in the mesh reactors that optimised heat transfer to the packed particles. The early work of Loison and Chauvin utilised such a method of packing. Studying early German and B.C.U.R.A. work suggests diffculties with dry packing loads that reflect attempts to utilise a sufficiently representative

sample size which overcomes inhomegenities between different sample fractions. These features of sample loading will be discussed in subsequent sections.

5.4 Mesh furnace design configurations

The basic concept of the mesh reactor in analogy to the domestic light filament is a simple one in theory. On initial application of electrical power to the cold filament there is little resistance to the flow of current and temperature rises rapidly. However, as temperature rises, the changing mesh resistance and increased heat losses causes a slowing of the rate of temperature rise.

The rate of equilibration to the peak temperature and its linearity depends in a complex manner on the ratio of heat input to heat losses. For a large ratio of heat input to heat losses, temperature rise is both rapid and linear over a major part of the initial period.

To maintain heating rates independant of final temperature requires two stage power application as shown by fig 29 (from ref 19). The magnitude of power demanded depends on the mesh mass, specific heat, electrical resistivity, gas atmosphere surrounding the mesh, external pressure, peak temperature required, coal loaded on to the mesh surfaces and the rate of cooling by radiation, convection (to gas) and conduction down the relatively massive electrodes holding the mesh. Reference to figures 30-32 should illustrate the basic features of the system.

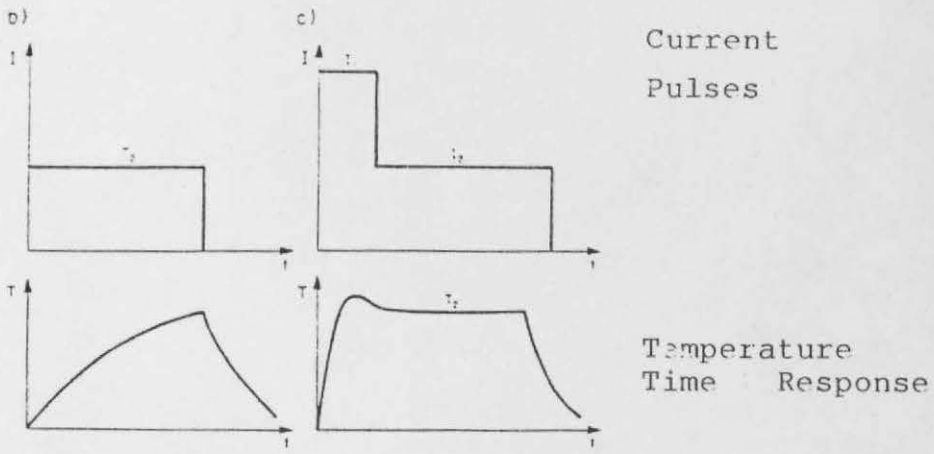

Fig 29 The captive sample technique: (a) pyrolysis apparatus (b) single-pulse T-t response (c) double-pulse T-t response.

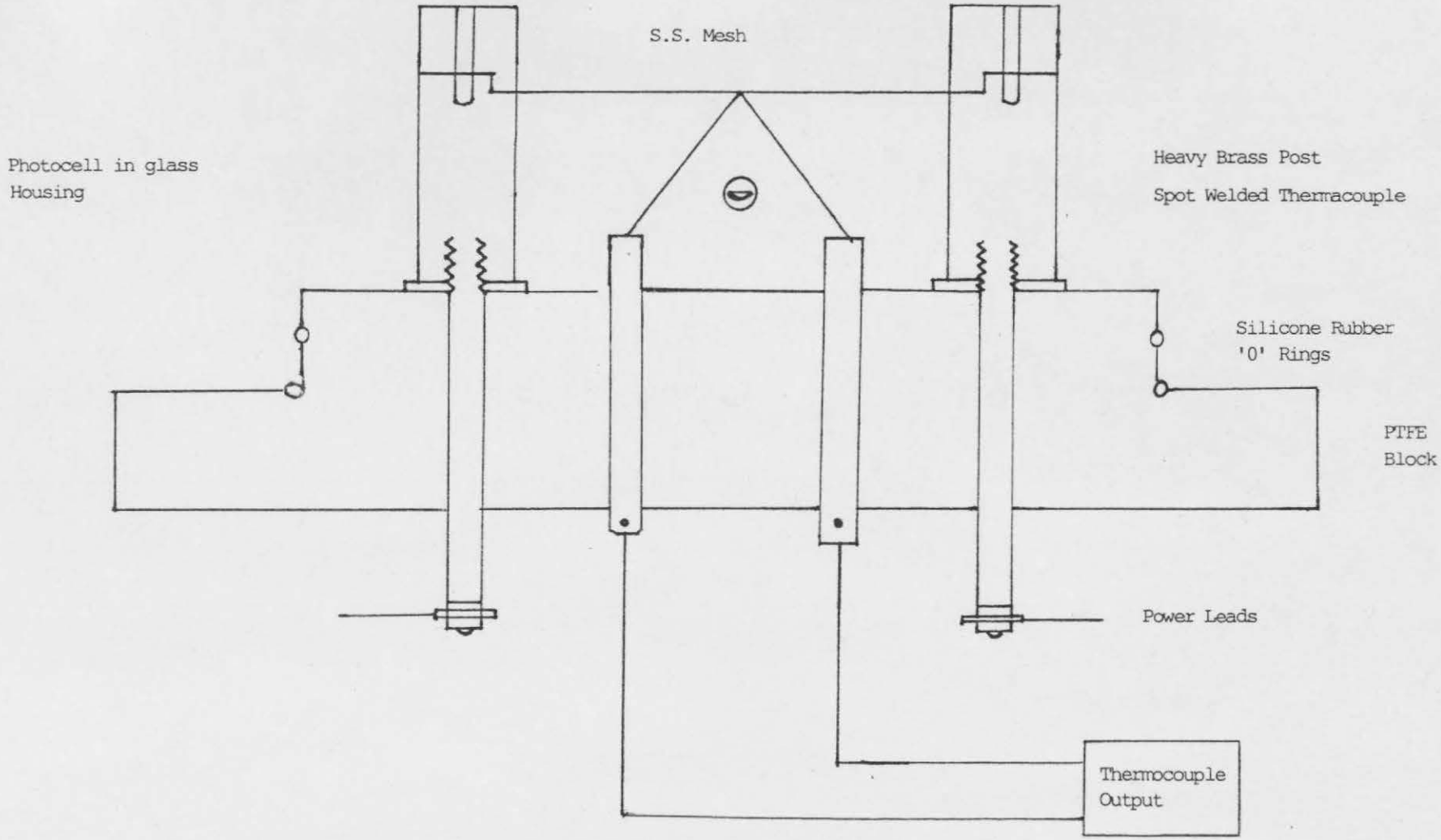

Fig. 30 Mesh Strip Furnace Detail

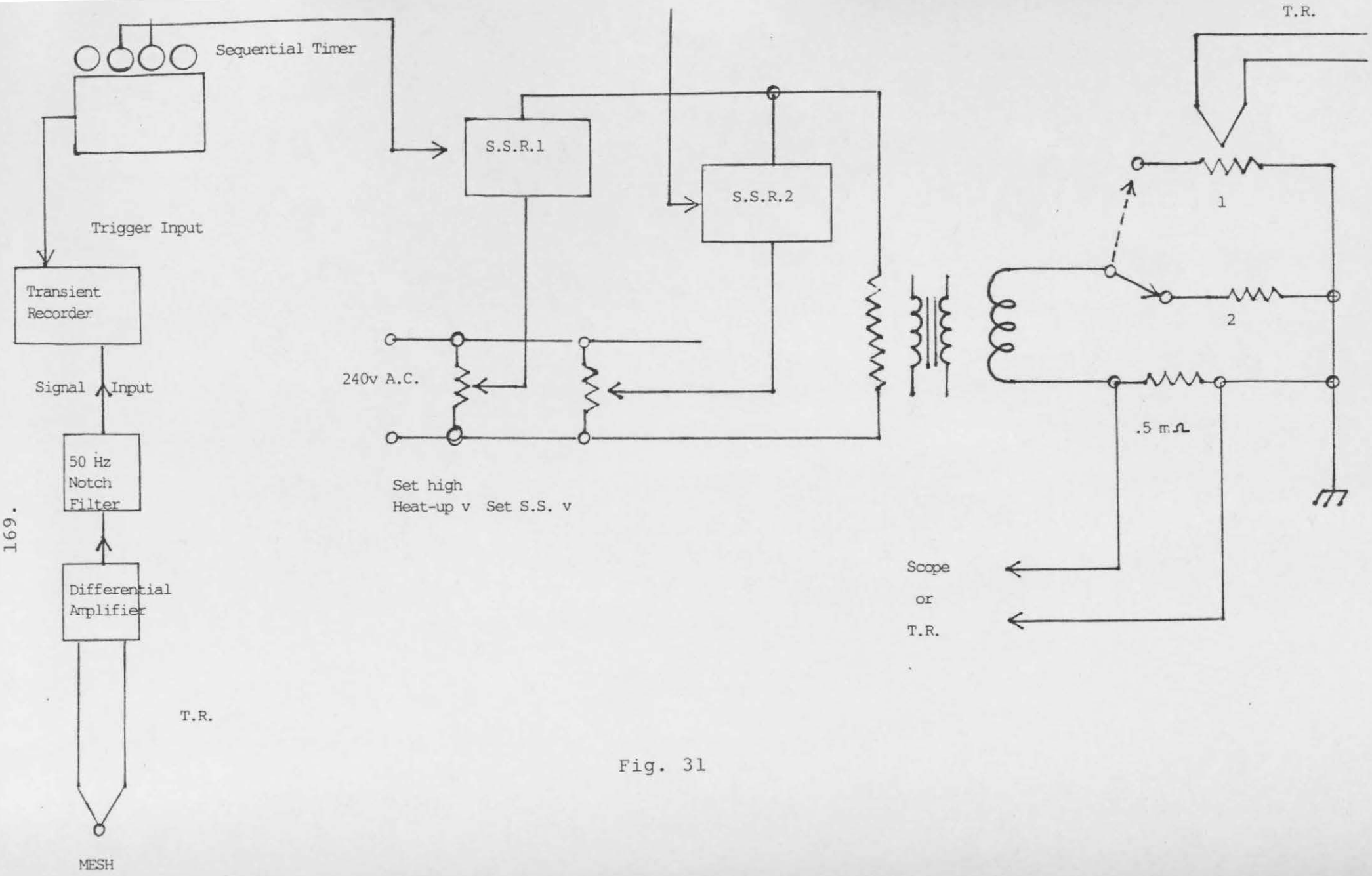
Sequential Timer
S.S.R.1
S.S.R.2
Trigger Input
Transient Recorder
Signal Input
240v A.C.
50 Hz Notch Filter
Differential Amplifier
T.R.
MESH
Set high Heat-up v
Set S.S. v
T.R.
1
2
.5 mΩ
Scope or T.R.

Fig. 31

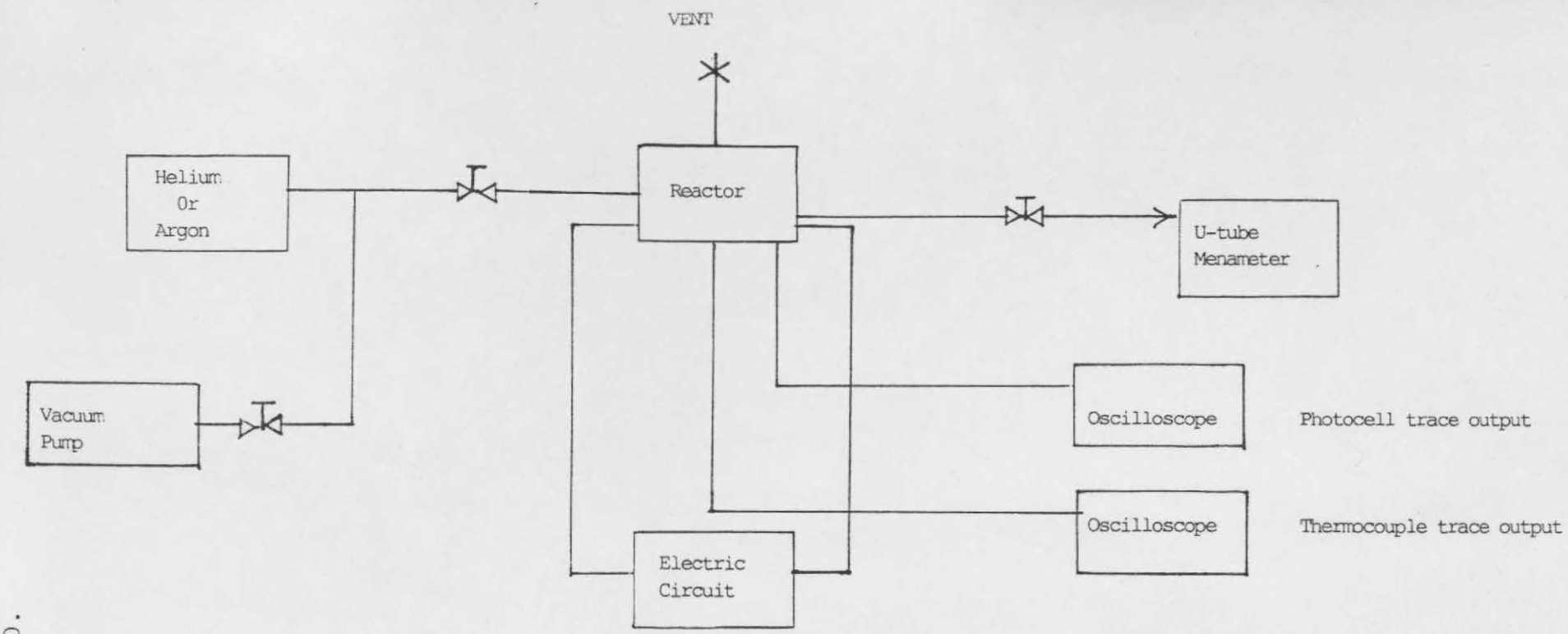

1). Digital Thermocouple Output
2). Ramp Heating Rate Settings
3). Final Temperature Settings

Fig. Pyrolysis Experimental Equipment

Fig. 32

Reference to the literature[46,215-217,158] will show a variety of mesh reactor designs which result in a variety of temperature time responses. Some such as Hamilton, Niksa and Freihaut used programmable power systems to achieve the desired temperature/time programs. However, those that do not possess some form of servo system of feedback control cannot reproduce linear temperature rises at the lower heating rates (<1000^{o}C/S, dependant on mesh configuration and power supply).

The importance of ensuring linear heating of the coal particulate/mesh system stems from considerations of the kinetics of the reaction processes. Consider a chemical decomposition as follows:

$aC \dashrightarrow$ products

For a first order process,

$$\text{rate of reaction} = r = -\frac{1}{a}.\frac{d}{dt}[C] = k_a(T)[C] \quad (1)$$

defining, $k(T) \equiv a.k_a(T)$

$$R = -\frac{d[C]}{dt} = k(T)[C] \quad (2)$$

and noting $k(T) = A \exp(-E_A/RT)$

$$-\frac{d[C]}{[C]} = A \exp(-E_A|RT) \quad (3)$$

$$\text{i.e. } \ln\frac{[C]o}{[C]} = \int_o^t A \exp(-E|RT)\, dt \quad (4)$$

For an isothermal experiment the above yields the relation

$C(t) = Co\,[1-\exp[-t\ A \exp(-E|RT)]$

In the above case, [Co] = maximum initial concentration of reactant which decomposes. In the case of coal this is replaced by a commonly used fractional decomposition parameter which is usually measured by gravimetric means (e.g. weight loss).

Thus F = fraction of undercomposed coal

$$= 1 - \frac{V}{Vo} = 1 - \frac{\text{mass loss at time (t)}}{\text{Ultimate mass loss}}$$

Thus F varies from 1 $\longrightarrow$ 0 as the coal decomposition proceeds (f (T/time)).

Eqn (4) is recast as follows by the preceding definition:

$$-\ln \frac{(Vo-V)}{(Vo)} = \int_o^t A \exp(-E_A/RT) \quad (4a)$$

In a non-isothermal experiment where temperature rises as some function of time, the R.H.S. of Eqn (4a) cannot be analytically integrated, unless the relationship is hyperbolic.[214] However, a linear variation in T/t is both simple to implement in a heating circuit and also minimises any differences in reaction rate existing between the beginning and end of the reaction with respect to isothermal experiments.

Thus for an imposed heating rate, $\frac{dT}{dt} = m$

$$-\ln \frac{(Vo-V)}{(Vo)} = \frac{A}{m} \int_{To}^{T} \exp(-E_A/RT) \quad (5)$$

Reference to the literature will provide numerous approximations for the integration of the R.H.S. of Eqn (5). One such approximation used for the single overall reaction model study will be used later. For the present, the above analysis highlights the requirement for linearity of imposed heating ramp in the mesh reactor.

5.4.1 Initial mesh configuration

Extensive development was conducted stage by stage on all aspects of the electrically heated mesh. This included investigations of mesh loading, temperature programme, lags in measured

temperature and power programming. Initial tests revealed the operating ranges of heating rates and mesh weights sustainable by the power delivered from a 12V transformer operating off a 50 Hz mains supply at 240V. The transformer was capable of delivering 70A at steady state conditions, but could sustain much higher heating currents at the very early stages of power application to the cold mesh. Thus, high heating rates were possible at largely linear profile by presetting voltages and durations of power supply in the 2 heating pulse periods.

Tests of power delivered under constant current conditions (by variation of a series resistance) and under constant voltage conditions (preset by variac control) indicated that the latter was desirable from the viewpoint of stability and predictability. Constant current operation resulted in instabilities reflected by overshoots and undershoots of temperature in the temperature/time profile. These deviations in temperature and lags in thermocouple readings of the mesh temperature were detected by a Silicon photocell. The operating range of the photocell with minor amplification of output signal was possible from 450^{o}C-<1200^{o}C. Larger amplification of the signal and operation under conditions of low external light extended the bottom range to 400^{o}C. However, this was achieved at the cost of unstable signal output. The photocell suffered saturation in its output at temperatures greater than 800^{o}C and thus its most useful range was limited to 450-800^{o}C. The photocell being hardy, of small size (~ 5mm diameter including housing) and of very fast response was found to be extremely useful in the developmental design of the system including improvements in experimental technique.

The initial electrical aspects of the system is depicted in figure 31 . By operating under A.C. heating conditions, it was possible to obtain accurate metering of the period of power supply to the mesh system by means of the zero crossing solid state thyristor switches. Thus overshoots and undershoots in temperature were avoided. (Comparison with stored profiles of the photocell output to the latter traces also aided in the detection of temperature time deviations). Time resolution was limited to 10ms intervals. Time control of the processes of power delivery, including triggering of the digital transient recorder (digital storage of fast rising Temp/time signal) was under the control of a preset pulse sequence delay generator. The latter could be preset for simultaneous or sequential operation with a time control over events ranging from microseconds to 999 seconds. It was used also in high speed photography studies for controlling the simultaneous operation of a cine camera along with power delivery to the mesh system.

Tests with side insertion of thermocouple wires to the mesh of various wire diameters indicated that 50 μm diameter Chromel-Alumel were the most suitable from the viewpoint of physical handling and ability to follow profiles up to 5000^{o}C/S. But tests with the photocell showed up lags which were found to vary with heating rate and peak temperature reached (see figure 33). These experimentally estimated lags are in agreement with lags estimated by P. Arendt of the Berbau group (refer P Arendt thesis) and the variation of heating lags with peak temperature agrees with a similar study of electrically heated sections. (ref: Green S. J. and Hunt, T. W., "Accuracy and response of thermocouples for surface and fluid temperature measurements"; source of

Fig:33 Thermocouple lags estimated by photocell.
Argon atmosphere

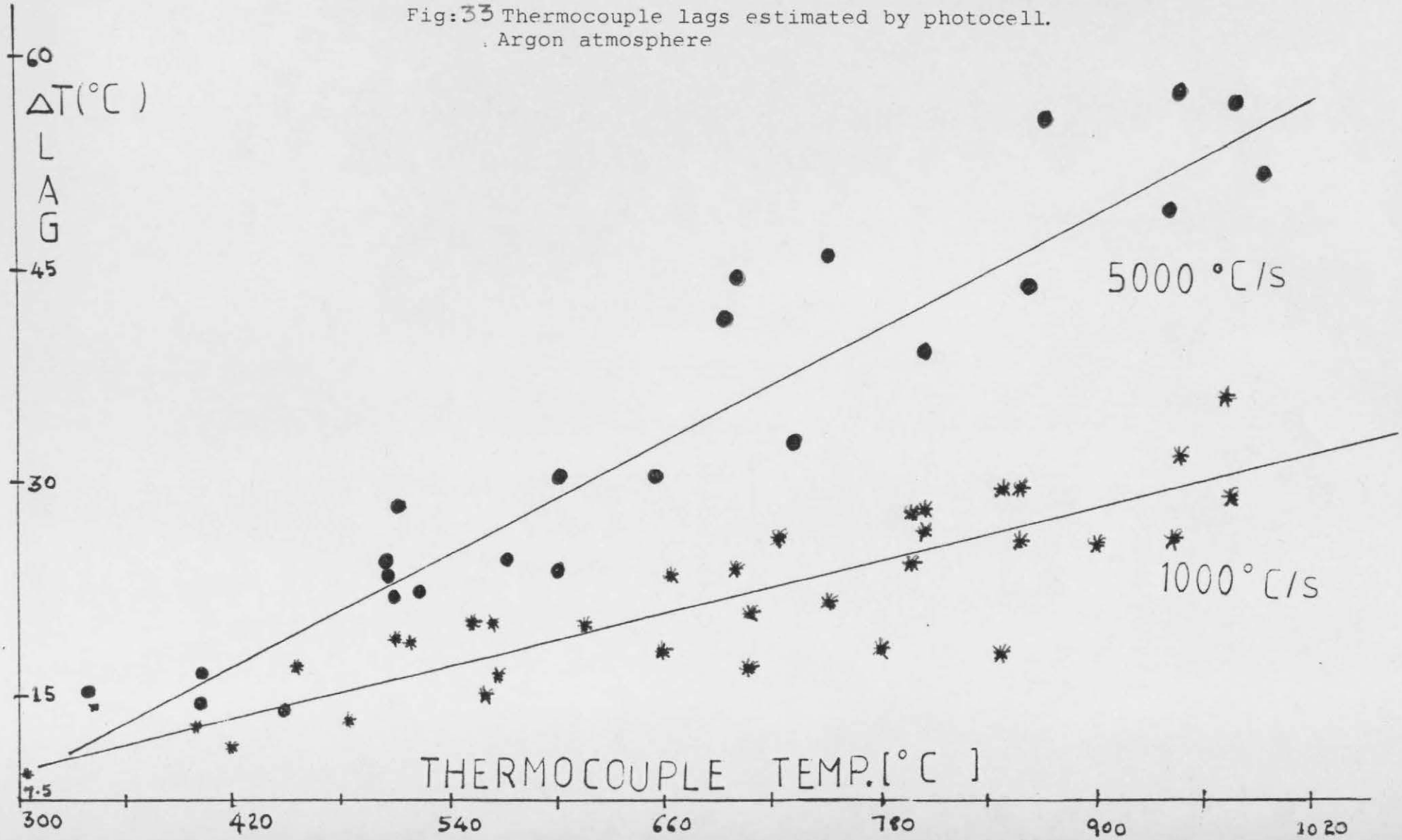

reference not available). The latter is a result of increased radiation losses at the higher temperatures.

Whilst many useful experiments and information was obtained from this design of the mesh system, non linerarities of heating profile at the lower heating rates and suspected inaccuracies of temperature profiles at the lower temperatures (<400^{o}C) and the higher temperatures (>800^{o}C) led to the design of an improved system. By comparison of the linearised output of the mesh electrical resistance variation with temperature and photocell and thermocouple outputs a feedback control system of power delivery was implemented. The system was designed by R. Holt of the Houldsworth School to whom the author is indebted for its final conception. In the former system adjustments to the power settings (voltages) had to be made following coal loading to the mesh based on rough calculations and previous experience. Thus the temperature/time profile could depart occasionally from pre-set values based on the unloaded mesh. In the new system, the feedback capability allowed automatic matching of the power demanded by the extra load to the desired heating ramp profile stored electronically.

The former electrical system was also employed for early studies of single coal particles using graphite rods as both particle holder and heat source. These early studies provided visual and photographic information of a different kind from the mesh photomicrographic studies which was developed by the author for studying the physical kinetic aspects of coal Pyrolysis.

5.4.2 Stage 2 mesh configuration

The major components of the final system consisted of power control by phase angle power metering, triac power switching coupled to a zero crossing detecting circuit (prevents instabilities due to high frequency rf. Noise generated by switching of large currents), an apto isolator switch (isolates activiting circuit from solid state triac switch), sensing elements, reference heating profiles and comparator circuits. (Refer fig. 34)

Essentially phase angle power control allows the thyristor power switch to be activated at a specific point in each half cycle of the A. C. waveform, of a magnitude determined by the power demands of the heating cycle (Refer fig 35 which shows the heating voltage waveforms for 5000^{o}C/S heating rate to a steady state temperature of 300^{o}C).

Using either thermocouple or mesh resistance or photocell response as sensor, the output of the sensor is compared to the output of the electronically generated temperature programmer and any difference, amplified by a differential amplifier. The amplified difference or error signal is applied to the phase angle power control in proportion to the error signal such that, the earlier in the mains half cycle the thyristors are switched on, the greater the average power supplied to the mesh during the half cycle (refer fig 35).

The mechanism of the above power metering is achieved as follows. At every zero crossing voltage of the A.C. supply, a zero crossing detector produces a pulse which is used to reset the output voltage of a 100Hz ramp generator. (The temperature

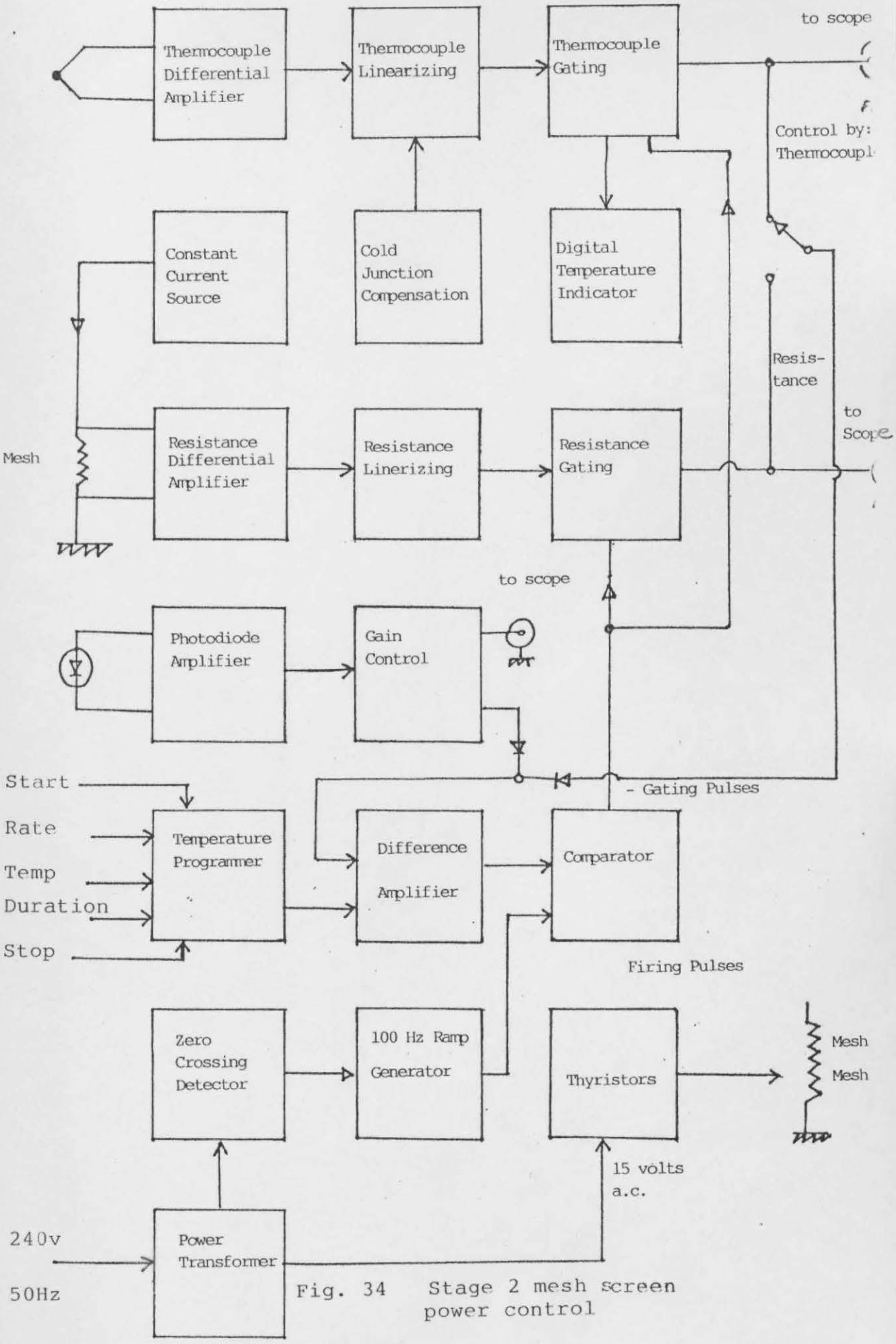

Fig. 34 Stage 2 mesh screen power control

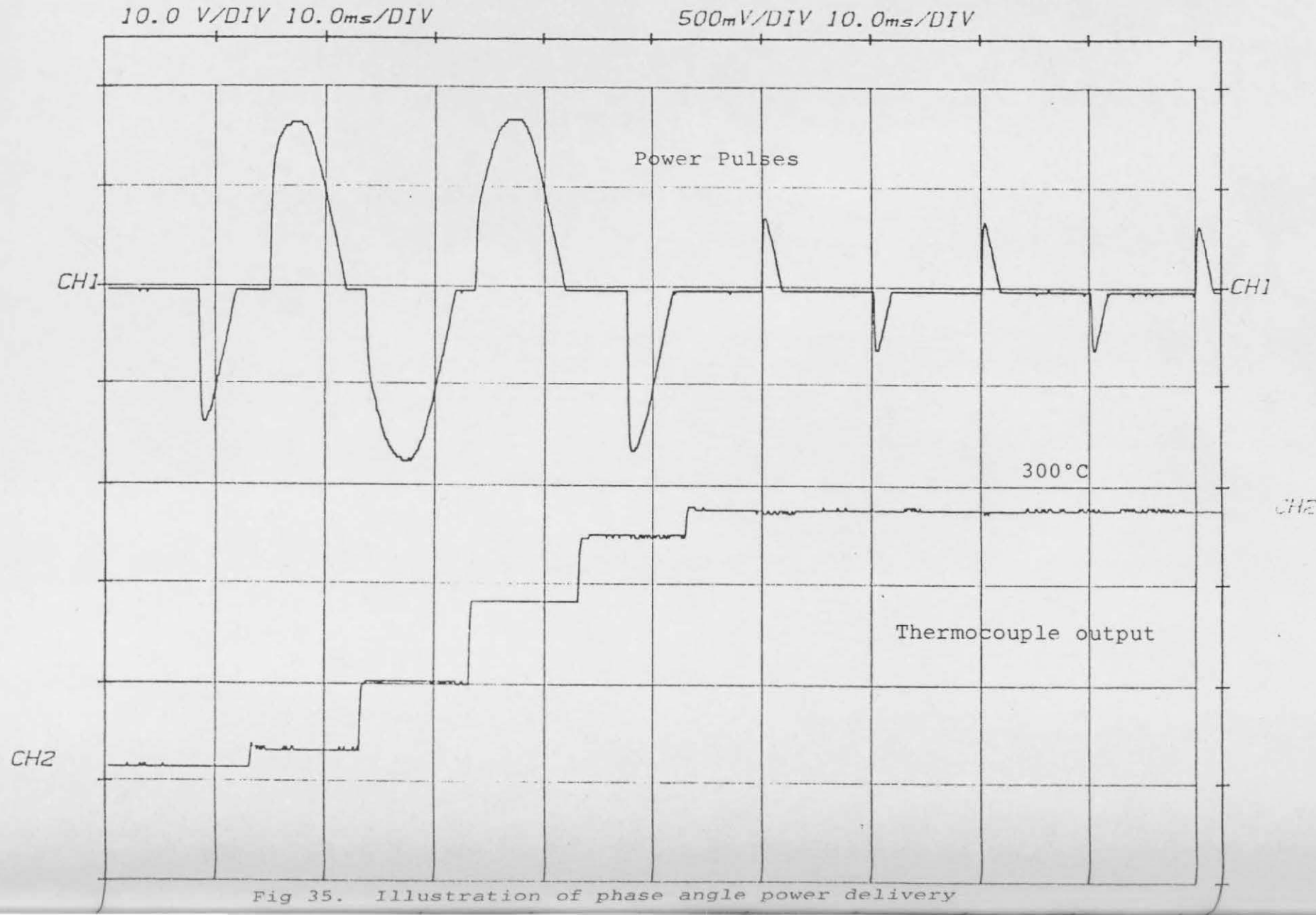

Fig 35. Illustration of phase angle power delivery

programmer was set to produce a control voltage for the heating circuit with 5V being equivalent to 1000^{o}C. On starting the heating program, following a preset delay of 2s the electronically generated ramp starts rising to reach a steady peak voltage value corresponding to the steady state temperature chosen. The period of the steady state temperature is preset by a calibrated 10 turn dial (0-100 seconds, in 20 ms time resolution period). At the end of the preset period, the output voltage falls to zero and the programmer is reset for the next sequence). The output of the generator then falls to zero volts linearly in 10 ms (for mains frequency of 50 Hz). At this time another pulse arrives from the zero crossing detector to reset the ramp generator. A comparator circuit compares the error signal from a difference amplifier with the instantaneous ramp voltage. Thus, when the ramp voltage falls below the error signal level, the output of the comparator produces a negative signal, which switches on the opto-coupled triac switch. The output terminals of the triac are connected to the power thyristor gates and one of these is triggered on. The arrangement of the circuit precludes firing of the power thyristor switches earlier than 2ms after the zero crossing. This provides sufficient time for temperature measurements by any one of the sensors mentioned. Thus temperature measurements are made undisturbed by the heating currents flowing in the mesh. The sensor amplifier is enabled by a pulse from the comparator for the measurements to take place.

5.4.2.1 Temperature sensing elements

(a) The thermocouple which is spot welded to the mesh was used for feedback control of the circuit at heating rates <1000°C/S. Earlier work (vide infra) had indicated significant temperature lags at the higher heating rates by comparison of the output profiles of the photocell to steady state temperature and transient pulse profiles of the thermocouple output.

A series of heating pulse tests on thermocouples of different wire diameters suggested that the response time of the thermocouple was a complex function of bead diameter, imposed heating rate, film heat transfer coefficient and thermal properties of the gas surrounding the thermocouple. Where there was intermittent contact between surface and bead as may occur following mesh movements during heating or under vacuum conditions, significant errors were detected (Refer to a comprehensive analysis by Niksa, ref: 216 and his thesis for vacuum effects).

These early studies were confirmed by calculations and comparison of profiles generated by the new feedback system controlled by resistance output sensing or by photocell output control, both of which are near instantaneous in their response. Calculations of time constants for imposed heating rate of 1000°C/S in an argon atmosphere for various bead diameters resulted in estimated temperature lags of 29°C for 50 μm bead size, 75°C for 100 μm bead size and 45°C for 75 μm bead size.

Spot welding of the thermocouple improved on these figures but for the 50 μm wire diameter thermocouple, lags were still apparent, which is a reflection of heat losses down the bare wires

during heating and the complex geometry of the mesh/thermocouple system. A calculation was done of steady state error under conditions of natural convection for wire diameter, 50 μm. An error of ± 11.5°C was found for a peak temperature of 1000°C.

Experiments were conducted on Analar grade metals of Sb, Tin and Pb (using a cine camera) at the supposed melting points of these metals at particle sizes of 75-90 μm loaded onto the mesh and subjected to transient heating and steady state temperature profiles. The errors at steady state were found to be as follows:

Tin, (mp = 231.9°C) steady state error ± 1.2°C

Pb, (mp = 327.3°C) steady state error ± 4.2°C

Sb, (mp = 630.5°C) steady state error ± 6.7°C

These values suggest a steady state error dependant on the temperature driving force difference which appears to be in accord with the value calculated for 1000°C, peak temperature (± 11.5°C).

Transient lags estimated by the melting point method were more variable than those estimated by recourse to photocell comparisons. The following results were obtained:

dT/dt°C/S	T peak°C	lag (°C)	Gas
1019	630°C	25.5 ±12°C	Argon
1031	630°C	40.5 ±13.8°C	"
980	630°C	33 ±13°C	"

Clearly the thermocouple control circuit could not be used for heating rates >900°C/S. However, it is reliable at lower heating rates. The thermocouple signals were amplified by a

differential amplifier. A linearizing network of diodes and resistors were used to produce a linear output with respect to the temperature range spanned. Cold temperature compensation was provided by a sensor adjacent to the thermocouple terminals. Measurement of temperature was conducted by means of a gating circuit driven by pulses which coincide with the thyristor firing pulses which disables the thermocouple amplifier during the period of application of heating current to the mesh. The thermocouple output drives a digital temperature display. The temperature profile may be displayed on a suitable display device.

(b) Resistance temperature measurement

By passing a stabilised current of 0.5A through the mesh dynamic resistance measurements of the mesh may be made. The voltage across the terminal posts was amplified by a differential amplifier. The amplified signal was linearized by a network of diodes and resistors and a control dial on the front panel of the equipment allows the signal level to be adjusted to agree with the thermocouple signal. This was found to be necessary owing to the variable resistances of different meshes. Measurements were conducted by applying the gating technique as described before. Like the thermocouple output voltage signal, the output may be used to control temperature level of the mesh.

Measurements of contact resistances dissipated at the point of connection to the brass electrode posts indicated $<\pm 0.5\%$ of the total resistance. Thus the average mesh temperature measured by this method was reasonable and available over the full temperature range employed for the study.

(c) Silicon photocell control

As there was no electrical connection between the mesh and the photocell sensor, gating of the output signal was not necessary for measurement and control. It's use was restricted to temperatures >450^{o}C and may be used in conjunction with thermocouple control by adjusting the gain of the photocell amplifier to match the latter's output to the output voltage of the thermocouple amplifier at a set point. By employing an arrangement of precision rectifier circuits the photocell could then take control of the mesh heating current at any time when the photocell amplifier output was greater that of the thermocouple amplifier output, (at higher temperatures the photocell output is large relative to the thermocouple output). It was thus possible to supress overshoots of mesh temperature even at high heating rates using the thermocouple as master for the early part of the heating cycle when the photocell output is relatively low. (Refer to figs 36 & 37 for illustration of sensor output profiles).

5.5 Photomicrography studies

A technique was developed for studying the dynamic transformations of single and multiple particle assemblies within the mesh folds, on it's surface or of particles held within the mesh holes. A Bolex Electric cine camera with a speed of 50 frames per second was used to obtain 16mm cine films. Exposure times were dictated by rotation speed of the prism at the camera position behind the camera lens. Tests were conducted on a digital watch of 1ms time resolution and a conservative estimate of steady state time resolution per frame was found to be 19.24ms

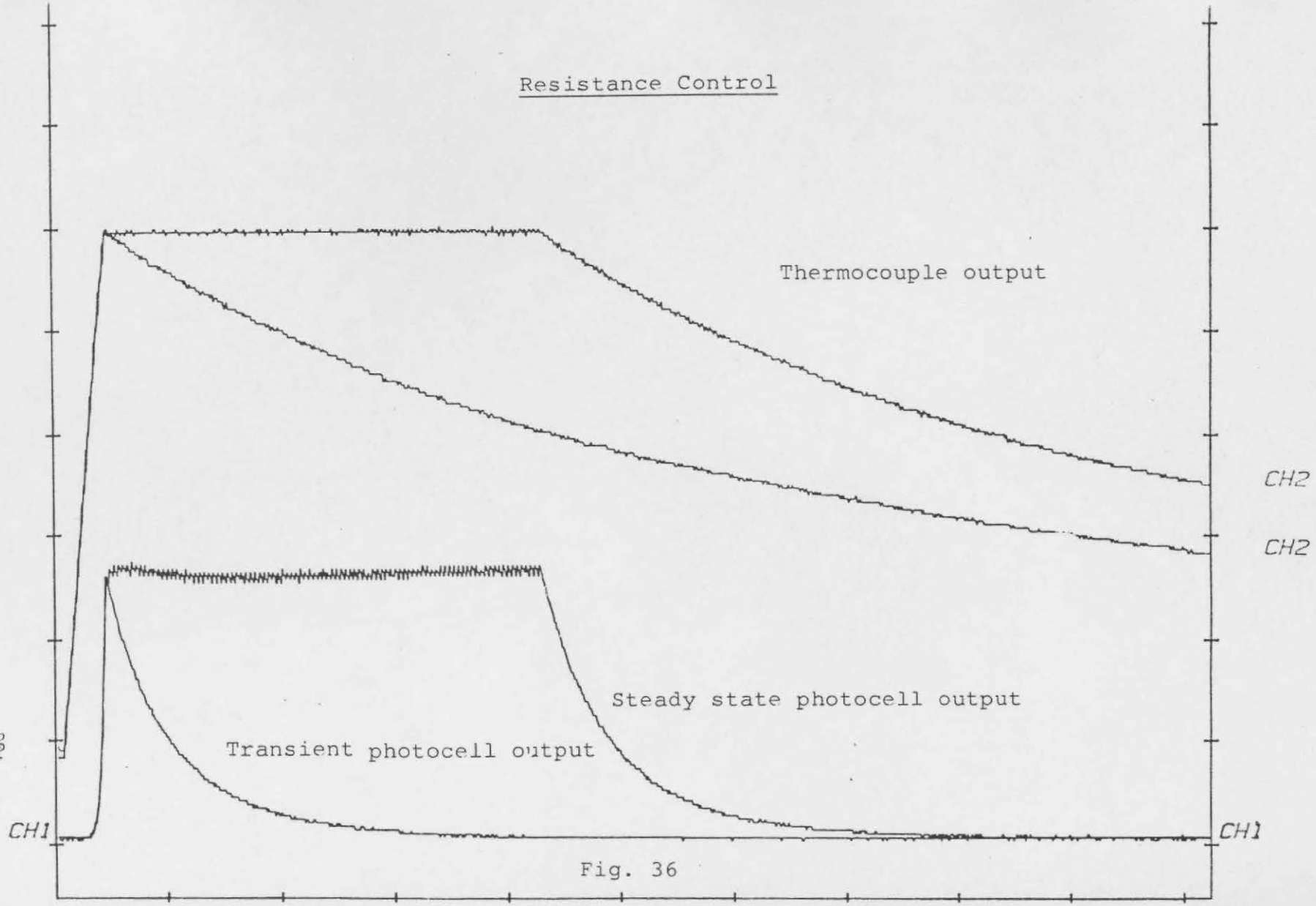
Resistance Control
Thermocouple output
CH2
CH2
Steady state photocell output
Transient photocell output
CH2
CH1
CH1

Fig. 36

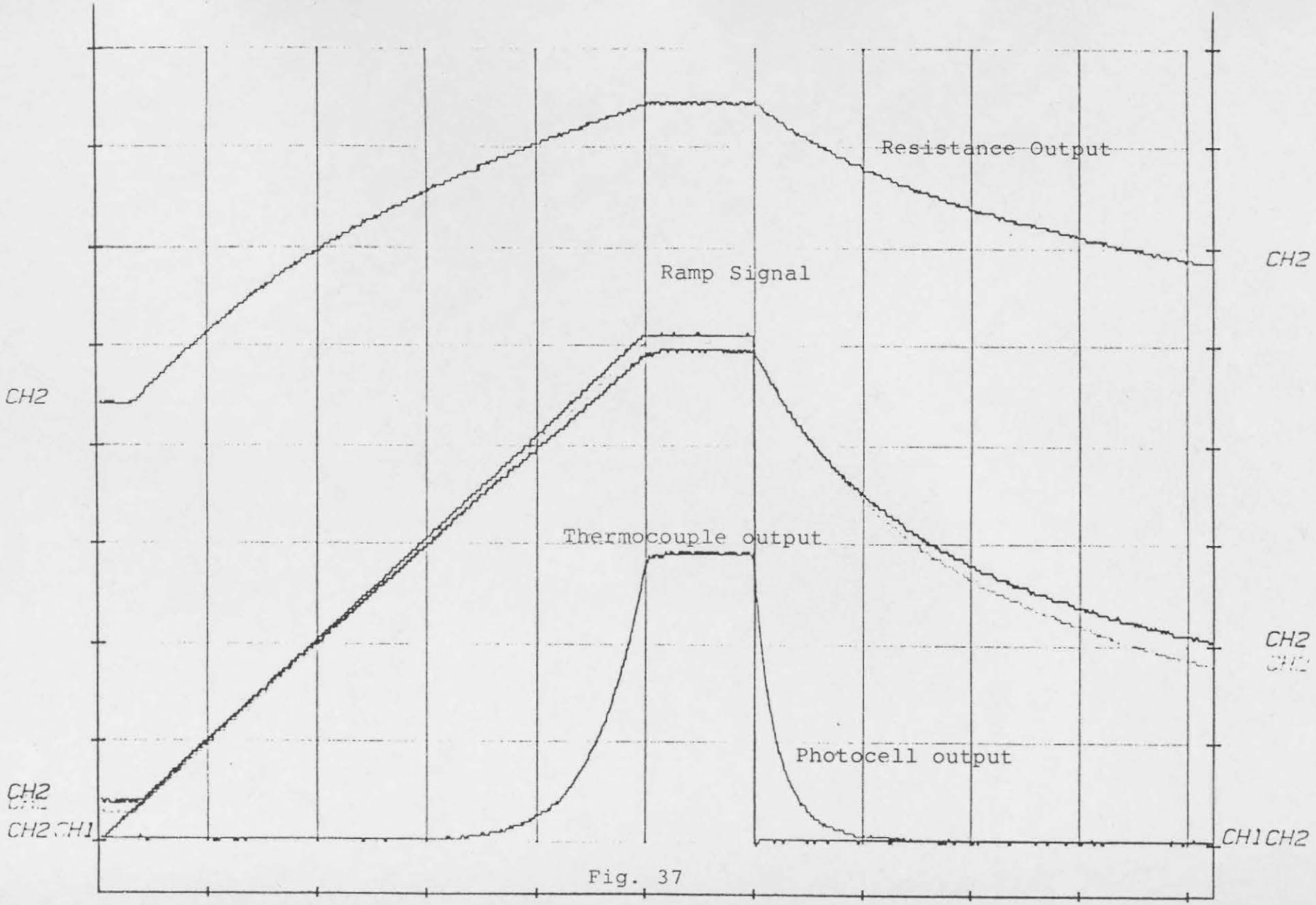
Resistance Output
Ramp Signal
Thermocouple output
Photocell output
CH2
CH2
CH2
CH2
CH2
CH2
CH1
CH1
CH2

Fig. 37

± 3.8ms. A delay time of 2 seconds was found to be sufficient from the moment of camera activation to power delivery to the mesh to allow stable steady state operation of the filming speed.

Extensive tests with the system indicated that both transmitted light and reflected light photography was possible down to 50μm particle sizes. Owing to the limited depth of field of high magnification systems, techniques were developed for keeping the mesh/particle system flat during the period of heating. The information obtained by either method of photo-micrography were different in quality and kind. Reflected light photography was more difficult in terms of limited depth of field and light requirements. However, observation of surface flow on particle surfaces, dynamic blow hole formation and other features were possible with this method.

Size changes including porosity changes of the reacting particle was more amenable by means of transmitted light photography. Optical glass fibre guided light source was used for this method. Focus and visual observation was much helped by a high quality ground glass screen available for this purpose in the Bolex camera.

The optical system consisted of a light microscope system with a high numerical aperture (X4 magnification) and an eyepiece of X10-X17 magnification. The camera lens was removed and focus was made possible by movement of the microscope tube stem. The microscope system was stabilised on a heavy metal platform to reduce vibrational disturbances. The Bolex camera was mounted on a heavy tripod frame with the possibility of 3 way movement at the camera head.

The particle diameter was estimated by means of projection of the developed 16mm film on to a white paper sheet. The image was approximated to an ellipsoid and an equivalent mean diameter, de of a sphere of the same volume was estimated by the following formulae:

$$de = (D_v \times d_h^2)^{1/3} \quad \text{where} \quad D_v = \text{vertical axis length}$$

$$d_h = \text{horizontal axis length}$$

Frame by frame inspection was possible by means of the projector system available. Many useful observations were also made by means of purely visual observations in both the mesh system and the use of a graphite rod holder. Information so collated was useful in adjunct to SEM studies of partially reacted coal particles at various temperature time histories.

5.6 Mesh loading variations

The following loading variations were attempted:

1) Slurry load (7-20mg) on to mesh of 50μm holes and 50μm wire diameter as well as meshes of 75 μm hole diameters and 50 μm wire diameter. The latter packing allowed better contact between coal particles and mesh surfaces for the 75-90 μm fractions.

2) 'Dry' loads of coal particles in both meshes of sample sizes 3-10mg.

In both the above cases contact between particles and mesh surfaces was enhanced by applying a tension to the brass posts by drawing them towards the centre of the reactor (fractionally)

before fixing the mesh in place. The former studies coupled with the photography studies suggested significant heat and mass transfer problems which led to the development of a unique method of particle loading as follows:

(3) particles of size 75-90 μm were loaded by pressing them into the holes of the 75 μm holes of the 200 mesh stainless steel screen mesh. This was done by careful brushing of the particles on to a previously double folded mesh. This was followed by gentle rolling of a firm plastic cylinder over the mesh surface. Excess particles were brushed off and the mesh/coal/thermocouple composite was carefully folded for weighing in a sartorius analytical balance. The latter technique allowed loadings of about 2mg sample sizes. The middle section of the fold was left free of particles so that no particle surface came into contact with each other which can lead to particle agglomeration or hinder tar evolution.

The technique allowed the best contact of coal particles to the mesh surfaces such that the mesh completely surrounds the particles and remains in contact with the mesh wires during the period of heating. Any particles falling off the holes during handling or heating largely fell on free mesh surfaces.

However, great care was needed in handling procedures and considerably increased the complexity of the mesh technique. Estimates of errors stemming from particle loss during fixation of mesh to the electrodes was found necessary. Consequently the errors were larger in yield measurements, particularly at temperatures below coal melting ($<350^{o}C$) and fragmentation of highly reacted char particles at high temperatures ($>900^{o}C$).

The mesh size used was 5cm x 5cm, of type 304 stainless steel (same type used by Menster[155] et al). The composition was as follows:

C = 0.05%; Si = 0.6%; Mn = 0.8%;

Cr = 18.5%; Ni = 10%; Balance = Fe.

The mesh undergoes decarbonization at 400-600^{o}C which embrittles the mesh. All mesh screens were prefired at high temperatures in flowing Argon gas to ensure as near constant properties as possible between meshes before particle loadings.

5.7 Fluidised bed configuration and design

Extensive development and study of various feed geometries, coal feed technique and sampling procedures led to a design of a fluidised bed Pyrolysis system sketched out in fig 38.

The system consisted of a N_2 fluidised sand bed with probes for measurement of temperature displayed on a digital Jenway device and a 1.0 mm diameter tube probe for tests on gas distribution profiles. A feed delivery system consisting of a tube of double skin dips just below the bed surface. Feed was injected batchwise through the central tube by means of a pulse of 'N_2' gas metered through a 3 way PTFE valve connected to a glass feed hopper. Reproducible coal feeds of about 90mg were injected by this means into the fluidised bed. The outer skin of the feed tube was cooled by a very small flow of air to ensure injected coal feed did not cake during its passage through the inner tube. A smooth ceramic diffuser was attached to the

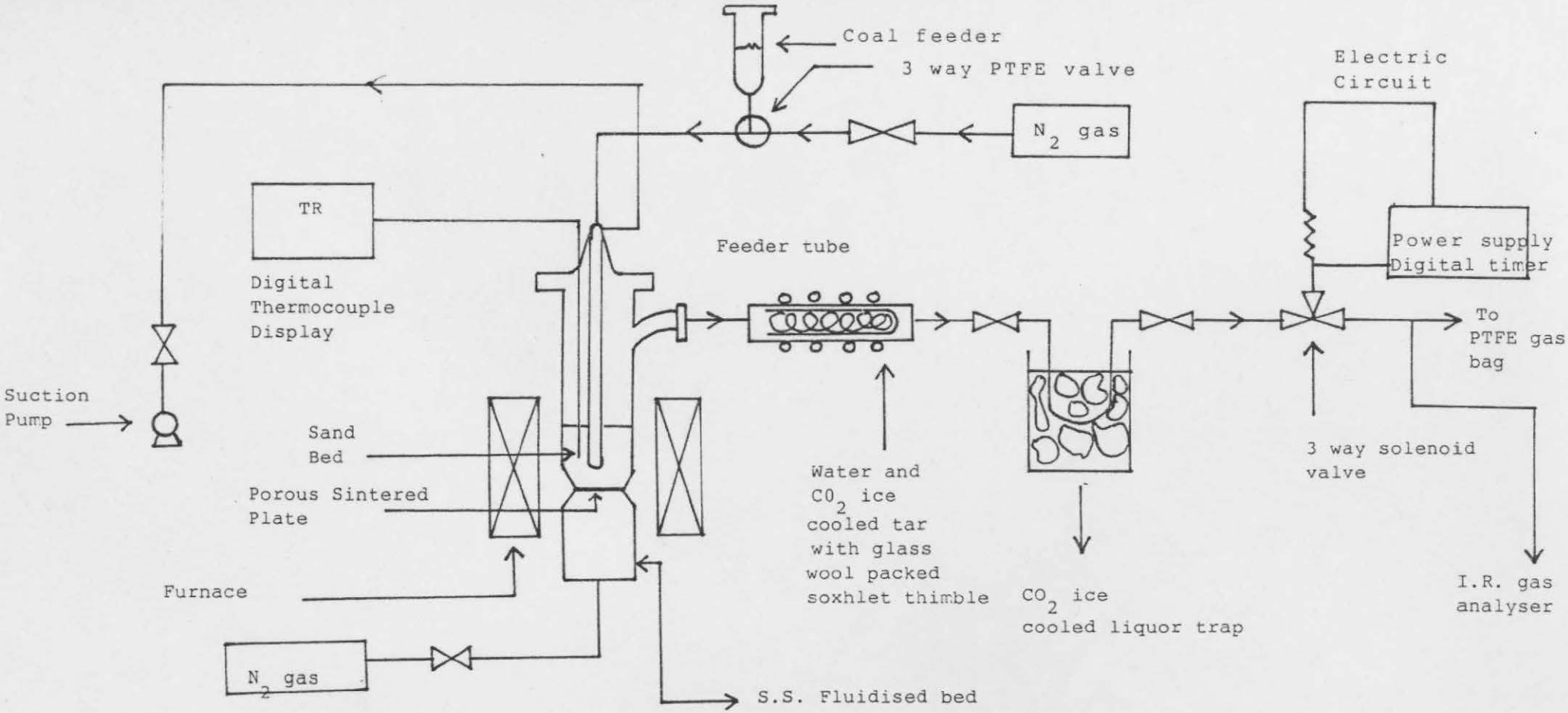

Fig.38 Fluidized-Bed pyrolyser system

bottom of the feeder tube that ensured dispersion of the relatively concentrated feed pulse.

The bed consisted of silica sand of particle size 89-125 μm The inner diameter of the fluidised reactor was 4.0cm with a total height of 19.0cm and an offtake side arm for effluent flow at about 14cm. Slumped bed height ranged from 2.5 to 3.7 cm with a bed weight of 42-57g. Runs were performed at near atmospheric pressure (102-108 kPa).

Minimum fluidisation velocities calculated by commonly used correlations underestimated the Umf values compared to experimentally determined values determined by pressure drop measurements. On average runs were conducted at 5-8 times Umf. Owing to caking of even the weakly caking coals used with the sand particles, the use of high fluidisation velocities was required at the intermediate temperatures (500-750^{o}C). A similar effect was noted by Tyler et al,[125] which by comparison with largely agglomeration free fluidisation with larger sand particles suggest a momentum effect.

The bed was heated by an electric furnace which attained steady state conditions within periods of 1-3 hrs depending on temperature of bed required.

The effluent stream was passed through a water cooled stainless steel tube packed with a glass fibre thimble filled with glass wool. The tar trap was covered by solid CO_2 ice pieces during the run periods. A liquor trap followed the tar trap also cooled by CO_2 ice. The remaining liquids free effluent passed through a 3 way solenoid valve which vents to the

atmosphere normally, but is activated during Pyrolysis runs to flow into a sampling system consisting either of a gas proof teflon bag or an on-line CO and H/C I.R. gas analyser.

The time for sampling was controlled by a programmable timer capable of sampling times ranging from 0.5-128 seconds. Sampling times and flows were accurately metered, the latter by a calibrated rotameter at the fluidising gas input side and a wet drum meter at the output side. The sampling times required for total gas collection was determined from concentration/time curves generated by the I.R. gas analyser, recorded on a multi-chart recorder. These curves were useful for determining problems such as defluidisation brought about by excessive bed agglomeration or feed tube blockage at the higher temperatures.

It was possible to detect H_2S gas by use of wetted lead acetate paper placed in the path of the effluent gas stream. The concentration was estimated from a precalibrated H_2S colorimeter. Lead acetate reacts with H_2S to produce a dark brown/purple black deposit by the following reaction:

$$Pb\ (C_2H_3O_2)_2 + H_2S \longrightarrow PbS + 2C_2H_4O_2$$

The tar in the thimble/glass fibre composite was extracted with THF in a Soxhlet apparatus. It was then dried using a rotary vacuum evaporator and finally under flowing N_2 whilst being heated gently in a glass pyrex flask. It was thus possible to estimate tar yields gravimetrically. A fine mesh basket preceded the tar trap to trap any elutriated char particles (6-10% of char was elutriated depending on bed temperature and degree of char sand agglomeration).

Total yields were found by weighing the feeder tube before and after coal feeding and the char/sand composite at the end of the run. Liquids yield were also estimated gravimetrically.

5.8 Gas analysis

The gas yields were detected by G.C. injection of samples from the gas bag and from known gas flows during the sampling runs. Syringe sampling was also conducted from the mesh reactor under both vacuum and static diluent gas pressure. The mesh reactor volume was then backfilled to an excess pressure of 4-10 mm Hg above room pressure, measured by a U-tube manometer. Room temperature and pressure readings were noted on the days that gas sampling was conducted. (The mesh system did not allow light liquids collection (BTX, ammoniacal liquor and H_2O) as in the fluidised bed system. Further, tar recovery proved to be difficult in the mesh reactor owing to the limited quantities generated. Early work conducted with a glass fibre filter paper at the effluent stream of the mesh reactor led to interesting observations of qualitative tar evolution behaviour).

Gas chromatography analysis of the gas collected was conducted on appropriate G.C. columns. H_2 and CO_2 were detected on silica gel columns using a TC detector and Argon carrier gas stream. H_2 and CO were detected on molecular sieve columns using a similar arrangement as for the silica gel.

Hydrocarbon gases were analysed on columns fitted with FID detectors. Two columns were used, a n-Octane Porasil C column

and a Phenyl Isocyanate column. A maximum of 16 gases were detected ranging from C_1-C_5 H/C gases. The best separation was obtained on the phenylisocyanate column maintained at around room temperature (19-25^{o}C). However, C_3H_6 and n-C_4H_{10} evolved together and could only be resolved on the N-Octane column. In the latter column C_2H_6 and C_2H_4 appeared together as a composite including the C_4 unsaturates. Total detection from a single injection took about 40 minutes for complete separation.

The identification of the gases were simulated by dummy runs on prepared gas mixtures and observing their elution times in sequence and finally as a composite mixture. It was apparent however that other heavier gases/liquids were not being detected owing to their low vapour pressures. Gases such as HCN, ammonia H_2O vapour and others of trace quantities could not be detected by the analytical system employed.

Because of the low concentrations of CO and CO_2 in the mesh reactor system coupled to the much lower sensitivity of the TC detector compared to the FID detector, these gases produced variable results, especially at the lower temperatures. Recourse to the fluidised bed results clearly indicate that these gases were significant components of the gas composition over a wide temperature range for the coals used in this work.

CHAPTER 6

INTERPRETATION AND OVERVIEW OF RESULTS

6.1 Analytical and petrographic coal properties

Proximate analysis and ultimate analytical data (Perkin Elmer 240C Elemental Analyser), including petrographic analysis was collated. (A quantitative analysis was performed by A Carr of LRS, British Gas PLC). A quanlitative analysis was performed on Markham Main coal (75/90 μm particles) by the author using a technique suggested by A. H. V. Smith of British Coal. Observations indicated the presence of significant pyrites inclusions. A significant part of the Inertinite group of macerals was dominated by Semifusinite, followed by massive macrinite and micrinite.

Proximate Analysis (75/90 μm)

	M Main (Rank 700)	Goldthorpe (Rank 800)
H_2O	3.61%	3.70%
Ash	2.37%	1.56%
VM (daf)	38.42%	40.99%
FC (daf)	54.99%	54.01%

Ultimate Elemental Analysis, M Main (Wt %)

75/90 μm	90/125 μm	150/212 μm	
81.32 (daf)	74.8 (db)	81.78 (daf)	C
5.49 (daf)	5.5 (db)	5.28 (daf)	H
1.79 (daf)	2.1 (db)	1.86 (daf)	N
9.96 (daf)		9.32 (daf)	O
1.44 (daf)		1.35 (daf)	S (total)

Markham Main Maceral Composition (Vol %)

	75/90 μm	90/125 μm	150/212 μm
Vitrinite	78	79	68 (71)*
Inertinite	13	9	21 (21)*
Exinite	9	12	11 (8)*

* MRS data

Goldthorpe Elemental Analysis (75/90 μm)

79.95	C (daf)
5.75	H "
1.98	N "
11.84	O "
0.79	S " (total)

	Goldthorpe (75/90)	M Main (75/90)
B S Swelling No:	1-1½	1-1½
C.V.	7326 cal/g	7322 cal/g
H/C	0.87	0.81
O/C	0.0919	0.1115
Apparent molecular formulae	$C_{100} H_{87} N_2 S_{0.4} O_{11}$	$C_{100} H_{81} N_2 S_{0.7} O_9$

6.2 Initial Studies and Results

Initially, several tests were conducted on the mesh reactor using meshes of various sizes, configuration and mesh hole size. Studies were conducted under both constant current mode (by using an external resistor) and constant voltage mode (using variacs to set the voltages for 2 stage heating).

A series of studies were conducted or temperature variations of the mesh using simultaneously side inserted thermocouple bead and spot welded thermocouple. (A design to spot weld thermocouple on to the mesh was constructed and spot welds made using a high magnification microscope stage for viewing).

The studies indicated that for 50 micron wire Chromel Alumel thermocouples, and heating conducted under flowing argon gas:

1) Placing the bead so that it was slightly above bottom fold resulted in a temperature 12-14^{o}C above that indicated by the spot welded thermocouple. (This was an effect noted by Freihaut et al as well, and in the view of the author is probably due to a combination of convection and mesh geometry effect). It was also noted that the thermocouple moved about in this position resulting in variable readings at the peak temperature.

2) By wedging the bead more firmly between the top and bottom folds of the mesh, the agreement between the two thermocouples was found to be $\pm 2^{o}$C.

3) Significant temperature lags were found for case of vacuum runs with the side inserted thermocouple.

4) Near the mesh edges and near the electrode posts, the mesh was cooler than the central region by $\pm$7-14^{o}C and $\pm$23-25^{o}C in the worst cases.

Thus only a central two thirds of the mesh was of uniform temperature and coal particles had to be loaded into this area by some means. (Refer to Ch 5 for estimates of steady state and transient errors).

Initial studies were conducted on a small mesh (22mm x 30mm) using 53 μm coal particle size (high volatile 902 rank coal) to test for yield measurement efficiencies. A glass fibre filter was used to effect tar trapping. The results are indicated in figure (A). Here coal particles were brushed on to the mesh surface (hole size 51 microns) with a brush, the excess brushed off and the mesh folded once before fixation to the brass electrodes.

Considerable scatter was found owing to particle loss during handling of the mesh. The results presented represent the least variable set among a set of runs and serves merely to illustrate certain trends and observations made during these initial studies intended to develop the mesh technique. It was observed that during Pyrolysis, the tars evolved with some force, with a 'hissing' evaporative effect. There was a cloud like evolution of tar aerosol with the lighter components carried off by the flowing argon gas stream. A flow of 1L/min was used which was found to be optimum for the reactor sufficient to maximuse tar trapping at the filter paper whilst minimising turbulence which causes evolving tars to redeposit over mesh surfaces. It was observed the cloud of tar nevertheless remains in the mesh vicinity for a time with the heaviest components sinking to the bottom of the reactor base. There was also some tar ('heavy' tar) depositing on the mesh electrode supports and lighter material coating the reactor sides.

Figure (A) indicates that the 'lighter' tar trapped by the glass fibre filter exhibits a maximum at about 450^{o}C. It was found after many trials that complete tar recovery was difficult to achieve. Aluminium foil liners were used along with methylene

Fig.A
Cumulative Volatile Yield vs Peak Temperature

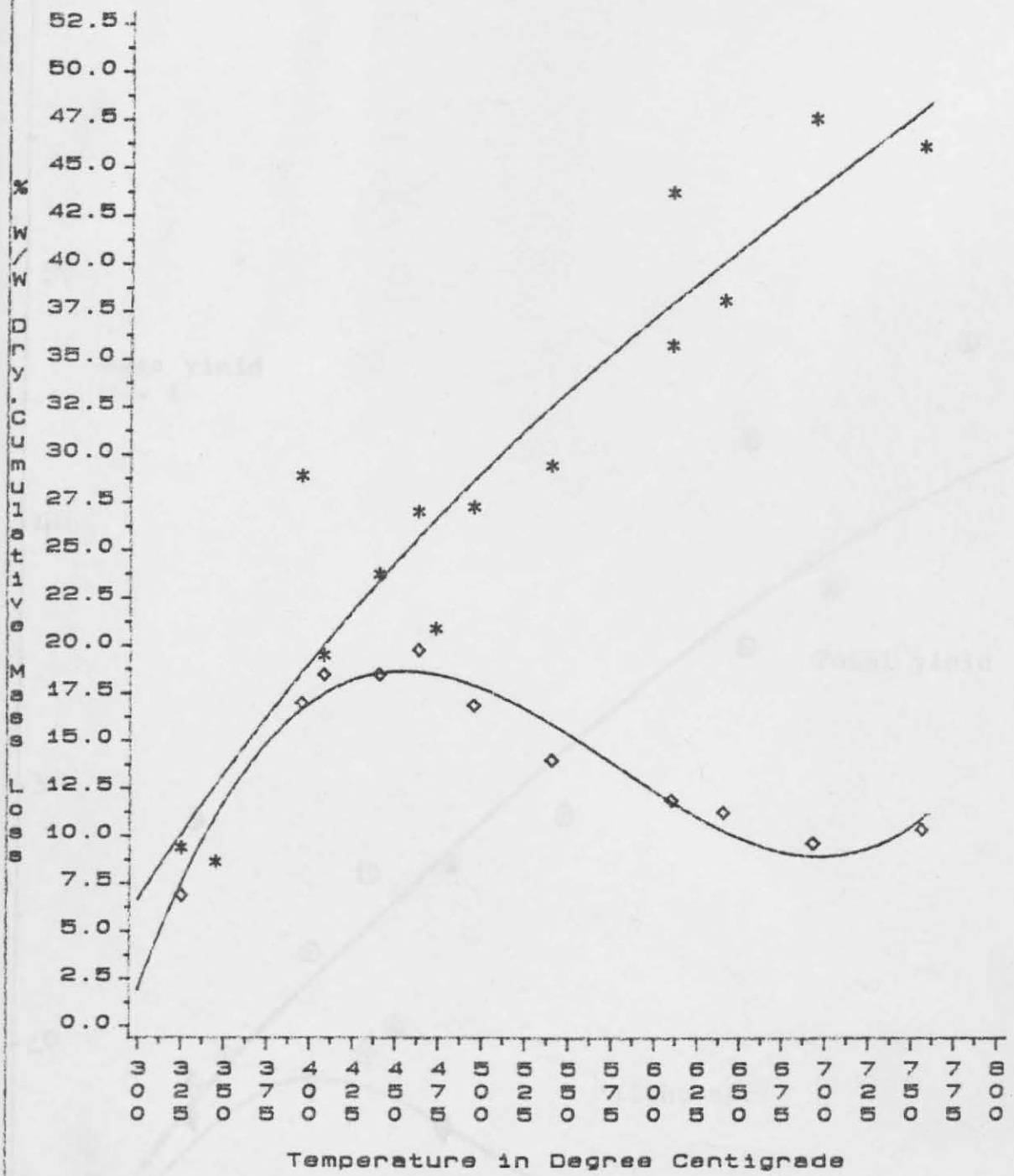

Nonisothermal Expts./(time=10/20ms)
60 micron mesh;Dp=63.0 microns
Coal Rank 902;Atm;Argon
Cumulative yield,Star symbol
Light tar yield,Diamond symbol
dT/dt=6000 Deg C/s +

chloride solvent washing of the reactor walls. However, tar recovery proved to be a time consuming affair and subject to considerable weighing error and incomplete recovery was the rule rather than the norm. In subsequent runs, tar was recovered by solvent washing of the reactor components by high purity Tetrahydrofuran (THF) solvent and stored in glass vials in a dessicator. Tar yield was estimated by difference between total volatile yield and where this was conducted gas yield Corrections were made for Pyrolytic H_2O formation and liquor by recourse to an emperical formulae provided by Probert et al and liquor yield (H_2O + BTX + other liquids) from fluidized bed work. [Probert found that for T>500^{o}C up to 1000^{o}C, Pyrolytic H_2O could be correlated by H_2O (mass %, daf) = 19.7 O C + 1.64]. An experimentally determined tar yield for Markham Main coal was determined from a composite of runs from long and short residence times and differing loading of coal particulate packing geometry for comparative purposes.

Before moving on to the main results to be discussed, a number of qualitative and quantitative trends of interest are noted at this stage. With regard to tar evolution a peak yield of light tar was noted around 425-475^{o}C as noted. Observations of the tars evolved indicated the following trends with reference to Markham Main (Rank 700) coal. (dp=75/90 μm, atmospheric conditions, mass slurry of loads 5-21mg tightly packed into a 75 μm mesh reactor and dried overnight in a vacuum oven):

< 290°C mesh discoloured and oily with very light patches (light yellow) on the filter paper. A strong smell of H/C and or thiophenic material was evident.

<412°C light sunflower yellow oil patch noted on the filter. Glass sides smeared with oily film (Tar yield - 13.4%)

459°C light and heavy tar evolved. Heavy tar of a light khaki brown colour and the light tars were grey/brown/smokey in character. (Tar yield - 16.9%)

607°C large evolution of mainly dark brown tar (Tar yield - 14.7%).

783°C Tar colour on filter paper indicated blackish brown streaks in the middle intermixed with chocolate brown tar. On the outer edges of the filter was the bright sunflower yellow oils/tar noted at lower temperatures (<412°C).

845°C Very dark brown tar was evolved with more of the black/brown tar noted as well as the light yellow oils/vapours.

A noticeable feature, particularly noted for the case of low loadings (1-2mg pressed into 75 μm hole mesh and double folded) was the following:

At the higher temperatures (>700°C), the tars smearing the sides of the reactor vessel had the form of an inverted funnel. The 'funnel' consisted of lighter gradations of brown coloured tar at the outer edges with darker tar towards the centre of the smear. In the centre of the smear was found the dark brown/black tars noted earlier.

Reference to a number of holographic studies of coal particle ignition studies[225,216] show, for the majority of particles, an attached spherical volatile flame with long soot-like trails ahead of the onion shaped top of the flame. A number of studies

conducted by the author on the mesh, of partially Pyrolysed char indicated a similar characteristic, to be discussed later. The preceding observations along with figure (A) indicate:

1) Tar evolution consists of a range of tar types with the character of the tar changing with temperature.

2) The colour of the tar at the higher temperatures indicate oxygenated groups (aromatic ether linked tars?) evolving.

3) The light coloured, sunflower yellow oils/tars suggest, possibly sulfer containing species of a light molecular weight fraction. Their increased reappearance at higher temperatures (>800^{o}C) suggest that some cracking of light components may be occurring.

4) The tar evolution appears to dominate the overall weight loss at the earlier temperatures <500^{o}C. However, the peak noted below this temperature is also an artifact arising from the increasing appearance of heavy tar at these temperatures which end up on the reactor base, thus missing the filter.

5) It was noted that at higher heating rates >1000^{o}C/S in atmosphere, the tar evolution was rapid, emitting with a hissing noise. The velocity of projection was also observed to be higher at the higher temperatures.

Studies of coal loaded onto the 50 μm mesh simulating the experimental conditions of Loison & Chauvin[157] Paul Arendt Freihaut and others[225,216] showed up different characteristics of mass loss and tar evolution characteristics compared to

the 75 um mesh loadings. (The results of figure A were obtained from conditions approximating to the single particle case. Refer to section 5.6 for packing conditions). In the case of the 50 um mesh screens, at high loadings (5-12mg, flowing diluent argon or helium gas), the total yields and tar evolution characteristics were shifted to higher temperatures and times.

Thus, the light sunflower yellow oils were first noticed at temperatures 438-452^{o}C. Rapid evolution of heavy tars occurred only at temperatures >550^{o}C. At high temperatures, >700^{o}C tar evolution became as violent and as rapid as that observed for the 75 micron mesh at lower temperatures (vide infra).

Fig M1A and M1 represent the total volatile yields for the 50 and 75 micron mesh as a function of peak temperature and 'isothermal' peak holding times at the peak temperature. (Conditions were 1000^{o}C/S heating rate of the mesh/coal composite, with argon gas flow at atmospheric pressure. 6-11mg for 50 micron mesh and 5-13mg for 75 micron mesh).

Figures MM1H H5 and MM50 show the cumulative volatile yield during the period of mesh/coal heating to the peak temperature followed immediately by convective and radiative cooling to the surroundings, including conductive cooling down the heavy brass electrodes, (residence time at peak temperature, 10 milli-seconds and a cooling rate of 200-250^{o}C/S). Some tests were conducted with gas cooled injection of a blast of N_2 or Argon at the mesh/coal composite at the point of heating current cut off at the peak temperature. (The cooling gas was ducted through a metal coil

dipped in a liquid N_2 bath). The coolant stream was initiated by a voltage pulse to a solenoid valve (± 10ms response time) at the end of the heating period, the whole sequence of operation being controlled by the sequential timer (vide infra). Cooling rates of 440°C/S were achieved at atmospheric flow conditions and 1110°C/S for vacuum conditions (<40 torrs). Several runs indicated little effect on ultimate volatile yield for this extra cooling rate. Thus further development of a cooling quench system was abandoned. (There is however a maximum delay of 20 milli-seconds between heating current switch off and coolant injection)

Figures MM1HE, MM5H (1000°C/S and 5000°C/S in helium blanket, 75/90 μm) including figures MMG and MM1G (1000°C/S, 90/125 μm and 150/212 um) show the total yields at heating up in helium gas at fairly low coal loadings (3-8.0 mg). Figure MV refers to total volatile yield at vacuum conditions (0.5-5 Torrs) and atmospheric conditions and long residence time at the peak temperature (t = 9.5s). Some runs were conducted at 200°C/S in both helium and Argon gas streams as well as vacuum. However, the mesh system heated up at grossly non linear rates at the higher temperatures (>600-650°C). This was an effect noted for so called 'programmed' heating driven mesh systems such as that used by Niksa. Subsequent development of a feedback control heating system overcame these problems at a later stage (refer Ch 5).

6.3 Analysis of stage one mesh reactor studies

The characteristics of the curves indicate considerable variation and individually reflects various characteristics reported by others who have utilised the mesh technique.

Figure MIA and MI indicate low mass losses at temperatures below 500°C, even for a residence time of 10s for the 50 um mesh case. The character of the curves are similar to that reported by a number of studies (N. Berkowitz,[83] Wiser et al using static packed beds). At higher temperatures there is increased mass loss during heat up followed by a rapidly rising mass loss as a function of isothermal heating time at the peak temperature. The cumulative yield approaches an asymptote at times and rates depending on the peak temperature reached. These are similar to the curves reported by Niksa using a similar mesh reactor. The form of the curves would suggest a two component or a maximum of 3 component volatalising system (reminiscent of the maceral mass loss curves, (refer figure MAC)). (See figure N.1 for Niksa curves).

Reference to figure MV for the 50 um mesh also indicate an enhanced mass loss at temperatures 700° C for the case of vacuum runs where the coal/mesh composite was heated for 9.5 seconds at the peak temperature. (Heating rate of the mesh system was 1000°C/S). This is in accord with results reported by Suuberg for Montana Lignite coal) who observed enhanced mass loss at temperatures above 800° C for the vacuum case for similar coal packing conditions. Niksa observed enhanced mass losses for the higher heating rates at long residence times (30s) at temperatures above 625-650°C for one coal under high vacuum. (Base case was 100°C/S, where in his system heating profiles had to be adjusted by hand to ensure linearity refer to figure 25). For another coal he found enhanced mass losses throughout the temperature range with the enhancement increasing at temperatures 700° C. In both case heating rates of 10^4K/S made minimal improvement in yield at the higher temperatures (750°C). It must be noted Niksa uniquely reports enhanced yields as an effect

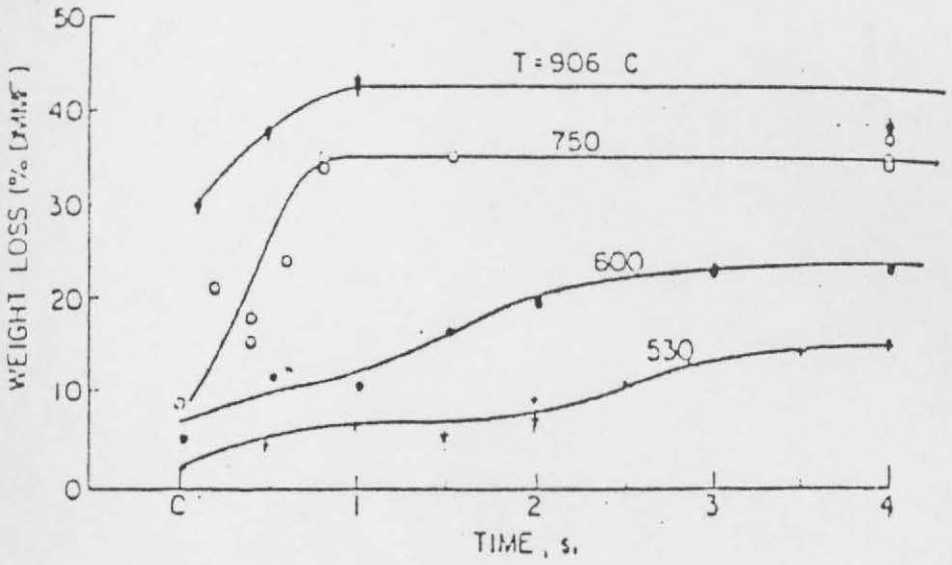

Fig. N.1

Re: Niksa: 0.19 MPa pressure

Transient and isothermal yields

Fig.MIA
Cumulative Volatile Yield vs Time at Final Temperature

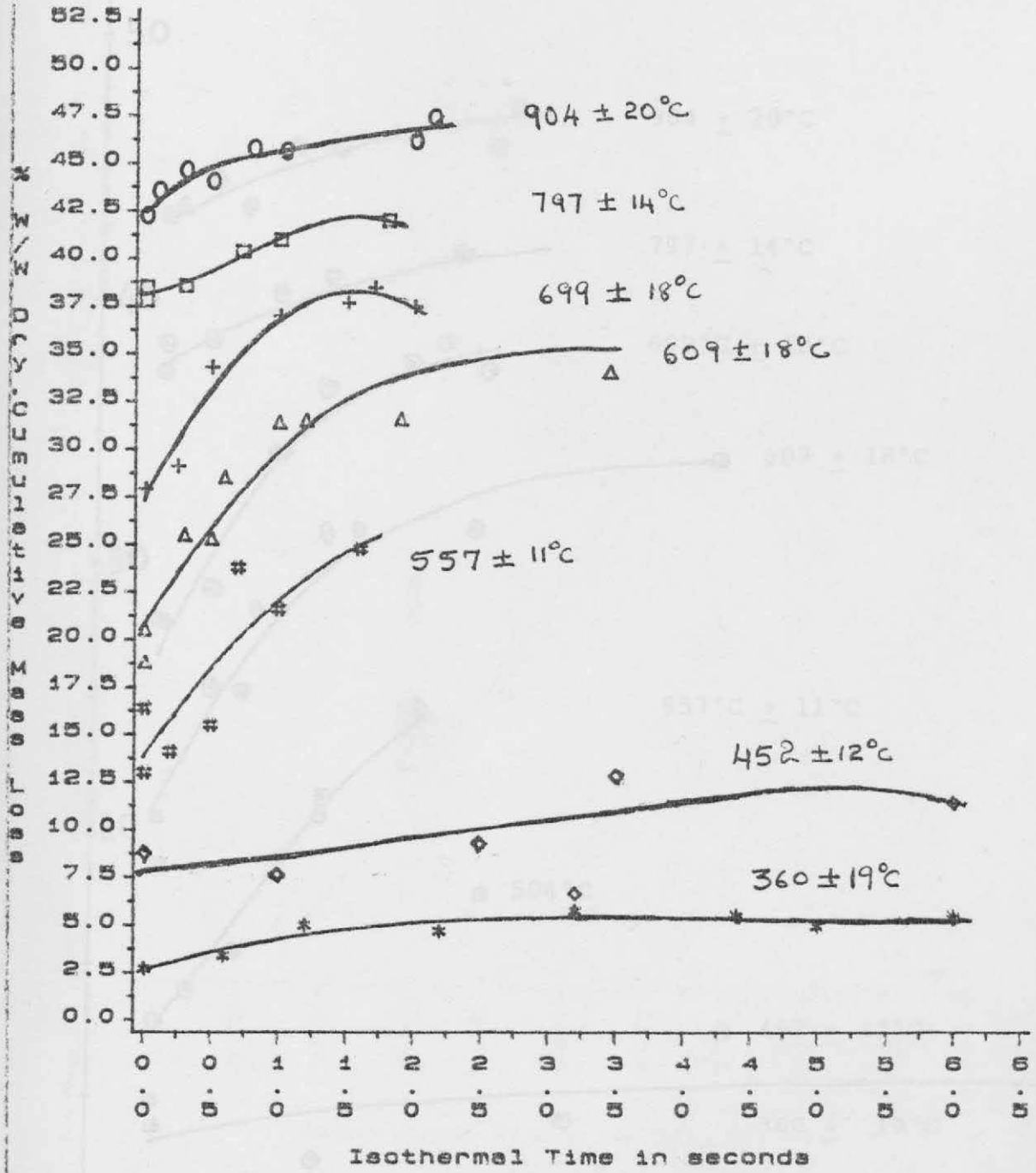

Isothermal Expts/Variable res.times
50 micron mesh
Load=5.0–13.0mg
Variable residence times at peak T
M.Main Coal
Atm/Argon gas/Dp=75/90,microns
dT/dt=973 Deg C/s + 42.0 Deg C/s

Fig.MM50
Cumulative Volatile Yield vs Final Mesh Temperature

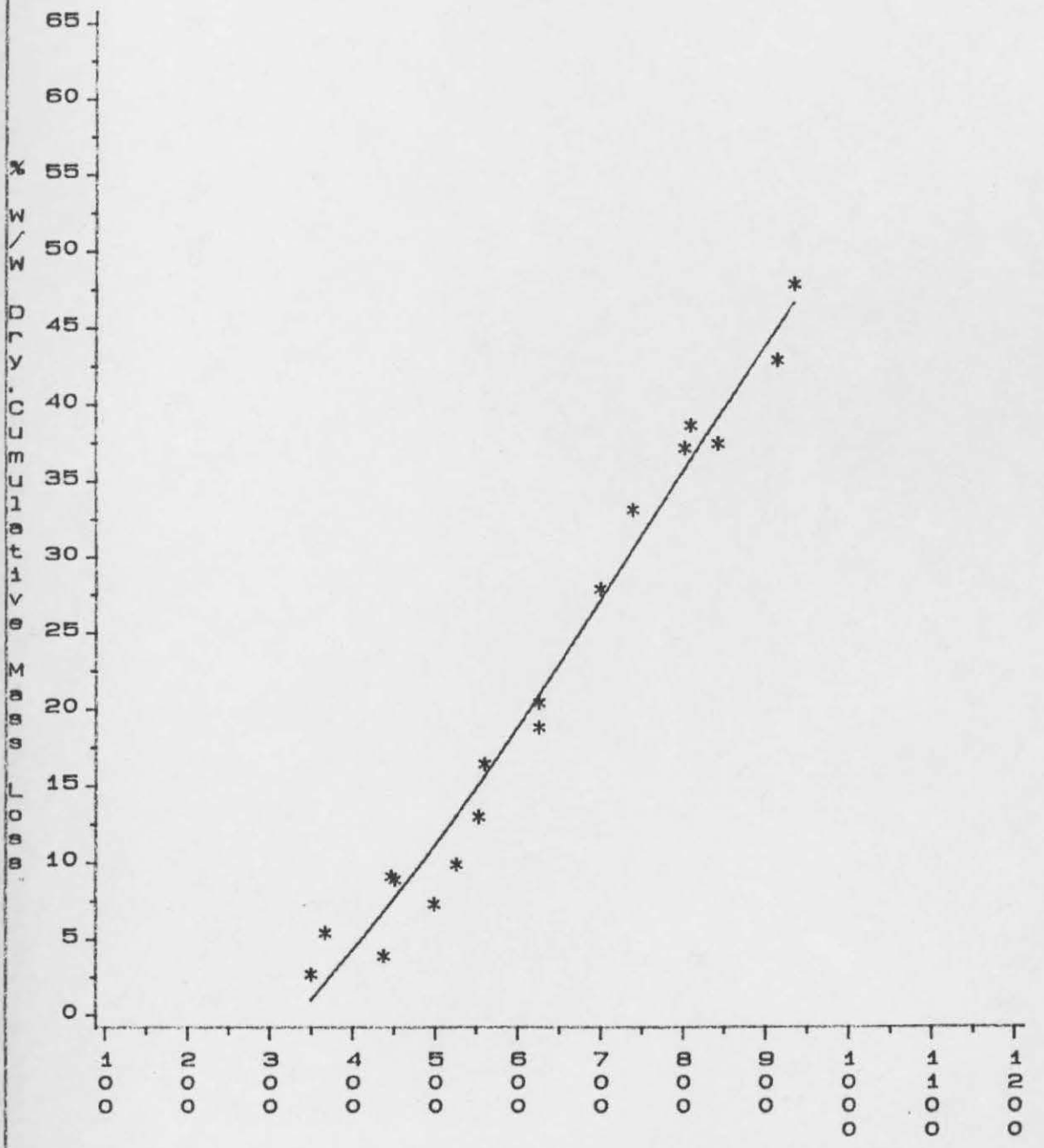

Note: This refers to yields for case MIA at 10/20ms

Nonisothermal Expts
50 micron mesh
Load=3.0-12.0mg
Residence Time at Peak T=10/20ms
M.Main Coal
Atm.(Argon)/Dp=75/90,microns
dT/dt=1043 Deg C/s +55.0 Deg C/s

Fig.MI
Cumulative Volatile Yield vs Time at Final Temperature

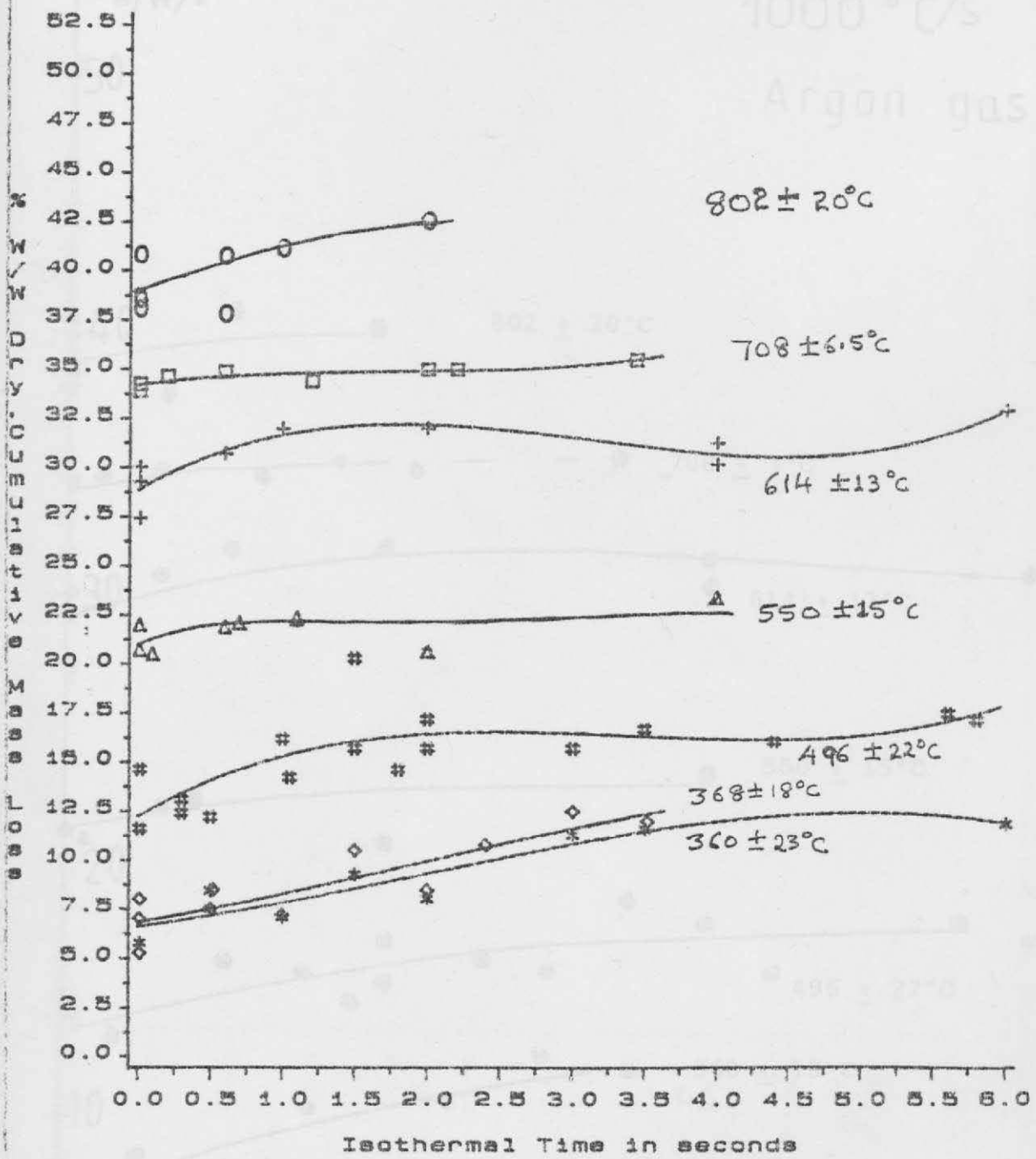

Isothermal Expts/Variable res.times
75 micron mesh
Load=4.0–10.0mg/10–20mg
Variable residence times at peak T
M.Main Coal
Atm/Argon gas/Dp=75/90,microns
dT/dt=992 Deg C/s + 27.0 Deg C/s

Fig.H5
Cumulative Volatile Yield vs Final Mesh Temperature

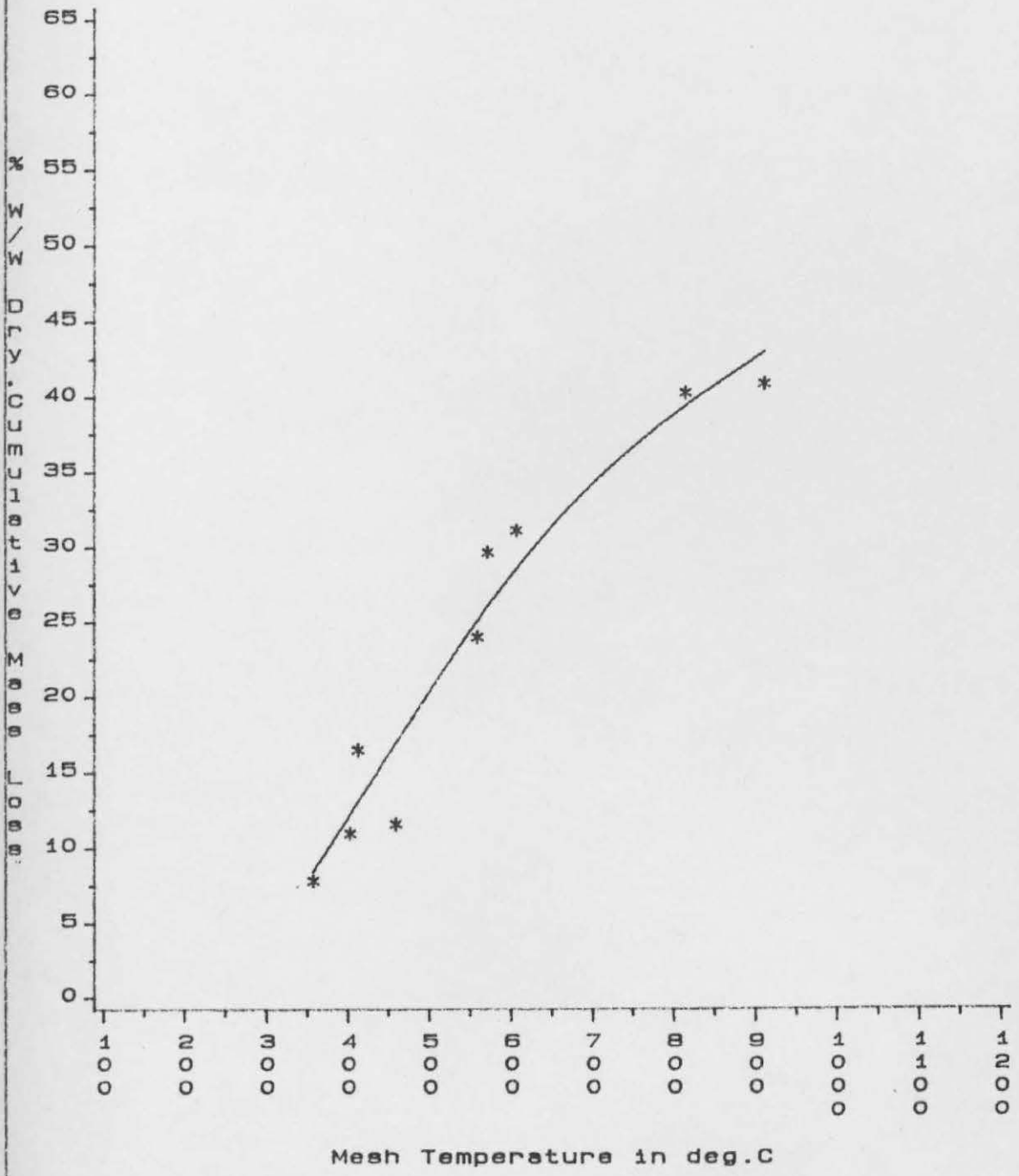

Note: This refers to yields for case of Fig. MI at 10/20ms

Nonisothermal Expts.
75 micron mesh
High Loadings(10.9-21.0mg)
Residence Time at Peak T=10/20ms
M.Main Coal
Atm.P/Dp=75/90,microns
dT/dt=5696 Deg C/s +507.0 Deg C/s

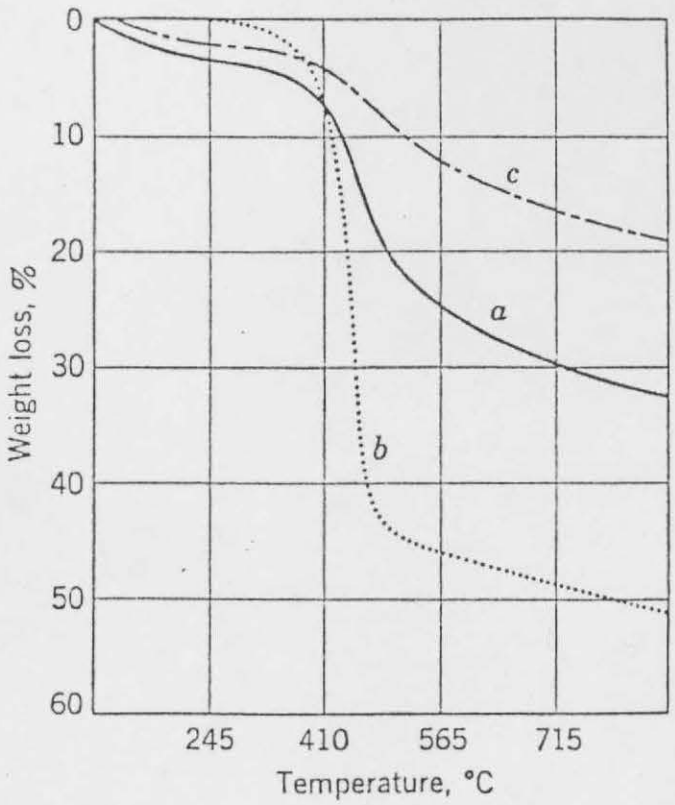

Fig. MAC Weight-loss curves of petrographic components. *a*. Vitrinite; *b*. exinite; *c*. micrinite.

Re: Kroger et al

Fig.MV

Cumulative Volatile Yield vs Peak Temperature(Yield at 9.5 seconds)

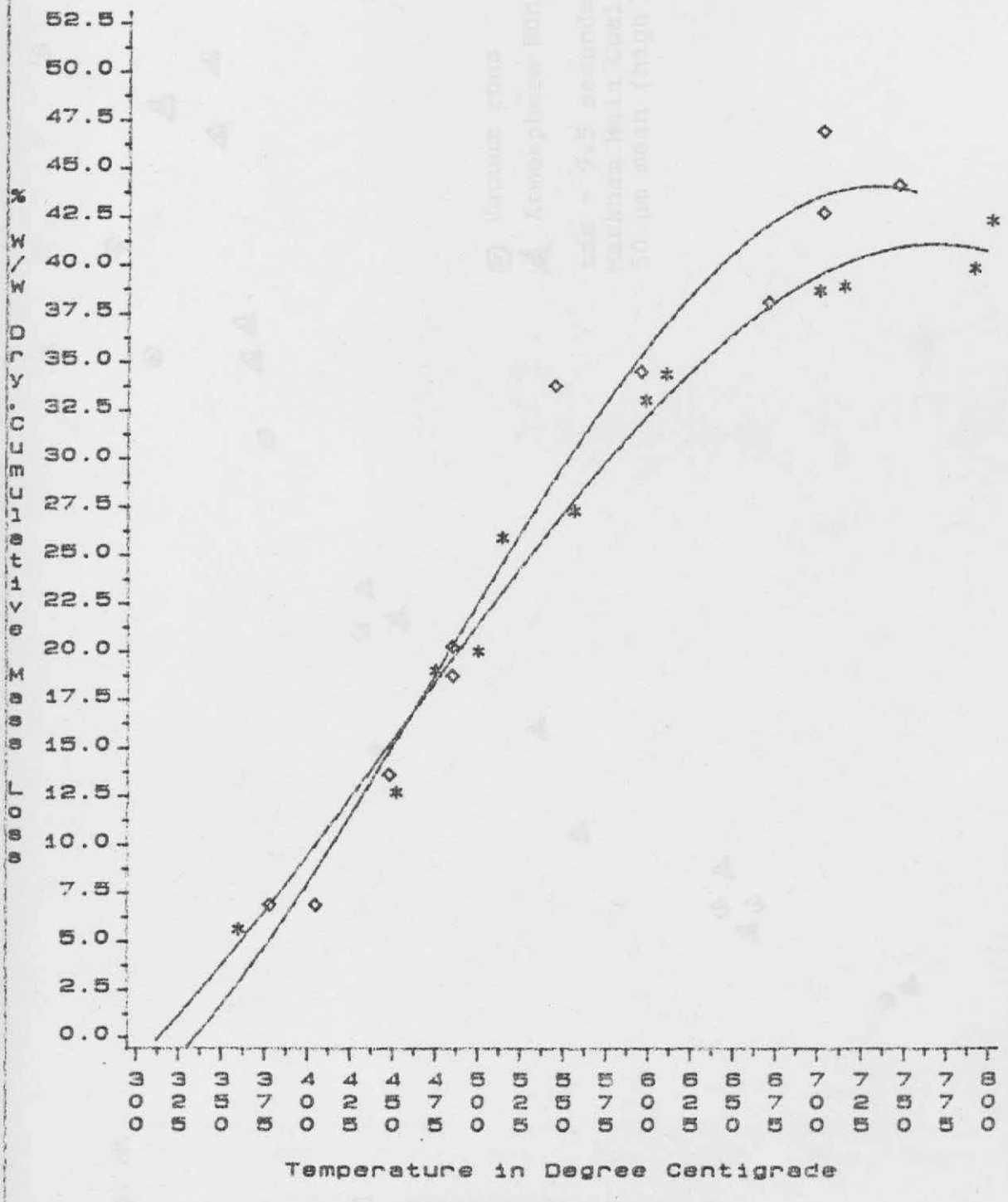

Isothermal Expts./(time=9.50 sec.)
50 micron mesh;Dp=75/90 microns
M.Main Coal;dT/dt=1000 Deg C/s
Atmospheric Runs,star symbol
Vacuum Runs,diamond symbol

Fig.TarM

Mesh tar yields,50 & 75 micron mesh,Atmospheric pressure

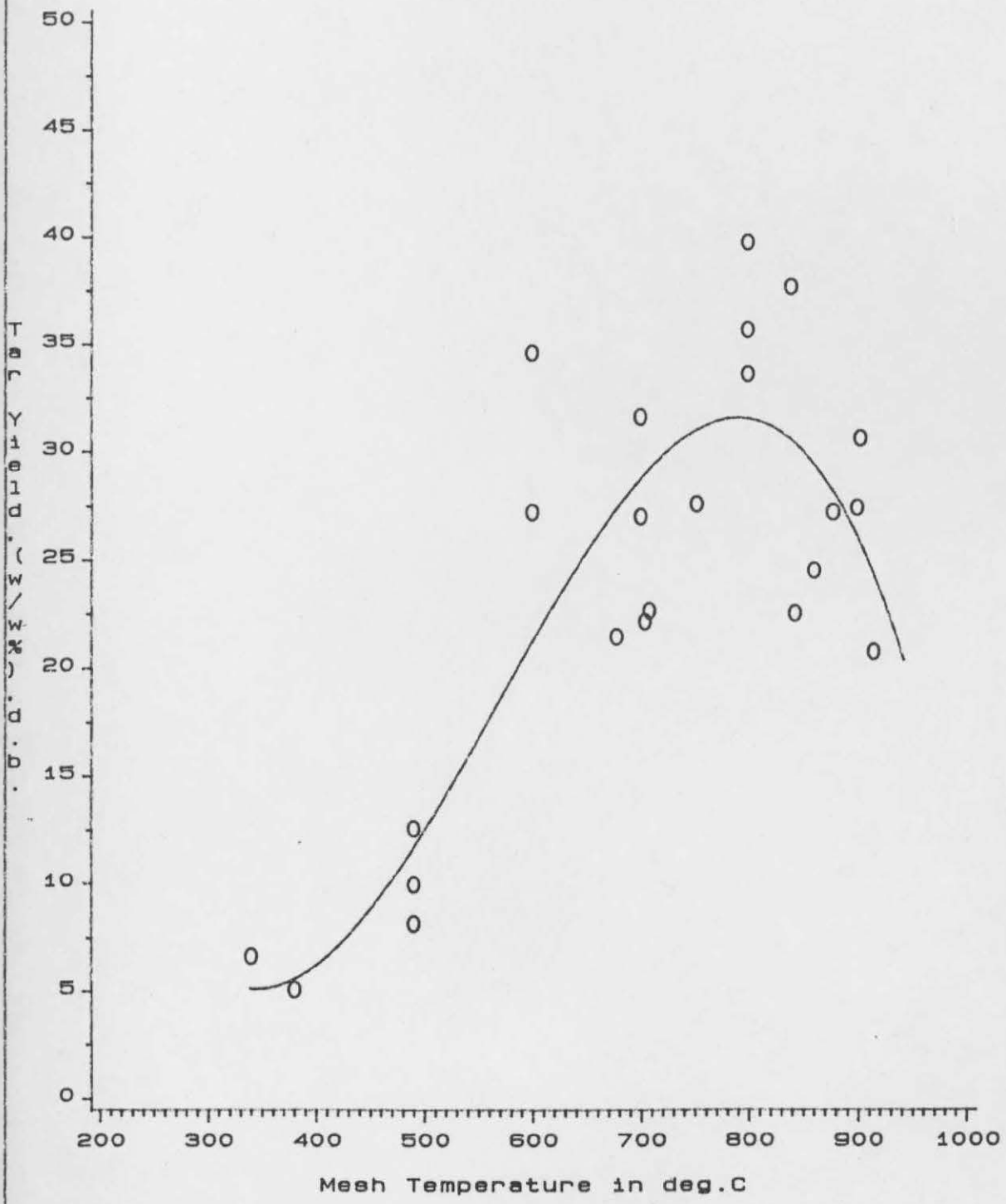

Markham Main Coal:Dp=75/90uM
Cumulative Tar Yield(d.b.)
Residence time at peak Temp.=10ms-1.0s
Results from mixture of mesh types and residence times at the peak temperature

Fig.MM1H
Cumulative Volatile Yield vs Final Mesh Temperature

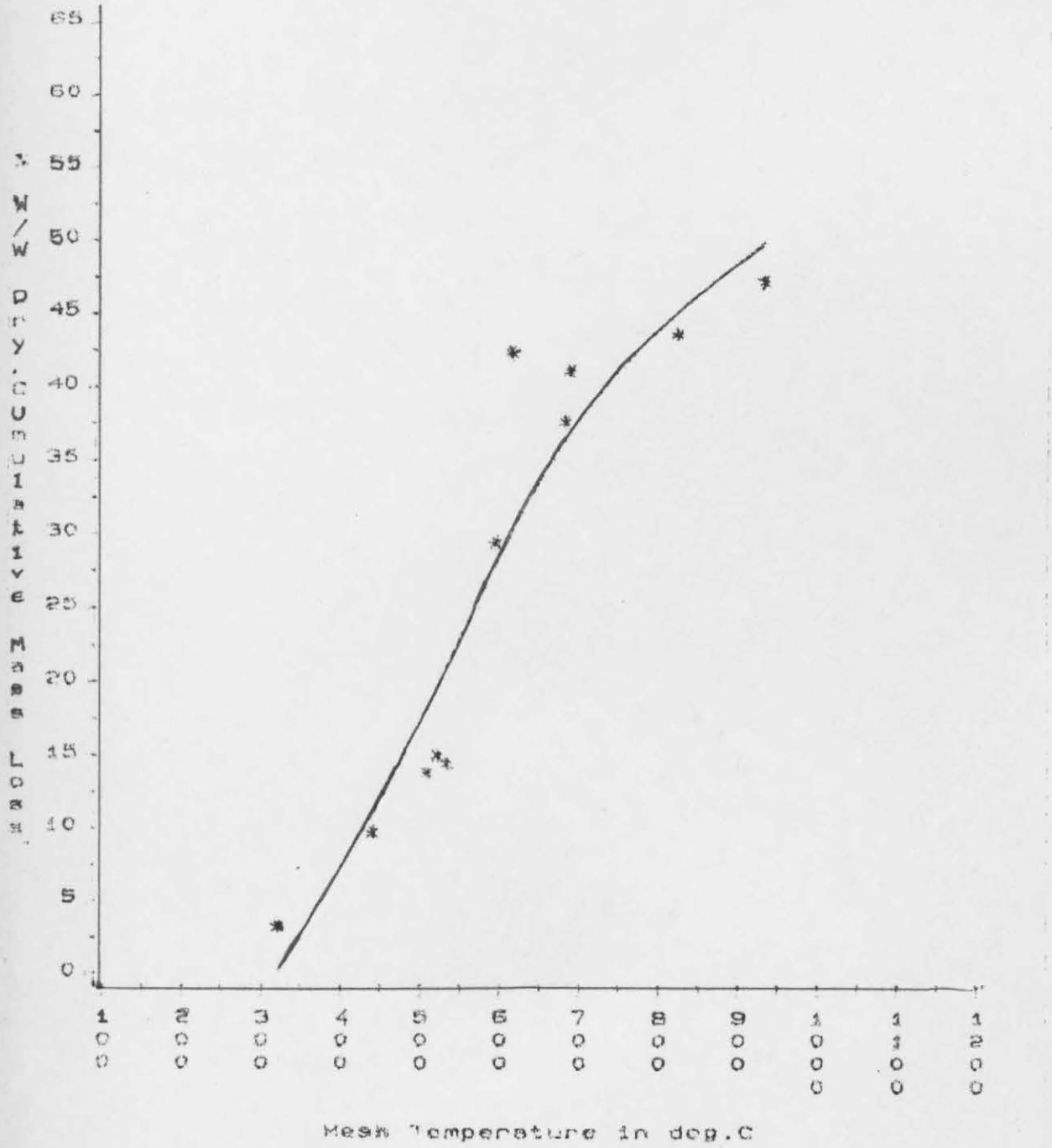

Nonisothermal Expts
50 micron mesh
Load=3.0-8.2mg
Residence Time at Peak T=10/20ms
U.Main Coal
Atm.(Helium) /Dp=75 /90,microns
dT/dt=1000 Deg C/s +45.0 Deg C/s

Fig.MM5H
Cumulative Volatile Yield vs Final Mesh Temperature

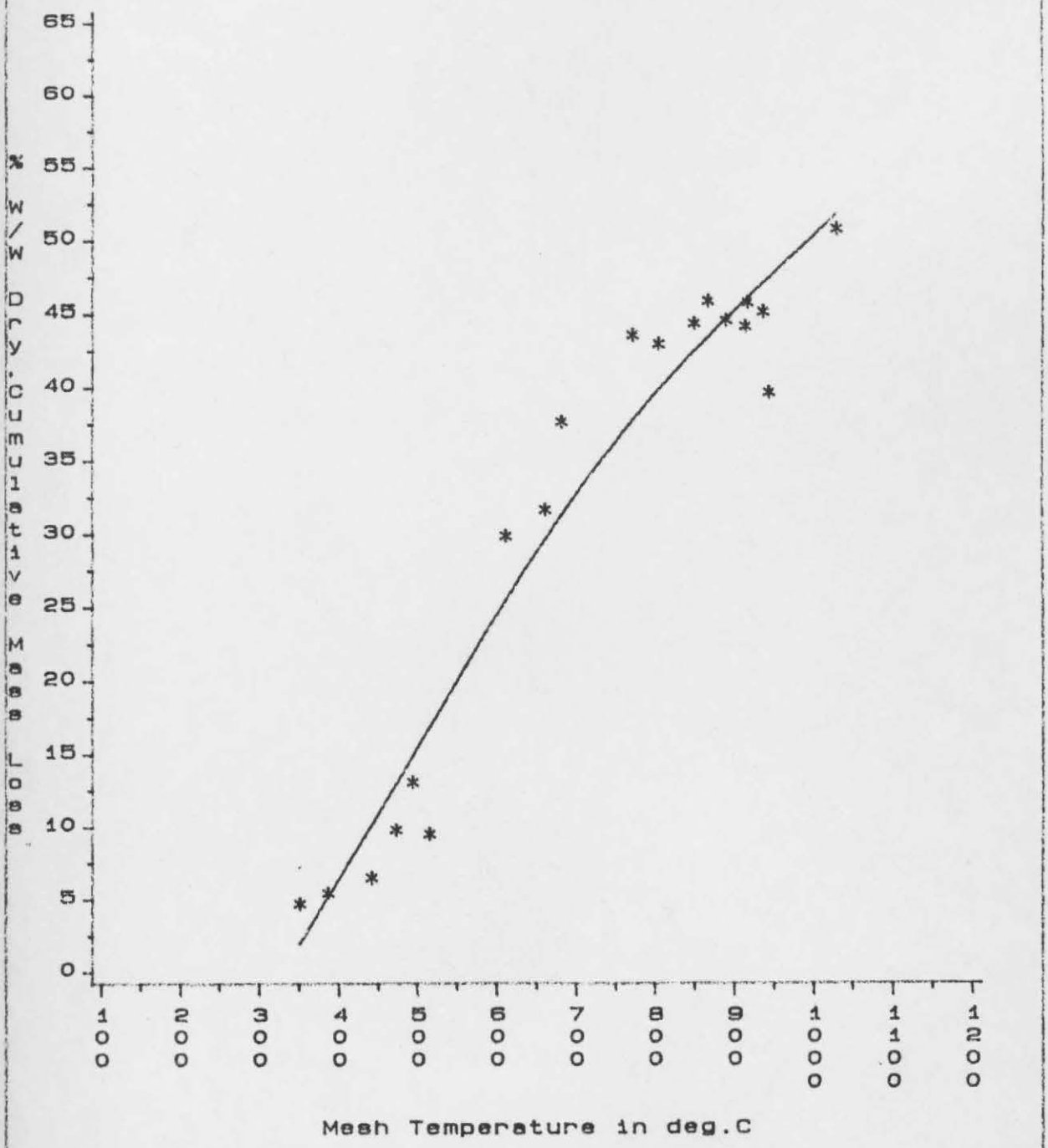

Nonisothermal Expts
50 micron mesh
Load=3.0-6.8mg
Residence Time at Peak T=10/20ms
M.Main Coal
Atm.(Helium)/Dp=75/90,microns
dT/dt=5000 Deg C/s +65.0 Deg C/s

Fig.MMG
Cumulative Volatile Yield vs Final Mesh Temperature

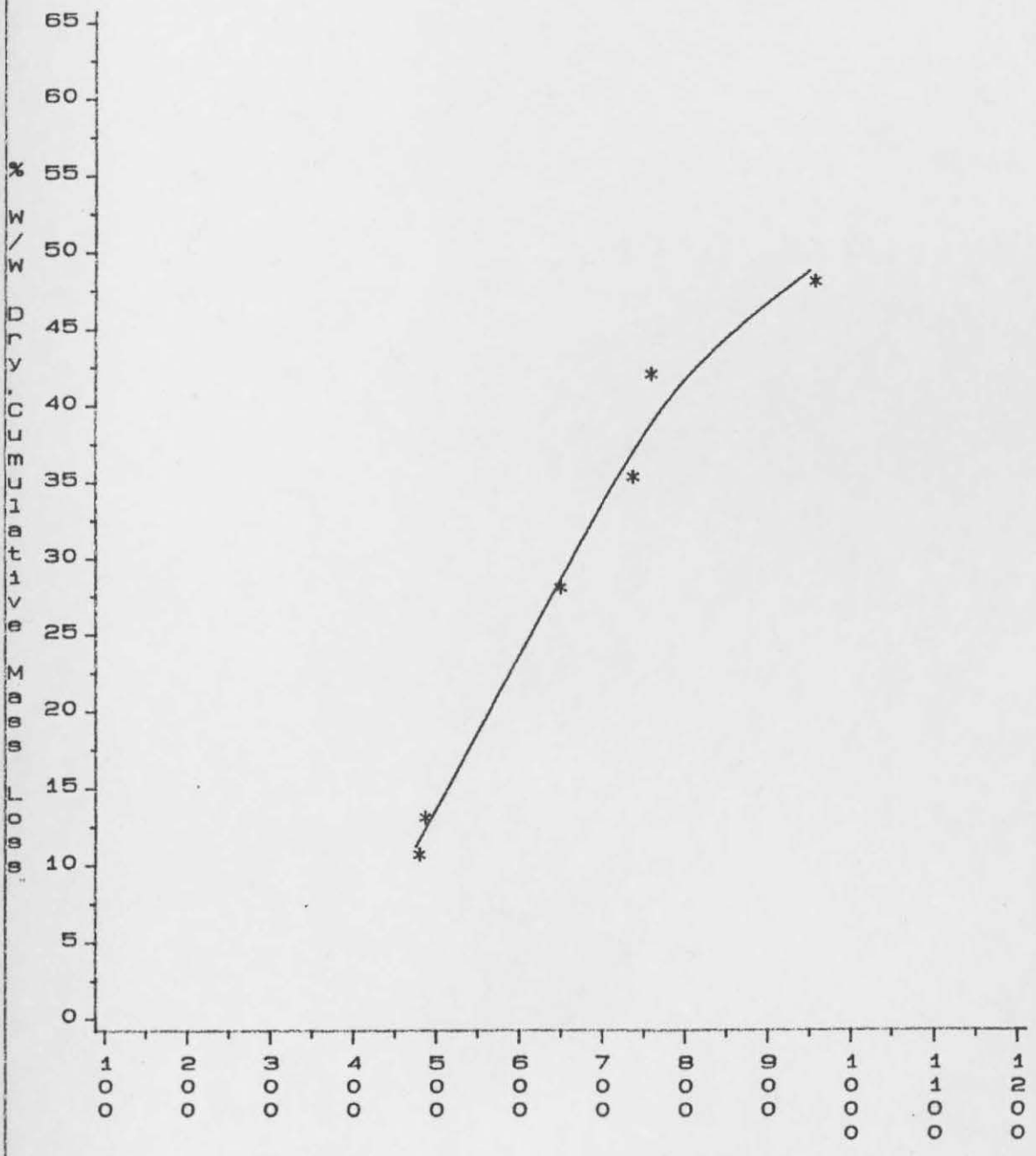

Nonisothermal Expts
50 micron mesh
Load=3.0–7.0mg
Residence Time at Peak T=10/20ms
M.Main Coal
Atm.(Helium)/Dp=90/150,microns
dT/dt=1000 Deg C/s +69.0 Deg C/s

Fig.MMLG
Cumulative Volatile Yield vs Final Mesh Temperature

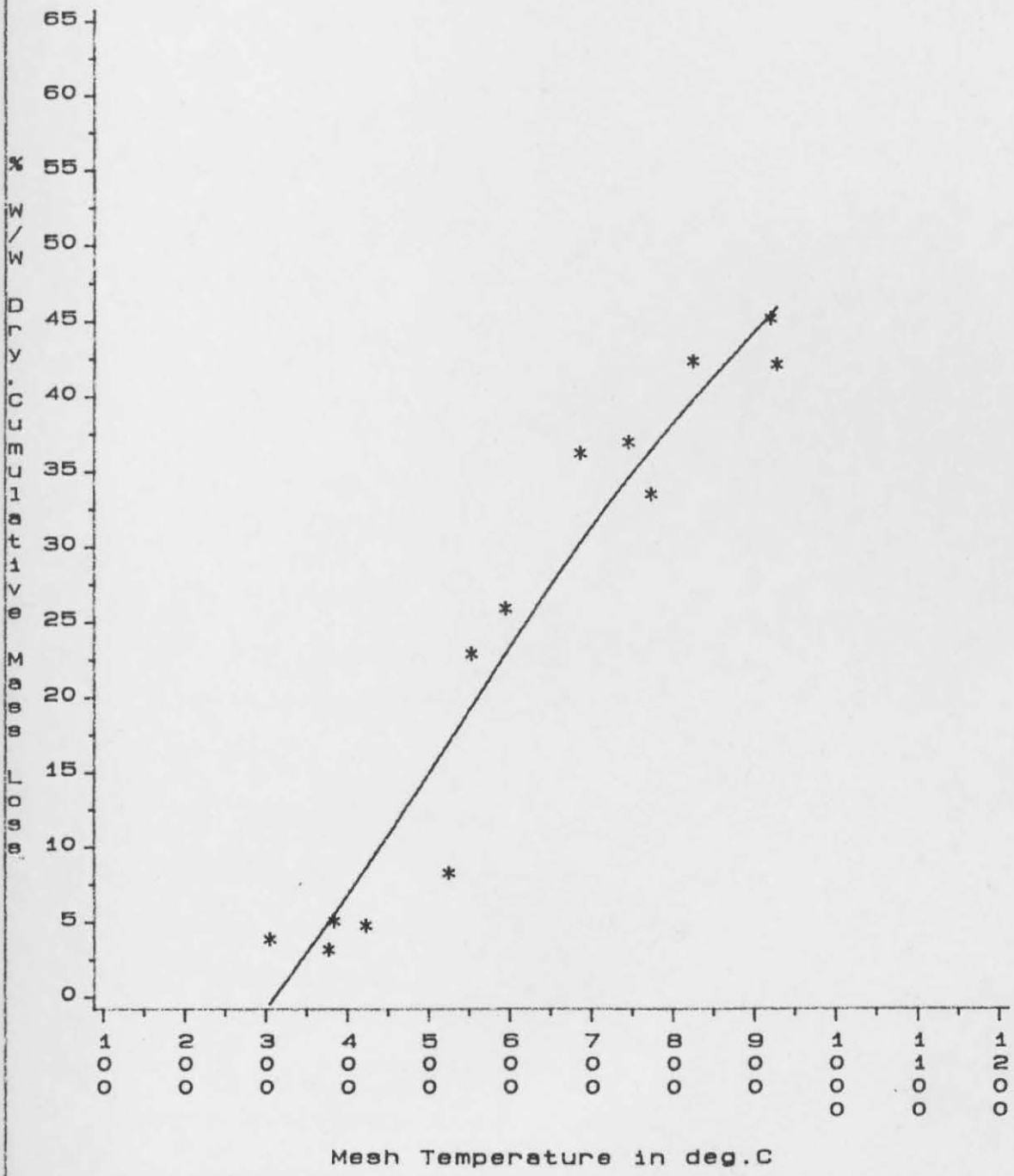

Nonisothermal Expts
50 micron mesh
Load=3.1-6.0mg
Residence Time at Peak T=10/20ms
M.Main Coal
Atm.(Helium)/Dp=150/212,microns
dT/dt=1000 Deg C/s +69.0 Deg C/s

originating from a heating rate effect (for vacuum conditions, t=30s at peak temperature and for heating rates <10,000°C/S).

Reference to fig MI will indicate however a singular effect and that is that the initial, very rapid mass loss observed during heat up completely dominates the yield/temperature/time curves in the case of the 75 um mesh. At temperatures below 500°C there is a small degasification period observed, less noticeable at the higher temperatures. A second striking observation is the enhanced mass yields noted at longer residence times ($\sim$ 4-5%) below 800-900°C, for the 50 μm mesh compared to the 75 μm mesh case.

This can be explained with reference to the mesh loading characteristics. In the case of the 50 μm mesh, the particles are more loosely packed. Thus particles are heated essentially by heat conduction through the gas film boundary layer surrounding them. At lower temperatures it is likely that oily material of low thermal conductivity inhibits heat transfer by thickening the boundary layer. At higher temperatures, heat transfer is enhanced by radiation as well as a much enhanced particle mesh surface contact owing to enhanced particle swelling at these temperatures. (The latter is shown by SEM micrographs).

In the case of the 75 μm mesh, particles are in better contact with the mesh surface and for tight packings, essentially independant of interphase heat transfer. Whilst heat transfer is much improved, char particle surfaces provide areas for redoposition of liquids and cracking reactions both of which can lead to increased solids deposition. This probably explains the differences in ultimate yields for the two meshes.

To obtain an order of magnitude idea of possible particle lags a simplified heat transfer model was considered. Essentially, for particles of diameter larger than mesh hole size and loosely dispersed, the particles may be considered to be bathed in diluent gas. For fine particles <200 μm, the Reynolds number for flow around static particles will be low. Thus the system may be approximated to one in which the particle is surrounded by a near immobile medium and effective heat exchange between the particle and surroundings is via a boundary layer of gas surrounding the particle. For the case of low Biot number, and assuming the theoretical value of Nusselts number = 2 for a single particle in a stagnant medium, the following analysis was conducted.

For a body submerged in a fluid whose temperature varies linearly with time, the following relationship holds (Reference: Heat transfer for Engineers, H. Y. Wong), namely:

$$Tp = Tf + mt - \frac{Sp\ Cp\ Vp}{h_c\ Ap} + \left[\frac{Sp\ Vp\ Cp\ m}{h_c\ Ap}\right] \exp\left[\frac{-hc\ Ap}{Sp\ Cp\ Vp}\right]$$

m = assumed heating rate of low thermal capacity gas = 1000°C/S; Sp = particle density; Vp = Volume of body; Ap = surface area of particle; h_c = convective heat transfer coefficient. Tf = Temperature of gas fluid. Making a correction for vapour efflux[55] from particle surface, (1/3 h_c) and for Argon gas diluent the following was obtained for a particle of 82.5 um diameter:

T_f(°C)	t_h(heating time)	Tp (particle temperature at t_h)
700	0.7	642°C
600	0.60	492°C
550	0.55	542°C
500	0.50	442°C
452	0.452	374°C
360	0.36	302°C

The above simplified analysis indicated that the particle temperature was lagging the imposed heating rate of the fluid surrounding the particle, roughly approximating to the weight loss trends noted for both 75 μm and 50 μm mesh. Thus, for the 50 μm mesh, set for a peak temperature of 708 ± 6.5°C, the ultimate mass yields corresponds closely to that reached by the 75 μm mesh heated to 614 ± 13°C for short isothermal residence time (⩽1.2s) (the temperature of the particle was estimated to be 642°C for a final demanded temperature of 700°C at a heating time of 0.7s). The analysis also indicated that the rate at which heat is conducted to the particle surface is dependant on the gas properties surrounding the particle. Thus helium, which has a higher thermal conductivity than argon gas should provide less resistance to the interphase heat transfer. Reference to fig MM1H indicates that this is so, evidenced by the higher mass losses noted for heating in helium gas.

A further problem is the growth of particulate mass by sintering. The coalescence of neighbouring particles by vapour deposition at the necks of contacting, softened coal particles may give rise to the physically controlled phenomena of particle agglomeration kinetics. This will depend on such factors as particle size and shape, size of neck and the rate of its growth dictated by the surface tension forces tied to viscuous flow of the tar liquids. As the viscosity of tar like material is known to exhibit an exponential temperature dependance, of the form $n = n_o \exp(-E_A/RT)$, it is quite possible that the form of the mass loss curves may reflect some such phenomena.

Clearly, the curves illustrate a mass transfer resistance effect in the case of high loadings for the 75 μm mesh, despite the initial rapid mass loss observed during heat up. Thus, at long residence times, the 50 μm mesh weight losses are higher by about 4-5% for similar peak temperatures. In order to minimise heat transfer and mass transfer effects, coal loadings, mesh types and heating rate variations were carried out.

It was finally decided to adopt a double folded 75 μm mesh with the particles pressed into the mesh surface as described earlier in Chapter 5. The heating circuitry was also improved to ensure linear heating rates at low heating rates as discussed earlier. A heat transfer model incorporating transient heating coupled to chemical reaction was also simulated to test for the effects of imposed heating rate and other external conditions on the temporal and spatial variations of the particle. This will be discussed in subsequent sections.

6.4 Effect of heating rate and pressure variations on overall Pyrolysis yields

1-2mg of coal particles loaded onto a 5 x 5 cm, 75 μm hole mesh were heated to varied peak temperatures and residence times (250-1140^{o}C and 20ms-10s) at heating rates of 10 , 200, 1000 and 5000^{o}C/S. Most of the results reported refer to heating rates of 10^{o}C/S and 5000^{o}C/S for the Goldthorpe coal and 1000 and 5000^{o}C/S for the Markham Main coal. Pressure was varied between 0.5-5 Torr (vacuum runs) and atmospheric pressure. Gas collection was conducted in-situ which led to problems of tar deposition at atmospheric pressure runs, particularly at the high temperatures.

For the atmospheric pressure runs, the vessel was partially evacuated to avoid overpressurising the reactor during the run. As there was no injection loop available on the FID G.C., frequent calibrations of the G.C. and multiple injections were required to ensure reproducibility. Typical errors for the gas analysis were in the range 15-25% of the quoted values. However, as the trends and magnitude of the results indicate, the values obtained are comparable to extant data on other coals and enabled much information to be collated which clearly delineate the effects of heating rate and pressure on various classes of gas yields.

Such information coupled to a very substantially comprehensive yield distribution from the fluidised bed provides a reasonable basis for comparative study of various process variables and the initiation of a data base for local Bituminous coals. Figures MA1 to GV10 show the overall yield as a function of the conditions labelled. The fluidised bed volatile yields are noted (figures M1 to G1). Some of the gas yields from the mesh reactor fitted by an independant, single reaction, nonisothermal model is shown in figures i to xxxi . Others are tabulated (refer tables T1 to T3). Elemental analysis of collected tars from the mesh rector (accumulated over several runs and stored in THF solvent) and fluidised bed reactor, including char elemental analysis from the mesh reactor is presented (figs MM1C to GT). Gel permeation chromatography was performed courtesy of the Chemistry department for tars from both the mesh reactor and fluidised bed. The number average molecular weight of the tars were plotted as a function of peak Pyrolysis temperature (fig MOLW).

Fig.MA1
Cumulative Volatile Yield vs Final Mesh Temperature

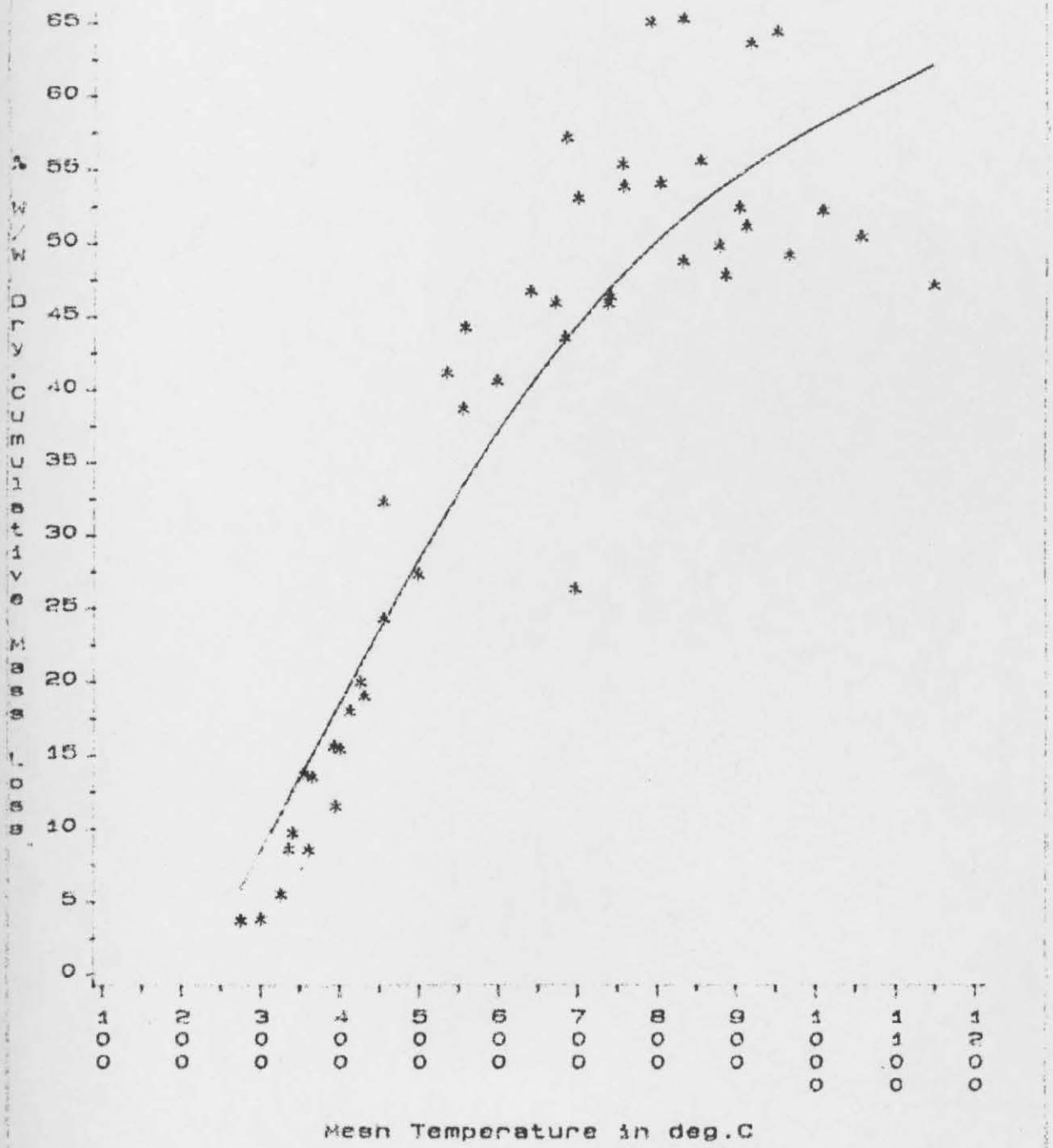

Nonisothermal Expts.
75 micron mesh
Low Loadings
Residence Time at Peak T=10/20ms
M.Main Coal
Atm.P/Dp=75/90,microns
dT/dt=1000 Deg C/s

Fig.MV1
Cumulative Volatile Yield vs Final Mesh Temperature

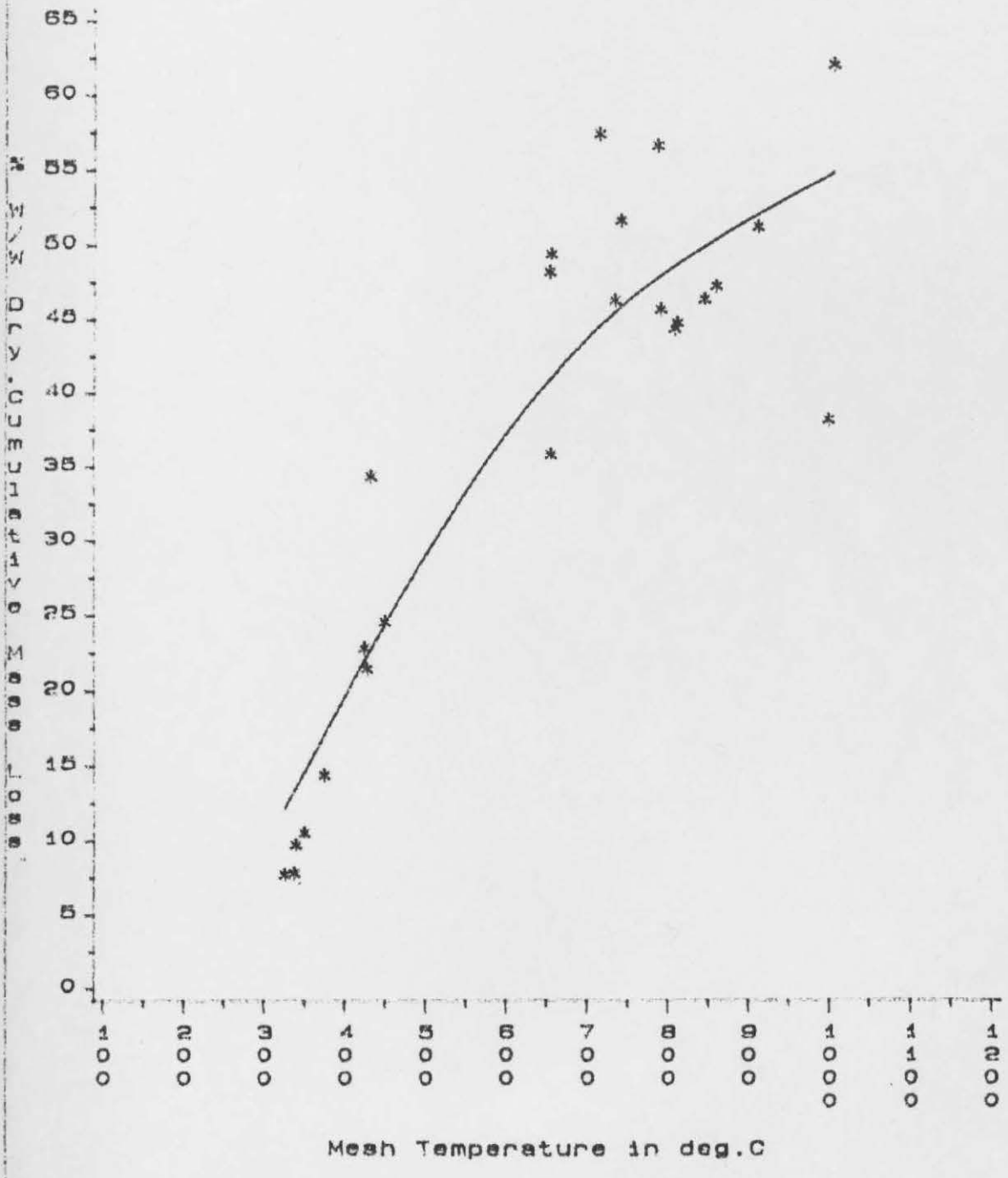

Nonisothermal Expts.
75 micron mesh
Low Loadings
Residence Time at Peak T=10/20ms
M.Main Coal
Vacuum/Dp=75/90,microns
dT/dt=1000 Deg C/s + 60.0 Deg C/s

Fig. MIV
Cumulative Volatile Yield vs Final Mesh Temperature

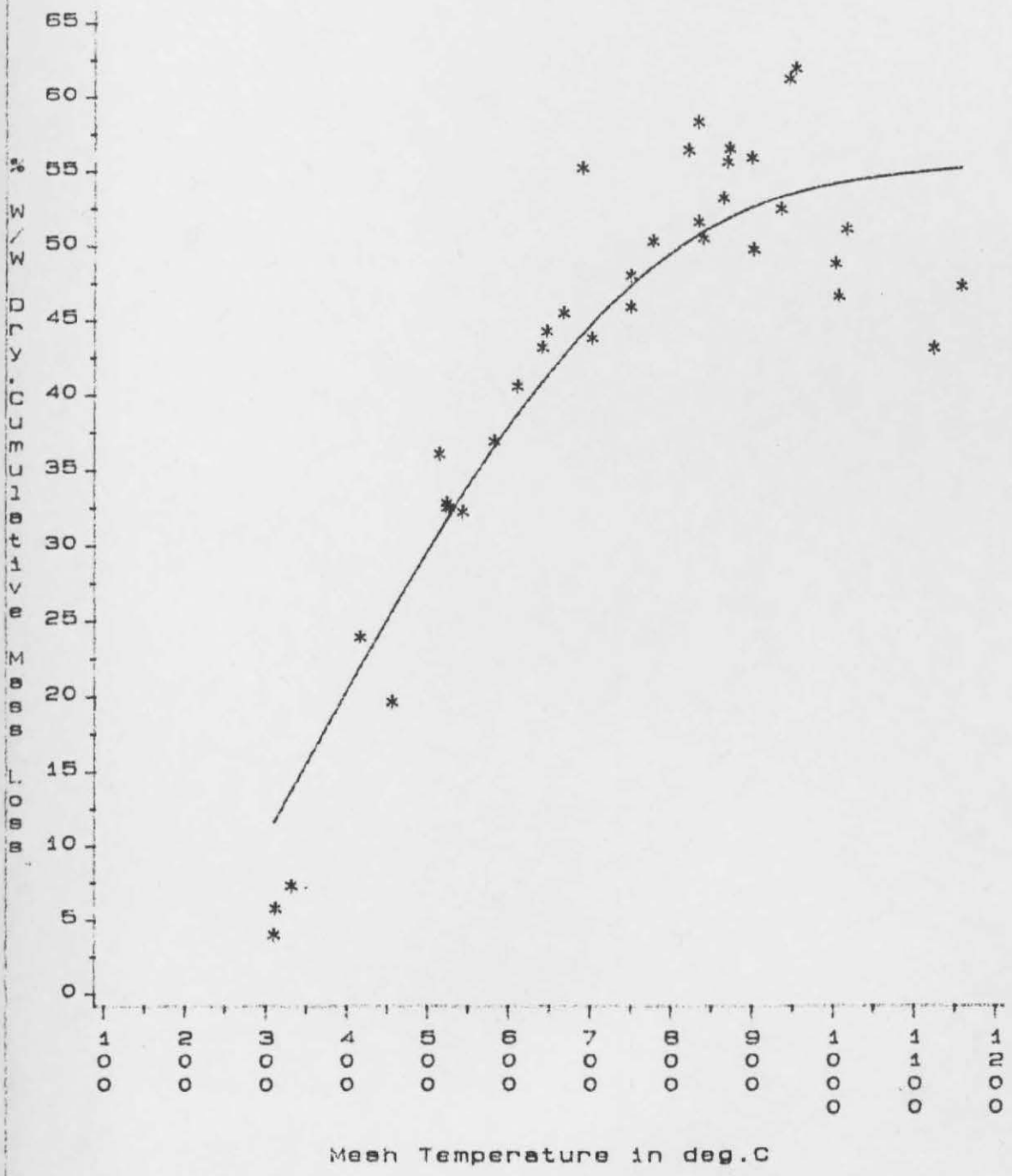

Nonisothermal Expts/Long res. time
75 micron mesh
Load=1.1-2.6mg
Residence Time at Peak T=2.5s
M.Main Coal
Vacuum/Dp=75/90,microns
dT/dt=1005 Deg C/s + 42.0 Deg C/s

Fig.MA5
Cumulative Volatile Yield vs Final Mesh Temperature

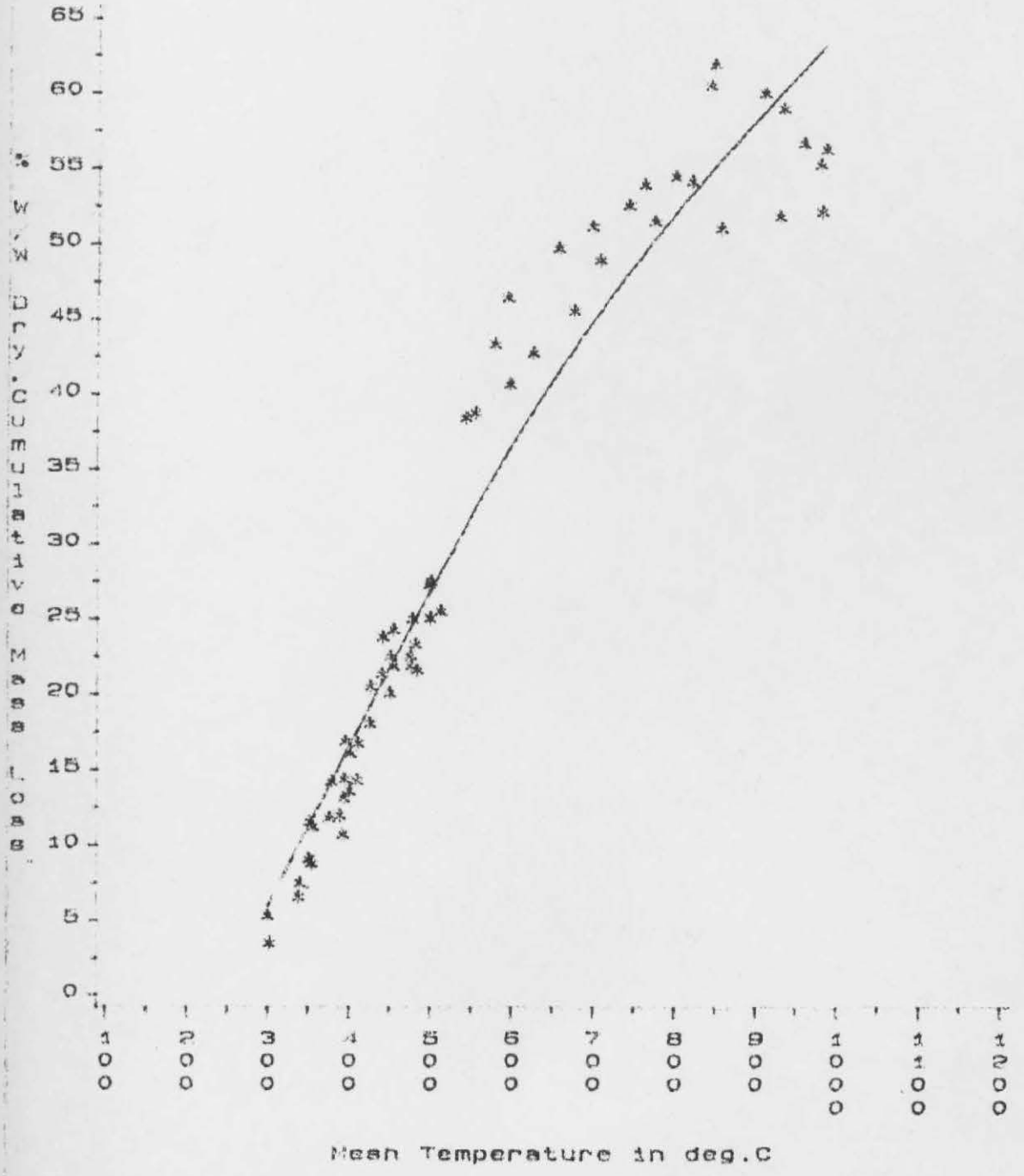

Nonisothermal Expts.
75 micron mesh
Low Loadings
Residence Time at Peak T=10/20ms
M.Main Coal
Atm.P/Dp=75/90,microns
dT/dt=5000 Deg C/s

Fig.5L
Cumulative Volatile Yield vs Final Mesh Temperature

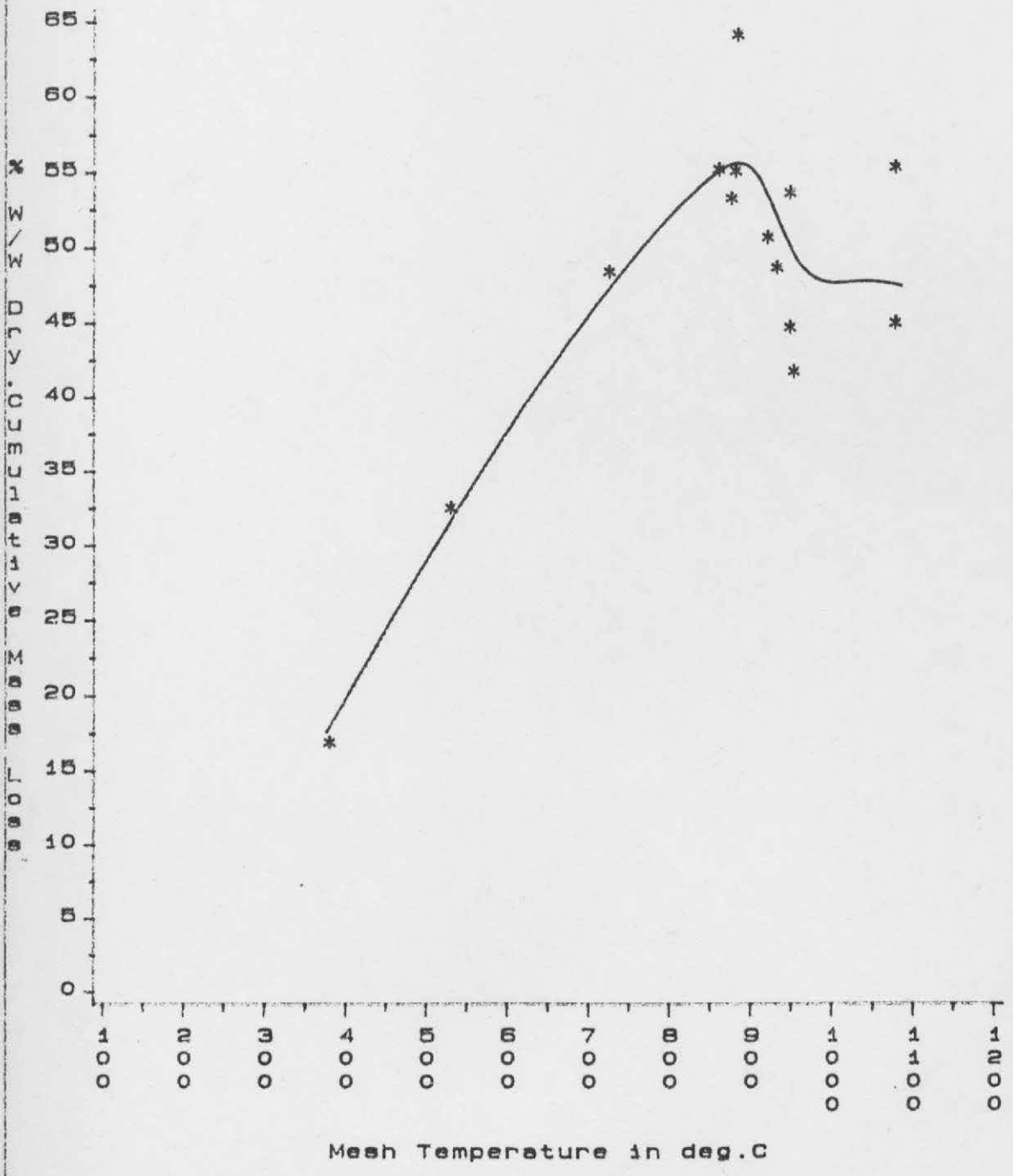

Nonisothermal Expts.
75 micron mesh
Low Loadings(1.0–2.1mg)
Residence Time at Peak T=2.5/4ss
M.Main Coal
Atm.P/Dp=75/90,microns
dT/dt=5000 Deg C/s +52.0 Deg C/s

Fig. MV5
Cumulative Volatile Yield vs Final Mesh Temperature

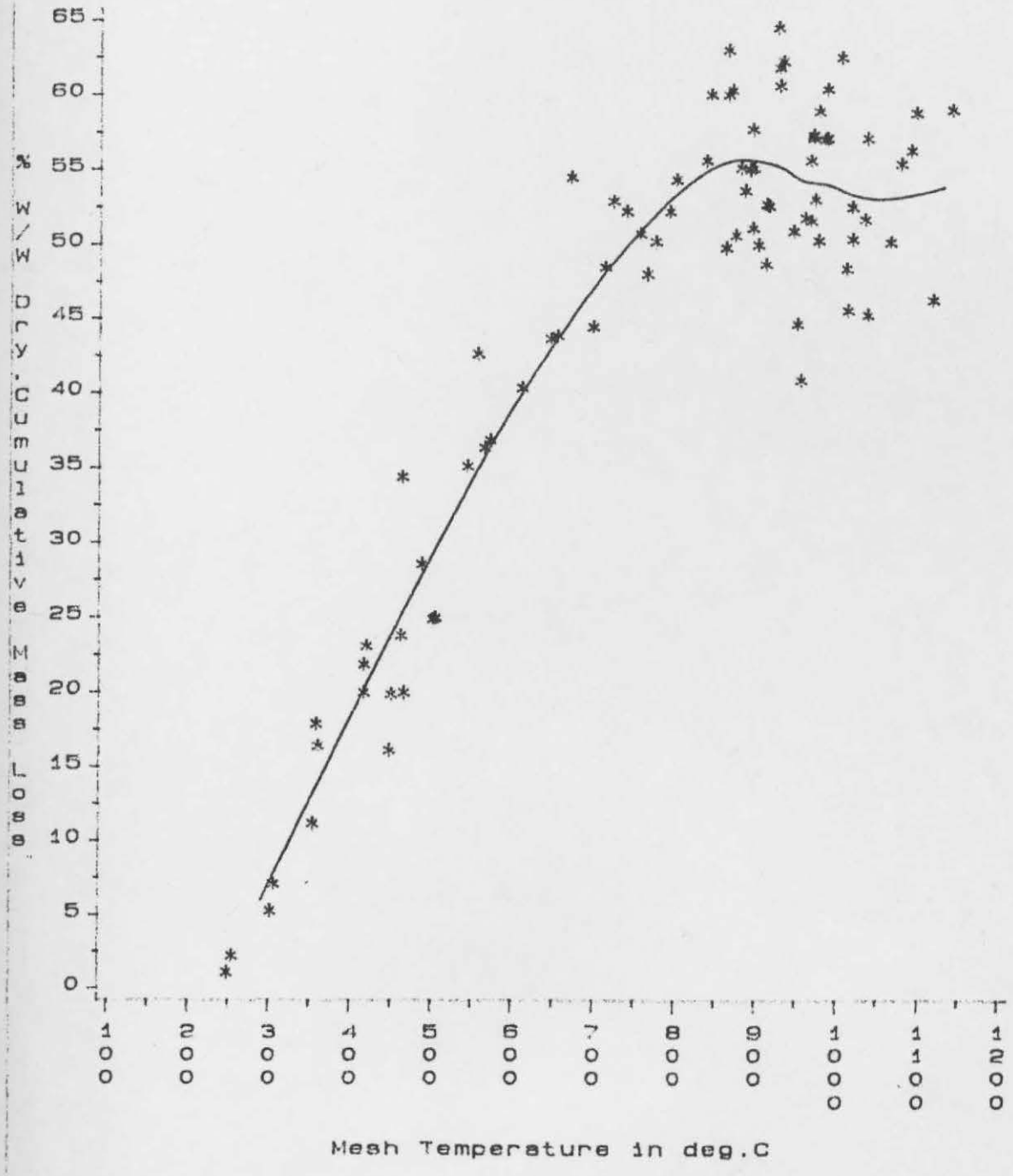

Nonisothermal Expts/Long res. time
75 micron mesh
Load=1.1-2.8mg
Residence Time at Peak T=2.5s/4.0s
M.Main Coal
Vacuum/Dp=75/90,microns
dT/dt=5098 Deg C/s +189.0 Deg C/s

Fig.H1
Cumulative Volatile Yield vs Final Mesh Temperature

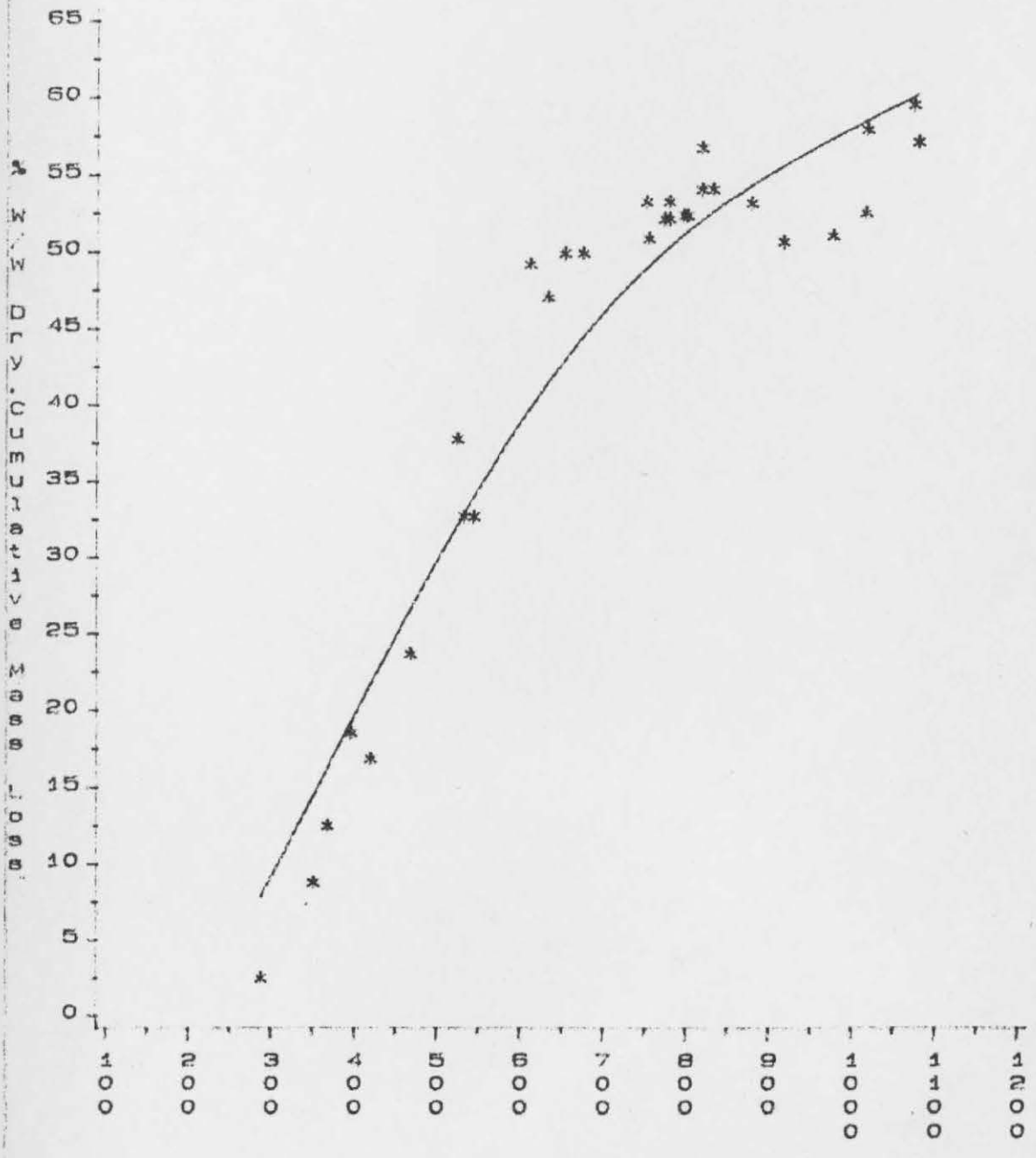

Nonisothermal Expts.
75 micron mesh
Low Loadings
Residence Time at Peak T=10/20ms
Goldthorpe Coal
Atm.P/Dp=75/90,microns
dT/dt=5000 Deg C/s + 48.0 Deg C/s

Fig.GV1
Cumulative Volatile Yield vs Final Mesh Temperature

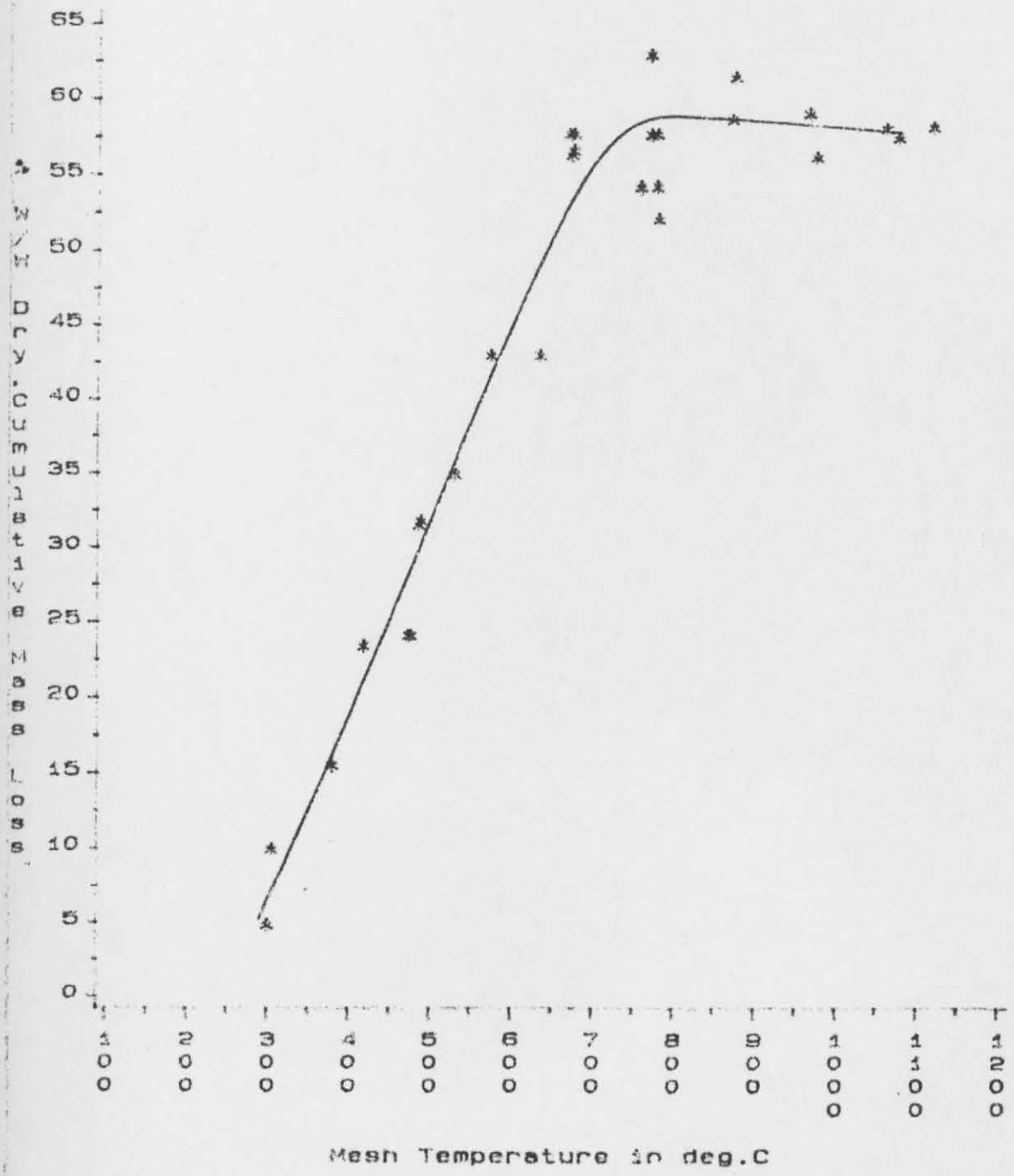

Nonisothermal Expts.
75 micron mesh
Low Loadings
Residence Time at Peak T=10/20ms
Goldthorpe Coal
Vacuum/Dp=75/90,microns
dT/dt=5000 Deg C/s

Fig.G10
Cumulative Volatile Yield vs Final Mesh Temperature

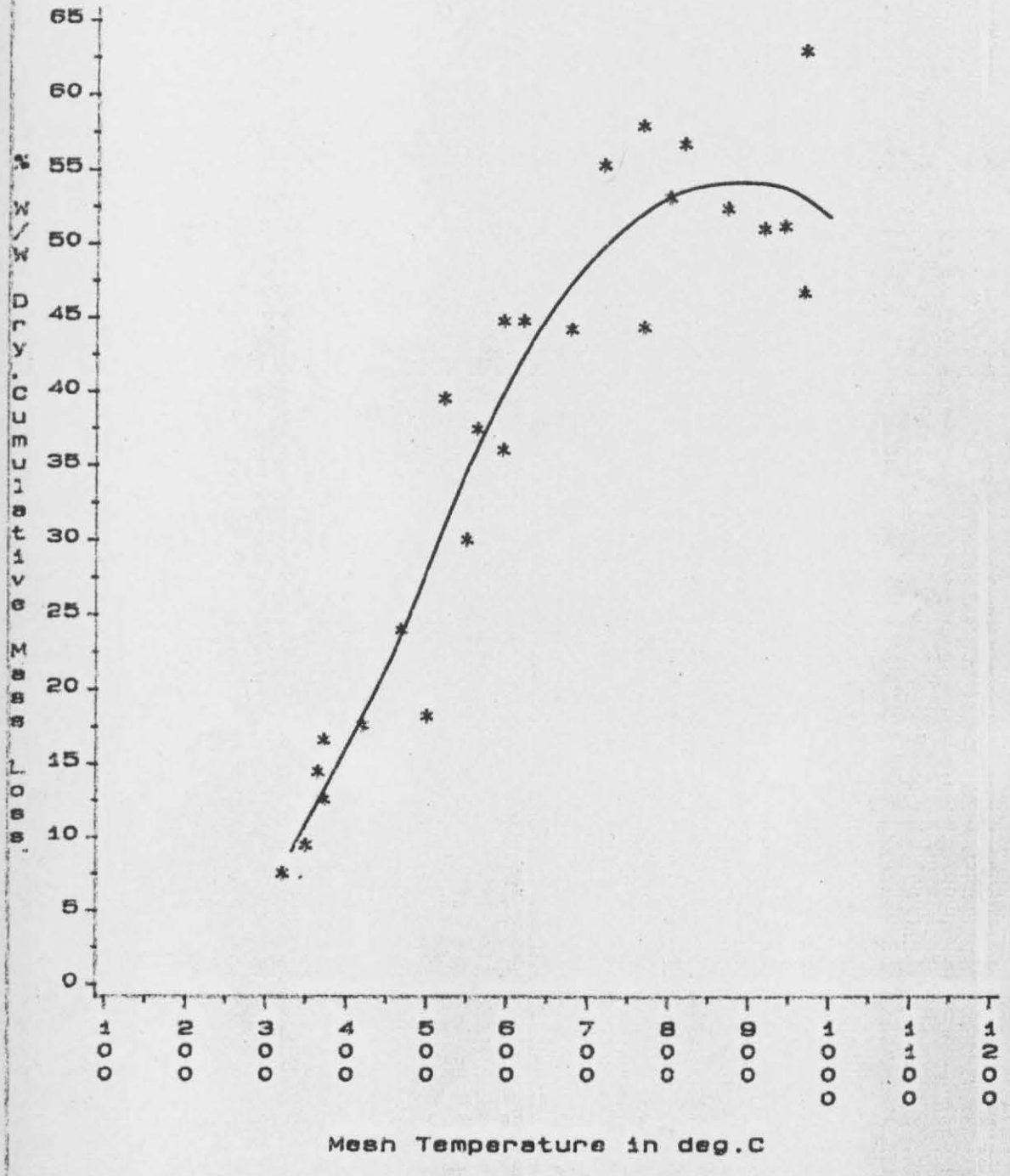

Nonisothermal Expts.
75 micron mesh
Low Loadings
Residence Time at Peak T=10/20ms
Goldthorpe Coal
Atm.P/Dp=75/90,microns
dT/dt=10 Deg C/s

Fig.GV10
Cumulative Volatile Yield vs Final Mesh Temperature

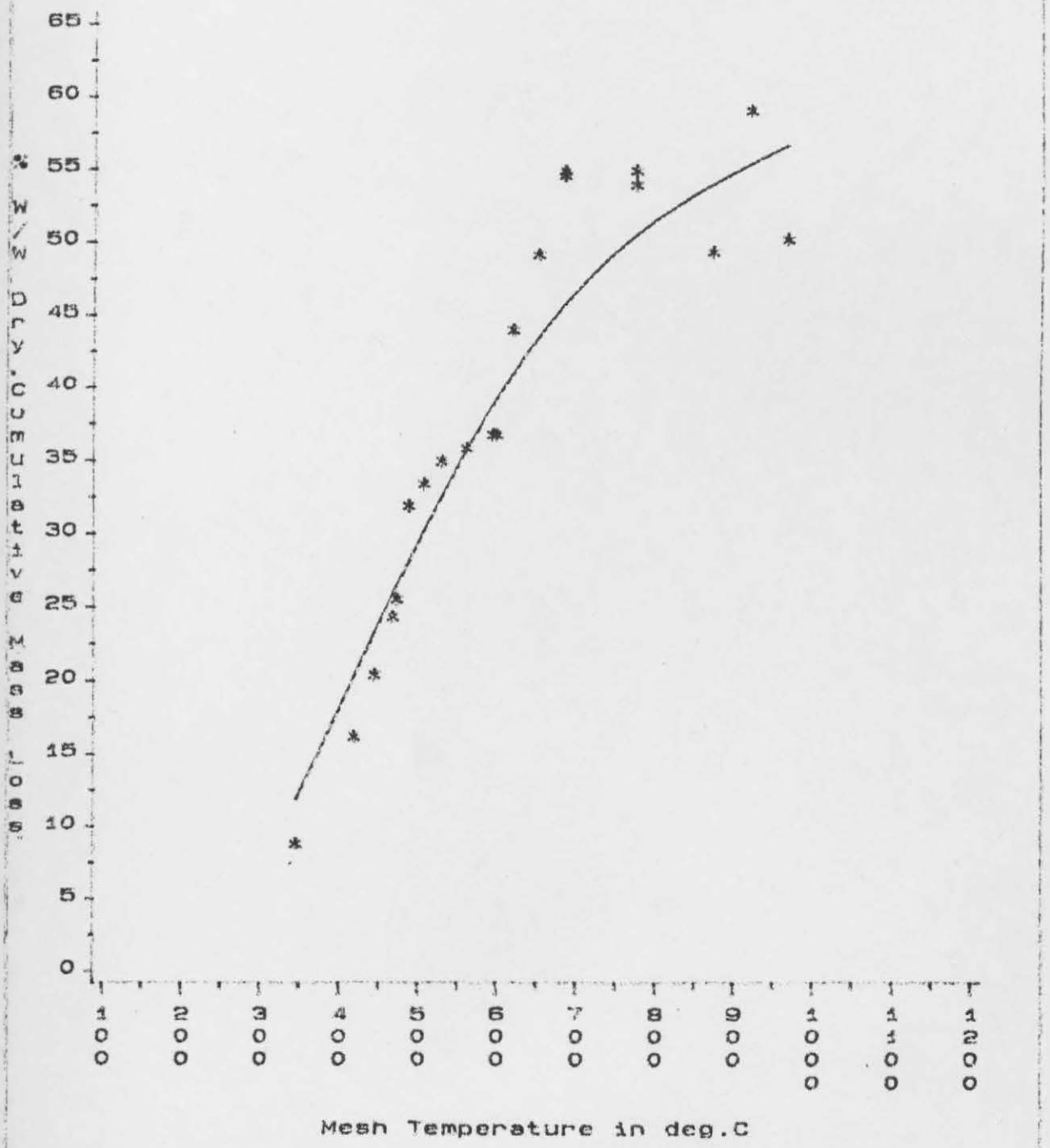

Nonisothermal Expts.
75 micron mesh
Low Loadings
Residence Time at Peak T=10/20ms
Goldthorpe Coal
Vacuum/Dp=75/90,microns
dT/dt=10 Deg C/s

Fig.M1
Cumulative Product Composition vs Bed Temperature

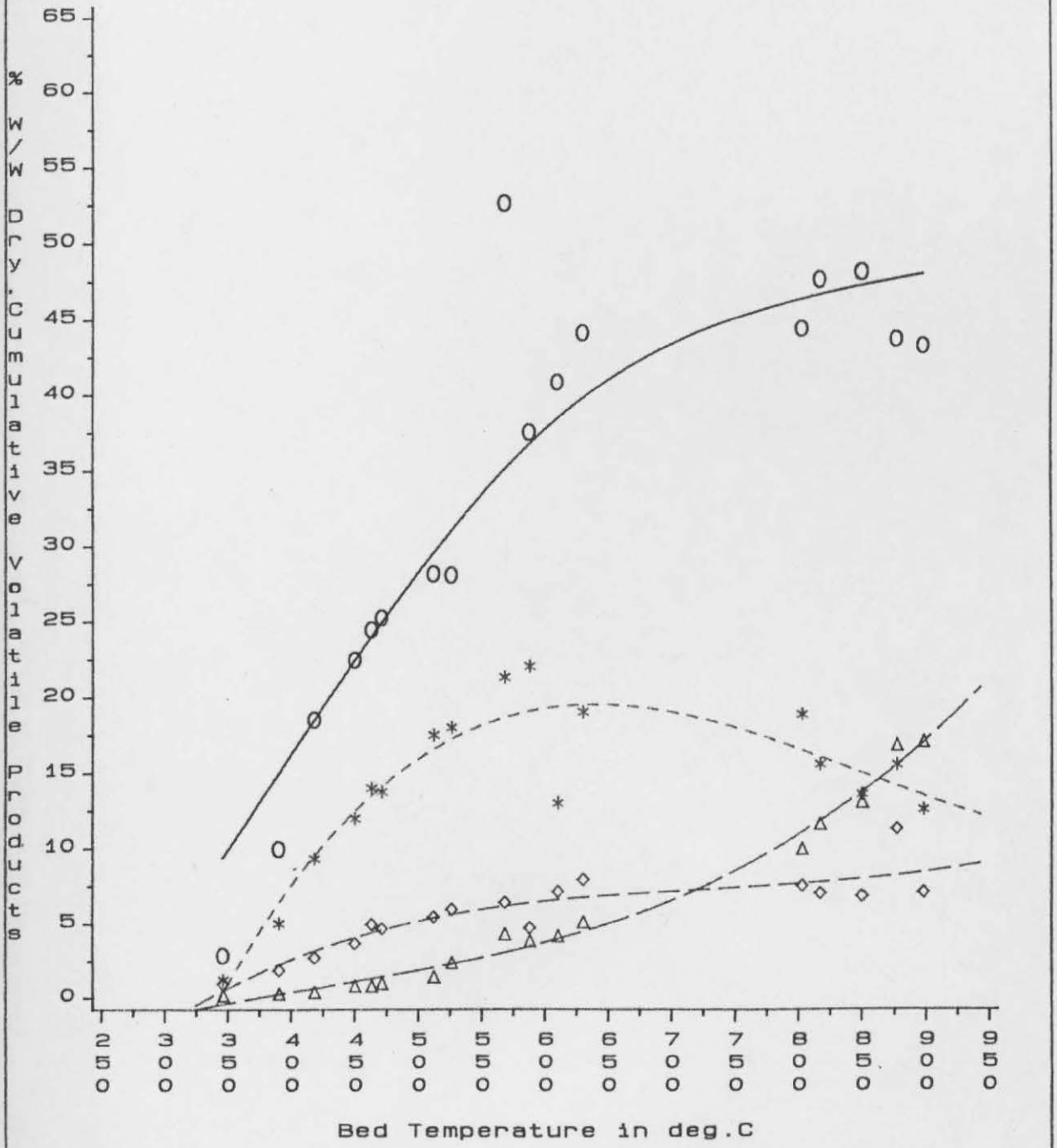

Total Volatiles Yield O
Tar Yield *
Liquids Yield △
Gas Yield ◇

M.Main Coal,75/90 microns
Atm.pressure,N2 Fluidising gas
Fluidised Sand Bed

Fig.G1
Cumulative Product Composition vs Bed Temperature

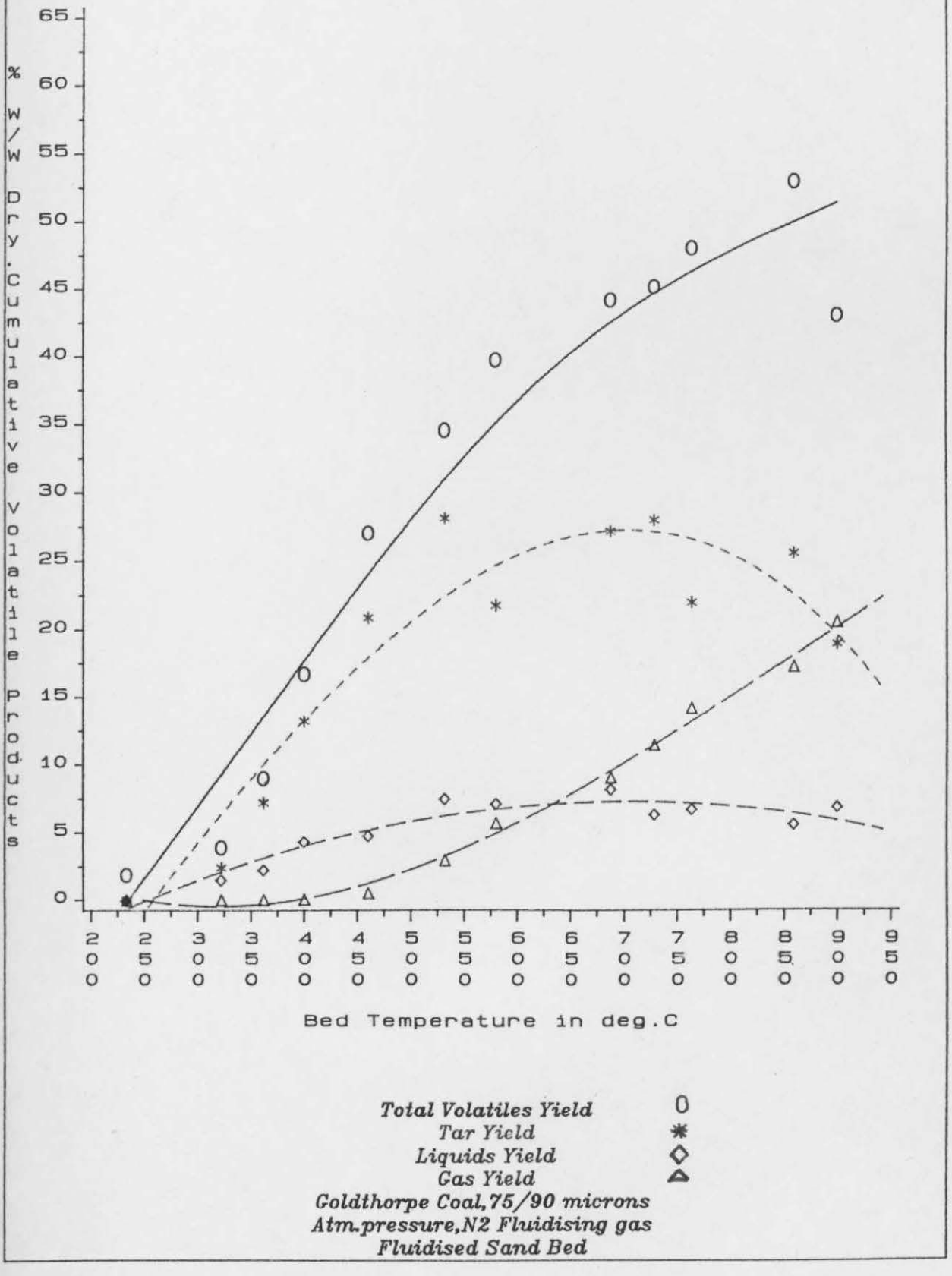

Fig. MMIC
Fractional elemental composition vs Temperature

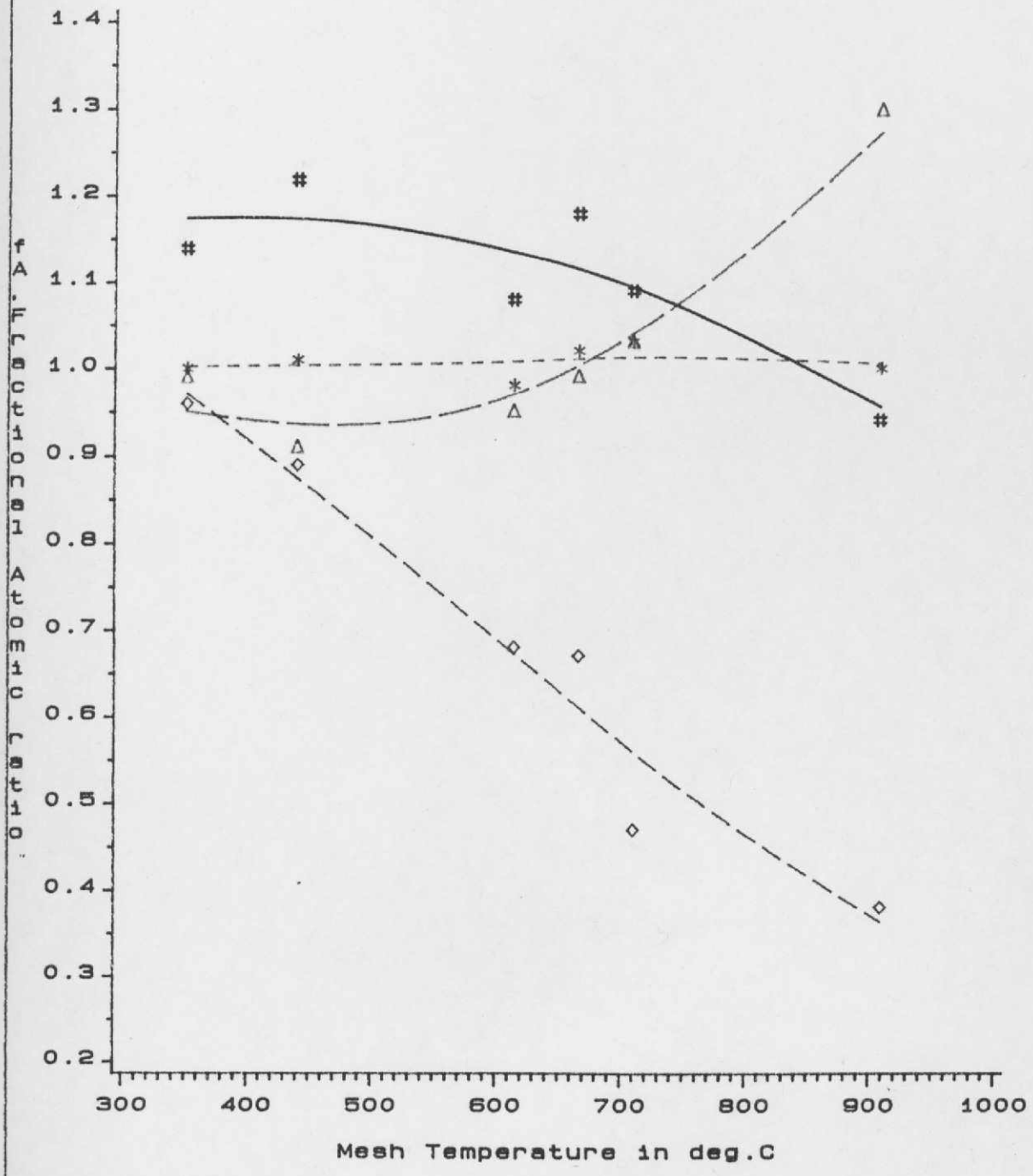

fA(Nitrogen) #
fA(Carbon) *
fA(Hydrogen) ◇
fA(O2+S) △

Markham Main Char
Atm.Pressure,75/90 microns
dT/dt=1000 degC/sec

Fig. MMP
Fractional elemental composition vs Temperature

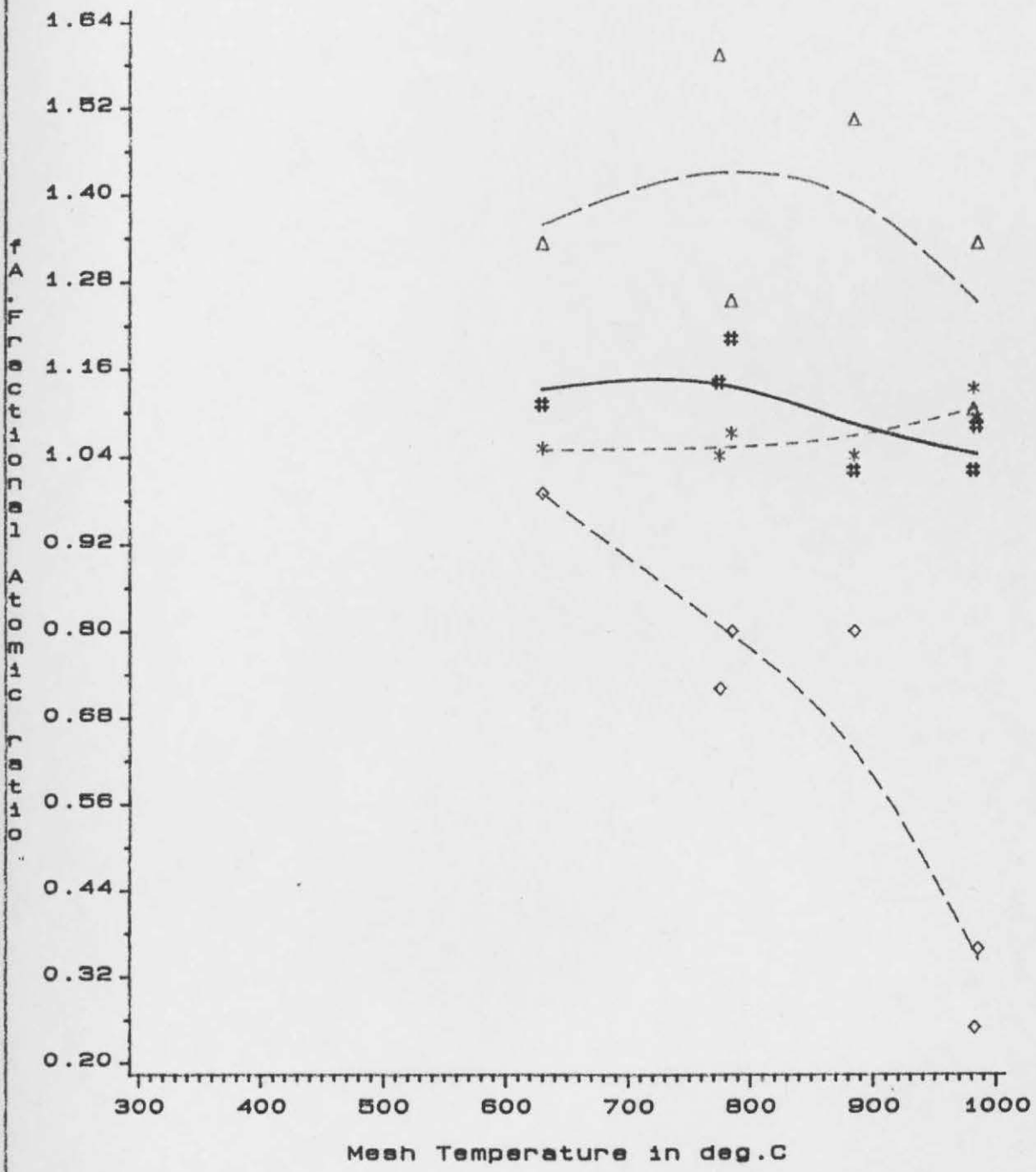

fA(Nitrogen)
fA(Carbon)
fA(Hydrogen)
fA(O2+S)

Markham Main Char
Pressure=20 bar,90/150 microns
dT/dt=1000 degC/sec

Fig. MMAM
Fractional elemental composition vs Temperature

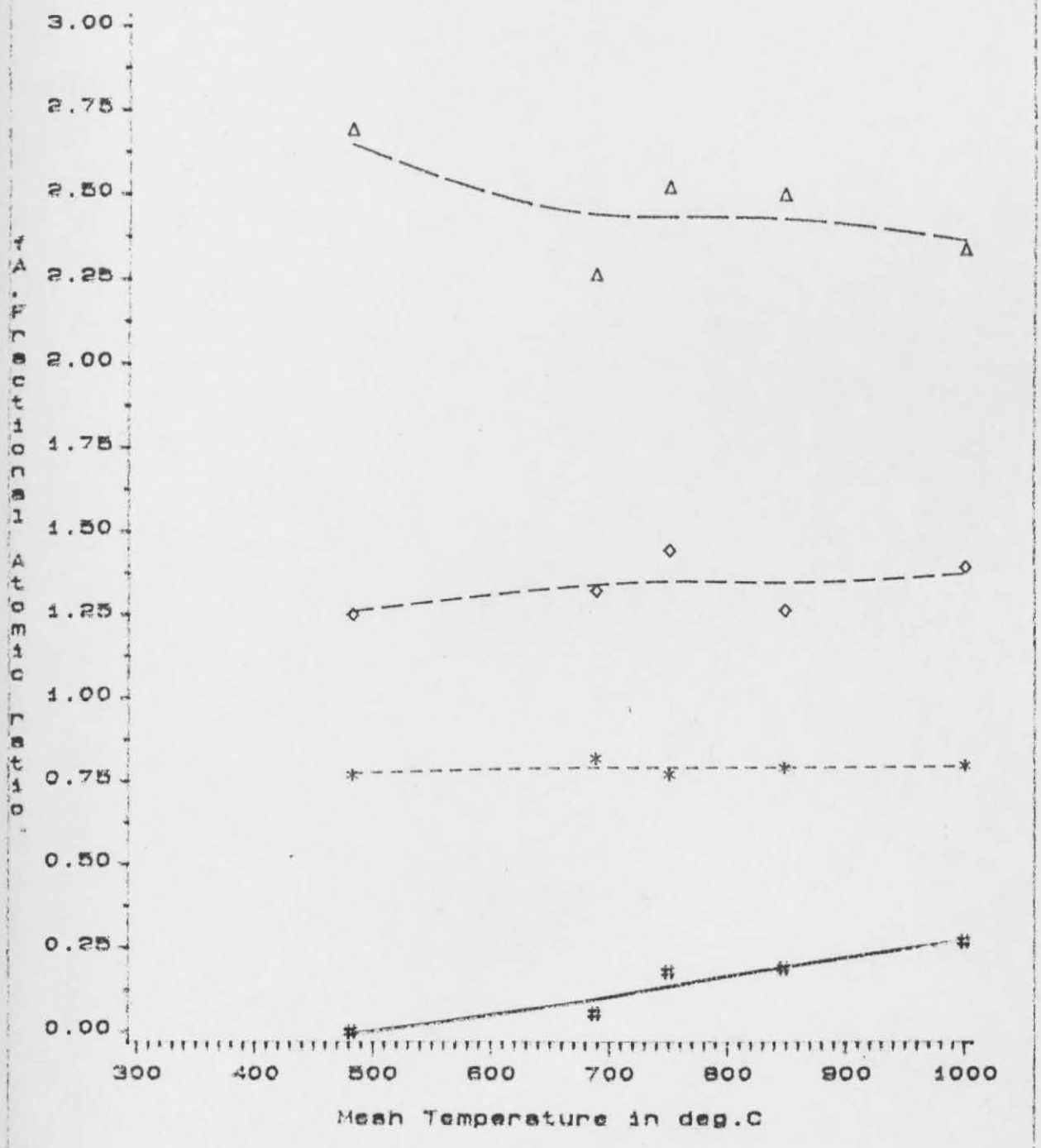

Fig. MMVM
Fractional elemental composition vs Temperature

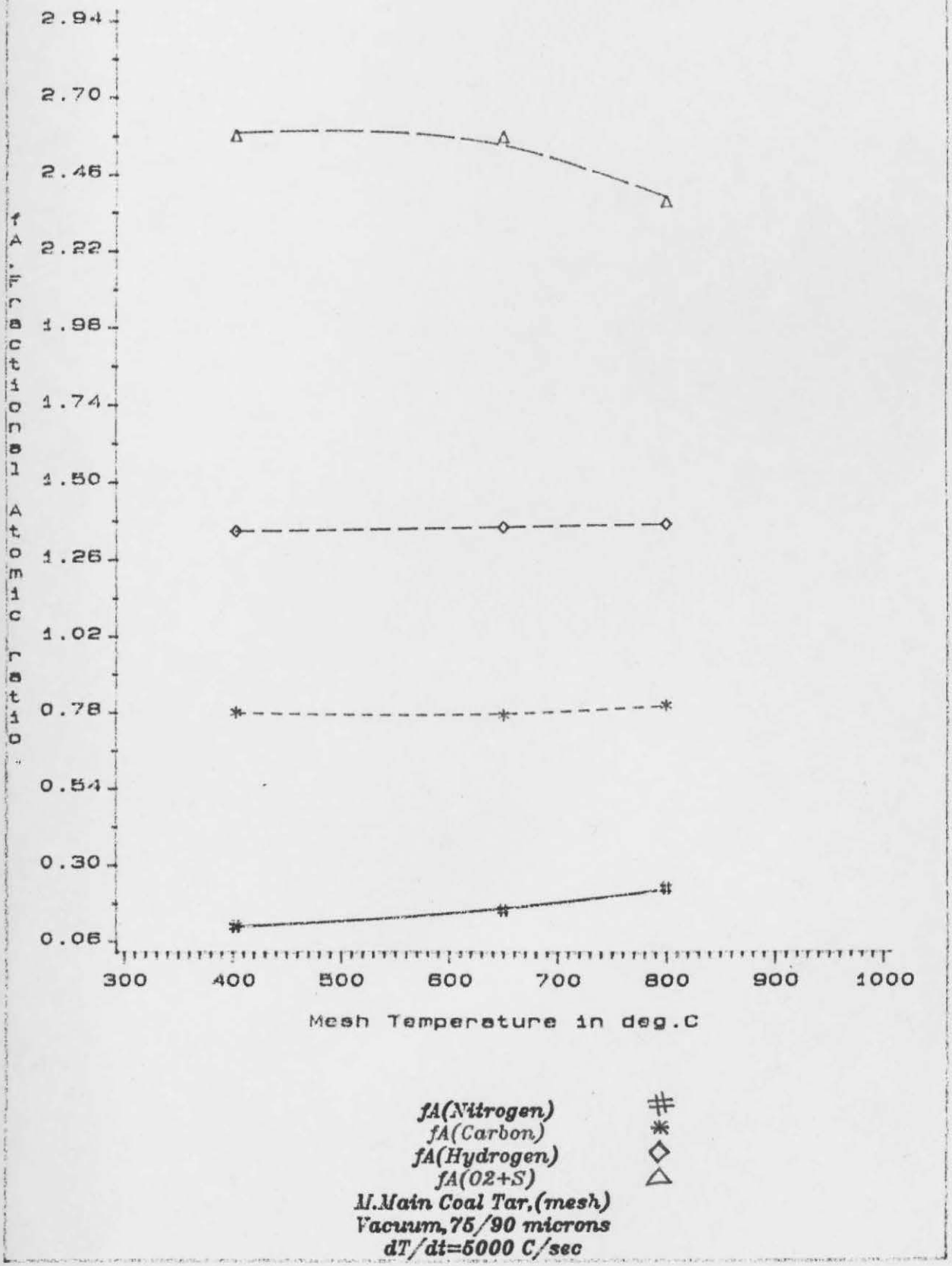

Fig. MMVI
Fractional elemental composition vs Temperature

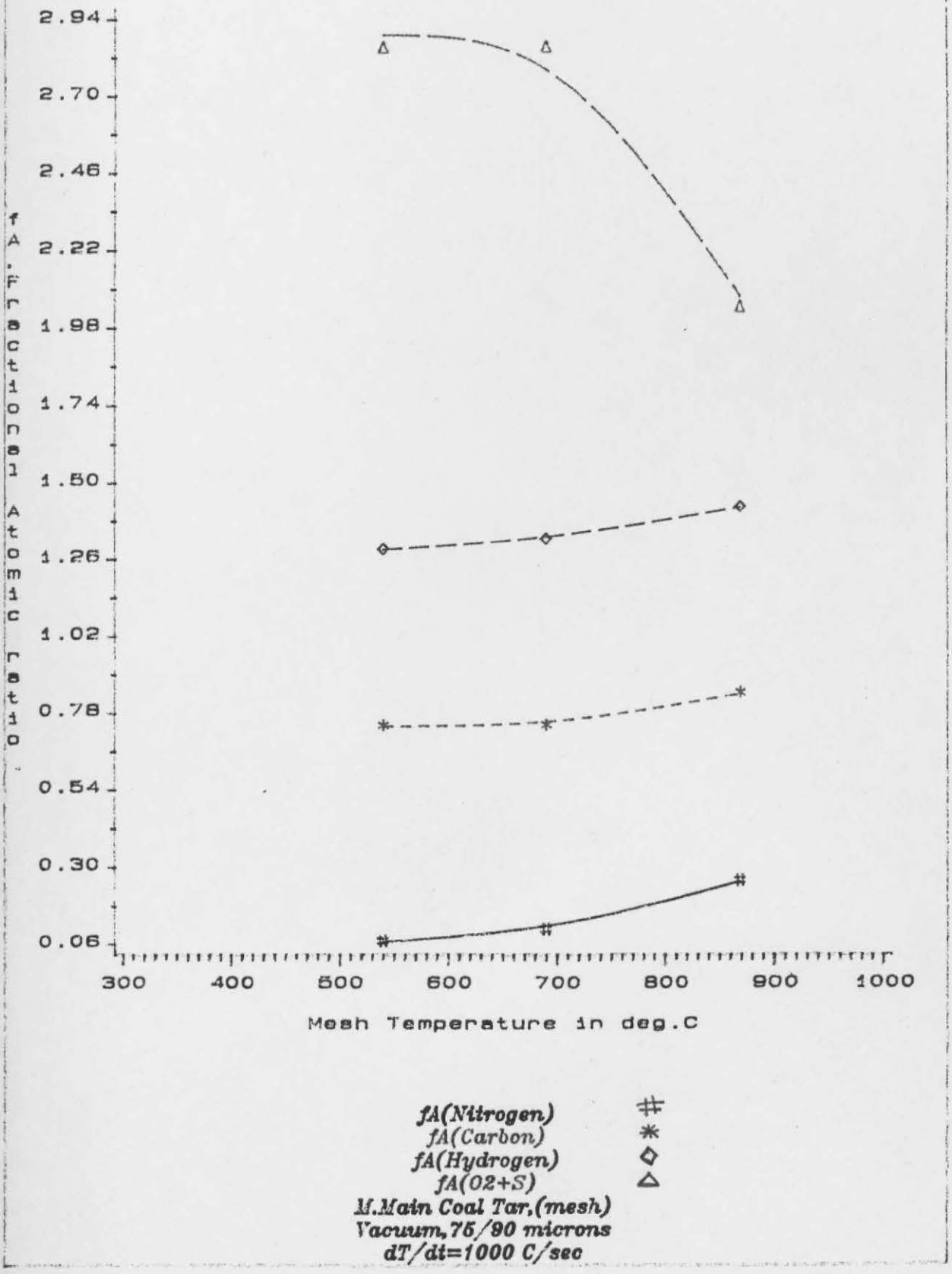

Fig. FBA
Fractional elemental composition vs Temperature

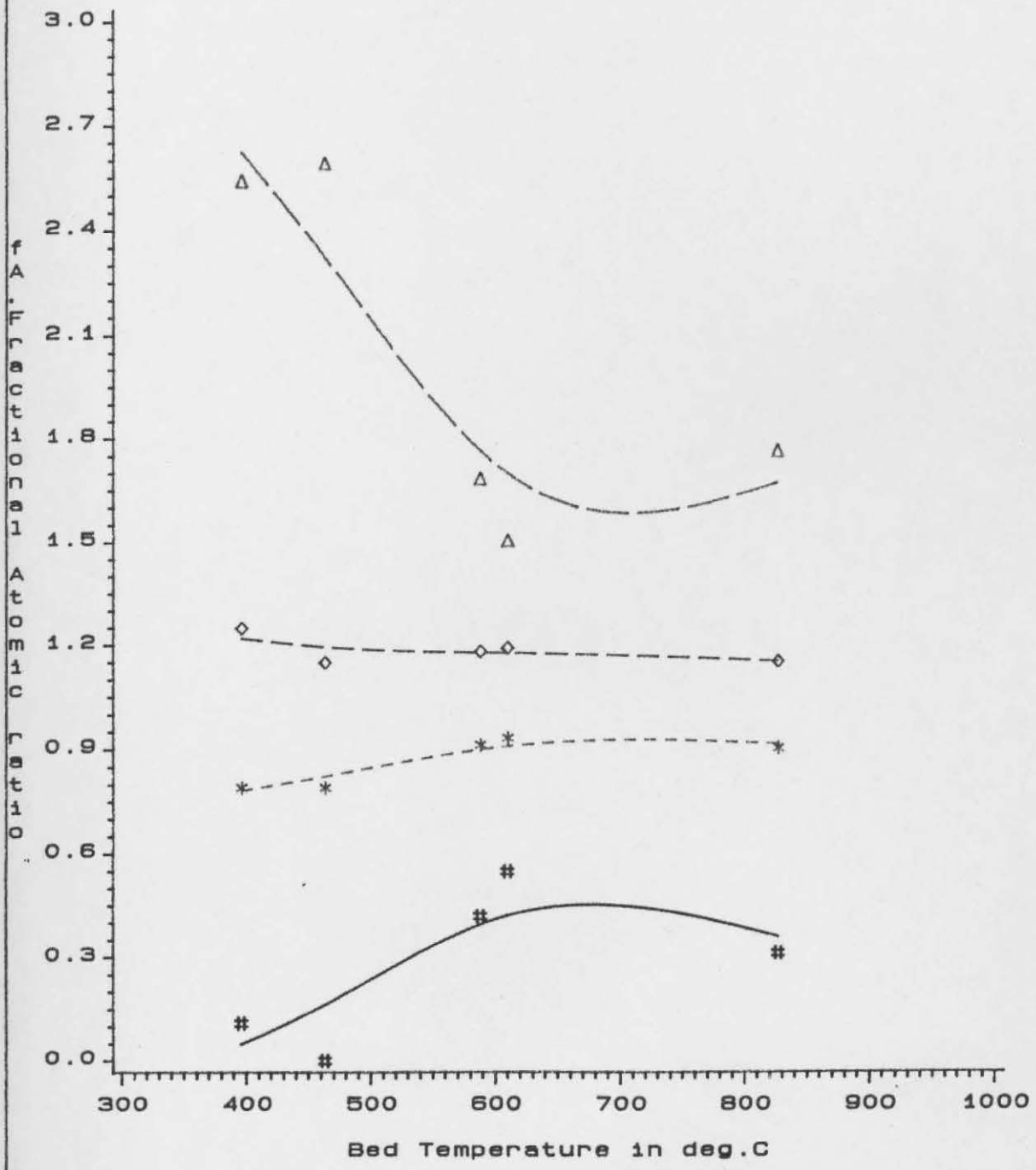

fA(Nitrogen) #
fA(Carbon) *
fA(Hydrogen) ◇
fA(02+S) △

M.Main Coal Tar,(F.B.)
Atm.Pressure,75/90 microns
Fluidised Bed

Fig. FBG
Fractional elemental composition vs Temperature

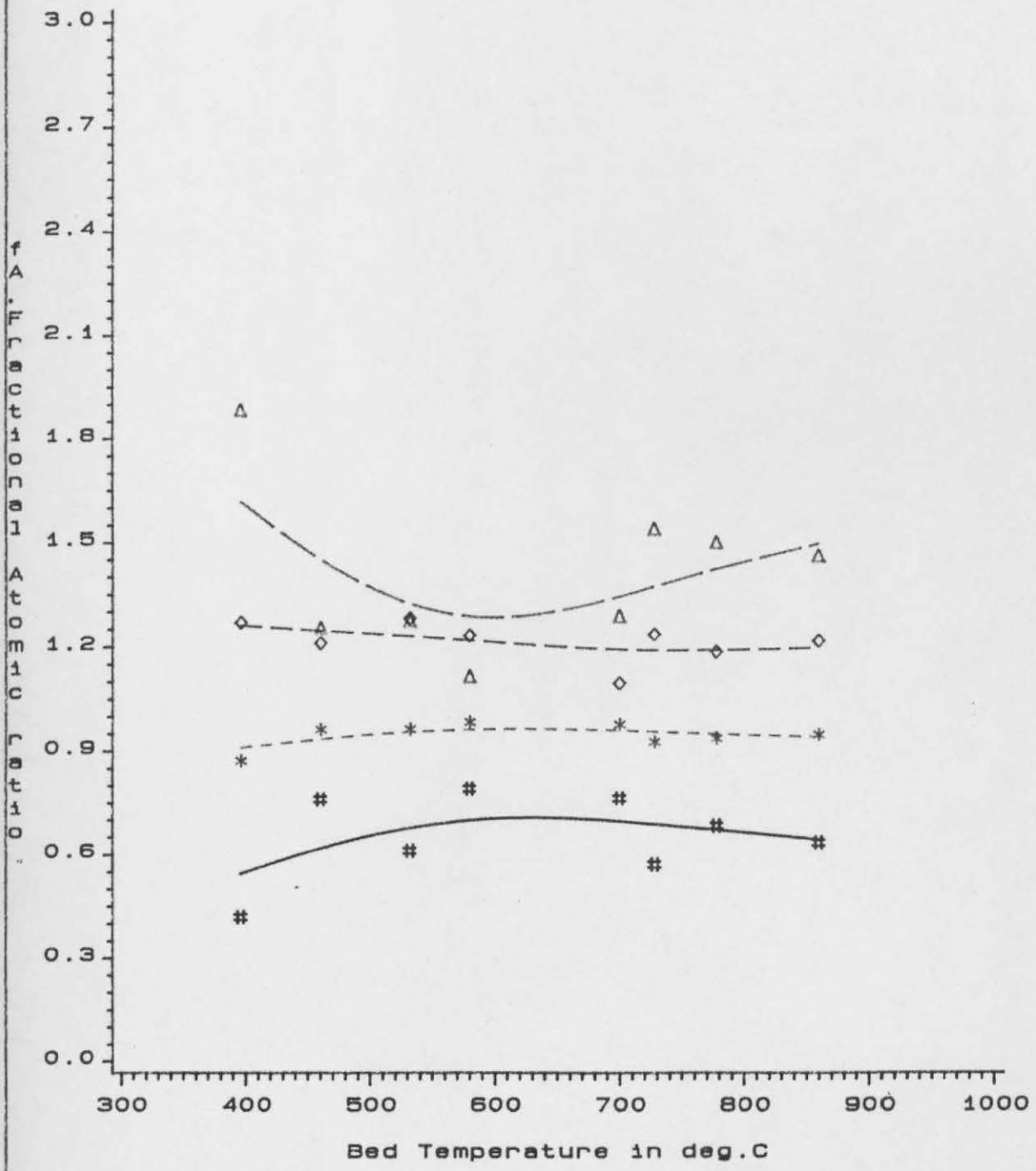

fA(Nitrogen) #
fA(Carbon) *
fA(Hydrogen) ◇
fA(O2+S) △

Goldthorpe Coal Tar,(F.B.)
Atm.Pressure,75/90 microns
Fluidised Bed

Fig.M2
Elemental composition vs Temperaperature

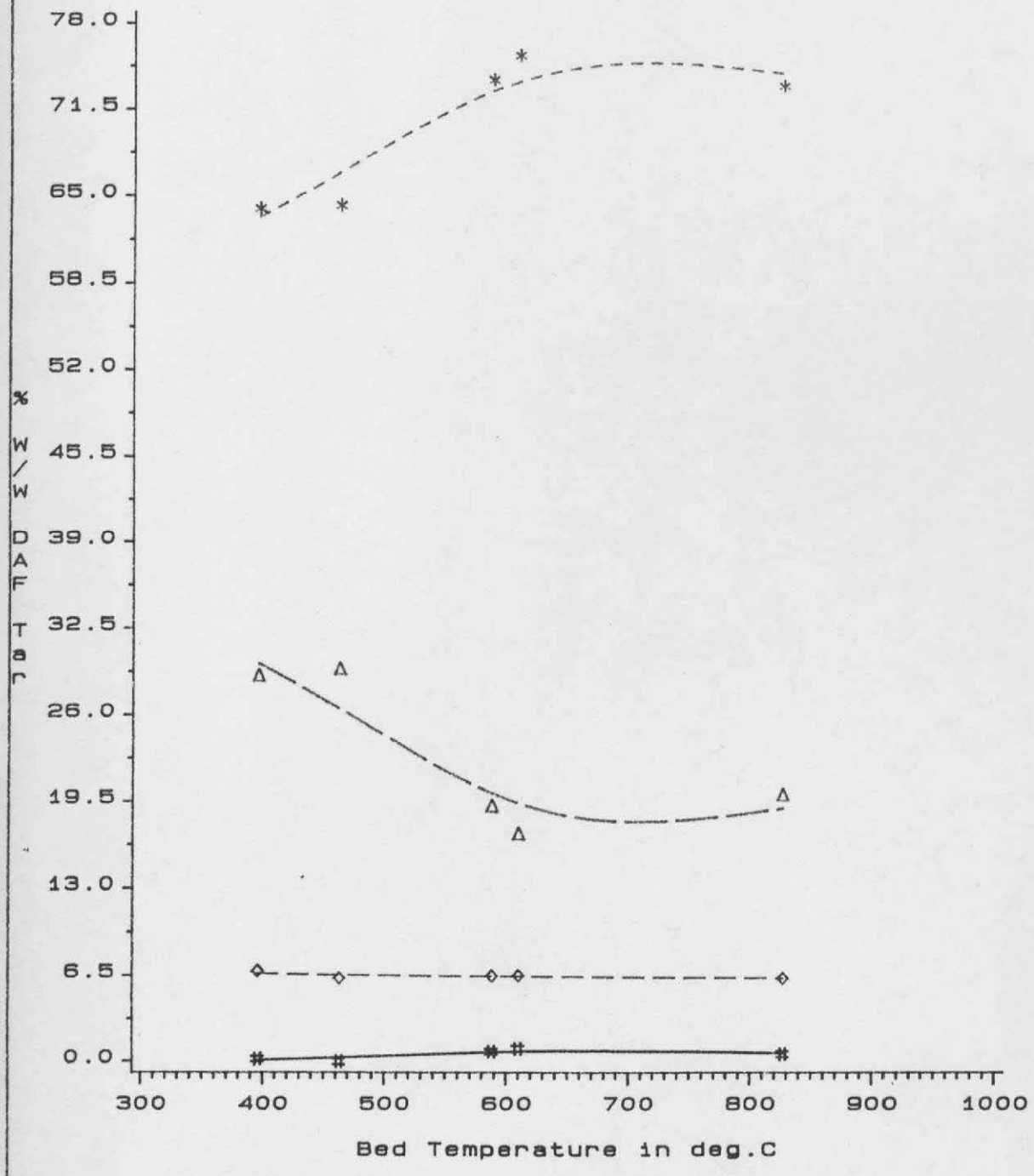

Nitrogen
Carbon
Hydrogen
02+S

M.Main Coal Tar,(F.B.)
Atm.pressure,75/90,microns
Fluidised Bed

Fig.GT
Elemental composition vs Temperature of Bed

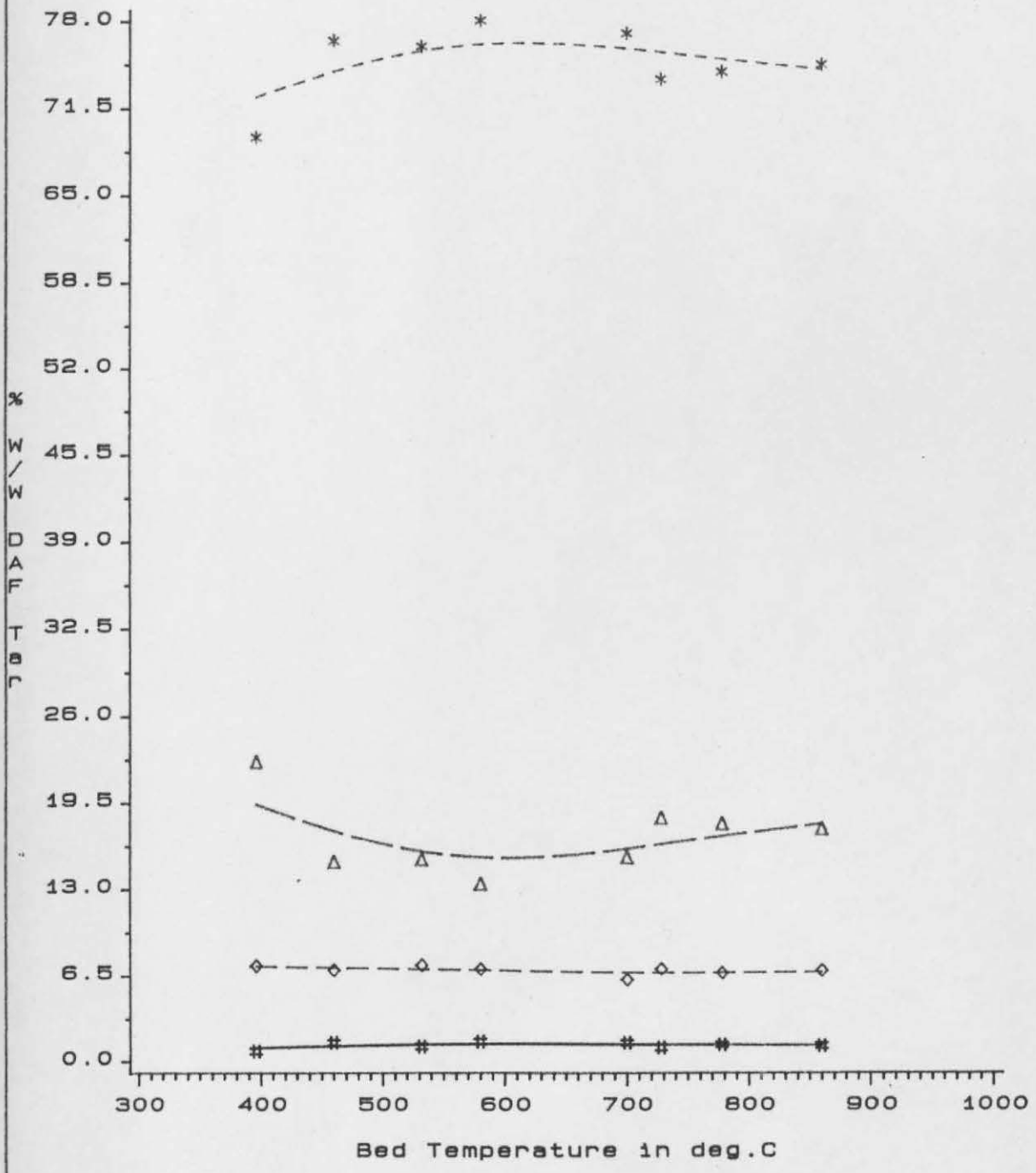

Nitrogen #
Carbon *
Hydrogen ◇
O2+S △

Goldthorpe Coal Tar,(F.B.)
Atm.pressure,75/90,microns
Fluidised Bed

Fig.MOLW

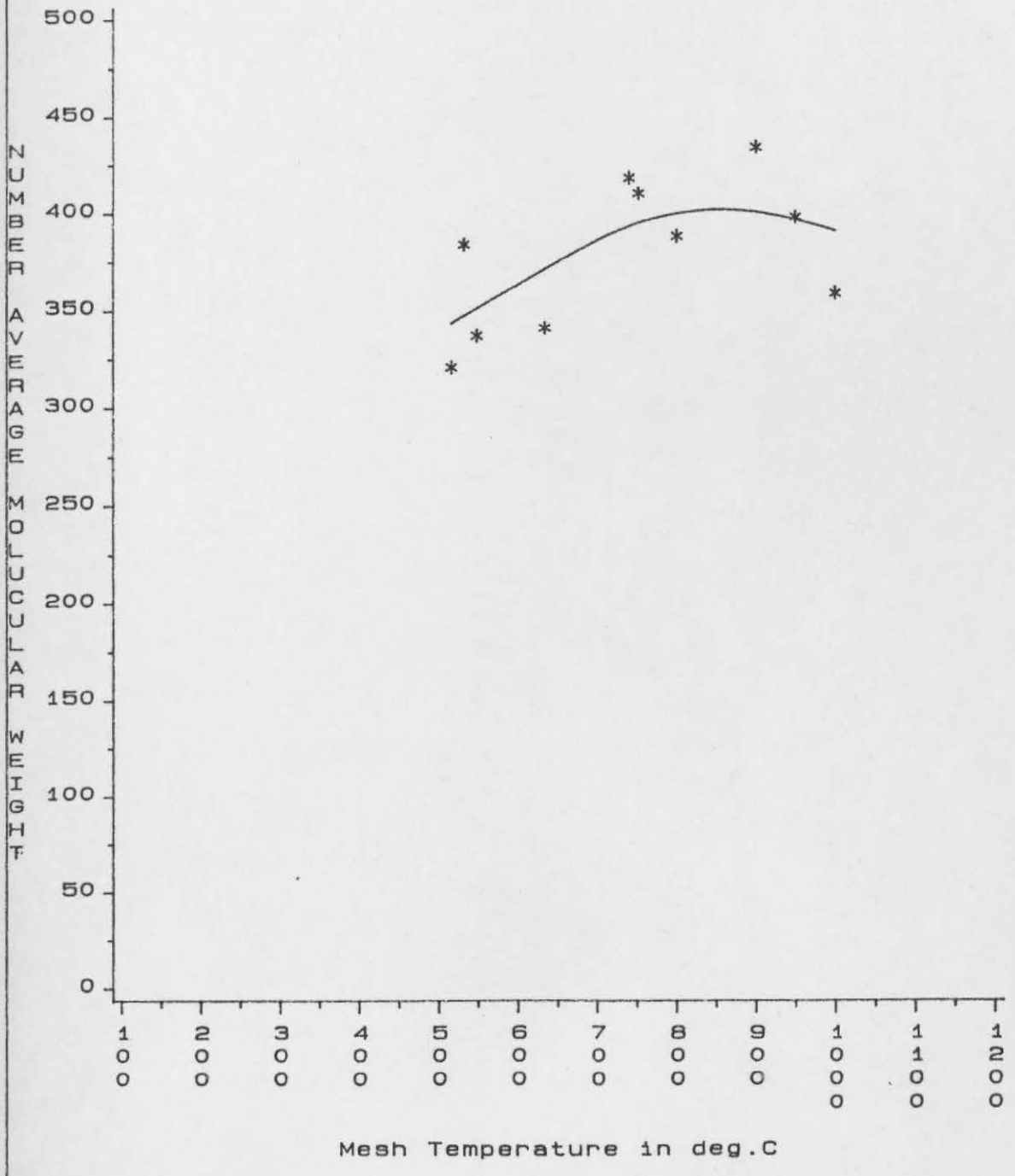

Mesh Expts.
75 micron mesh
Variable Loadings

M.Main Coal
Atm.P&Vacuum /Dp=75/90,microns
dT/dt=1000-5000C/s

The curves have been fitted by a curve fitting routine using the cubic spline method and do not represent model fits (apart from gas yields for the mesh), which will be described in the next chapter. The fitted data was useful for comparative purposes for assessing trends with regard to the variables of heating rate, pressure and residence time variations. It can be seen that weight loss is rapid and occurs substantially during the heat up period. Thus further heating at the peak temperature makes little difference to the ultimate yield (apart from an effect on gas distribution). Reference to higher mass load (75 um) curves (fig MI) will indicate a very low rate of degasification in the asymplotic period. The scatter in the data is such that the low rate of degasification is not revealed in the low mass load studies. However, the gas analysis results indicate that substantial evolution of light gaseous species occur throughout the temperature range of their appearance and most of the evolution occurs during the heat up time of the particle, including their short residence time at the peak temperature (10-40 milliseconds). Nonetheless, there is an increase in gas yield with residence time at the peak temperature revealed by the gas analysis which reflect process parameters such as heating rate, external pressure and residence time at the peak temperature. By representing products such as CH_4, C_2H_4 and C_3H_6, H_2 and C_2H_2 as representative of particular groups of species such as saturates, unsaturates, char degasification and ring fragmentation and/or soot precursor species (C_2H_2 and C_4 unsaturates), some trends may be elucidated. This will be described in later sections.

The overall mass loss curves reveal features which are substantially different from those such as revealed by heating the coal in loose packings in the 50 μm mesh screen. In the latter case the yield is a function of two time scales, a heating up time scale (nonisothermal yields) and an isothermal time scale (heating time at the peak temperature). In the low mass load studies where particles are heated at the same rate as the containing mesh reactor, most of the mass loss occurs during heat up to peak temperature. This is in agreement with more recent studies conducted in entrained flow reactors where conditions are conducive to better heat transfer.[57] Freihaut et al in their studies, using the mesh technique also concluded that substantial mass loss occurs during particle heat up.

The following trends are noted:

1) Ultimate yield is independant of imposed heating rate for medium heat fluxes and rapid quenching of products. This is revealed by the fluidised bed results which show agreement with the mesh results over the temperature range 300-650^{o}C. . However, at higher temperature substantial sooting is observed with the fluidised bed, with high acetylene, C_4 unsaturates and allene formation. Extensive sooting and cracking of products over char covered surfaces lead to diminished total yields at the higher temperatures for the fluidised bed.

2) External pressure has minimal effect on total mass yields provided product removal is not inhibited. (This is true over pressure conditions from low vacuum (0.5-5 torrs) to 1 atmosphere and 75/90 μm particles of the high volatile,

low caking coals used in this study). A small effect of enhanced yield is observed for the Markham Main coal at longer residence times under vacuum conditions over the temperature range 600-850^{o}C. A similar enhancement in yield is observed for the Goldthorpe coal at short residence times for the vacuum runs at 5000^{o}C/S. However, this is not clearly distinguishable within the scatter exhibited by the data.

3) The curves do not reveal an inflexion at low temperatures (around 450-600^{o}C) such as exhibited by yield curves using loose packings. Such inflexions in the overall yield curves are noted for the case of loose packings in the 50 μm case where it is suspected that heat transfer effects operate. Reference to Suuberg's study [19] will reveal that this inflexion (over 400-700^{o}C) disappears as the pressure of the diluent He gas surrounding the coal particles is increased from 1 atm to 69 atm. (Refer to fig (SUA)). The increase in pressure must lead to an increase in interphase heat transfer from the low pressure case, thus diminishing any temperature lags between particulate phase and the heated gas phase.

Extant curves on weight losses in the fluidised bed also reveal high yields at low temperatures (400-500^{o}C). Thus the yield curves for the fluidised bed agree substantially with the mesh yield curves. However, Tyler et al did note a diminished yield at lower temperatures (below 650^{o}C) which was attributed to residence time differences of the char in two different fluidised bed systems. This may arise

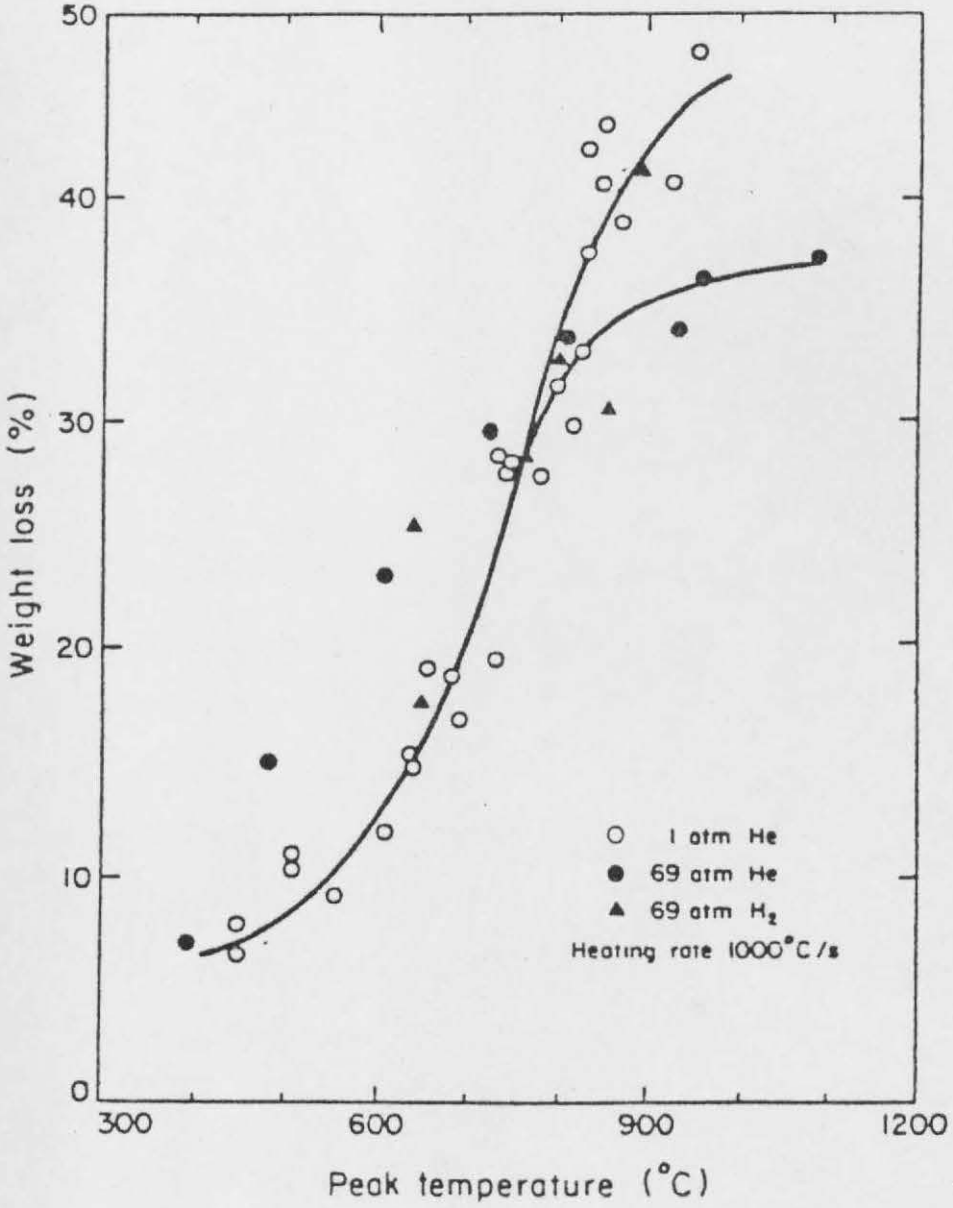

Fig. SUA Weight loss vs. peak temperature for pyrolysis and hydropyrolysis of a bituminous coal "Pittsburgh No. 8 Re: Suuberg et al.

from differences of techniques used to measure yield. In the lower yield case, char was withdrawn and yield measured by the ash tracer method, whereas in the other case direct weighing of the bed was performed. Nonetheless, this does not explain the agreement in yield noted at the higher temperatures. Both yield curves, however, do not show inflexions at the lower temperatures in agreement with the yield curves obtained by the author.

4) Some of the curves in the mesh reactor indicate a depression of yield at high temperatures (>850^{o}C in Goldthorpe case and 950^{o}C in the Markham Main case). Whilst this could not be clearly delineated, it is apparent that a different kind of rection may be operating at these temperatures. The appearance of higher yields of C_4 unsaturates (Butadiene, cis and trans Butene, But-1-ene), allene and C_2H_2 at these temperatures suggest cracking reactions occurring which is substantially accelerated in the fluidised bed reactor at lower temperatures (700-900^{o}C). Further, the elemental analysis reveals increasing heteratom removal from the char such as 'N' and O_2 & S at the higher temperatures. These polar groups attached to thermally resistant structures may lead to repolymerization and thus char forming reactions in competition with removal of products by radical stabilisation routes. In fact reference to the elemental distribution data for the M. M. char (figs MMIC and MMP) show indications of 'O_2 + S' heteroatom trapping in the char.

5) The elemental analysis of the tars evolved from the mesh at high heating rates show enrichment in 'H' relative to the parent coal and somewhat higher than tars from the fluidised bed. There appears to be minimal variation in 'H' and 'C' content with temperature, heating rate or external pressure for the mesh tars in agreement with the slight variations in Number Average Molecular weights obtained from a mix of reaction conditions. The removal of 'O' and 'S' species (obtained by difference) at the higher temperatures and the increasing appearance of 'N' in the tars at higher temperatures may account for the diminished molecular weights of tars at the high temperatures. These trends suggest some cracking/fragmentation of ring structures at high temperatures evidenced by the high CO gaseous evolution at these temperatures.

The number average molecular weight distribution for the fluidised bed tars show similarity to the mesh tars only at the lower temperatures (400^{o}C). At higher temperatures there is a shift to lower molecular weight distributions reflected by the increased loss of heteroatoms (O + S) and 'H' including increased 'C' content of the tars. The fluidised bed tar distribution curves obtained are almost identical in their variations with temperature to that reported by Tyler et al[125] but the elemental changes with regard to 'C' and heteroatom variations are different (The latter may be due to reporting N along with O + S which show differing characteristics in their evolution behaviour, refer figs(TY1-TY3) for Tyler's results).

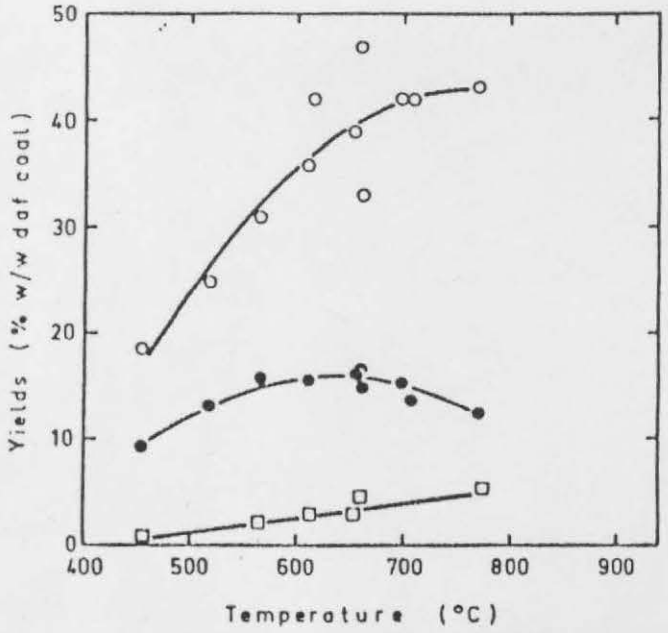

Effect of temperature on pyrolysis yields from Blair Athol coal. ●, tar; ○, total volatile matter; □, C_1–C_3 hydrocarbon

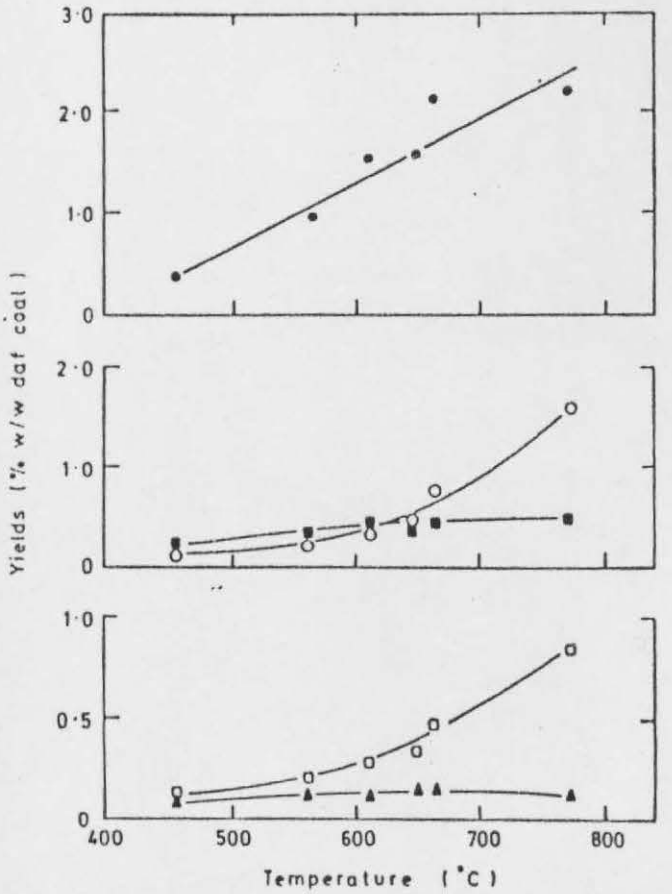

Effect of temperature on hydrocarbon gas yields from Blair Athol coal. ●, CH_4; ○, C_2H_4; ■, C_2H_6; □, C_3H_6; ▲, C_3H_8

Fig. TYL1

Fig. TYL2.

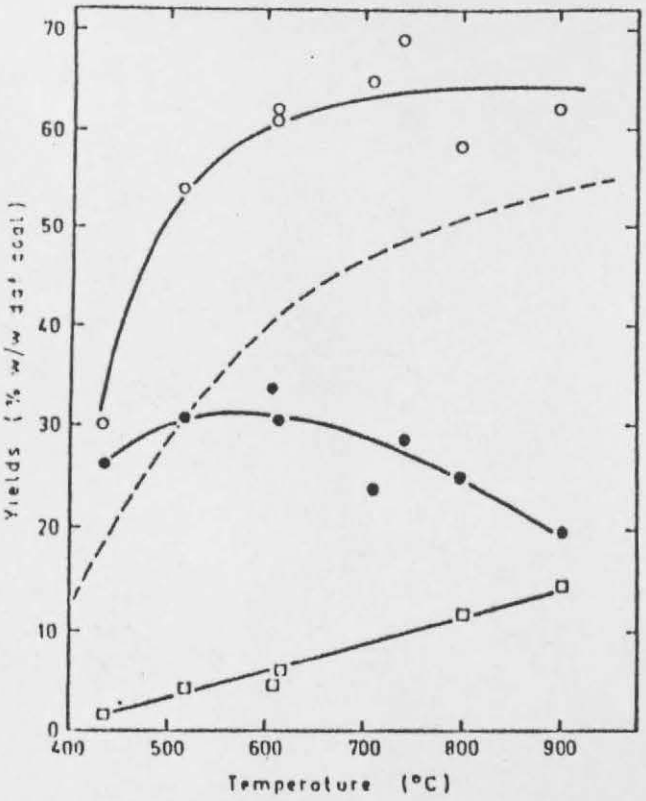

Effect of temperature on pyrolysis yields from Pittsburgh coal. ●, tar; ○, total volatile matter; □, $C_1 - C_3$ hydrocarbons; - - - -, data for grid heating[10], corrected to a daf basis after allowing for coal moisture

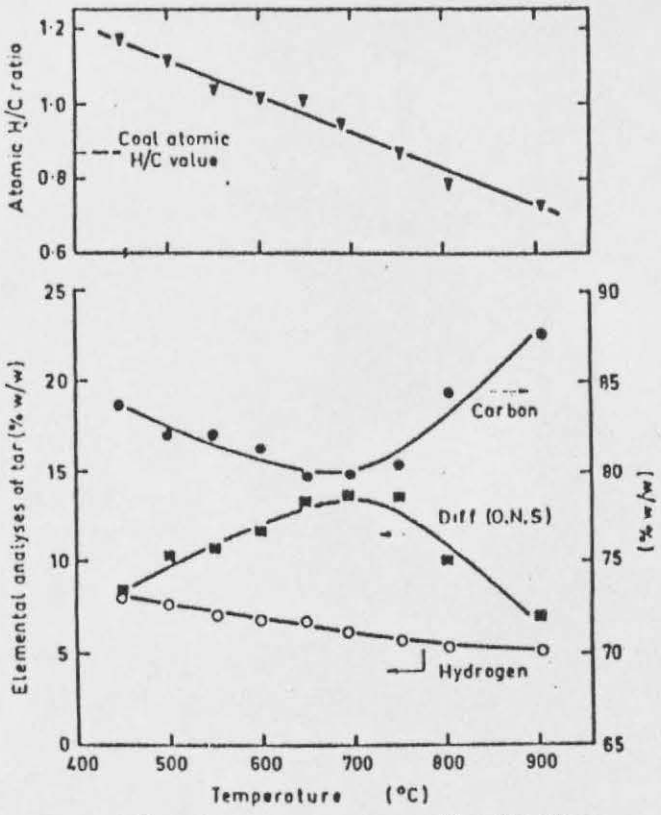

Effect of temperature on composition of tars from Liddell B coal

Fig. TYL3

Figs. TYL1 - TYL3 from Tyler et al

6) The gas evolution characteristics show significant variations with heating rate, pressure and residence times at peak temperature. Such clear variations, especially those associated with heating rate are not revealed in the case of loose packings, as employed by Anthony anmd Howard, Suuberg et al and others. (Refer to Elliott, ref. 33 page 720 for a comparison of gas yields as a function of heating rate variations. Refer to table H2 for comparison between 50 um (loose packing case) and 75 um mesh gas yields (single particle case).) Reference to table H1 indicates several trends as follows:

a) At the higher heating rates higher unsaturates are being formed, C_2H_4 and C_3H_6 being significantly sensitive indicators of this effect. Correspondingly there is significantly larger saturates being formed at the lower heating rates for both vacuum and atmospheric conditions, revealed by a significant increase in CH_4.

b) The quantity of gases formed at lower heating rates exceed those at the higher heating rates. (however, severe cracking which can occur at high temperatures at atmospheric pressure under the conditions of gas collection used in this study, and occasional tar redeposition can lead to excess gas yields at higher heating rates. Thus the vacuum gas yields are more reliable indicators of yield variations). The excess gas yield at low heating rates over the high heating rate case narrows with temperature increase.

c) More H_2 is being formed at the lower heating rates to a significant extent. The increase of H_2 with peak temperature residence times is significantly larger for

TABLE H1

TABLE GOLDTHORPE COAL; GASES; COMPARISON AT DIFFERENT HEATING RATES

Temp °C	CH4	C2H4	C3H6	C2H2	H2	Total Sats	Total Unsats	Total H/C	Heating Rate °C/S	Pressure	Time
475	0.034	0.015	0.011	-	-	0.038	0.026	0.064	5000	A	20ms
458	0.141	0.046	0.055	-	0.0031	0.260	0.101	0.361	5000	A	6.0s
475	0.147	0.050	0.041	-	-	0.28	0.09	0.37	10	A	10s
473	0.059	0.018	0.017	-	-	0.13	0.03	0.16	10	V	20ms
472	0.032	0.011	0.008	-	-	0.047	0.019	0.066	5000	V	20ms
475	0.172	0.055	0.047			0.31	0.10	0.41	5000	V	10 s
460	0.182	0.048	0.050	-	0.0017	0.39	0.12	0.51	Fluidised Bed		
594	0.3869	0.109	0.096	-	0.0104	0.828	0.247	1.075	5000	V	20ms
603	1.259	0.470	0.568	0.0367	0.0769	2.064	1.286	3.3498	5000	A	6.0s
597	1.424	0.241	0.148	0.0022	0.073	2.153	0.417	2.569	10	A	10.0s
595	0.588	0.120	0.098	-	0.0071	1.020	0.218	1.238	10	V	20ms
580	1.233	0.345	0.257	0.00048	0.055	2.177	0.871	3.048	Fluidised Bed		
670	0.937	0.202	0.158	0.007	0.032	1.51	0.40	1.91	5000	V	20ms
673	1.582	0.265	0.191	0.028	0.156	2.15	0.51	2.66	5000	V	10
685	1.509	0.216	0.142	0.002	0.091	2.173	0.386	2.559	10	V	20ms
680	1.635	0.248	0.195	0.0032	0.088	2.399	0.475	2.875	10	A	20ms
688	1.470	0.864	0.798	0.005	0.293	2.46	2.21	4.67	Fluidised Bed		
773	0.909	0.266	0.318	0.031	0.046	1.432	0.722	2.154	5000	V	20ms
769	1.682	0.368	0.263	0.059	0.457	2.197	0.812	3.009	5000	V	10 s
773	2.263	0.366	0.318	0.011	0.991	3.032	0.76	3.788	10	V	10 s
770	2.684	0.410	0.262	0.0099	0.802	3.534	0.716	4.250	10	A	20ms
774	2.697	0.695	0.329	0.0294	2.037	3.52	1.201	4.722	10	A	10 s
755	1.852	1.310	0.698	0.041	0.269	2.559	2.524	5.083	5000	A	20ms
742	1.460	1.226	0.613	0.08	0.455	2.152	2.212	4.364	5000	A	6.0s
769	1.740	1.624	0.819	0.118	0.824	2.69	3.08	5.77	Fluidised Bed		
870	1.693	0.421	0.254	0.051	0.319	2.25	0.84	3.09	5000	V	20ms
873	1.752	0.728	0.386	0.088	0.992	2.43	1.43	3.86	5000	V	6.0s
870	2.372	0.451	0.226	0.014	0.965	3.20	0.74	3.94	10	V	20ms
872	2.604	0.483	0.285	0.0124	1.450	3.462	0.892	4.354	10	A	20ms
873	2.955	1.037	0.366	0.029	2.037	3.520	1.201	4.721	10	A	10 s
864	2.424	0.747	0.284	0.014	3.088	3.14	1.14	4.28	10	V	10 s
872	2.220	1.016	0.879	0.032	0.392	3.11	2.96	6.07	5000	A	20ms
884	2.372	2.301	0.810	0.123	2.409	2.938	3.786	6.72	5000	A	6.0s
875	2.453	2.215	0.415	0.099	1.765	3.715	3.367	6.882	5000	A	6.0s
877	1.656	1.647	0.372	0.239	1.268	1.74	2.43	4.17	Fluidised Bed		
971	1.774	0.460	0.306	0.088	0.613	2.31	1.05	3.36	5000	V	20ms
973	1.837	1.386	0.442	0.0787	2.743	2.19	2.07	4.26	5000	V	10 s
968	2.219	0.670	0.267	0.049	2.37	2.9	1.09	3.99	10	V	20ms
969	2.673	0.776	0.263	0.0625	2.825	3.357	1.251	4.60	10	A	20ms
975	2.994	1.347	0.170	0.019	4.329	3.44	1.62	5.06	10	V	10 s
900	1.645	1.823	0.292	0.169	1.477	1.922	2.494	4.42	Fluidised Bed		

Note: A = Atmospheric pressures
V = Vacuum pressure

The above table illustrates the effects of heating rate on gas yield for comparable conditions of pressure and time. The fluidised yields are included for comparison.

Table H2

MARKHAM MAIN COAL
Comparison of gas yields for differing heating conditions

Temp	CH4	C2H4	C3H6	C2H2	H2	Total Sats	Total Unsats	Total H/C	Heating °C/S	Pressure	Time
409	0.070	-	0.002	-	0.001	0.077	0.0056	0.083	1000	ATM	9.5 s
400	0.011	0.003	0.0018	-	-	0.045	0.014	0.059		Fluid Bed	
417	0.011	0.003	0.00	-	-	0.023	0.003	0.026	5000	VAC	2.5 s
417	0.019	0.003	0	-	-	0.235	0.003	0.026	5000	Vac	2.5 s
475	0.106	-	0.042	-	0.005	0.240	0.047	0.287		ATM	9.5 s
471	0.159	0.028	0.051		0.003	0.330	0.102	0.432		Fluid Bed	
476	0.107	0.044	0.041	-	-	0.199	0.085	0.284	5000	ATM	6.0 s
476	(0.031)	(0.014)	(0.018)		(0.0015)	0.056	0.032	0.088	5000	ATM	20ms
488	0.062	0.009	0	-	-	0.089	0.009	0.098	5000	VAC	2.5 s
588	0.843	-	0.124	0.0026	0.048	1.359	0.219	1.578	50μ	ATM	9.5 s
588	0.858	0.213	0.280	0.0007	0.061	1.396	0.628	2.024		Fluid Bed	
575	0.717	0.218	0.165	-	0.033	1.183	0.383	1.566	5000	ATM	6.0 s
573	(0.179)	(0.079)	(0.105)	-	0.009	0.322	0.203	0.525	5000	ATM	20ms
746	0.72664	-	0.154	0.0018	0.385	1.217	0.233	1.450	50μ	ATM	9.5s
749	1.484	0.833	0.605	0.033	0.377	2.000	1.669	3.670	5000	ATM	6.0 s
735	1.432	0.878	0.580	0.027	0.133	1.957	1.654	3.611	5000	ATM	20ms
819	0.953	-	0.277	0.0024	0.437	1.438	0.359	1.797	50μ	ATM	9.5 s
817	1.814	1.470	0.698	0.115	0.727	2.399	2.578	4.977		Fluid Bed	
813	1.292	0.485	0.131	0.032	0.471	1.746	0.844	2.590	5000	VAC	2.5 s
803									5000	VAC	20ms
858	0.840	-	0.214	0.0024	0.555	1.268	0.298	1.566	50μ	ATM	9.5 s
877	2.245	1.625	0.367	0.236	1.250	2.547	2.393	4.940		Fluid Bed	
863	2.872	1.498	0.772	0.073	1.399	3.437	2.616	6.053	5000	ATM	6.0 s
856	1.695	1.141	0.699	0.108	0.497	2.096	2.168	4.265	5000	ATM	20ms
866									5000	VAC	20ms
874											
921	0.232	-	0.130	0.013	0.673	0.791	0.218	1.008	50μ	ATM	9.5 s
928	2.981	1.592	0.721	0.219	1.620	2.967	2.836	5.803	5000	ATM	6.0 s
920	2.875	1.874	1.087	0.149	0.839	3.553	3.686	7.239	5000	ATM	20ms
930	1.709	0.802	0.744	0.314	2.042	2.461	2.082	4.543	5000	VAC	6.0 s

Note: Comparison of gas yields for 50 um mesh (high load at residence time = 9.5s) to fluidised bed yields (vapour residence time 1-3 seconds) and transient yields in 75 mesh (5,000°C/S; (t_{ss} 2.5 secs and 20 ms). All runs at atmospheric pressure and residence time conditions. Gas yields for packing in 75 um mesh (single particle simulation).

the H_2 than for the CH_4 at higher temperatures (>870°C). This suggests that the pool of methyl groups or bridge structures giving rise to CH_4 is both limited and in the latter case probably reduced by cracking at an earlier stage. There may be however, a significant content of aromatic 'H' left in the semicoke which may be split off during annealing of the charring structure.

d) Below 500°C, the quantities of H/C gases and their distribution (apart from C_4 unsaturates) appears to be comparable for longer residence times (6-10s) for all heating rates and external pressure conditions to the fluidised bed yields. At higher temperatures, the unsaturates content increase considerably in the fluidised bed gas yields which suggest the onset of cracking of volatile components in the hot gas carrier stream (residence times of Vapours 1-3 seconds). The appearance of significant acetylene at high temperaures (>770°C) in the fluidised bed and at >880°C for the atmospheric mesh runs at high heating rates suggest significant cracking at the temperatures noted.

The appearance of C_4 unsaturates at relatively low temperatures (362-460°C) in the fluidised bed and also in 50 μm mesh reactor (Markham Main coal; vacuum conditions and sufficient mass loads and residence times (9.5s) to detect the relatively low concentrations of these compared to the 75 μm low load studies) suggest that these may arise from long chain polymethylene units hypothised to be present in high volatile coals by Calkins et al.[199-202] The acceleration

Fig.fbg1
Fluidised bed gas yields vs Temperature

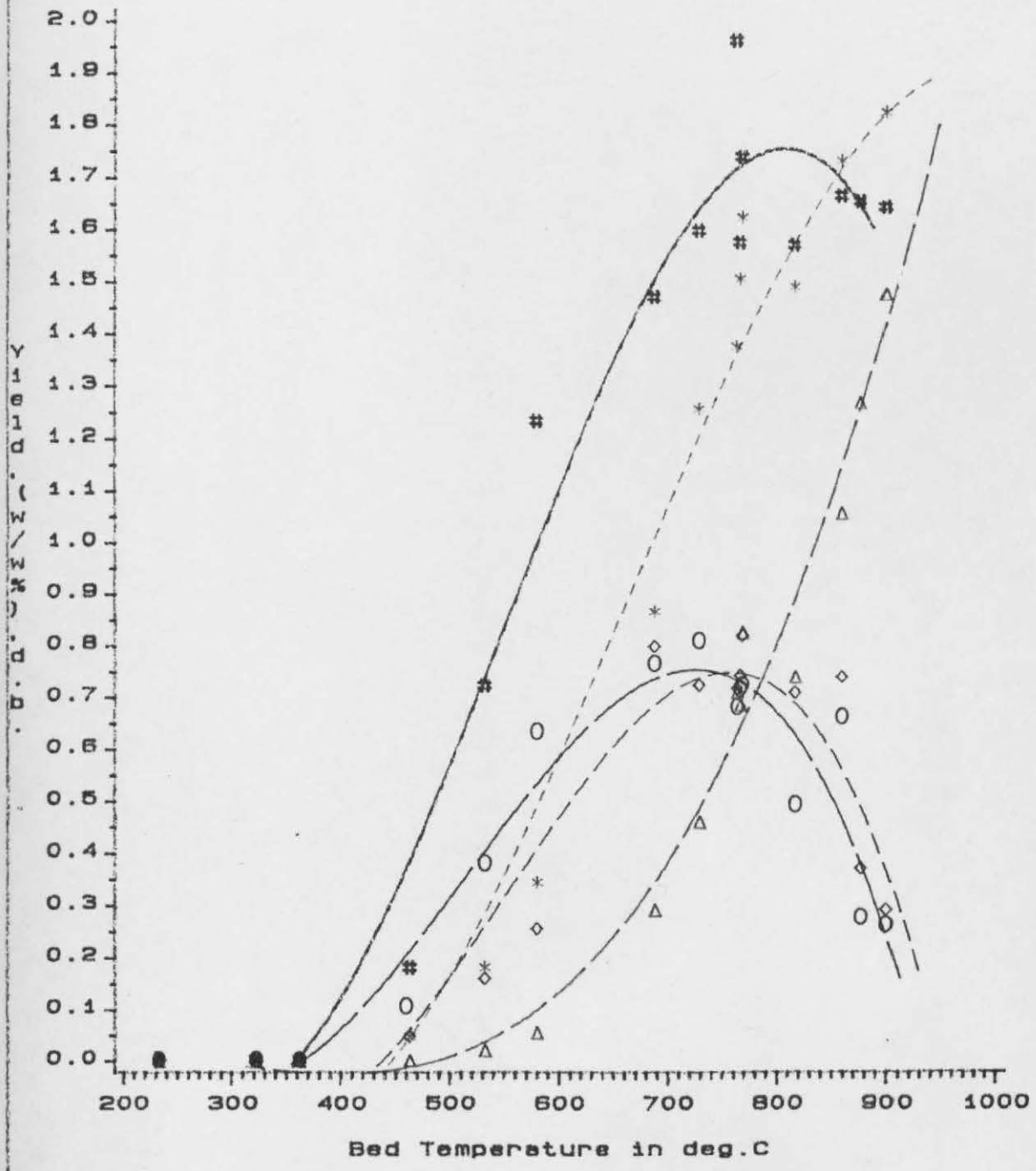

Goldthorpe Coal:Dp=75/90uM
CH4 GAS(Hash symbol)
C2H4 GAS(Star symbol)
C3H6 GAS(Diamond symbol)
H2 GAS(Triangle symbol)
C2H6 GAS(Circle symbol)

Fig.fbg2
Fluidised bed gas yields vs Temperature

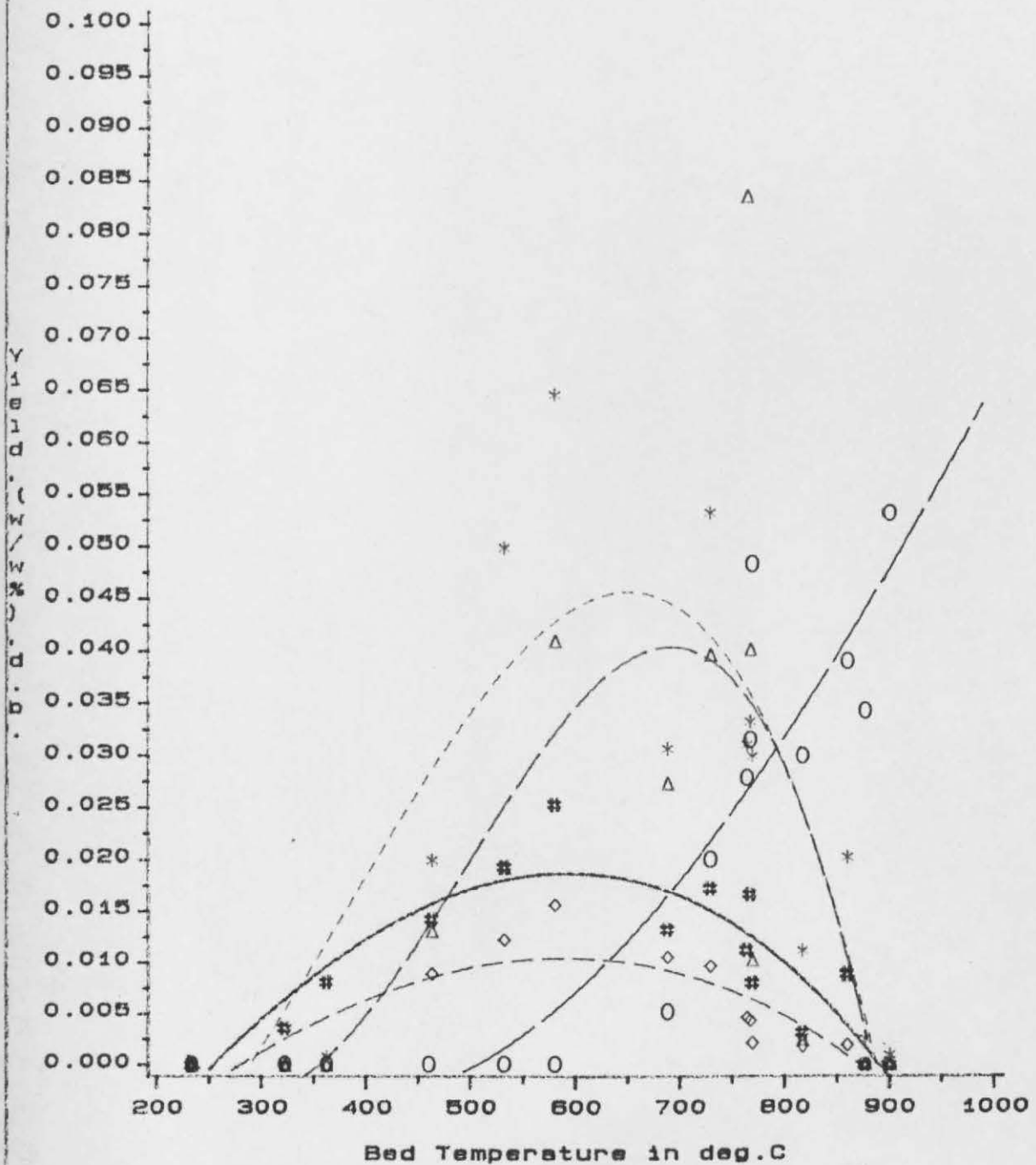

Goldthorpe Coal:Dp=75/90uM
i-C4H10 GAS(Hash symbol)
n-C4H10 GAS(Star symbol)
i-C5H12 GAS(Diamond symbol)
n-C5H12 GAS(Triangle symbol)
Allene(Circle symbol)

Fig.fbg3
Fluidised bed gas yields vs Temperature

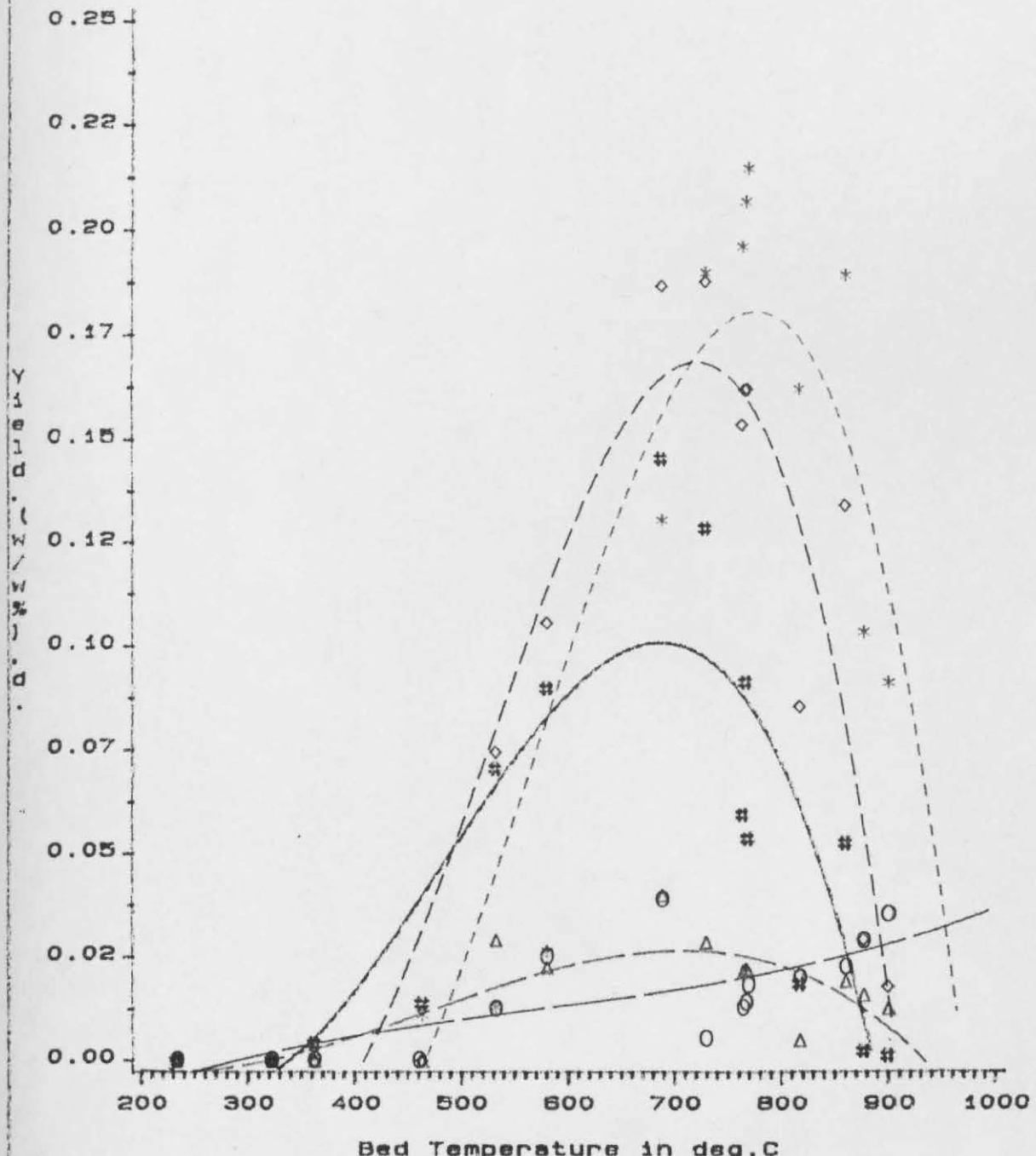

Goldthorpe Coal:Dp=75/90uM
But-1-ene(Hash symbol)
1,3 Butadiene(Star symbol)
Trans-Butene(Diamond symbol)
Cis-Butene(Triangle symbol)
Pentene(Circle symbol)

Fig.fbg4
Fluidised bed gas yields vs Temperature

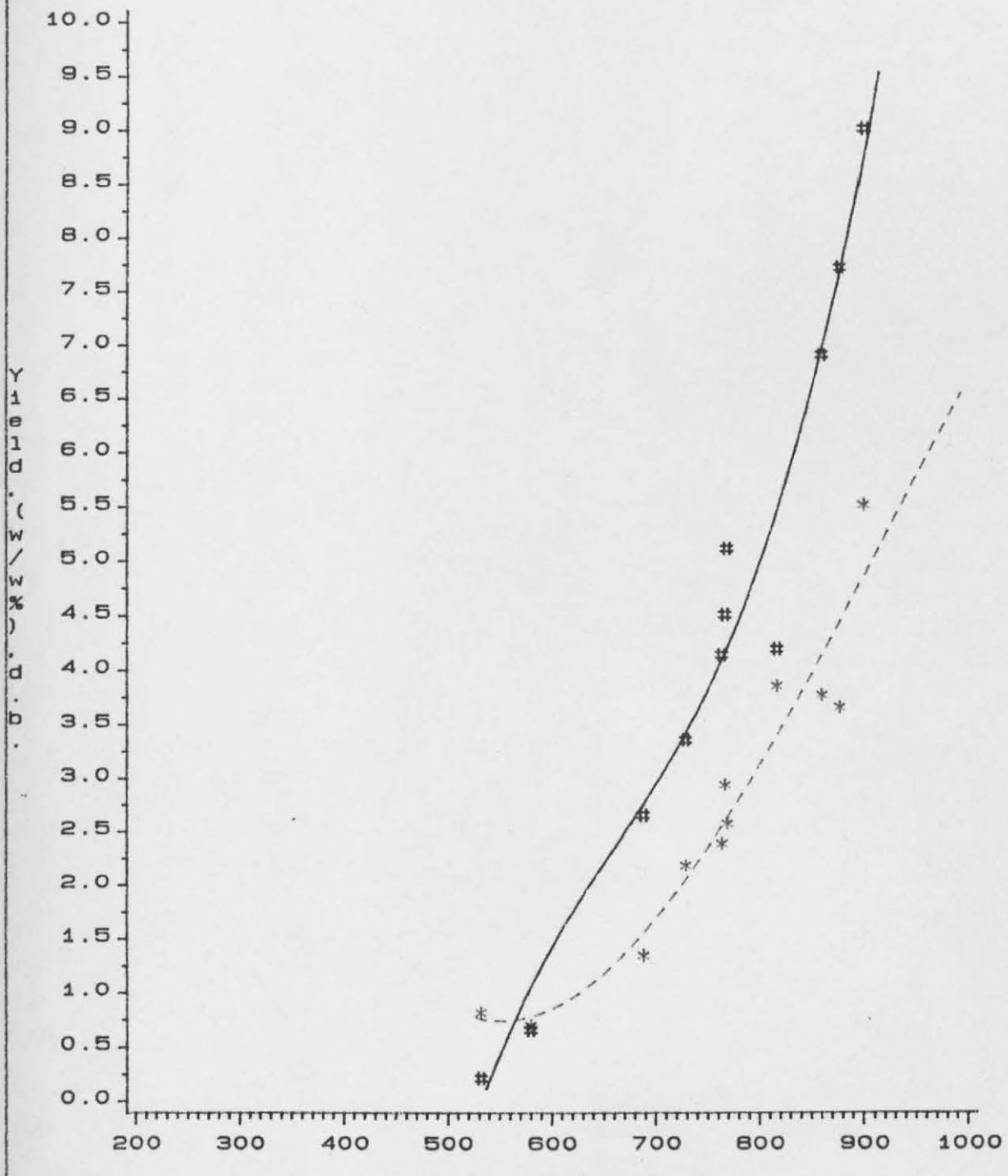

Goldthorpe Coal:Dp=75/90uM
CO GAS(Hash symbol)
CO2 GAS(Star symbol)

Fig.fbg5
Fluidised bed gas yields vs Temperature

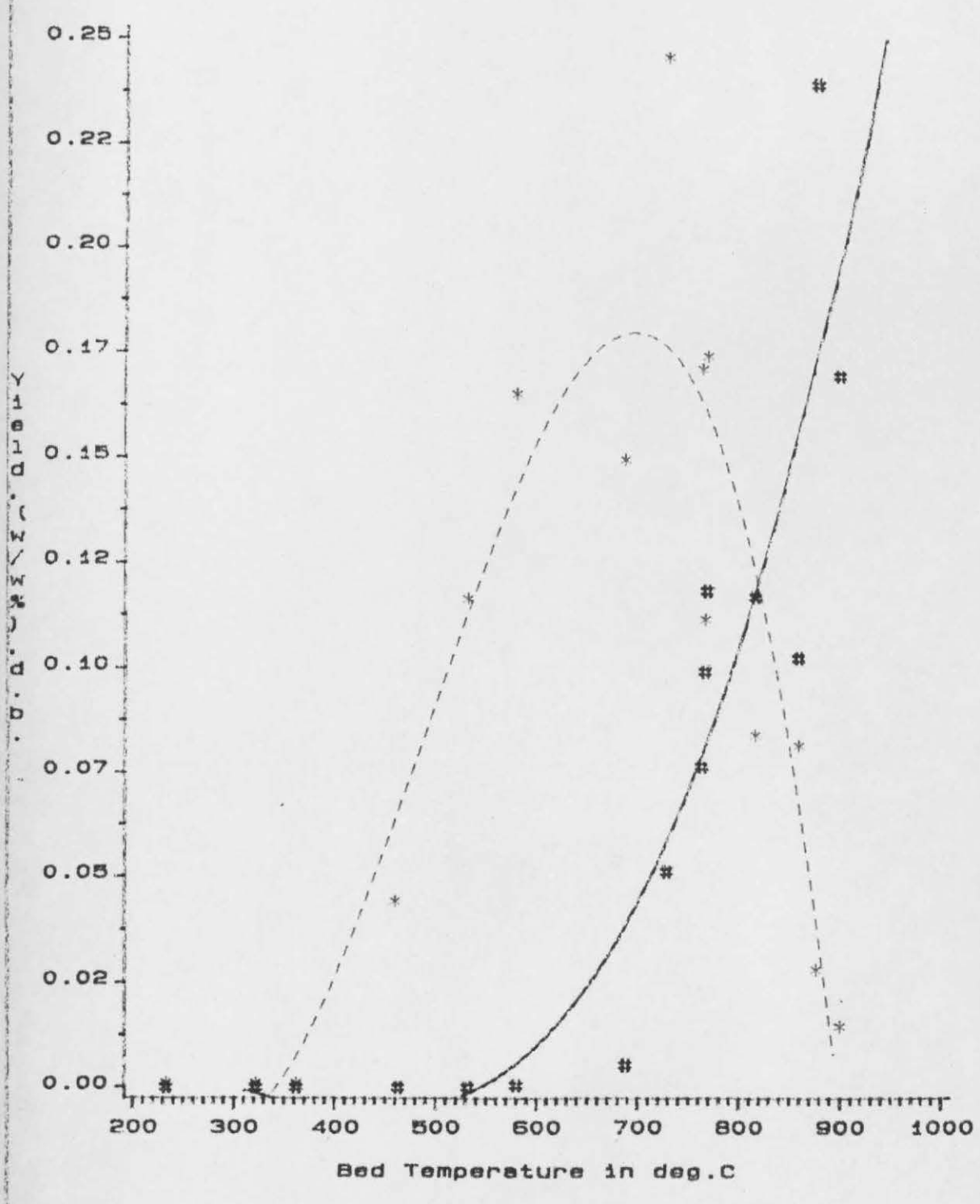

Goldthorpe Coal:Dp=75/90uM
C2H2 GAS(Hash symbol)
C2H6 GAS(Star symbol)

Fig.MM1
Fluidised bed gas yields vs Temperature

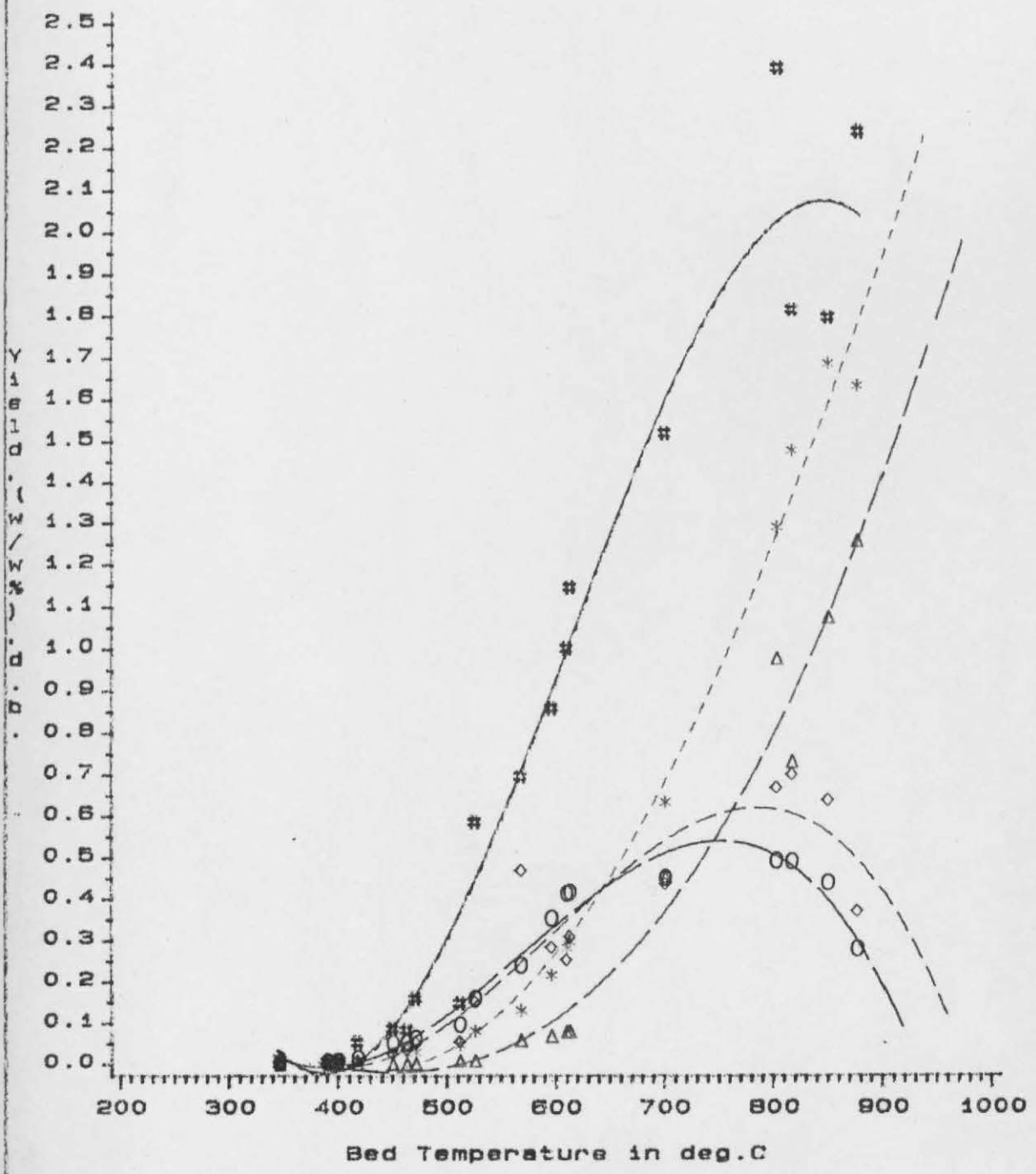

M.Main Coal:Dp=75/90uM
CH4 GAS(Hash symbol)
C2H4 GAS(Star symbol)
C3H6 GAS(Diamond symbol)
H2 GAS(Triangle symbol)
C2H6 GAS(Circle symbol)

Fig.mmg2
Fluidised bed gas yields vs Temperature

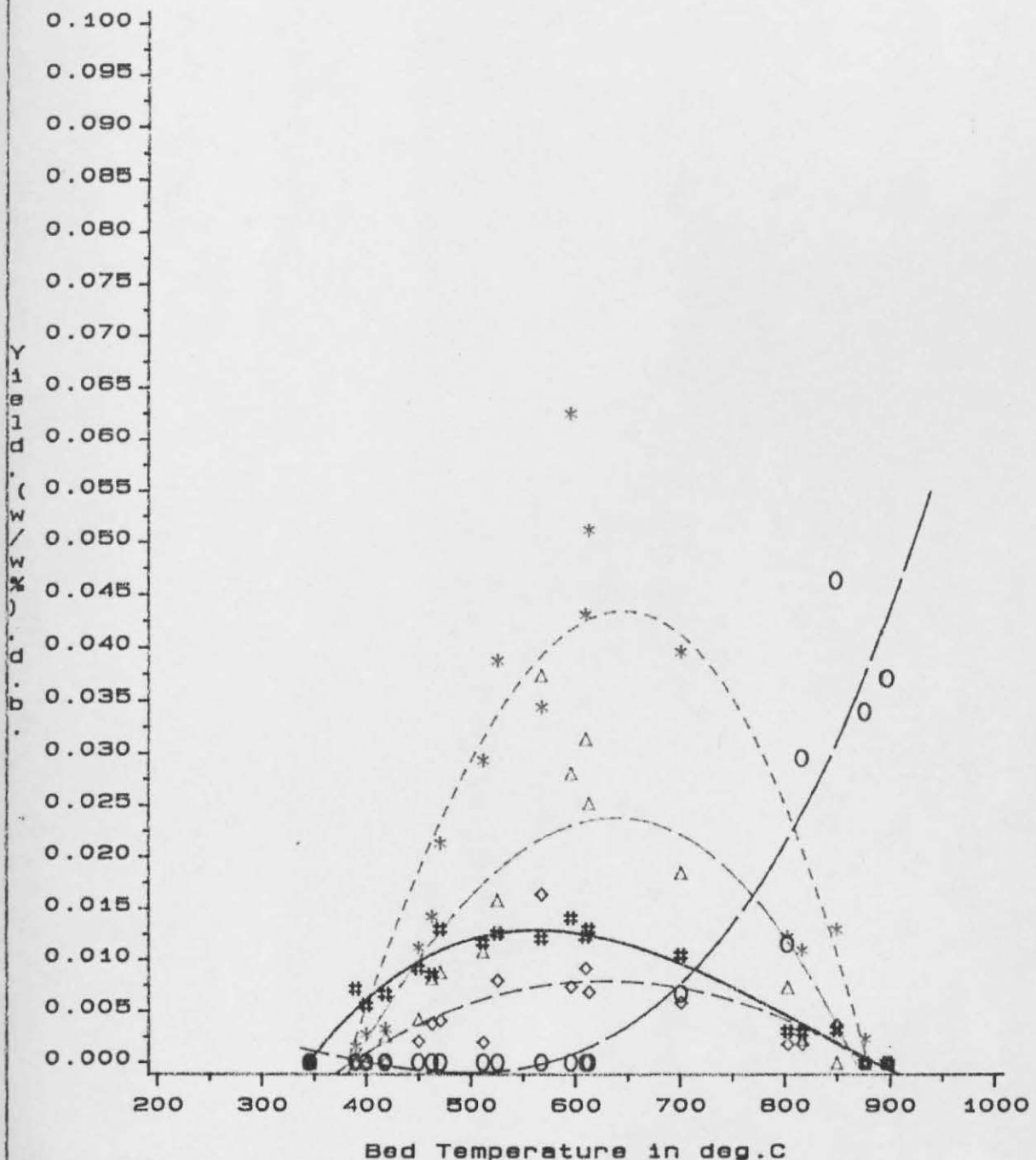

Markham Main Coal:Dp=75/90uM
i-C4H10 GAS(Hash symbol)
n-C4H10 GAS(Star symbol)
i-C5H12 GAS(Diamond symbol)
n-C5H12 GAS(Triangle symbol)
Allene(Circle symbol)

Fig.mmg5
Fluidised bed gas yields vs Temperature

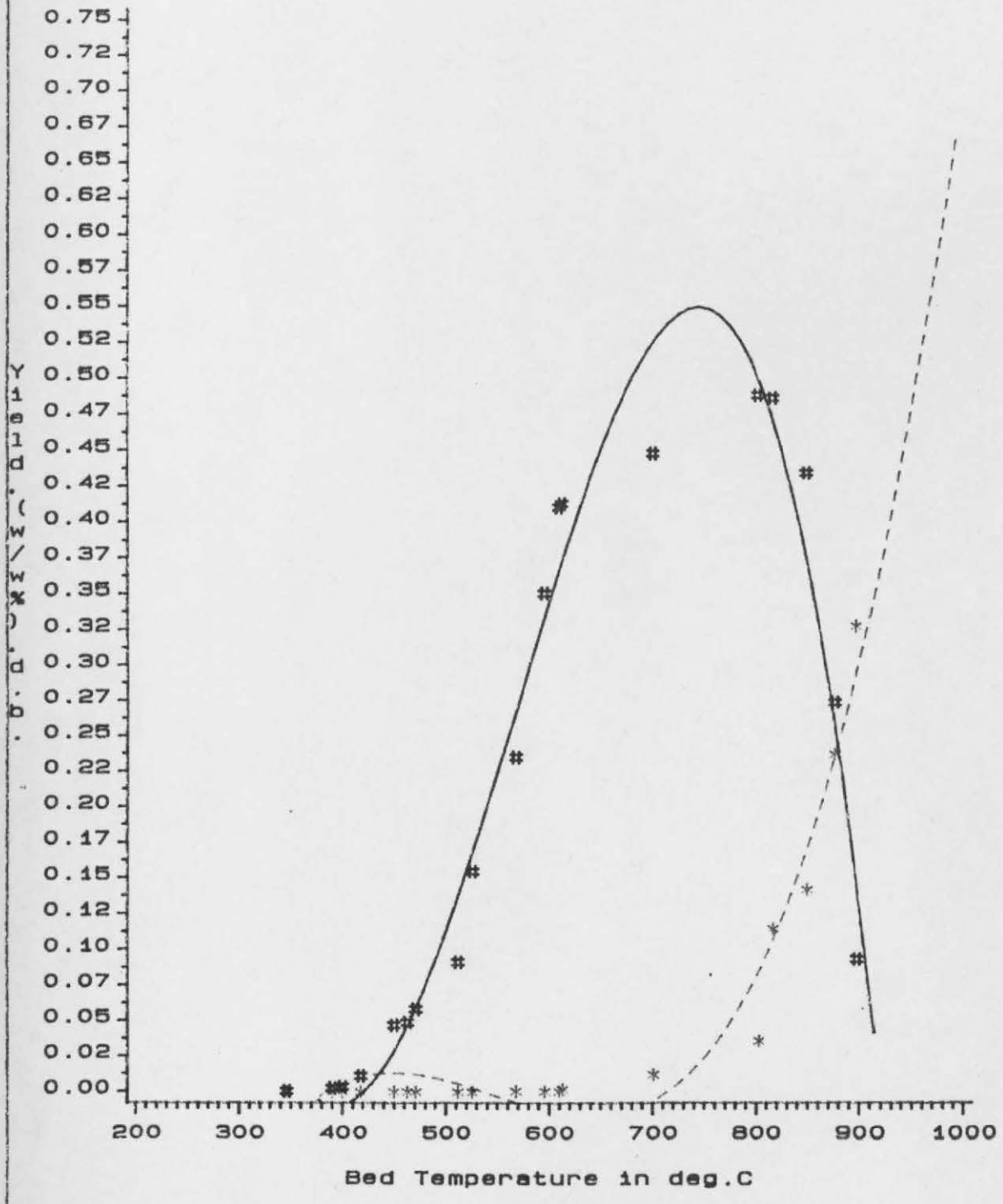

Markham Main Coal:Dp=75/90uM
C2H6 GAS(Hash symbol)
C2H2 GAS(Star symbol)

Fig.mmg3
Fluidised bed gas yields vs Temperature

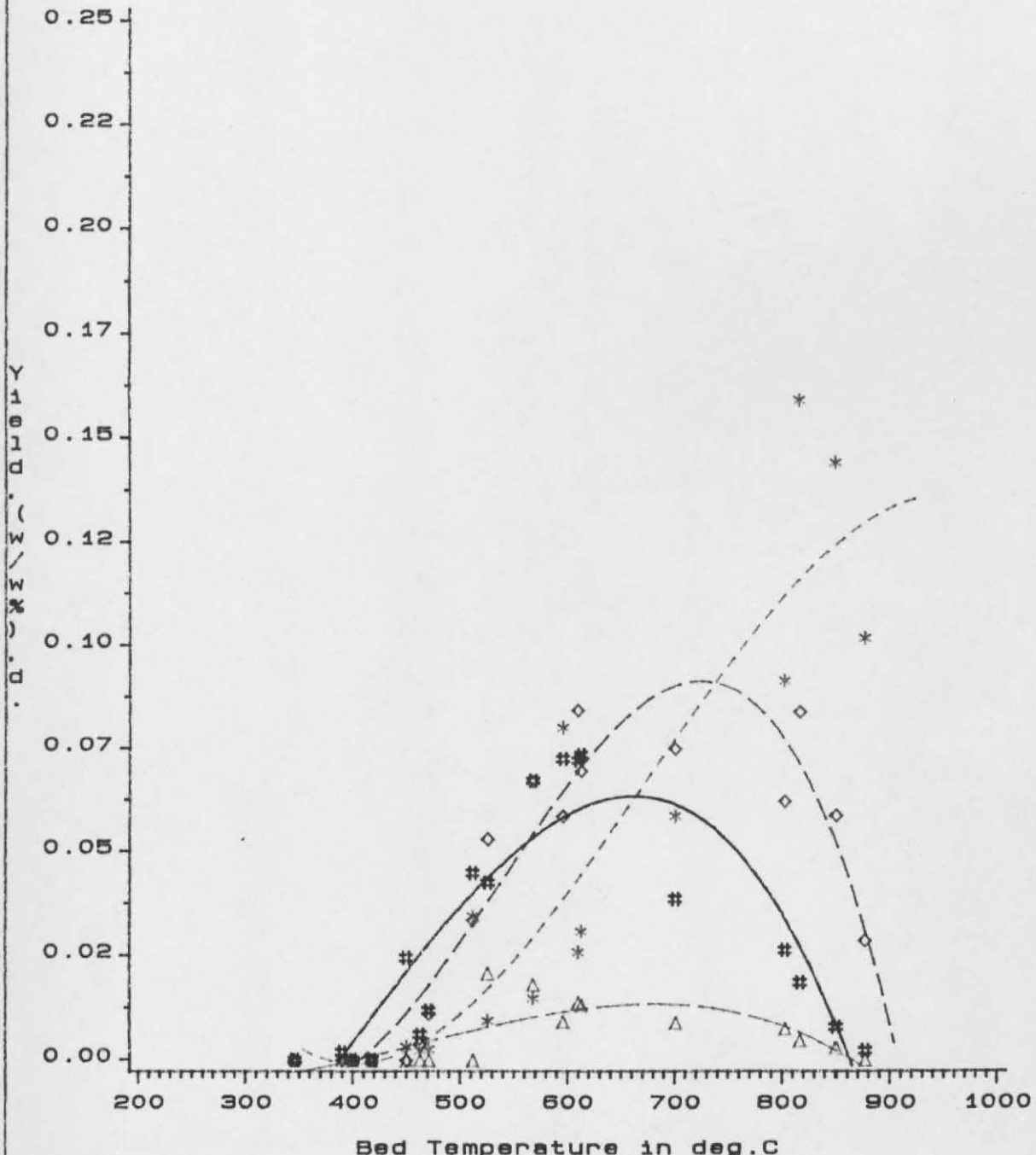

Markham Main Coal:Dp=75/90uM
But-1-ene(Hash symbol)
1,3 Butadiene(Star symbol)
Trans-Butene(Diamond symbol)
Cis-Butene(Triangle symbol)
Pentene(Circle symbol)

Fig.mmg4
Fluidised bed gas yields vs Temperature

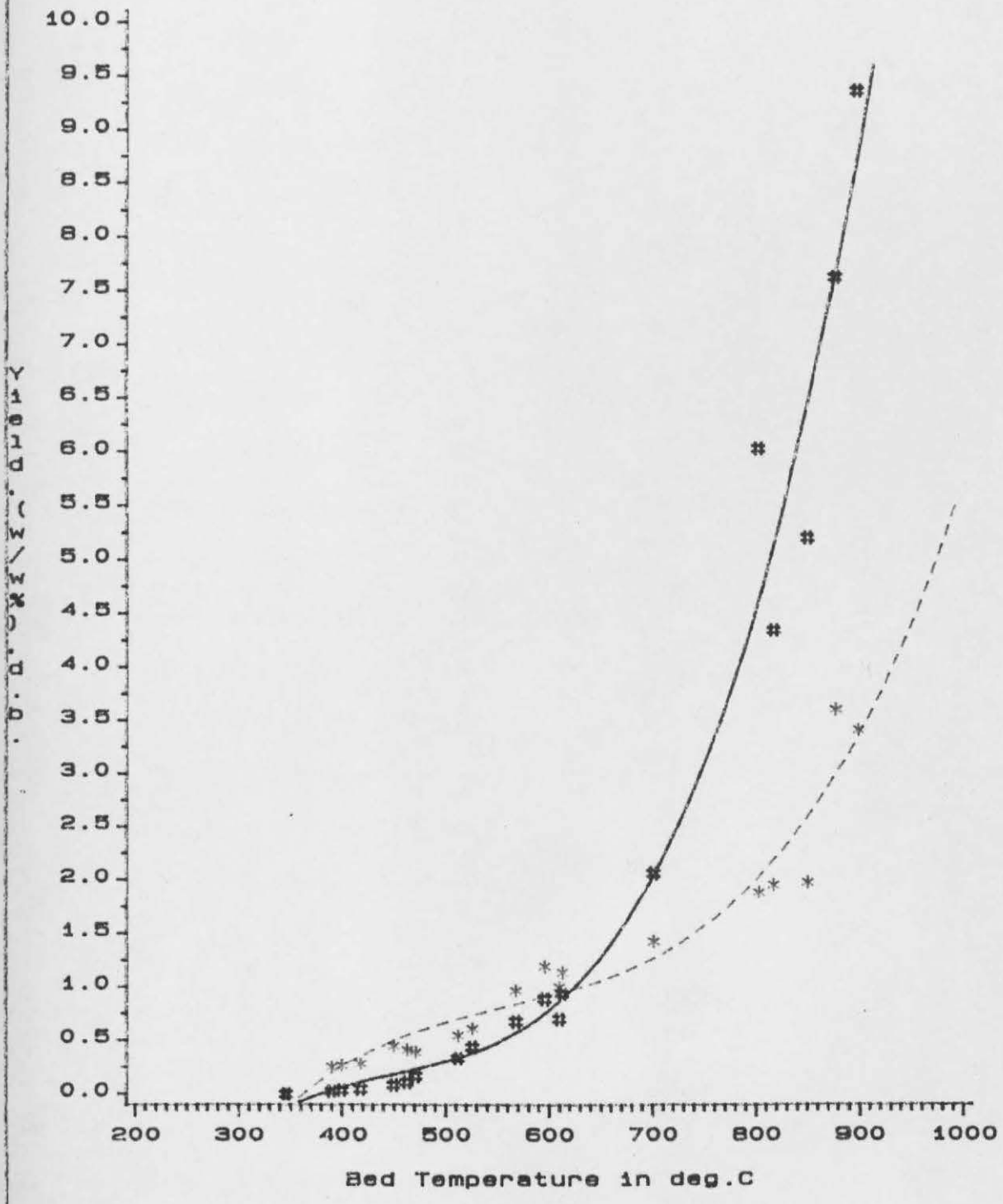

Markham Main Coal:Dp=75/90uM
CO GAS(Hash symbol)
CO2 GAS(Star symbol)

and distribution of C_4 unsaturates in both reactors reflect possible hydroaromatic and/or naphthenic ring fragmentation as well as thermodynamic equilibrium distributions with temperature. Refer to figures fbg1 to mmg4 for the F.B. gas yields.

The large concentration of H_2 released at lower heating rates and long residence times compared to the fluidised bed reveals some subtleties of heating rate effects which may be related to the movement of lamallae during the char annealing stage.

At atmospheric pressures, the gas yield is higher for all heating rates and the unsaturate yield increases significantly with residence time. This suggests the possibility of competitive reactions and or cracking reactions caused by diffusion limitations of the vapour product precursors out of the softened liquefied coal. At high heating rates and better heat transfer to the particles, evaporation limitation of the heavy tarry material may set in leading to enhanced cracking of the rapidly formed products. There is some suggestion of this evidenced by the higher rate of increase of C_2 H_2 at longer residence times for the high heating rate cases.

The features and results noted above will be discussed in more detail in the ensuing chapter. Reference to FTIR spectra results as well scanning electron micrograph and high speed photograpy studies will provide some insights into the processes occuring during pyrolytic decomposition. Model fits to some of the data as well as numerical heat transfer simulations have been conducted to get a feel for the various

parameters that reflect the yield distributions obtained.

CHAPTER 7

MODEL RESULTS AND ANALYSIS

7.1 Overall single reaction model

The single reaction model represents the simplest case of reaction rate analysis of solid state decomposition reactions. The model, assuming unimolecular first order decomposition kinetics has been applied to both coal and oil shale studies. In the case of a particle heating up at a known rate, assuming reaction to occur uniformly throughout the particle volume, the following analysis holds:

For each reaction i, the Pyrolysis rate is:

$$\frac{dVi}{dt} = k_i e^{-E_i/RT} \ (V_i^* - V_i)$$

where V_i^* represents ultimate realisable yield, obtained from the highest temperature and residence time of interest.

V_i = yield at time t

T = ^oK and R = gas constant.

For the case of an imposed linear heating rate, the equation reduces to the following,

$$-\ln\left(\frac{V_i^* - V}{V_i^*}\right) = \int_{To}^{T} \frac{ki}{m} \ e^{-Ei/RT} \ dT$$

(refer Ch 5 for derivation and explanation).

A number of approximations for the integral on the R.H.S. is available,[220] and the one derived by Coats and Redfern, widely applied in nonisothermal reaction kinetics was applied, yielding,

$$-\ln\left(\frac{V_i^*-V}{V_i^*}\right) = \frac{kRT^2}{m E_i}\left(1-\frac{2RT}{E_i}\right)\exp\left(^{-Ei}/_{RT}\right)$$

or $$\ln\left\{\frac{-m\ \ln(1-Vi/Vi^*)}{RT^2}\right\} - \ln\left(1-\frac{2RT}{E_i}\right) \approx \ln\frac{ki}{E} - \frac{E^i}{RT}$$

The values of E_i and ki were obtained by iterative least square fitting of the data to the last equation. The above equations may be recast to include heating and cooling time including isothermal residence time at the peak temperature. However, as reaction actually starts at some intermediate stage of the heat up stage and pressure drived and/or diffusive flow can drive the volatile products away from the surface, the use of such adjustment is quite arbitrary. Reference to the high speed photography results later will provide some idea of the uncertainties involved.

The overall model was applied independantly to the overall individual gas yields as well as to total yields. Solomon et al[143] used a similar analysis by applying the isothermal version of the single reaction model to his mesh yield data.

Yield data from the case of nonisothermal runs were fitted by the above equation including some of the gas data. The model fitted curves are shown in figures (M15) to (M21). Figures (i) to (xxxi) represent model fits to the gas yield data for the conditions referred to. Representative values of rate parameters are tabulated below.

Goldthorpe coal, 5000°C/S, vacuum conditions:

Volatile product	E_i (kJ/mole)	k_i (1/S)
CH_4	52.2	1.09×10^4
C_2H_6	45.8	9.49×10^3
C_2H_4	50.6	5.14×10^3

Volatile product	E_i (kJ/mole)	k_i (^{1}/S)
C_3H_8	40.7	4.9×10^3
C_3H_6	52.0	1.31×10^4
H_2	98.7	4.9×10^5
C_2H_2	80.41	9.71×10^4
But-1-ene	31.21	6.52×10^2
CH_4	59.2	85
C_2H_6	47.4	1.13×10^4
C_2H_4	56.8	2.0×10^4
C_3H_8	36.2	3.85×10^3
C_3H_6	31.4	1.38×10^4
But-1-ene	37.2	2.65×10^3
H2	140.1	1.49×10^8
C_2H_2	98.3	7.1×10^6
M. Main, 5000^{o}C/S, Atm		
CH_4	65.7	4.1×10^5
C_2H_6	40.3	2.13×10^3
C_2H_4	64.7	2.86×10^4
C_3H_8	28.7	6.99×10^2
C_3H_6	49.2	1.69×10^3
H_2	96.6	3.7×10^5
C_2H_2	94.6	4.6×10^5
Allene	38.7	1.34×10^3

Comparable values and trends were observed for other conditions tested in the mesh reactor.

The values obtained by the above independant single reaction model are comparable to those reported by Solomon et al [143] for temperature range of 300-1250^{o}C and residence times of 3-180 seconds

in the mesh reactor. Their results for H_2 and H/C (total of light gases) are as follows:

H_2, E_i = 106KJ/mole $k_i = 3.6 \times 10^3$ (S^{-1})

H/C, E_i = 66.6 kJ/mole k_i = 290 (S^{-1})

Similarly low values of rate parameters were reported for other species.

Rate parameters were also found for overall yields (total yields) and showed better fits to the data. In the case of the gases best fits were obtained for unsaturates as well as CH_4, H_2, C_2H_2 and where sufficient data was available to allene. However, C_3H_6 and C_3H_8 were generally poorly fitted mainly due to data scatter, but particularly due to cracking of these gases at high reaction temperatures. Variations in the adjustable parameter V_i^* produced minor variations in E_i, but more substantial variations in the pre-exponential factor.

Representative values of rate parameters for total volatile yields were as follows:

Goldthorpe coal; 5000°C/S; Atmospheric pressure, E_i = 25.84 KJ/mole, $k_i = 1.64 \times 10^3$ (S^{-1})

M. Main coal; 1000°C/S; Atmospheric pressure, E_i = 26.77 KJ/mole, $k_i = 3.8 \times 10^2$ (S^{-1})

Goldthorpe, vacuum; 5000°C/S, E_i = 26.3; $k_i = 2.05 \times 10^3$ (S^{-1})

M. Main, Atmospheric pressure, 5000°C/S, E_i = 26.29 KJ/mole, $k_i = 1.79 \times 10^3$ (S^{-1})

The rate parameters show relative insensitivity to individual types of volatile gases, coal type, pressure conditions and heating rate. For the overall yields, the preexponential factor shows a proportional relationship to heating rate such that higher heating

FIG. M.15

NONISOTHERMAL MODEL FIT TO EXPERIMENTAL DATA

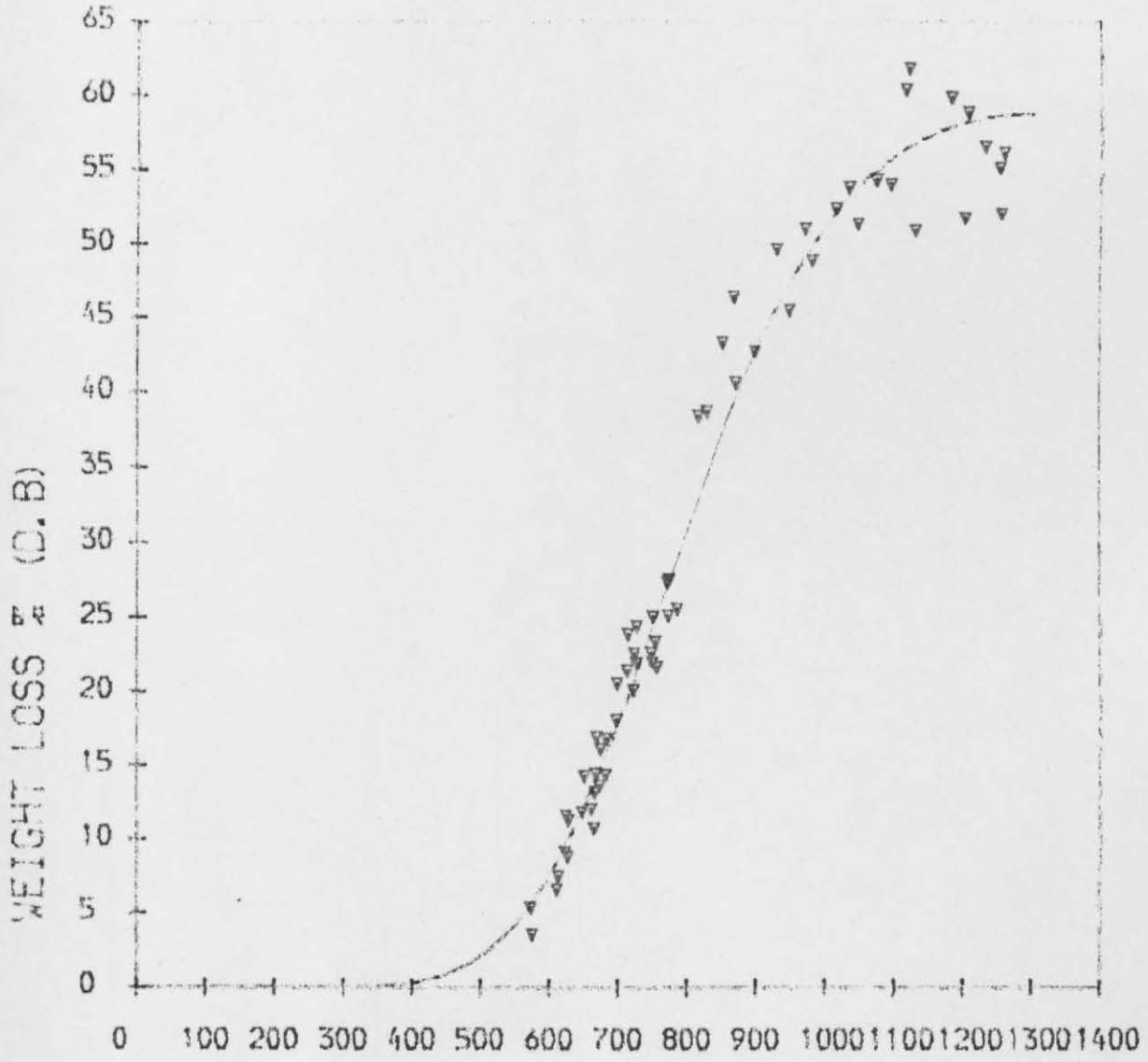

COAL TYPE. Markham Maim

MESH TYPE. 75 um

RESIDENCE TIME CHARACTER. 10/20 ms

PARTICLE SIZE. 75/90

HEATING RATE. 5,000°C/S

PRESURE OF RUN. ATM

Eo = 26.29 kJ/mole

A = 0.179×10^4 s

FIG.M16

NONISOTHERMAL MODEL FIT TO EXPERIMENTAL DATA

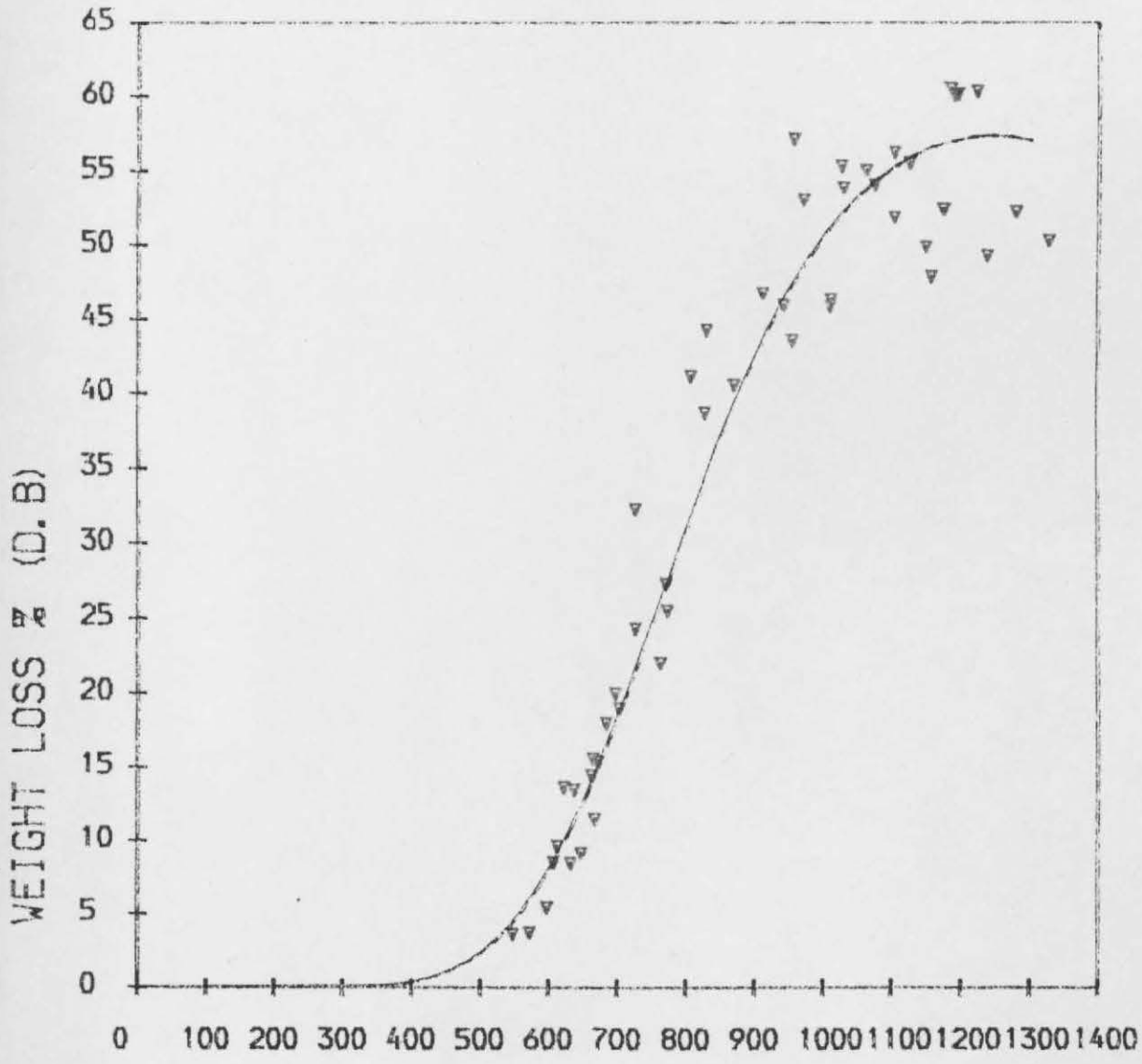

COAL TYPE, Markham Main

MESH TYPE, 75 um

RESIDENCE TIME CHARACTER, 10/20ms

PARTICLE SIZE, 75/90 um

HEATING RATE, 1,000°C/S

PRESURE OF RUN, ATM

Eo = 26.77 kJ/mole

A = 3.8×10^{2} s^{-1}

FIG. M. 17

NONISOTHERMAL MODEL FIT TO EXPERIMENTAL DATA

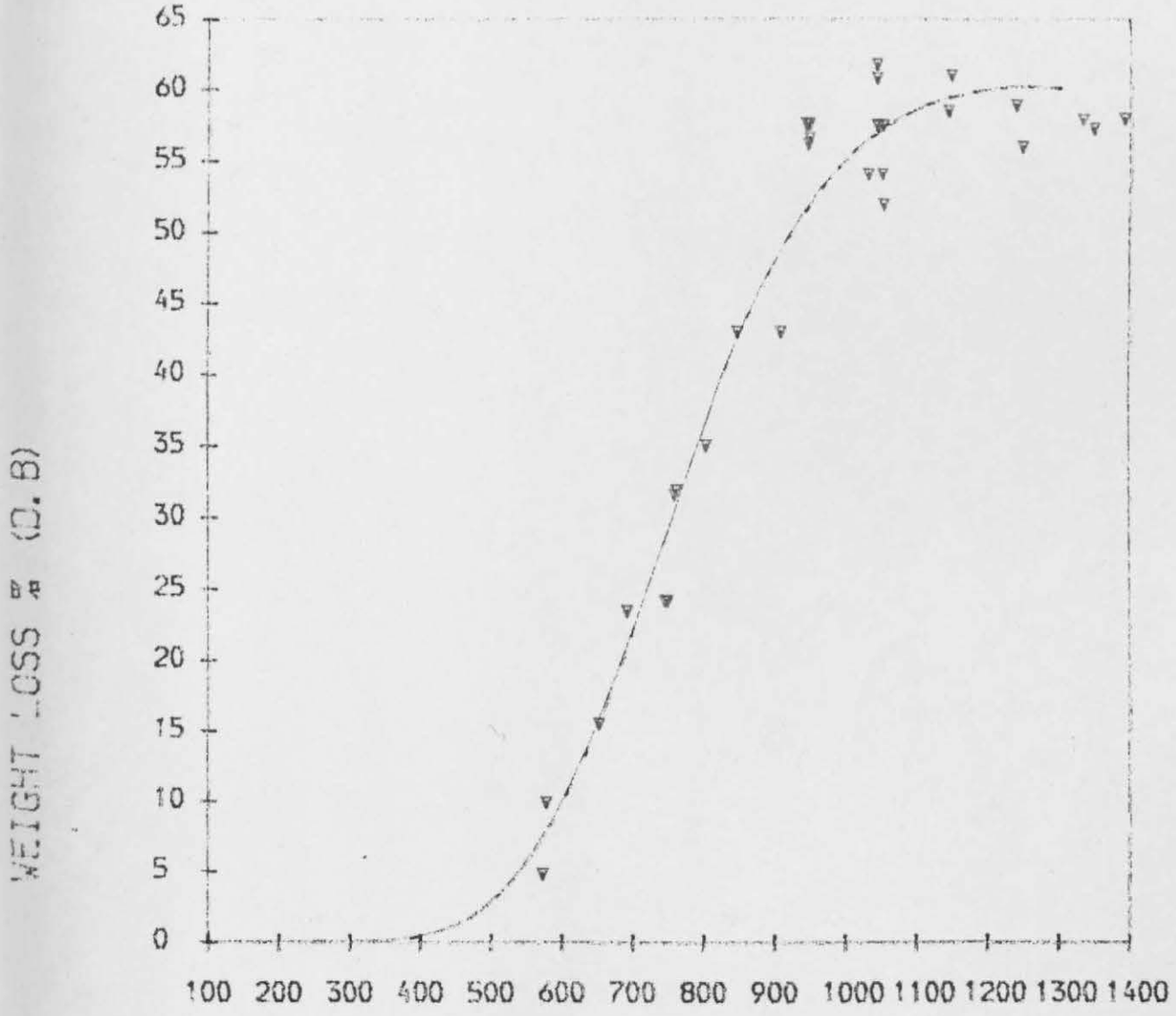

Eo = 26.77 kJ/mole

A = 3.8×10^2 S^{-1}

COAL TYPE. Markham Main
MESH TYPE. 75 um
RESIDENCE TIME CHARACTER. 10/20ms
PARTICLE SIZE. 75/90 um
HEATING RATE. 1,000°C/S
PRESURE OF RUN. ATM

FIG. M.18

NONISOTHERMAL MODEL FIT TO EXPERIMENTAL DATA

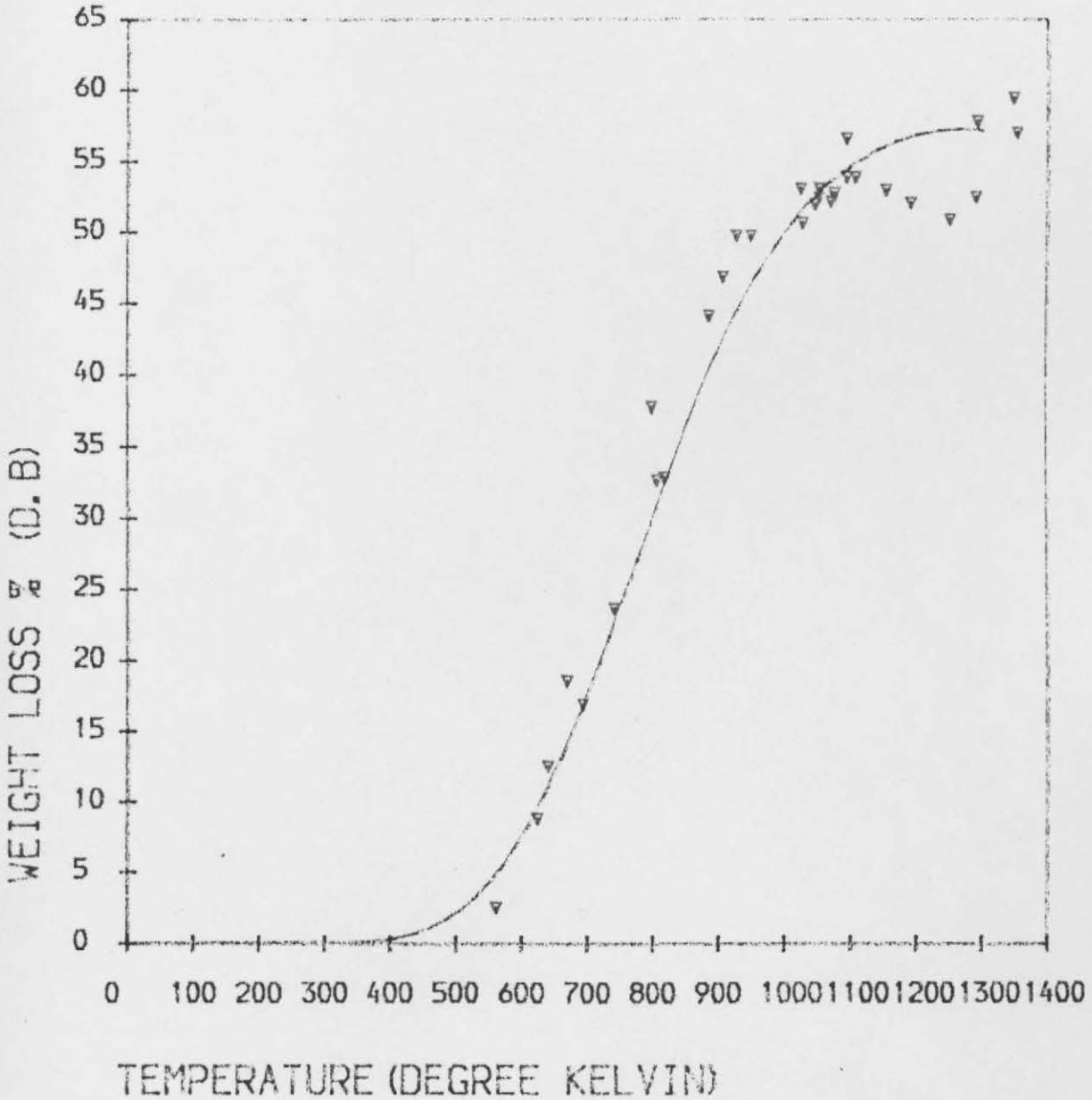

COAL TYPE, Goldthorpe

MESH TYPE, 75 um

RESIDENCE TIME CHARACTER, 10/20

PARTICLE SIZE, 75/90 um

HEATING RATE, 5000°C/S

PRESURE OF RUN, ATM

Eo = 25.84 kJ/mole

A = 0.164×10^{4} S^{-}

FIG. M.19

NONISOTHERMAL MODEL FIT TO EXPERIMENTAL DATA

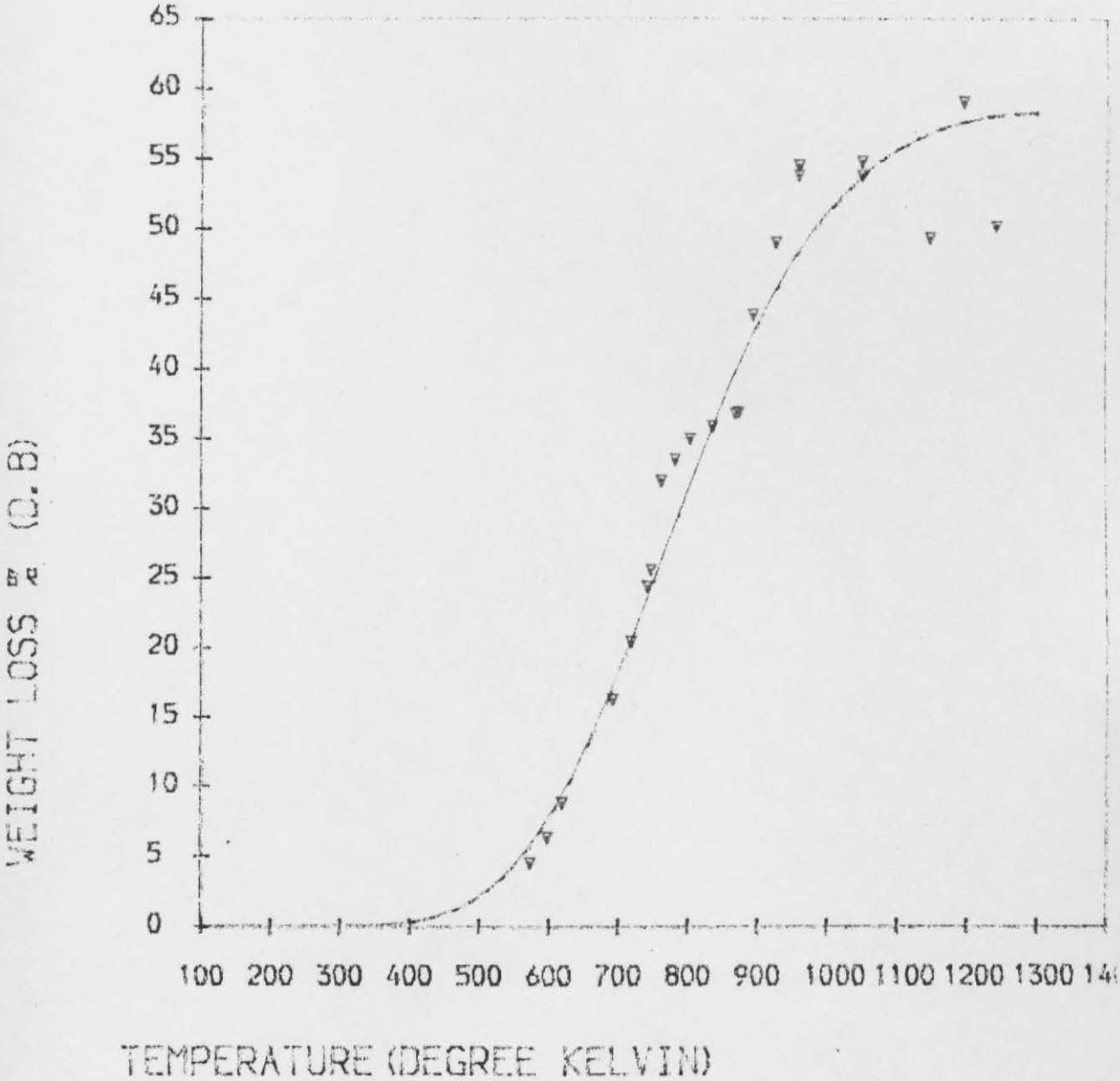

COAL TYPE, Goldthorpe
MESH TYPE, 75 um
RESIDENCE TIME CHARACTER, 10/20 ms
PARTICLE SIZE, 75/90 um
HEATING RATE, 10°C/S
PRESURE OF RUN, Vacuum

FIG. M.20

NONISOTHERMAL MODEL FIT TO EXPERIMENTAL DATA

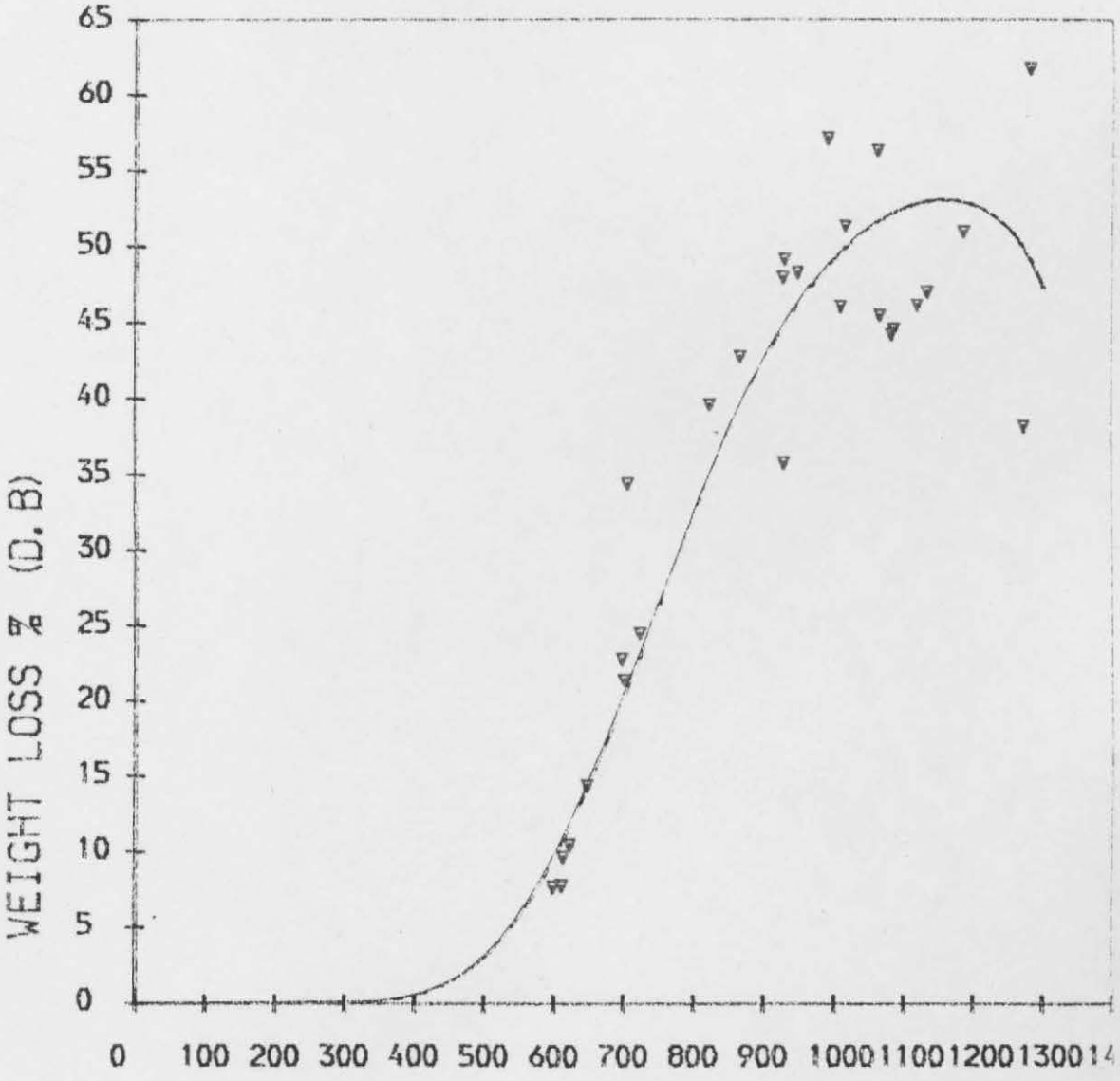

COAL TYPE: Markham Main
MESH TYPE: 75 um
RESIDENCE TIME CHARACTER: 10/20
PARTICLE SIZE: 75/90°
HEATING RATE: 1,000°C/S
PRESURE OF RUN: Vacuum

FIG. M.21

NONISOTHERMAL MODEL FIT TO EXPERIMENTAL DATA

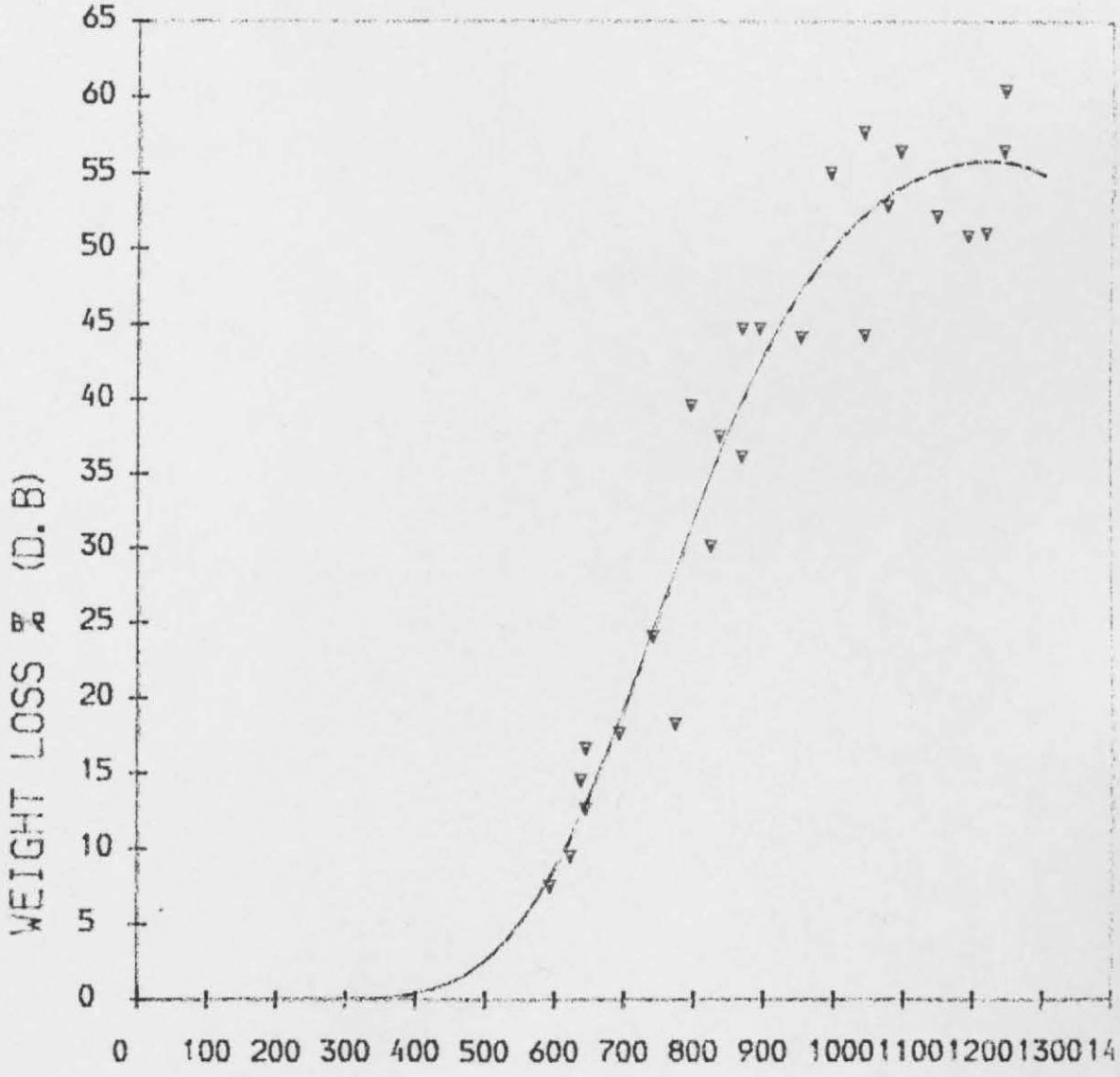

COAL TYPE, Goldthorpe
MESH TYPE, 75 um
RESIDENCE TIME CHARACTER, 10/20 ms.
PARTICLE SIZE, 75/90
HEATING RATE, 10°C/S
PRESURE OF RUN, ATM

Graphs i - xxi represent a selection of product gases fitted by the nonisothermal, single reaction model equation. The yields so fitted represent cumulative mass yields obtained by heating the coal particles to the peak temperature followed immediately by cooling. (Residence time at peak temperature 10/20 ms).

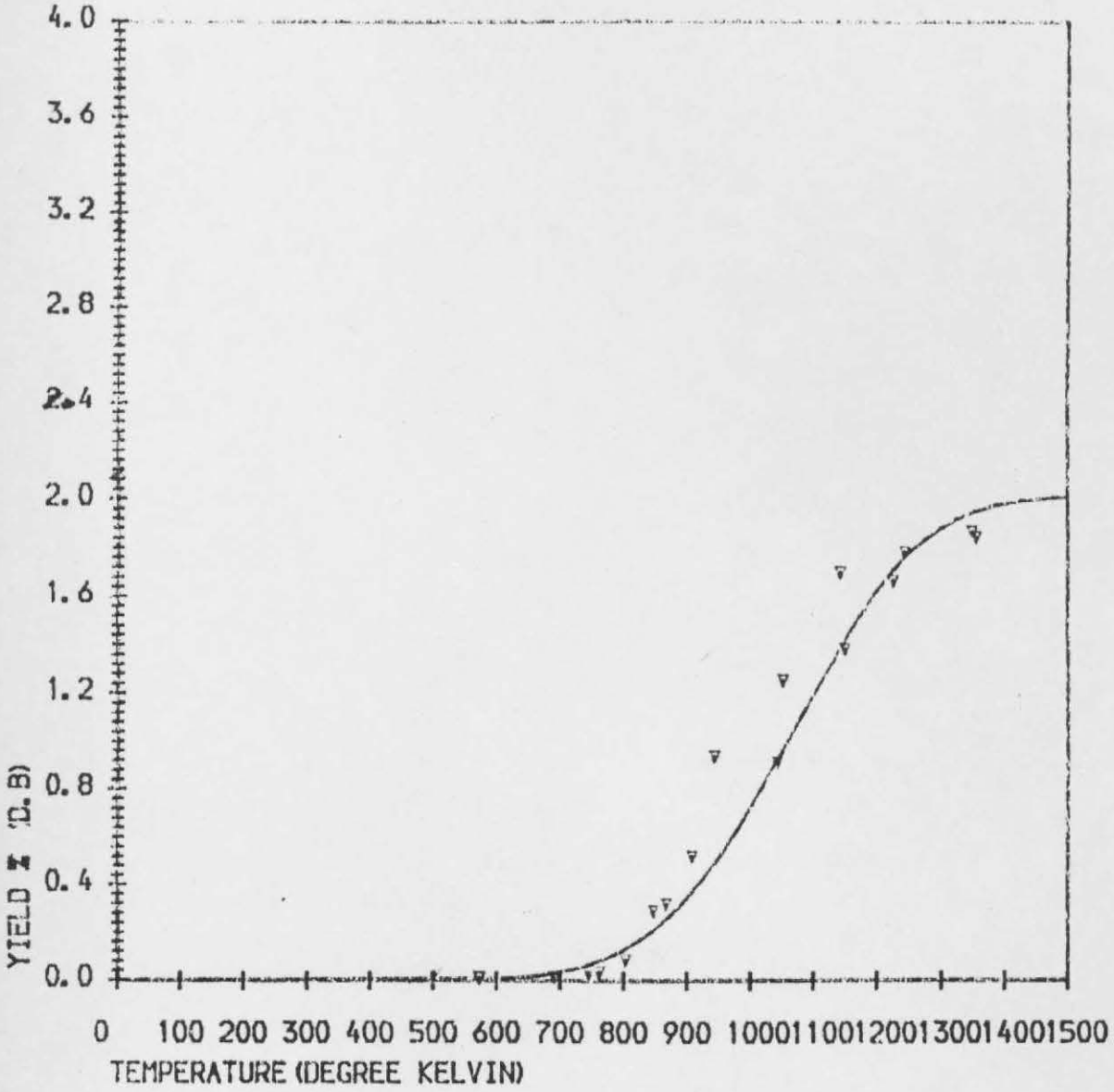

Goldthorpe
5,000°C/S
Vacuum
CH_4

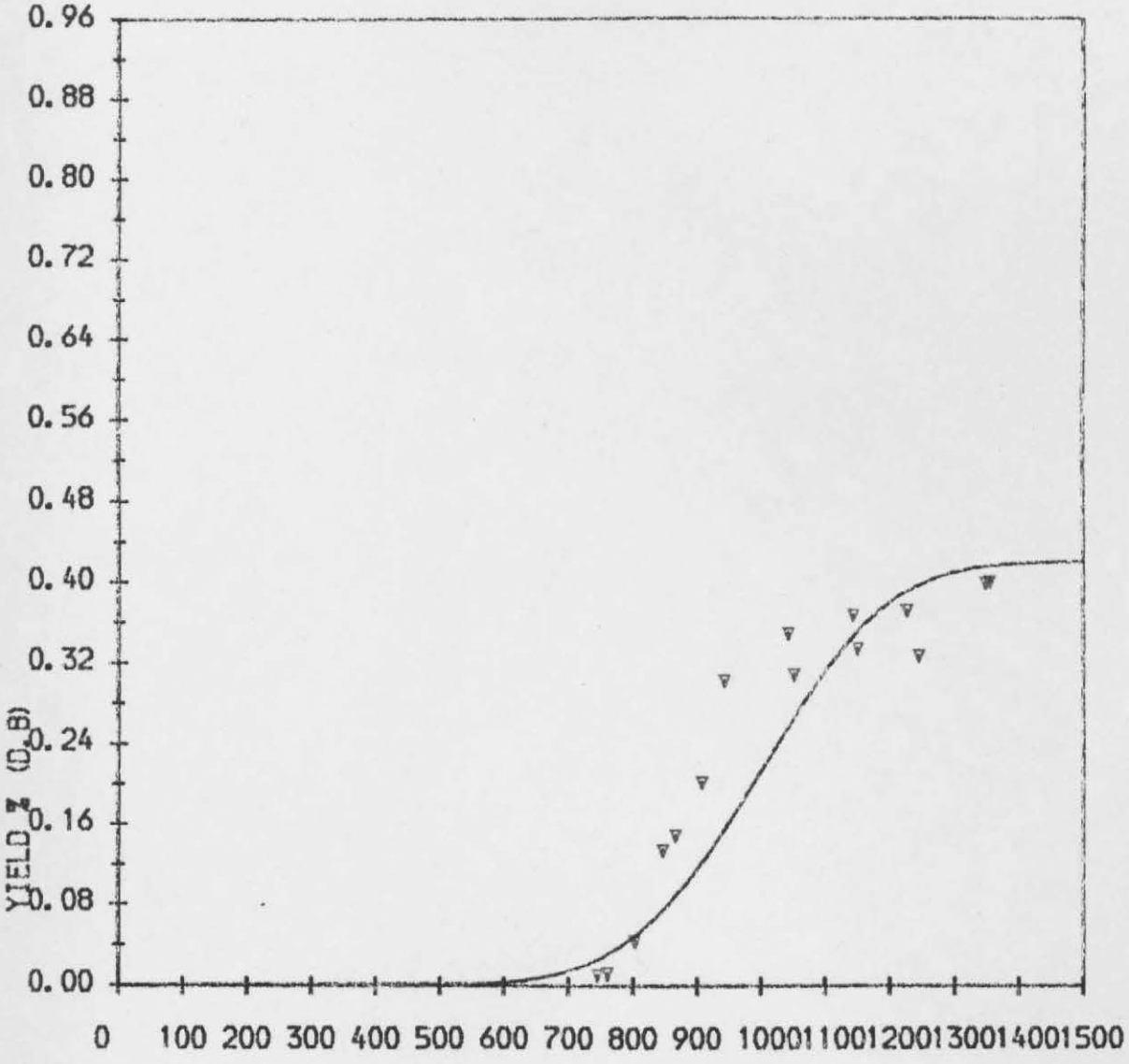

Goldthorpe
5,000°C/S
Vacuum
$C_2 H_6$

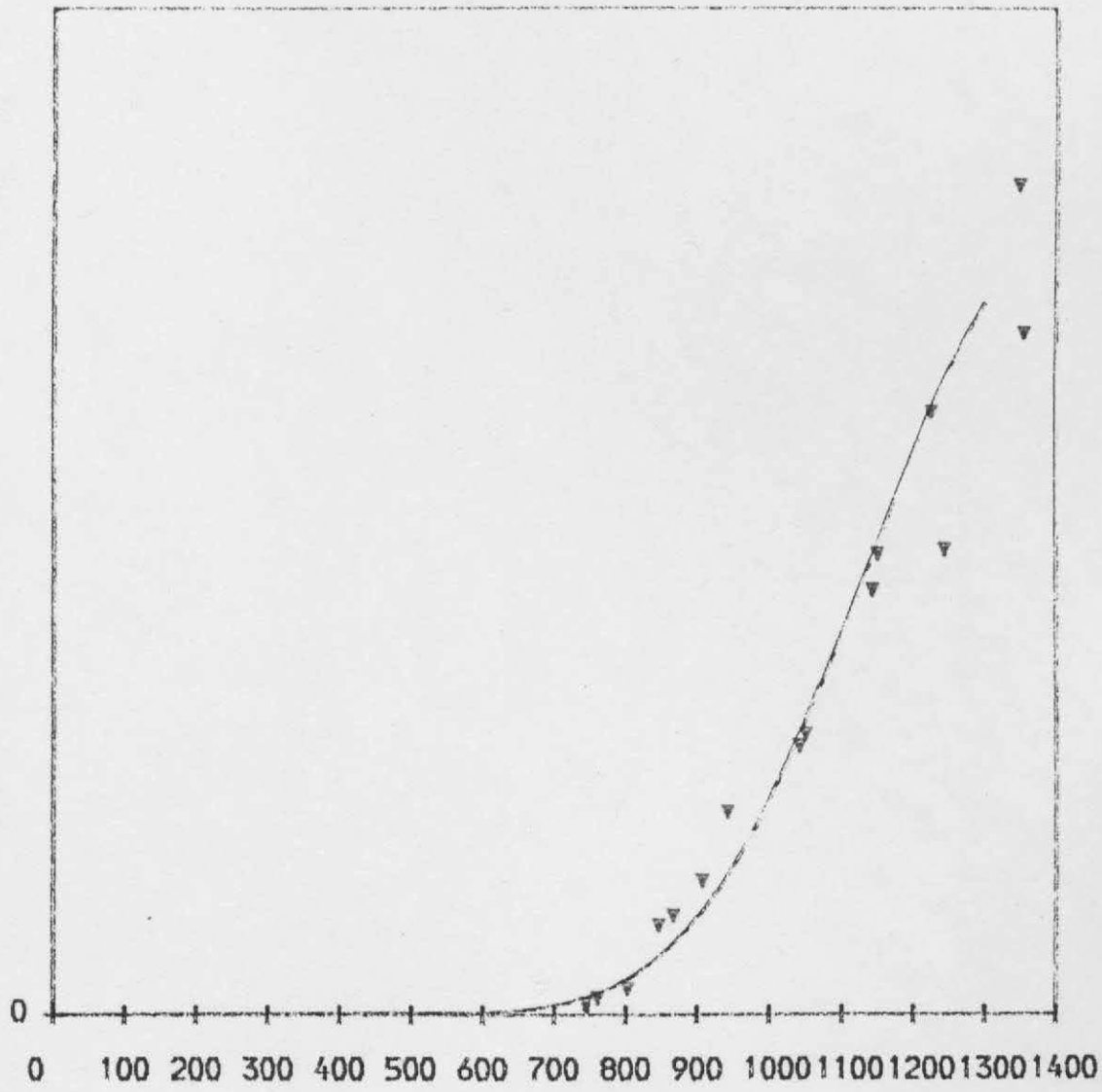

Goldthorpe
5,000°C/S
Vacuum
$C_2 H_4$

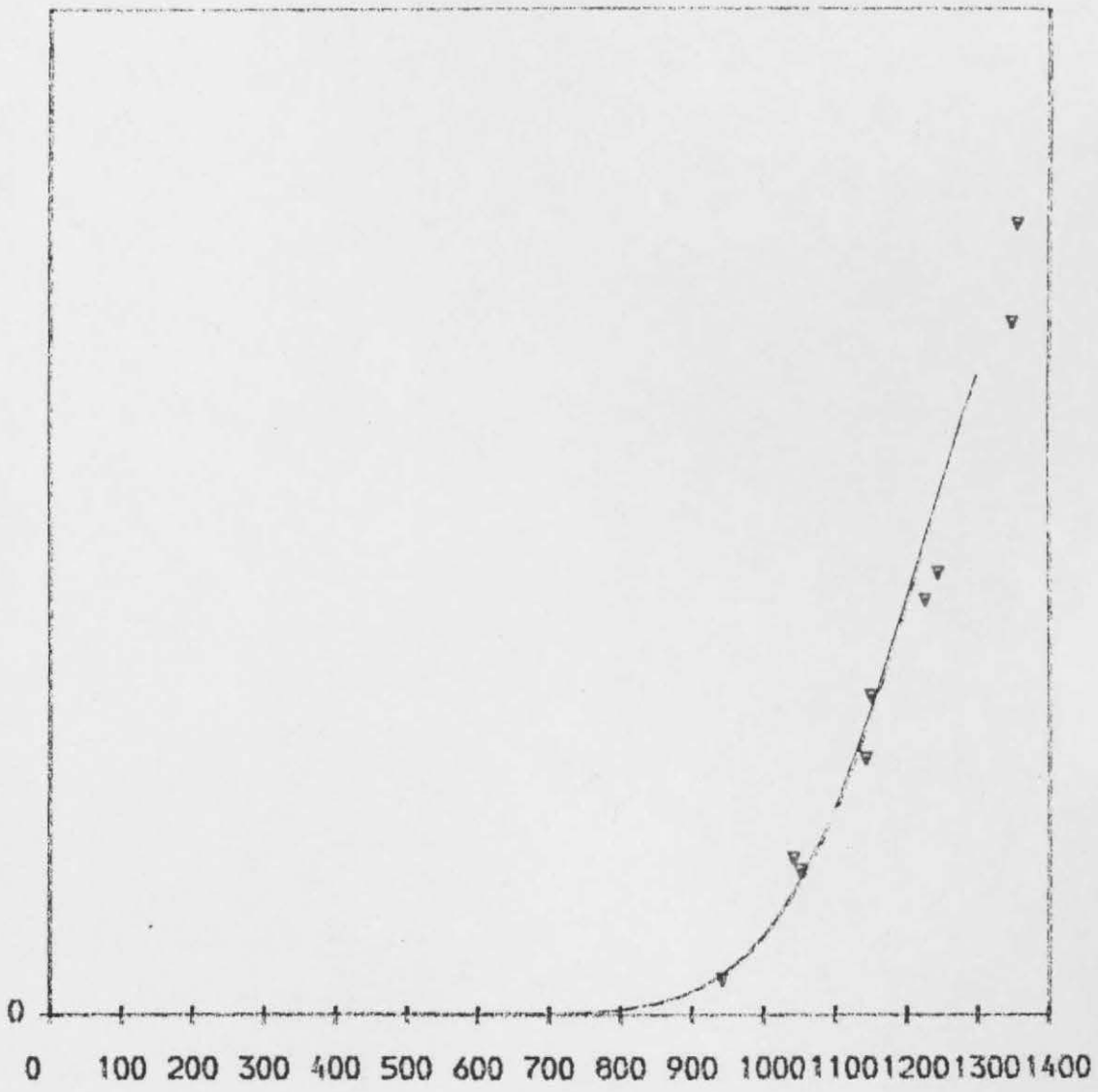

Goldthorpe
5,000°C/S
Vacuum
C_2 H_2

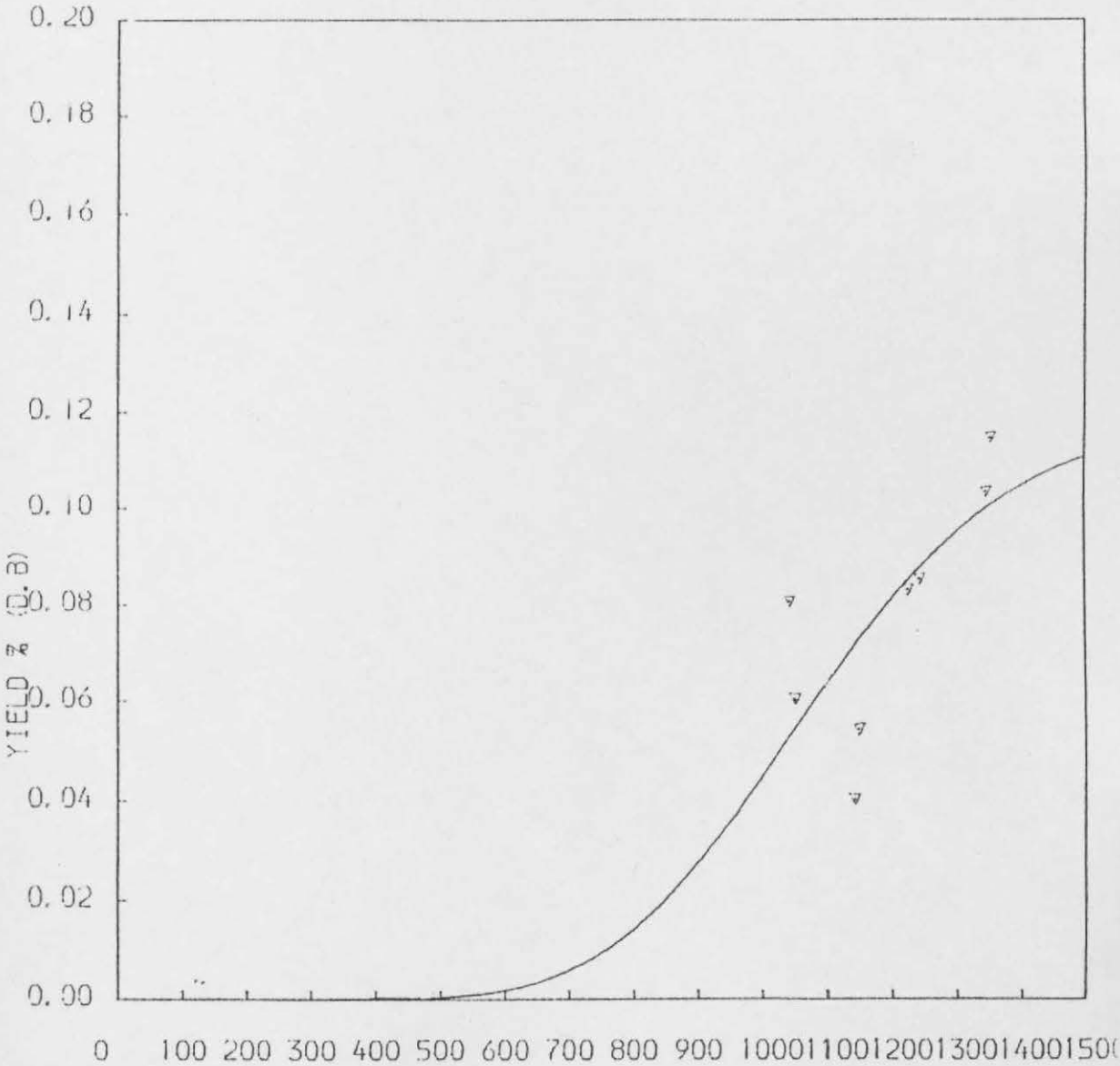

Goldthorpe

5,000°C/S
Vacuum
Butadiene

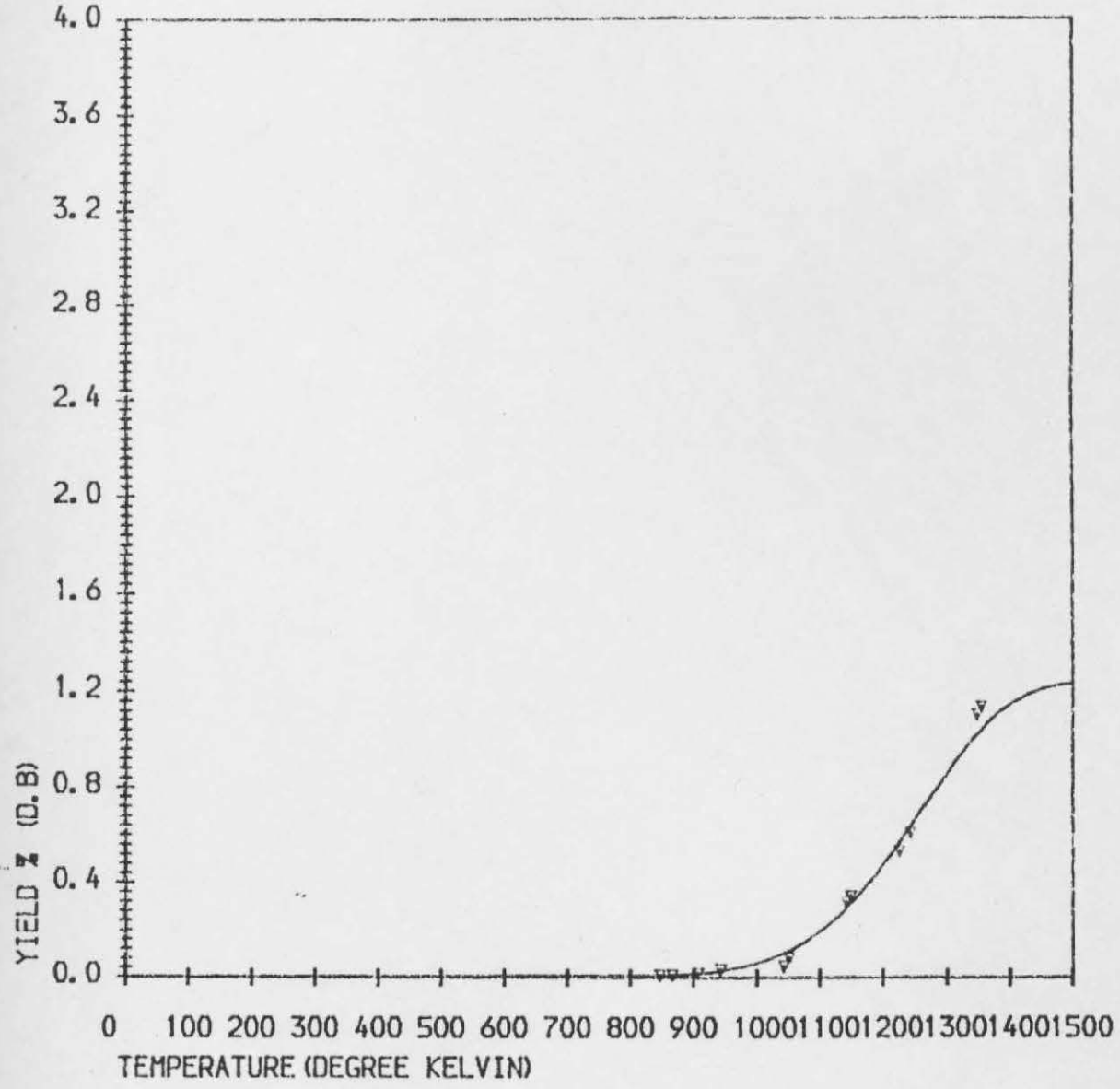

Goldthorpe
5,000°C/S
Vacuum
H_2

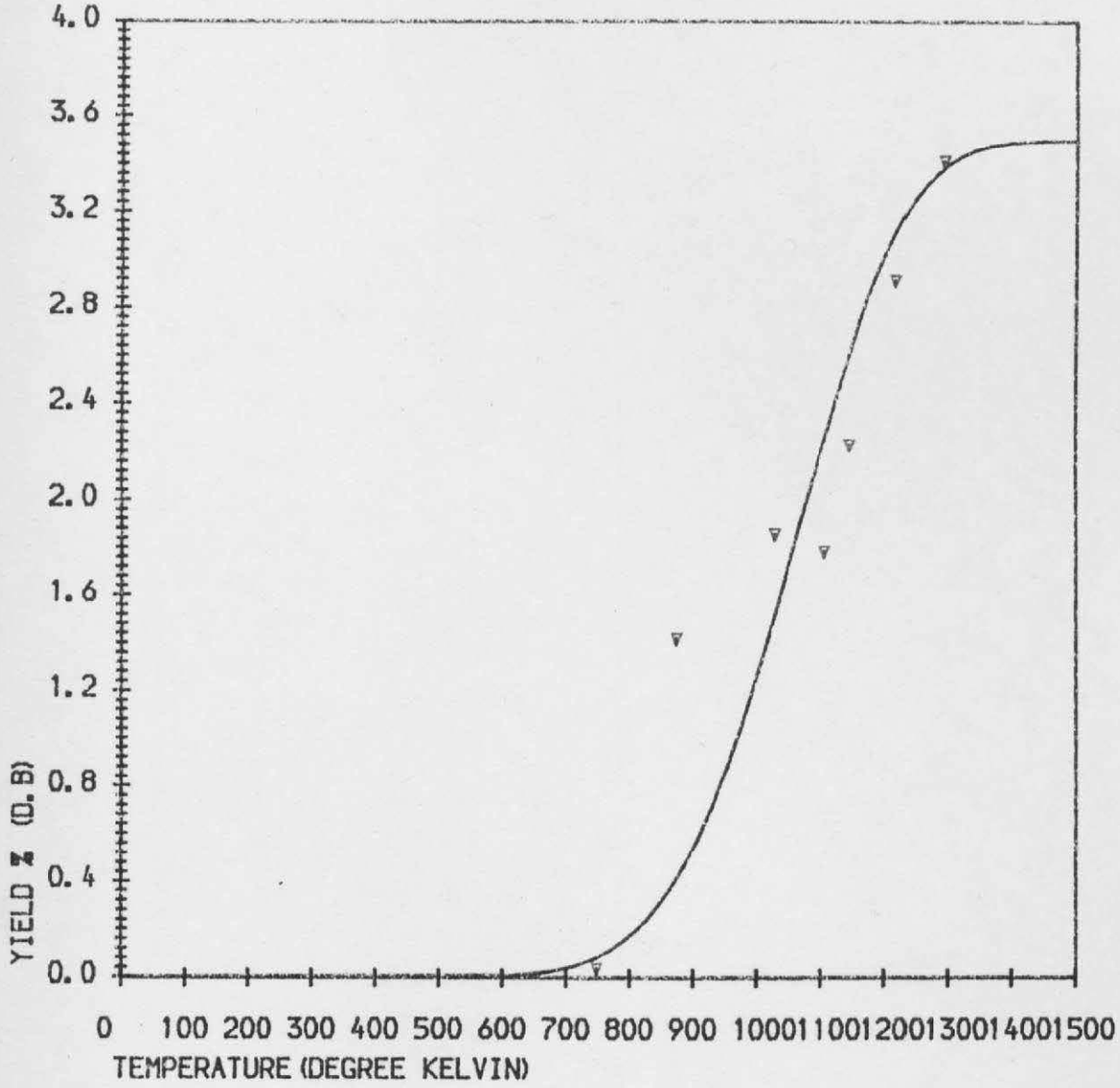

Goldthorpe
5,000°C/S
Atmosphere
CH_4

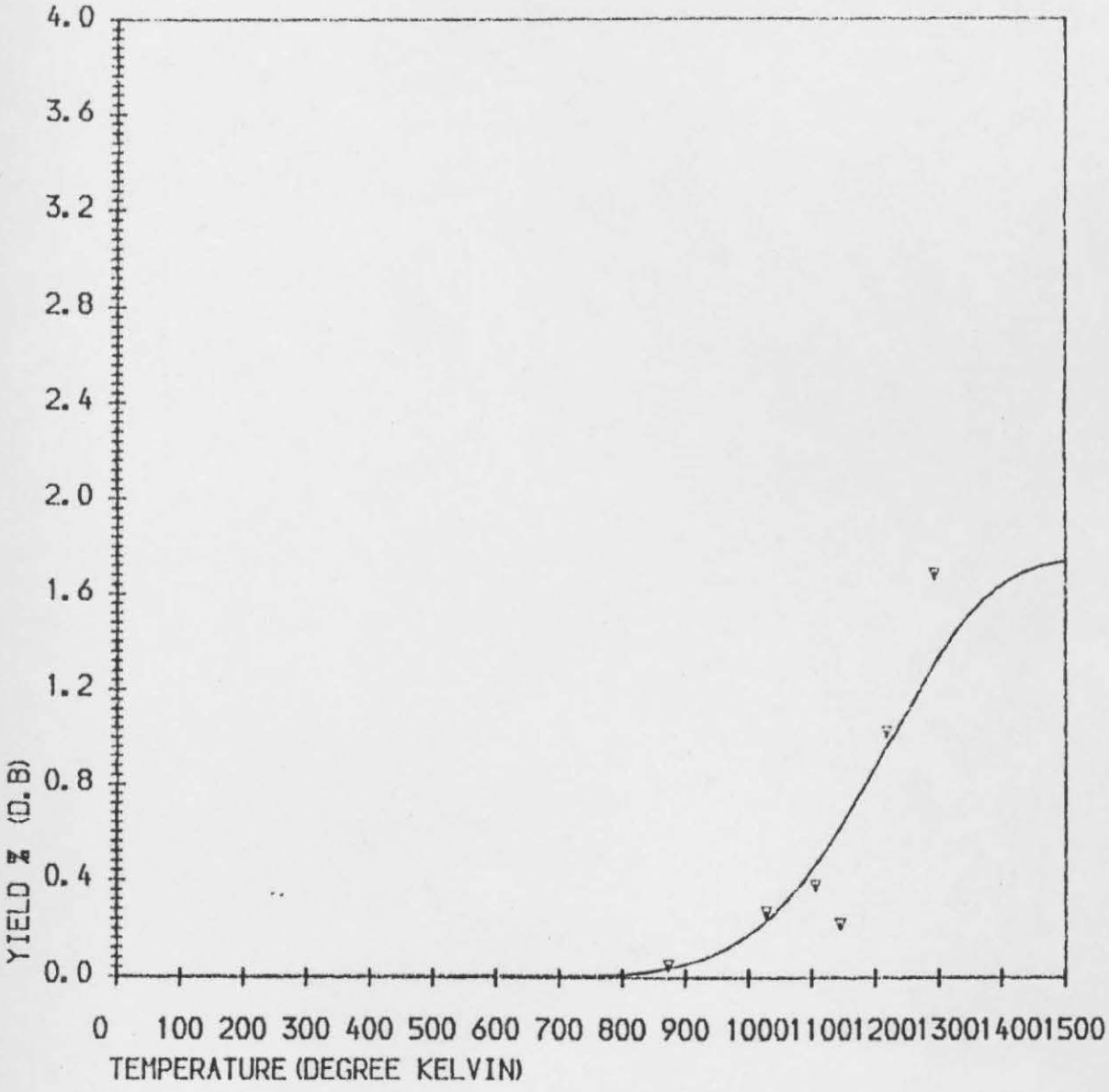

Goldthorpe

5,000°C/S

ATM.P

H_2 gas

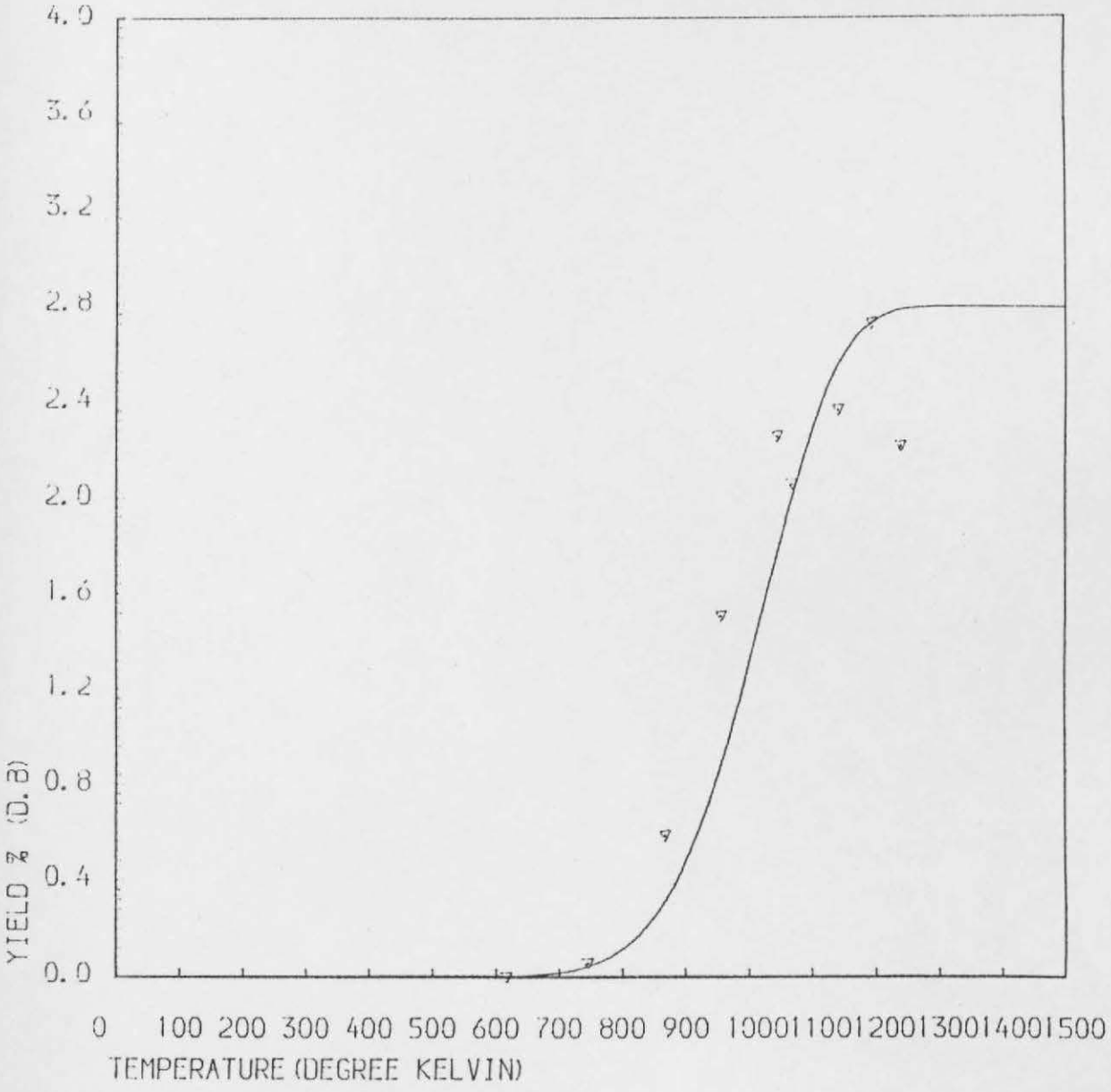

Goldthorpe
CH_4
10°C/S
Vacuum

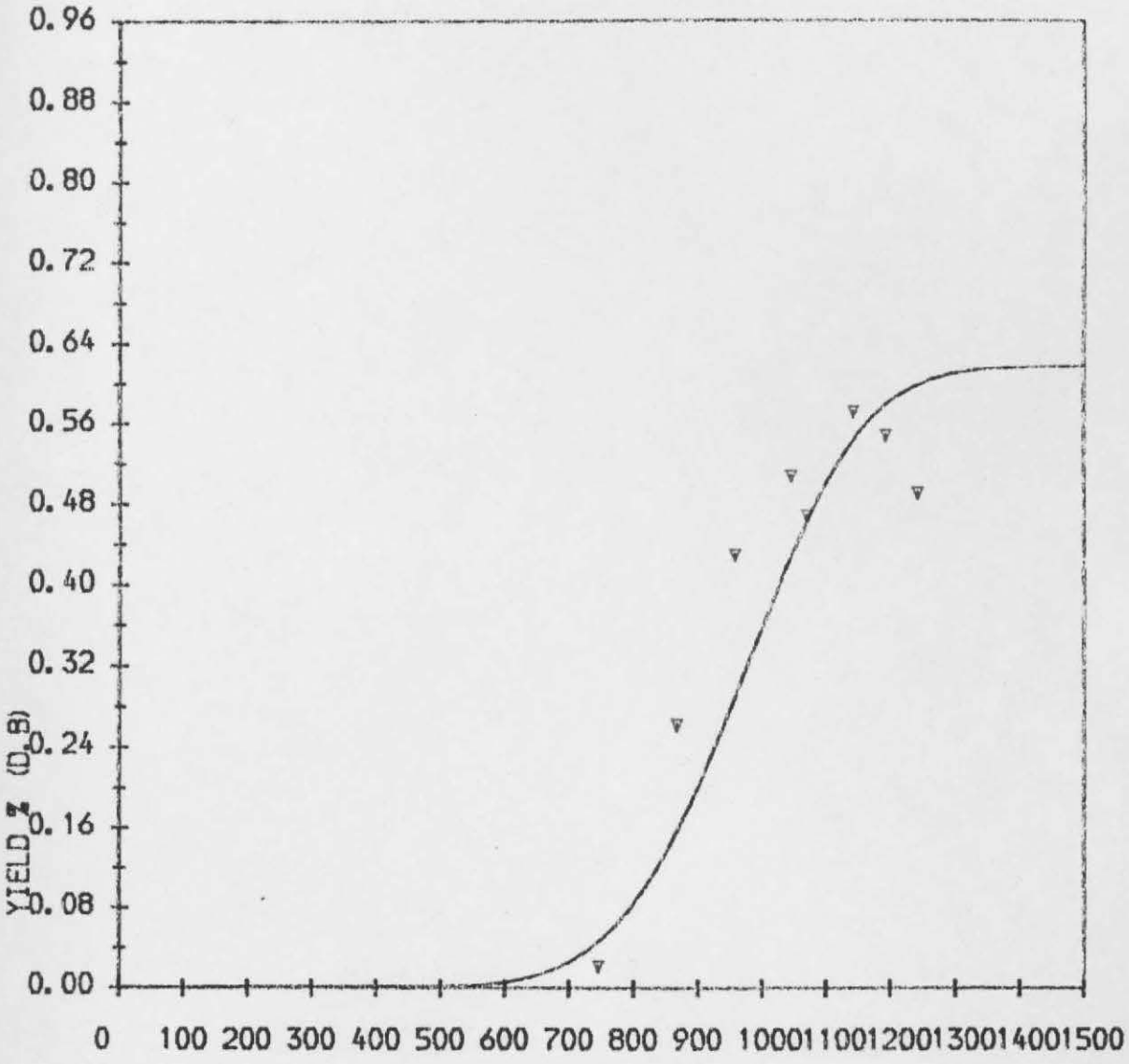

Goldthorpe
10°C/S
$C_2 H_6$
Vacuum

TEMPERATURE (DEGREE KELVIN)

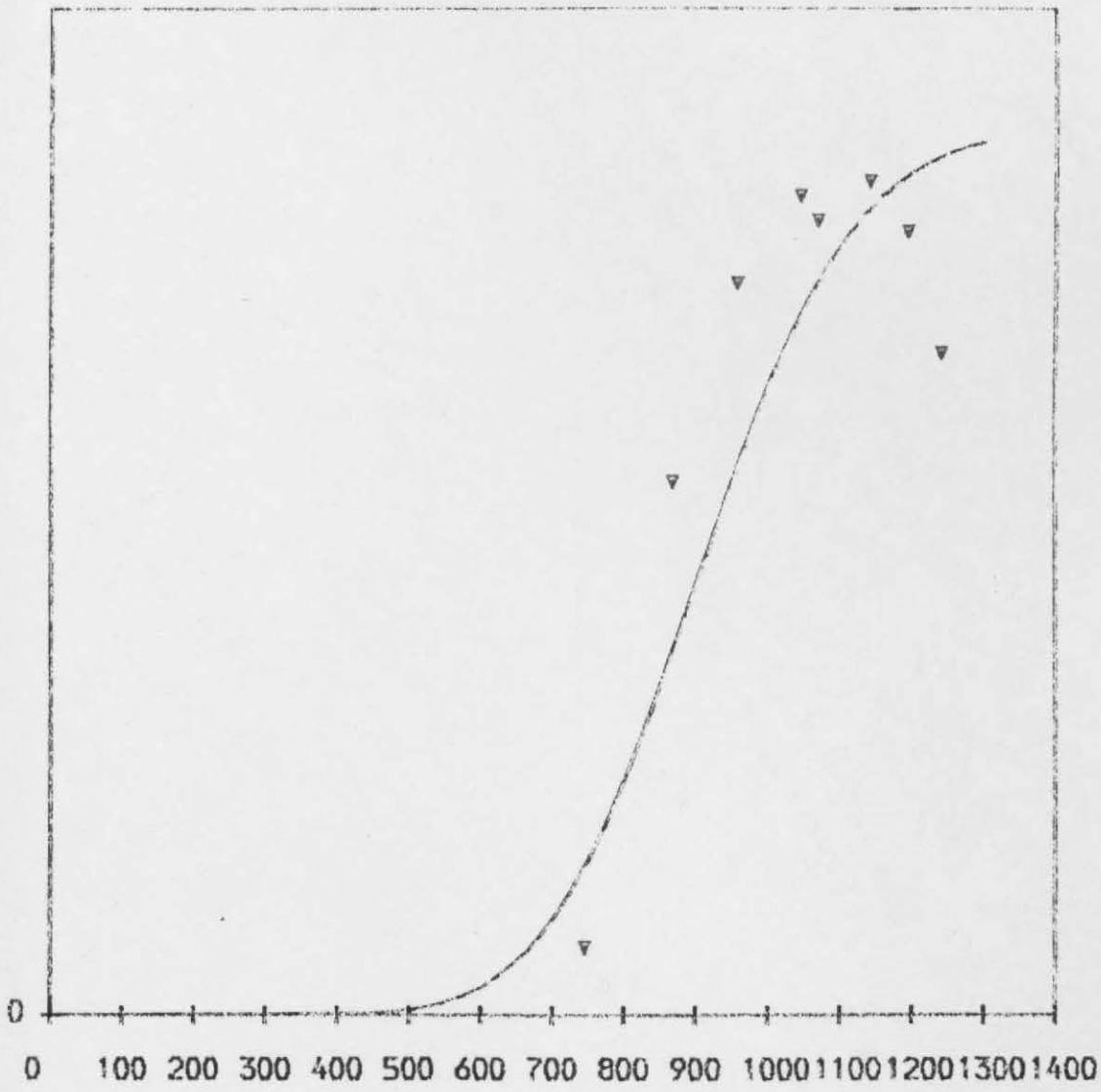

Goldthorpe
10°C/S
Vacuum
$C_3 H_8$

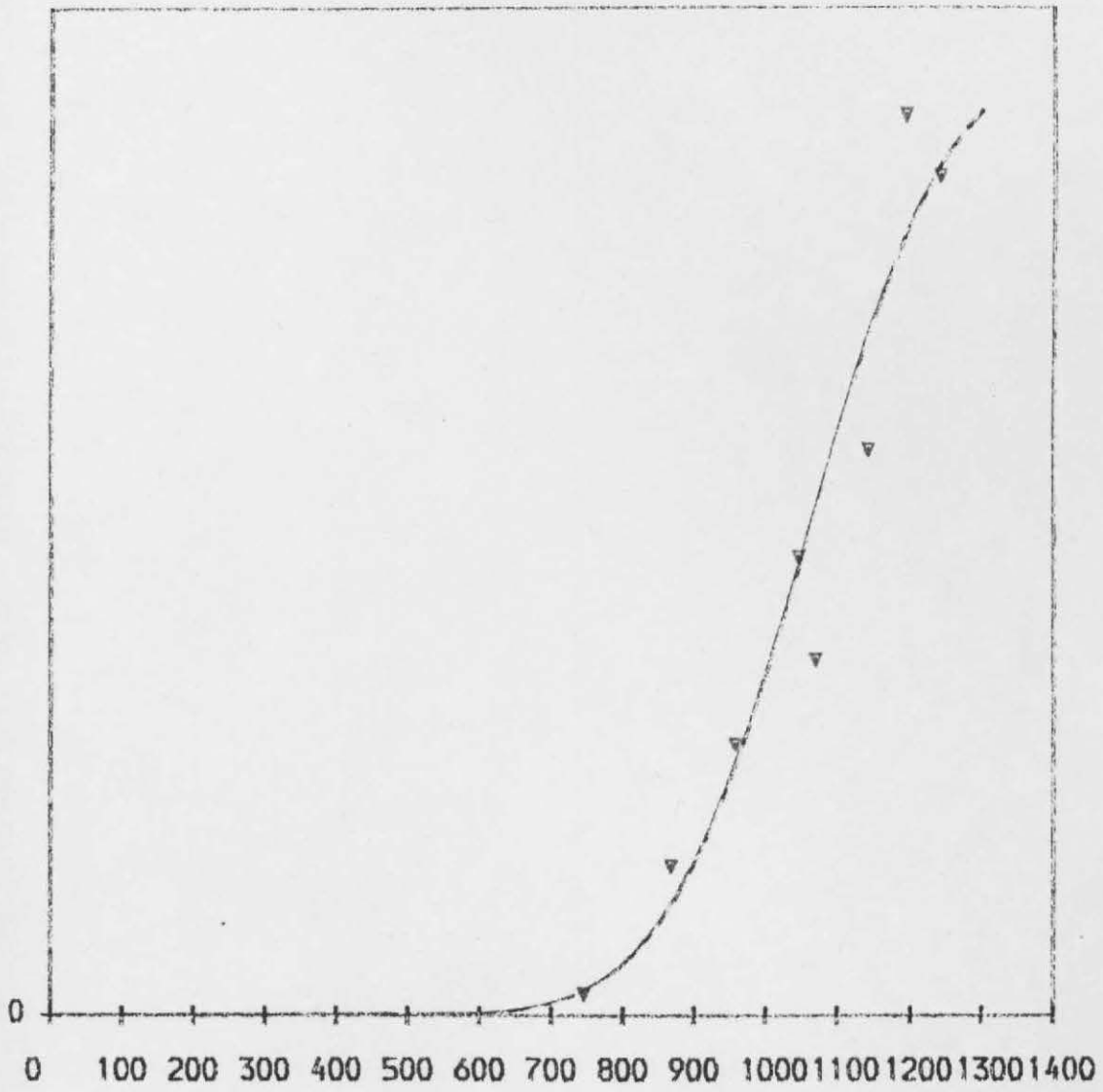

Goldthorpe
10°C/S
Vacuum
$C_2 H_4$

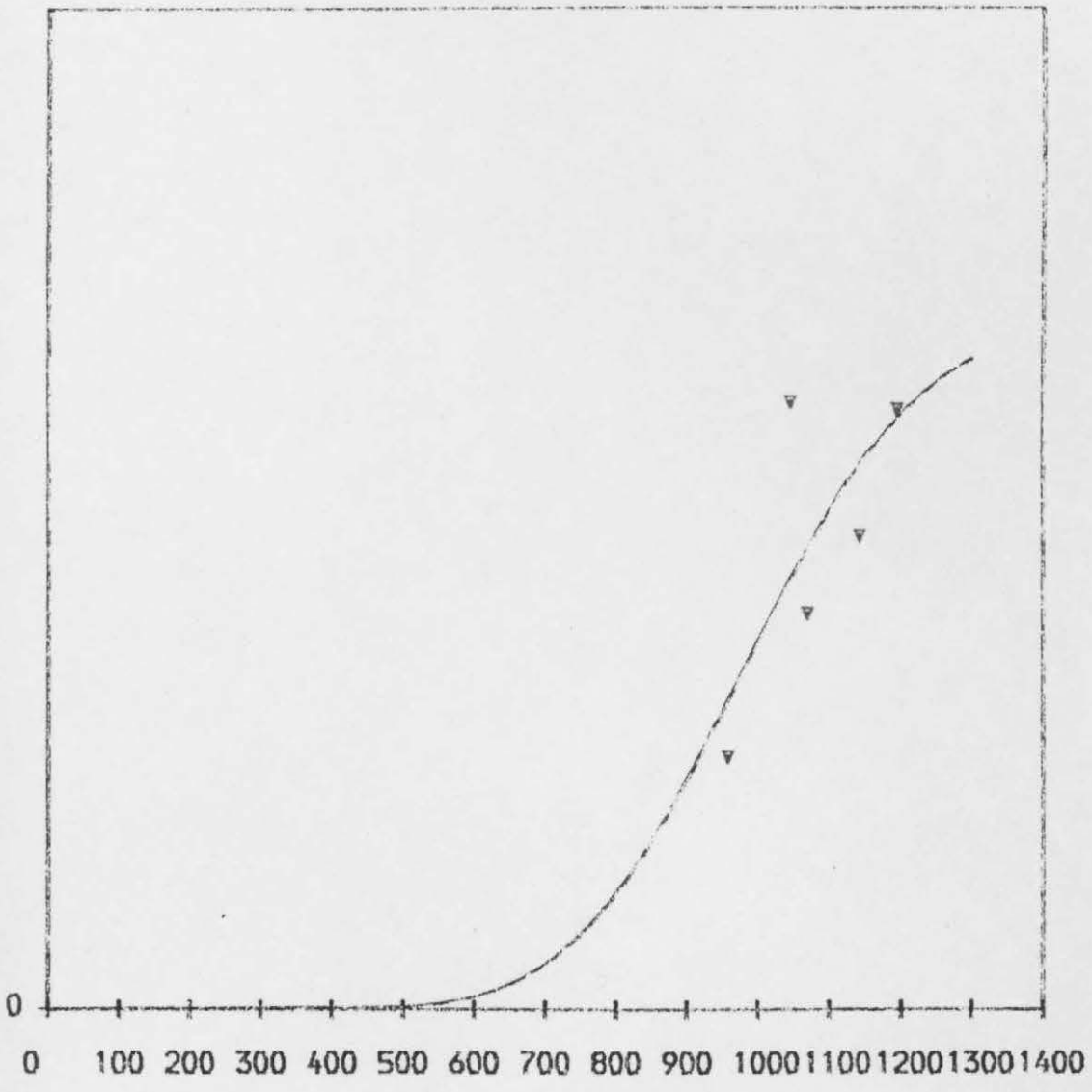

Goldthorpe
10°C/S
Bit-1-ene
Vacuum

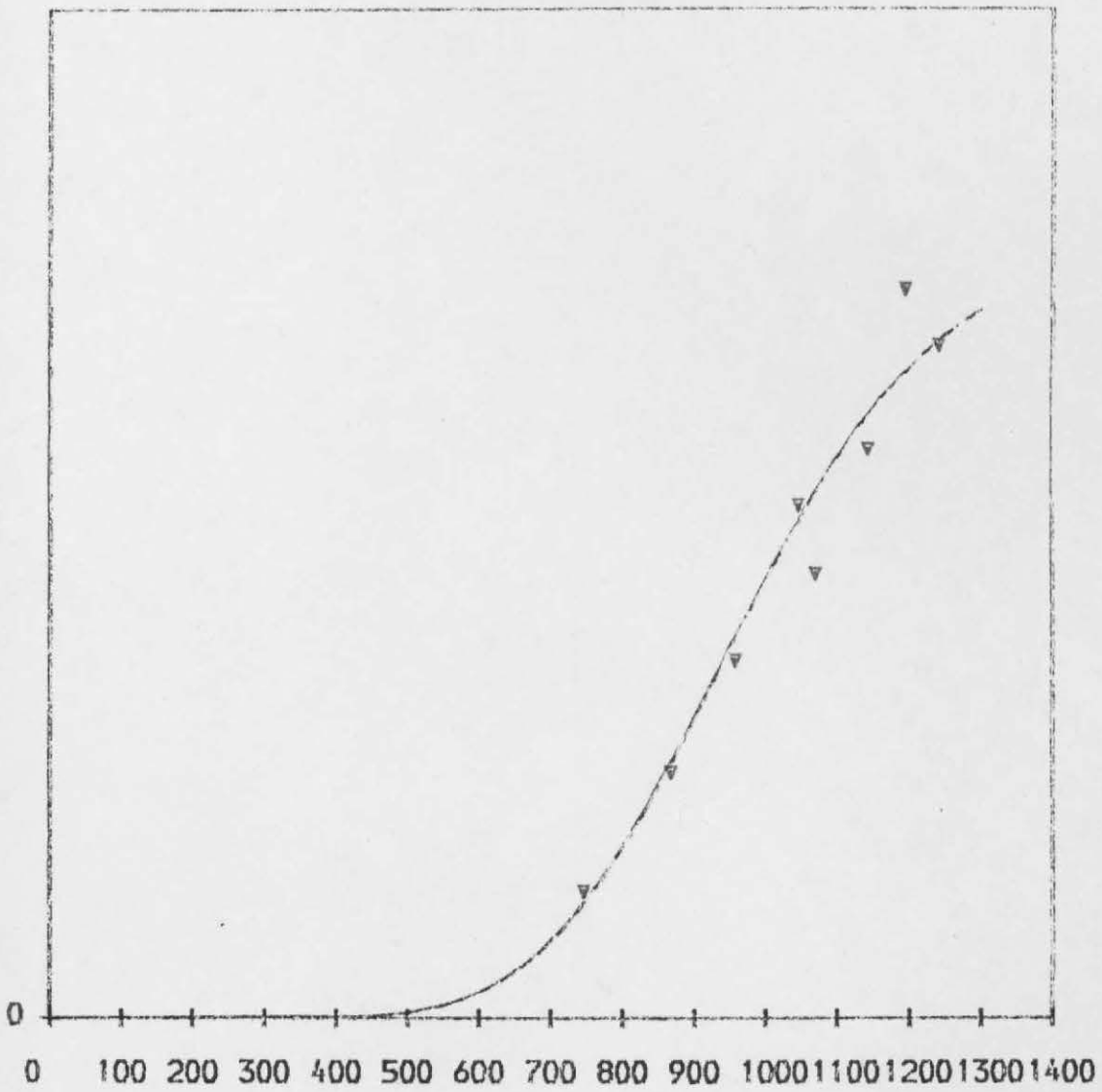

Goldthorpe
10°C/S
Vacuum
C_3H_6

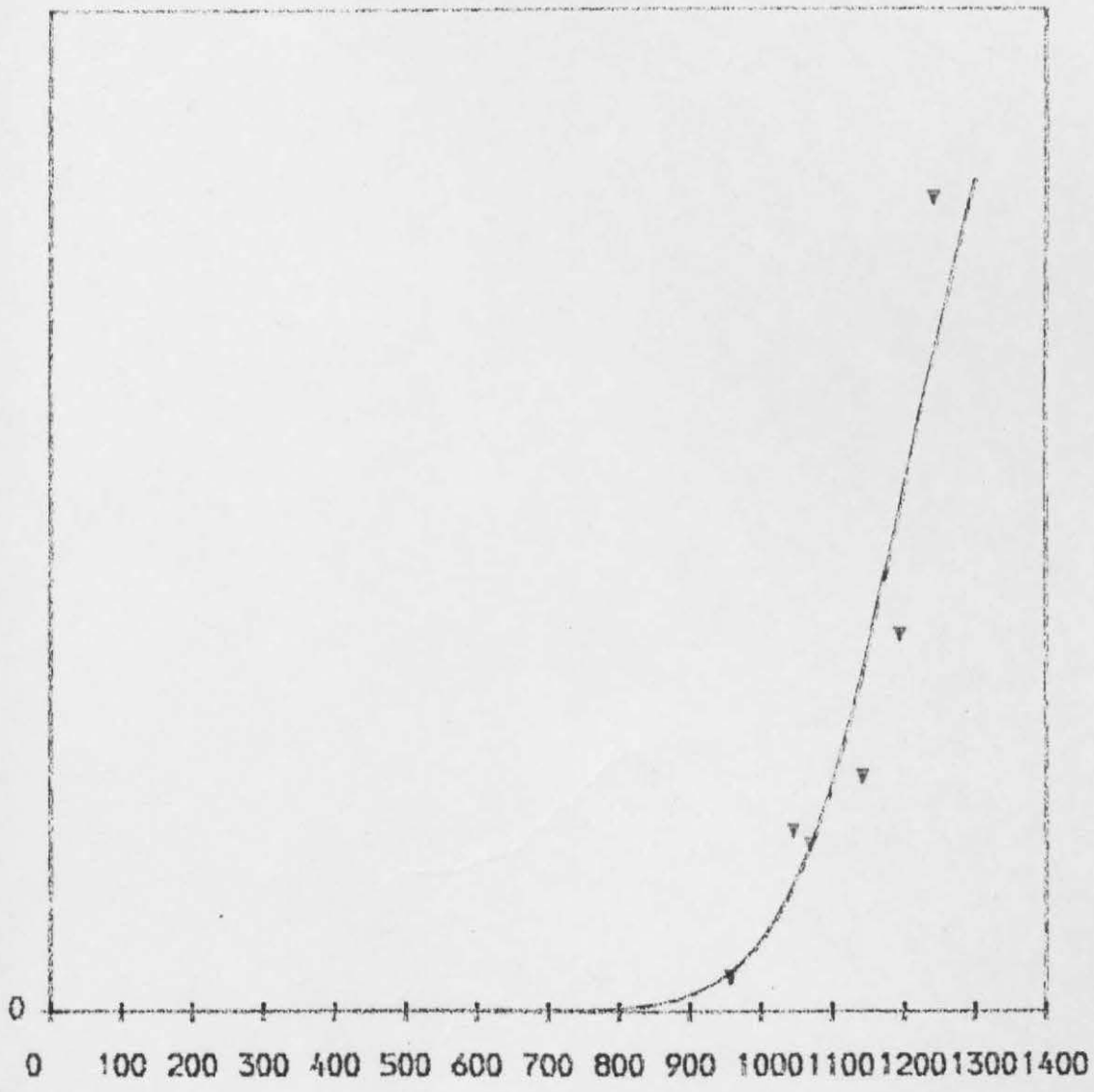

Goldthorpe
Vacuum
10°C/S
C_2 H_2

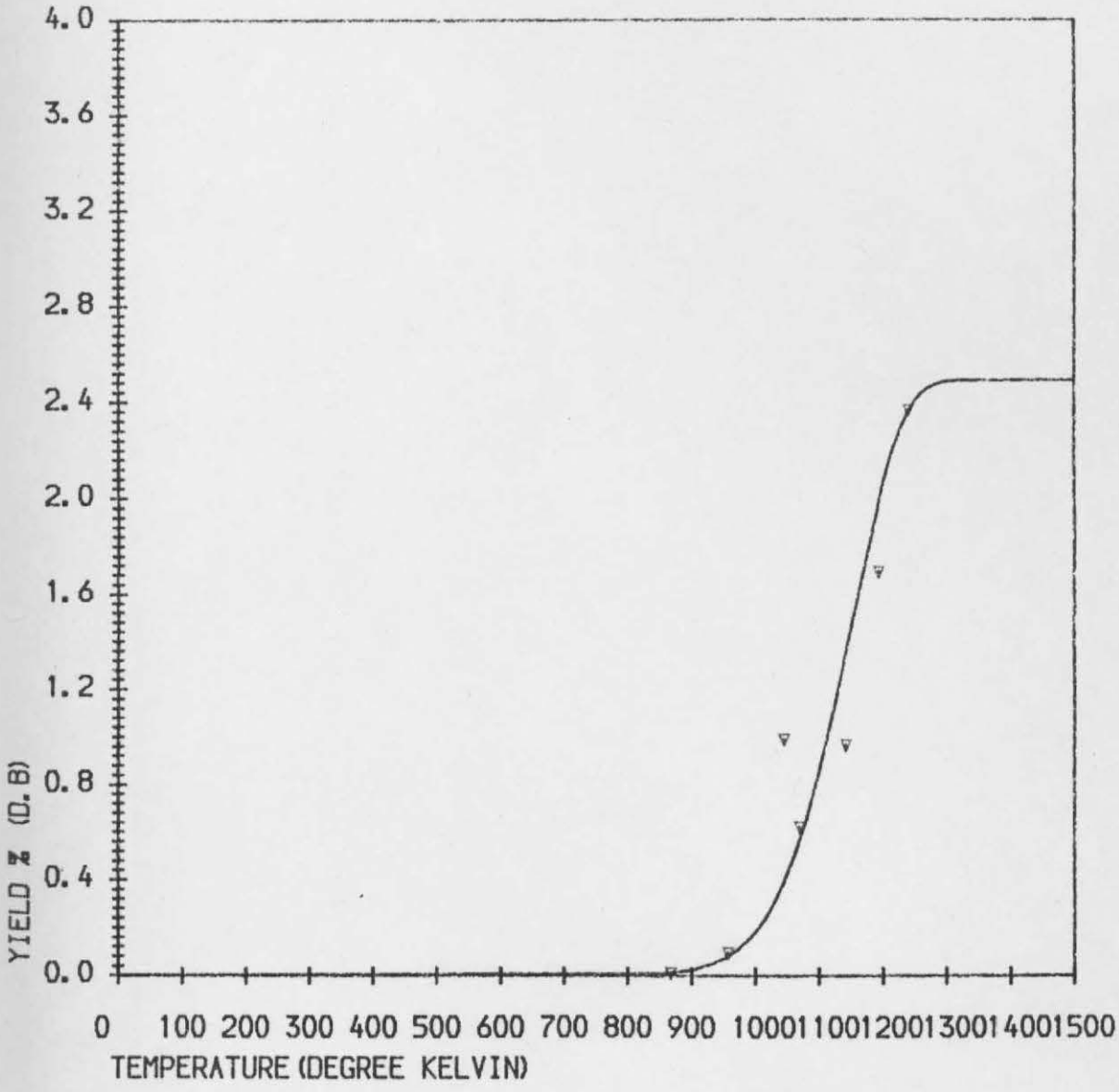

Goldthorpe
10°C/S
Vacuum
H_2

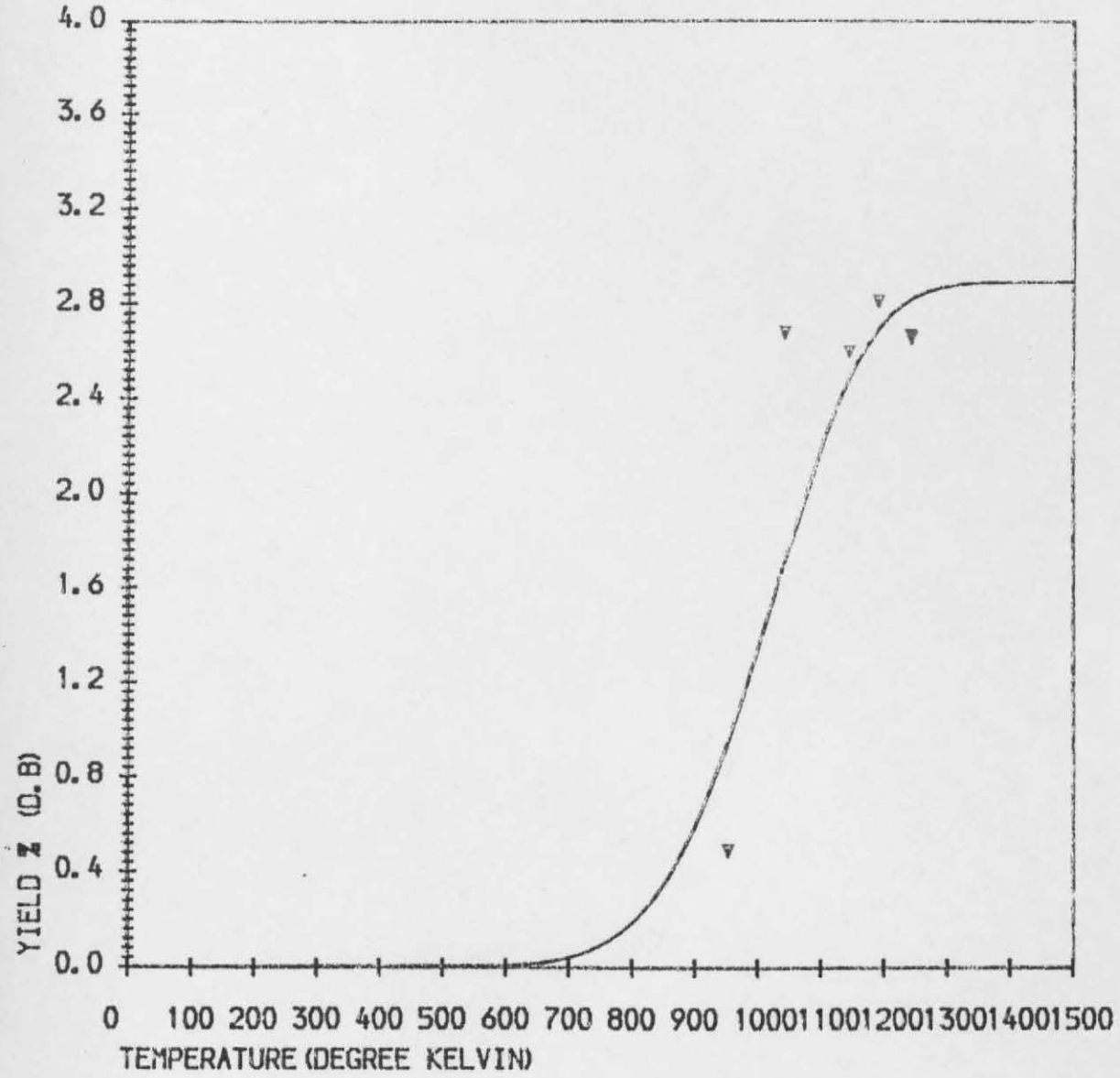

Goldthorpe
10°C/S
Atm. P $C_2 H_6$

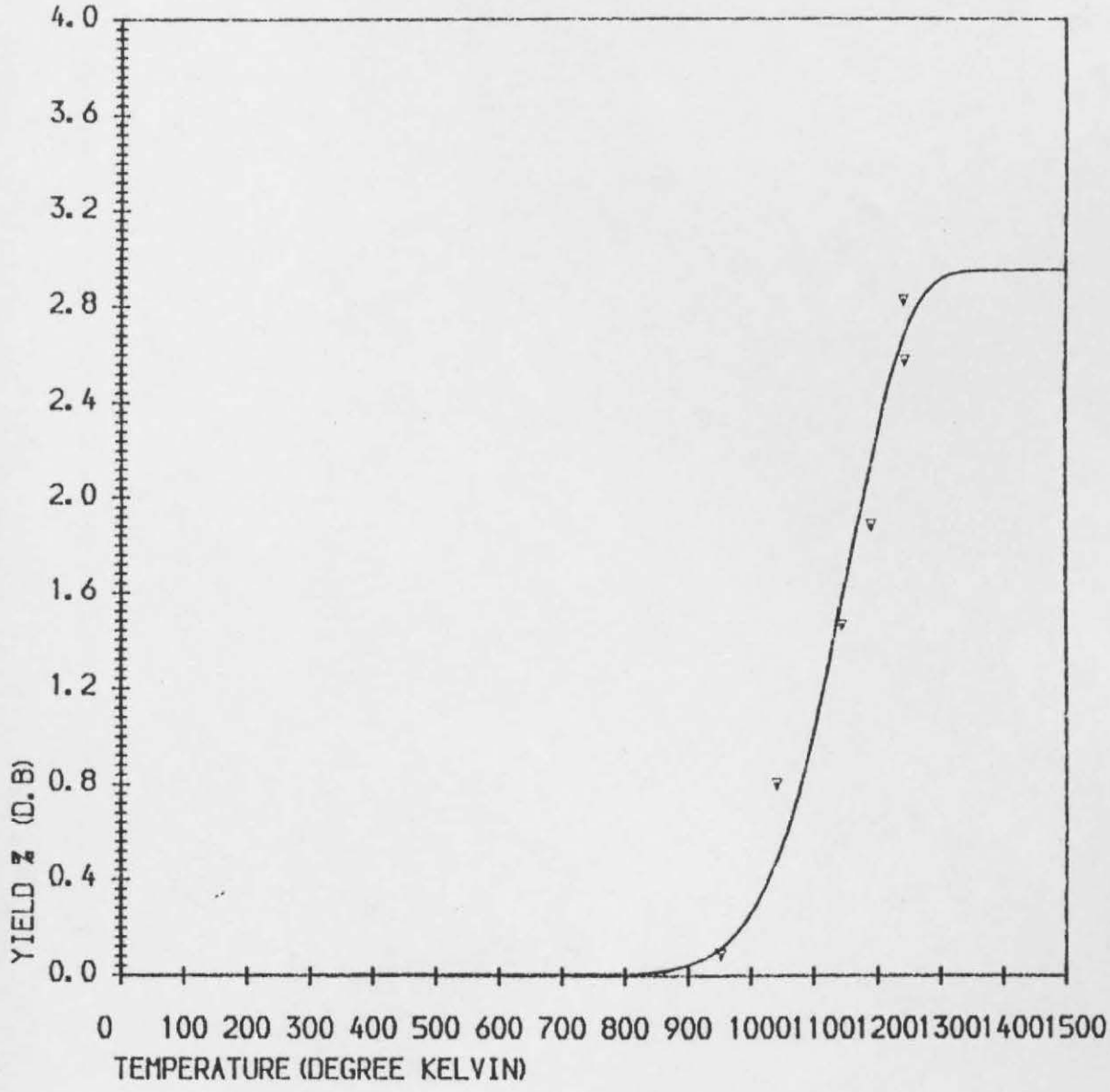

Goldthorpe
10°C/S
Atm. P
H_2

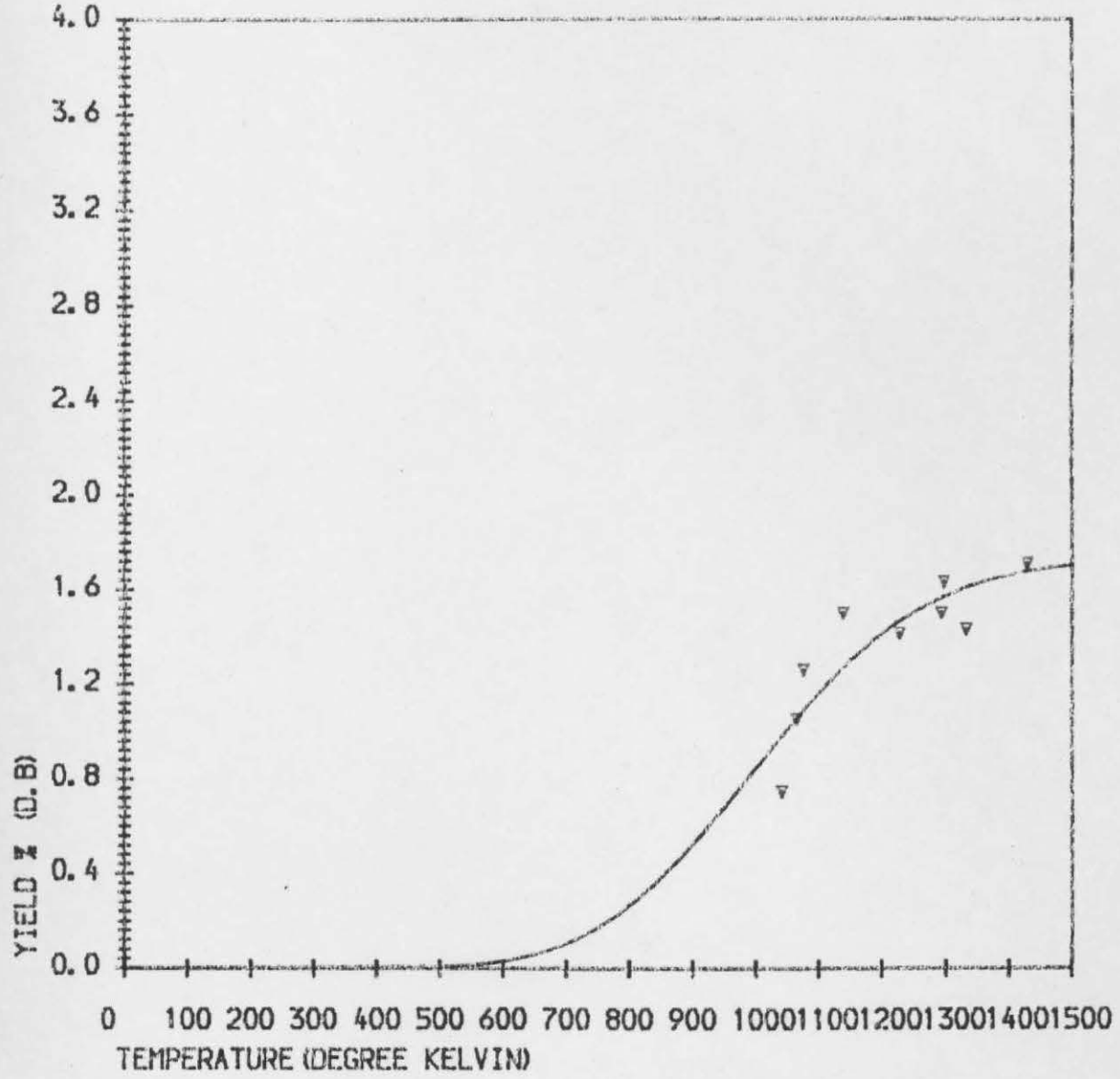

Markham Main
5,000°C/S
Vacuum
CH_4 gas

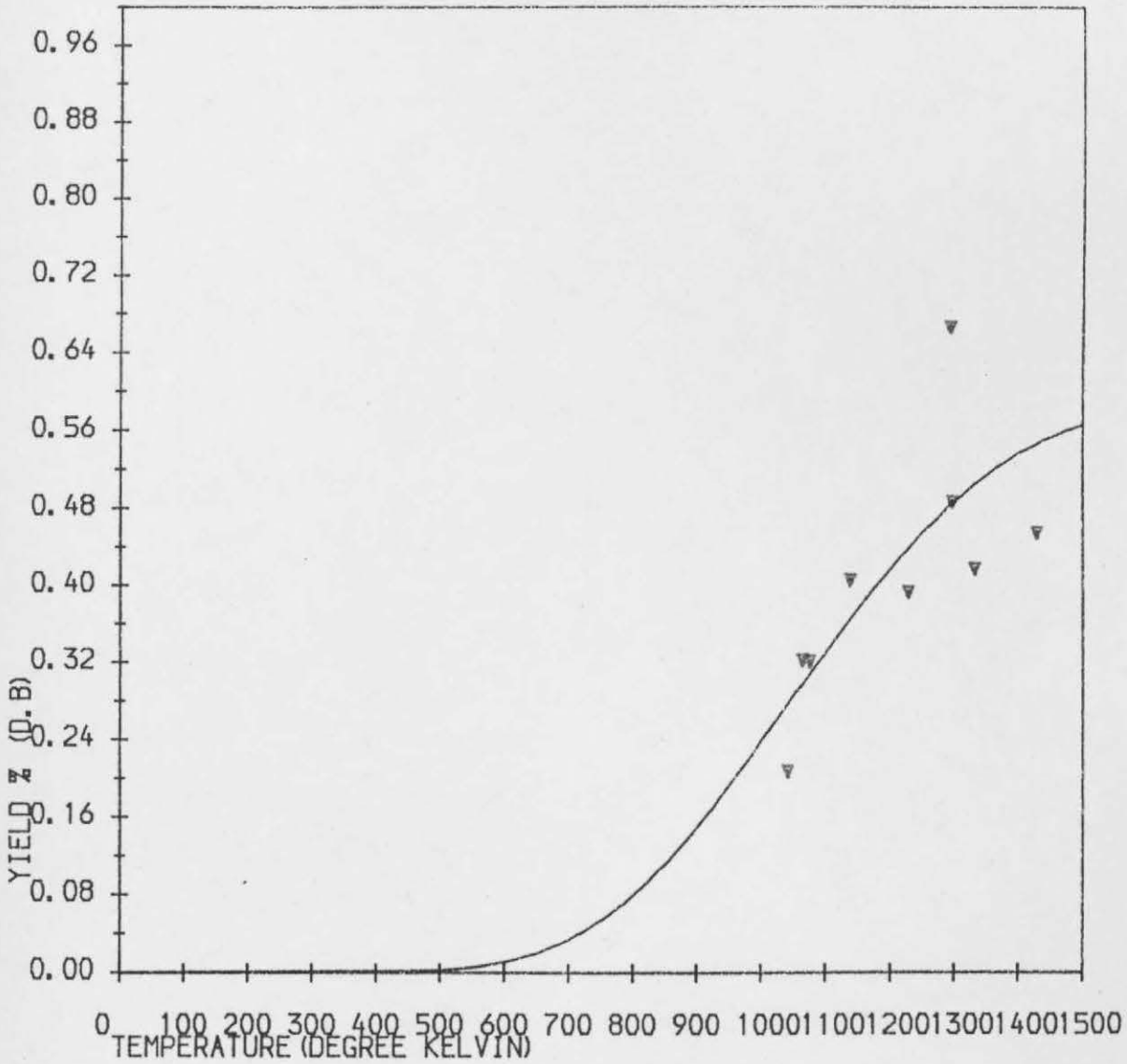

Markham Main
5,000°C/S
$C_2 H_6$
Vacuum

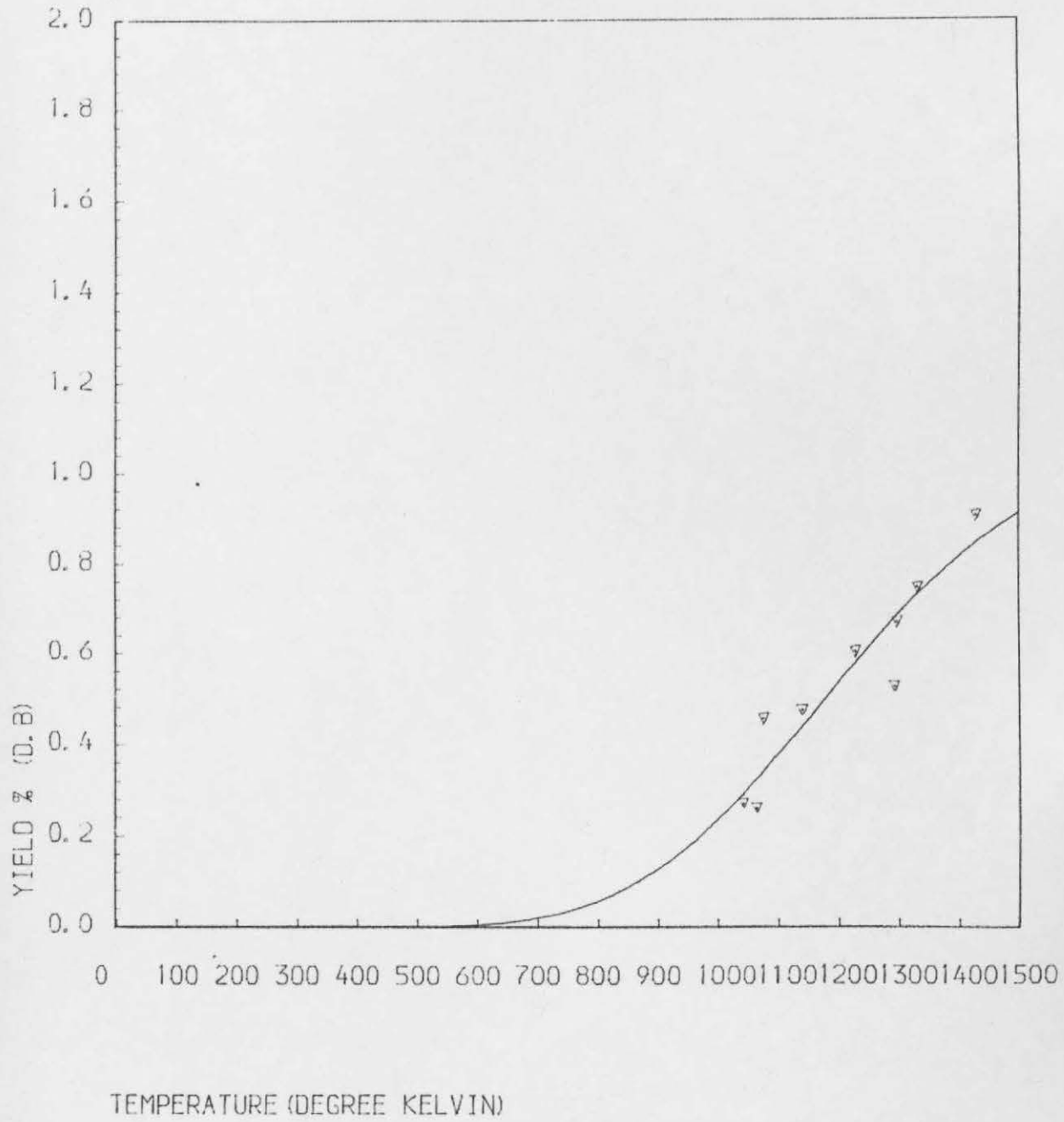

Markham Main
$C_2 H_4$
5.000°C/S
Vacuum

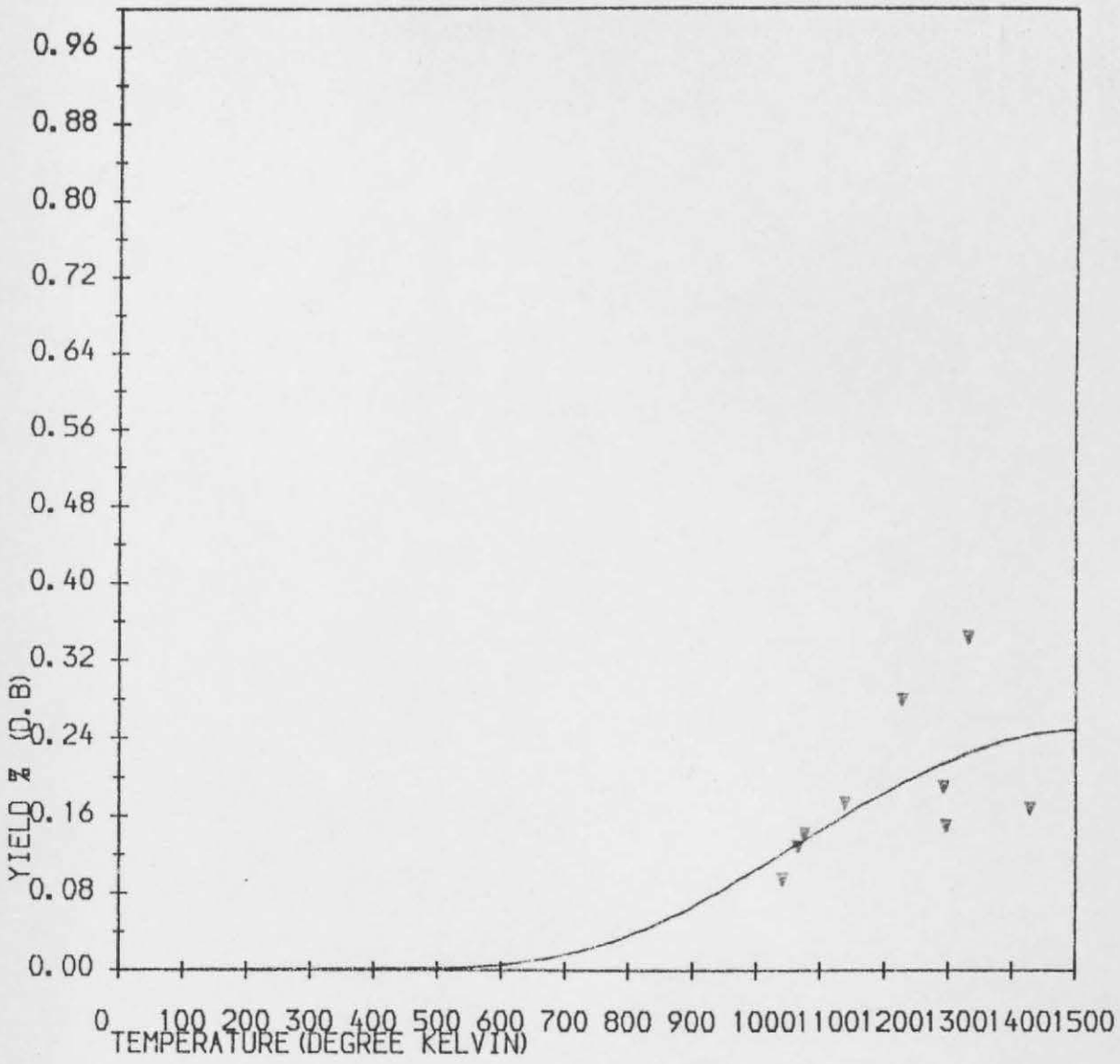

Markham Main
5,000°C/S
$C_3 H_8$
Vacuum

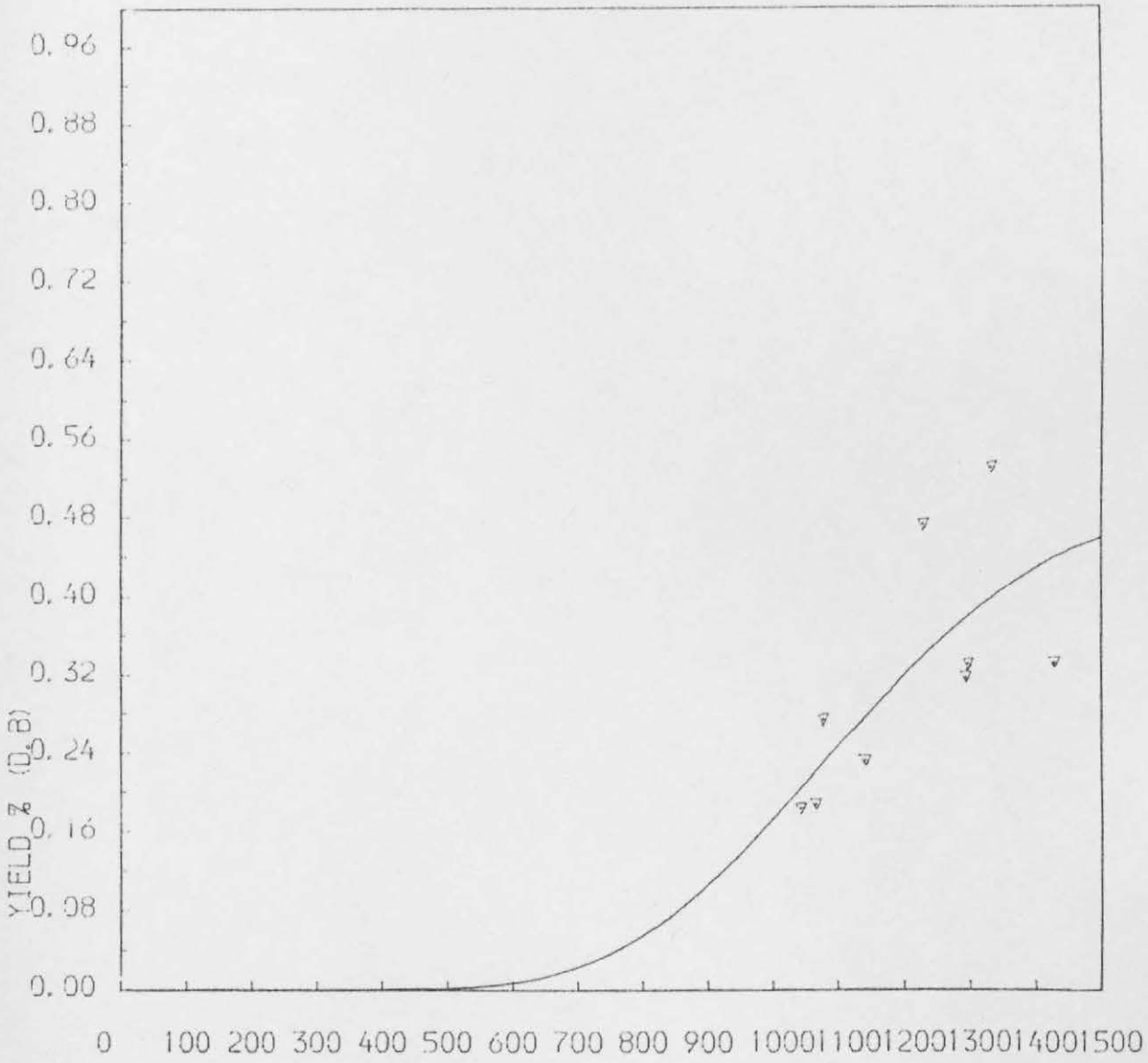

Markham Main

5,000°C/S
Vacuum
C_3H_6

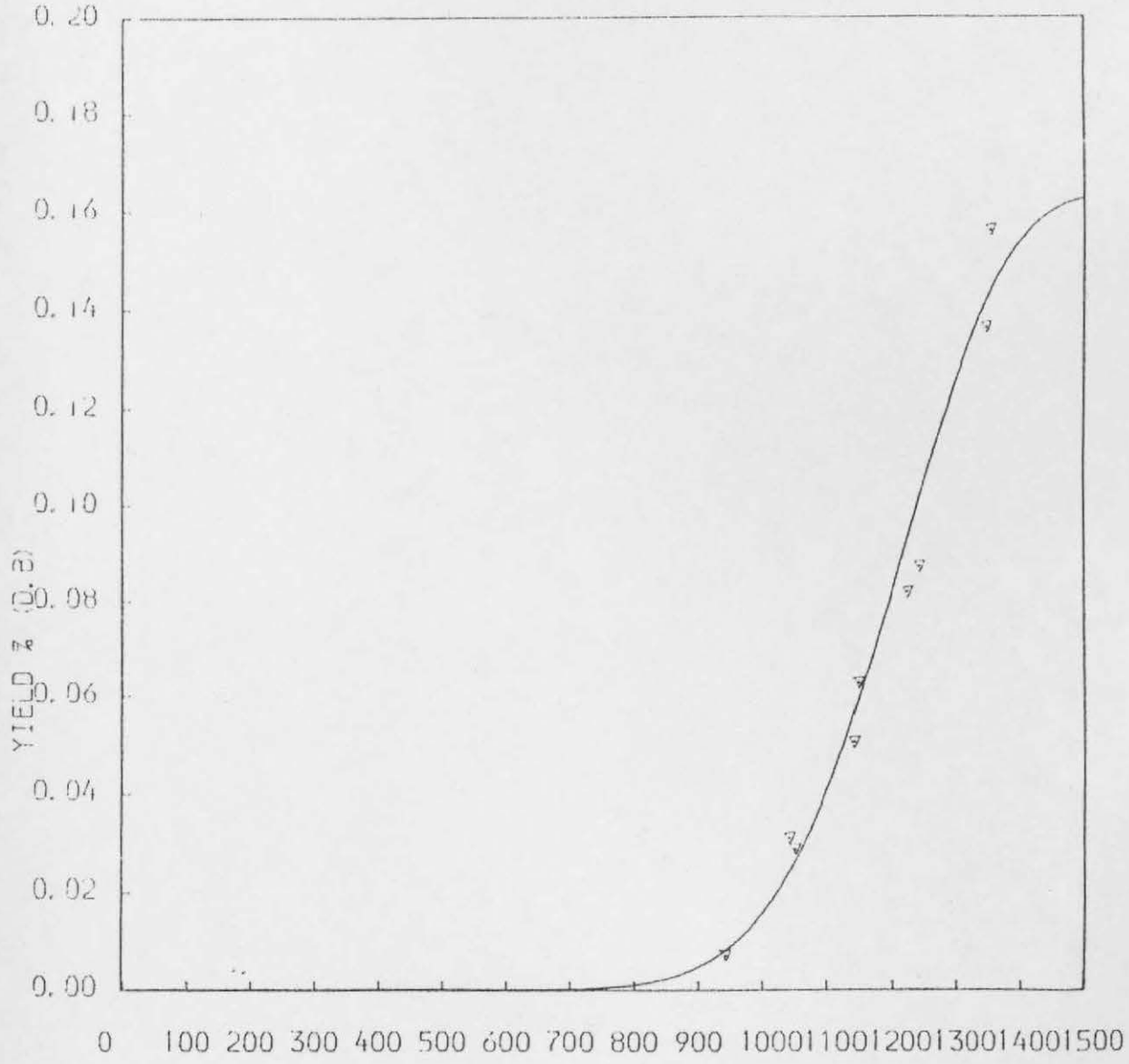
0.20
0.18
0.16
0.14
0.12
0.10
0.08
0.06
0.04
0.02
0.00
YIELD
0
100 200 300 400 500 600 700 800 900 1000 1100 1200 1300 1400 1500
TEMPERATURE (DEGREE KELVIN)
Goldthorpe
5,000°C/S
Vacuum
$C_2 H_2$

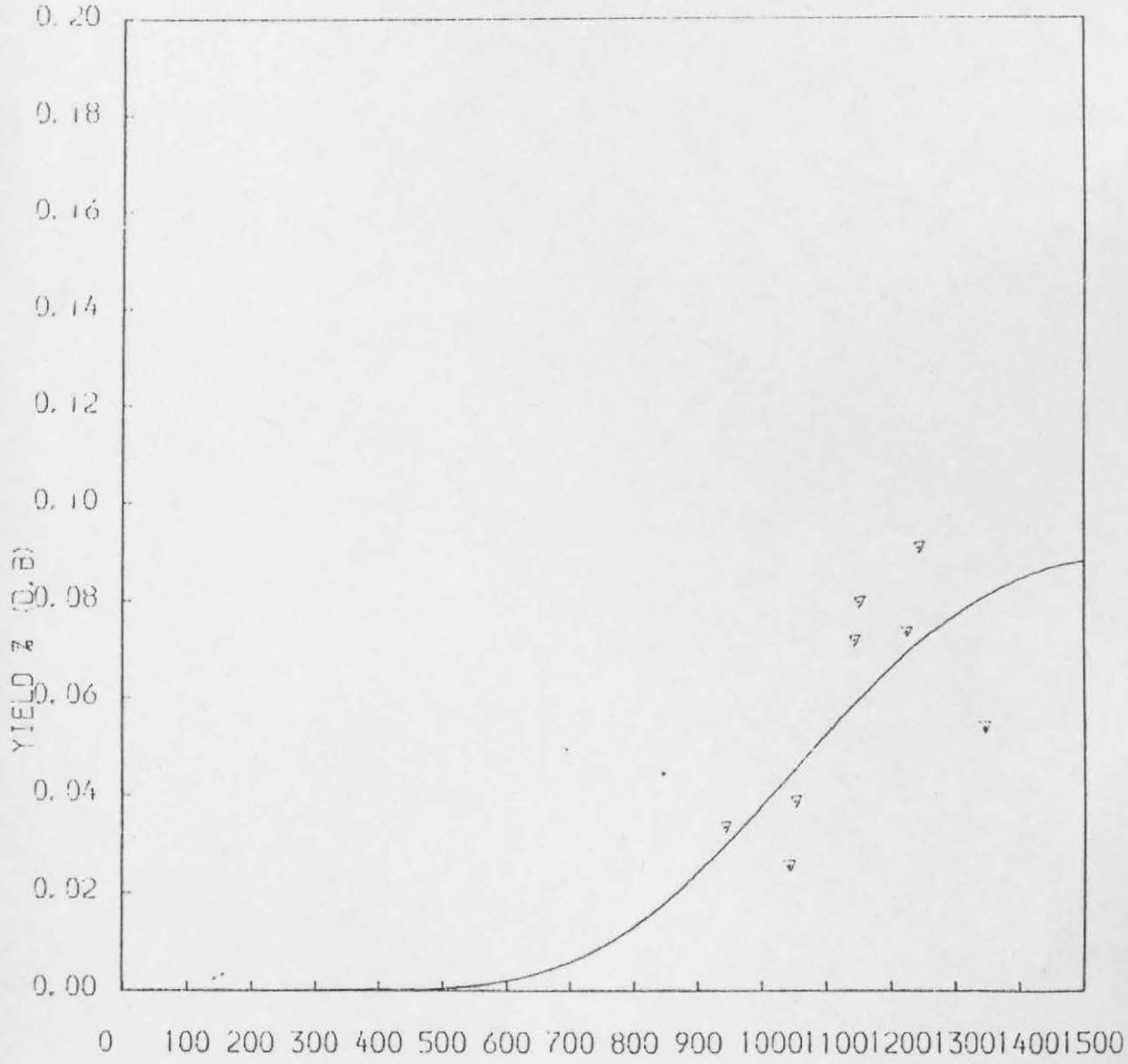

GOLDTHORPE
5,000°C/S
Vacuum
But-1-ene

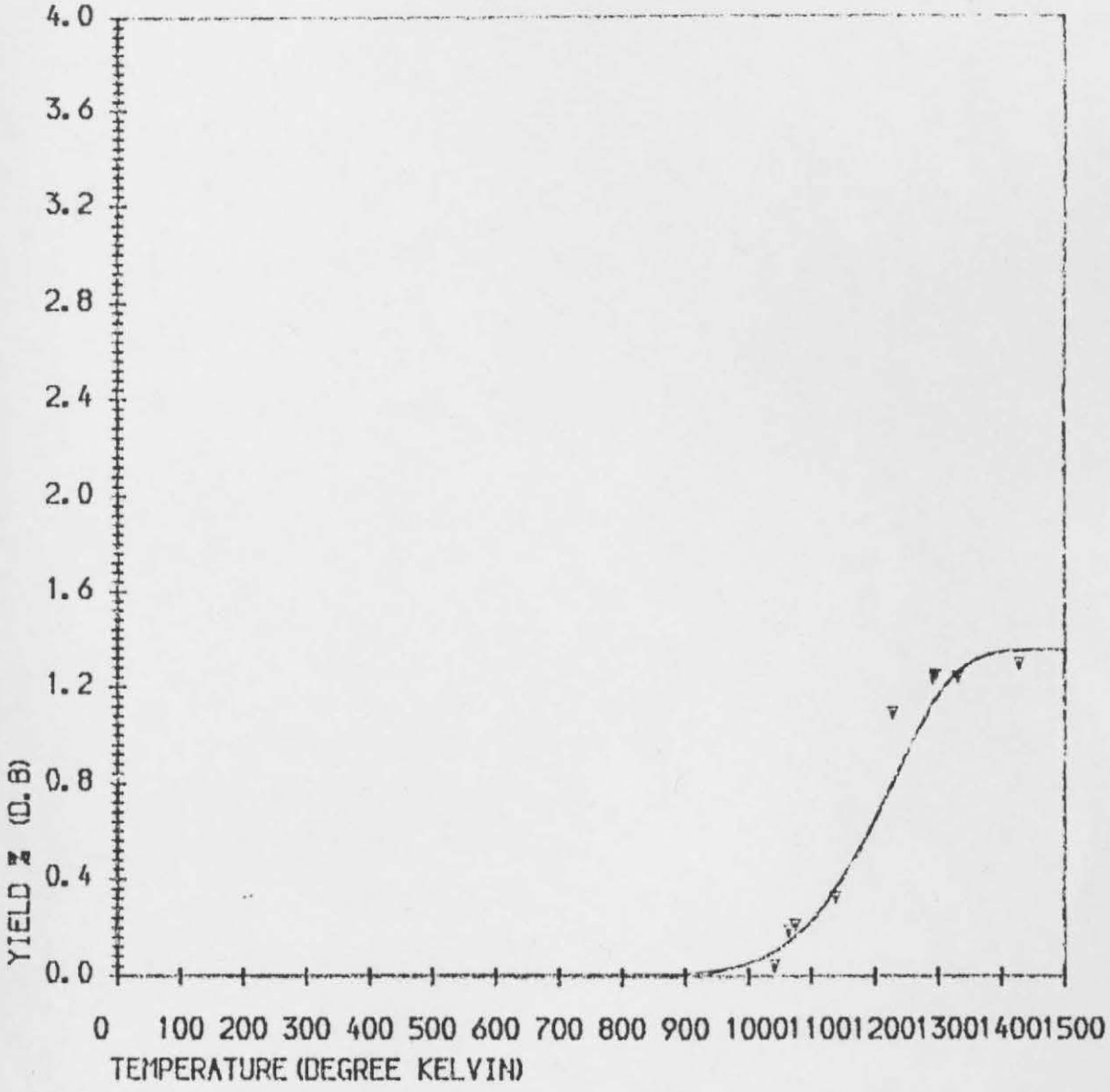

Markham Main
5,000°C/S
H_2 gas
Vacuum

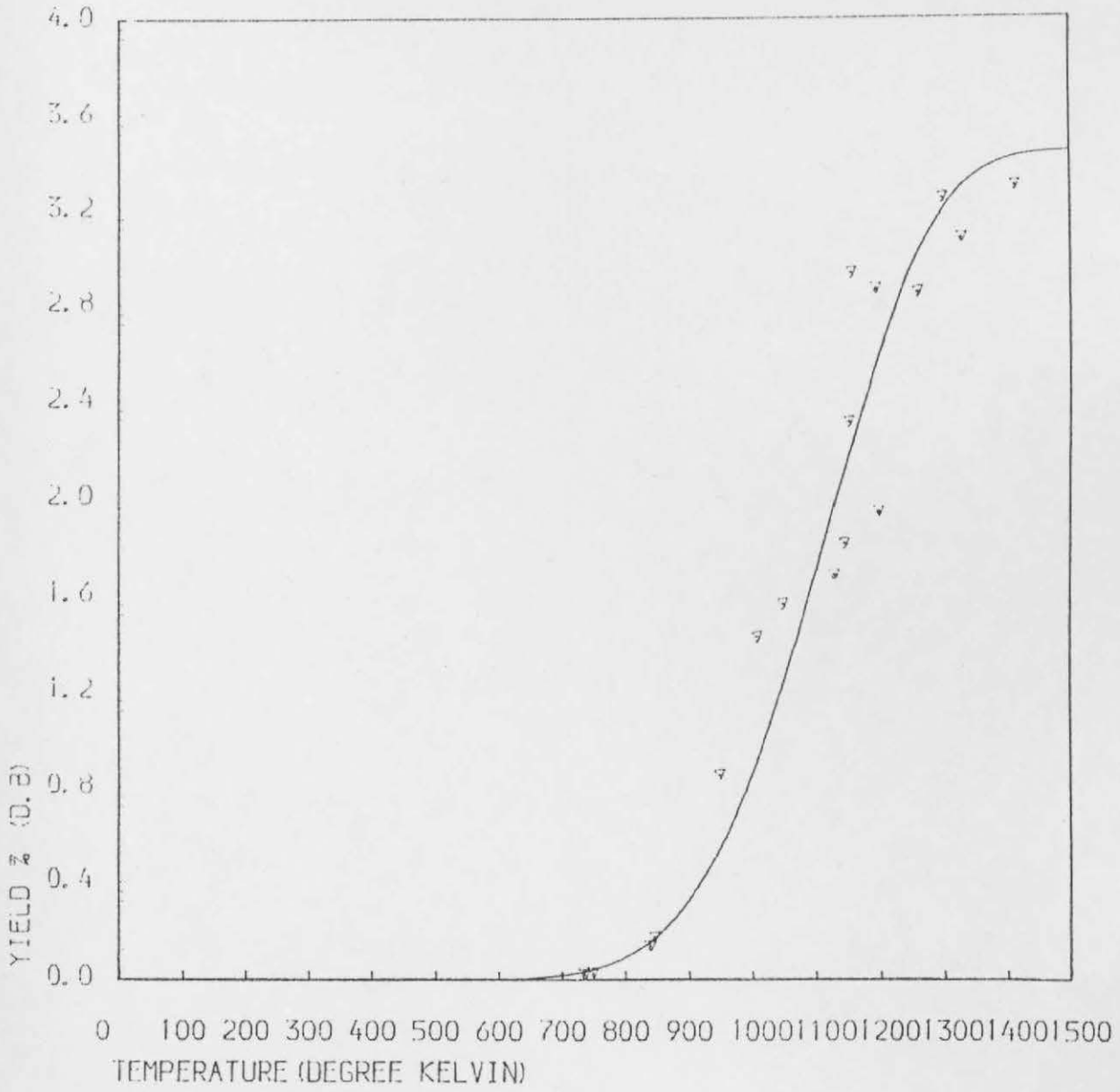

Markham Main
5,000°C/S
Atmosphere
CH_4

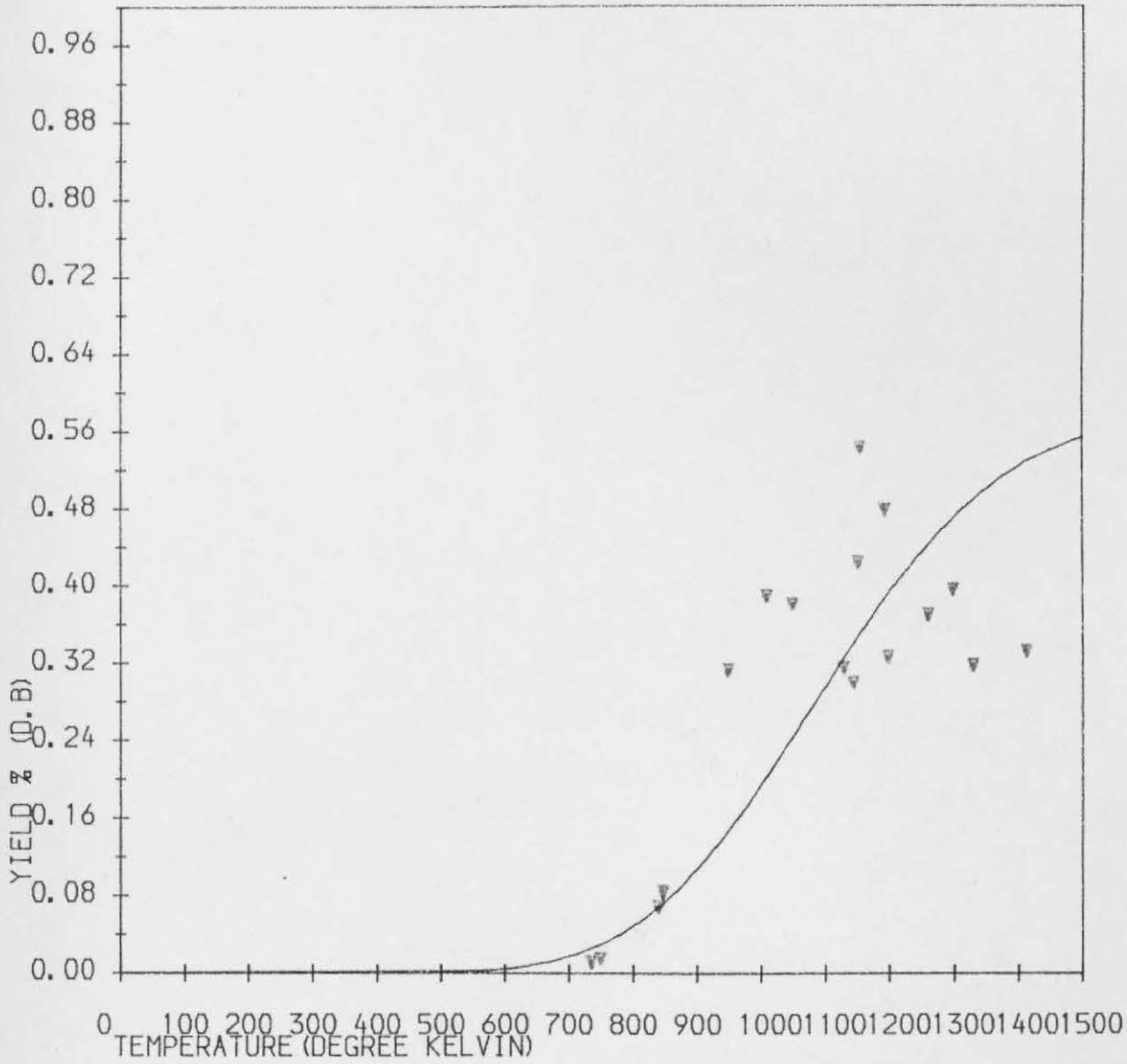

Markham Main
5,000°C/S
$C_2 H_6$
Atmosphere

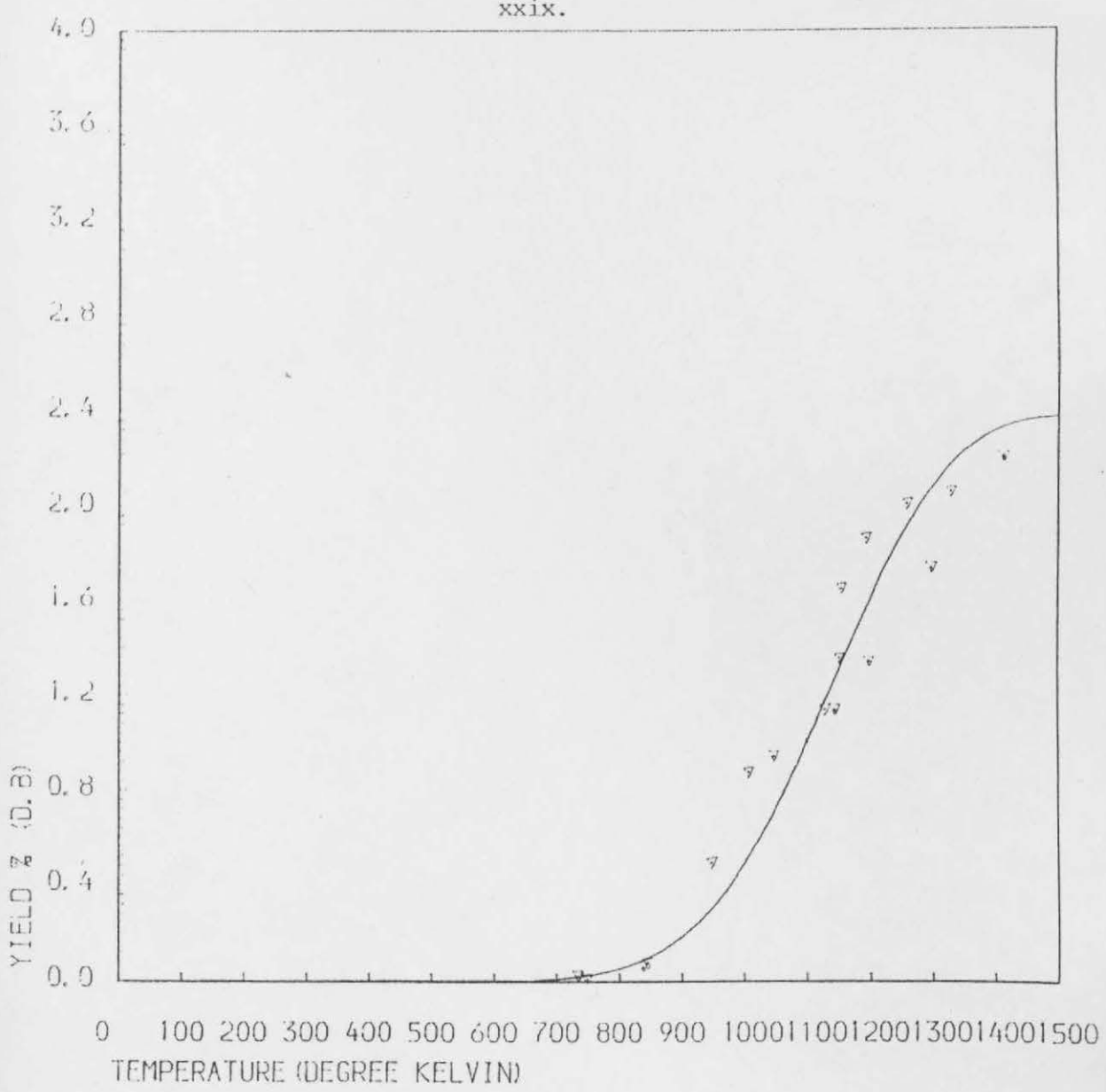

Markham Main

5,000°C/S

$C_2 H_4$

Atmosphere

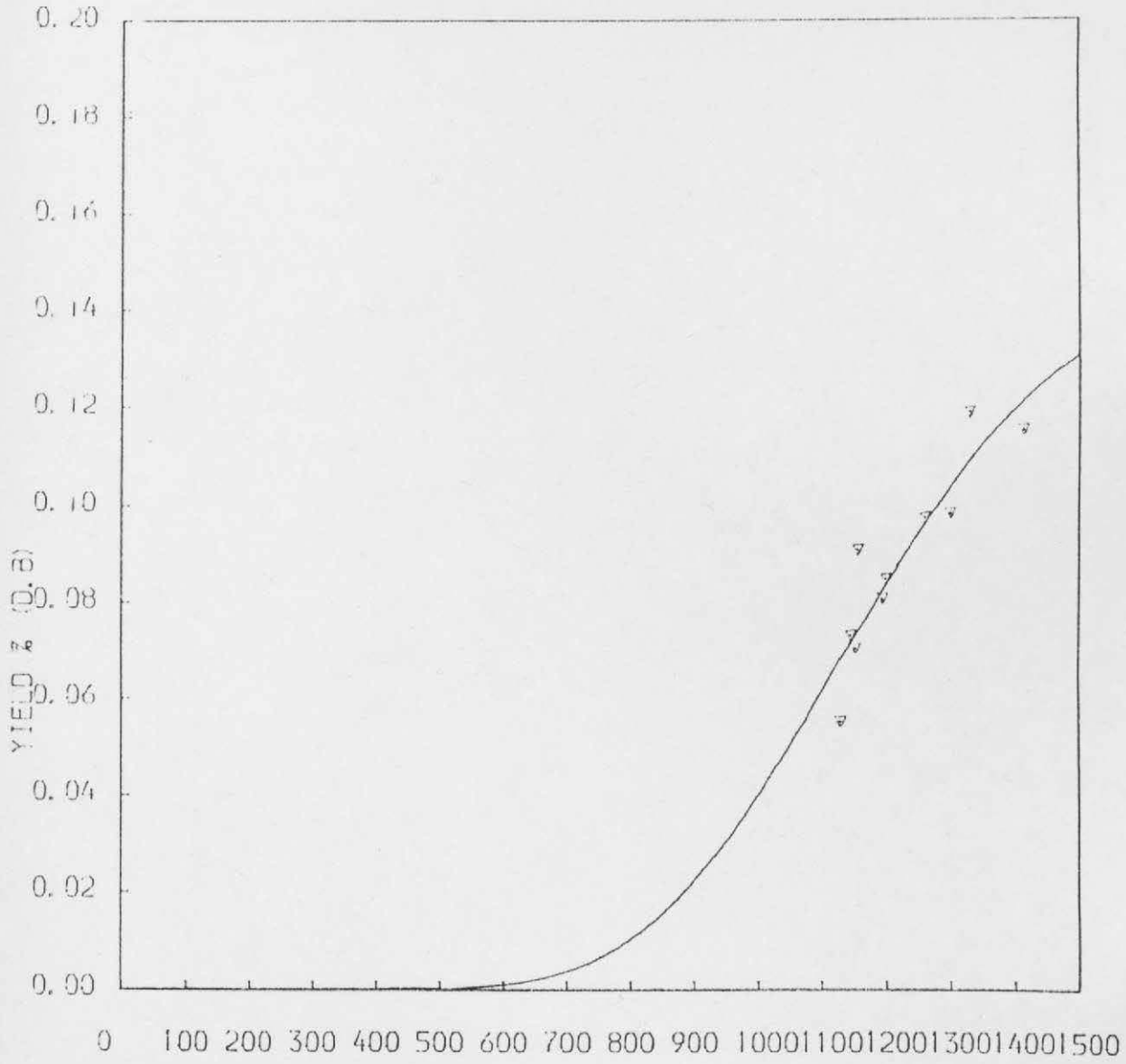

Allene
Markham Main
5.000°C/S
Atmosphere

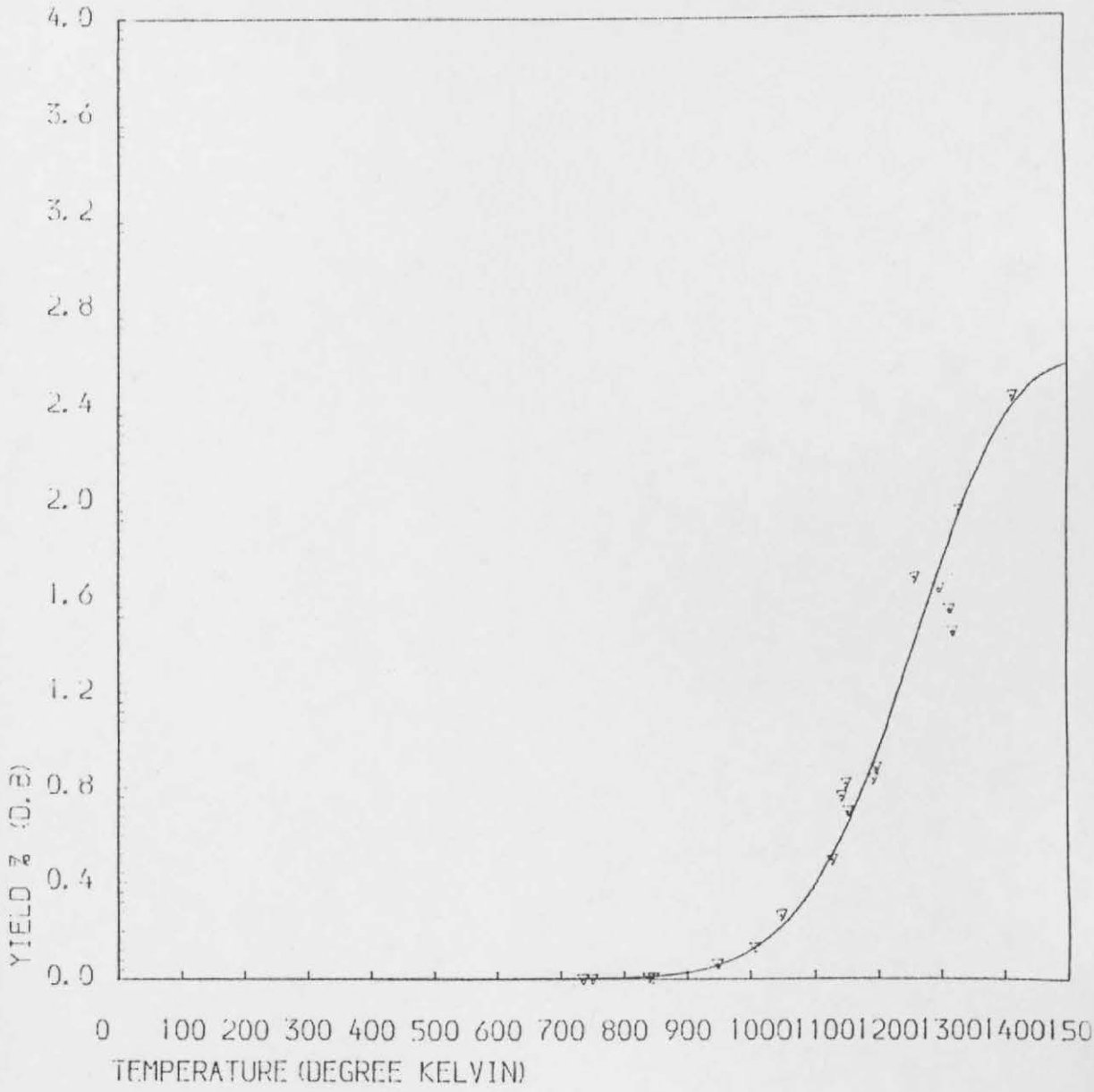

Markham Main
5,000°C/s
H_2
Atmosphere

Goldthorpe Coal 10 C/s t = 06/sec P=Atmosphere

Temperature deg.C	Allene w/w%	CO w/w%	CO2 w/w%
587.0	----		
774.0	----	6.131	2.952
873.0	0.041	9.986	3.121
875.0	0.094	6.721	3.779
924.0	-----	-----	-----

T.2

Goldthorpe coal = 10 C/s t = 10/20 ms P = Atmosphere

Temperature Deg.C	Allene w/w%	CO w/w%	CO2 w/w%
680.0	-----		
770.0	-----		
872.0	0.025	2.236	3.309
918.0	0.061	7.313	5.109
969.0	0.037	8.359	4.447
971.0	0.086	9.040	5.386

rates produce higher k_i values, whilst the activation energies remain relatively insensitive.

It is not clear how these relatively low values of rate parameters can be reconciled to chemical reaction parameters and may represent physically limited processes such as latent heat of vaporization of liquid H/C or other diffusion process such as bubble transport in the coal melt. Similarly, low values have been obtained for light H/C gases evolved during very high heating rate coal Pyrolysis in shock tubes. (Refer literature review, reference to Doolan et al).

As regards insensitivity to the classes of gases, it is noted that for each type of curve, the form of the curve with regard to temperature is similar for similar classes of gases. However, for low heating rates, the rate of production of gases such as CH_4 and H_2 show steeper slopes, and is partly due to increased formation of these gases at these heating rates. Insensitivity to coal type may be due to the fact that both coals are high volatile, low swelling bituminous coals from the Carboniferous period. Differences in behaviour occur for CO and CO_2 evolution, which is dependant on the 'O' content of the two coals. Reference to the fluidised bed will show up these differences with Goldthorpe producing more CO_x due to its higher 'O' content.

As the TC detector used to detect CO and CO_2 gases was much less sensitive to CO and CO_2 relative to H_2, these gases were only reliably reported for the high temperatures in the case of the mesh reactor. Some authors have detected a two step behaviour for these gases; especially for the high volatile, low rank coals.

However, infra red gas analysis used for the fluidised bed reactor indicated that an initial CO peak was noted before the main CO evolution at later times for the case of coal particles exposed to the atmosphere. This initial minor peak was found to be absent for coal particles that were prepared and stored under inert gas. It is well known that coal, especially fine particulate coal rapidly takes up atmospheric 'O' with the consequent formation of carbonylic, carbonyl, etheric and other groups which can then decompose at lowish temperatures.

Hence for those cases of multistep behaviour observed for some coals in the evolution of CO_x groups, care needs to have been taken to ensure that such behaviour did not reflect effects noted above. The results suggest as noted in earlier discussions, marked evolution of a number of products simultaneously during the heat up period for temperatures >450^{o}C. (Minor quantities of CH_4 were detected down to temperatures as low as 250^{o}C; however they were of such low concentrations as to be unreliably quantified and may arise from desorbed/trapped fragments of coalification). This suggests independant parallel evolution of components from a variety of functional groups present in the reacting coal structure. (There are competitive processes operating as well, noted by the effects of heating rate on product distribution).

Further, the data for overall yields in particular approach asymptotes which are dependant on the peak temperature of treatment. This implies that V_i^* exhibits a temperature dependence that is not compatible with the mathematical treatment implied by the single reaction model.

To overcome this, the parallel independant reaction model was invoked by Anthony and Howard. This was claimed to represent a more realistic description of the Pyrolysis process. By introducing a probability density function of a distribution of activation energies representing a large set of reactions which go to completion at a rate dependant on the temperature/time history sustained by the particles, data was fitted successfully by this model. The thrust of the equation derived is that the time required to achieve a certain degree of completion of decomposition decreases strongly at high temperatures and is correspondingly so large at low temperatures as to be practically unattainable in laboratory time scales. This explains the fact that residual char/semicoke produced at lower temperatures can yield additional volatile matter at high temperatures. The latter is thought to be generated by reactions with activation energies so large as to be immeasurably slow at lower temperatures. This philosophy however does not preclude the possibility of product distribution being influenced by competitive reactions, such as secondary reaction pathways. (As the author's results illustrate, heating rate exerts an influence as well).

To assess the efficacy of the parallel reaction model to fit the yield data, the latter was fitted to the parallel, multiple reaction model as well.

7.2 The multiple parallel reaction model

Starting with the single reaction equation,

$\frac{dV_i}{dt} = k_i (V_i^* - V_i)$(1); for a large number of reaction

sources, the activation energy E may be approximated by a continuous distribution function, F(E). Thus, F(E)dE represents the fraction of the total potential mass loss V^* with a mean activation energy Eo between E and E + dE,

$$\text{i.e. } V_i^* = dV^* = V^* F(E)dE$$

$$\text{where } \int_0^\infty F(E)dE = 1$$

The yield for each reaction for all reactions is obtained by integrating equation (1) over all values of E.

The resulting equation is:

$$\frac{V^*-V}{V^*} = \int_0^\infty \exp\left(-\int_0^t k_i \exp(-E/RT)dt\right) f(E)dE$$

The distribution function was for reasons of mathematical tractability assumed to be approximated by a gaussian distribution of activation energies. Pitt fitted his data ($>10_s$) by a stepwise procedure and obtained a bell shaped distribution. Other possible distributions such as a Rossin-Ramler distribution may be equally appropriate. Thus $f(E) = \frac{1}{\sigma(2)^{1/2}} \exp\left(-\frac{(E-Eo)^2}{2\sigma^2}\right)$

where σ = standard deviation of the gaussian distribution. The integration of the activation energy is sufficiently accurate over the range Eo $\pm$ 2σ and thus, the integration limits may be replaced by E + 2σ & E - 2σ.

For the case of an imposed linear heating rate, the non-isothermal version of the equation is,

$$\frac{V^*-V}{V^*} = \frac{1}{\sigma(2\pi)^{1/2}} \int_{Eo-2\sigma}^{Eo+2\sigma} \exp\left(\frac{k_i}{m}\int_{To}^{T} \exp(-E/RT)dT\right)$$

$$* \exp\left(-0.5\left(\frac{E-Eo}{\sigma}\right)^2\right) dE$$

By utilising the Coats-Redfern approximation for the exponential

integral over the temperature range of interest (as in the single nonisothermal model), a more tractable equation is derived (Ref: E. Nuttall et al, 1983, American Chemical Society). Thus the expression used by the author for correlating yield data was as follows:

$$\frac{V^*-V}{V^*} = \frac{1}{6(2\pi)^{\frac{1}{2}}} \int_{E_o-2\sigma}^{E_o+2\sigma} \exp\left(-\frac{k_i RT^2}{mE}\left(\exp(-E/RT)\left(1-\frac{2RT}{E}\right)\right)\right.$$

$$\left. * \exp\left(-0.5\left(\frac{E-Eo}{\sigma}\right)^2\right)\right) dE$$

where m = constant heating rate. The preceding equation was fitted to the yield data by a numerical optimization procedure, using a Numerical Algorithm routine Eo4FDF in conjunction with a calling routine, DO1AHF to perform the integration. Essentially, starting from initial guessed values of the parameters σ, Eo, k_i and V*, the data was fitted to the equation until the residual sum of squares of the differences between observed and calculated values reaches a minimum for the non linear function considered. (The author acknowledges kind assistance from Mr Jacoby of the Computer studies department for introduction to a number of NAG numerical routines used in this study).

The above equation may be applied to individual gas species as demonstrated by others (ref: [223] ; quoting Weimar and Ngan). The equation may also be recast to include heating, cooling and isothermal residence times at the peak temperature as in the single reaction model.

The overall yield for a selection of conditions were fitted to the data, indicated by reference to figures (P15) to (P18). Tabulated below are the values of rate parameters obtained. (The numbers in brackets refer to the single reaction model results).

Coal	Conditions	E_o (KJ/mole)	σ (KJ/mole)	k_i (S^{-1})
M.M.	1000°C/S	187.8	29.8	1.438×10^{13}
	1 Atm P	or	or	or
	V*=58.5	120.5	30.8	7.464×10^{7}
	(V*=61.5)	(26.77)	-	(3.8×10^{2})
M.M.	5000°C/S	105.4	24.3	4.152×10^{8}
	1 Atm P			
	V*=62.5			
	(V*=62.5)	(26.29)	-	(1.79×10^{3})
Gold	5000°C/S	107.6	30.7	6.143×10^{7}
	1 Atm P			
	V*=62.5			
	(V*=62.5)	(25.84)	-	(1.64×10^{3})
Gold	5000°C/S	104.0	23.9	6.83×10^{7}
	Vacuum			
	V*=62.5			
	(V*=62.5)	(26.63)	-	(2.05×10^{3})

Fitting of the equation to C_2H_4 for the case of Goldthorpe coal, (10°C/S; vacuum) produced, E = 187.4 KJ/mole, $k_i = 0.588 \times 10^{13}$

σ = 24.7 KJ/mole

Comparable figures for the single reaction model was E = 56.8 KJ/mole, $k_i = 0.2 \times 10^{5}$. Comparable data for Lignite reported by Anthony and Howard are as follows:

Fig. P15

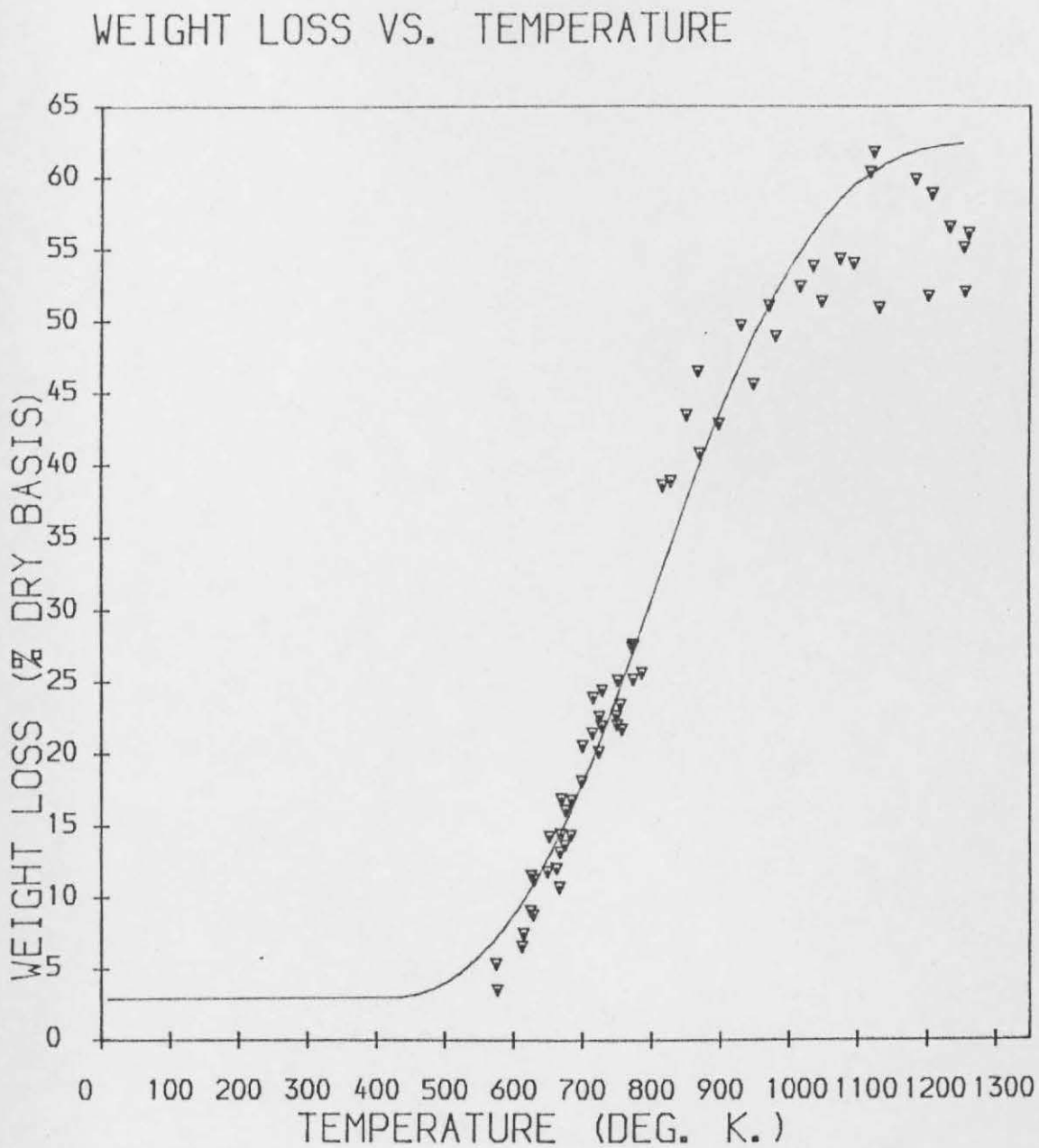

COAL TYPE: Markham Main
MESH TYPE: 75 um
RESIDENCE TIME CHARACTER: 10/20 ms
PARTICLE SIZE: 75/90 um
HEATING RATE: 5,000°C/S
PRESURE OF RUN: ATM

Eo = 105.4 kJ/mole
σ = 24.3 kJ/mole
A = 4.152×10^{8} S^{-1}

Fig P.16

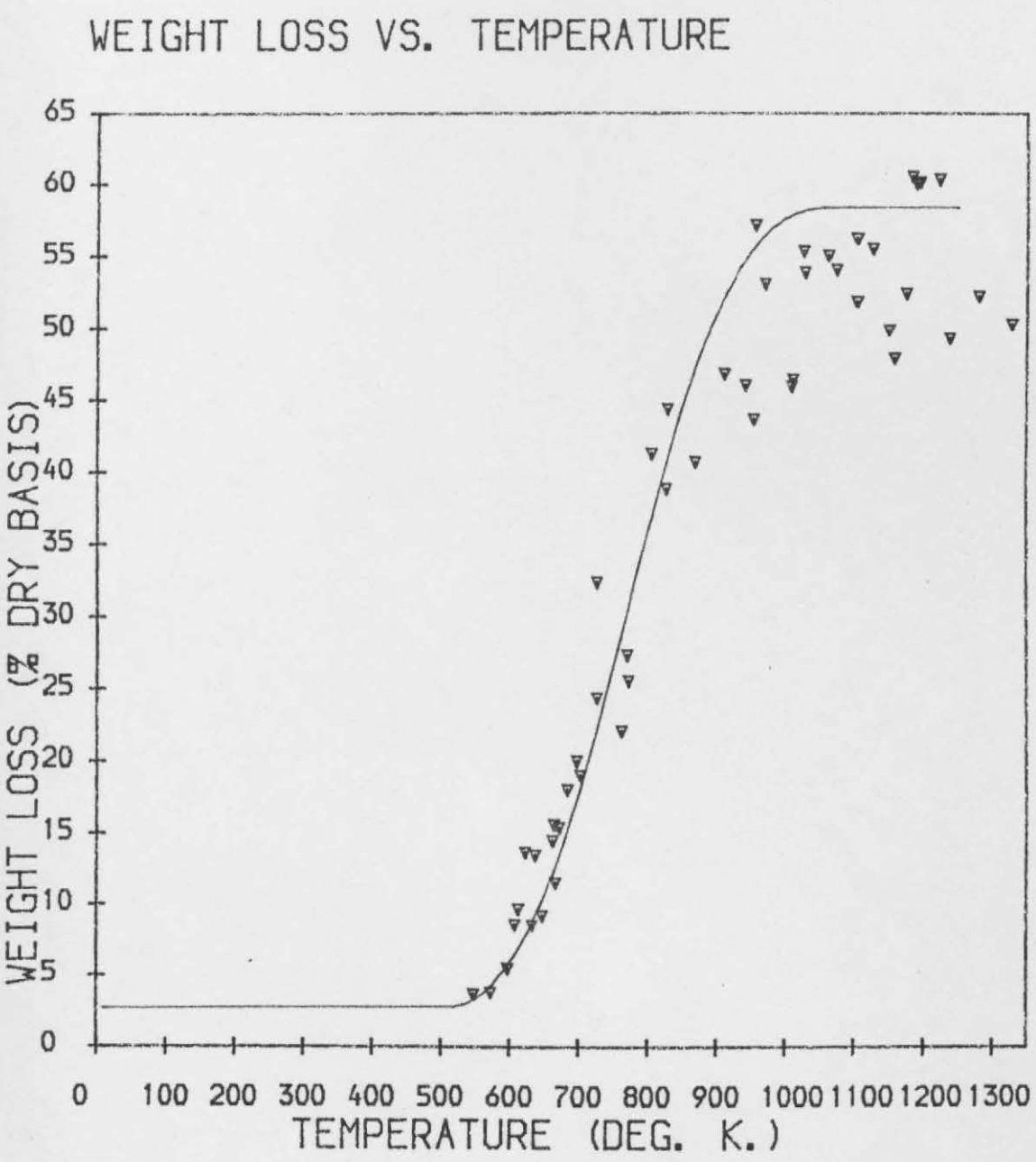

COAL TYPE, Markham Main

MESH TYPE, 75 um

RESIDENCE TIME CHARACTER, 10/20 ms

PARTICLE SIZE, 75 um

HEATING RATE, 1,000°C/S

PRESURE OF RUN, ATM

Eo = 187.8 kJ/mole

σ = 29.8 kJ/mole

A = 1.439×10^{13} S^{-1}

Vo = 58.5

Fig. P17

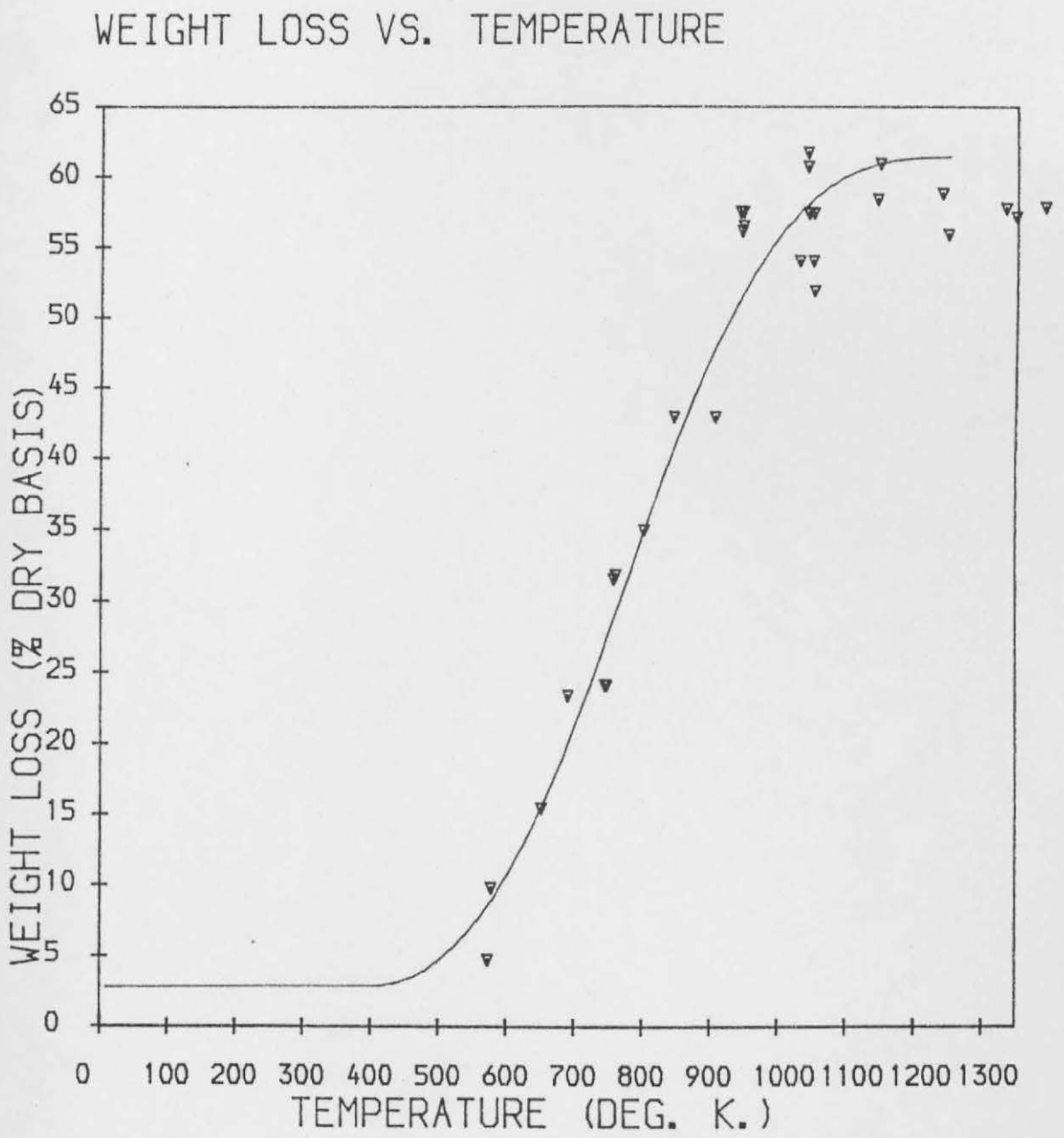

COAL TYPE. Goldthorpe

MESH TYPE. 75 um

RESIDENCE TIME CHARACTER. 10/20 ms

PARTICLE SIZE. 75/90 um

HEATING RATE. 5,000°C/S

PRESURE OF RUN. Vacuum

Eo = 104 kJ/mole

A = 0.239×10^{2} kJ/mole

$\sigma = 6.831 \times 10^{7}\ s^{-1}$

Fig. P18

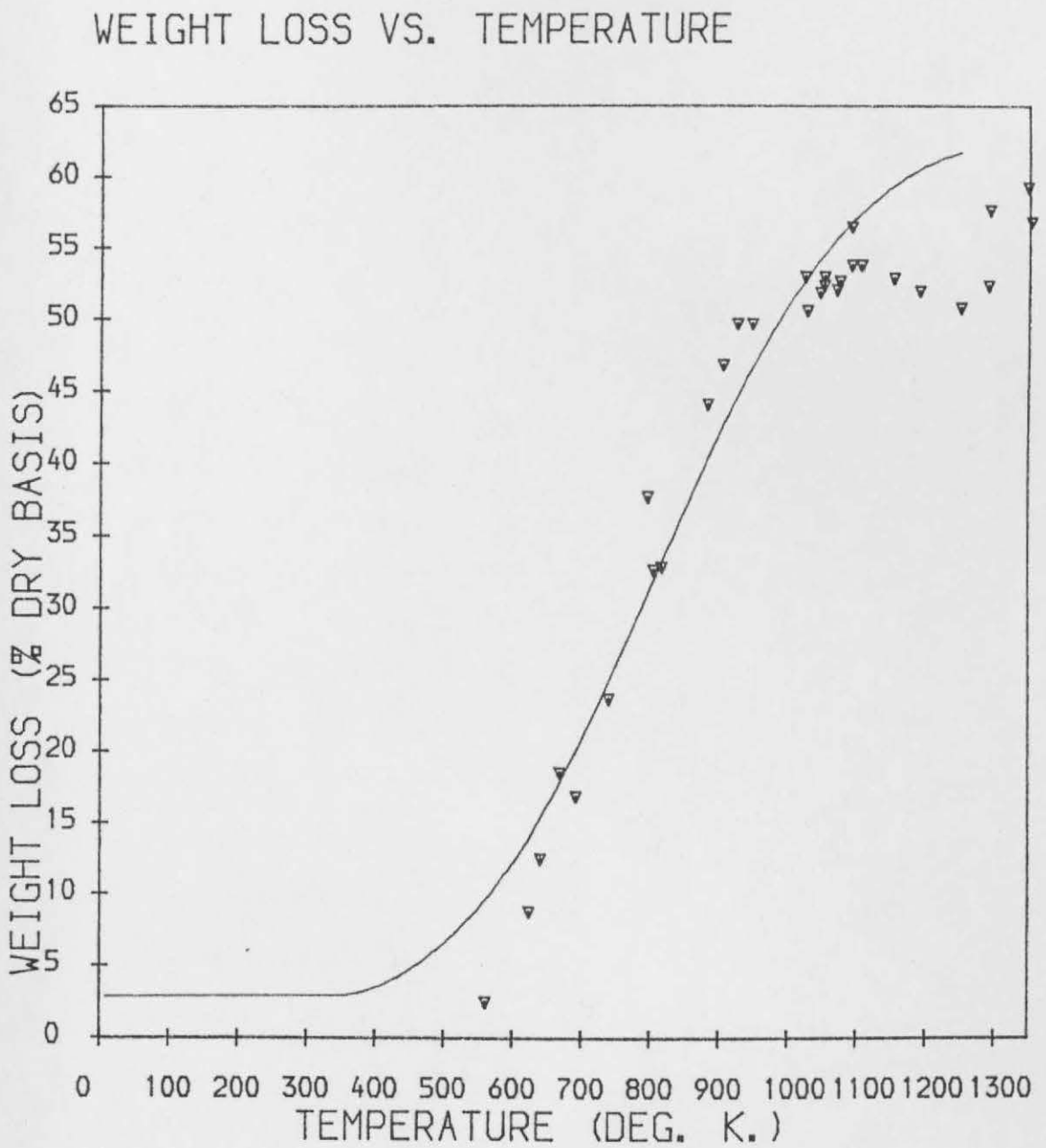

COAL TYPE, Goldthorpe

MESH TYPE, 75 um

RESIDENCE TIME CHARACTER, 10/20 ms

PARTICLE SIZE, 75/90 um

HEATING RATE, 5,000°C/S

PRESURE OF RUN, ATM

Eo = 107.6 kJ/mole

A = 6.143×10^{7} S^{-1}

σ = 30.7 kJ/mole

V*(%)	k_i (S^{-1})	E_o (KJ/mole)	σ (KJ/mole)
40.6	1.07×10^{10}	203.8	39.25
40.6	1.67×10^{13}	235.6	45.65

The above illustrates the observation noted by the author and others[221] that differing initial guesses for the fitted parameters caused the non least square regression routine to converge to more than one set of parameter values that fit the data. Statistical refinement of the fits would reduce the number of fits to two sets as noted by Serio et al.[221] For the present study the model was used merely to acquire a feel for the rate parameters obtained for comparison purposes with the single reaction model. Thus the fits represent an initial first approximation.

A feature of the two sets of parameters when compared to the data fits indicated the following. Whilst the lower rate parameter values (120.5, σ = 30.8, $k_i = 7.464 \times 10^7$) and the higher rate parameter (187.8, σ = 29.6, $k_i = 1.438 \times 10^{13}$) values fitted the data, the former resulted in a higher yields at the lower temperatures than the latter. Also, as comparison between the appropriate curves show, the single reaction model fits the overall yields better over most of the temperature range than does the more complex multiple reaction model.

The compensation effect noted between pre-exponential factor and activation energy allows for multiple solutions noted. (In the case of the single reaction model, whilst this compensation effect arise from the values obtained for various classes of compounds, the regression is relatively insensitive to initial guesses).

7.3 General comments on the model parameters

From the viewpoint of simplicity of data correlation, the single reaction model appears to be preferrable. Both models illustrate trends in the data with similar facility. However, the multiple regression produces rate parameters approaching those suggested by chemical reaction control. This could arise from the increased number of adjustable parameters compared to the single reaction model (the nonisothermal model noted herein requires only 2 adjustable parameters E and V*). A mathematical analysis of the multiple reaction model by Antal et al[224] concluded that the model was no more than a sophisticated curve fitting device.

Perusal of the literature also indicates that the model appears to be insensitive to coal rank. Thus, Ciuryla et al[223] working with lignitic and bituminous coals (atmospheric pressure, 40-160^{o}C/min) reported relatively narrow range of rate parameter values which fitted the different coal types. Other reported data also suggest this relative insensitivity. There is a suggestion that either the Pyrolysis mechanism for coals are very similar or the model is unable to distinguish among different Pyrolysis mechanisms. Weimar and Ngan, who applied the parallel model to both gas yields and overall yields to 3 different coal ranks (5 coals; Lignitic, subbituminous and Bituminous coals) found this insensitivity to coal type to operate for each class of volatiles. He reports that the mean activation energies increase in the order CO_2, CO (first peak), CH_4, CO (second peak) and H_2.

Reference to the single, independant reaction model results show a consistent trend of increase in E_i in the order $H_2 > C_2H_2 > CH_4 > C_2H_4$ for the two coals studies for heating rates of $10^{o}C/S$ and $5000^{o}C/S$ including vacuum and atmospheric conditions. The latter case holds for closely related ranks of coals (low rank high volatile Bituminous coals) of fine particle size compared to that reported by Weimer and Ngan.

It is interesting to note the relatively high activation energies predicted by the single reaction model for H_2 and C_2H_2. These products are evolved at the higher temperature range relative to the others and represent classes of compounds arising from cracking reactions. (It is however possible for H_2 to arise at the lower temperatures from hydroaromatic structures in atomic form as hypothesised by Mazumdar et al and also by lamallae movement at the higher temperatures as suggested by Berkowitz).

Reference to the review on coal structure by the author has indicated the possibility of facile release of large range of compounds of wide molecular mass by disruption of weak bonds such as hydrogen bonds, electron donor interactions and Wander Waal interactions between the relatively planar coal macromolecules. A high proportion of clatharated material present as such in the coal was posited as a distinct possibility by a number of authors. The single reaction model fitted to the data suggest values of Activation energy in the region of 25-26 KJ/mole, of the order of magnitude noted for 'H' bonds. Coupled to the dominant, rapid rate of mass loss observed by the yield curves there appears to be some grounds for the use of the independant single reaction model in correlating yield data compared to more complex models such as the multiple reaction model.

The yield results and the form of the curves (overall yields) suggest the possibility of different temperature regimes for different classes of reaction. Thus, an early low activation energy, rapid depolymerization along with breakage of weak carboxylic and other weak chemical bonds may be followed by a series of parallel and competitive reactions at intermediate temperatures giving rise to light gaseous species along with high temperature tar. At higher temperatures, competitive reactions such as repolymerization and cracking may dominate as indicated by the 'dips' or minima noted at temperatures >850^{o}C. Menster's curves show these effects more clearly (refer fig. 26), but could arise from severe evaporative limitations caused by rapid temperature rise and thus, much increased product generation relative to evaporation. Nonetheless, his conditions of small particle size (44-53 μm) and vacuum operation would diminish any mass transfer effect.

The effect of high unsaturate yields at high heating rates suggest the possibility that diffusion limitation, particularly of heavier precursor molecules giving rise to the lighter products may be occurring. The liquefaction of the coal particle, enhanced by high heating rates will have a profound effect on the mass transport of volatiles through the melt. The transient viscosity of the coal in its plastic state regulates the dynamics of bubble nucleation growth, and diffusion of the light species through the coal melt. The diffusion coefficients of various gas species in the melt vary over several magnitudes with respect to both molecular size and direction in the nonisotropic coal structure.

Figures fbgv1 - m54 represent a selection of cumulative gas yields obtained at the stated conditions of pressure, residence time, peak temperature and coal type. The data has been fitted by a cubic regression routine using a statistical analysis systems package (SAS).

Fig.fbgv1
Mesh gas yields vs Peak mesh Temperature
5000 C/s##.VACUUM

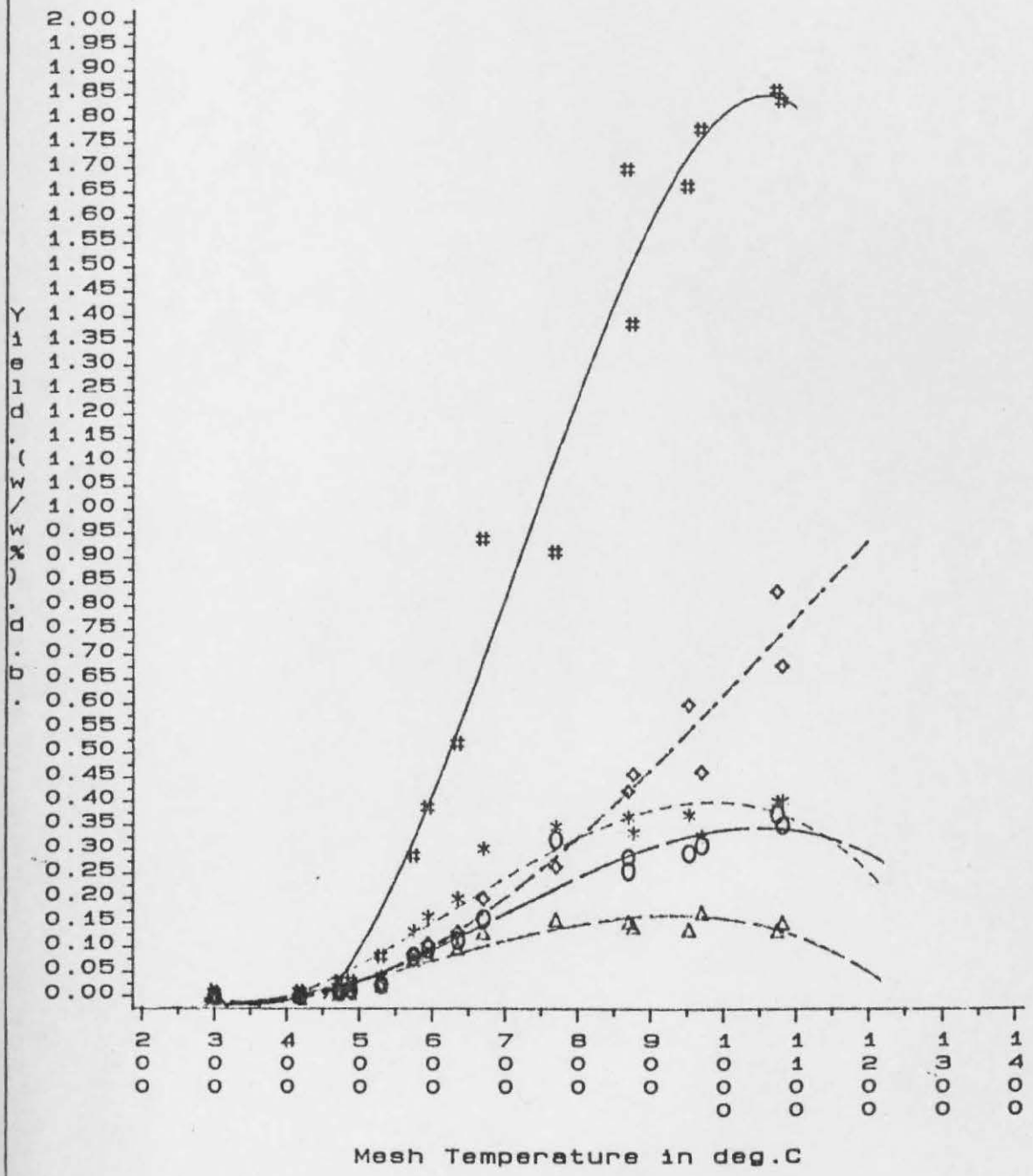

Goldthorpe Coal:Dp=75/90uM
CH4 GAS(Hash symbol)
C2H6 GAS(Star symbol)
C2H4 GAS(Diamond symbol)
C3H8 GAS(Triangle symbol)
C3H6 GAS(Circle symbol)
Residence time=10/20ms

Fig.fbgv2
Mesh gas yields vs Peak mesh Temperature
5000 C/s##,VACUUM

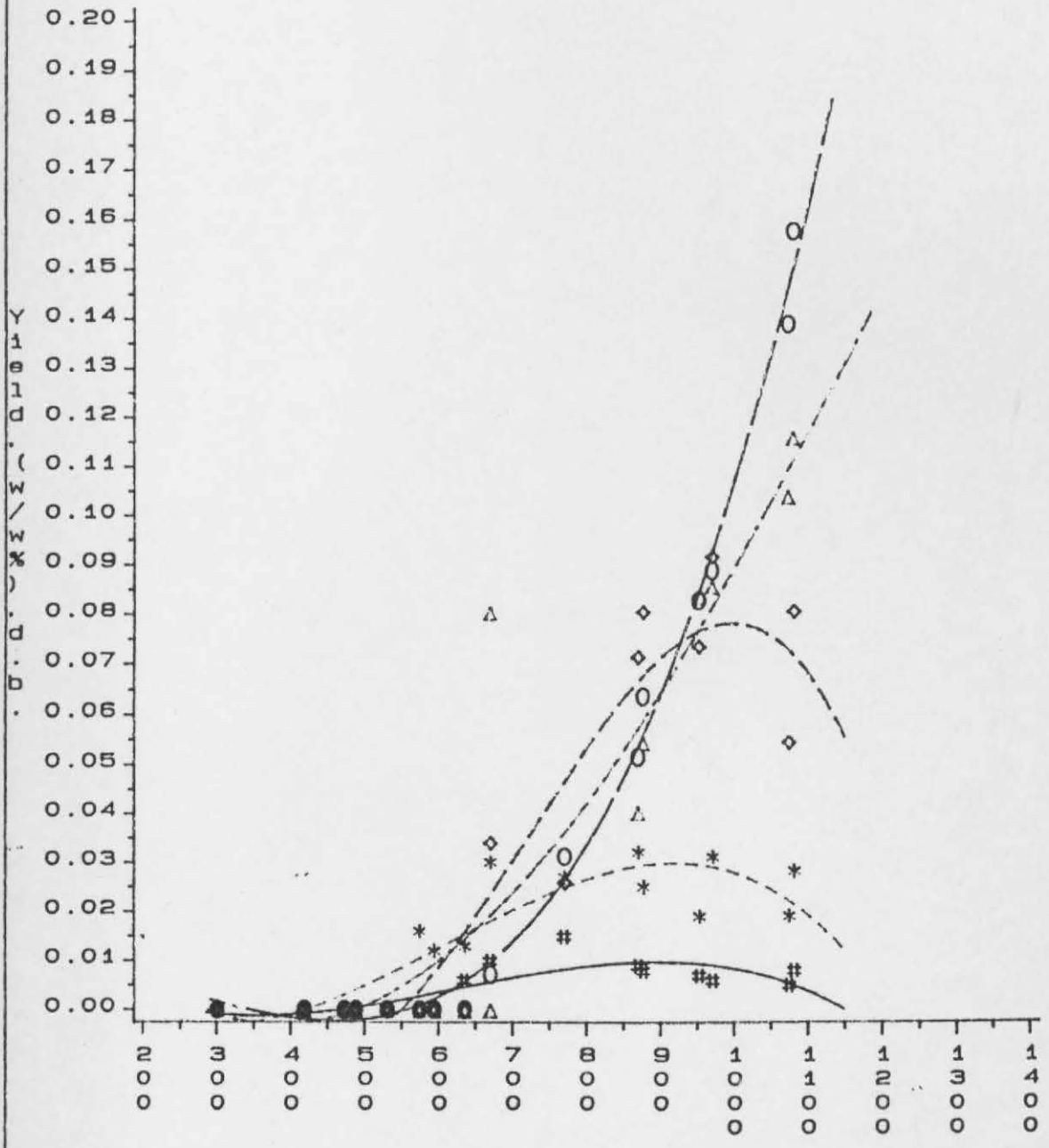

Goldthorpe Coal:Dp=75/90uM
I-C4H10 GAS(Hash symbol)
N-C4H10 GAS(Star symbol)
BUT-1-ENE GAS(Diamond symbol)
1,3 BUTADIENE GAS(Triangle symbol)
C2H2 GAS(Circle symbol)
Residence time=10/20ms

Fig.fbgv3
Mesh gas yields vs Peak mesh Temperature
5000 C/s##,VACUUM

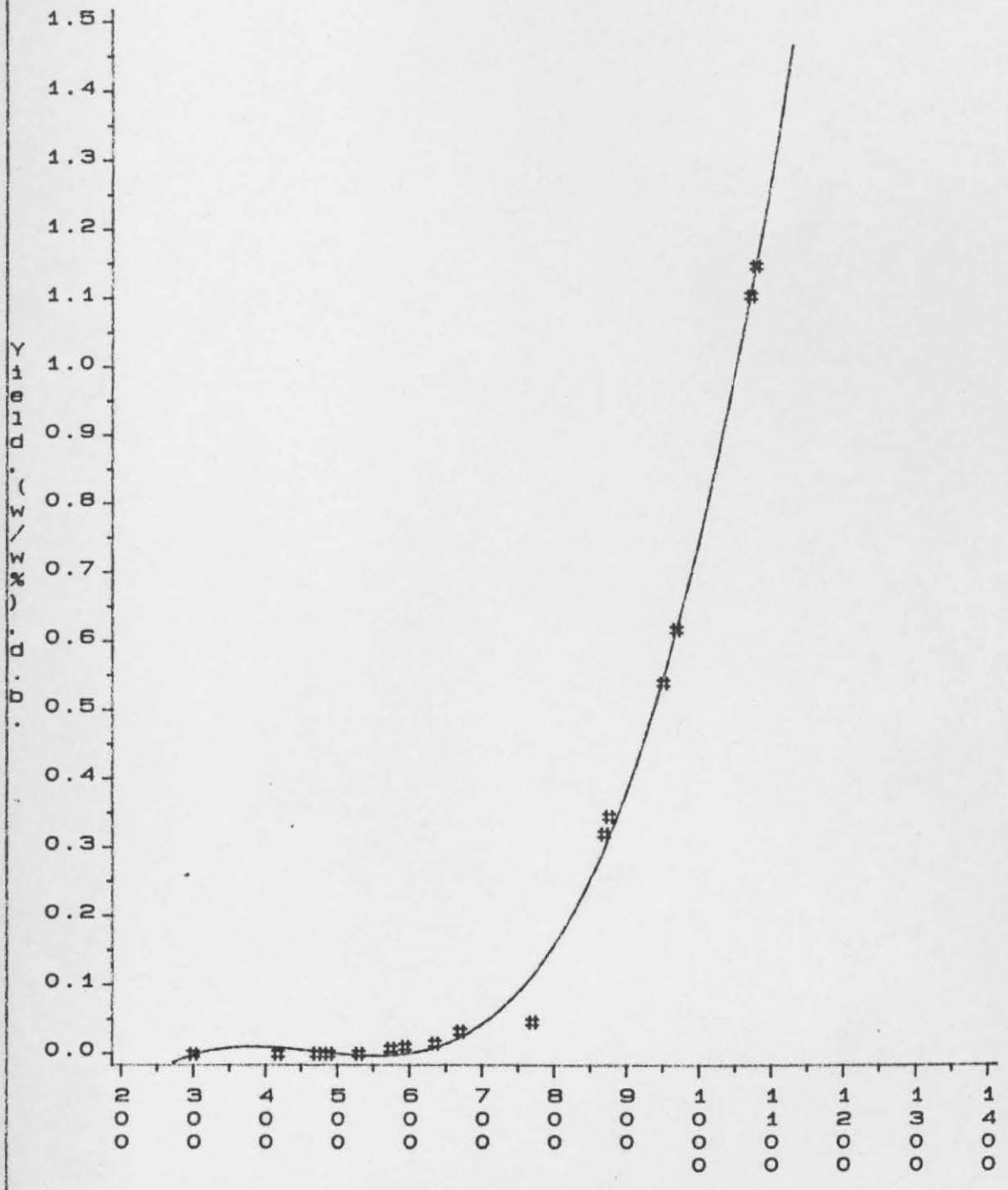

Goldthorpe Coal:Dp=75/90uM
H2 GAS(Hash symbol)
Residence time=10/20ms

Fig.mvg1
Mesh gas yields vs Peak mesh Temperature
5000 C/s##.VACUUM

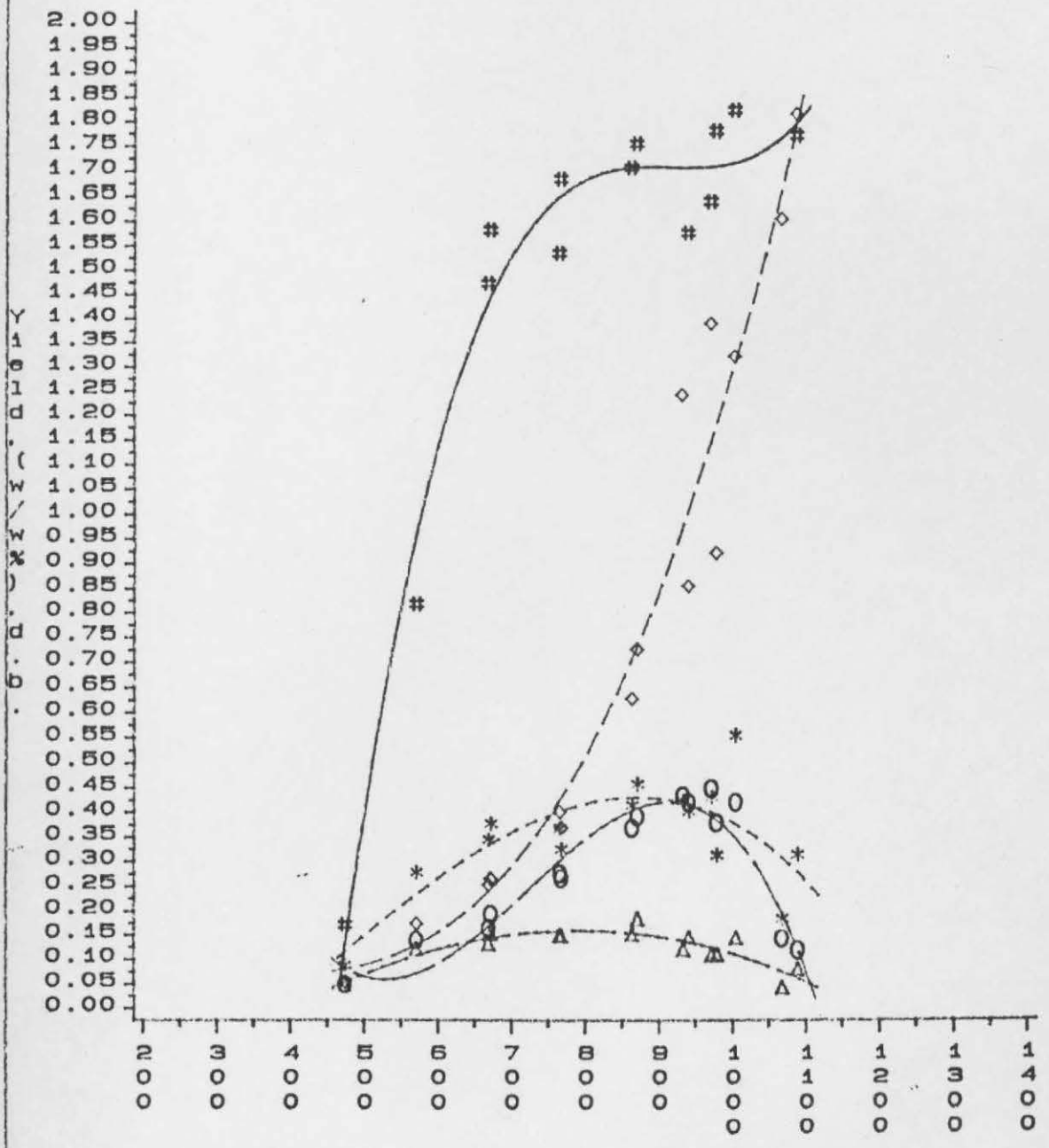

Goldthorpe Coal:Dp=75/90uM.
CH4 GAS(Hash symbol)
C2H6 GAS(Star symbol)
C2H4 GAS(Diamond symbol)
C3H8 GAS(Triangle symbol)
C3H6 GAS(Circle symbol)
Residence time=06/10 seconds

Fig.mgv2
Mesh gas yields vs Peak mesh Temperature
5000 C/s##,VACUUM

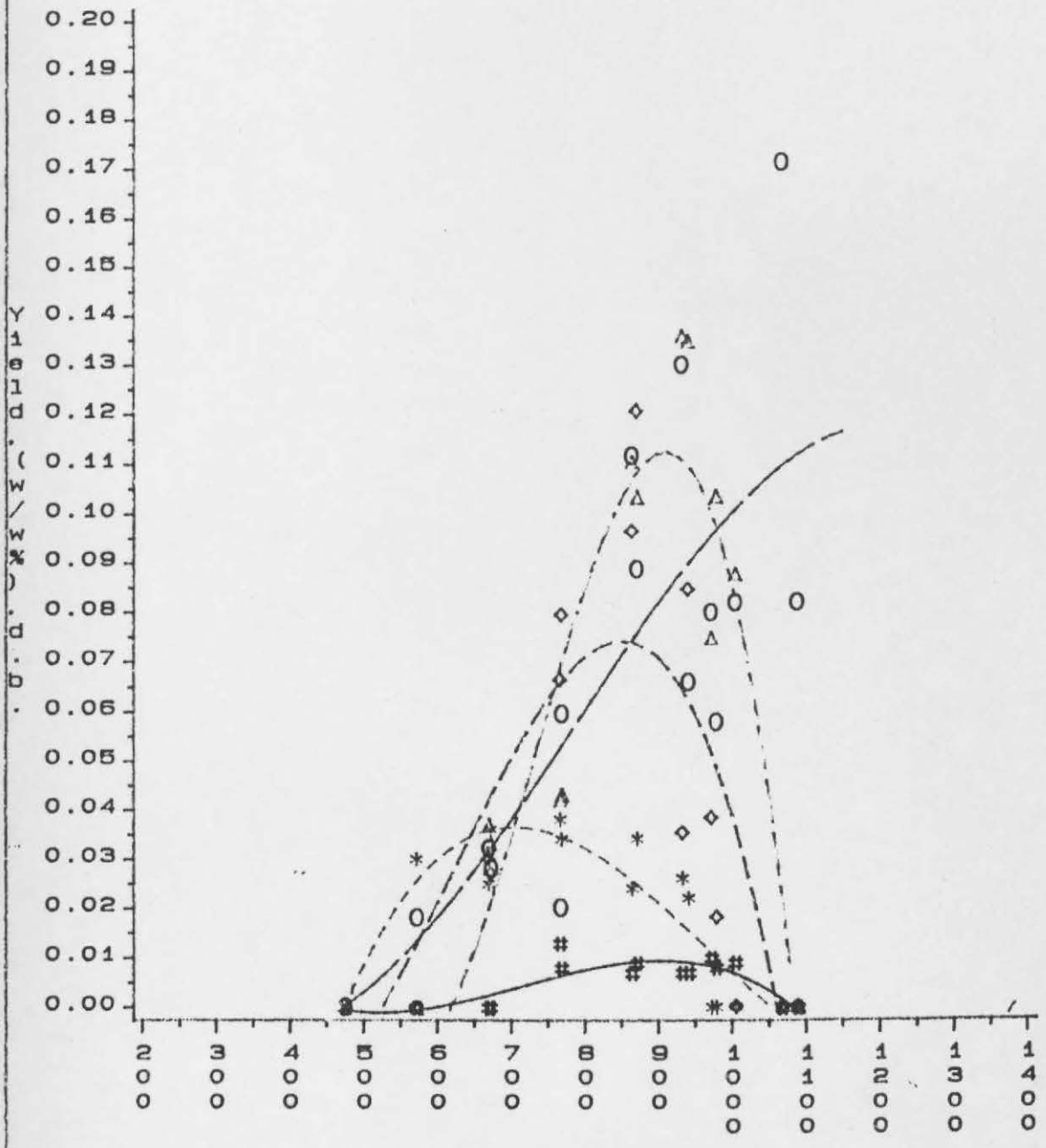

Goldthorpe Coal:Dp=75/90uM
I-C4H10 GAS(Hash symbol)
N-C4H10 GAS(Star symbol)
BUT-1-ENE GAS(Diamond symbol)
1,3 BUTADIENE GAS(Triangle symbol)
C2H2 GAS(Circle symbol)
Residence time=06/10 seconds:P=Vacuum)

Fig.mgv3
Mesh gas yields vs Peak mesh Temperature

5000 C/s##.VACUUM

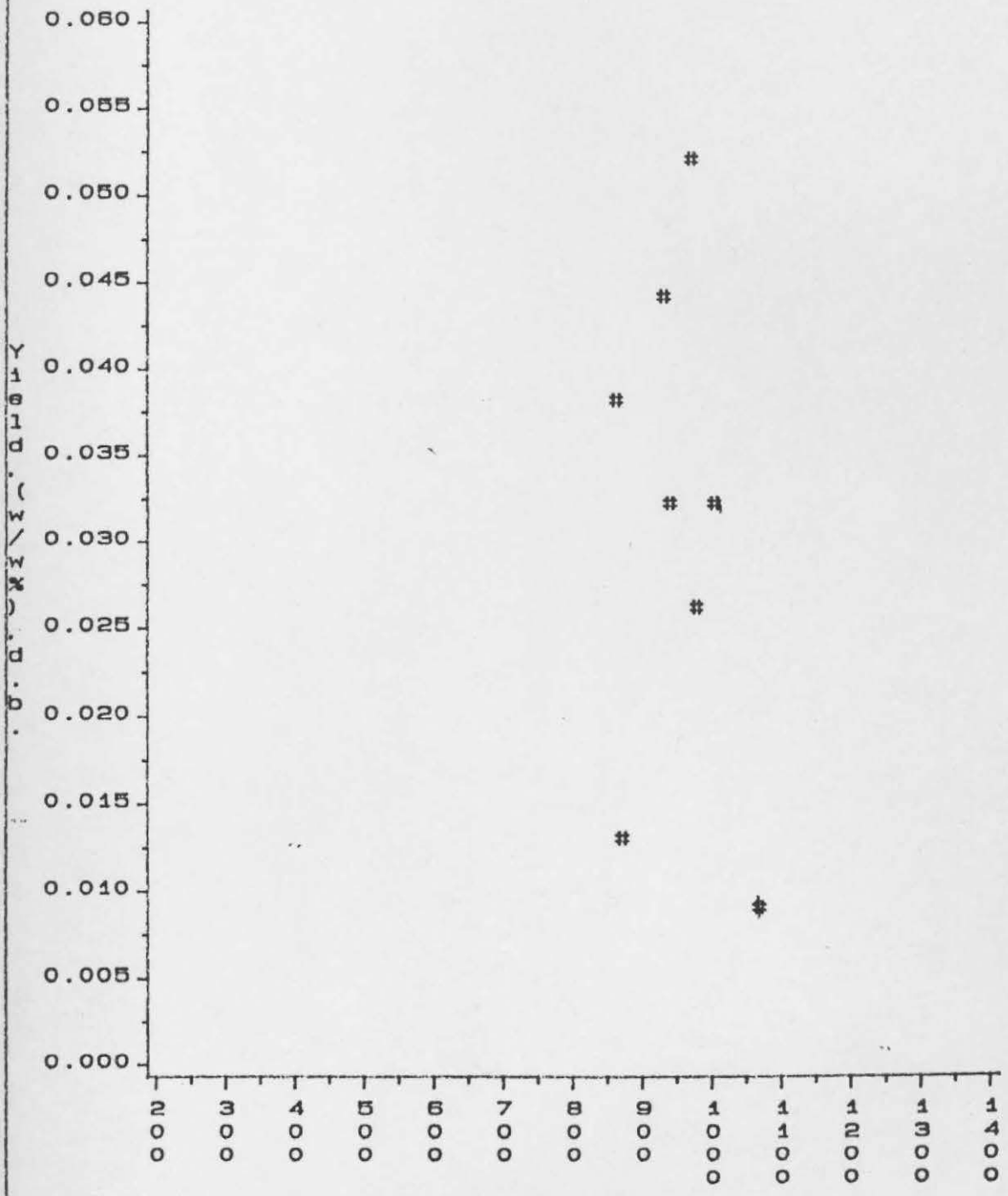

Goldthorpe Coal:Dp=75/90uM
Allene GAS(Hash symbol)
Residence time=06/10s:P=Vacuum

Fig.MGV5
Mesh gas yields vs Peak mesh Temperature

5000 C/s##.VACUUM

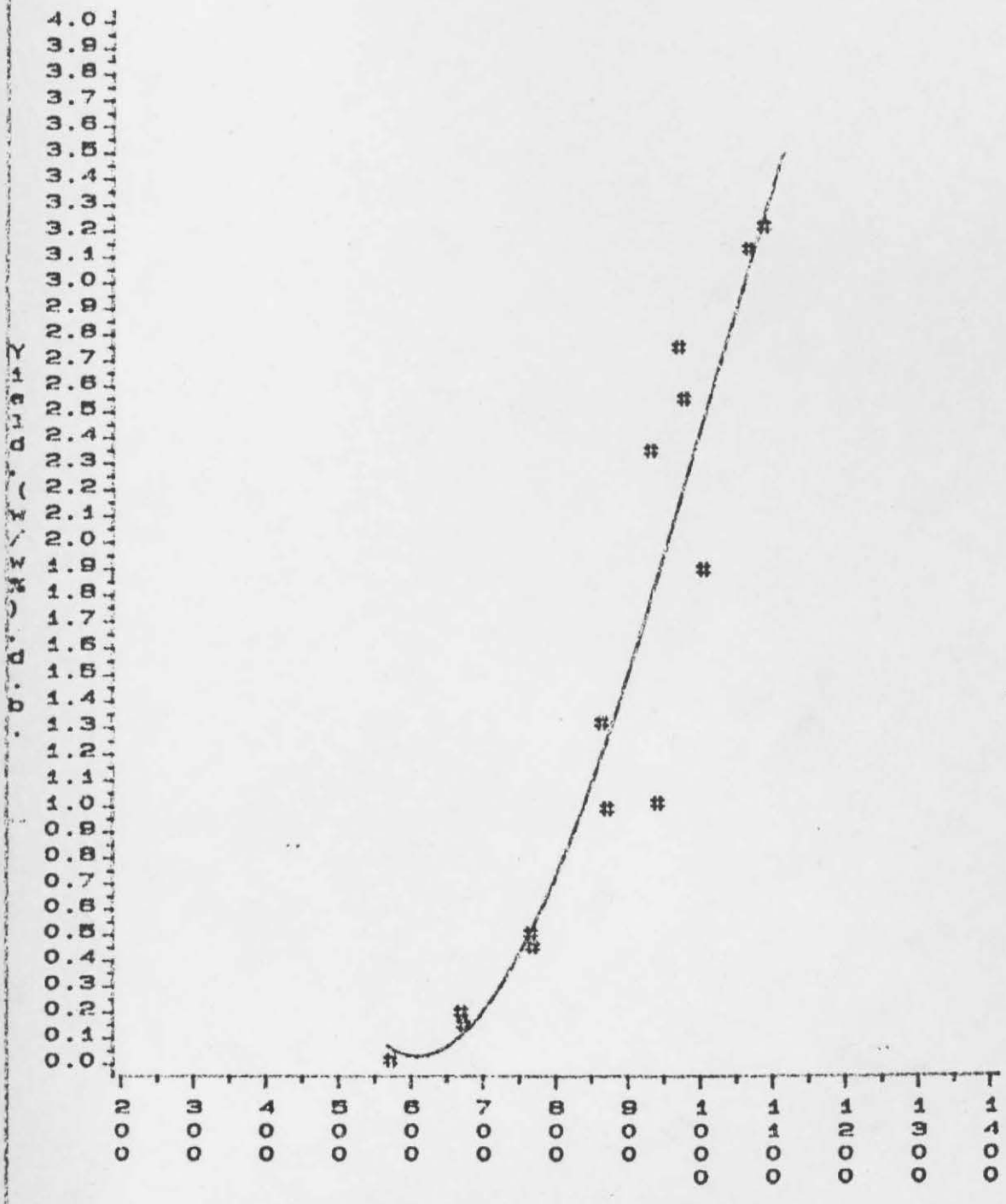

Goldthorpe Coal:Dp=75/90uM
H2 GAS(Hash symbol)
Residence time=06/10s:P=Vacuum

Fig.g5a1
Mesh gas yields vs Peak mesh Temperature

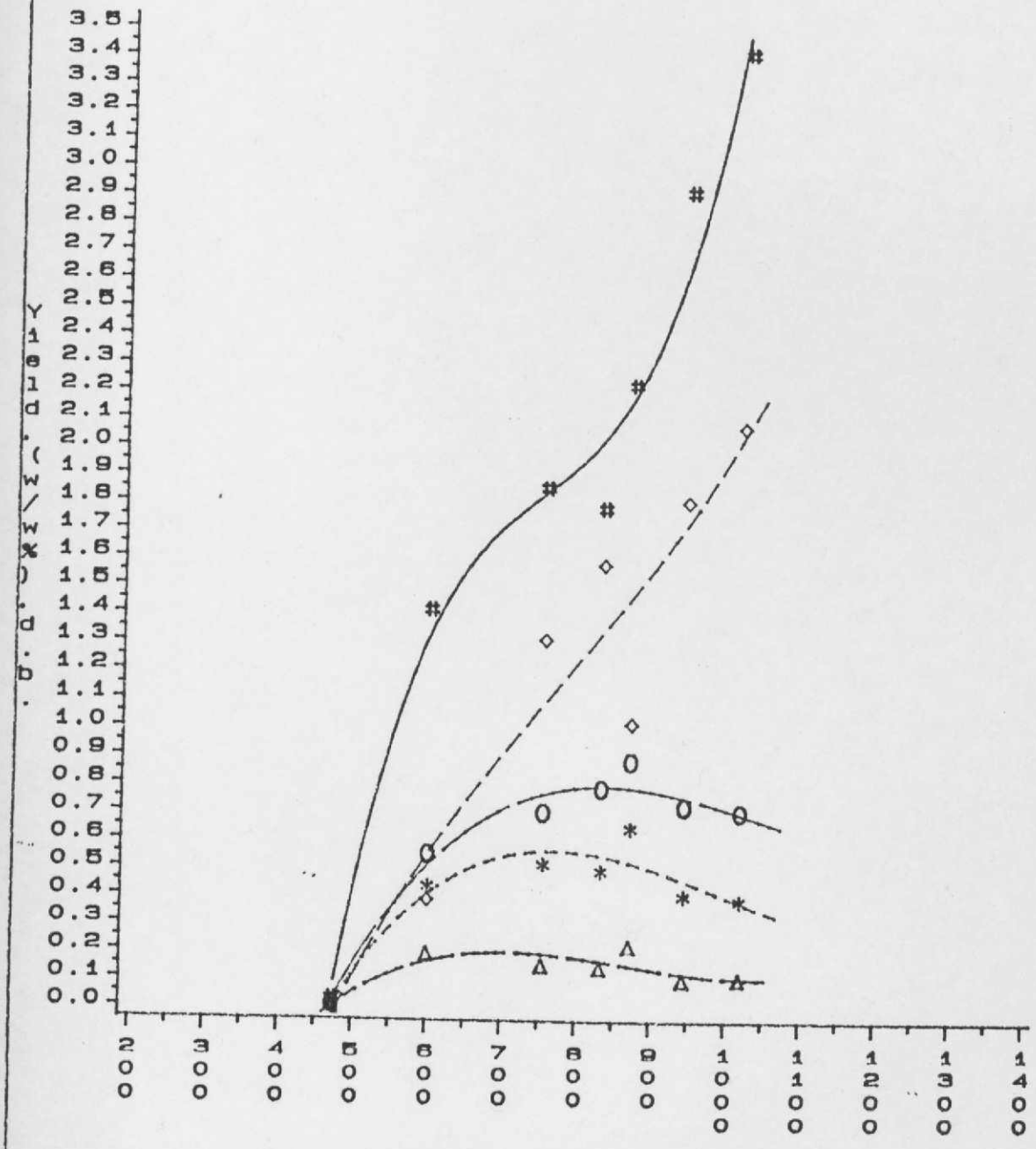

Goldthorpe Coal:Dp=75/90uM:(5000 C/s)
CH4 GAS(Hash symbol)
C2H6 GAS(Star symbol)
C2H4 GAS(Diamond symbol)
C3H8 GAS(Triangle symbol)
C3H6 GAS(Circle symbol)
Residence time=10/20 ms:P=Atm.

Fig.g5a2
Mesh gas yields vs Peak mesh Temperature

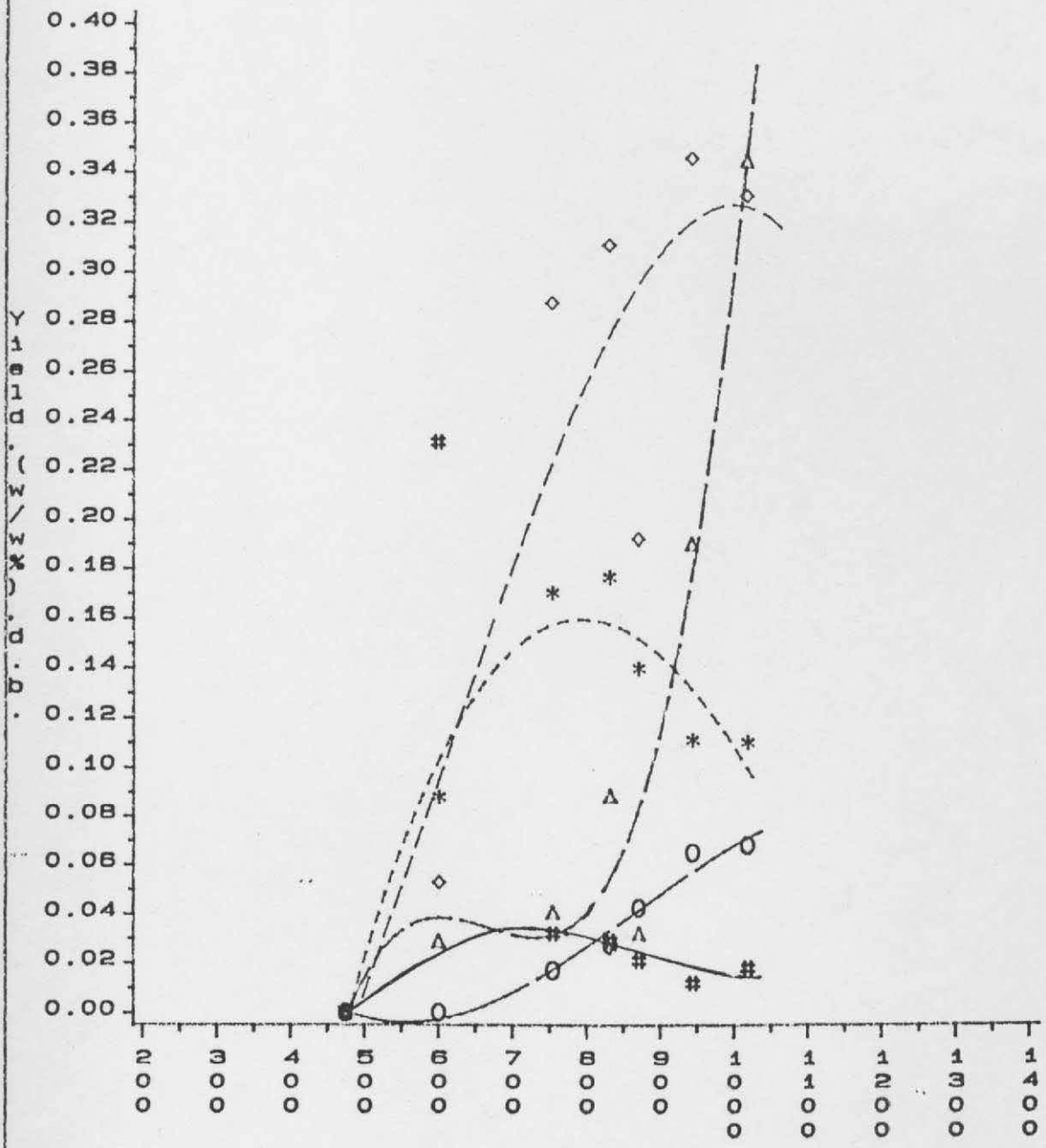

Goldthorpe Coal:Dp=75/90uM:5000 C/s
N-C4H10 GAS(Hash symbol)
BUT-1-ENE GAS(Star symbol)
1,3 BUTADIENE GAS(Diamond symbol)
C2H2 GAS(Triangle symbol)
ALLENE GAS(Circle symbol)
Residence time=10/20 ms:P=Atm.

Fig.g5a3
Mesh gas yields vs Peak mesh Temperature
Heating Rate=5000 C/s:Atm.Pressure

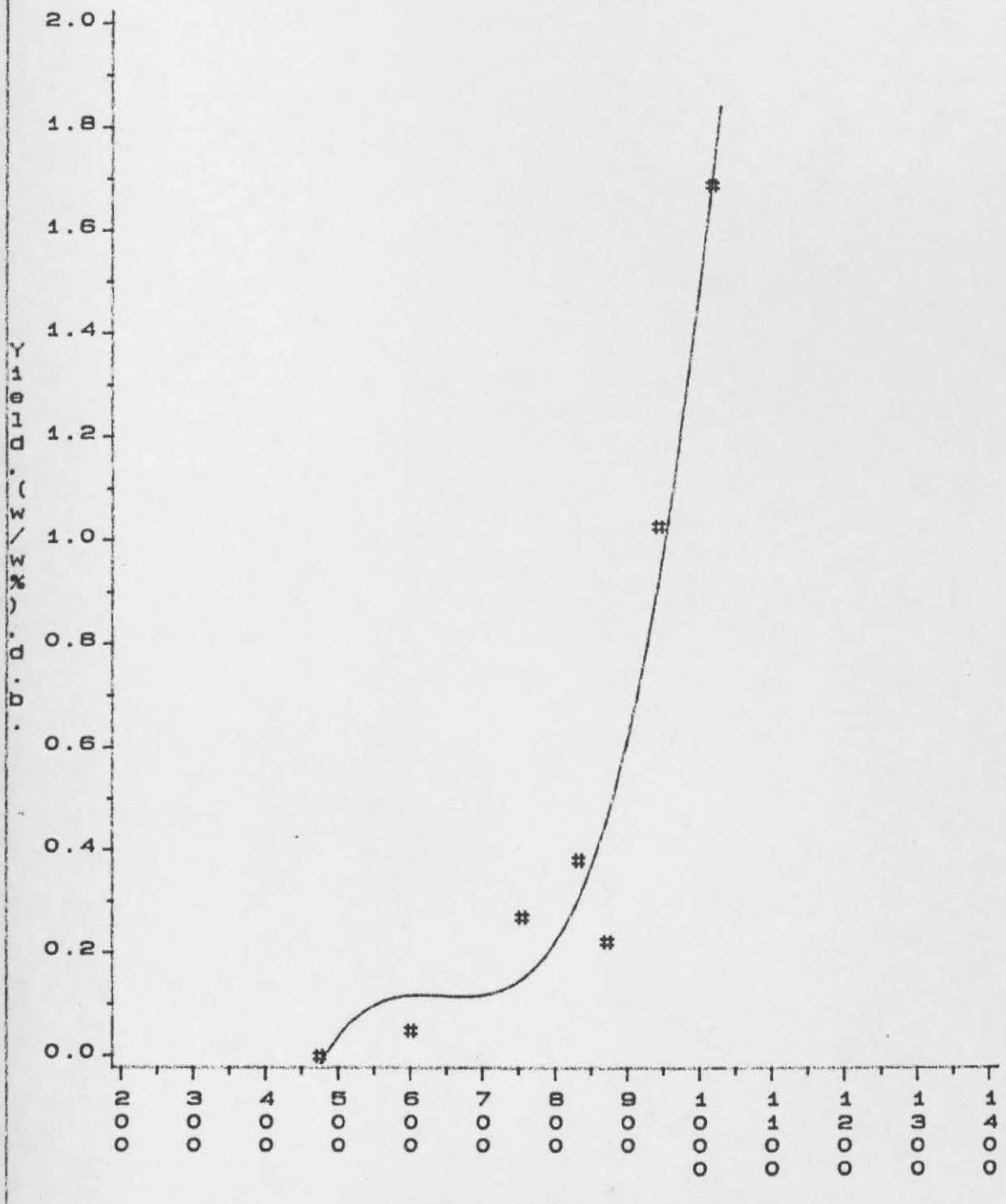

Goldthorpe Coal:Dp=75/90uM
H2 GAS(Hash symbol)
Residence time=10/20 ms:P=Atm

Fig.lg5a1
Mesh gas yields vs Peak mesh Temperature

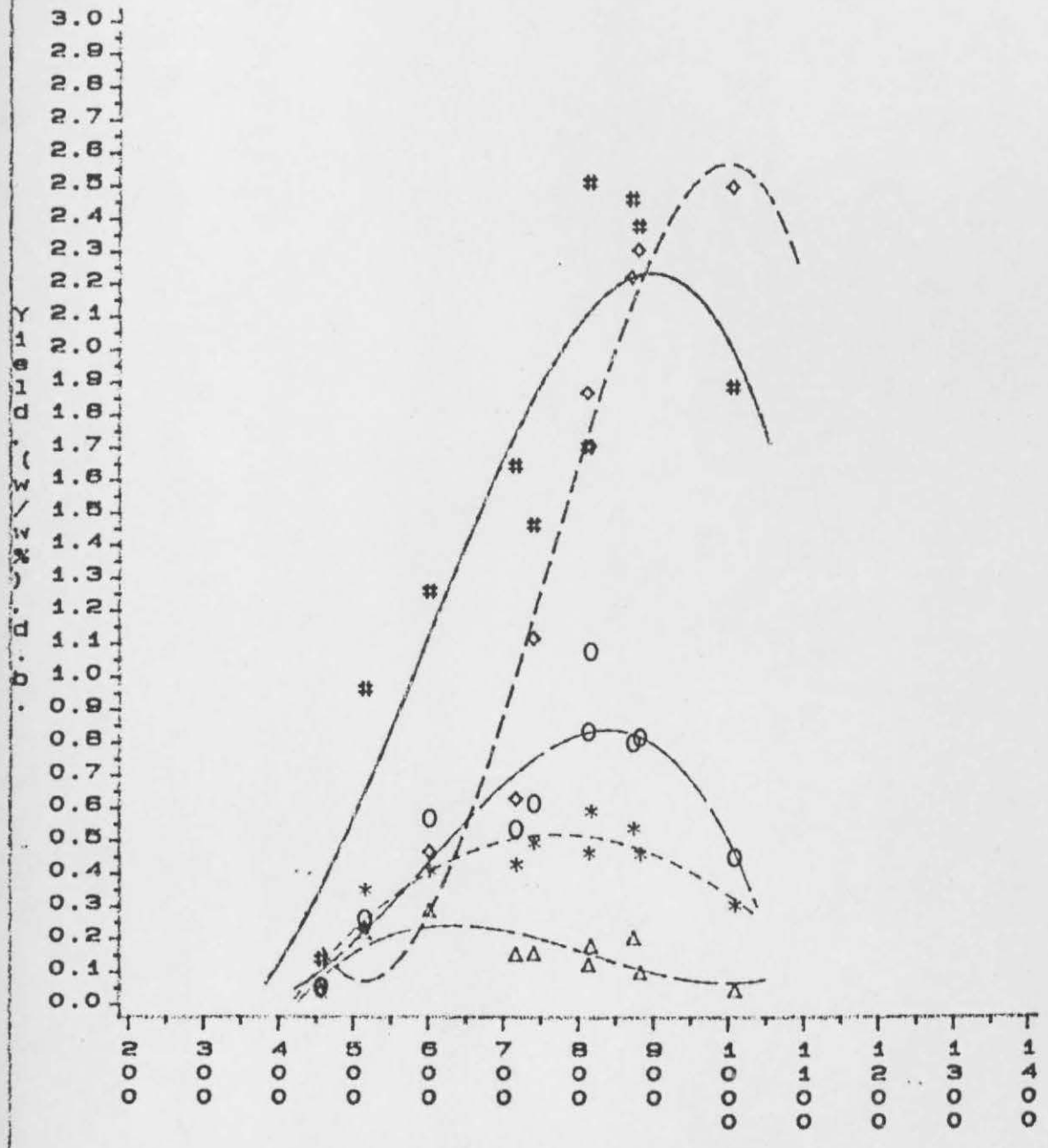

Goldthorpe Coal:Dp=75/90um:(5000 C/s)
CH4 GAS(Hash symbol)
C2H6 GAS(Star symbol)
C2H4 GAS(Diamond symbol)
C3H8 GAS(Triangle symbol)
C3H6 GAS(Circle symbol)
Residence time=6/10 s:P=Atm.

Fig.lg5a2
Mesh gas yields vs Peak mesh Temperature

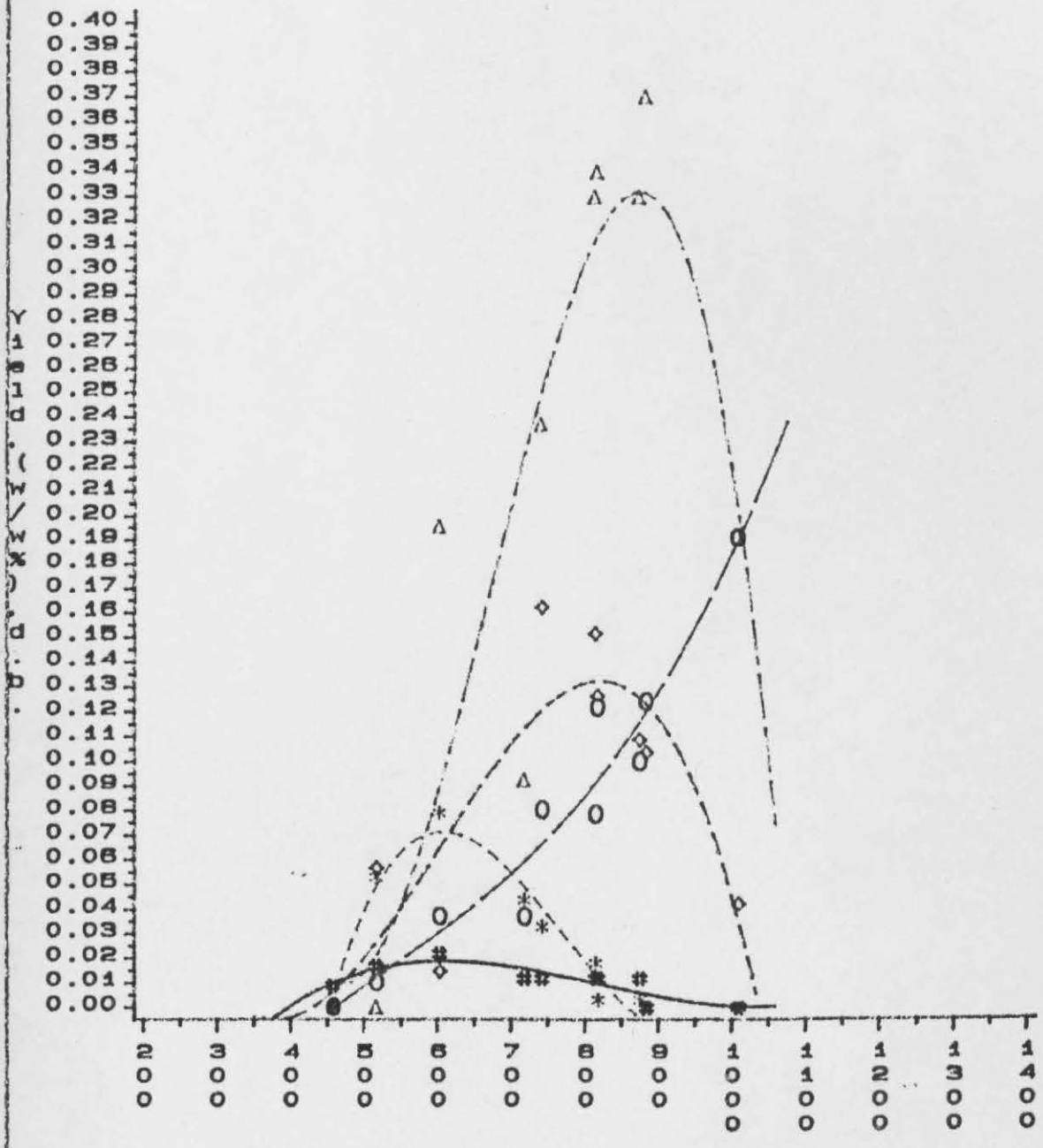

Coldthorpe Coal:Dp=75/90uM:5000 C/s
I-C4H10 GAS(Hash symbol)
N-C4H10 GAS(Star symbol)
BUT-1-ENE GAS(Diamond symbol)
1,3 BUTADIENE GAS(Triangle symbol)
C2H2 GAS(Circle symbol)
Residence time=06/10 seconds:P=Atm.)

Fig.lg5a3
Mesh gas yields vs Peak mesh Temperature

Heating Rate=5000 C/s:Atm.Pressure

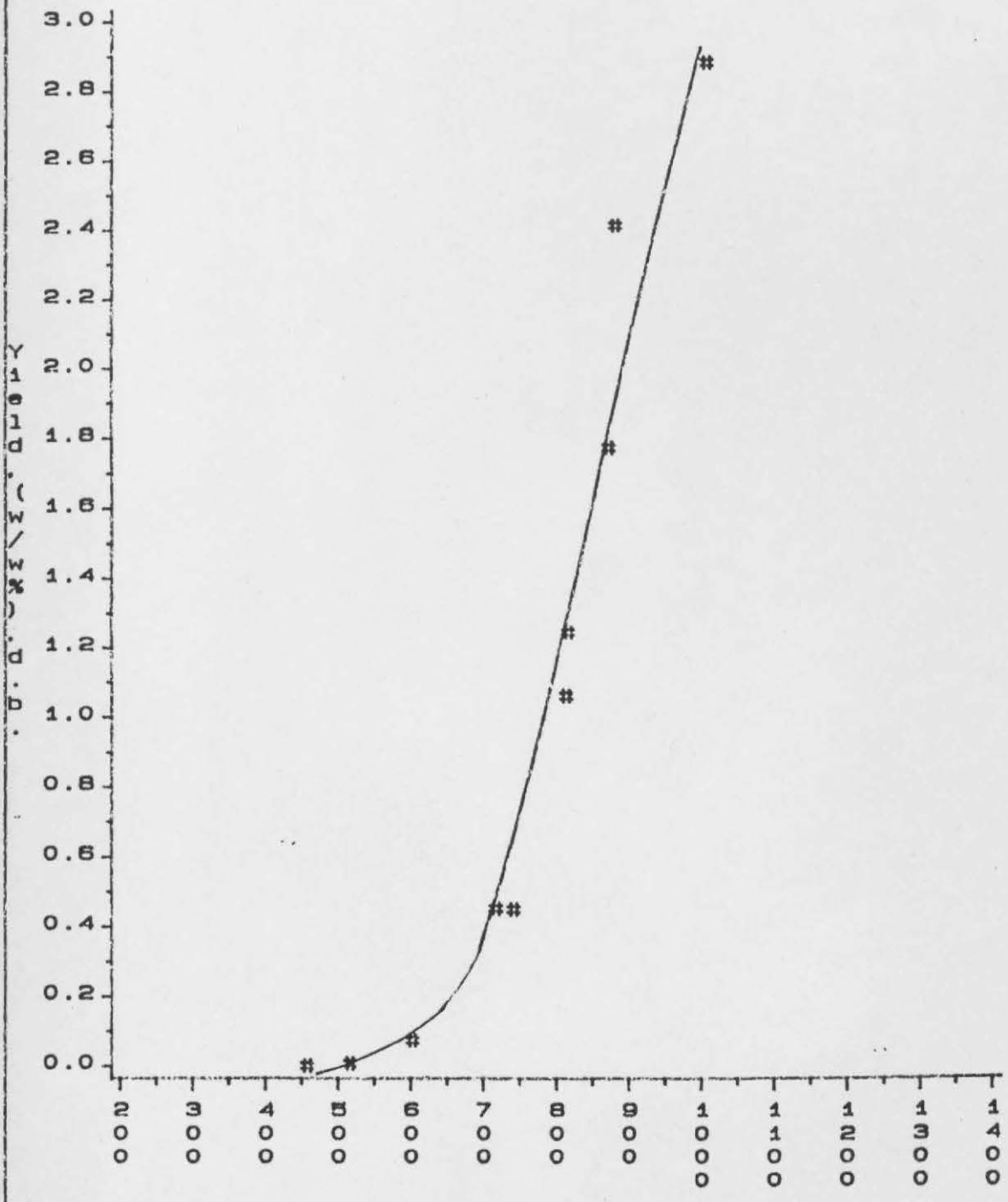

Goldthorpe Coal:Dp=75/90uM
H2 GAS(Hash symbol)
Residence time=6/10 seconds:P=Atm.

Fig.lg5a4
Mesh gas yields vs Peak mesh Temperature
Heating Rate=5000 C/s:Atm.Pressure

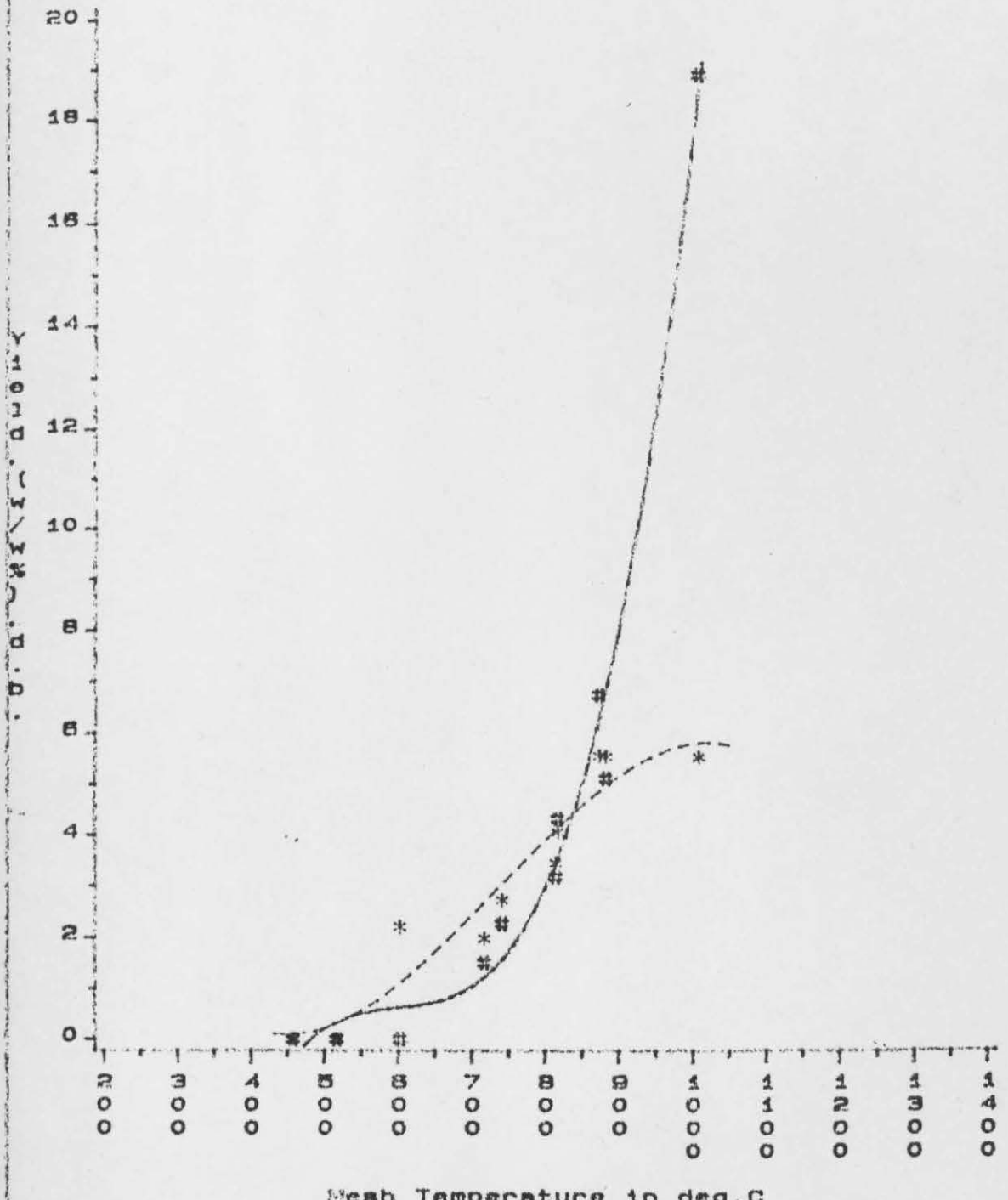

Goldthorpe Coal:Dp=75/90uM
CO GAS(Hash symbol)
CO2 GAS(Star symbol)
Residence time=6/10 seconds:P=1atm.

Fig.g1v1
Mesh gas yields vs Peak mesh Temperature
10 C/s##,VACUUM

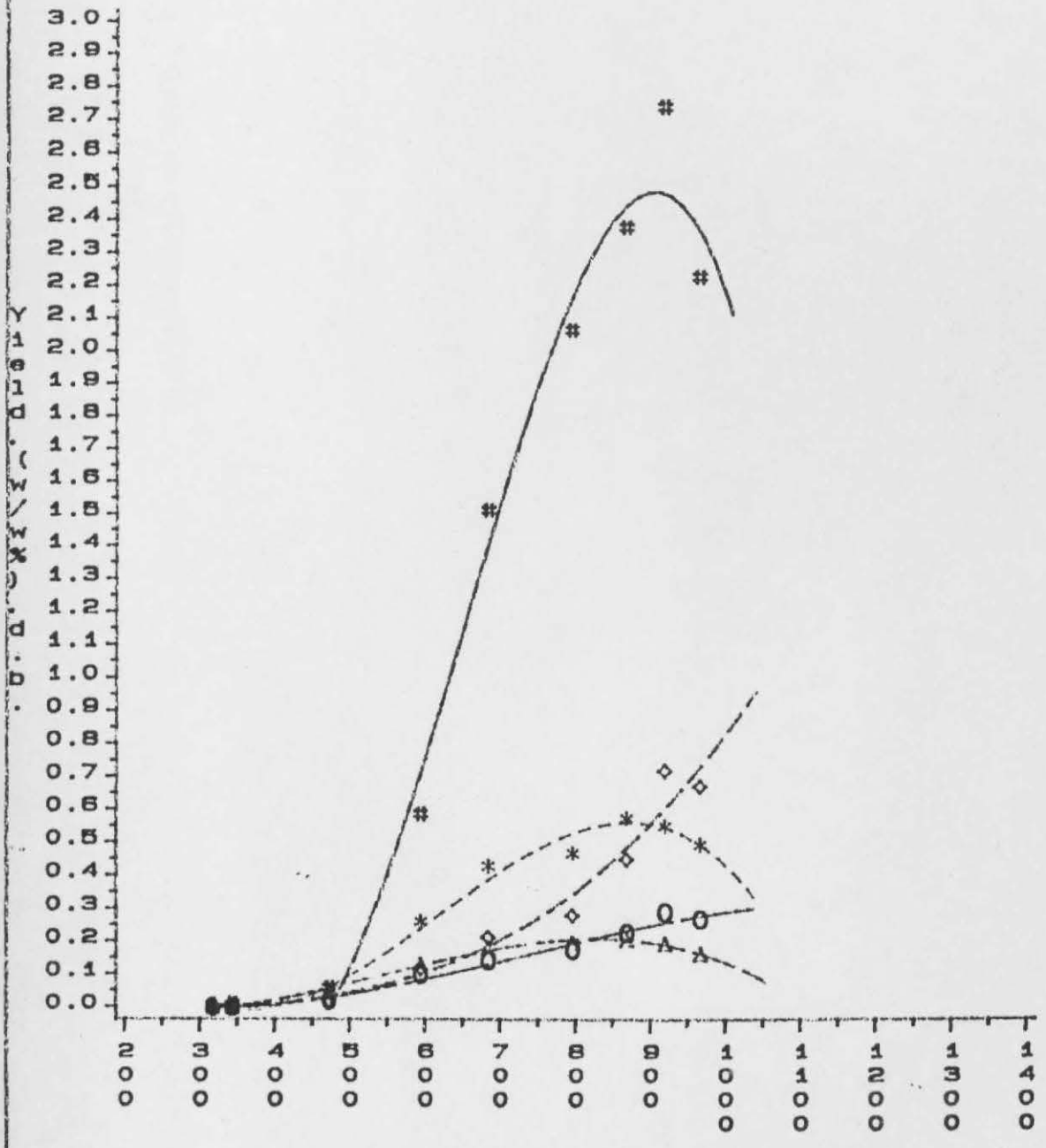

Goldthorpe Coal:Dp=75/90uM
CH4 GAS(Hash symbol)
C2H6 GAS(Star symbol)
C2H4 GAS(Diamond symbol)
C3H8 GAS(Triangle symbol)
C3H6 GAS(Circle symbol)
Residence time=10/20ms:P=Vacuum

Fig.g1v2
Mesh gas yields vs Peak mesh Temperature
10 C/s##,VACUUM

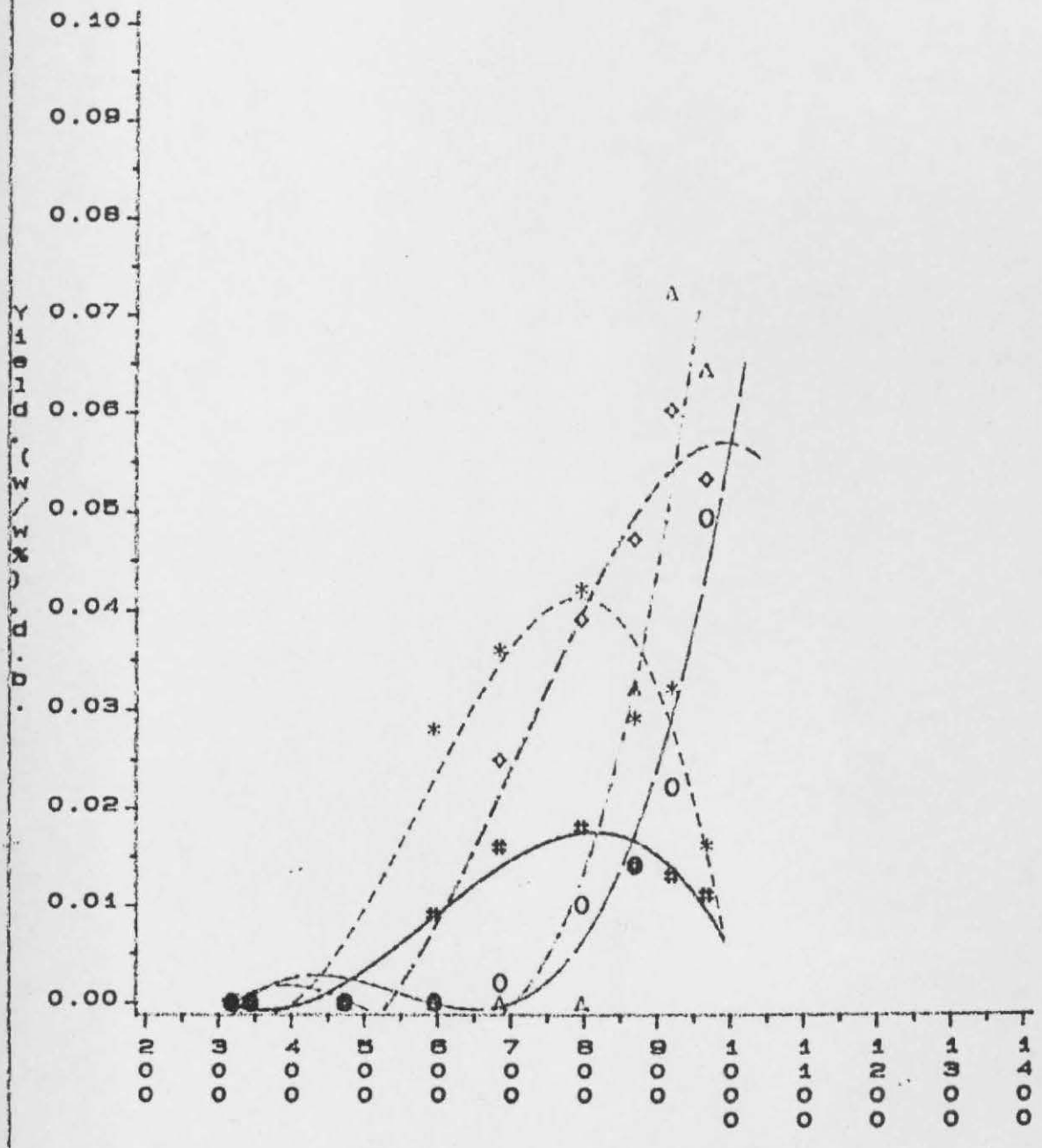

Goldthorpe Coal:Dp=75/90uM
I-C4H10 GAS(Hash symbol)
N-C4H10 GAS(Star symbol)
BUT-1-ENE GAS(Diamond symbol)
1,3 BUTADIENE GAS(Triangle symbol)
C2H2 GAS(Circle symbol)
Residence time=10/20ms :P=Vacuum

Fig.g1v3
Mesh gas yields vs Peak mesh Temperature

10 C/s##.VACUUM

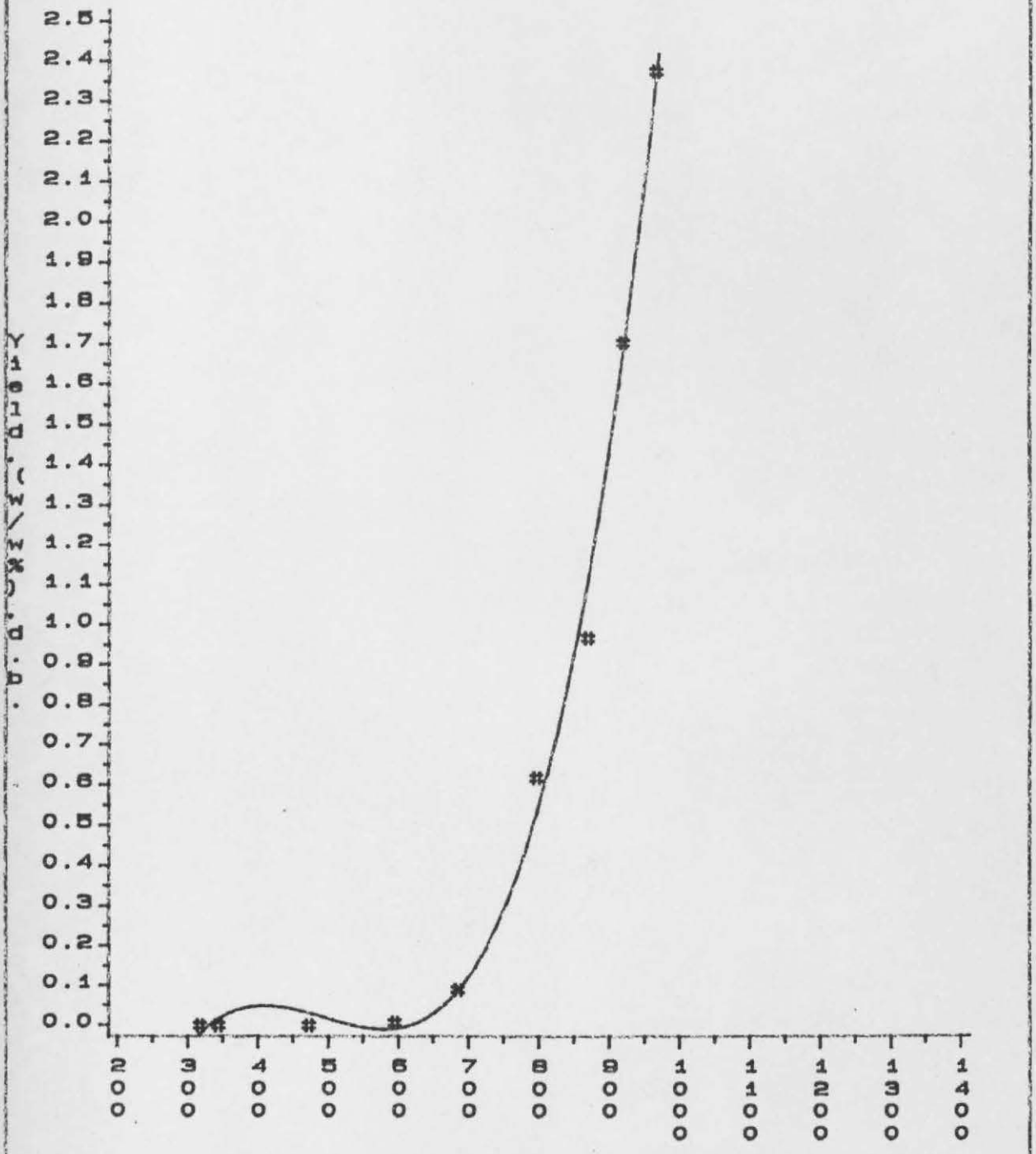

Goldthorpe Coal:Dp=75/90uM
H2 GAS(Hash symbol)
Residence time=10/20ms:P=Vacuum

Fig.g1A1
Mesh gas yields vs Peak mesh Temperature

10 C/###.ATMOSPHERE

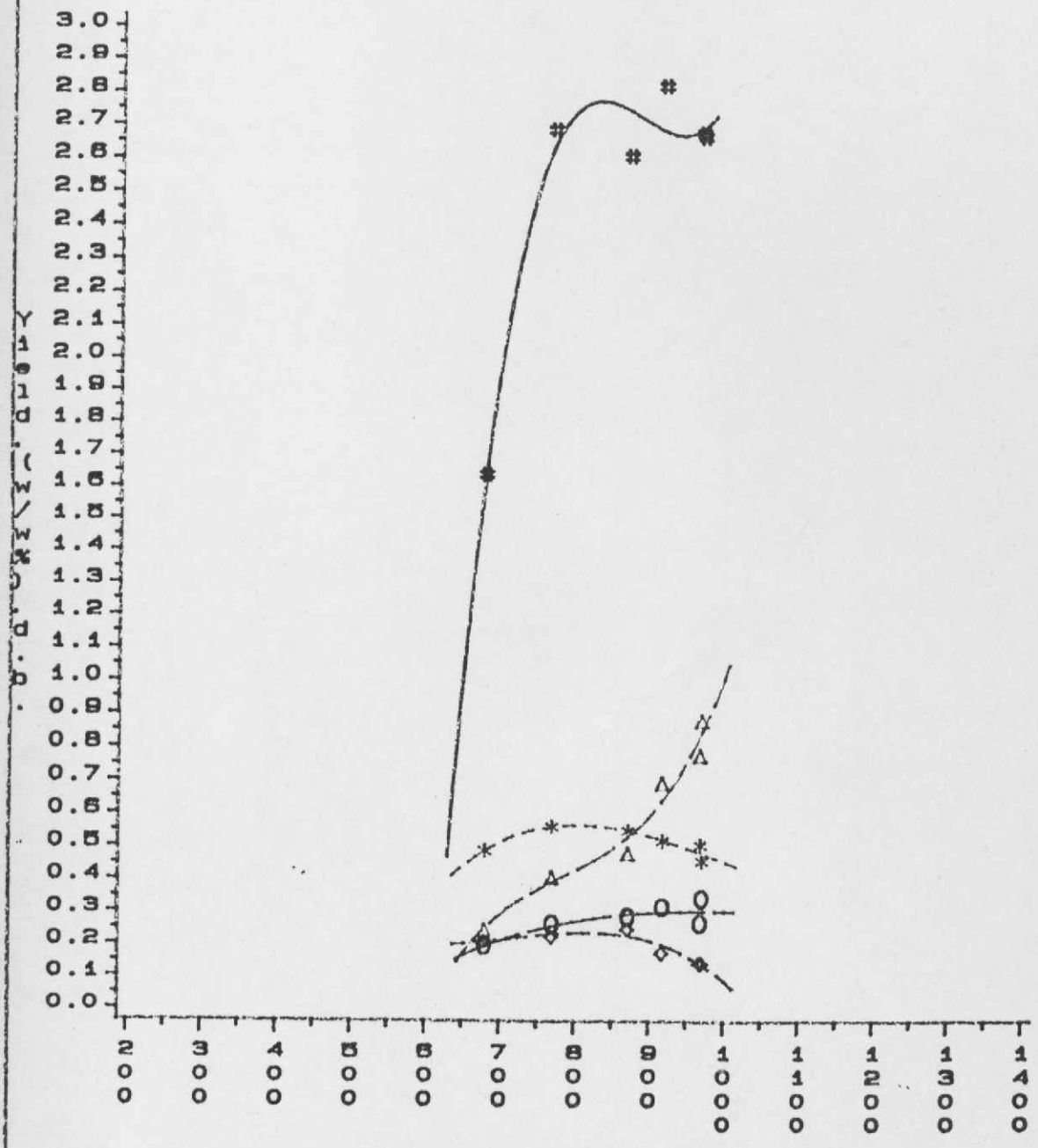

Goldthorpe Coal:Dp=75/90uM
CH4 GAS(Hash symbol)
C2H6 GAS(Star symbol)
C3H8 GAS(Diamond symbol)
C2H4 GAS(Triangle symbol)
C3H6 GAS(Circle symbol)
Residence time=10/20ms:P=Atm

Fig.g1a2
Mesh gas yields vs Peak mesh Temperature
10 C/s##,ATMOSPHERE

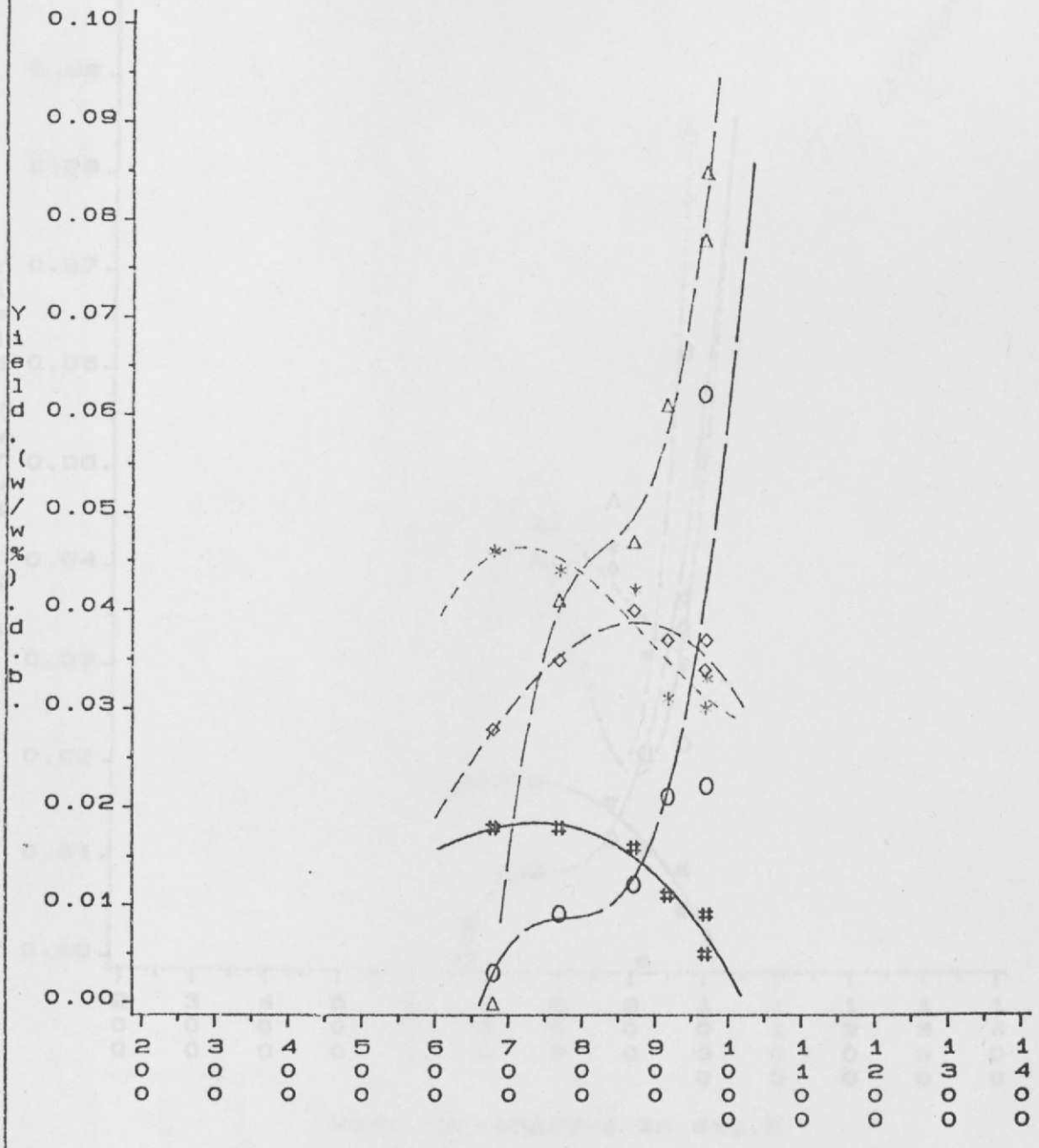

Goldthorpe Coal:Dp=75/90uM
I-C4H10 GAS(Hash symbol)
N-C4H10 GAS(Star symbol)
BUT-1-ENE GAS(Diamond symbol)
1,3 BUTADIENE GAS(Triangle symbol)
C2H2 GAS(Circle symbol)
Residence time=10/20ms :P=Atm

Fig.g1a3
Mesh gas yields vs Peak mesh Temperature

10 C/s##.ATMOSPHERE

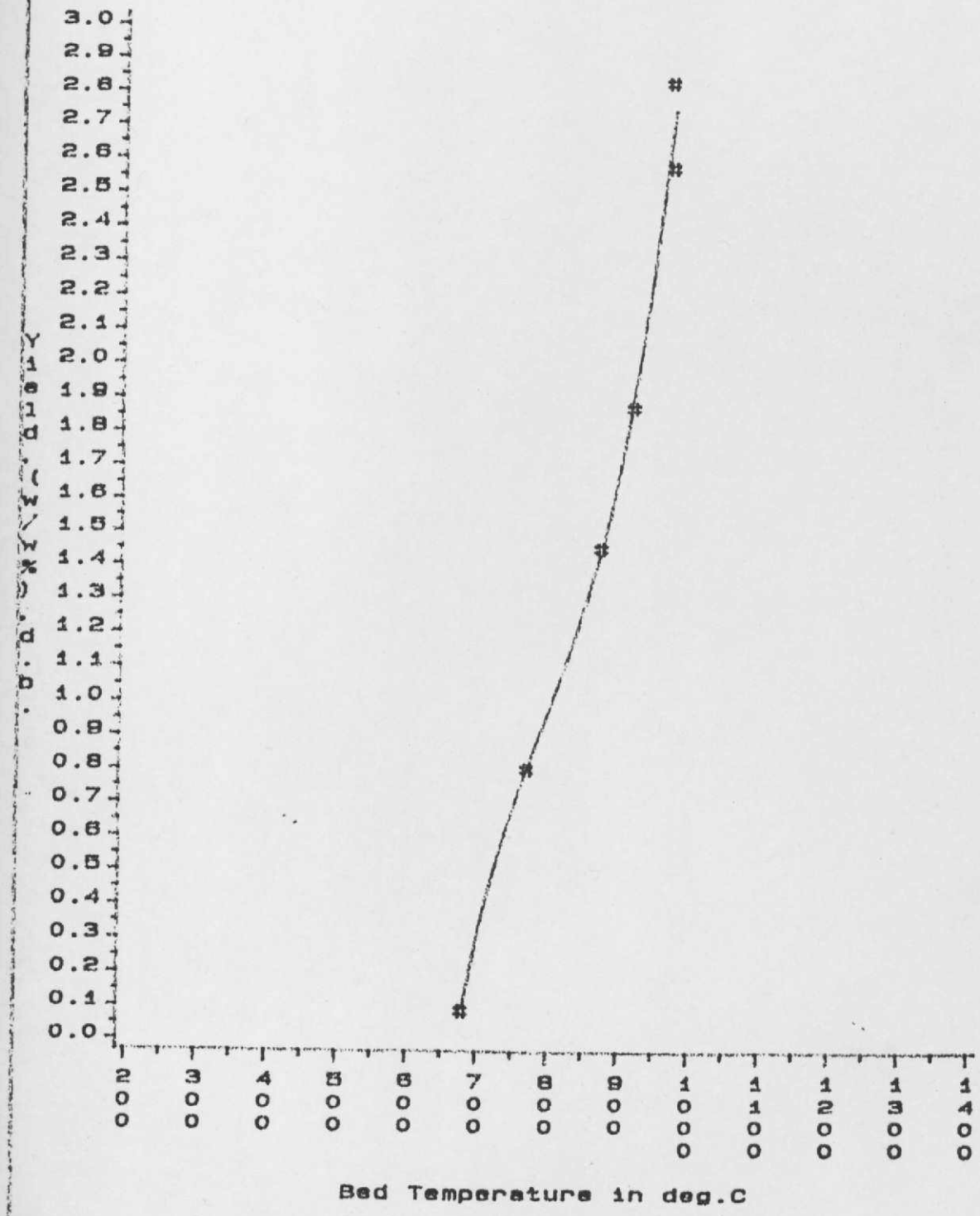

Goldthorpe Coal:Dp=75/90uM
H2 GAS(Hash symbol)
Residence time=10/20ms:P=1tm.

Fig.g1A11
Mesh gas yields vs Peak mesh Temperature
10 C/s.##.ATMOSPHERE

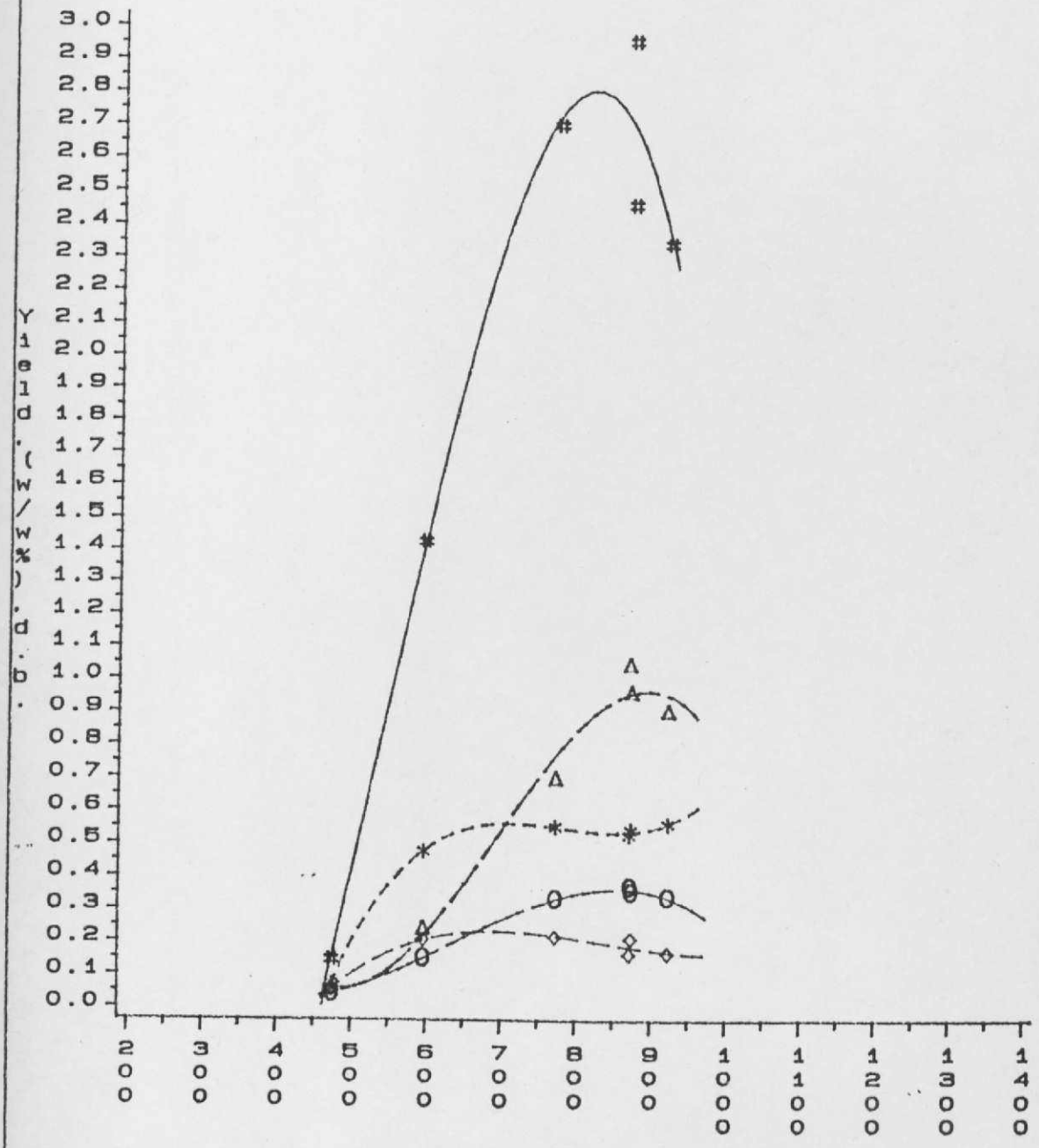

Goldthorpe Coal:Dp=75/90uM
CH4 GAS(Hash symbol)
C2H6 GAS(Star symbol)
C3H8 GAS(Diamond symbol)
C2H4 GAS(Triangle symbol)
C3H6 GAS(Circle symbol)
Residence time=6/10sec:P=Atm.

Fig.g1al2
Mesh gas yields vs Peak mesh Temperature
10 C/s,##,ATMOSPHERE

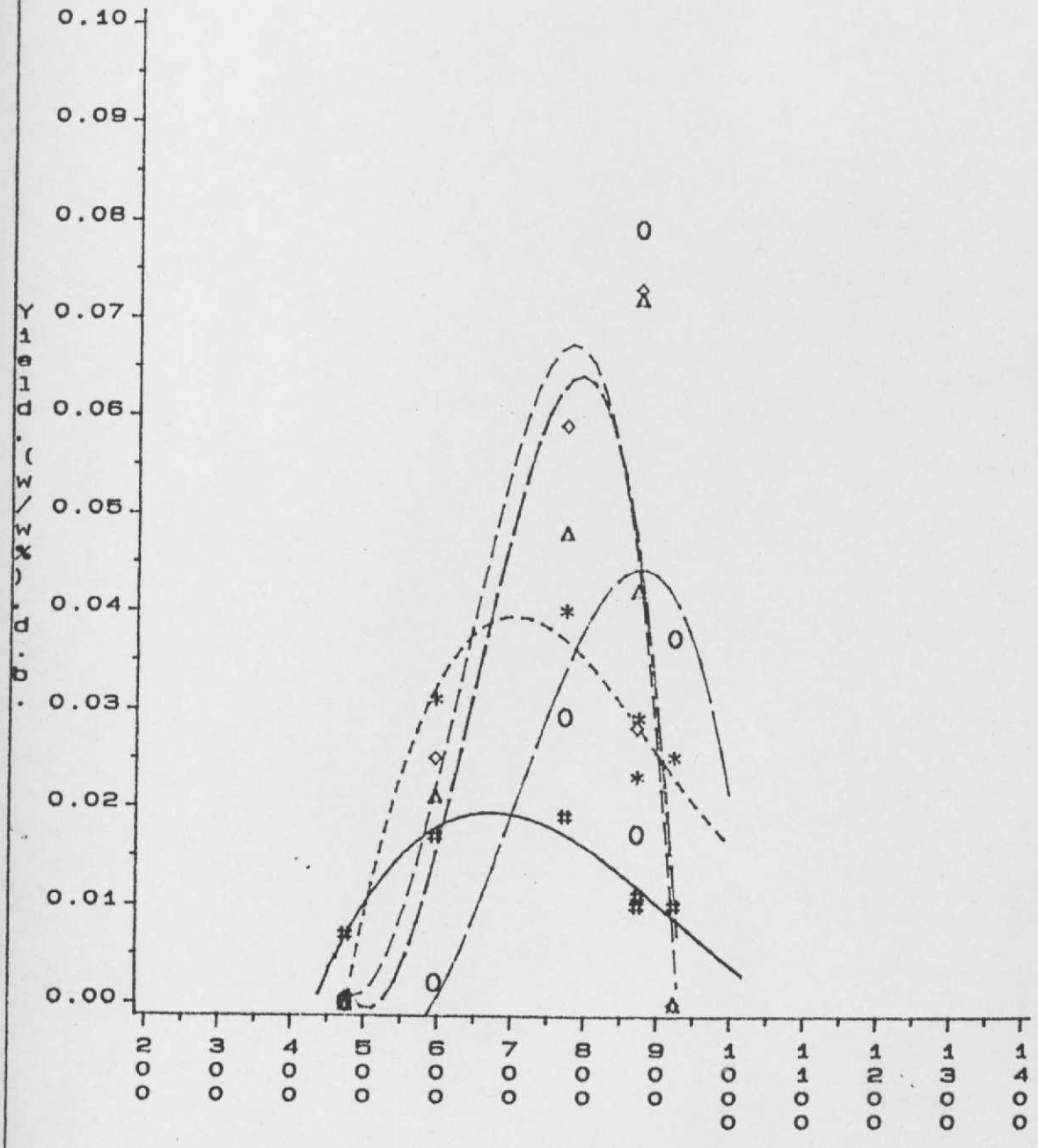

Goldthorpe Coal:Dp=75/90uM
I-C4H10 GAS(Hash symbol)
N-C4H10 GAS(Star symbol)
BUT-1-ENE GAS(Diamond symbol)
1,3 BUTADIENE GAS(Triangle symbol)
C2H2 GAS(Circle symbol)
Residence time=6/10s :P=Atm

Fig.g1al3
Mesh gas yields vs Peak mesh Temperature

10 C/s.##.ATMOSPHERE

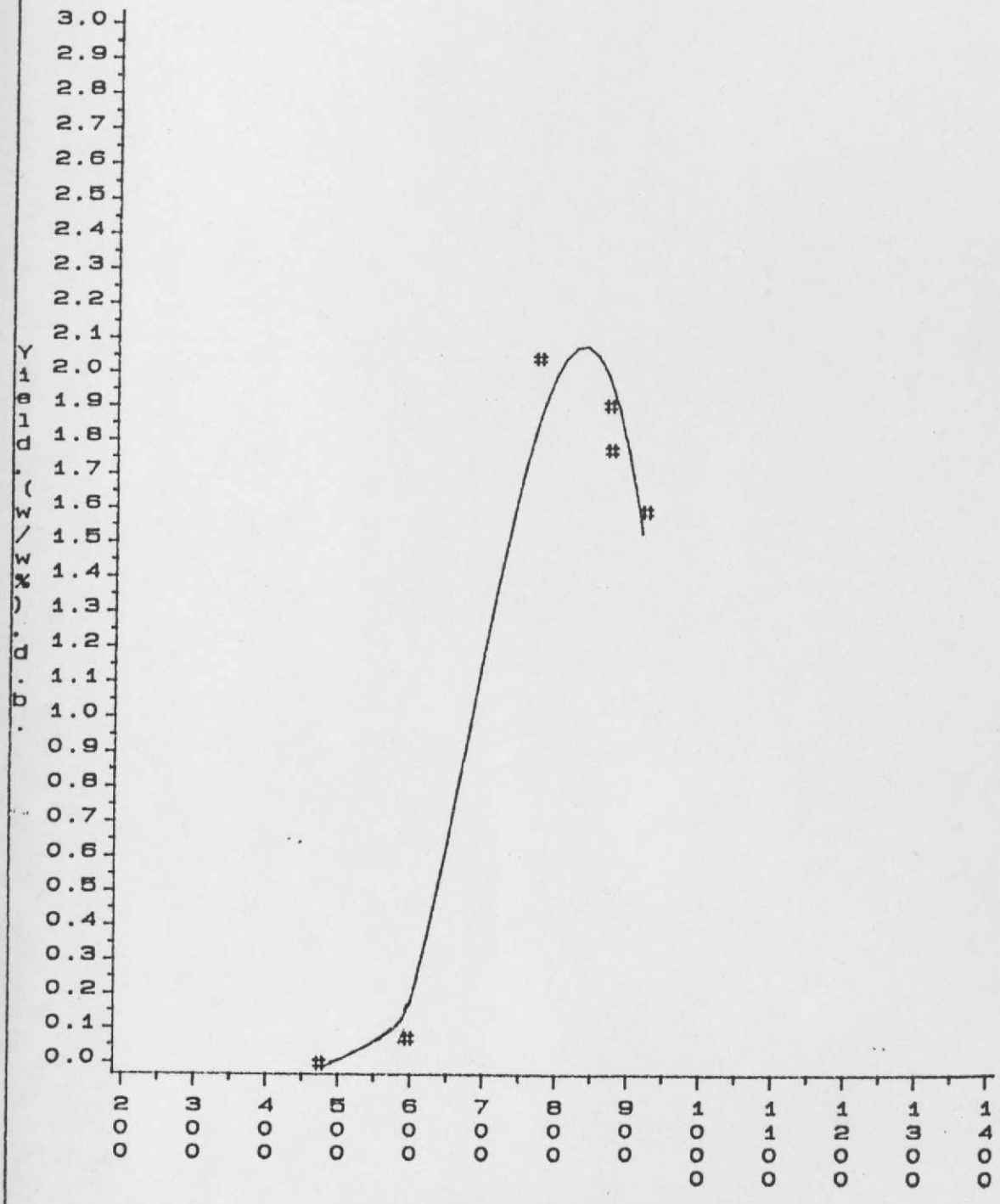

Goldthorpe Coal:Dp=75/90uM
H2 GAS(Hash symbol)
Residence time=6/10sec:P=Atm.

Fig.m51
Mesh gas yields vs Peak mesh Temperature
Heating Rate=5000 C/s

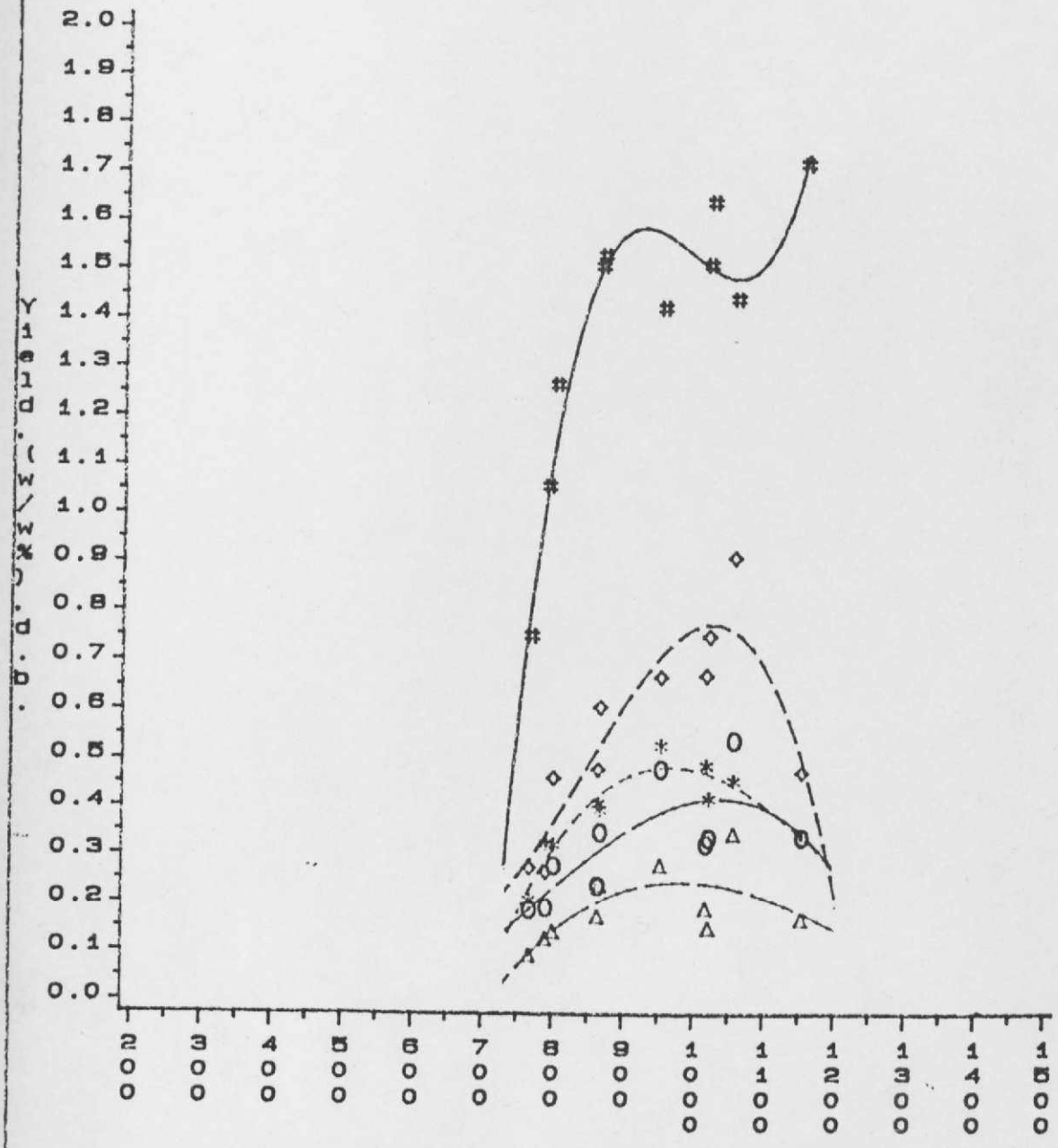

M.Main Coal:Dp=75/90uM
CH4 GAS(Hash symbol)
C2H6 GAS(Star symbol)
C2H4 GAS(Diamond symbol)
C3H8 GAS(Triangle symbol)
C3H6 GAS(Circle symbol)
Residence time=10/20ms:(P=Vacuum)

Fig.m52
Mesh gas yields vs Peak mesh Temperature

Heating Rate=5000 C/s;Vacuum

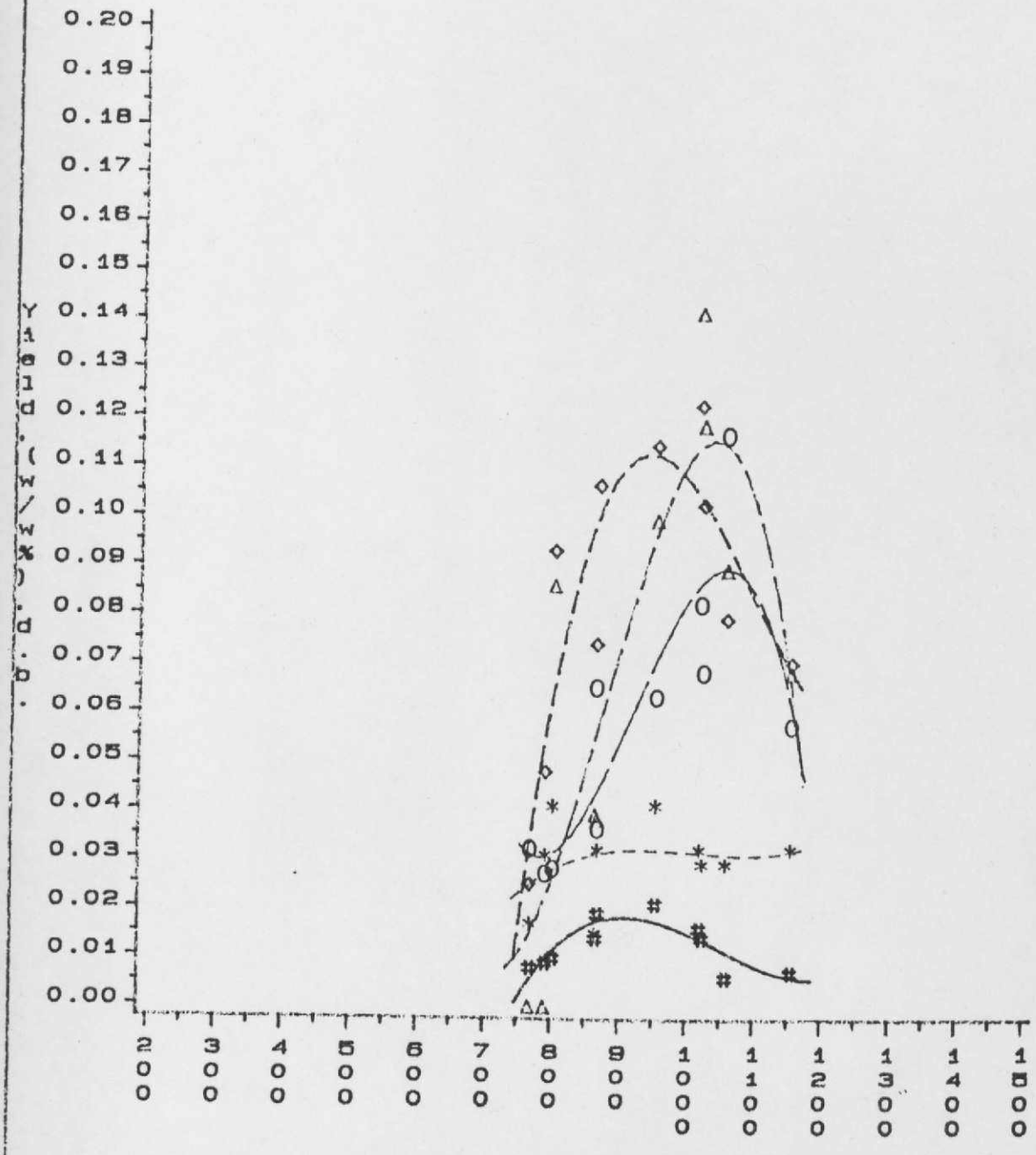

Markham Main Coal:Dp=75/90uM
I-C4H10 GAS(Hash symbol)
N-C4H10 GAS(Star symbol)
BUT-1-ENE GAS(Diamond symbol)
1,3 BUTADIENE GAS(Triangle symbol)
C2H2 GAS(Circle symbol)
Residence time=10/20ms

Fig.LM51
Mesh gas yields vs Peak mesh Temperature

Heating Rate=5000 C/s

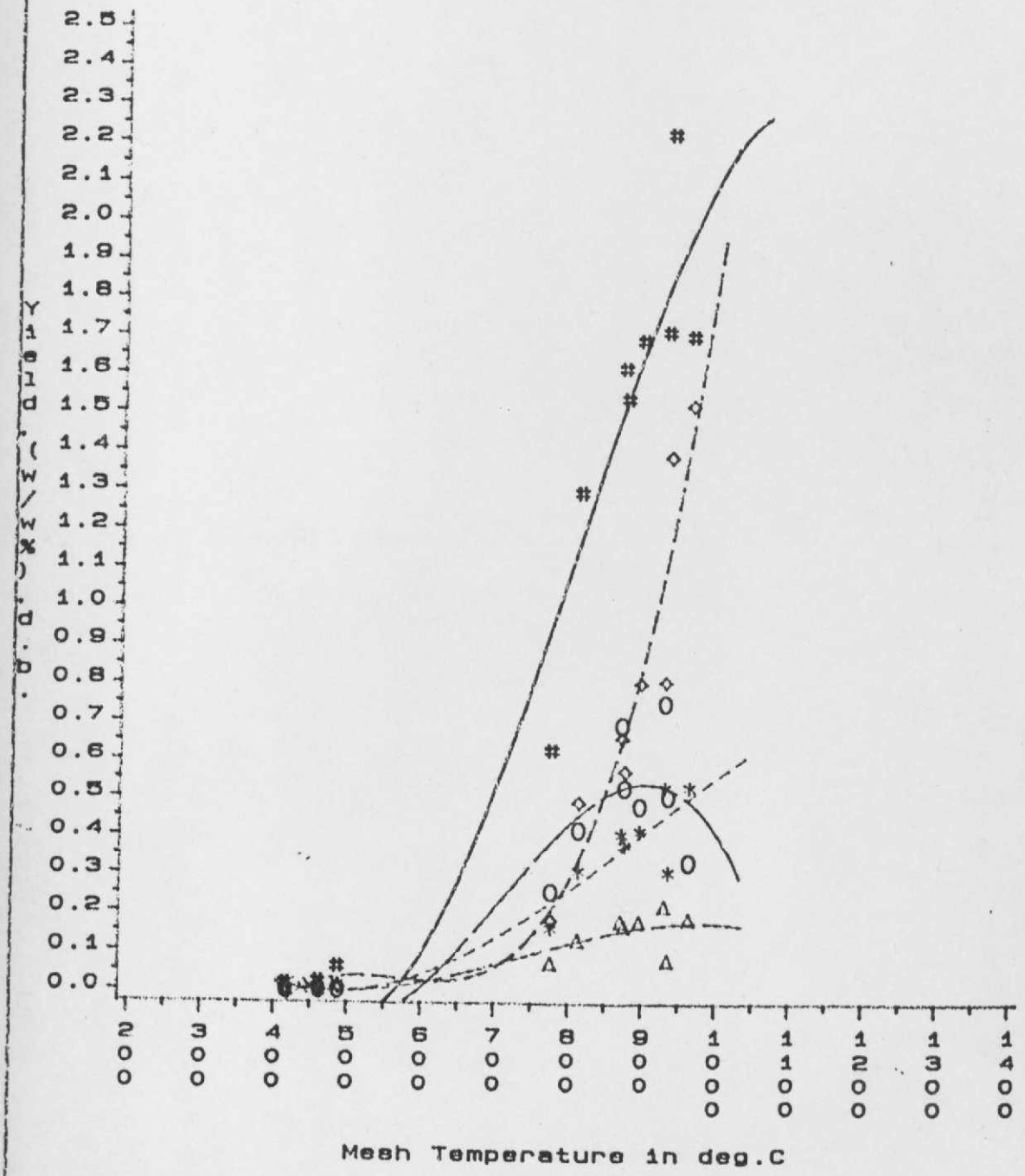

M.Main Coal:Dp=75/90uM
CH4 GAS(Hash symbol)
C2H6 GAS(Star symbol)
C2H4 GAS(Diamond symbol)
C3H8 GAS(Triangle symbol)
C3H6 GAS(Circle symbol)
Residence time=2.50sec:(P=Vacuum)

Fig.1m52
Mesh gas yields vs Peak mesh Temperature
Heating Rate=5000 C/s;Vacuum

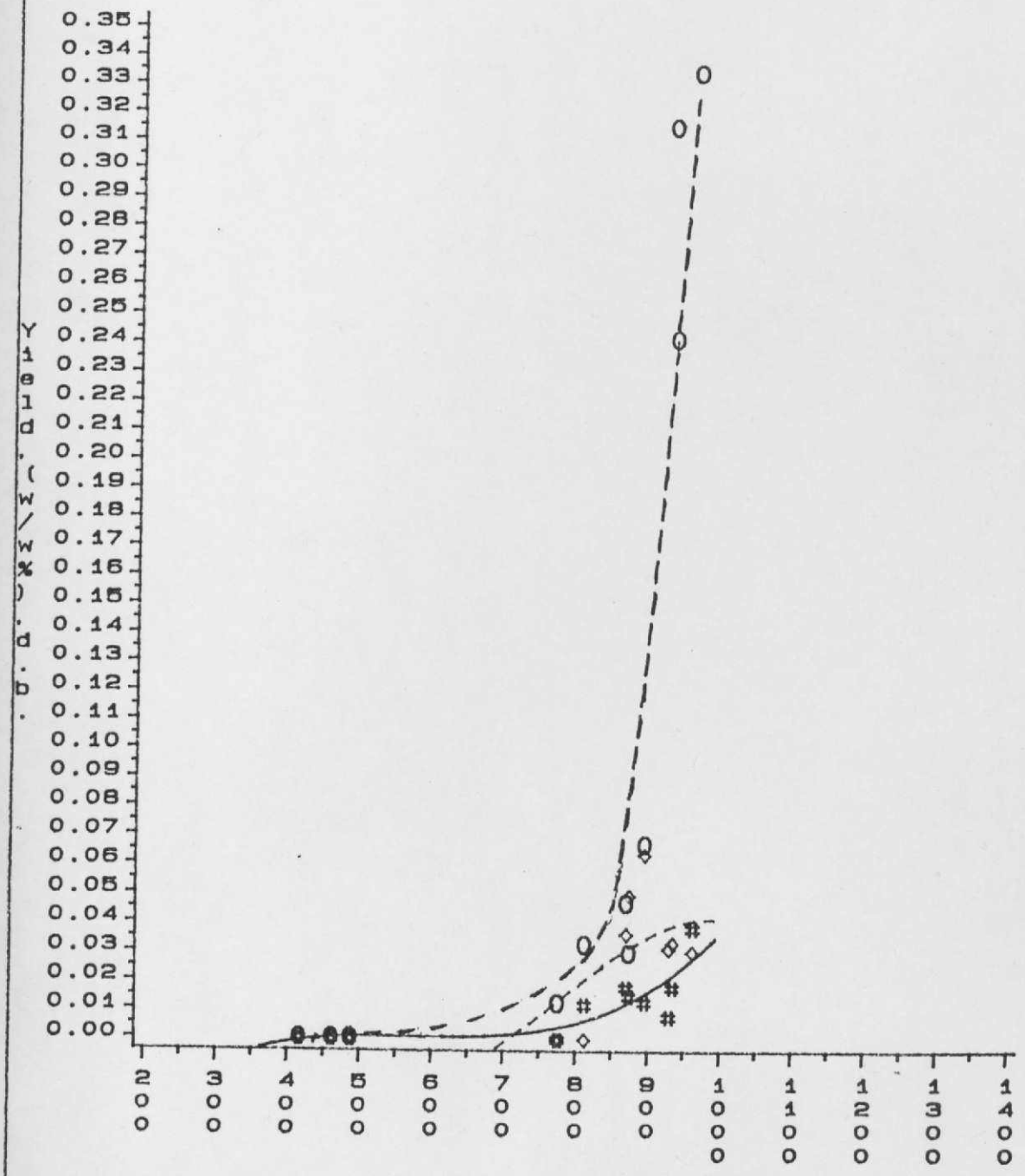

Markham Main Coal:Dp=75/90uM
I-C4H10 GAS(Hash symbol)
BUT-1-ENE GAS(Diamond symbol)
C2H2 GAS(Circle symbol)
Residence time=2.50sec

Fig.1m53
Mesh gas yields vs Peak mesh Temperature
Heating Rate=5000 C/s:Vacuum

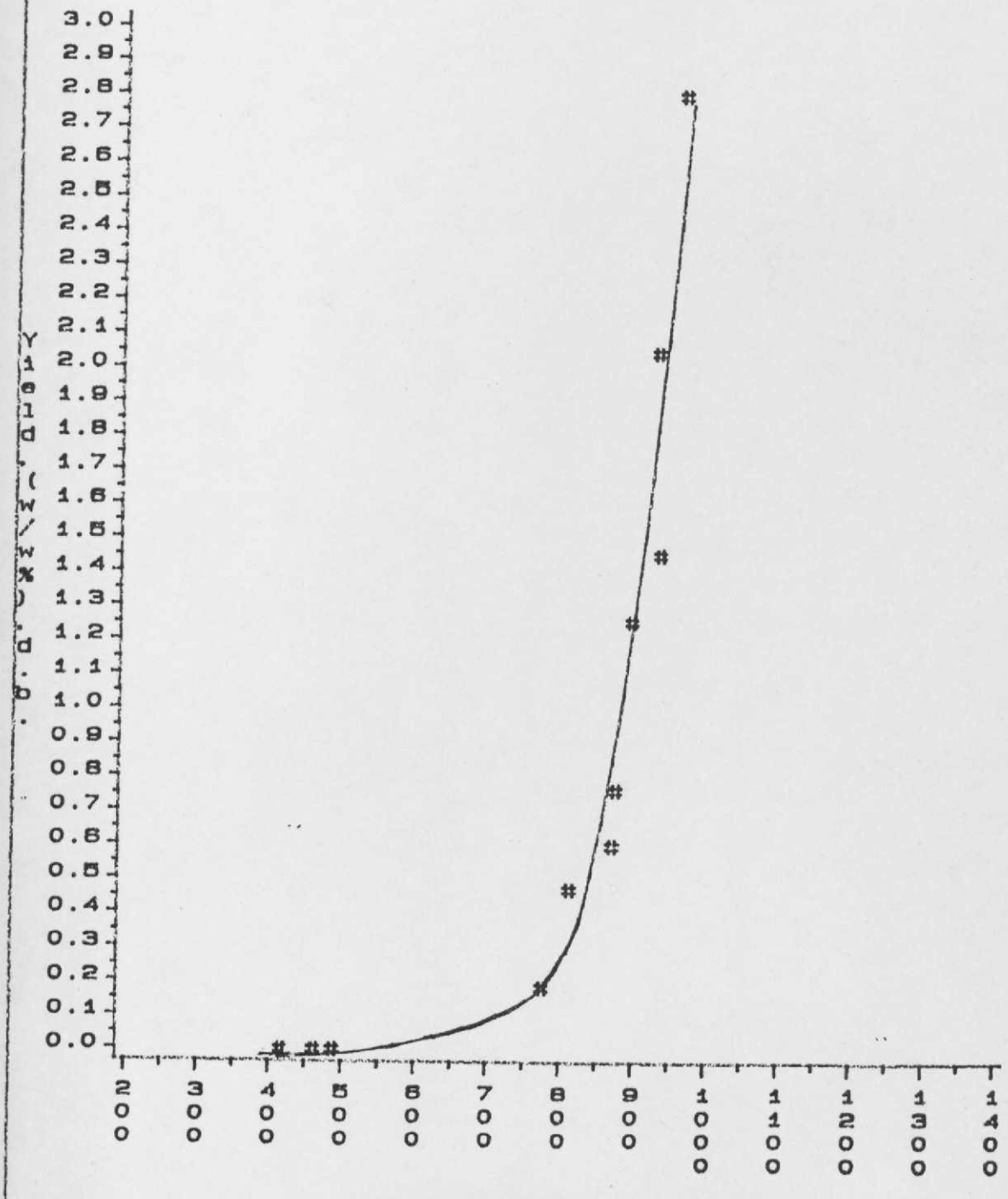

Markham Main Coal:Dp=75/90uM
H2 GAS(Hash symbol)
Residence time=2.5sec.

Fig.ma51
Mesh gas yields vs Peak mesh Temperature
Heating Rate=5000 C/s:Atmosphere

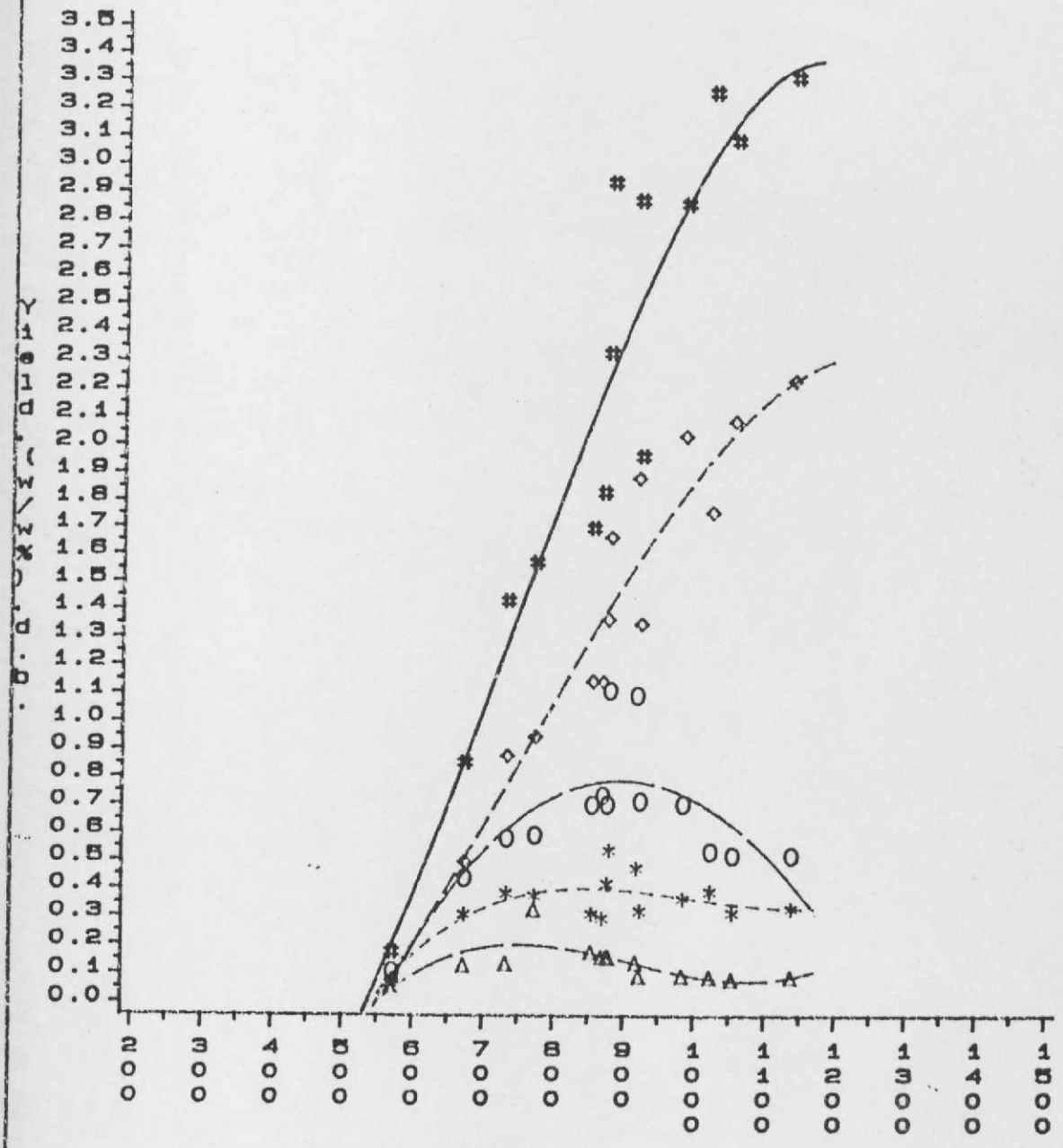

M.Main Coal:Dp=75/90uM
CH4 GAS(Hash symbol)
C2H6 GAS(Star symbol)
C2H4 GAS(Diamond symbol)
C3H8 GAS(Triangle symbol)
C3H6 GAS(Circle symbol)
Residence time=10/20ms:(P=Atm.)

Fig.ma52
Mesh gas yields vs Peak mesh Temperature
Heating Rate=5000 C/s;Atmosphere

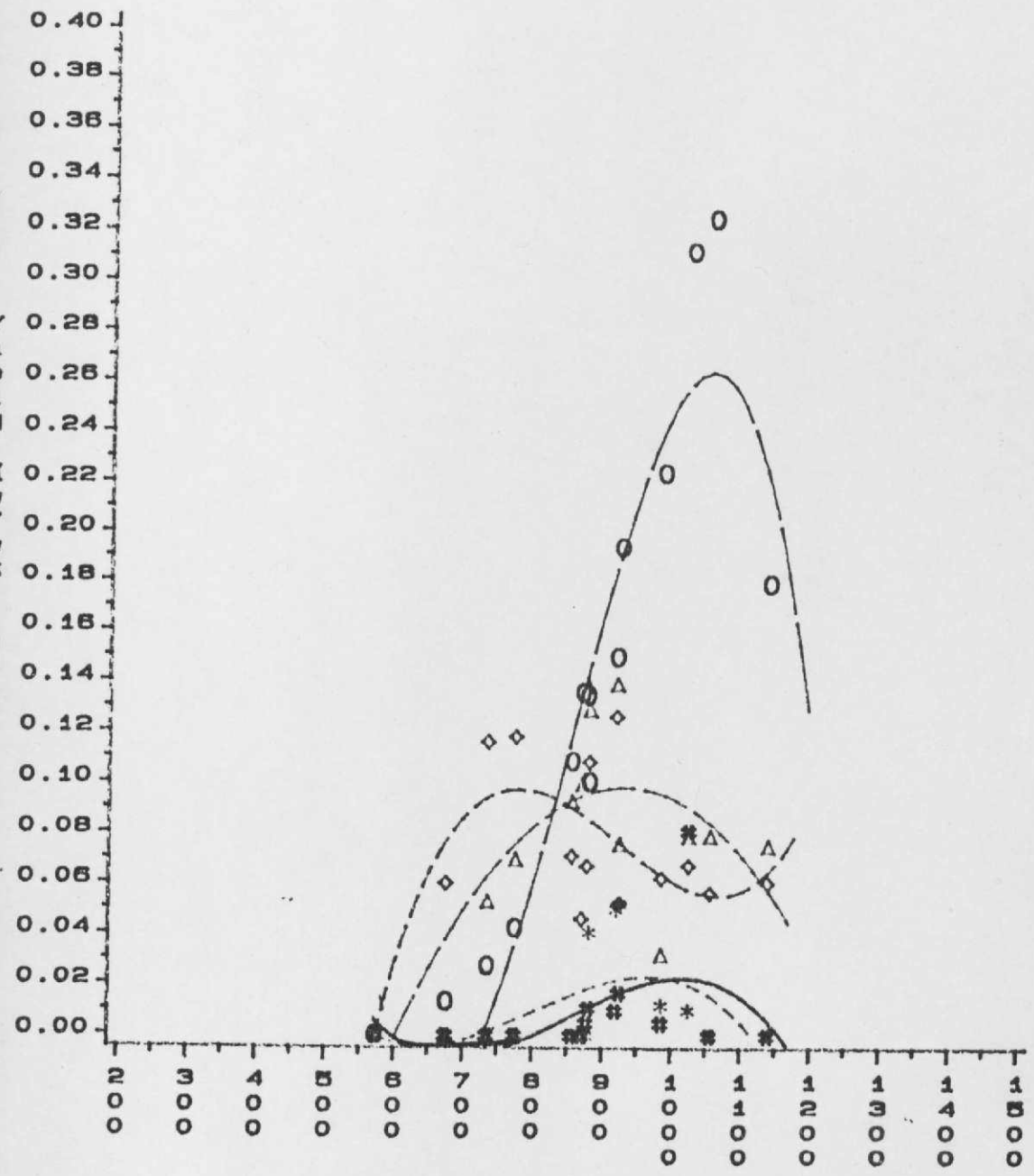

Markham Main Coal:Dp=75/90uM
I-C4H10 GAS(Hash symbol)
N-C4H10 GAS(Star symbol)
BUT-1-ENE GAS(Diamond symbol)
1,3 BUTADIENE GAS(Triangle symbol)
C2H2 GAS(Circle symbol)
Residence time=10/20ms

Fig.ma53
Mesh gas yields vs Peak mesh Temperature

Heating Rate=5000 C/s:Atmosphere

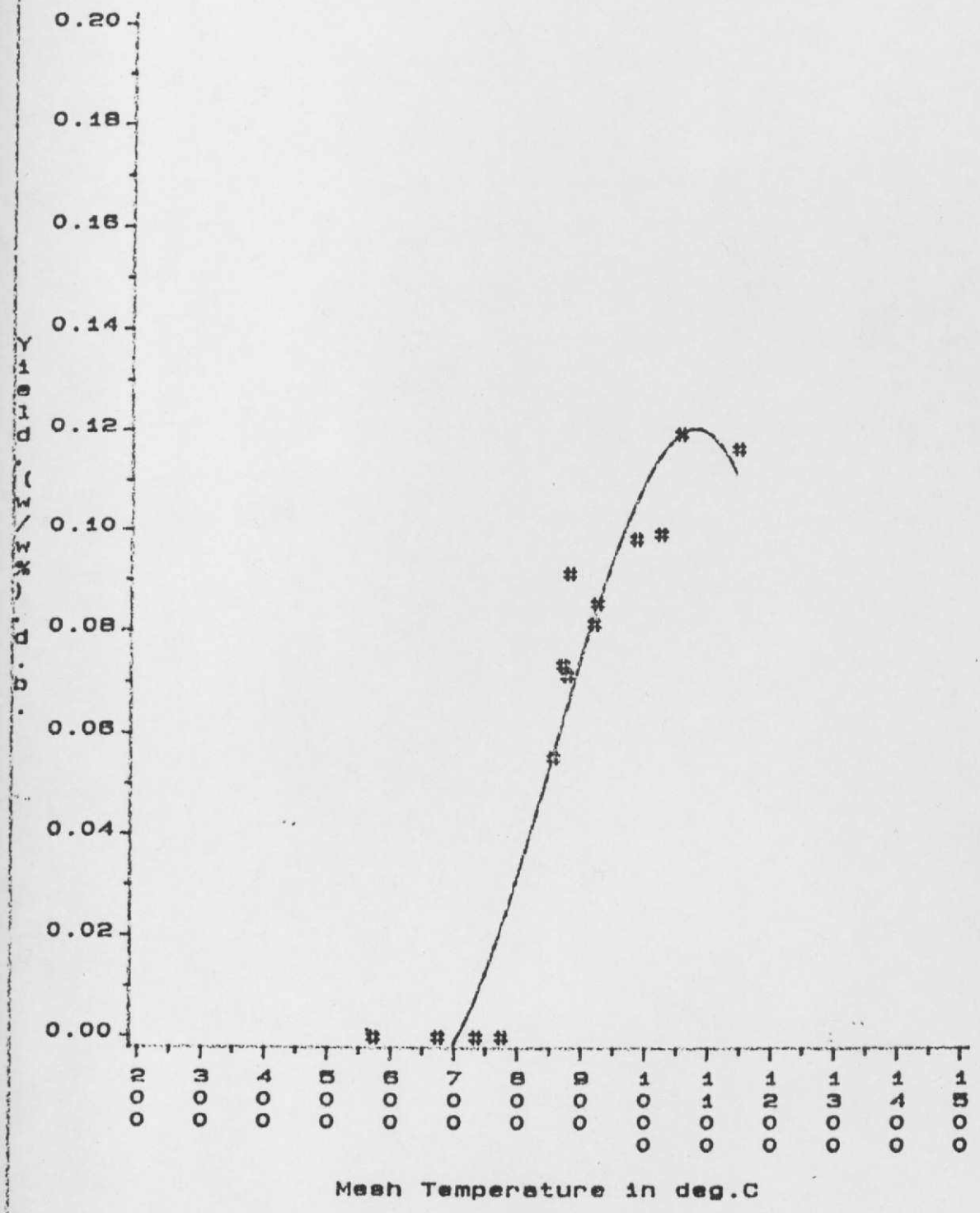

Markham Main Coal:Dp=75/90ul

ALLENE GAS(Star symbol)

Fig.m54
Mesh gas yields vs Peak mesh Temperature
Heating Rate=5000 C/s:Atmosphere

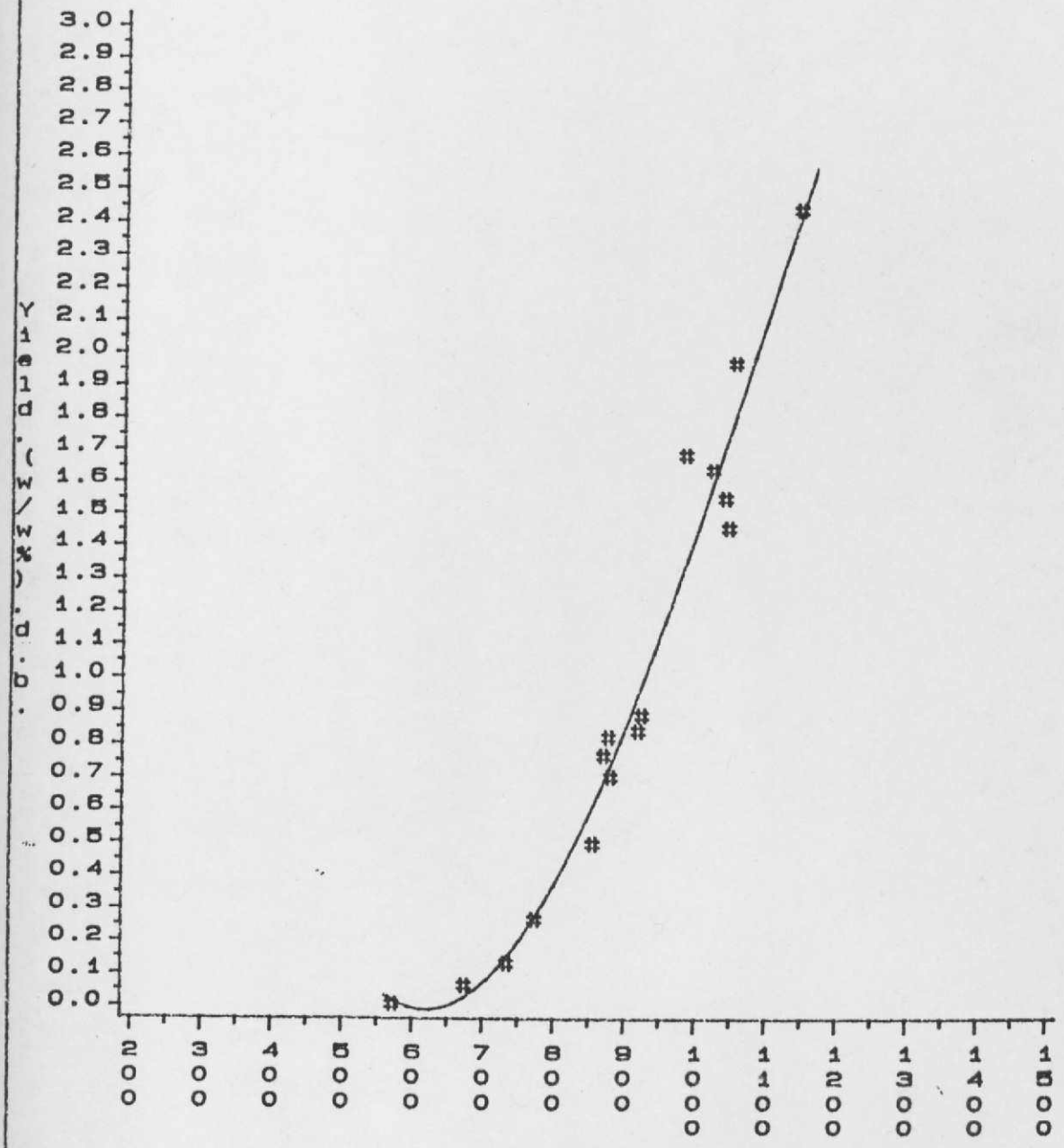

Markham Main Coal:Dp=75/90uM
H2 GAS(Hash symbol)

Residence time=10/20ms

The large surface areas presented by swelling, gas filled bubbles to partially dissolved gases diffusing through the melt may provide scope for extensive secondary reactions at the bubble interphase. Rapid generation of a wide range of tarry products by a low energy process may lead, at high heating rates to an evaporative limitation of the heavy species leading to enhanced cracking reactions. This may operate as evidenced by the results for conditions, even where mass transfer is enhanced by vacuum conditions of gas collection. Alternatively, even smaller particle sizes may be required to avoid diffusion limited conditions.

Clearly a more comprehensive model which incorporates sets of parallel, competing and repolymerization reactions must be the key to a realistic description of coal Pyrolysis over the temperature range and conditions of interest.

7.4 Heat transfer modelling

In order to get a handle on the ranges of conditions experienced by the particle during rapid heating by a variety of heat sources such as convective, conductive and other mechanisms of heat transfer, a heat transfer model was assessed.

The unsteady partial differential equation describing conductive heat transport for a solid sphere is:

$$\frac{\delta T}{\delta t} = \frac{k_s}{\rho_s C_p}\left[\frac{\delta^2 T}{\delta r^2} + \left(\frac{2}{r}\right)\frac{\delta T}{\delta r}\right] - \beta \text{ (Reaction Heat Source)}$$

$$\beta = \frac{\text{Heat of reaction of V i}}{\frac{dV}{dt} i \; C_p}$$

The global Pyrolysis rate was assumed to follow an overall 1st order reaction of the multiple, parallel reaction model of the form:

$$\frac{dV}{dt} = k_o \exp(-E/RT) * (V^* F(E)dE - V)$$

and F(E) = gaussian distribution as described earlier.

The values used for the numerical solution are tabulated in the appendix. They represent average values from an exhaustive search in the literature of transport properties of coal.

The equation was solved for the case of the following boundary conditions at the particle surface:

1) $\frac{dT}{dt}$ = constant, (1000 & 5000^{o}K/S)

2) Convective boundary condition, $\frac{\delta T}{\delta r} = \frac{h_c}{k_s} (T_E - T_s)$

Other conditions such as constant external temperature and constant heat flux were available with options to choose any of the required conditions. Reaction rate could be switched off as desired. Case (1) approximates particle heat up in the mesh and case (2) the fluidised bed and similar reactors. Two sets of reaction rate parameters were employed to test for the effect of activation energy on the spatial reaction behaviour.

Set (1) $k_o = 1.63 \times 10^{13}\ S^{-1}$

$E_A = 213$ KJ/mole

$\sigma = 19.8$ KJ/mole

Set (2) $k_o = 1.08 \times 10^8$

$E_A = 108$ KJ/mole

$\sigma = 24.3$ KJ/mole

$V^* = 0.60$ (ultimate yield) in both cases.

The initial conditions prevailing within the particle was assumed to be uniform at 298°K. Integration of the heat transport equation was carried out in conjunction with the reaction rate term by numerical procedure in the NAG Library routine D03PGF.

Freihaut et al[225] reported solutions to the coupled partial differential equation for the case of constant external temperature and a simple single reaction model.

The simulations indicated the following:

1) For the case 1000°C/S and 5000°C/S start of reaction result in increased temperature gradients, about 57°C for the 1000°C/S case at 0.6s into heating time to a peak temperature of 1000°C, and about 117°C for the 5000°C/S at 0.2s.

2) For the case of reaction heat switched off, the temperature lags between particle centre and surface (for particle radius = 80 μm) was found to be ~19°C for 1000°C/S and about 93°C for 5000°C/S heating rate. (The measured temperature lags estimated for a 75-100 μm thermocouple bead by the photocell responses was about 29°C for 1000°C/S and ~ 89°C for the case of 5000°C/S. For coal particles of much lower thermal diffusivity but presumable higher heat absorptivity, these figures appear to be reasonable).

3) For the case of large activation energy, the reaction zone penetration was diminished with respect to the low activation energy case. This is consistant with the results of Freihaut et al who found the same. Thus low pre-exponential factors and activation energies result in a more uniform reaction zone throughout the particle volume as has been noted also for liquid droplets.(226)

4) For the case of convection heating, the choice of heat transfer coefficient (medium flux, Nu = 2) temperature and concentration gradients were small ($\sim$ 9-10^{o}C at 509^{o}C) with the reaction only 75% complete by 1s (Temperature reached 510^{o}C).

At higher temperatures in the flow reactors, significant radiative fluxes will contribute to the external driving heat force. This may give rise to temperature gradients for sufficiently high heat fluxes.

At temperatures above 750^{o}-800^{o}C considerable sooting was noted in the fluidised bed reactor with consequent increase in C_2H_2 formation. Fragments of soot particles were seen to literally blast through the tar trap train into the gas bag. The soot structure ranged from powdery/fine particulate spherulitic 'C' to hard shiny deposits at the top of the reactor exit.

The model estimates reaction times of 120 milliseconds for the 5000^{o}C/S case and about 440 milliseconds for the 1000^{o}C/S case. Simulations by Prado et al (Reference: NATO ASI series, edited by Lahaye & Prado, series No 137, 1987) using the parallel reaction model for 80 μm coal particles and furnace temperatures of 1400-1800K,

calculate devolatalization times of 8-14 milliseconds. Measurement of Pyrolysis times by observation of the volatile flame estimates devolatalization times of 1-17 ms. However, as the authors high speed photography results show, (see photographs of volatile ignition and detachment), this method will seriously underestimate devolataliation times as Pyrolysis proceeds somewhat before ignition of volatile bubble is observed.

7.5 High speed photography experiments

The photomicrography experiments highlight some aspects of devolatalization behaviour which aid in the understanding of the physical processes occurring during Pyrolysis.

Photomicrographs P1 show Pyrolysis, ignition and combustion of a char particle trapped between 50 μm mesh wires. These pictures of incidental relevance to rapid Pyrolysis, reveal features that would not have been observed without the assistance of volatile ignition noted. The particle, M. Main of about 250 μm size melted in the range 336-358^{o}C at a heating rate of the mesh of 1060^{o}C/S to a peak temperature of 1007^{o}C. Most of the volatile evolution, consequent free swelling and ignition and burning of the volatile bubble around the particle occured during heat up to peak temperature.

The approximate temperature of maximum swelling occurred at about 645-666^{o}C represented by frames 9 and 10 (counting from the top L.H.S.). The moment of ignition of volatile cloud was not clearly delineated, but probably occurred at temperatures between 666-687^{o}C. The fuzzy appearance and enhanced size of

P.1 (50 um grid) Coal Particle undergoing
devolatalization, ignition and volatile flame detachment

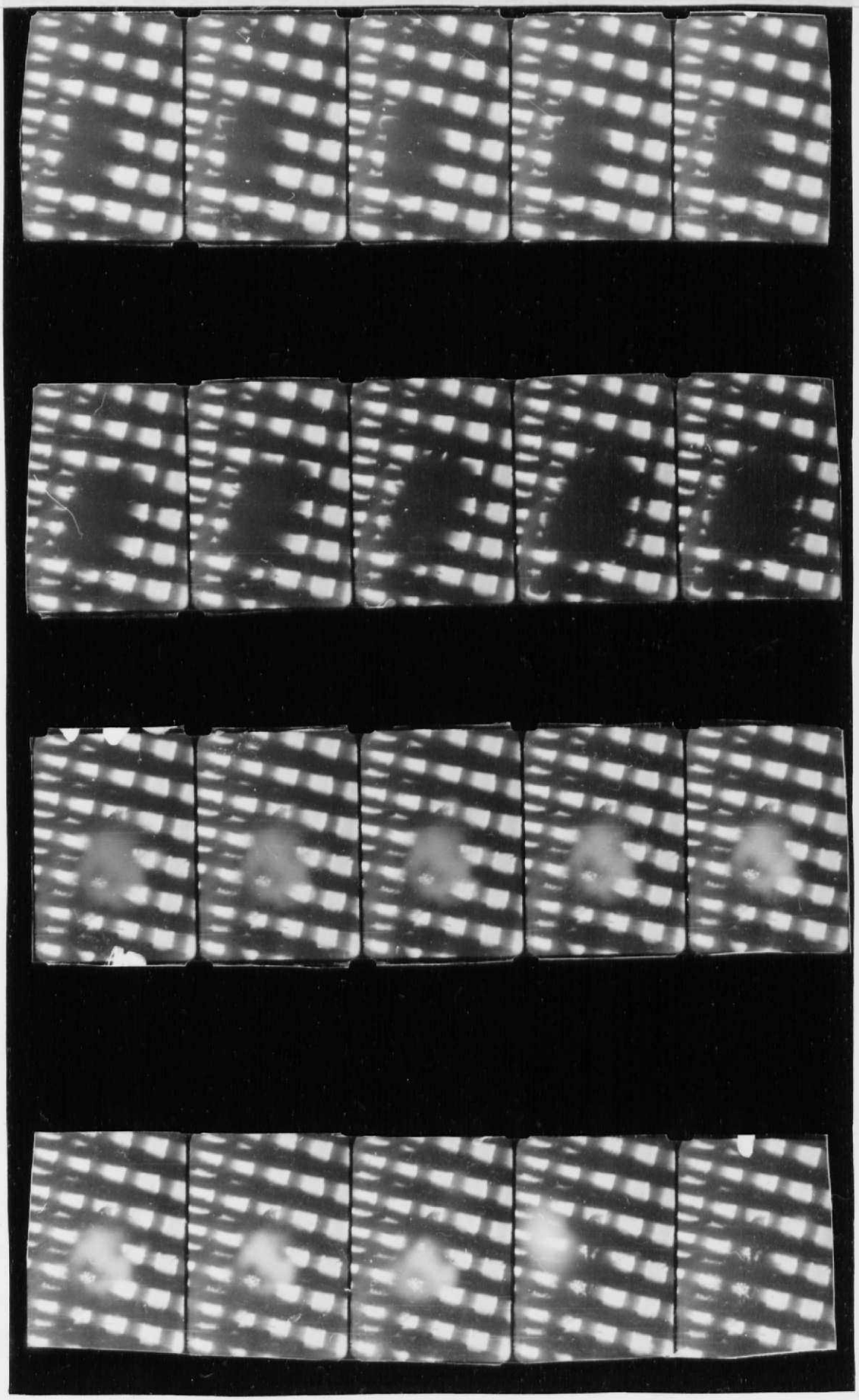

the particles arises partly from a continuously vaporising vapour cloud surrounding the coal particle. The volatile flame was seen to fluctuate over the particle surface revealing areas of high web-like porosity where the solid matrix had been burnt away. The volatile cloud detaches from the particle surface at about 210-230 milliseconds after ignition at about 850°C. This is a unique picture, only noted in X-ray studies and quartz reactor fluidised bed studies before. Holographic studies of devolatalising coal particles heated rapidly through flames show a variety of devolatalisation behaviour, among which is that of volatile cloud either surrounding the coal particle or issuing from some part of it at a distance away. Entrained flow combustion studies have shown the effects of volatile bubble burning and soot trails coming off them. Thus, such behaviour indicates that both freely moving and fixed particles exhibit this phenomena.

The importance of these pictures with regard to Pyrolysis is the observation of the residence time of this volatile cloud around the particle. It is clear from these pictures that considerable scope exist for secondary cracking reactions of relatively low vapour pressure volatile products on the particle surface and around it. The residence time of these vapours around the heated coal particle/mesh surface probably explain the phenomena of enhanced gas yield including unsaturates at long residence times at the peak temperature. It is not clear if volatile detachment as observed for combusting volatile cloud does occurr in the case of pure Pyrolysis. This could explain why total overall mass yields do not show enhancement at long residence times compared to short residence times (other than gases).

P.2 50 um grid Free swelling pyrolysis of coal particle

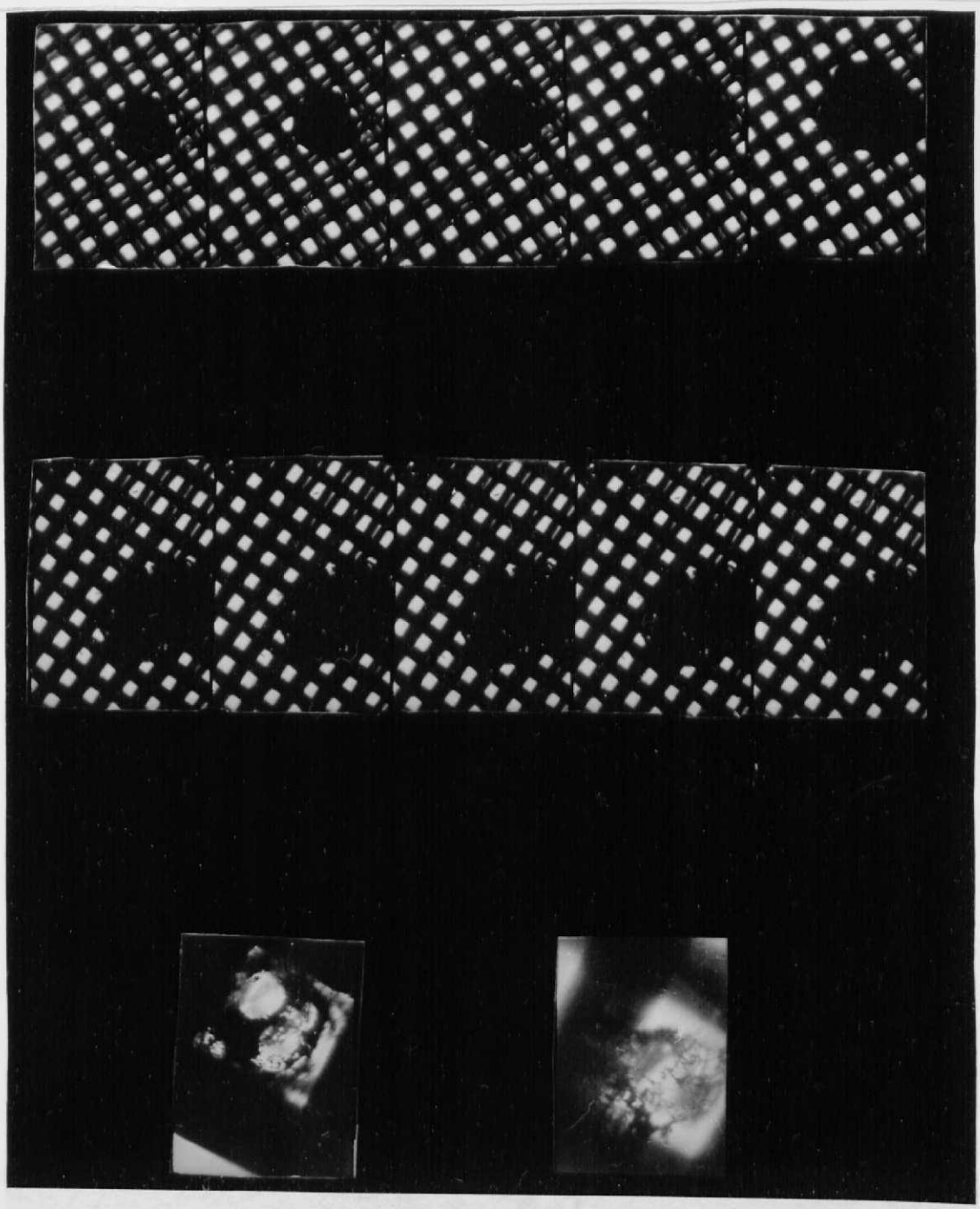

Char type found after pyrolysis to 1000°C at 1000°C/s
(dp = 150/212 um; 150 um mesh hole sizes)

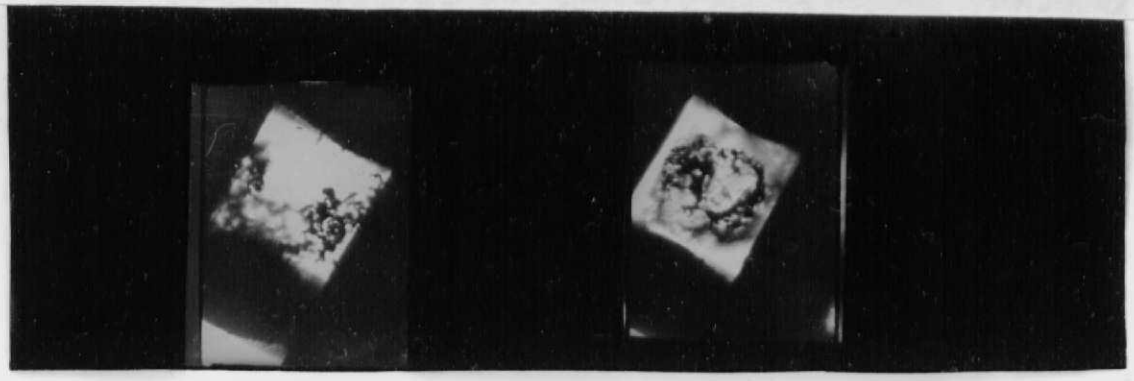

The latter is partly due to the early rapid removal of heavy products from the particle and the ensuing slow char/coke transition degasification, apart from data scatter.

However, runs conducted under transmitted light conditions have indicated a gradual acceleration of porous cellular structure with increased residence time at the peak temperature leaving a very porous cellular structure at the end. This is quite akin to the highly porous cellular char seen beneath the volatile flame as it detaches from the char surfaces.

Reference to micrographs P2 shows Pyrolysis of a particle heated to 886^{o}C at 985^{o}C/S in flowing Argon gas. The particle melts/softens at about 332^{o}C with rapid swelling occurring up to a maximum at about 499-540^{o}C. The particle was observed to be rolling about its position up to temperatures of 581-623^{o}C. Cessation of movement occurred at about 644^{o}C. The percentage volume change observed was high $\sim$ 397%. (% volumetric swelling occurred over the range 98%-155% in most cases). The second set of frames show the holes developed over the surface from volatile jets issued at about 0.24-0.36 s into the steady state time at the peak temperature.

Reflected light studies suggest a heavy liquid flux moving violently over the rounded, softened coal with long strands of heavy liquids being whipped about. (Reference to some of the SEM pictures show these long strands dangling from the 'unpeeled' coal surfaces. Some very long liquid crystal-like material are also seen extruding from softened coal mass for both entrained high temperature char from the fluidised bed, as well as low temperature mesh char/coal). Surrounding the heavy volatile

flux over the curved coal/char surface is a haze of aerosol like, evaporating material continuously streaming in a bubble like cloud around the softened particle. One can see the heavy volatile flux thinning and thickening through the'aerosol' haze, the latter presumably due to newly generated liquids from within the Pyrolysing coal material.

Frequently, the observation of rapidly inflating coal particles evolving material over a large number of 'jet' holes could be seen. In one case the author observed a violent burst of volatile efflux followed by collapse of the softened, now 'excavated' particle into a doughnut shape (the top caved in without tearing). The particle surface had the appearance of a golfball with jagged indentations where the holes were located. The overall appearance of the char indicated a rough 'concrete'-like look, grey/metallic in colour. This type of char approximates to the thick walled cenopheres seen in other studies of SEM reported elsewhere. (Usually stem from a mixture of Vitrinite, Exinite and Inertinite maceral type).

A range of char types were produced as indicated by the 4 char pieces shown in P2. (Particles of 150-212 μm Pyrolysed in a 150 μm hole mesh to 1000^{o}C at a 1000^{o}C/S).

Photography also revealed that particles loosely held in the 50 μm mesh (55-70 μm particles) were jetting across the mesh surface in straight lines in all directions. This may explain the phenomena of tars deposited near the mesh posts as well as heat transfer problems associated with particle congregation at colder regions of the mesh and/or in heaps. (Reference to the

SEM micrographs will show agglomeration necks being formed between adjacent softened particles in the 50 μm mesh case). The particles are often seen 'unfurling' strands of volatile vapour as they jet about. A 110 μm particle was observed to move at an average speed of 0.23 cm/s across the mesh until trapped in a hole in the mesh screen.

For the M. Main coal particles studies, occassionally under Pyrolysis and char ignition conditions, red smears were noted over large areas of the char surface. This could possibly arise from Pyritic (FeS) interactions with the char. A Attar has highlighted the importance of sulphur bearing structures in the coal interacting and diffusing through the solid/semicoke structure. These smears/stains suggest some form of melting/solid state diffusive reaction within the char.

One feature noted in the study was the persistance of significant Pyrolysis well into the steady state peak temperature residence times for the 50 μm mesh case. Studies of particles fixed in the mesh holes indicate earlier melting, swelling and reaction occurring during the heat up period. Thus a 75/90 μm placed placed within a 75 μm mesh and heated to 800^{o}C at 850^{o}C/S showed a melting range over 275-290^{o}C and violent surface flux beginning at 330-345. The particle was also observed to swell in a 3-D sense retaining its blocky appearance apart from rounding of the particle edges indicated by heavy liquids flow over its surface.

A coal particle Pyrolysed in the 75 μm mesh to 780^{o}C, kept for 1.00s cooled and then repyrolysed to 905^{o}C showed renewed heavy liquid flux over its surface. Some authors (Prof Beer et al

T = 545°C t_{ss} = 100ms Markham Main; Atm. High load; 75 um mesh

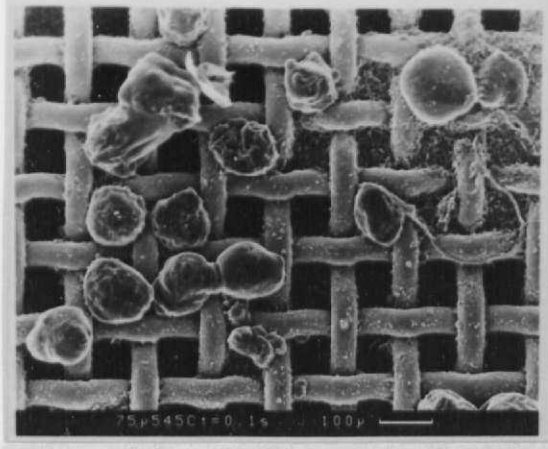

T = 275°C t_{ss} = 2.5 sec. Goldthorpe; Vacuum 200°C/S; 75 um mesh

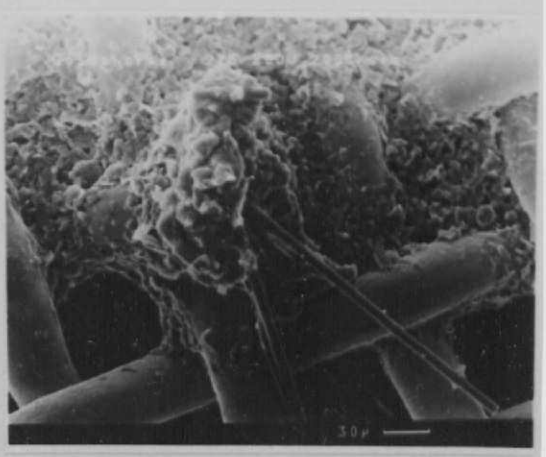

T = 425°C t_{ss} = 20ms Goldthorpe; Atm 10°C/S; 75 um mesh

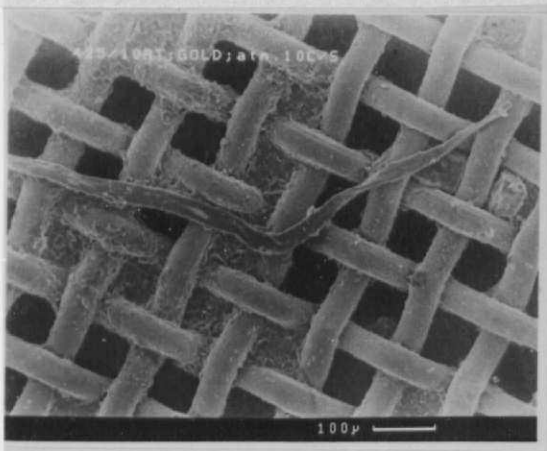

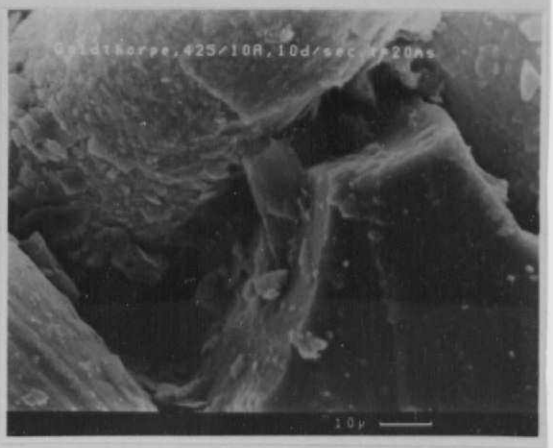

T = 450°C t_{ss} = 20ms Markham Main, Vacuum 1000°C/S; 75 um mesh

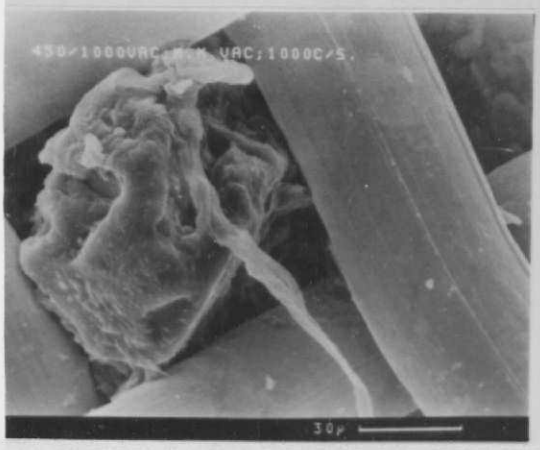

T = 300°C; Vacuum t_{ss} = 40 ms. 5,000°C/S; 75 um mesh

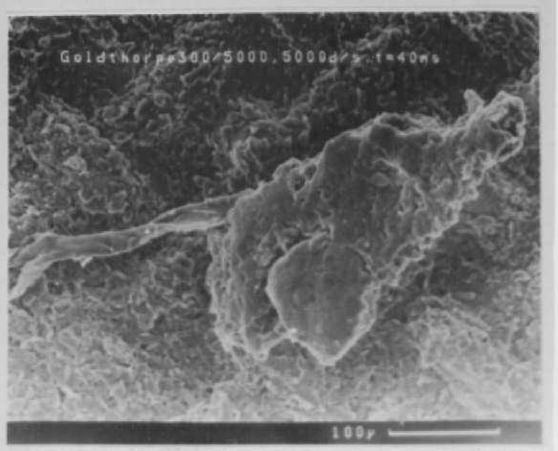

Goldthorpe Coal

T = 250°C 200°C/S t_{ss} = 10s 75um mesh

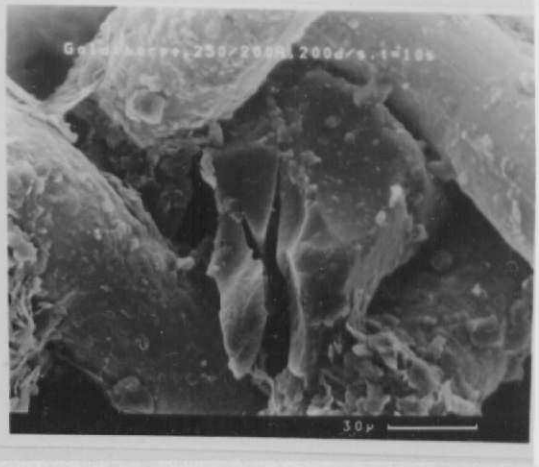

T = 350°C 200°C/S t_{ss} = 10s 75 um mesh

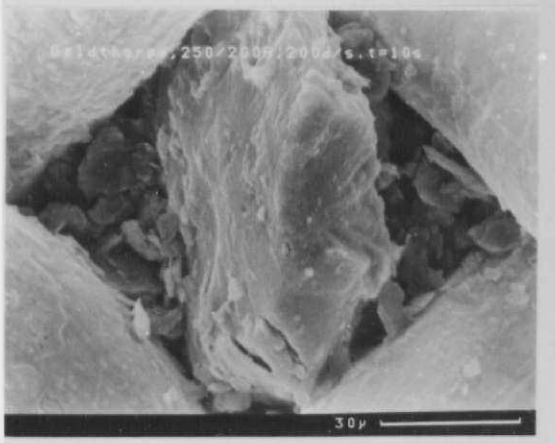

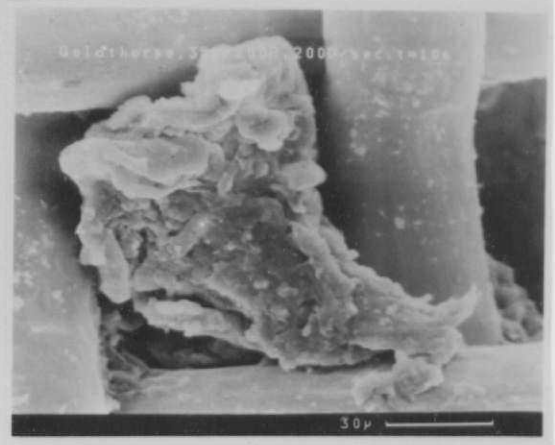

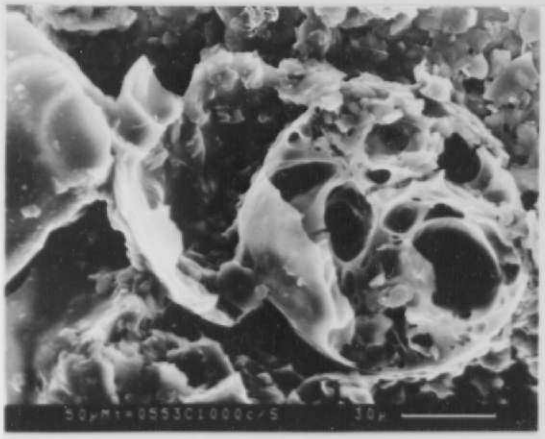

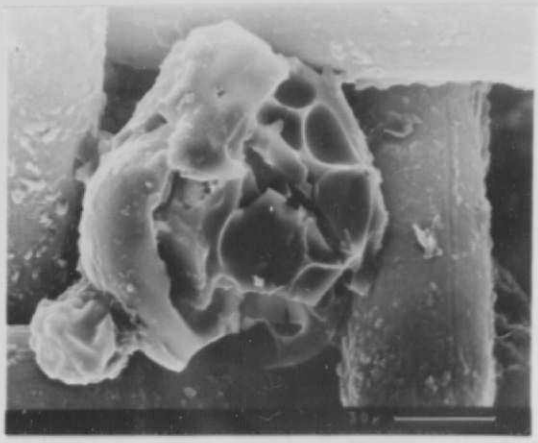

T = 553°C 1000°C/S t_{ss} = 10ms

T = 425°C 10°C/S t_{ss} = 10ms 75 um mesh

50 um mesh

of MIT) have reported high particle rotations during coal slurry combustion during the Pyrolysis stage. Whilst some of the long strands hanging from the particle surfaces give the appearance that this may have happened, the author holds that this rotation effect is more likely to be caused by the 'whipping' motion of the heavy viscuous liquids over the rounded coal surfaces during its period of accelerating fluidity or decaying viscosity.

Reference to some of the SEM pictures, particularly those from the fluidised bed (entrained bed char 472°C char caught in the mesh basket at the tar trap) show signs of multiple shells. Careful perusal of the SEM pictures over a range of temperatures indicate the following possibility.

Initially, at low temperatures differential expansion of the particles occur such that the planes along the bedding plane part like stacked sandwiches (250-300°C). Some particles literally start fragmenting along fault planes. Occassionally, long 'rodlets' are seen extruding from between the planes/cracks, or through the coal melt (see Goldthorpe coal, 275°C, 200°C/S, fluidised bed entrained char, 740°C and Goldthorpe, 425°C 10°C/S). At higher temperatures some of these planes split wide apart in the manner of curved, V shaped petals, still retaining their original shape, but at an early softened state. At higher temperatures >425°C as volatile liquids gather between the plates, and they soften and flow these shells liquefy and flow over each other. For those particles with gaping holes material is continually being 'spat' out in the form of liquid droplets as well as heavy liquid flow over the outer surfaces. Eventually the outer surfaces coke by evaporation whilst the insides remain fairly reactive and 'greasy' looking.

Fluidised Bed Char

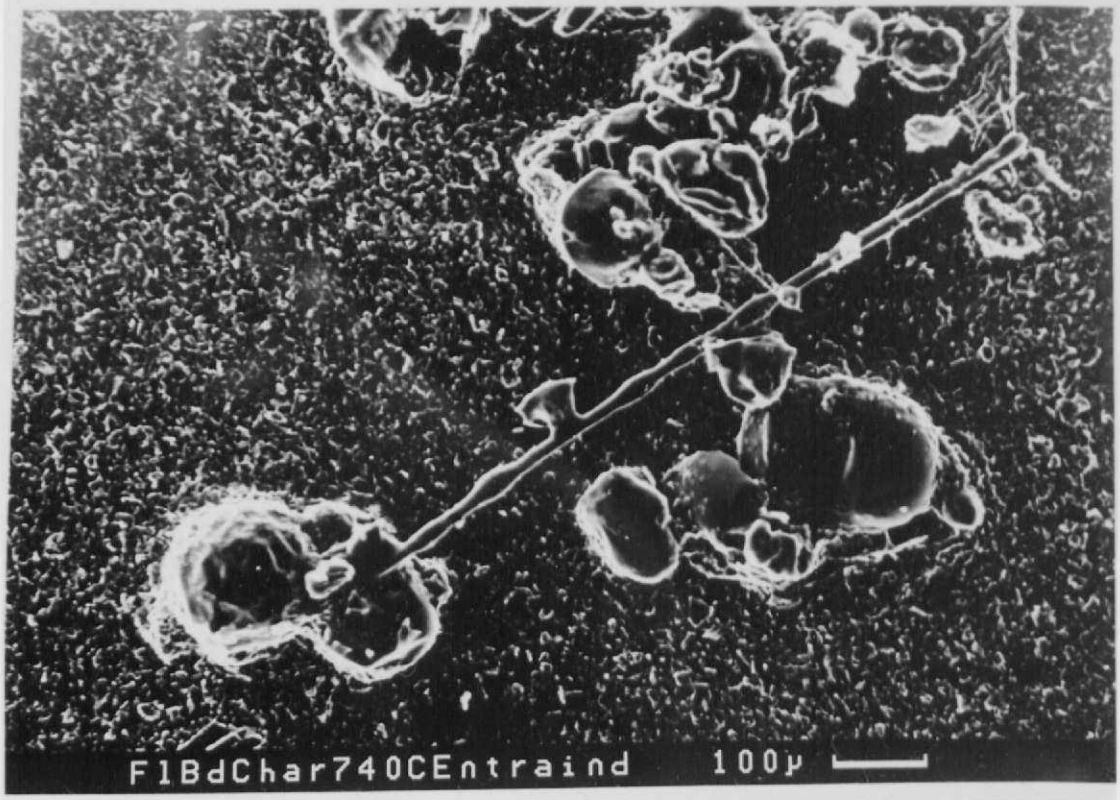

Markham Main Char; T_{bed} = 740°C; Entrained Char

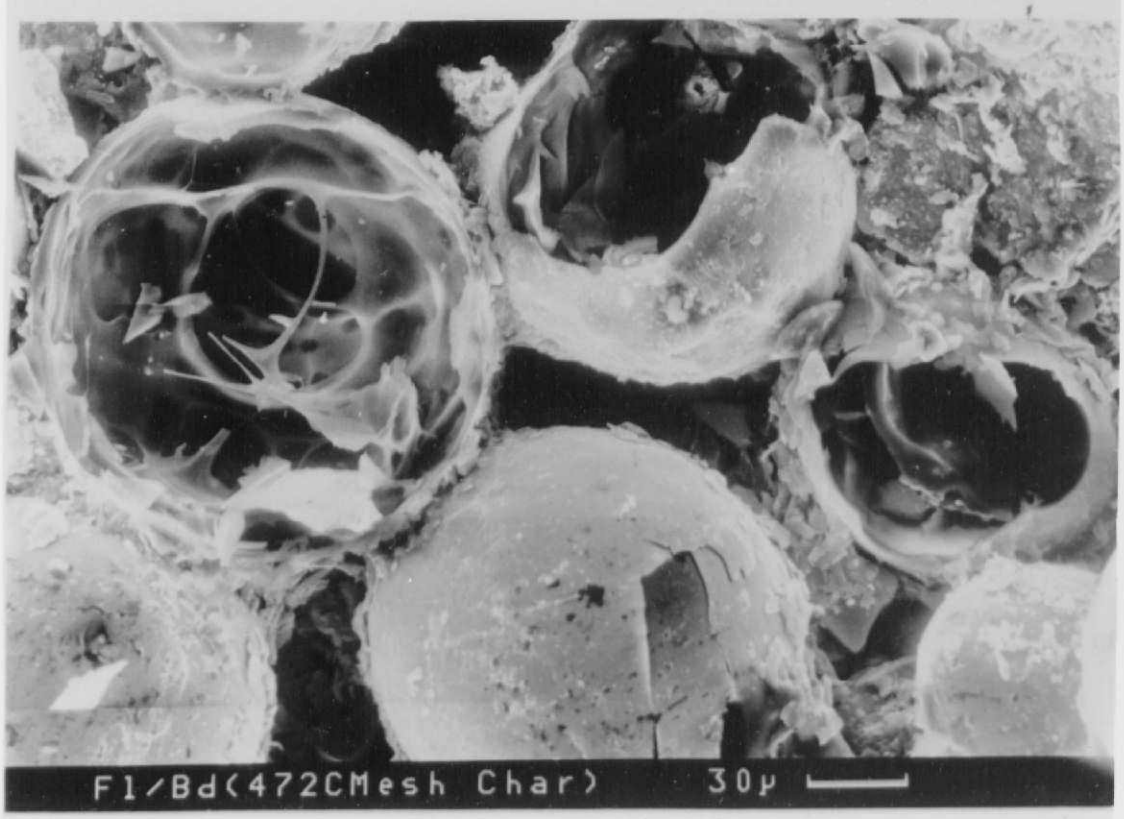

Markham Main Char; T_{bed} = 472°C; Entrained Char
(Char collected in mesh basket at tar trap)

The author has seen volatile bubbles of very thin skin being formed from these greasy looking 'cheesecake' structures under the influence of heating by the viewing electron beam. (Occasionally the liquid 'C' coating used for the SEM which is solvent based can give rise to this effect and has to be distinguished from the real thing).

Overall, many of the features shown by the SEM studies are novel features, not noted elsewhere in the literature by the author. Further there is evidence of coal softening, (melting of trapped components?) and reaction at lowish temperatures in the case of particles loaded into the holes of the mesh and heated. (This is confirmed by comparison of low heating rate studies to the high heating rate SEM at equivalent temperatures).

The last set of high speed photography results show the case of a 150-212 μm particle heated at 1014^{o}C/S to a temperature of 1004^{o}C in a 150 μm hole mesh. Melting was observed at about 244^{o}C-266^{o}C and the appearance of either extruded material or 'peeled' surface material at about 288^{o}C. The softened particle was seen to shrink at an early stage suggesting fast expulsion of volatiles and shrinkage continues along with much volatile flux and hole development throughout the heating stage. Finally fragmentation of the particle began to occur about 0.155 seconds into the steady state temperature.

The latter lengthy shrinking stage and increasing viscosity of the heavy liquid flux with rising temperature provide room for lamallae annealing, accompanied possibly, by H_2 evolution. This may explain the high 'H_2' release observed for the 10^{o}C/S

P.3 Single particle pyrolysis in 150 um hole mesh

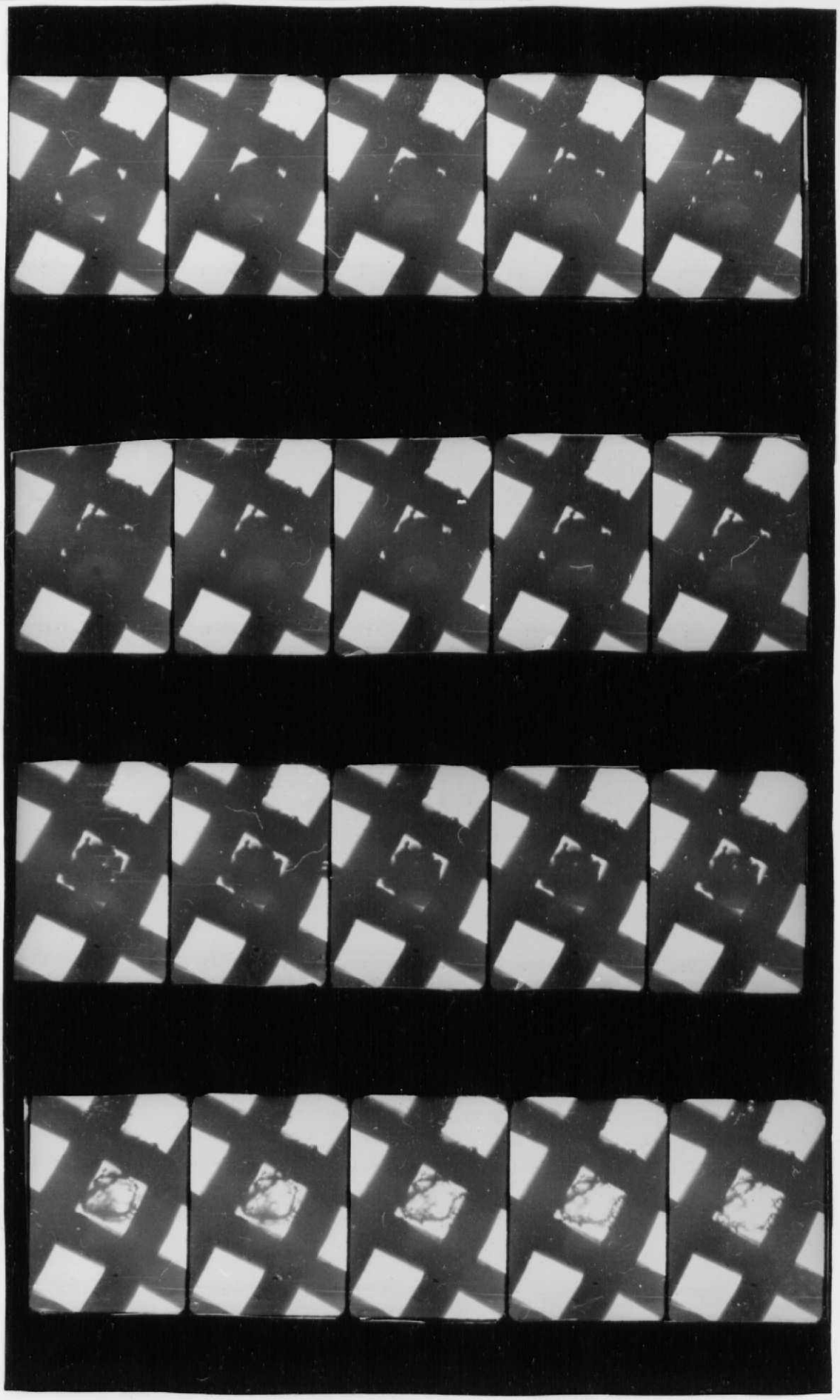

$dT/_{dt}$ = 1060°C/s; T_f = 1007°C

case compared to the 5000°C/S case where there is less time for these reactions to occur as well as less room for correct orientation for lamallae annealing to occur.

The observation of low temperature tar evolution and other material (napthenes, octenes, etc) has been hinted at in the literature review. A recent paper on tar evolution (Cannon S. A. et al, Fuel, 1987, Vol 66, Jan, pp 51) for a suite of U.S.A. coals suggest evolution of tar molecules at temperatures as low as 130°C and continued maximum evolution was reached at about 400-470°C.

A further study (M. S. Seehra et al Fuel, 1986, Vol 65, September pp 1315) suggest 3 temperature stages of Pyrolysis indicated by E.S.R. studies of radical spin concentrations. Thus the following was noted:

Stage 1. 3°C-277°C small increase in spin concentration with an activation energy of 16.7 KJ/mole (from the temperature dependance of spin concentrations). This was thought to be associated with CO_x & H_2O release from weak C, H & O bonds. (In accordance with the author's review this is possibly associated with 'H' bond breakage, carboxylic and carbonyl group release as suggested by Berkowitz).

Stage 2. 277°C-427°C Here the spin concentration actually decreases (the low yield of H_2 in this region may owe its lack of appearance to 'H' stabilization of light volatile species beginning to be generated in this region, eg, CO_x C_1, C_2 and C_3 H/C gases.)

Stage 3. 427^{o}C-627^{o}C free radical concentration (equated to spin concentrations) increase in this region with an activation energy of 104.7 KJ/mole.

The above appears to vindicate the hypothesis put forward by the author in the literature review on likely temperature trends parameterising the Pyrolysis process.

7.6 FTIR spectra analysis

FTIR spectra contain a number of useful pointers towards possible reactions occurring during Pyrolysis. Spectra of mainly tars from the mesh (atmospheric P and vacuum) as well as from the fluidized bed was obtained.

The trends suggested by the spectra indicate the following for the coals:

Whilst the Aliphatic CH_2 and CH_3 stretching at 2850/2920 cm^{-1} appear to be similar for both coals there appears to be more aromatic 'H' in M. Main coal indicated by the aromatic C-H stretch bands at 750, 850 and 3040-3050^{-1}. (The 750 cm^{-1} bond is enhanced relative to C-H stretch at 850 cm^{-1} suggesting decreased substitution to the ring structure).

The band absorptions at 460, 470, 537, 910/950 and 1010 cm^{-1} suggest more mineral matter presence in M. Main coal relative to Goldthorpe indicated by higher kaolinite and Fe minerals (shoulder at 1090-1100).

The bands at near 650 and 695 cm^{-1} suggest that both coals contain similar contents of long chain or side chain unsaturates.

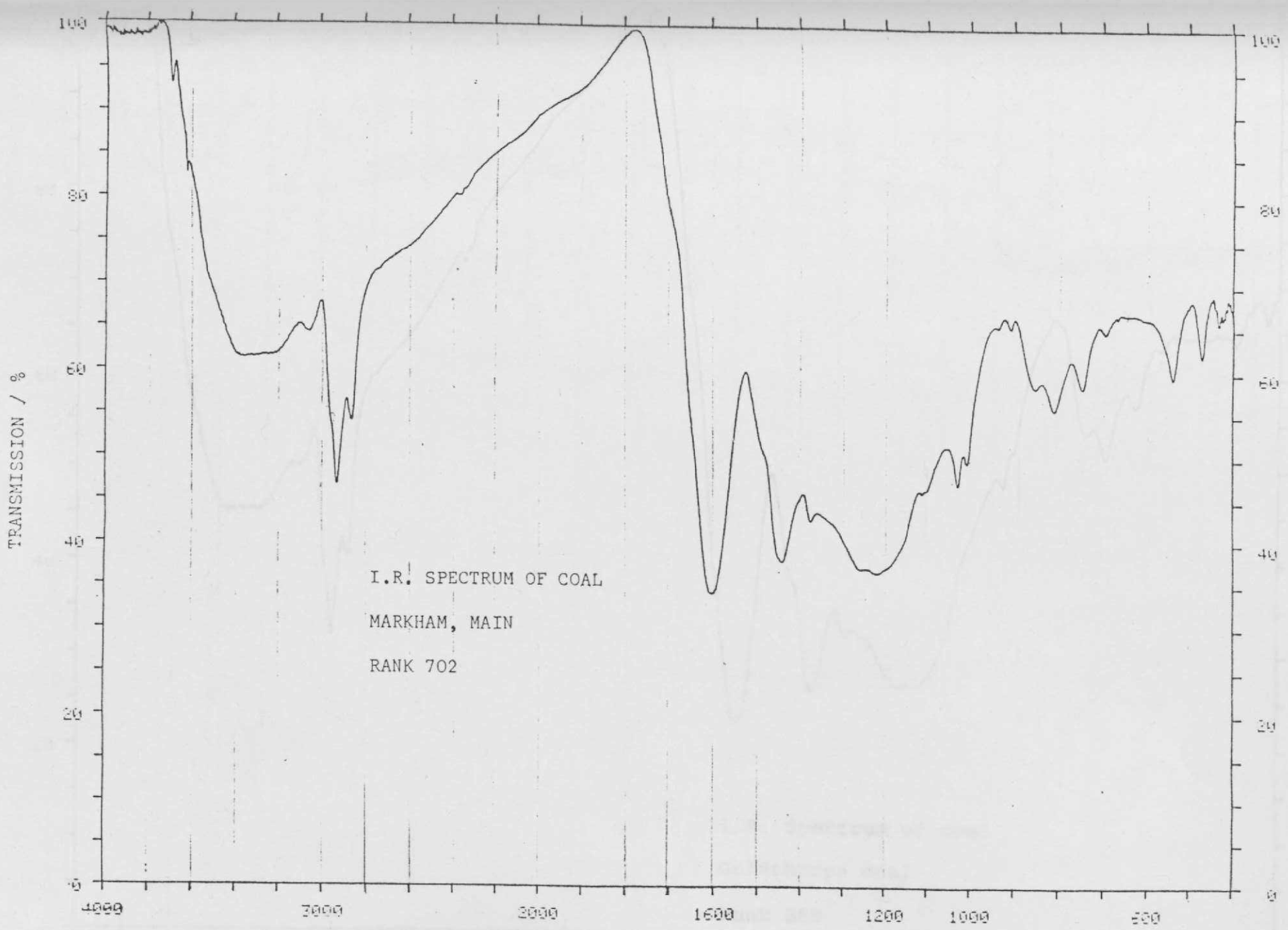
TRANSMISSION / %
100
80
60
40
20
0
4000
3000
2000
1600
1200
1000
500
I.R. SPECTRUM OF COAL
MARKHAM, MAIN
RANK 702
WAVE NUMBER / cm-1

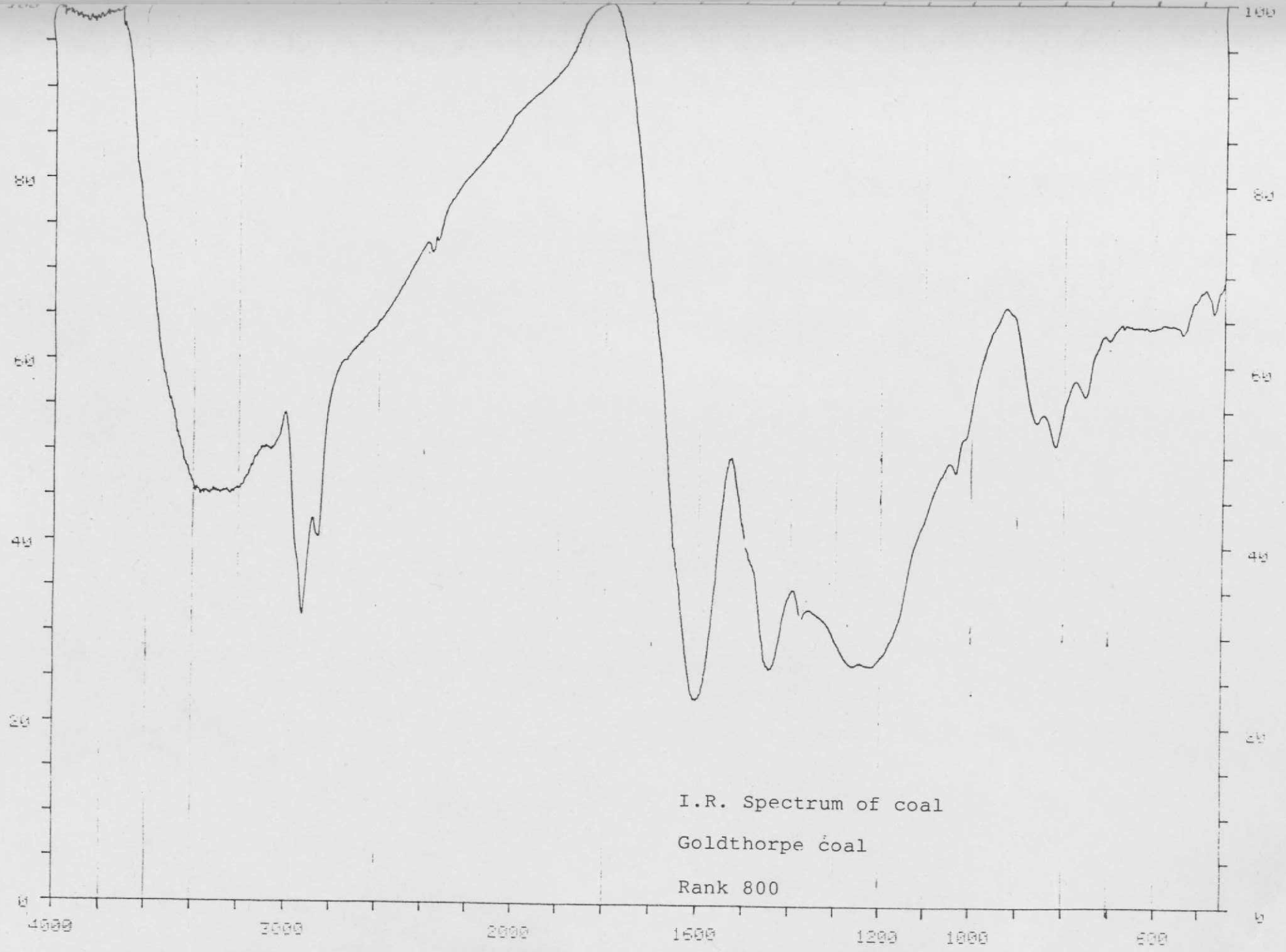

I.R. Spectrum of coal

Goldthorpe coal

Rank 800

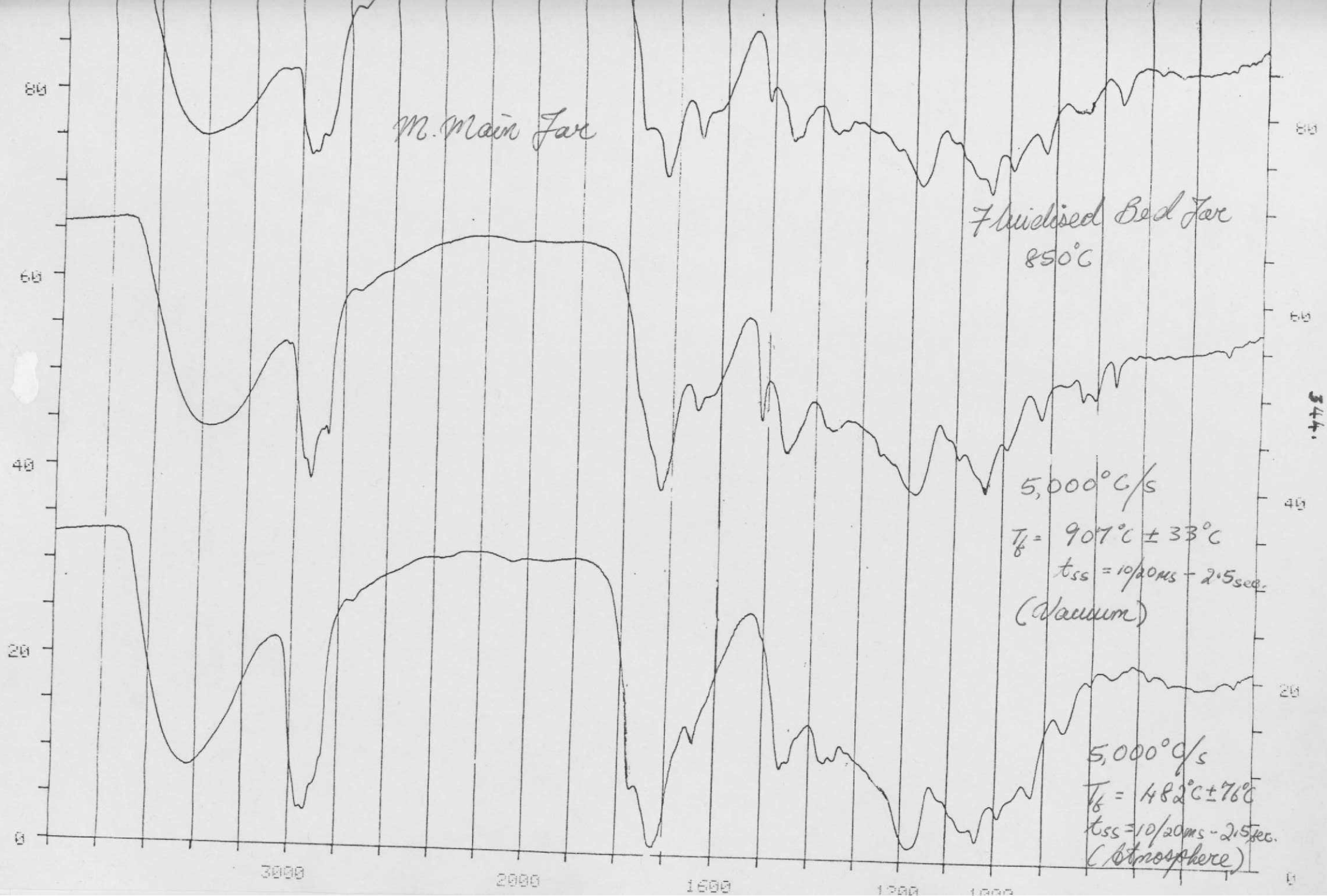
M. Main Jar
Fluidised Bed Jar
850°C
5,000°C/s
T_f = 907°C ± 33°C
t_{ss} = 10/20ms - 2.5sec.
(Vacuum)
5,000°C/s
T_f = 482°C ± 76°C
t_{ss} = 10/20ms - 2.5sec.
(Atmosphere)
80
60
40
20
0
3000
2000
1600
1200
1000

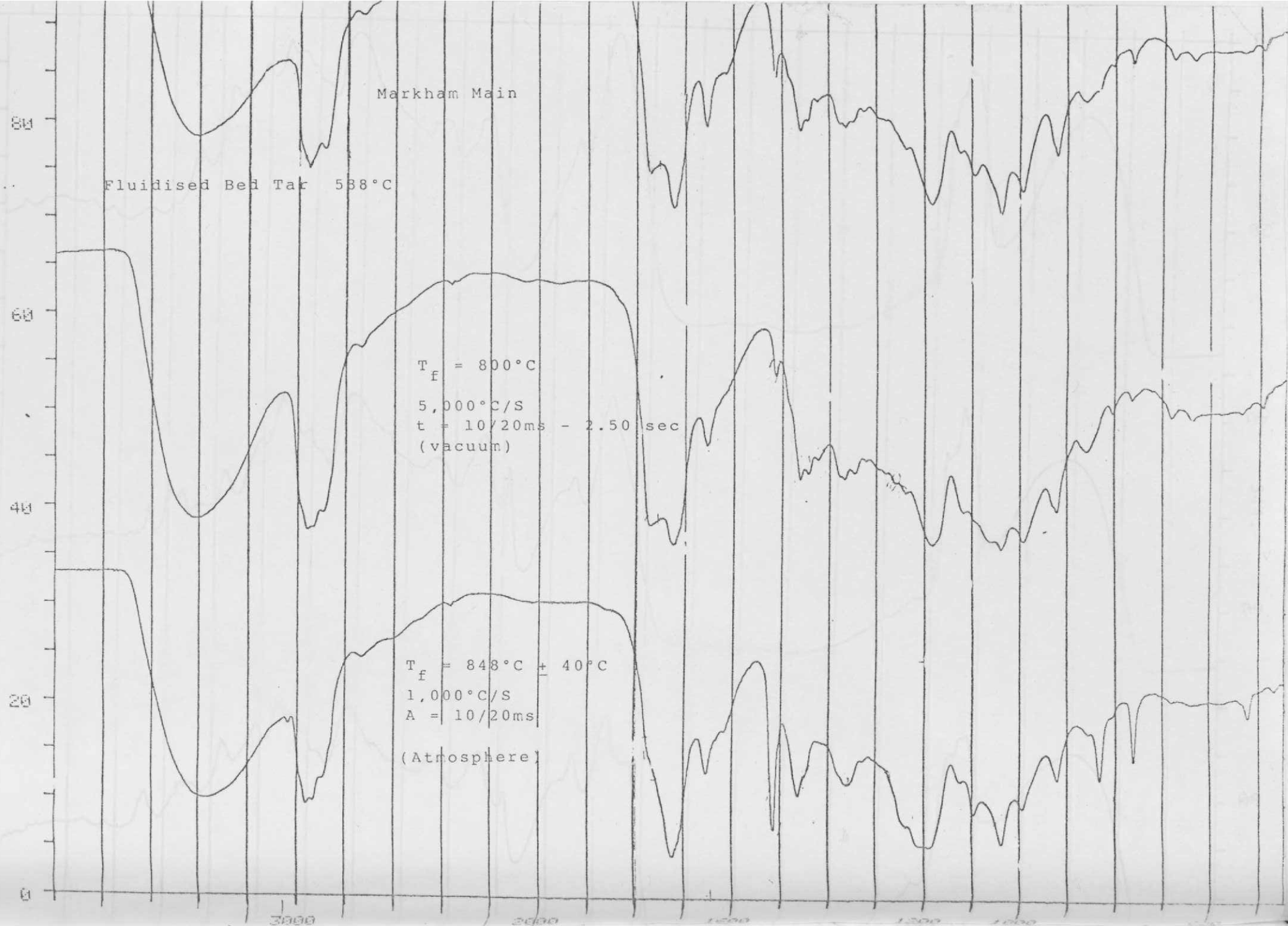
Markham Main
Fluidised Bed Tar 538°C
80
60
40
20
0
T_f = 800°C
5,000°C/S
t = 10/20ms - 2.50 sec
(vacuum)
T_f = 848°C ± 40°C
1,000°C/S
A = 10/20ms
(Atmosphere)
3000

The absorptions near 3650 and 3610 cm^{-1} suggest free phenolic 'OH' groups in M. Main, not noted in Goldthorpe.

The relative intensities of the bands at 1230 & 1270/1265 (Aryl-o-stretching) and 1440/1450 cm^{-1} (CH_2 substitution/bridge structures) indicate that the CH_2 bridges are relatively higher than etheric bridges for both coals.

Comparison of the tars from the fluidised bed (391°C), vacuum tar (400°C) and atmospheric mesh tar (482°C ± 76°C) of the M. Main coal indicate,

1) Great deal of similarity between all three tars. However, the atmospheric mesh tar had suffered increased loss of aliphatic groups including some ether and alkene groups.

2) More carboxylic/ester groups have been last for the fluidised bed reactor tar.

3) A peak at 1650 cm^{-1} for the atm mesh tar suggest some 'H' bonded N appearing in the tar. (In fact the elemental composition shows a small 'N' content in the tar at this temperature).

Surprisingly the Goldthorpe fluidised tar at 400°C suggest a larger fused ring system for this tar relative to the M. Main tar, (Both tars have similar No. Av. Mw. 667 for M.M. and 683-764 for Goldthorpe). The Goldthorpe tar suggest different distribution of unsaturated aliphatic groups.

Note: (Residual contamination by THF solvent in the case of tars, may be responsible for the ketonic band noted at 1710cm^{-1} and the possible shift of the aromatic band at 1600cm^{-1} down to 1650cm^{-1} assigned above to NH bonding.)

The Aryl O-O-R stretch at 1250/1260 cm^{-1} is enhanced relative to M.M. tars which suggest the possibility of polymerization condensation reactions suffered by the Gold tars or simply more ether bridge structure in the Gold coal. (Assuming the similarity between spectra of coal and its tar, it is possible that tar represents a sampling of the coal structure relative enhanced in 'H' structures). There is suggestion of some aromatic ether or quinonic structure by the strong C-O stretch at 1030 cm^{-1}. For Goldthorpe tar the NH band appears at the 588°C tar (In fact elemental distribution suggest enhanced 'N' in Gold tar relative to M.M. tar). There is also suggestion of enhanced loss of aliphatic CH_3 and CH_2 groups relative to M. Main coal tar.

Comparison of M. Main tars from mesh (atmosphere, 5000°C/S, 848°C), vacuum (5000°C/S, 800°C) and fluidised bed tar (850°C) indicate;

1) Long chain unsaturated groups (polymethylene units suggested by Calkins et al?) shows decomposition in the order Atm > FB > VAC.

2) Ring substitution shows diminished nature and thus possibility of increased condensation, in the order, Atm > FB > VAC.

3) Aromatic ether stretch is enhanced for all three tars in the same order.

4) Almost complete loss of carboxyl/ester groups in atm tar and partially removed in FB tar, but still present for vacuum tar.

5) Most of the aliphatic ether groups are gone for all tars and suggest that the only surviving etheric groups are in ring structures.

Overall the spectra indicates a highly aromatic tar from the Atm mesh tar with most of the aliphatic ethers, carboxylic/ esters and a good deal of Aliphatics cracked off relative to the vacuum tars with the fluidised bed tars showing an intermediate character.

Apparently the vacuum tars are largely undisturbed (minimal cracking) apart from some loss of CH_3 groups, aliphatic ether, followed by some ring condensation. Some aryl ether linkages appear to have broken. At higher temperatures ($907^{o}C$) the vacuum tar shows signs of increased condensation, increased loss of CH_3 groups including signs of significant cracking of long chain unsaturates.

The removal of long chain unsaturate groups (bands at 650 695cm^{-} in the mesh reactor and the fluidised bed at these temperatures (850°C) suggest that the increased appearance of C_4 unsaturates in the gases at these temperatures could arise from cracking of aliphatic groups followed by ring closure as well as hydroaromatic ring breakage.. The latter was contened by Vastola et al (refer review) and the former by Calkins and Tyler.

The above trends are in accord with the observation noted earlier of increased unsaturates production and cracking reactions at high heating rate, Atmospheric conditions relative to lower heating rate and vacuum conditions. The FTIR results suggest then remarkable similarity between tars for all conditions of operation below $400^{o}C$, but suggests increased loss of aliphatics

in the case of FB which arises from the hot, quench flow stream proximity. There is suggestion of condensation reactions occurring at high temperatures by the formation of new aromatic ether linkages. Recourse to the elemental char distribution suggests this possibility. There is also a clear suggestion that at higher temperatures diffusion or evaporation limitations may apply for increased external pressure relative to vacuum.

Observations of high speed photography of volatile jets and calculations from a simple model of radial flux from a spherical coal particle (ref: Atimtay and M. Azhakesan) suggest radial flux velocities of the order 6-9.3 cm/s for the case of 120 milli-seconds devolatalization times and 39-7-86.8 cm/s for 20ms and temperatures over 770-1094^{o}C. (Blair et al estimated jet velocities of 45 cm/s for their larger particles; $V_R \propto$ dp).

Flash Pyrolysis of partially reacted mesh char in atmosphere resulted in a huge violent evolution of tarry material ejected several tens of cms into the air followed by a blue flame ignition and later yellowish/blue flame over the mesh surface. The ejection of the tar vapours suggest quite rapid removal of some of the lighter components and some carryover of heavy material from the reaction zone. It is, hence possible that it is the heavy tars coating the swollen coal surface tht contribute to the repoly-merization reactions which also incidentally contain the highly reactive polar heteroatoms fixed in the fused ring structures. The lighter tar components evaporating into the vapour bubble around the particle may undergo cracking reactions, dependant on the rate of their removal by diluent flow or reduced pressure.

CHAPTER 8

CONCLUSION

The phenomena underlying rapid coal Pyrolysis has been investigated from a number of viewpoints. Physical kinetic studies of coal transformation under thermal heating conditions have been conducted allied to scanning electron micrographic studies and visual observations. They have resulted in unique observations of aspects of the Pyrolysis process and may throw some light on the structure of coal. By integrating analytical probes such as FTIR spectroscopy, elemental analysis and Gel permeation chromatography with the above, including parametric kinetic modelling data has been presented on various aspects of rapid coal Pyrolysis.

8.1 Features of rapid Pyrolysis

By separating out the effects of extraparticle mass transfer (due to high coal particulate packings), improving the rate of supply of energy to the target volume of the particulate (by packing it in a form that approaches the single particle case within the containing screen), it was possible to elucidate the effect of heating rate on Pyrolysis.

Heating rate for the above conditions result in overall total yields, insensitive to heating rate for the medium heat fluxes and fast quenching of reaction products. However, the yield distribution, particularly for the gases show that high heating rates result in greater unsaturates production. Low heating rates result in enhanced CH_4 and H_2 yields, the latter

continuing to increase at the higher temperatures whilst CH_4 appears to reach an asymptotic yield. Thermodynamic Considerations imply CH_4 cracking at temperatures 900°C.

For the coals tested high quantities of CO were obtained at the higher temperatures and suggest the possibility of self catalysed gasification of the char. Rapid release of a range of heavy liquid products at an early stage suggest that the so called 'depolymerization' step is a low activation energy process reflecting either:

1) Latent heat of vaporization of H/C

2) or 'H' bond and other such like bond breakage.

The SEM micrographs suggest quite striking phenomena of liquid crystal-like exudations from softened coal particles at relatively low temperatures (300°C). (Most particles however retain their blocky solid shape with partial reaction over parts of the particle up to 425°C).

Comparison of the fluidised bed data to the mesh screen data suggest overestimates of mass loss at the lower temperatures of the mesh yield (300°C) stemming from both mesh handling and fragmentation through cracks induced by particle expansion and rumpling due to heating. But over the temperature range 300-700°C overall yield is similar for both reactor systems. At higher temperatures, severe sooting by tar cracking reduces ultimate yield in the fluidised bed.

The tar yield data shows good correlation to atomic H/C ratio suggested by the Australian work.f From the fluidised bed data, at about 600°C.

Markham Main H/C = 0.81	Experimental tar yield = 22%
Goldthorpe H/C = 0.87	Experimental tar yield = 27%

(See reference 124), figure 6). This appears to be reconciled. with the contention that tar yield was found to correlate with Aliphatic content of precursor coal by Durie et al[124] and Solomon et al among others.

The heat transfer modelling suggested levels of heating lags between particle surface and centre of $\sim 93^{o}C$ for $5000^{o}C/S$ heating rate applied to a coal particle of 160 μm in diameter. SEM pictures of the coal particles for lower heating rates at comparable final temperatures do not indicate significant temperature lags for the 75-90 μm particles used here.

The gas yield curves fitted by the independant single reactio model suggest trends in pseudo activation parameters that reflect different classes of reactions occurring at different temperatures.

The efficacy of the multiple, independant model in fitting the data does not appear to improve the understanding of the overal mechanism of Pyrolysis. The sensitivity of the yield distribution suggest some form of competing reactions superimposed on the parallel evolution of a large number of products at intermediate temperatures.

At higher temperatures there appears a significant increase in the number of gas types. The FTIR analysis suggest, by the pattern of functional groups removed from the tar, that they represent part of the coal structure and are precursors for the formation of light gaseous species.

It is apparent from the form of the 'dips' noted at the high temperatures ($>850^{o}C$) coupled with the increased appearance of aromatic ether linkages in the tar and increased aromaticity suggested by FTIR that recondensation reactions are operating at these temperatures.

Lamallae annealing probably leads to H_2 evolution, C_2H_2 formation, polymethylene cracking and CO formation by ring fragmentation and/or self gasification, particularly at low heating rates.

Overall, therefore it appears that the Pyrolytic decomposition scheme is a product of initial rapid depolymerization followed by a series of parallel, competing and repolymerization reactions. It is also likely that at high heating rates, chemical reaction time no longer controls the overall chemistry. The enhanced diffusion of minimally disturbed tar under vacuum conditions compared to atmospheric pressure suggests this possibility.

8.2 Future Work

It would be prudent to test the conclusions concerning heating rate effects on product yield and distribution over a larger range of coal types. It may be that under the conditions of rapid Pyrolysis Bituminous coals of a wide variety exhibit relative insensitivity to Pyrolysis conditions. To assess the mechanism of Pyrolysis eventually, it is necessary to conduct parameter variations such as choosing extremes of heating rate, pressure and coal type under conditions free of transport limitations. It is also important to work on a scale sufficient to generate analytical data such as CO_x evolution, molecular weight analysis and other structural probes such as FTIR and NMR spectroscopy. The use of transient rapid reaction analysis probes such as time of flight mass spectrometry may be useful in elucidating the relevant activation steps operating over the temperature interval of interest. It is also likely that a dynamic bubble nucleation model with secondary reactions occurring at the bubble/melt interphase may need to be coupled to the chemical product generation model.

APPENDIX

Values used for heat transfer simulations were as follows:

V^* = 0.60 (ultimate yield)

ΔH = 780×10^{3} J/kg (Endothermic heat of reaction)

ks = 0.2413 J/mks (thermal conductivity of solid)

αs = 3.6×10^{-3} m/s (Thermal diffusivity of solid)

H = 731 J/sm K or 229 J/sm K (gas convective heat transfer coefficient)

ρ_s = 1000 kg/m^3 (solid density)

r = 80 um (particle radius)

TE = Equilibrium, external driving force temperature (°K)

REFERENCES FOR THESIS

1. Prof Ian Fells "The Options until 2030" Energy World, February 1982.

2. Amory B. Lovins "World Energy Strategies".

3. Probert S. D. and Russell P. B. "Fuel Consumption problems, Price trends and prospects for Britain" Applied Energy, 22 (1986), 119-144.

4. Brian Locke "Feedstocks and Fuels from coal: The need for process changes" Energy World, February 1982.

5. "Synfuels Developments in Western Europe" Petroleum Times, August 1981 page 13.

6. Challis A. A. L. "The 1982 Robens Coal Science Lecture: Coal: fossil and future" Journal of the Institute of Energy June 1983 page 55.

7. Klass D. L. and Chambers W. C. "Energy from coal gasification" Hydrocarbon Processing, April 1977 page 135.

8. Berman M. "Power Engineering, October 1981, page 50.

9. Jane J. Priestley "Industrial gas heating".

10. Snam M. Redman "UK Coal gasification - projects and operations" Petroleum Times, August 1981, page 17.

11. Dierck E. A. and Jurgen W. Stodelhofer "The industrial role of coal chemistry" Chemistry and Industry, 7th February 1983, page 113.

12. Probstein R. F. "Synthetic Fuels" 1982, McGraw Hill Book company.

13. Badziock & Hawksley, BCURA, Monthly Bulletin, Vol. 25, No. 8, Aug. 1981.

14. Johnson G. R. "A study of the mechanism of flash Pyrolysis of single particles of coal" Ph. D. Thesis, June 1985.

15. Desypris, J. et al
"An investigation of the flash pyroloysis of some coals". Fuel

16. "Targets defined for basic research in coal" September 22nd 1980, C & E N.

17. Julian Szekely et al "Gas-solid Reactions", Academic Press 1976.

18. John L. Cox "Concern over coal sampes" Fuel, 1984, Vol 63 July, page 1030.

19. G. R. Gavalas "Coal Pyrolysis" Coal Science and Technology series, No 4.

20. Richard C. Neavel "Coal structure and coal science: Overview and recommendations" Advances in Chemistry series 192, 1981. Eds; Martin L. Gobarty and K. Ouchi.

21. E. Beier "Gas exchange of black coal and other substances when stored for decades in contact with air" 1983 International Conference on Coal Science.

22. N. E. Cooke and P. S. Khendhadia and E. Furimsky "Investigation to develop methods for removal of oxygen from coals". The Canadian journal of chemical engineering, Volume 63, February 1985.

23. Karsner G. G. and Perlmutter D. D. "Effects of drying and Oxidation on Coal Pore Structure" 1982, American Chemical Society.

24. Guy Lengelle "Surface Temperature and Condensed phase reactions of propellants and combustible materials". The Combustion Institute; Deuxieme Symposium European Sur la Combustion, Orleans, France, 1975.

25. Antonin Blazek "Thermal Analysis" Van Nostrand Reinhold Co; London.

26. Bernard J. A. and Bradley J. N. 'Combustion'.

27. J. Lede et al "Flash Pyrolysis of wood in a cyclone reactor" 1986,

28. R. G. Graham "The Ultra rapid fluidized reactor: application to determine the kinetics of the fast Pyrolysis (ultra-pyrolysis) of cellulose"

29. Karl Heinrick Van Heek "Kinetics of Coal Pyrolysis as Basics for Design of Industrial Reactors" Chem. Eng. 7 (1984) 319-327.

30. Martin Hertzberg and Daniel L. N. G. "A microscopic and kinetic study of coal particle devolatalization in a laser beam". Fundamentals of the Physical-Chemistry of Pulverized Coal : Edited by J. Lahaye and G. Prade 1987.

31. Antal paper. (see Ref. 203)

32. Simons G. A. "The influence of fluid transport during Pyrolysis" 1983 International Conference on Coal Science; Proceedings August 15-19, 1983.

33. Chemistry of Coal Utilization, 2nd Supplementary Volume, Ed Martin A. Elliott (page 1311)

34. Talwalker A. T. "A topical report on coal Pyrolysis" Institute of Gas Technology, Contract No: DE-AC21-82 MC19316. U.S.A; DOE/MC 19316-1408.

35. Peter R. Solomon et al "Very Rapid Pyrolysis" Fuel, 1986, Vol 65, February page 182.

36. Michael J. Shires & Gellender M. "Gasified Coal-starting point for chemical manufacture" Chemistry International 1980, No 6, page 5-11.

37. Harry W. Parker "Liquid Synfuels Via Pyrolysis of Coal in Association with Electric Power Generation" Energy Progress (Vol. 2, No 1), March 1982, page 4-8.

38. Walter C. Patterson "Coming on at the gasworks end" The Guardian, October 23rd 1987.

39. Clare Bishop and Peter Maitlis "Chemical Industry Flirts with an old flame" New Scientist, 28th April 1983.

40. Rochus F. Quinkler "Synfuel developments in Western Europe" Petroleum Times, August 1981, page 13-20.

41. Chris Cunningham "Can coal gasification pick up steam?" New Scientist, 8th October 1981, page 106-109.

42. IRAM Berman "Synthetic fuel programs and developments" Power Engineering, October 1981, page 50-58.

43. McCullough G. R. et al "Shellcoal Gasification Process" Energy Progress (Vol 2, No 2) June 1982 page 69-72.

44. Klass D. L. and Chambers W. C. "Energy from coal gasification" Hydrocarbon Processing, April 1977, page 135-141.

45. Richard C. Bailie "Energy Conversion Engineering" Energy Science and Technology series No 1 1978.

46. Thomas B. Reed and James P. Diebold "Heat Transfer Mechanisms for Analytical Pyrolysis" Analytical Pyrolysis Techniques and Applications, Edited by Kent J. Voorhees.

47. Daniel J. Maloney and Robert G. Jenkins "Coupled heat and mass transport and chemical kinetic rate limitations during coal rapid Pyrolysis" 20th Symposium (Internation) on Combustion/The Combustion Institute, 1984, page 1435-1443.

48. Brewster B. S. and Seader J. D. "Measuring Temperature in a Flowing Gas-solids Suspension with a Thermocouple" A.I.Ch.E. Journal (Vol 30, No 4) July 1984, page 676-678.

Ibid; "Coal particle Suspensions in Vertical Downflow" A.I.Ch.E. Journal (Vol 30, No 6) November 1984, page 996.

49. Robert J. Flaxman and William L. H. Hallett "Flow and particle heating in an entrained flow reactor" Fuel, 1987, Vol 66, May, page 607-611.

50. Ching-Yi Tsai and Alan W. Scaroni "Pyrolysis during the initial stages of pulverized-coal combustion" 20th Symposium (International) on Combustion/The Combustion Institute, 1984, pages 1455-1462.

51. Arcot R. Balakrishnan and David C. T. Pei "Heat transfer in gas-solid packed bed systems. 1 A critical review" Ind Eng Chem Process Des Dev, Vol 18, No 1, 1979.

52. Gloria Bennett and Martin Luther "Thermal Analyses in support of laser Pyrolysis coal characterization studies" Los Alamos Lab Report LA-9188-MS 1981.

53. Given P. H. "Thermal decomposition of organic substances" Monthly Bulletin, Vol XVI, No 6 June 1952.

54. Borsch-Supan et al "Endothermic gasification of a solid by thermal radiation absorbed in depth" International Journal of Heat and Mass Transfer, Vol 27, No 8, page 117-1182, 1984.

55. Kalson A. P. "Effect of vapour efflux from a spherical particle on heat transfer from a hot gas" Ind Eng Chem Fundem 1983, 22, 357-358.

Ibid "Response to comments" Ind Eng Chem Fundem 1984, 23, page 269.

56. Mills A. F. et al "Analysis of coal particles undergoing rapid Pyrolysis".

57. F. Verfuss et al "Determinations of Heat of Reaction During the Rapid Devolatalization of Hard Coal" Erdol und Kohle, No 7, July 1982, page 332-336.

58. Yellow P. C. "Kinetics of the thermal decomposition of coal" b.c.u.r.a. monthly Bulletin, Vol XXIX, No 9, September 1965.

59. Studier M. H., Hayatsu R., Winans R. E. "Analytical methods for coal and coal products" Vol II Edited by Karr A. Ch 21.

60. Kirov N. Y. and Stephens J. N. "Physical aspects of coal carbonization" Research Monograph, 1967.

61. John M. Lytle et al "Effect of microstructure on the size and shape of coal particles during comminution" Fuel, 1983, Vol 62, November, page 1304

62. Pang, H. M. and Ridgeway K. "Mechanism of sieving: effect of particle size and shape" I. Chem. E. Symposium series No 69, page 163.

63. Cooling D. R. "The hardness of coal and its associated minerals" b.c.u.r.a. monthly Bulletin Vol XXIX, No 12, December 1965.

64. Goyal A. and Gidaspon D. "Simulation of Entrained flow hydropyrolysis reactors" Preprints of the American chemical society, Vol 27, No 1, 1982, page 57.

65. Douglas Smoot L. et al "Mixing and reaction of pulverized coal in an entrained gasifier" Preprints of the American Chemical Society, Vol 27, No 1, 1982, page 77.

66. Stanley Singer "Pulverized coal combustion, Recent developments" Energy Technology Review No 90, 1984, page 45.

67. Gillings D. W. "Carbonized Fuels from non caking coals. Recent results of research and development". The coke oven managers year book, 1957, page 175.

68. Peters W. and Bertling H. "Kinetics of the rapid degasification of coals" Fuel, 1965.

69. Atitmay A. "Combustion of Volatile matter in fluidised beds". Fluidisation, 1980, edited by Grace J. R. and Matsen J. M.

70. Stubington J. F. "The role of coal volatiles in fluidised bed combustion" Journal of the Institute of Energy, Dec 1980.

71. Azhahesan M. "The combustion behaviour of coals in an atmospheric fluidised bed" Msc dissertation, Leeds University 1981.

72. Essenhigh R. H. "Coal Combustion" review in Coal conversion technology, edited by Wen C. Y. and Stanley E.

73. Wendt J. O. L. "Fundamental coal combustion mechanisms and pollutant formation in furnaces" Prog Energy Combust Sci, Vol 6, page 201-222, 1980.

74. Massey, L. G. "Coal gasification" in Coal Conversion Technology, Edited by Wen C. Y. and Stanley Lee E. page 313-427.

75. Dent F. J. et al "An Investigation into the Catalytic Synthesis of Methane by town gas manufacture" 49th Report of the Joint Research Committee of the Gas Research Board and the University of Leeds, GRB20, 1945.

76. Johnson J. L. "Coal Gasification" L. G. Massey, Ed., Advances in Chemistry Series 131, American Chemical Society, Washington D.C., 1974.

77. Brown H. R. and Waters P. L. "The function of solvent extraction products in the coking process II - A theory of the mechanism of thermal softening" Fuel, 1966, Vol 45, page 41-59.

78. Kanury, M.A. "Introduction to Combustion Phenomena"
Combustion Science and Technology
Book Series, Volume 2.

79. Gomes, W. "Definition of rate Constant and Activation Energy In Solid State Reactions"
Nature, 192, 865 -866, 1961

80. Taplin, J.H. "Significance of Experimental Rate Constants"
Nature, 194, 471-472, 1962.

81. NCB Review 1976

82. Joiner, J.R. and Kovach J.J. "Sasol Two and Three"
Energy Progress (Volume 2, No. 2) June, 1982, Page 66-68

83. Berkowitz, N. "The Chemistry of Coal". Coal Science and Technology Series, 7 Elsevier, 1985.

84. Francis, E.H. "British Coalfields". Sci. Prog., Oxford (1979), 66, 1-23

85. Undergraduate Notes, Department of Applied Chemistry, Brighton Polytechnic, Author, J.W. Webb

86. Stack's textbook of Coal Petrology, 1982 edition

87. Amir Attar and Francois Dupuis "Data on Distribution of Organic Sulphur Functional Groups in Coals".
American Chemical Society, 1981.

88. Joseph Haggin "Interest in Coal Chemistry Intensifies"
C & EN, Aug. 9, 1982 Page 17-26

89. Kessler F.M., "Interpretation of the Chemical Compostion of Bituminous Coal Macerals".
Fuel, 1973, Vol. 52, July, Page 191-197

90. Coal Structure, edited by Robert A. Meyers.

91. Paul B. Weisz "The Science of the possible" Chemtech, February 1982.

92. Harris L. A. and Yust C. S. "The ultrafine structure of coal Determined by Electron microscopy in Coal Structure, Eds., Martin L. Gobarty and Ouchi K., 1982.

93. Fitzgerald D. "8th Arthur Duckham Research Fellowship report (1955-1956)" Publication No 516, The Institute of gas engineers.

94. Whitehurst D. D. "A Primer on the Chemistry and Constitution of Coal" 1978 ACS publication.

95. Collins C. J. et al Fuel, 1977, 56, 107.

96. Leon Petrakis & Grandy D. W. "Fuel"1981, Vol 60, Feb, 115.

97. Robert M. Davidson "Molecular Structure of Coal" Report No ICTIS/TR08, 1980, IEA Coal Research.

98. "Coal Structure" Edited by Gobarty M. L. and Ouchi K., ACS series, 192.

99. Gibson J. "The 1977 Robens Coal Science Lecture" Journal of the Institute of Fuel, June 1978 page 67-81.

100. Wheeler R. V. "Destructive Distillation" The Institute of Fuel, October 1938.

101. Hayatsu R. et al "Trapped organic compounds and aromatic units in coals" Fuel, 1978, Vol 57, September.

102. Peter H. Given et al "The concept of a mobile or molecular phase within the macromolecular network of coals: A debate" Fuel, 1986, Vol 65, February, 155-162.

103. Anna Marzcek et al"Mechanism of swelling and extraction and coal structure" Fuel, 1983, Vol 62, August, 977.

104. Peter H. Given "Concepts of Coal STructure in relation to combustion behaviour" Prog. Energy Combust. Sa., 1984, Vol 10, page 149-158.

105. Painter P. C. et al "FTIR study of hydrogen bonding in coal" Fuel, 1987, Vol 66, July, 973-978.

106. Alan Grint et al "Role and Composition of mobile phase in coal", Fuel, 1985, Vol 64, October, 1355-1361.

107. Spiro C. L. "Space filling models for coal: A molecular description of coal plasticity" Fuel, 1981, Vol 60, December 1121-1126.

Ibid, Fuel, 1982, Vol 61, November, page 1080-1084.

108. Oberlin A. "Carbonization and graphitization" Carbon Vol 22, No 6, page 521-541, 1984.

109. John A. G. Drake et al, Fuel, 1984, Vol 63, May.

110. Danuta Bodzek et al "Molecular components of coal and coal structure" Fuel, 1981, Vol 60, January, 47-51.

111. Tsai C. S. Coal Science series No 2.

112. 1983 International Conference on Coal Science Proceedings.

113. Kim S. S. et al "Application of ESR for Coal Pyrolysis and Quench Solvent Evaluation" - A.C.S. preprints; Vol 27, No 3-4, September 1982.

114. Je J. H. and Jai Young Lee "A study on the deposition of Pyrolytic carbons from hydrocarbons" Carbon, Vol 22, No 6, page 563-570, 1984.

115. Coal research in CSIRO, No 29, June 1966. "Carbons from cracking of coal tars" page 8-10.

116. Philip L. Walker "Carbon, an old but new material: the continuing story" Chemistry and Industry, 18th September 1982 page 683-691.

117. Philip L. Walker "Structure of coals and their conversion to gaseous fuels" Fuel, Vol 60, September 1981, page 801-802.

118. Dirk W. Van Krevelen "Development of coal research - a review" Fuel, Vol 61, September 1982, page 786-790.

119. Brown and Waters P. L. "The Function of Solvent Extraction products in the Coking Process II - A theory of the mechanism of Thermal Softening" Fuel, Vol 45, January 1966, page 41-59.

120. Harold Juntgen "Review of the Kinetics of Pyrolysis and Hydropyrolysis in relation to the chemical constitution of coal" Fuel, Vol 63, June, 1983, page 731-737.

121. Solomon P. R. "Coal structure and thermal decomposition" in "New approaches in coal chemistry" A.C.S. Symposium Series 169, 1981, page 61.

122. Coal research in C.S.I.R.O., No 17, August 1962, page 1-6.

123. Teichmüller M. and Durand B. "Fluorescence microscopical rank studies on liptinites and vitrinites in Peat and Coals, and comparison with results of the Rock-Eval Pyrolysis" International Journal of Coal Geology, 2, 1983, page 197-230.

124. D. Duayne Whitehurst, Editor "Coal liquefaction fundamentals" A.C.S. Symposium Series, 139, 1980.

125. Tyler R. J. "Devolatalization of bituminous coals by flash Pyrolysis" Fuel, 1980, Vol 59, April, page 218-226.

126. Henk L. C. Meuzelaar et al "Characterization of coal maceral concentrates by Curie-point Pyrolysis mass spectrometry" International Journal of Coal Geology, 4(1984), page 143-171.

127. Fenton G. W. and Smith A. H. V. "Petrological studies of British Bituminous coals in relation to utilization, with special reference to carbonization" in "Residential Conference on Science in the use of coal" April, 1958.

128. Claus F. K. Diessel "Carbonization reactions of Inertinite macerals in Australian coals" Fuel, 1983, Vol 62, August, page 883-892.

129. Ching-Yi Tsai and Scaroni A. W. "Pyrolysis during the inital stages of pulverized-coal combustion" 20th Symposium on Combustion, August 1984.

130. Hamilton L. H. "Char morphology and behaviour of Australian Vitrinites of various ranks Pyrolysed at various heating rates" Fuel, 1981, Vol 60, October, page 909-913

Ibid, 1980, Vol 59, February, page 112-116.

131. Anson et al "Structure and surface area of pulverized coal during combustion" Combustion and Flame, 16, 265-274, (1971).

132. N. Oka et al "The influence of rank and maceral composition on ignition and char burnout of pulverized coal" (Private copy).

133. Newall H. E. and Sinnatt F. S. "The carbonisation of coal in the form of fine particles - 1, The production of cenospheres Fuel in Science and Practice, December 1924, page 424-434 - "The study of cenospheres II & III" ibid, 5, 335, (1926) and 6, 118, (1927).

134. Khan M. R. and Jenkins G. R. "Swelling and plastic properties of coal devolatalized at elevated pressures: An examination of the influence of coal type" Fuel, 1986, Vol 65, May, page 725-731.

135. Ergun et al "Microscopic studies of rate of thermal decomposition of petrographic components of coal" Fuel, 1958.

136. Macrae, J. C. "The thermal decomposition of spore exines from Bituminous coal" Vol 22, No 5, Fuel in Science and Practice, page 117-129.

137. Girling G. W. "Evolution of volatile hydrocarbons from coal" J. appl. Chem., 13th February 1963, page 77-91.

138. Kekin N. A. et al "Behaviour of coals upon heating in a high vacuum and in caking mechanism" Koks i Khimiya, No 1, page 3-8, 1984.

139. Arendt P. and Karl-Heinrich Van Heek "Comparative investigations of coal Pyrolysis under inert gas and H_2 at low and high heating rates and pressures up to 10 mPa" Fuel, 1981, Vol 60, September, page 779-794.

140. Sundaram, M. S. et al "Flash Pyrolysis of coal in reactive and non reactive gaseous environments" A.C.S. preprints, 28(5), 1983.

141. Rau E. and Robertson J. A. "The use of the microsample strip furnace in coal research" Fuel, 45, 73 (1966).

142. Blair D. W. et al "Evolution of Nitrogen and other species during controlled Pyrolysis of coal" 16th Symposium (International) on Combustion.

143. Solomon P. R. and Colket M. B. "Coal devolatalization" 17th Symposium (International) on Combustion.

144. Waters P. L. "Fractional thermogravimetric analysis" Analytical Chemistry, Vol 32, No 7, June 1960, page 852-858.

145. Roy C. et al "Vacuum Pyrolysis of Prince Mine coal, Nova Scotia, Canada" Fuel, 1985, Vol 64, December, page 1662-1666.

146. Solomon P. R. and Hsiang-Hui King "Tar evolution from coal and model polymers: theory and experiment" Fuel, 1984, Vol 63, September.

147. Gat N. et al "Coal Pyrolysis under rapid heating with a C W laser" Meeting of the Central States Section of the Combustion Institute, Lexington, KY, March, 1983.

148. ---------- "On Internal Temperature gradients in a Pyrolysing coal particle" Combust. Sci. and Tech., 1986, Vol 49, page 297-303.

149. Khay C. Teo & Watkinson P. A. "Charaterization of Pyrolysis tars from Canadian coals" Fuel, 1987, Vol 66, August, page 1123-1132.

150. Kopp O. C. and Harris L. A. "Initial volatalization temperatures and average volatalization rates of coal - their relationship to coal rank and other characteristics" International Journal of Coal Geology, 3 (1984), page 333-348.

151. Glen H. Ko et al "Correlation of tar yields from rapid Pyrolysis with coal type and pressure" Fuel, 1987, Vol 66, August, page 118-1122.

152. Mookerjea S. K. and Mazumdar B. K. "Some aspects of the low temperature Pyrolysis behaviour of coal" Fuel.

153. Furimsky E. et al "Effect of Coal rank on structure of tars from low temperature Pyrolysis of Canadian Coals" Ind. Eng. Chem. Prod. Res. Dev. 1984, 23, page 134-140.

154. Freihaut J. D. et al "A parametric investigation of tar release in coal devolatalization" 19th Symposium (International) on Combustion, The Combustion Institute, 1982, page 1159-1167.

155. Menster M. et al, Preprints, Am. Chem. Soc. Div., Fuel Chem., 14(5), 94 (1970).

---------- Coal gasification, Advances in Chemistry Series, 131, 1974, page 1-8.

156. Suuberg E. M. et al "Product composition and formation kinetics in rapid Pyrolysis of pulverized coal - implications for combustion" 17th Symposium (International) on combustion. Combustion Institute, page 117-130.

157. Loison R. and Chauvin R. "Rapid Pyrolysis of Coal" Chemie et Industrie, Vol 91, No 3, March 1964, page 269-274.

158. Freihaut J. D. et al "Reaction induced temperature deviations during coal devolatalization in a heated grid" American Chemical Society, Division of Fuel Chemistry, Preprints, Vol 27, No 2, 1982.

---------- "Evolution of fuel Nitrogen during the vacuum thermal devolatalization of coal" Preprints, Am. Chem. Soc. Div. of Fuel Chemistry, Vol 26, No 3, page 18-44.

159. Juntgen H. and Van Heek K. H. "Gas release from coal as a function of the rate of heating" Fuel.

160. Jixi Romovacek and Jaroslav Kubat "Characterization of coal substance by Pyrolysis-gas chromatography" Analytical Chemistry, Vol 40, No 7, June 1968, page 1119-1126.

161. Solomon P. R. and David G. Hamblen "Finding order in coal Pyrolysis kinetics" Prog. Energy Combust Sci. 1983, Vol 9, page 323-361.

162. Street P. J. et al, Fuel, 48, 343, (1969).

163. Solomon et al "Coal gasification reactions with on-line in-situ FTIR analysis" 2nd quarterly report, DOE/FE/05122--T2, 30th March, 1982.

164. Solomon et al, 2nd quarterly report, DOE contract No DE-AC22-82PC50254, November 20th 1982.

165. Brown and Waters "Chloroform Entracts of coal" Coal Research in C.S.I.R.O., No 29, June 1966.

166. Geoffrey Fynes et al, Fuel, 1984, Vol 63, July, page 897-903.

167. Vastola F. J. and McGahen L. J., Fuel, 1987, Vol 66, July, page 886-889.

168. Karn F. S. et al, Fuel, 1972, Vol 51, April, page 113-115.

169. Agreda V. H. et al "Coal devolatalization and elemental release in batch and laminar flow furnace reactors" Am. Inst. Chem. Engrs., 1980, page 87.

170. Dormans H. N. M. and Van Krevelen D. W., Fuel, Vol 39, 1960, page 273-292.

171. Wolfs et al, Fuel, Vol 39, 1960, page 25-39.

172. Chermin H. A. G. and Van Krevelen D. W., Fuel, Vol 36, 1957, page 85-104.

173. Van Krevelen et al, Fuel, Vol 35, 1956, page 462-475.

174. Thiessen R. and Sprunk G. C., Fuel, Vol XIII, No 4, page 116-125.

175. Fitzgerald D., Transactions of the Faraday Society, No 399, Vol 52, Part 3, March 1956.

176. Van Krevelen et al, Fuel XXX-LL, 1951, page 253-259.

177. Macrae J. C. and Finlayson P. C., Proceedings of the Residential Conference on Science in the use of Coal (Sheffield, April, 1958), page C-15.

178. Waters P. L., Fuel, Vol 41, 1962, page 3-4.

179. Fong W. S. et al, Fuel, 1986, Vol 65, February, page 195-201.
---------- , ibid, page 251-254.

180. Hurst N. W. and Jones T. A., Fire and materials, Vol 9, No 1, 1985.

181. Badziock S., B.C.U.R.A. Monthly Bulletin, Vol XXV, No 8, August, 1961.

182. Idris Jones N., Journal of the Institute of Fuel, January 1964, page 3-11.

183. David Gray et al, "Problems in pulverized coal and char combustion" in "Coal gasification", edited by L. G. Massey.

184. Klose W. and Lent M., 1983 International Conference on coal science, page 517-520.

185. Pitt C. J., Fuel, Vol 41 , 1962, page 267

186. Farbory Goodarzi et al, Fuel, Vol 57, May 1978, page 273.

187. Isao Mochida and Harry Marsh, Fuel, Vol 58, September 1979, page 626.

188. Lewis I. C., Carbon, Vol 20, No 6, page 519-529, 1982.

189. Walker P. L., Carbon, Vol 24, No 4, 1986, page 379-386.

190. Peter S. Maa et al, Fuel, 1975, Vol 54, January, page 62-69.

191. Delert H. H. "Chemical characteristics of the thermal decomposition of Bituminous coals" Fuel, Vol , 1968 & 1969, page 433-448.

192. Peet N. J. et al, "The rapid carbonization of high organic sulphur New Zealand coals" Fuel, Vol , 1969, page 259.

193. Yaw D. Yeboah et al, Ind. Eng. Chem. Process Des. Dev., 1982, 21, page 324-330.

194. Alan A. Herod and Cathryn A. Smith, Fuel, 1985, Vol 64, February, page 28..

195. Thomas M. G. et al, Fuel, 1982, Vol 61, August, page 761.

196. Thomas W. Lester et al, Fuel, 1982, Vol 61, June, page 493.

197. Doolan K. R. et al, 19th Symposium (International) on combustion, 1982, page 1131-1138.

198. Teo K. C. and Watkinson, Fuel, 1986, Vol 65, July, page 949-959,.

199. Calkins W. H. et al, Fuel, 1984, Vol 63, August, page 1113-1118.

200. Calkins W. H. and Tyler J. R., Ibid, page 1119-1112.

201. Calkins W. H., Ibid, page 1125-1129.

202. Calkins W. H. and Sparkman W., International Journal of coal Geology, 6 (1986), page 1-19.

203. Antal M. J. et al, Combustion Science and Technology, 1980, Vol 21, page 141-152.

204. W. Davies et al, Sheffield U

205. J. Verfus Et al, Erdol und Kohle, Erdas Vereinigt mit Brenstoff-Chemie (35) No 7, July 1982, page 332-336.

206. Unger P. E. and Suuberg E. M., 18th Symposium (International) on Combustion. The Combustion Institute, 1981, page 1203.

207. Juntgen and Van Heek K. H., Fuel Processing Technology, 2, (1979), page 261-293.

208. Solomon P. R. and Hsiang-Hui King., Fuel, 1984, Vol 63, September, page 1302-1311.

209. Attar A., A.I.Ch.E. Journal, Vol 24, No 1, 1978, page 106-115.

210. Russel B. W. et al, A.I.Ch.E. Journal, Vol 25, No 1, January 1979, page 65-80.

211. Gavalas G. R. and Wilks K. A., A.I.Ch.E. Journal (Vol 26 No 2), March 1980, page 201-212.

212. Devanathan N. and Sa ena S. C., Ind. Eng. Chem. Res. 1987, 26, page 539-548.

213. Cussler S. L., Chemtech, July 1986, page 422.

214. Salvador F. et al, Journal of Chemical Education, Vol 61, No 10, October 1984, page 921.

215. Suuberg E.M. et al, 17th Intl. Symp. on Combustion, 1978.

216. Niksa S. J. et al, Fuel, 1982, Vol 61, December, page 1207.

217. Hamilton L. H. et al, Fuel, 1979, Vol 58, December, page 873.

218. Wagner R. et al, Fuel, 1985, Vol 64, April, page 571-573.

219. Peters A. W. P. G. et al, I.Chem.E. Symposium Series No 69 page 1-57.

220. Agràwal and Sivasubramaniam, A.I.Ch.E. Journal July 1987, Vol 33, No 7.

221. Serio M. A. et al, Ind. Eng. Chem. Res. 1987, 26, 1831-1838.

222. Jamaluddin et al, Combustion and Flame, 62:85-89, 1985, page 85-89.

223. Ciuryla V. T. et al, Fuel, 1979, Vol 58, October, page 748-754.

224. Antal M. J. et al, Preprints, Division of Fuel Chem. Vol 23, A.C.S., March (1977).

225. Freihaut J. D. et al, Preprints, Division of Fuel Chem. Vol 22 (1), 173, National Meeting, A.C.S., March 1977.

226. WilliamsA., Combustion and Flame, 1973.